

FROM RECHARGE TO REEF:  
ASSESSING THE SOURCES, QUANTITY, AND TRANSPORT OF  
GROUNDWATER ON TUTUILA ISLAND, AMERICAN SAMOA

A DISSERTATION SUBMITTED TO THE GRADUATE DIVISION OF  
THE UNIVERSITY OF HAWAII AT MĀNOA IN PARTIAL  
FULFILLMENT OF THE REQUIREMENTS FOR THE DEGREE OF

DOCTOR OF PHILOSOPHY  
IN  
EARTH AND PLANETARY SCIENCES

MAY 2019

By  
Christopher K. Shuler

Dissertation Committee:  
Aly I. El-Kadi, Chairperson  
Henrietta Dulai  
Craig R. Glenn  
Scot Izuka  
Celia Smith

*"Only when the well is dry, will we know the worth of water."*  
- Benjamin Franklin

## ACKNOWLEDGEMENTS

To quote one of my first graduate mentors, Dr. Alex Messina,

*“The fundamental social unit of the Fa’a Samoa, or the Samoan way of life is the aiga, or extended family. All success and prosperity is shared equally with each member, as it is recognized that no individual succeeds without the full support of the aiga.”*

Throughout the preparation of this dissertation I have been supported by an incredible network of people across the Samoan and Hawaiian island chains. It is with much alofa and aloha that I extend my deepest gratitude to the many individuals and agencies who were all essential for making this work possible.

Firstly, I must thank my committee chair and main adviser, Aly I. El-Kadi as well as my dissertation committee, Henrietta Dulai, Craig R. Glenn, Scot Izuka, and Celia Smith for always supporting me as I explored my ideas, no matter how obscure. I would like to thank the porespace crew, Joe Fackrell, James Bishop, and Christine Waters, for teaching me how to be a real graduate student, and I would also like to thank the GG grad student ohana for plenty of good beach days and Friday evenings at TGs. This work would not have been possible without the collaboration of the American Samoa Power Authority, the American Samoa EPA, the American Samoa Community College and Land Grant, and the Coral Reef Advisory Group. Additionally, I would like to thank all of the individuals who acted as research colleagues, mentors, or arm-chair advisers, including Paul Eyre, Tim Bodell, Katrina Mariner, Will Spitzenberg, Mia Comerios, Ian Gurr, Mark Schmaedic, Hideo Hatori, Kristine Bucchianeri, Mia Comeros, Marike Sudek, Alice Lawrence, Matt Erickson, Taylor Viti, Eric Welch, Olkeba Leta, Brytne Otuhaka, April Kam, Patricia Hirakawa, Rosie Alegado, Dan Amato, Veronica Gibson, Lydia Baker, Nalani Olgun, Alan Mair, Ito, and Alex Messina. I would also like to give my appreciation to Barbara Guieb, Kevin Nishimura, John Matassa, Arlene Sullivan, Susan Van Gorder and Lily Shao for teaching me essential skills in navigating university bureaucracy.

I want to dedicate this work to Utu Abe Malae, former ASPA executive director and likely the most effective champion of water resources sustainability in American Samoa.

I would also like to acknowledge funding and support provided by NOAA’s Pacific Regional Integrated Sciences and Assessments Program (Pacific RISA), the USGS Water Resources Research Institute Program, The US-EPA Region IX Making a Visible Difference Program, The Arcs Foundation, and the UH-Manoa Geology and Geophysics Department.

I thank my family, the in-laws, and the outlaws, for their continual encouragement, and especially, I thank my incredible wife who has remained supportive, reassuring, and inspiring throughout these long years of graduate student pay. I would also like to acknowledge my newborn daughter, who through her mere existence has pushed me to pull it all together and finish this work. Finally, I would like to thank the people of American Samoa for their friendliness, welcoming nature, and curiosity that has allowed my research to be enjoyable, successful, and I hope, impactful.

## ABSTRACT

On high volcanic islands, groundwater resources are essential for maintaining human habitability and for sustaining coastal and aquatic ecosystems. On the island of Tutuila in American Samoa, groundwater is the only source of drinking water to over 90% of the island's approximately 60,000 residents. However, the island's population faces numerous water quality and water quantity challenges including well salinization, aquifer contamination by anthropogenic sources, and environmental water quality degradation. The purpose of this work is to contribute to new understanding of these issues in tropical island environments, and specifically for the island of Tutuila, by exploring a wide range of hydrogeologic phenomena through presentation of six individual chapters; each of which targets a small set of the territory's most critical water resources management questions. This dissertation commences in its Introduction and concludes in its Appendices with a comprehensive literature review on the topic of American Samoan hydrogeology, which is contextualized as a conceptual hydrogeologic model that supports the other studies presented here as individual chapters. Chapter 2 details the application of geochemical and biological tracers to determine the mechanism of contamination in wells on Tutuila's Tafuna-Leone Plain that have caused one of the longest standing boil-water-notices in U.S. history. Chapter 3 explores surface water - groundwater interaction in one of the island's steepest watersheds and uses natural environmental tracers to quantify submarine groundwater discharge (SGD) and associated nutrient loading. This study shows how comprehensive, tracer-based field assessment of SGD can be complimented by watershed modeling to develop a conceptual hydrogeologic model of groundwater-surface water interaction and to quantify coastal nutrient loading by multiple hydrologic pathways. Chapter 4, expands upon the techniques used in Chapter 3 and also examines macroalgal tissue parameters to quantify the impact of land-based, nutrient-pollution sources on four separate watersheds spanning a human-impact gradient. Chapter 5 presents the development and results of a water budget assessment of Tutuila Island, specifically designed to estimate spatially distributed groundwater recharge, and including effects of future climate change. Chapter 6 presents a distinctive approach to groundwater modeling; instead of focusing on model results, this chapter focuses on the vertically-integrated, cloud-based, and process oriented collaborative modeling framework applied jointly between researchers and water utility staff at the American Samoa Power Authority to develop a cooperative groundwater modeling process. As a case study, this chapter shows how the collaborative approach can be applied to develop modeling products that have greater longevity and applicability to the needs of resource managers. Each of the individual chapters in this dissertation is linked through the common goal of seeking to provide researchers, water resource managers, and policy makers with applied science tools that can be used to improve water resources sustainability in American Samoa and throughout the Pacific.

# Table of Contents

Chapter 1:.....	1
Introduction and Conceptual Hydrogeologic Model .....	1
1.1 Background and Motivation .....	1
1.2 Dissertation Significance, Objectives, and Outline .....	2
1.3 Geographic Setting .....	4
1.3.1 Regional Setting.....	4
1.3.2 Regional Geologic History .....	5
1.4 Geology of Tutuila.....	6
1.4.1 Pleistocene Volcanic Shields.....	6
1.4.2 Sedimentary Units and Changes in Sea Level.....	8
1.4.3 Holocene Leone Volcanics.....	9
1.5 Updated Conceptual Hydrogeologic Model of Tutuila, American Samoa .....	9
1.5.1 General Conceptual Hydrogeologic Model of Basalt Islands .....	10
1.5.2 Hydrogeologic Units on Tutuila .....	12
1.5.3 Groundwater Occurrence in Tutuila’s Hydrogeologic Units.....	13
1.5.4 Conceptual Model Summary .....	20
Chapter 2:.....	21
Isotopes, Microbes, and Turbidity: A Multi-Tracer Approach to Understanding Recharge Dynamics and Groundwater Contamination in a Basaltic Island Aquifer ...	21
Abstract.....	21
2.1 Introduction.....	22
2.1.1 Study Location.....	25
2.2 Methods .....	27
2.2.1 Turbidity, Rainfall, and Video Log Data.....	27
2.2.2 Indicator Bacteria on Annual Scales.....	28
2.2.3 Water Isotopes in Precipitation and Groundwater .....	28
2.3 Results.....	29
2.3.1 Results: Groundwater Turbidity and Response to Rainfall .....	29
2.3.2 Results: Indicator Bacteria in GUDI and non-GUDI Wells.....	32
2.3.3. Results: Water Isotopes in Precipitation and Groundwater .....	35

2.4 Discussion.....	39
2.4.1 Expected Groundwater Travel Times .....	39
2.4.2 Isotope Mixing Model: Recent-Rainfall and Old-Groundwater Fractions.....	43
2.5 Conclusions.....	46
References: Chapter 2.....	47
Chapter 3:.....	50
Understanding Surface Water - Groundwater Interaction, Submarine Groundwater Discharge, and Associated Nutrient Loading in a Small Tropical Island Watershed .....	50
Abstract.....	50
3.1 Introduction.....	51
3.2 Study Area .....	53
3.3 Methods .....	55
3.3.1 Water Sampling and Stream Gauging Methods.....	55
3.3.2 Radon-Based SGD Measurement .....	56
3.3.3 Watershed and Land-Use Modeling.....	58
3.4. Results.....	61
3.4.1 Conceptual Hydrogeologic Model.....	61
3.4.2 Characterization of Baseflow Components .....	62
3.4.3 SGD Rates and Nutrient Fluxes.....	64
3.4.4 Nearshore Water Quality.....	68
3.4.5 SWAT Model Results.....	68
3.5 Discussion.....	74
3.5.1 Implications for Natural Resources Management .....	74
3.5.2 Conceptual Model Implications.....	75
3.5.3 Nitrogen Source Tracing.....	75
3.5.4 SWAT Model Applicability.....	76
3.5.5 Assumptions and Limitations of the SWAT Model .....	77
3.6 Conclusions.....	79
References: Chapter 3.....	80
Chapter 4:.....	89
Assessment of Terrigenous Nutrient Loading to Coastal Ecosystems along a Human Land-Use Gradient, Tutuila, American Samoa.....	89
Abstract.....	89

4.1. Introduction.....	90
4.1.1 Study Location descriptions .....	92
4.2. Materials and Methods.....	94
4.2.1 Water Sample Collection and Analysis.....	94
4.2.2 Time-Series and Survey Based <sup>222</sup> Rn Measurements .....	97
4.2.3 SGD and Nutrient Flux Calculations .....	97
4.2.4 In Situ Algal Survey.....	98
4.2.5 Algal Deployments .....	99
4.3. Results.....	100
4.3.1 Water Quality Results: Nutrient Levels .....	100
4.3.2 Water Quality Results: Nitrate Isotopes.....	101
4.3.3 Water Quality Results: Nearshore – Offshore Gradient.....	101
4.3.4 Hypnea Deployment Results .....	104
4.3.5 In-situ Algal Survey Results .....	104
4.3.6 SGD Rates and Associated Nutrient Fluxes .....	106
4.3.7 Stream Baseflow Estimates and Associated Nutrient Fluxes .....	108
4.3.8 Validation of SGD Measurements .....	109
4.4. Discussion.....	111
4.4.1 Nutrient Levels in Coastal Management Context.....	111
4.4.2 Comparison of Watersheds Along an Expected Land Use Gradient .....	112
4.4.3 Management Considerations and Future Directions.....	116
4.5. Conclusions.....	117
References: Chapter 4.....	118
Chapter 5:.....	126
Groundwater Recharge for Tutuila, American Samoa Under Current and Projected Climate as Estimated with SWB2, a Soil Water Balance Model.....	126
Abstract.....	126
5.1 Introduction.....	127
5.1.1 Study Area .....	129
5.2 Methods .....	130
5.2.1 Gridded Monthly Precipitation .....	132
5.2.2 Rainfall Fragments.....	132

5.2.3 Land Use .....	134
5.2.4 Soils .....	135
5.2.5 Runoff to Rainfall Ratios .....	136
5.2.6 Direct Infiltration .....	139
5.2.7 Potential Evapotranspiration.....	141
5.2.8 Canopy Interception and Losses.....	142
5.2.9 Mountain Front Recharge .....	143
5.3 Results and Discussion .....	145
5.3.1 Future Climate Scenarios.....	149
5.3.2 Sensitivity Analysis.....	153
5.3.3 Comparison to Previous Tutuila Water Budget Studies.....	157
5.4 Summary and Conclusions .....	158
5.4.1 SWB Technology Transfer.....	162
References: Chapter 5 .....	163
Chapter 6:.....	166
Collaborative groundwater modeling: Open source, cloud-based, applied science at a small-island water utility scale .....	166
Abstract.....	166
6.1 Introduction.....	167
6.1.1 Objectives .....	169
6.2 Case Study Setting.....	169
6.2.1 Collaborative Groundwork .....	170
6.3 Methods .....	171
6.3.1 Modeling Framework .....	171
6.3.2 Cyber-infrastructure Framework .....	173
6.3.3 Weather Station Infrastructure .....	176
6.3.4 Stream Gauge Infrastructure.....	177
6.3.5 SWB2 Model Development.....	178
6.3.6 FloPy Model Development.....	179
6.4 Process Implementation and Discussion.....	180
6.4.1 Weather Data Process Implementation .....	180
6.4.2 Streamflow Data Process Implementation.....	180

6.4.3 SWB Implementation .....	183
6.4.4 FloPy Implementation .....	184
6.5 Conclusions.....	190
6.5.1 Continuing Work.....	190
6.5.2 Final Thoughts .....	191
References: Chapter 6.....	192
Appendix A: Conceptual Hydrologic Model Data .....	197
A1 Compilation and Interpretation of Subsurface Logs.....	197
A2 Examination of Lava Outcrops in Pleistocene Volcanic Rocks.....	208
A3 Interpretation of New Geophysics and Well Logging .....	212
A4 Hydrogeologic Data from Wells and Pumping Tests.....	215
A5 Numerically Modeled Values of Hydraulic Conductivity .....	222
A6 High-Level Spring Occurrence and Geochemistry.....	223
A7 Streamflow Analysis .....	228
Appendix B: Consolidated Aquifer and Well Monitoring Data.....	231
B1 Underutilized or Unexplored Areas .....	234
B2 Moderately Utilized Areas .....	247
B.2.1 Eastern Tutuila Region.....	248
B3 Heavily Developed Areas.....	265
REFERENCES: Chapter 1 and Appendices A and B .....	284
Appendix C: Supplementary Data .....	289
C1 Chapter 3 .....	289
C2 Chapter 4 .....	293

# Chapter 1:

## Introduction and Conceptual Hydrogeologic Model

### 1.1 Background and Motivation

Groundwater resources on high volcanic islands serve several important functions. Because surface water supplies are commonly limited in these settings, groundwater is often the primary water resource available for human needs. Natural groundwater discharge to coastal and terrestrial-aquatic ecosystems supports biodiversity by providing baseflow to streams, moderating salinity, and delivering nutrients or other dissolved constituents to reefs. Because of the isolated nature of oceanic islands, the importance of effectively utilizing, preserving, and protecting their limited groundwater resources is undeniable. Developing a well-informed and data-driven understanding of groundwater quality and quantity in island settings is a prerequisite for supporting ecosystem services and for developing sustainable water resource management strategies.

On Tutuila, the main island in the U.S. Territory of American Samoa, groundwater provides drinking water to over 90% of the island's approximately 60,000 residents (AS-DOC, 2013). In the past, overuse of groundwater from some of the island's aquifers caused salinization of wells, reduction in water quality, and necessitated abandonment of entire well fields. At present, island wide groundwater extraction rates, minus transmission losses, often cannot keep pace with municipal and industrial water demand, resulting in frequent interruptions to water service. A large range of hydraulic conductivities in the island's rocks causes production rate limitations in extremely low-conductivity areas, and groundwater contamination issues in highly conductive zones. Groundwater under the direct influence of surface water in the Tafuna-Leone Plain region (ASEPA, 2010) has afflicted portions of Tutuila with one of the longest-standing boil-water advisories in U.S. history (ASEPA, 2016). Additionally, water quality in many of the island's aquifers is threatened by anthropogenic contamination caused by prevalent non-point pollution sources (Shuler et al., 2017). Excessive nutrient delivery to reefs via the process of SGD is a plausible, yet understudied threat to the health of coastal ecosystems (Houk et al., 2013; Whitall and Holst, 2015). Compounding these issues is the fact that the island's landmass is quite small (less than 1/10<sup>th</sup> of Oahu, Hawaii); therefore, the total volume of freshwater storage is limited. To address these issues, quantitative hydrogeologic assessments are needed, and these assessments are fundamentally based on a well-informed understanding of the island's hydrogeology.

## 1.2 Dissertation Significance, Objectives, and Outline

The purpose of this work is to improve scientific understanding of hydrogeologic processes in tropical island environments, and on a local level, to address a set of American Samoa's most critical water resources management questions through applied scientific investigation of climatic, geologic, hydrologic, geochemical, and biological phenomena. American Samoa is located over 2000 miles away from the nearest continent, and with a total land area of only 199 km<sup>2</sup> (slightly larger than Washington, D.C.) any water resource challenge in the territory is a critical one. Currently the challenges faced in American Samoa include salinization of drinking water wells, anthropogenic contamination of aquifers, and degradation of environmental water quality. While these issues are complex and involve many stakeholders, this work seeks to contribute information towards their solutions by addressing a set of specific research questions that are carefully designed to consider some of the most pertinent needs of resource managers and stakeholders in American Samoa.

While the work presented in the following chapters is generally motivated by applied questions based on management priorities, the application of advanced, cross-cutting geochemical and numerical techniques as tracers of human impact provides a testing ground for these methodologies in this new setting, thereby furthering scientific knowledge regarding the utility of these techniques. However, the most significant contribution made by this work is in advancing the understanding of American Samoan hydrogeology. This may benefit future scientists, resource managers, and policy makers who strive to address the critical water resources challenges that lay ahead for the territory.

Chapter 1, *Introduction*, provides background on the study setting of Tutuila, American Samoa, and also introduces a conceptual hydrogeologic model to support the hydrogeologic framework upon which the other chapters are built.

Chapter 2, *Isotopes, Microbes, and Turbidity: A Multi-Tracer Approach to Understanding Recharge Dynamics and Groundwater Contamination in a Basaltic Island Aquifer*, applies geochemical and biological tracers including turbidity, fecal indicator bacteria, and water isotopes, to assess the mechanism of contamination in wells that have contributed to one of the longest-standing-boil water notices in U.S. history. The primary objective of this chapter is to determine if existing wells can be simply repaired or re-drilled, or if abandonment of the entire aquifer may be necessary.

Chapter 3, *Understanding Surface Water - Groundwater Interaction, Submarine Groundwater Discharge, and Associated Nutrient Loading in a Small Tropical Island Watershed*, shows how comprehensive, tracer-based field assessment of submarine groundwater discharge (SGD) can be complimented by watershed modeling to better understand groundwater-surface water interaction and watershed scale nutrient dynamics. The primary objective of this chapter is to quantify coastal nutrient loading from different anthropogenic sources as they contribute to terrestrial hydrologic pathways including surface runoff, lateral flow, baseflow, and SGD.

Chapter 4, *Assessment of Terrigenous Nutrient Loading to Coastal Ecosystems along a Human Land-Use Gradient, Tutuila, American Samoa*, expands the techniques used in Chapter 3 to four separate watersheds spanning a human-impact gradient, and also incorporates the assessment of macroalgal tissue parameters as a biological indicator of anthropogenic impact in these watersheds. The main objective of this chapter is to provide tools for coastal resource managers to detect or predict which nearshore areas may be at the highest risk of nutrient imbalance.

Chapter 5, *Groundwater Recharge for Tutuila, American Samoa Under Current and Projected Climate as Estimated with SWB2, a Soil Water Balance Model*, presents the development and results of a water budget assessment for Tutuila Island, specifically designed to estimate spatially distributed groundwater recharge. The main objective of this chapter, besides production of a groundwater recharge map, is assessing the effects of future climate change on groundwater resources.

Chapter 6, *Collaborative Groundwater Modeling: Open Source, Cloud-Based, Applied Science at a Small-Island Water Utility Scale*, takes a distinctive approach to groundwater modeling; instead of focusing on model results, this chapter focuses on a vertically-integrated, cloud-based, and process oriented collaborative modeling framework developed cooperatively between our research group and the American Samoa Power Authority. The main objective of this chapter is to present a case study that details the components in this process. These components include weather station and stream gauge installation, water budget modeling, and ongoing groundwater modeling. This case study shows how a collaborative approach can be applied to develop modeling products that have greater longevity and applicability to the needs of resource managers.

# 1.3 Geographic Setting

## 1.3.1 Regional Setting

Tutuila, the largest and most populous island in American Samoa, is located in the South Pacific Ocean near the coordinates of 14° 20' S and 170° 40' W (Fig. 1.1). The island has an area of 142 km<sup>2</sup> and a population of 56,000 residents (AS-DOC, 2013). Tutuila is within the South Pacific Convergence Zone, thus there is abundant rainfall year round. This region experiences some seasonality in precipitation with a wet season and a relatively less-wet season. Monthly average precipitation from November to March is roughly twice that of May to August's still significant rainfall amounts. Rainfall varies considerably with location and elevation (Fig. 1.2) and ranges between 1,800 to 5,000 mm/yr (70–200 in./yr) (Daly et al., 2006). Strong tropical storms and hurricanes also influence the region about once every other year, and an average of 25 to 30 significant thunderstorms affecting the island annually (Kennedy et al., 1987).

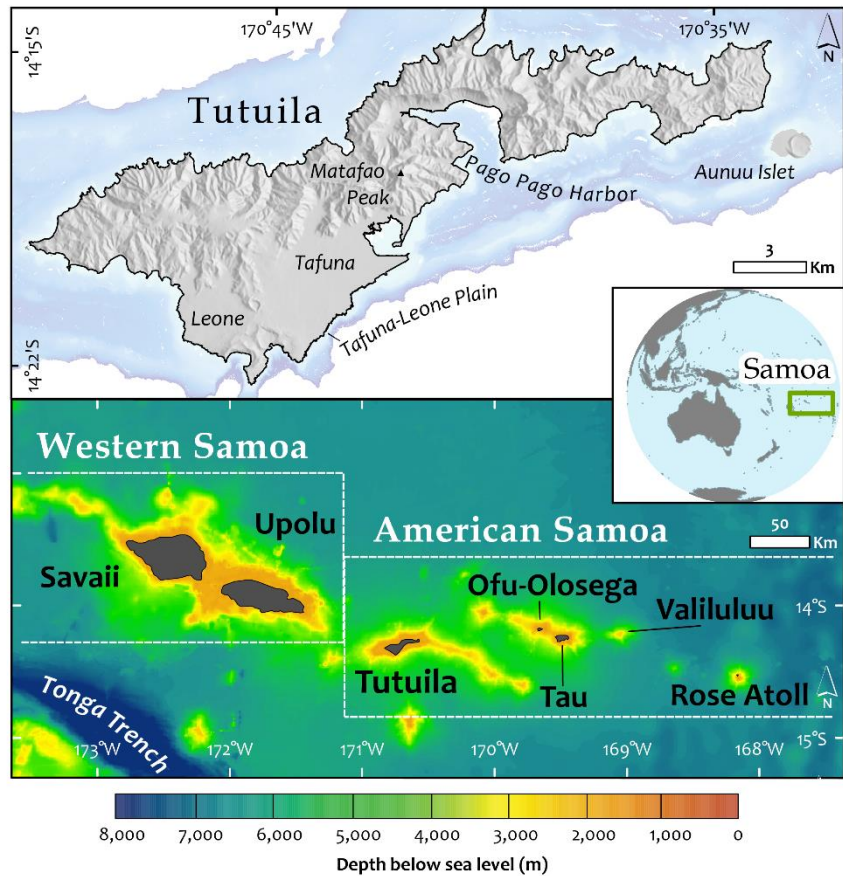


Figure 1.1. Bathymetric map of Samoan archipelago (bottom), and map of Tutuila Island (top). Divisions between Western and American Samoa are drawn to show political jurisdictions and do not constitute actual territorial boundaries. Regional location map shown in middle-right inset.

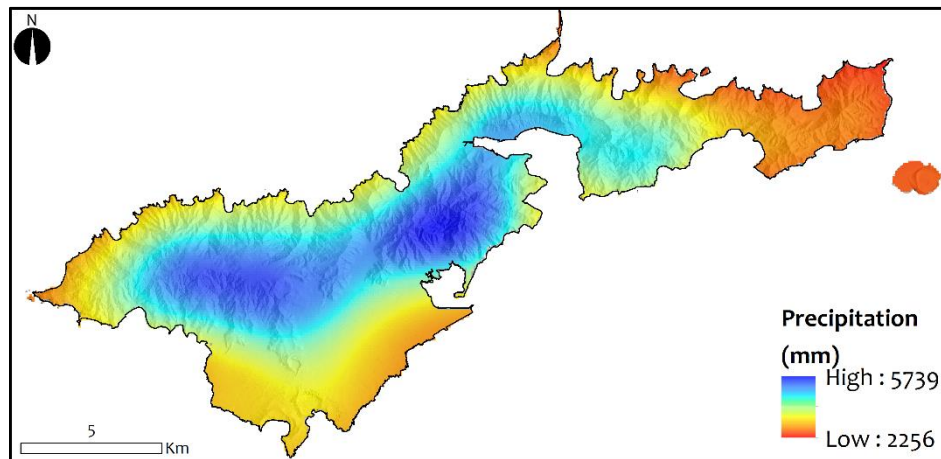


Figure 1.2. Average annual precipitation from climate data recorded from 1971 to 2000 (Daly et al. 2006).

Tutuila can be divided into two primary geographic regions: (1) an east-west trending series of Pleistocene age shield volcanoes that have eroded into a sharp 32 km long ridgeline, and (2) a geologically young (Holocene) series of lava and ash flows on the island's southwestern flank that primarily makes up the Tafuna-Leone Plain (Fig. 1.1). A north-south trending ridge of cinder cones bisects the plain, and the eastern (Tafuna) side of the plain is about twice the size (15 km<sup>2</sup>) of the western (Leone) side (8 km<sup>2</sup>). The older-volcanic shields generally rise 300 to 400 m above sea level with the island's highest point at the summit of Mt. Matafao (653 m). Only a third of the island has a slope of less than 30%, therefore, development density is high in the flatter areas such as the Tafuna-Leone Plain and the small alluvial-fill valleys that ring the island. The steeper parts of the landscape are heavily forested with tropical jungle.

### 1.3.2 Regional Geologic History

The Samoan Archipelago is located near the northern boundary of the Tonga Trench, at the crest of a plate flexure where the seafloor of the Pacific Plate begins to dip southward into the trench (Natland, 2003). Volcanism in the archipelago is likely controlled by both tectonic and hotspot processes, and the islands' eruptive history can be categorized into two distinct phases, respective of these processes. The first phase of Samoan volcanism is attributed to hot spot activity. This phase is thought to have constructed the shield volcanoes that make up the 'core' of each main Samoan island, similar to the way that other hot-spot chains in the Pacific, such as Hawaii, were created. As the Pacific Plate moves westward over a stationary mantle plume, the islands propagate eastward with the youngest island most proximal to the hot spot. Currently, the hot spot is thought to be underneath the volcanically active Vailuluu Seamount, about 20 miles east of Tau Island (Fig. 1.1). The oldest rocks from the chain were dredged from the submarine flanks of the island of Savaii and are dated to 5.2 millions of

years before present (Ma) (Koppers et al., 2008). On Upolu, older rocks range from 3.2 to 1.4 Ma, and Tutuila's older-volcanic mountains date from 1.5 to 1.0 Ma (Natland, 2003). The ages of the Manua islands (Ofu-Olosega and Tau) to the east of Tutuila are much younger, dating to 0.3 and 0.1 Ma (McDougall, 1985), and submarine eruptions from Valiluluu are ongoing (Johnson, 1977).

The second phase of Samoan volcanism is a rejuvenated phase (i.e., post-erosional phase) that probably occurred fairly contemporaneously throughout the late Pleistocene and Holocene on the islands of Savaii, Upolu, and Tutuila (Natland, 1980). The extent of this second phase of eruptions traverses the length of an approximately 300+ km long plate flexure zone across Savaii and Upolu, and to the eastern shore of Tutuila. On Tutuila, the rejuvenated phase created the Tafuna-Leone Plain on the shields' southwestern flank, and Aunuu Islet off of the eastern coast. Natland (2003) proposes this rejuvenated volcanism results from extensional fracturing caused by the structural effects of lithospheric bending as the Pacific Plate subducts into the Tonga Trench. Interestingly, this rejuvenated phase of volcanism is more voluminous on Savaii and Upolu and almost completely covered the original shields, thereby making them larger and creating domed edifices that are clearly less eroded than the highly dissected islands of Tutuila, Ofu, and Olosega. As a whole, the surficial appearance of the Samoan archipelago makes it appear that the more westerly islands (Savaii and Upolu) are younger, although they are not. This apparent discrepancy sparked much scientific debate regarding the validity of the mantle-plume hot-spot model until accurate dates from the Savaii undersea volcanic pile were measured (Koppers et al., 2008).

## **1.4 Geology of Tutuila**

### **1.4.1 Pleistocene Volcanic Shields**

In the Samoan archipelago, Tutuila is third in both size and age, having erupted 1-2 Ma from two or three parallel east-northeast trending rift zones on the ocean floor. During the island's hot-spot phase, four overlapping volcanic shields (Pago, Taputapu, Olomoana, and Alofau) (Fig. 1.3) were contemporaneously erupted over about a half-million years, starting around 1.5 Ma (Stearns, 1944; McDougall, 1985). These eruptions produced a complicated and heterogeneous assemblage of alkalic igneous rocks, in the form of thick lava flows, pyroclastic deposits, and crosscutting intrusive dikes and plugs. At its peak size, about 1.25 Ma, the island may have been nearly 45 km in length, 12 km in width, and about 1,500 m (5,000 ft) tall (Stearns, 1944). Also around that time, a large collapse in the center of the Pago Shield created the 9 km wide Pago Caldera. At the end of the Pleistocene Epoch, the caldera was deeply eroded by surface water, and inundated by the rising sea level, creating the fjord-like feature of Pago Pago Harbor. Stearns (1944) interpreted the nearly vertical north wall of the harbor as direct evidence of this collapse. After the collapse, additional eruptive activity inside of the caldera created a distinctive lithology consisting of low-permeability ponded flows, tuffs,

breccias, and trachyte intrusions that is collectively referred to as the Pago Inner-Caldera Unit. This unit postdates the Pago Outer-Caldera Unit, which is primarily composed of gently sloping lava flows and some pyroclastics (Stearns, 1944). The neighboring Alofau Shield may also have experienced a similar caldera collapse, whereas the westerly Taputapu Shield shows no evidence of such an event.

Tutuila's shield building phase ended about 1 Ma with the eruption of massive lava flows that filled several valleys, and the intrusion of numerous Trachyte plugs and dikes that remain today as the island's highest and most prominent peaks (Stearns, 1944; NPS, 2008). The shape of the original shields could be inferred from the existing island profile, as seen in the slopes of the long ridges that emanate from the island's central axis. These ridgelines often have slopes of about 15°, which corresponds to the dip of many individual lava flows measured on Tutuila by Eyre and Walker (1991). What remains of Tutuila today, after much subsidence below sea level, is the deeply eroded and weathered summit of the original island.

Rock samples from each shield were collected by McDougall (1985) to determine the potassium-argon ages of their flows. Though the dates suggest relatively contemporaneous eruptions, they do show that the Pago Shield (1.53–1.14 Ma) is probably slightly older than the Alofau and Olomoana Shields (1.11–1.48 Ma), and that the Taputapu Shield (1.01–1.25 Ma) is probably the youngest. Stearns (1944) also notes that the Taputapu flows appear to overlies the Pago flows in Aasu Valley, and the geomorphology of the Taputapu Shield shows it is younger than the Pago Shield, with less erosional dissection.

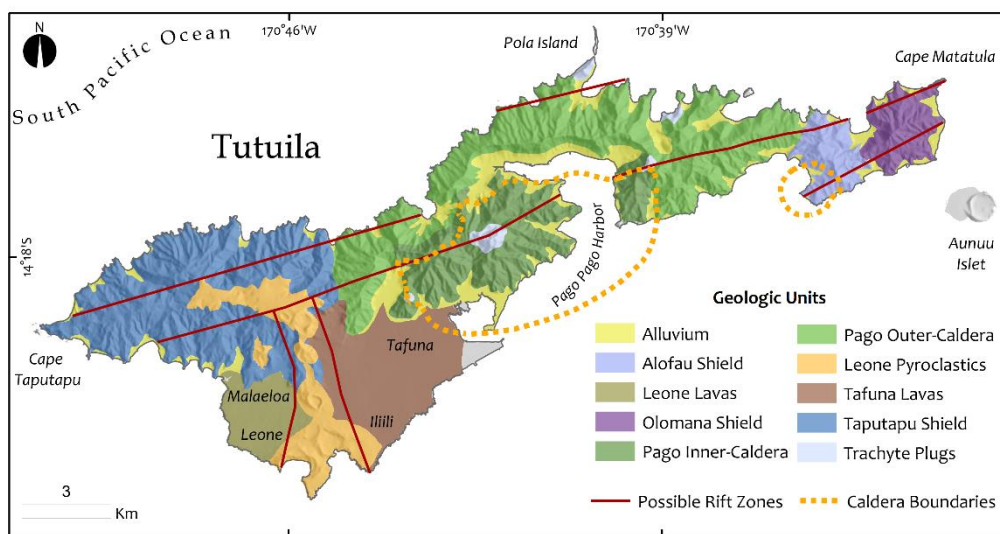


Figure 1.3. Simplified geology of Tutuila showing volcanic shields and inferred volcanic structures such as rift zones and caldera boundaries. Modified from Stearns (1944) and Knight Enterprises Inc. (2014).

## 1.4.2 Sedimentary Units and Changes in Sea Level

After the cessation of the shield-building phase, Tutuila experienced between 120 m to 800 m of isostatic submergence (Stearns, 1944). At some point during this interval, a Pleistocene-age barrier reef formed around much of the island. Behind the barrier reef, a lagoon environment allowed the growth of fringing reefs and the deposition of carbonates, marls, and terrestrial alluvium (Mayor, 1920). Next, there was a period where coral growth could not keep pace with the rate of the sea level rise, and the lagoon and barrier reef were drowned. Today these carbonate deposits form a submarine plateau that lies unconformably on the eroded upper surface of the older volcanic shields. Bathymetric data show that the top of the plateau occupies a remarkably uniform depth from -50 to -90 meters below sea level (Fig. 1.4). In 2015, a deep borehole was drilled showing two carbonate horizons in the Tafuna-Leone Plain region. The lower horizon ranges from -58 to -74 m below sea level and is thought to be a part of the carbonate bench. Radiocarbon dating shows the middle of the horizon is 10,300 years old. Above this horizon, the Leone Volcanic flows continue up to a depth of -15 m where a second carbonate layer is found. The layer is 9 m thick and was deposited during an interval between 7,000 and 4,400 years ago (Reinhard et al., 2019). This upper layer is probably one of many carbonate horizons or lenses that may have been interfingered with the Leone Volcanics. The existence of these horizons could result from a combination of the intermittent growth of the volcanic plain and global sea level fluctuations, which include a rise from -120 m at the end of the Pleistocene Epoch 12,000 years ago, and a +2 m high stand about 5,000 years ago (Nunn, 1998) (dates and elevations are approximate).

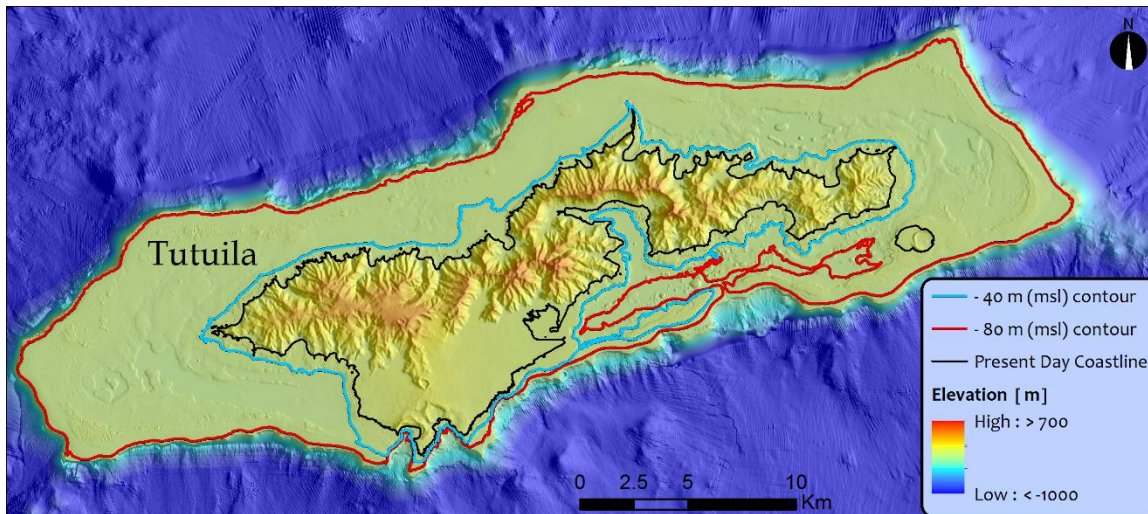


Figure 1.4. Bathymetry surrounding Tutuila (Lim et al. 2010). The sharp drop 3–7 km out from the coastline is interpreted as the former sub-aerial extent of the older shield volcano(s) prior to submergence. The flat area between -80 m and -40 m depth (*red and blue lines*) is the top of a carbonate rich sedimentary unit that is thought to have been deposited in a lagoon environment behind an ancient drowned barrier reef.

To the north of the Tafuna-Leone Plain area, and along the coastline of the rest of the island, are numerous deeply-incised valleys eroded into the older shields. The bottoms of many of these valleys are filled with terrestrial alluvium that collects as streams erode material from the mountains. The larger valleys also contain marine sediments and reef material, some rising to 2 m above the current sea level, which correlates with sea-level highstands within the last 5,000 years (Nunn, 1998). These alluvial wedges provide some of the limited flat land around the island for building villages, and most probably contain at least a small basal-lens aquifer.

### **1.4.3 Holocene Leone Volcanics**

After the last glacial period and until indigenous-historical times, Tutuila's rejuvenated volcanic phase produced eruptions along the southern flank and to the summit of the Taputapu Shield (Natland, 1980; Addison, 2006). Recent unpublished radiocarbon dates from the interbedded carbonate layers under the plain suggest that the rejuvenated phase eruptions began earlier than 10,000 years ago and continued until 4,000 years ago (Reinhard et al., 2019). Additionally, archeological excavation of a widespread red-ash layer throughout the plain indicates that pyroclastic eruptions were still occurring from around 650 to 750 years ago (Addison, 2014). These Holocene age lava flows, ash eruptions, and cinder cones, make up the Leone Volcanic Series.

The Leone Volcanic Series primarily originated from an approximately 7 km long north-south trending rift zone that is clearly demarcated as a ridge, topped with cinder and ash cones, running between the villages of Tafuna and Leone. The Tafuna-Leone Plain represents the bulk of the erupted material from Tutuila's rejuvenated phase, during which submarine eruptions erupted through the carbonate shelf, and ash deposits and lava deltas flowed down the flank of the older shields (Keating and Bolton, 1992). The pyroclastic cones closer to the sea have more ash in their compositions, indicating they were formed from explosive eruptions (likely due to intruding seawater), whereas the cinder cones and pahoehoe flows located farther north are indicative of subaerial effusive eruptions. Aunuu Islet, a small tuff cone 1.3 km off of the southeastern coast of Tutuila, was also created by submarine eruptions during this phase. It is interesting to note that the southern boundary of the Tafuna-Leone Plain is located at the edge of the carbonate shelf, which suggests that the rejuvenated volcanics must have flowed outwards until they reached the edge of the shelf where they cascaded down the submarine slope into the depths.

## **1.5 Updated Conceptual Hydrogeologic Model of Tutuila, American Samoa**

The foundation of any study involving groundwater, whether an analytical approach or a numerical model, inherently relies on basic assumptions of how water behaves in the

subsurface. Unlike surface water resources, which can be observed, sampled, and measured with relative freedom, groundwater resources generally remain hidden beneath thick layers of soil and rock, making them difficult and expensive to observe directly. The qualitative or pictorial representation of groundwater properties, aquifer mechanics, and subsurface water flow invoked when one considers unseen subsurface processes is termed a conceptual hydrogeologic model (Betancur et al., 2012). Such a model is constructed by integrating direct or indirect measurements, results of exploration activities, and the general knowledge of aquifer construction and groundwater movement. An effective conceptual model ideally constrains all factors that significantly control groundwater quality or quantity, such as anthropogenic and natural-geochemical influences, underlying geology, surface water characteristics, and climatic variability. While conceptual models are a necessary foundation for building more quantitative analyses, such as numerical models, they also stand as perpetual works in progress, subject to update or revision as information becomes available through new observations or results.

This chapter attempts to compile all currently available hydrologic information with recently acquired subsurface datasets to inform an updated conceptual hydrogeologic model of Tutuila's groundwater and surface water resources. Published reports, recently collected data, and studies from similar basaltic islands were integrated to explain groundwater behavior in Tutuila's already developed basal aquifers, and to update various hypotheses of high level groundwater occurrence where data limitations exist. Additional data are detailed in Appendix A of this dissertation. Although this work attempts to integrate all of Tutuila's pertinent and available hydrologic information, much still remains to be discovered about the island's groundwater and its subsurface structure. Ultimately, this model is intended to support and inform future efforts to quantitatively assess the sustainability of Tutuila's groundwater resources; tasks that include numerical modeling, exploration for new uncontaminated groundwater sources, and decision support tools for water resources management.

### **1.5.1 General Conceptual Hydrogeologic Model of Basalt Islands**

Generally, on basaltic oceanic islands, the primary freshwater resource is contained in a lens-shaped body near sea level within saturated rocks (Tribble, 2008). This basal freshwater lens is supported by the underlying seawater due to the contrasting densities between fresh water and salt water. The transition between fresh and salt water is marked by a zone of brackish water (the transition zone) that can vary in thickness and depth. A secondary freshwater resource described in basaltic island settings is high-level groundwater. It is distinctive from basal-lens groundwater as it is supported by low-permeability features such as dikes, perching layers, or low-conductivity country rock, and may or may not be hydraulically connected to underlying seawater. High-level groundwater has been observed and developed for use on other islands. However, on Tutuila no wells, except three in the

village of Aloaufou have definitively tapped high-level groundwater and its occurrence remains generally unconstrained.

Various conceptual models have been proposed for groundwater occurrence on volcanic islands and these generally fall into two categories: Hawaiian models and Canary Islands models (Join et al., 2016) (Fig. 1.5). The Hawaiian Model describes groundwater occurrence in two distinct systems, basal groundwater and high-level groundwater (Lau and Mink, 2006). On the other hand, the Canary Islands model (Custodio, 1989; Custodio and Cabrera, 2008) – alternately described as the ‘fully saturated vertically extensive freshwater body’ model (Izuka and Gingerich, 2003) – describes a single hydraulically connected basal groundwater body extending from sea level and supported to high elevations by low-conductivity aquifer material. The average hydraulic conductivity distribution in this model is believed to decrease with depth, which is justified by an assumed loss of porosity due to compaction and secondary mineralization, as well as increasing age and weathering.

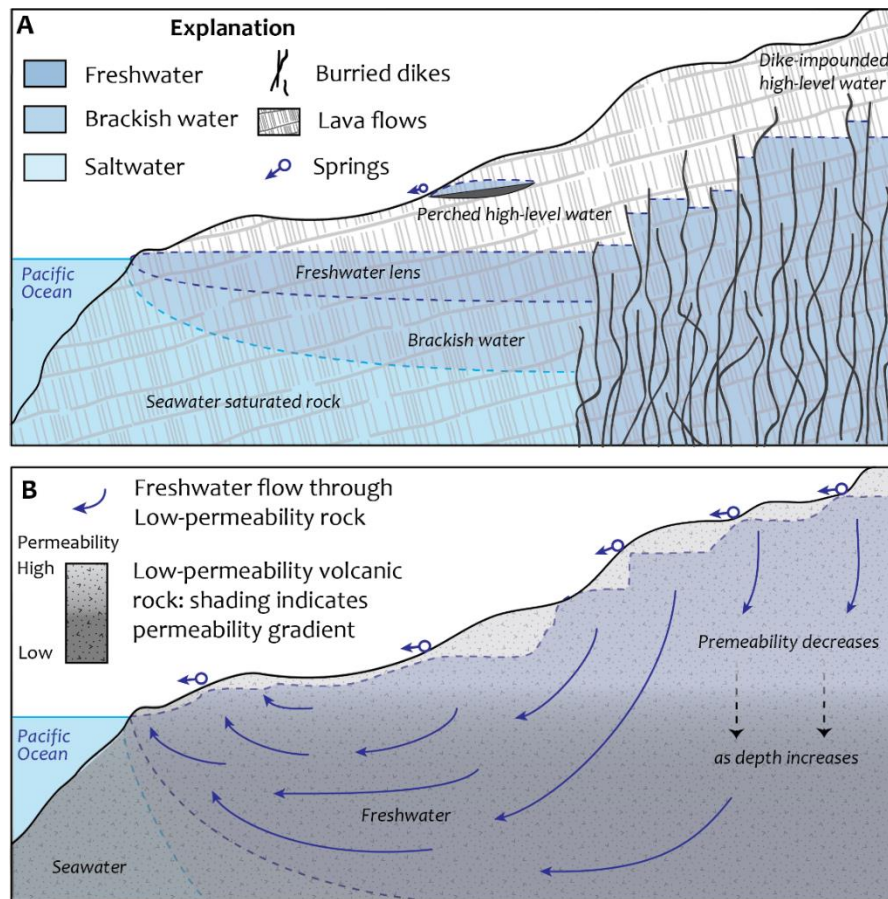


Figure 1.5: Two different conceptual models of groundwater occurrence on basaltic oceanic islands. The Hawaiian model (Lau and Mink, 2006), in *panel A*, consists of two disconnected groundwater systems, high-level and basal. The Canary Island model (Custodio, 1989), *panel B*, implies elevated and basal groundwater are hydraulically connected as a single system contained in low-permeability rock.

## 1.5.2 Hydrogeologic Units on Tutuila

Neither of the aforementioned conceptual models has been undeniably invoked to describe groundwater occurrence on Tutuila. However, they are not necessarily incompatible. Taken in perspective, a conceptual model is merely a simplification used to inform predictions or parameterization of numerical models. Real world subsurface conditions controlling groundwater movement and storage on Tutuila are heterogeneous and poorly constrained, thus it is possible and even likely, that different regions with distinct geologic histories may be more effectively parameterized on a regional scale by different conceptual models. This emphasizes the importance of interpreting data from different hydrogeologic units on an individual basis, as attempted in this work.

Izuka et al. (2007) delineated more than five hydrogeologic units for Western Tutuila based on what is known of the island's geologic construction (Fig. 1.6). The Taputapu and Pago Shields were consolidated into one low-conductivity unit – the Pleistocene Older-Volcanics Unit – as lack of data precluded their differentiation into separate hydrogeologic units. The Leone Volcanics were separated into the more hydraulically conductive Tafuna Unit on the eastern side of the plain and a less conductive Leone Unit on the western side. The rift zone running through the middle of the plain was classified as a Pyroclastic Unit with simulated dikes, and a wedge-shaped Reef Unit was located between the Leone Units and the Pleistocene Older-Volcanic Unit. The boundaries and characteristics of these units comprise the foundation of the hydrogeologic conceptual model of Tutuila. However, new geologic and hydrogeologic data presented in Appendix A may provide evidence for proposed updates to this conceptual model, such as considering each shield in the lower-conductivity unit separately.

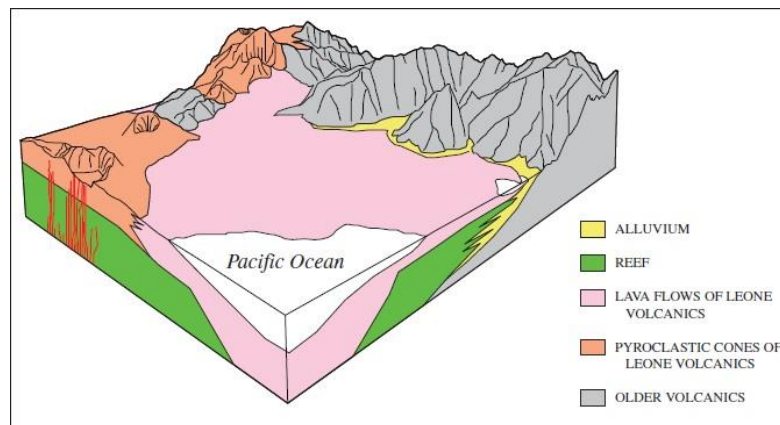


Figure 1.6. Conceptual hydrogeologic model of the Tafuna-Leone Plain region showing distinctive hydrogeologic units. Reprinted from Izuka et al. (2007) with permission.

## **1.5.3 Groundwater Occurrence in Tutuila's Hydrogeologic Units**

### **1.5.3.1 Holocene Leone Volcanics**

The young aquifers of the Tafuna-Leone Plain region are primarily composed of pahoehoe and a'ā lava flows with localized interfingerings of ash beds and/or sedimentary carbonate layers. These materials sit above the weathered edifice of the Taputapu shield, though the degree of water movement between the Leone and Taputapu units is unknown. Due to their young age and lack of weathering, the Leone Volcanic aquifers are generally very hydraulically conductive and hold a thin basal lens. A prevalence of fractures, clinker zones, and lava tubes provides a high secondary porosity to the region, making it favorable for groundwater development (Bentley, 1975). However, these features also make the Tafuna-Leone plain susceptible to groundwater contamination (Kennedy et al., 1987). Currently, the 24 wells in the plain region produce about 70% of the island's municipal water (RCWW, 2002). Wells in this area are generally designed to skim the top of the unconfined basal lens that floats (due to its lower density) on salt water within the saturated rock. Because the plain's geologic units are so conductive, the water table in the region is typically about 1 to 3 m above sea level (Izuka, 1999b). The unsaturated zone above the water table is often less than 35 m thick, allowing only minimal travel time for contaminant attenuation. Within the plain there are three subregions, which can be distinguished into different hydrogeologic units: (1) the Tafuna Plain, (2) the Leone Plain, and (3) the Leone Pyroclastics. Each of these units probably has a large degree of heterogeneity, as shown by the quickly alternating sequences of variably textured lavas and different types of pyroclastic materials seen in cores from two recently drilled deep exploratory boreholes (Tables A2 and A3). Visual inspection of the borehole core shows the Leone Series rocks in TGH-1 (on the Leone side of the plain) generally have a higher proportion of volcanoclastics (ash and cinder) than is seen in TGH-3 (on the Tafuna side), though the materials in both boreholes are still predominantly basalts from lava flows.

### **1.5.3.2 Tafuna Plain**

The structure of the Tafuna region has been described by Eyre and Walker (1991) as a lava delta (Walker, 1991) formed as molten rock flowed from sub-areal vents downgradient via long tongues and subsurface tubes. Sub-flow-surface transport of lava causes the exterior of the flow to dome and buckle and these forces create structures such as tumuli, lava rises, and lava tubes; when covered by successive flows it creates heterogeneity and preferential pathways for the movement of the water. When erupting, lava may flow over, around, or through topographic irregularities, which produces a heterogeneous subsurface distribution of less and more permeable zones. It should be noted that the Tafuna aquifer behaves as an unconfined aquifer, and the more permeable sections are probably still interconnected by fractures through the denser sections. The structural complexity of the Tafuna Lava Delta is

enhanced by the fact that the lavas rest on the uneven topography of ancient buried ridges, valleys, pinnacles, and sedimentary basins of Taputapu's ancient erosional surface. Despite this heterogeneity, the water table in the Tafuna plain sits fairly uniform at about 1 to 2 m above sea level, and varies during drier or rainier periods.

### **1.5.3.3 Leone Plain**

The Leone side of the plain is similar to the Tafuna side, though it contains more ash and pyroclastic material, blown westward by the southeasterly prevailing winds during explosive eruptions (Izuka et al., 2007). Extensive ash layers are observed in exposures on the Leone coast and in the borehole logs. These layers likely serve to reduce the vertical permeability of the unit, causing portions of the basal-lens to be locally or partially thickened, though no definitive measurements have been made to support this hypothesis. Nonetheless, aquifer test data does suggest that overall hydraulic conductivities are generally lower on the Leone side than on the Tafuna side, and the surface water contamination issues reported on the Tafuna Plain appear to be less prevalent on the Leone side (Kennedy et al., 1987). Water levels in the Leone Plain are similar to those on the Tafuna side and rise to about 3 m above sea level in wells near the Taputapu contact.

### **1.5.3.4 Leone Series Pyroclastics**

The north-south trending ridge running down the center of the Tafuna-Leone Plain is comprised of ash and cinder cones. The ridge is considered to be a rift zone emanating from the rejuvenation stage of the Leone Series eruptions. A highly weathered rock outcrop found in a Futiga cinder quarry suggests the rift zone is underlain by at least one relic ridge of Taputapu rocks, mantled by Holocene age pyroclastic deposits and interbedded lava flows. The subsurface structure of the area has not been explored thoroughly, and there is only one well (Well 178) developed within the pyroclastic unit. This heterogeneous unit contains materials that range from highly-permeable unconsolidated cinder to nearly impermeable indurated tuff, which may have a wide range of hydraulic properties (Izuka et al., 2007). Based on information in Izuka et al. (2007) and a recovery test of Well 178, the overall permeability of the pyroclastics is probably near to or less than the Leone side of the plain. Since ash cones are primarily distributed in the southern portion of the ridge, and cinder cones are primarily found in the more northerly section, it may be reasonable to assume that the northern section has higher hydraulic conductivities. Also in the central section of this ridge a shallow valley is found, which may be remnant of paleo-ridgelines from the Taputapu Shield. This valley displays a subdued topography, suggesting it is filled with either alluvium, recent lavas, or pyroclastic material. Although there are no borehole logs in this region, recently conducted MT geophysics alludes to the presence of either perched groundwater or a fully saturated subsurface in this area.

### 1.5.3.5 Malaeimi Valley

Malaeimi Valley is a unique area on Tutuila. Its upper sections are carved from Pago Shield rocks, and its lower section was flooded (or potentially dammed) with basalts from the Tafuna Lava Delta. Currently, the interior of the valley has a flat bottom and is filled with alluvial material. Thus, wells in the valley might be tapping aquifers in lower-conductivity Pleistocene rocks, alluvial fill, or highly-conductive Tafuna lavas depending on their location and depth. Historically, water table elevations were seen to vary spatially and temporally, and large drawdowns in response to pumping were observed in some wells (Eyre and Walker, 1991). Some high water levels were observed to be unstable and declined rapidly when pumped. In general, high drilling water levels in the Upper Malaeimi Wells are found to rapidly drop off further down the valley at wells near the valley mouth. While these observations could help to constrain the subsurface boundaries of the valley's different geologic units, it remains unclear how hydraulically connected these different zones are to each other.

Another interesting feature of Malaeimi Valley is that it receives a significant amount of additional water from the process of mountain front recharge (MFR). Streams flowing off of the flanks of the less permeable Pago Shield rocks quickly infiltrate into the more permeable alluvial valley fill and Leone series lavas at the bottom of the valley and add to the area's total recharge. This additional water increases the thickness of the basal lens in this area, as well as providing additional water supply for the lens downgradient from the MFR zone (Fig. 1.7). The elevated lens thickness in this area may act as a freshwater fence, not only reducing the potential for saltwater upconing in the MFR zone, but also for wells upgradient in the valley.

Although the hydrogeology of Malaeimi Valley is complex, this region has long been recognized as one that contains valuable water resource characteristics; due to the unique geology and relatively high recharge rate. Malaeimi Valley has been recognized as possessing all qualifications needed for designation as a "Special Management Area" under American Samoan Law, and its protection as a special management watershed would be a significant step forward in water resources management on Tutuila (Pedersen Planning Consultants, 2004).

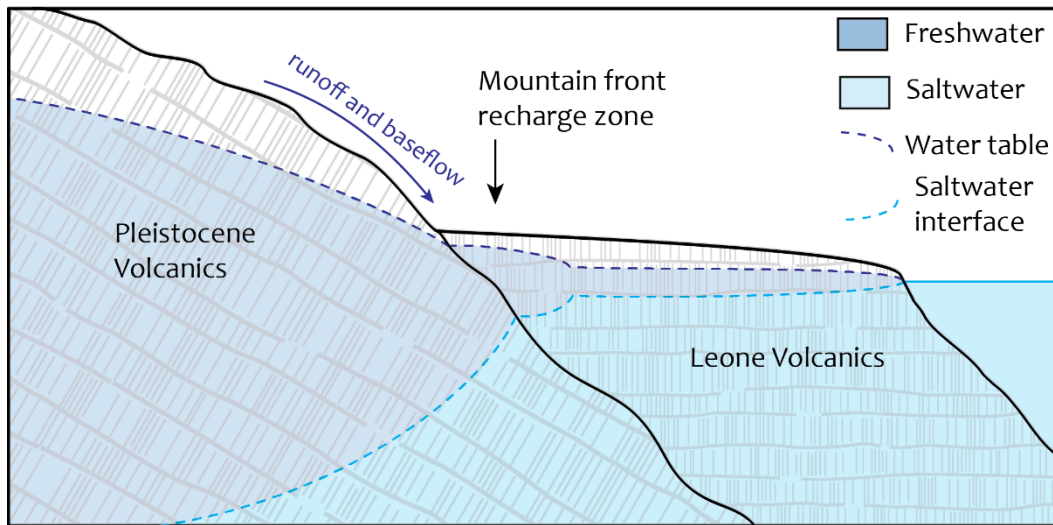


Figure 1.7: Diagram showing possible interaction of the basal lens in the mountain front recharge zone at the margin of the less-permeable Taputapu Shield and the more-permeable Tafuna-Leone Plain.

### 1.5.3.6 Pleistocene Volcanic Shields

The Pago, Taputapu, Alofa, and Olomoana shields make up what has been previously referred to as the Older-Volcanic Hydrogeologic Unit, the Pleistocene Unit, or the Low-Permeability Unit (Eyre, 1994; Izuka et al., 2007). These shields are in a basic sense, constructed of gently dipping a'a lava flows organized as an alternating sequence of more permeable rubble zones and less permeable massive sections (see Section 2.2). This sequence is complicated by the presence of cross-cutting dikes, interbedded pyroclastic sections, clay rich paleohorizons, and products of mass wasting or caldera collapse that all serve to disrupt the continuity of the lava-flow structures. This complex geology may manifest hydrogeologically as a heterogeneous permeability fabric where variably sized compartments of high permeability rubble or cinders are adjacent to beds or tongues of massive lavas and other low permeability features that act as perching layers or barriers to water movement.

The shields likely contain both high-level and basal groundwater bodies. However, the basal supply probably makes up the majority of the developable groundwater in this unit. Some existing wells in the Pleistocene rocks register elevated water levels, some of which when pumped, are subject to high drawdown. These high drawdowns could be caused by overall low hydraulic conductivities (if a purely basal system was tapped) or by limitations in the aquifer extent. Previous workers have generally classified Tutuila's older shields into a single hydrogeologic unit with uniform properties. However, recent observations are beginning to provide sufficient data to characterize the region into separate hydrogeologic units.

The Pago Shield itself has two distinctive geologic units, the Inner-Caldera and the Outer-Caldera. The Outer-Caldera Unit contains thin and thickly bedded a'a lava flows,

numerous dikes, vitric tuff beds, and potentially buried cinder beds; the Inner-Caldera Unit is composed primarily of ponded basalts, trachyte plugs and flows, as well as a relatively high fraction of volcanoclastics, breccias, and other products of mass wasting (Stearns, 1944; Knight, 2014). Both of these units contain numerous dikes and are thought to impound small quantities of high-level water behind these barriers (Keating and Bolton, 1992). In general, the composition and structure of the Outer-Caldera Unit suggests that it has better water transmitting properties than the Inner-Caldera Unit (Shuler et al., 2014). However, the available hydrological data does not show a clear difference in the performance of wells drilled in either unit, which is probably due to local scale heterogeneities.

Measured aquifer parameters and geologic information suggests that the Taputapu Shield may have a greater water development potential and higher average *K* values than the island's other shields. This hypothesis is supported by the following:

1. A limited number of recent aquifer tests show specific capacities and *K* values that are significantly higher than those measured in the other shields (Table 7).
2. The Taputapu Shield may have experienced less erosion and mass wasting, which are processes that serve to reduce connectivity between permeable zones. This is supported by the observations that it is younger (Tarling, 1965; McDougall, 1985), and has a lower average slope (22°) then the Pago Shield (28°) (Fig. 1.8).

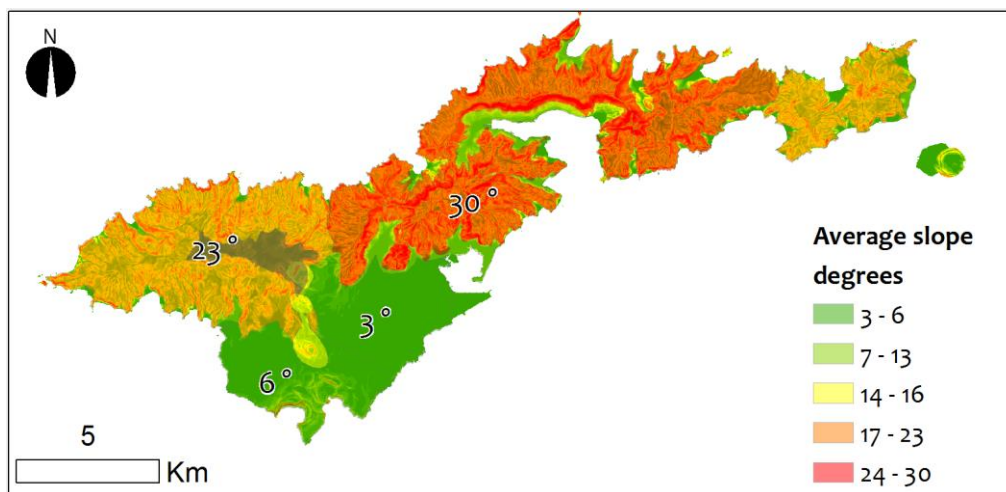


Figure 1.8. Average slope (°) of simplified geologic units. Taputapu shield slope excludes the subdued topography region covered by Holocene Aoloaou cinders (shown in grey).

3. McDougall (1985) hypothesizes that Taputapu and Olomoana are satellite shields of the main Pago Volcano, and therefore should have more high permeability flank lavas and less low permeability caldera related features (e.g., intrusives, ponded lavas, hydrothermal alteration). This is supported by gravity anomalies as measured by Machesky (1965). These show clear maxima (290 mGal) above the Pago Shield (Fig. 1.9), suggesting the Pago unit contains more impermeable intrusive bodies, such as

dike complexes or solidified magma chambers.

4. The inferred dike intensities as measured by Walker and Eyre (1995) and the locations of measured dikes by Stearns (1944) (Fig. 1.9) suggests a greater density of impermeable intrusive bodies in the Pago Shield.

Despite this evidence, the Taputapu Shield is nonetheless a large heterogeneous region, and more extensive aquifer testing should be performed to validate this hypothesis for specific areas.

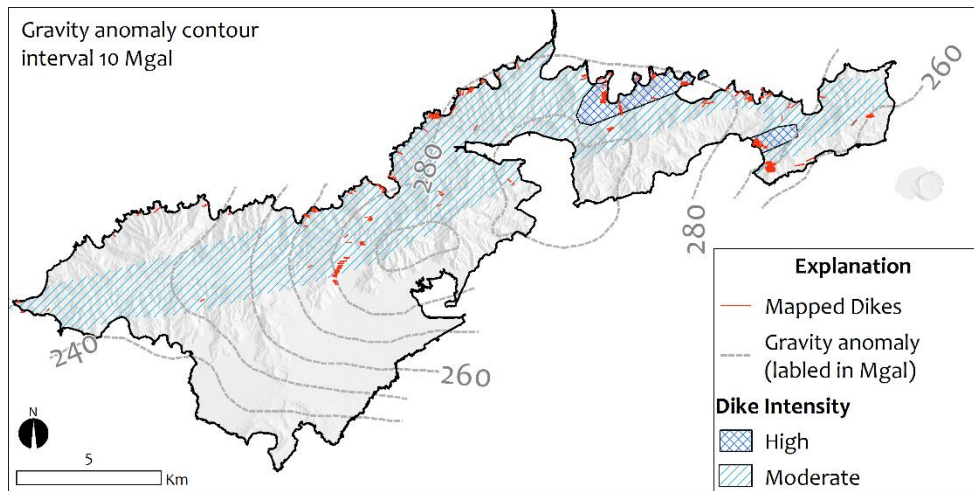


Figure 1.9. Geophysical and surface-mapping data showing inferred density of intrusive structures throughout Tutuila. Heavy cross-hatching indicates dike-complex areas and light hatching shows zones of moderate dike intensity from Walker and Eyre (1995). Bouguer gravity anomaly as measured by Machesky (1965) shows denser material nearer to the Pago Caldera. Also shown are locations of mapped dikes in outcrops by Stearns (1944).

### 1.5.3.7 Perched or Dike Impounded Aquifer at Aoloau

The 4.1 km<sup>2</sup> summit area at Aoloau is blanketed by layers of high permeability Holocene-age cinders. The permeable nature of this formation is indicated by observations of coarse cinder outcrops, domed topography, and a lack of runoff despite a high rainfall average (5,250 mm/yr). Aquitards within and below this unit are thought to consist of beds of fine ash, thermally welded tuff, lava flows, or paleo-horizons on the surface of the Taputapu Shield (Eyre and Walker, 1991). A known reservoir of elevated water has already been developed in the village of Aasu. The extensive nature and unique geologic setting of this high-level aquifer makes it unique on Tutuila. Three wells – two out of production (Wells 127 and 129) and one that is still producing (Well 128) – were drilled into the cinder unit. Well 128 currently produces about 35 to 40 GPM (190 m<sup>3</sup>/d). This elevated groundwater reservoir is inferred to be the source of multiple perennial springs that discharge from the margins of the subdued topography that define the unit. These springs have been well documented and

probably served as a source of village water prior to groundwater development. Geophysical cross-sections (Appendix A, Fig. A10) indicate the potential for shallow perched aquifers of similar occurrence in both the eastern (Aoloau Village) and the western (undeveloped) portions of the cinder cap.

The thickness of the cinder is likely to be variable and dependent on the underlying Taputapu topography and distance to source vents. A driller's log from Aasu Well 127, in the eastern portion of the unit, indicates the thickness of cinder deposits to be greater than 50 m (Eyre and Walker, 1991). The unit probably thins towards the west with increasing distance from visible vents. Approximately six million gallons per day of water recharges this area (Eyre and Walker, 1991). Since the subsurface geology of the Taputapu Shield has not been fully explored, it is also possible that the Aoloau aquifer is supported by dike-impounded groundwater from within the underlying shield. Future subsurface exploration of any part of this unit will help to constrain the quality and the quantity of the available resource.

#### **1.5.3.8 Valley-Fill Aquifers**

Numerous small alluvial-fill valleys ring the island and are often partially filled with eroded volcanic alluvium, mass-wasting debris, and marine sediments from ancient and contemporary reefs and shorelines. These valleys usually contain one or more perennial or intermittent streams. The streams may help to recharge small basal-lens aquifers contained within the alluvium or underlying Pleistocene rocks. Around the island there are about 40 inhabited alluvial valley-fill plains that range in area from approximately 0.005 km<sup>2</sup> to 0.5 km<sup>2</sup>. A dozen of the more populated valleys contain one to four municipal wells, drilled to provide water to the village as a satellite system. The aquifers that these systems tap are generally less hydraulically conductive than the Tafuna-Leone Plain aquifers, and their water quality varies greatly between areas. Many of the wells drilled in these units probably pass through the valley-fill and, depending on the open interval of the well, may also obtain water from the underlying Pleistocene volcanic rocks. Existing driller's logs may make it possible to interpret the thickness of the valley fill and hypothesize which geologic unit(s) the wells are developing. However, in many of the existing logs the location of the paleovalley bottom is ambiguous and the logs for many existing wells are missing. The available logs and aquifer tests indicate that materials and hydrologic properties are generally different between valleys, though in general, alluvial-valley fill has been inferred to typically have hydraulic conductivities that are higher than the older volcanics, but lower than the Leone Volcans (Izuka et al., 2007).

Additionally, the pattern of urban development in these villages often places residences, piggeries, and agriculture directly above the alluvial aquifers. These potential sources of contamination may affect the unprotected groundwater below. Nonetheless, the alluvial fill/Pleistocene volcanic aquifers provide an important source of water to isolated areas, and despite low observed and predicted yields from most of the formations, the demand in many of these small villages is currently fairly low.

## 1.5.4 Conceptual Model Summary

A two-stage eruptive history with shield-building and rejuvenated phases, compounded with high erosion rates, has made Tutuila's geologic structure complex and heterogeneous. This is seen by examining existing well performance with aquifer tests and water level observations. The presence of high-level water in the island's older shields is irrefutable, due to the presence of perennial streams, but the nature of the impounding structures remains poorly understood. A significant perched aquifer is observed below Aoloau Village, and numerous persistent springs support perennial baseflow throughout the island. Nonetheless, the type and locations of groundwater impounding structures remains unknown. These structures could be dikes, perching layers, low-connectivity matrix rock, or any combination of the above.

In general, the hydrologic connectivity between adjacent zones of variable permeability may be the primary controlling factor influencing the water resources availability of any given area. Conditions found during well drilling are likely to be site specific, in which case it will be difficult to predict the regional connectivity of any given location without extensive pump testing. In general, groundwater behavior in the Tafuna-Leone Plain region suggests that the connectivity between water bearing pockets is high. Therefore, the overall hydraulic conductivity of the region is probably controlled by the high-permeability zones resulting in a thin unconfined basal-lens. In the Pago, Olomana, and Alofau shields, connectivity between permeable zones is more variable but generally lower, which results in drilling and production head levels that vary greatly as well. Geologic and hydrologic evidence suggests the Taputapu Shield is more likely to display more favorable producing conditions than the Pago Shield. Nonetheless, the Taputapu region is large and heterogeneous, and the productivity of wells is predicted to vary greatly with site-specific conditions.

Long-term pump tests after drilling and continued collection of high-resolution water level data during production would be useful to assess the degree of connectivity between more permeable portions of the aquifers. However, interpretation of this type of data, which is always more limited than would be preferred, can be difficult and may yield non-unique solutions. If it is feasible for multiple exploratory wells to be planned and tested, the likelihood of finding a zone that sustainably produces a satisfactory volume of water will be increased. Continued collection of hydrologic data remains important for increasing the knowledge base that will ultimately contribute to further revisions of this conceptual hydrogeologic model.

References for Chapter 1 are included in Appendix B: References section.

## Chapter 2:

# Isotopes, Microbes, and Turbidity: A Multi-Tracer Approach to Understanding Recharge Dynamics and Groundwater Contamination in a Basaltic Island Aquifer

### **Abstract**

Wells designated as groundwater under the direct influence (GUDI) of surface water have caused an ongoing boil-water advisory afflicting the island of Tutuila, American Samoa for almost a decade. Regulatory testing at these wells found turbidity and indicator bacteria spikes correlated with heavy rainfall events. However, the mechanism of this contamination has, until now, remained unknown. Surface water may reach wells through improperly sealed well casings, or through the aquifer matrix itself. In this study, three independent surface water tracers, turbidity, indicator bacteria, and water isotopes were used to assess recharge timing and determine contamination mechanisms. Results from each method were reasonably consistent, revealing average GUDI well breakthrough times of  $37 \pm 21$  h for turbidity, 18 to 63 h for bacteria, and 1 to 5 days for water isotopes. These times match well with estimated subsurface flow rates through highly permeable aquifer materials. In contrast, where one well casing was found to be compromised, turbidity breakthrough was observed at 3 to 4 h. These results support local management decisions and show repairing or replacing wells will likely result in continued GUDI contamination. Additionally, differences in observed rainfall response for each tracer provide insight into the recharge dynamics and subsurface flow characteristics of this and other highly conductive young-basaltic aquifers.

As published in: Shuler, C. K., Dulai, H., DeWees, R., Kirs, M., Glenn, C. R., & El-Kadi, A. I. Isotopes, Microbes, and Turbidity: A Multi-Tracer Approach to Understanding Recharge Dynamics and Groundwater Contamination in a Basaltic Island Aquifer. *Groundwater Monitoring & Remediation*.

## 2.1 Introduction

Both groundwater and surface water resources are essential for providing drinking water to the world's increasing population. While groundwater makes up only 26% of global water use (FAO 2016), in many areas, use of groundwater offers advantages over surface water. Requirements for treating groundwater to a potable standard are often less stringent because aquifers typically provide natural filtration of particulates and generally long subsurface transit times that eventually inactivate surface-living pathogens. In the United States (U.S.), the U.S. Environmental Protection Agency (US-EPA) Surface Water Rule mandates municipal water from surface water sources be treated to remove or inactivate 99.9% (3-log) of protozoa, bacteria, and 99.99% (4-log) of viruses (US-EPA 1998). To achieve this level, filtration is typically necessary as high particulate loads can reduce the efficacy of chemical treatments. Likewise, the US-EPA Groundwater Rule mandates groundwater treatment to the same standard as surface water in sources where turbidity levels exceed 1 nephelometric turbidity unit (NTU) or microbial indicator bacteria, such as total coliforms (TC) and *Escherichia coli* (*E. coli*), are found. In these cases, the offending well is classified as groundwater under the direct influence of surface water (GUDI) (US-EPA 2006).

In the U.S. Territory of American Samoa, the main island of Tutuila is almost entirely reliant on groundwater. Forty-five municipal wells across the island provide at least 90% of the drinking water used by the island's ~60,000 residents (AS-DOC 2013). To determine GUDI status of Tutuila's wells, the island's water utility, American Samoa Power Authority (ASPA), performed a GUDI test at each well in the municipal system by assessing correlation between turbidity, indicator bacteria, and rainfall. Eight of Tutuila's highest producing wells located on the Tafuna-Leone Plain were found to be GUDI wells (e.g. Vold et al. 2013). Increasing the level of treatment for water produced by these wells has proven to be cost prohibitive, therefore in 2009 a boil-water advisory was issued over much of the island. As of this writing, the boil-water advisory remains in effect for large portions of the water delivery system.

Although surface water clearly reaches some of Tutuila's wells during heavy-rainfall, the mechanism of this contamination has yet to be identified. Two hypothesized mechanisms are (1) highly-permeable aquifer material that allows surface water to infiltrate and contaminate the entire aquifer, or (2) improperly constructed well casings or well packings that allow small amounts of localized surface water to infiltrate through the well bore itself (Fig. 2.1). If contamination primarily travels through faulty well seals, then repairing or replacing the wells would be cost effective and allow continued use of existing water delivery infrastructure. However, if the permeability of the entire aquifer is so high as to lack sufficient filtration capacity, abandonment of the entire well field or installation of costly surface water treatment facilities will be necessary to solve the issue. Therefore, developing a better understanding of the recharge dynamics in the Tafuna and Leone aquifers will benefit future groundwater management efforts on Tutuila.

In this study, the aforementioned hypotheses were tested by comparing levels of environmental tracers with rainfall records to determine the average travel time of surface water to each GUDI well. Three independent multi-tracer datasets were used (1) continuous profiles of turbidity levels obtained from the original ASPA GUDI well tests, (2) indicator bacteria concentrations sampled discretely at both GUDI and non-GUDI wells on a monthly basis, and (3) water isotope values in precipitation and groundwater sampled discretely over short and long time resolutions. Additionally, video logs of ASPA wells were obtained and examined to visually assess well construction and casing integrity.

Turbidity is an indirect measure of suspended particulates and colloids in water, thus in groundwater, turbidity levels are controlled by source water particulate load, aquifer filtration capacity, and the degree of sedimentation occurring along subsurface flow paths. Turbidity is commonly used as a tracer for understanding recharge dynamics and microbial contamination in karst systems (e.g., Massei et al. 2006; Pronk et al. 2009; Goldscheider et al. 2010). However, there are relatively few studies that address this parameter in basaltic aquifers (e.g., Levitt et al. 2005). Nonetheless, in young, highly-permeable basalts, such as those that make up the Tafuna-Leone Plain (Stearns 1944), lava tubes and high secondary porosity from prevalent fractures may support conduit and fracture flow similar to that of karstic aquifers (Kiernan et al. 2003). While the presence or absence of turbidity is a commonly used metric in regulatory water testing worldwide, its use as a tracer for assessing recharge dynamics in high-permeability basalt aquifers remains, to the authors' knowledge, a novel approach.

Presence of short-lived endogenous or soil bacteria species in groundwater indicates lack of aquifer filtration capacity and short groundwater travel time, as *E. coli* die off rates in this environment may be greater than 50% per day (Entry and Farmer 2001; Foppen and Schijven 2006). In tropical climates, *E. coli* and other coliforms in groundwater do not necessarily signify fecal contamination as they do in temperate climates (Byappanahalli and Fujioka 1998; Byappanahalli et al. 2012). However, when detected in wells, these organisms indicate a direct and rapid connection between production well pumps and surface waters or soils, which have been found to be significant sources of *E. coli* and TC in American Samoa (Kirs et al. 2017). Bacteriological tracers have previously been applied in numerous settings for determining groundwater travel times through preferential pathways that lie at the statistically-rapid end of flow-velocity distributions (Barrell & Rowland 1979; Taylor et al. 2004; Godfrey et al. 2005).

The isotopic composition ( $\delta^{18}\text{O}$  and  $\delta^2\text{H}$ ) of precipitation and groundwater is commonly used to assess recharge source, elevation, or timing. Water isotopes are widely applied globally, and there are numerous examples of their application in tropical environments to better understand recharge dynamics (Scholl et al. 2002; Rhodes et al. 2006; Fackrell 2016). Potential factors that affect  $\delta^{18}\text{O}$  and  $\delta^2\text{H}$  fractionation in rainfall include the temperature-dependence of vapor-liquid fractionation, shifts in water vapor-source regions,

or progressive enrichment due to Raleigh fractionation occurring as source vapor becomes progressively more 'rained out' with increasing elevation or distance from sources (Dansgaard 1964; Rozanski et al., 1993; Gat, 1996). At sites within the intertropical convergence zone, such as the Samoan Archipelago, distinctive seasonal fractionation effects have been observed. These effects have been attributed to either seasonal shifts in water vapor source regions (Cobb et al., 2007) or variability in rainfall type. For example, in Costa Rica, Rhodes et al. (2006) found that convective storms are more prevalent in the wet-season and produce isotopically depleted rainfall, whereas dry season trade-wind showers were seen to produce more isotopically enriched rainfall. Although the direct causes of this variability probably vary from region to region, observed and predictable seasonality in precipitation isotopes allows them to be applied in this study as a seasonal-scale tracer of groundwater recharge timing. While this intertropical seasonality effect has been used before to partition hydrographs and study surface-water dynamics (e.g. Birkel et al. 2016; Calderon and Uhlenbroo 2016), its use for assessing groundwater-contaminant transit times is, to the authors' knowledge, an innovative application.

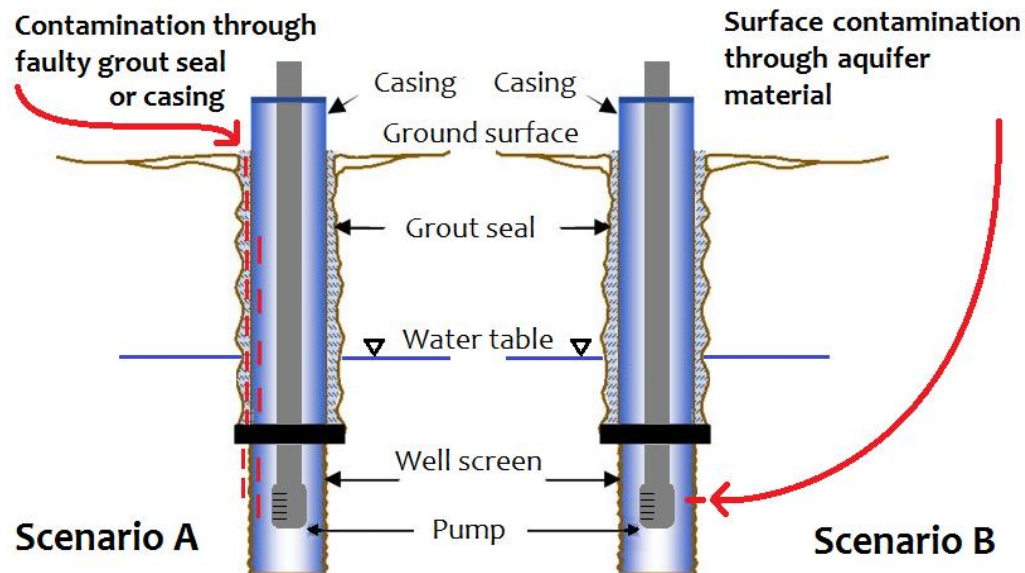


Figure 2.1: Hypothesized flow paths of surface derived contamination in GUDI wells. Scenario A shows contaminated water (*indicated by red lines*) entering a well through a poorly sealed packing or well casing, while Scenario B depicts contamination traveling to a well pump through highly permeable aquifer matrix.

### 2.1.1 Study Location

American Samoa encompasses the four smallest high-volcanic islands in the Samoan hot spot chain, which is located in the South Pacific about half-way between Hawaii and New Zealand (Fig. 2.2). Tutuila is the largest and most populous island in the territory, with a land area of 142 km<sup>2</sup> and a population density of almost 400 people/km<sup>2</sup>. Geologically, Tutuila can be divided into two primary lithologies, the older shields and the younger Tafuna-Leone Plain. The Pleistocene age shield volcanoes comprise the bulk of the island, and consist of four merged eruptive centers that have subsequently been eroded into a steep and heavily forested ridgeline (Stearns 1944). Aquifer tests on wells in the Pleistocene unit show relatively low hydraulic conductivities (*K*). On the shields' southwestern flank, Holocene age rejuvenated volcanism later accreted the Tafuna-Leone Plain, a 30 km<sup>2</sup> lava delta pocketed with a number of volcanic cones and craters, and containing lava tubes and high-secondary porosity from abundant fracturing (Keating and Bolton 1992; Izuka et al. 2007).

The Tafuna-Leone Plain can be divided into the predominantly thin bedded pahoehoe lava flows of the Tafuna Unit on the eastern side and the interbedded ash and lava layers that comprise the Leone Unit on the plain's western side. While permeabilities throughout the plain are generally higher than in the Pleistocene shields, *K* values in the Leone Unit are generally lower than in Tafuna due to enhanced deposition of volcanic ash driven by prevailing easterly winds from vents on the central plain. Soils on the Tafuna-Leone Plain are thin and in many places on the Tafuna side, bedrock outcrops directly at ground level (Nakamura 1984).

Tutuila's climate is hot and humid throughout the year, with average temperatures around 28 °C and annual rainfall ranging between 3000 and 6000 mm/year. High rainfall rates are common since much of Tutuila's precipitation is generated from convective cells (thunderstorms) forming within the South Pacific Convergence Zone. Heavy rainfall from frequent tropical cyclones is also common during the austral summer. Although there is a wetter season, which extends from October to May and a drier season that spans June to September, prevalent rainfall occurs throughout the year (Fig. 2.3).

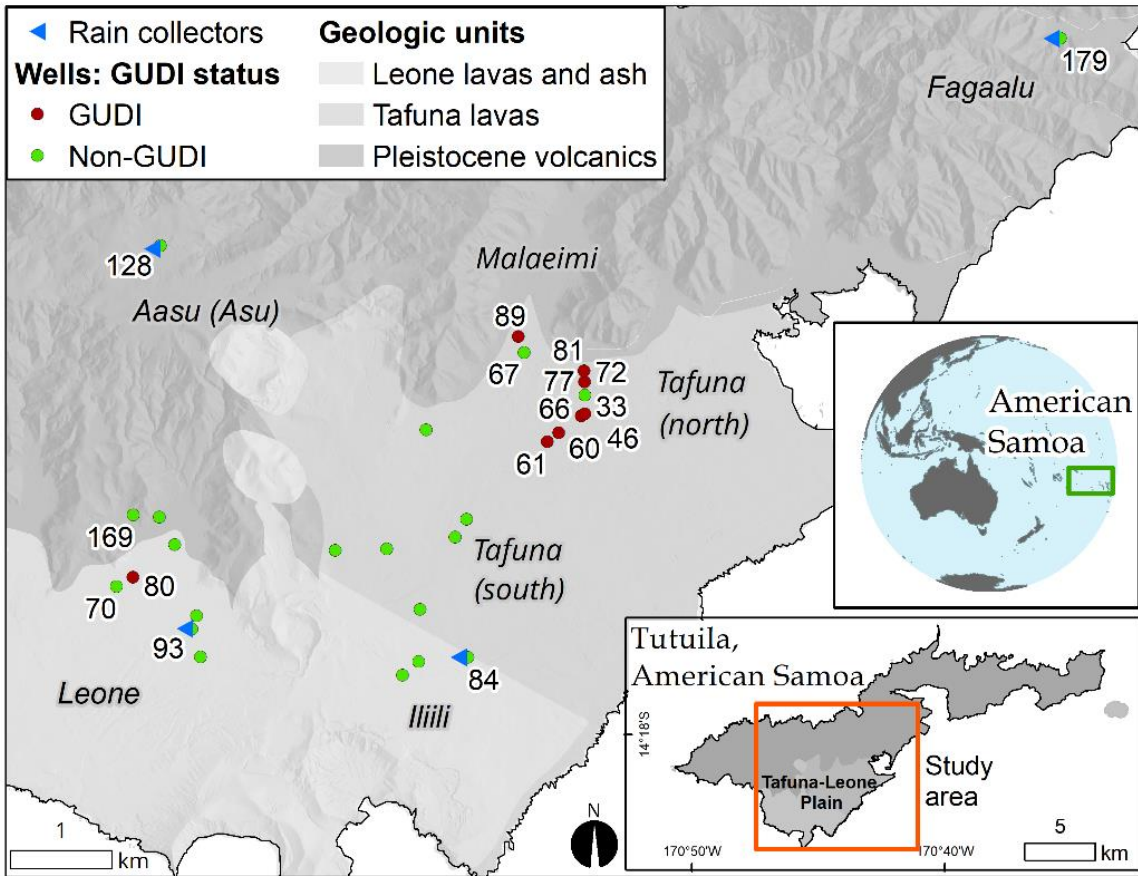


Figure 2.2: Study region, locations of municipal wells (*filled circles*), and simplified geologic units. Pertinent wells are labeled by ID number and are color coded by U.S. Environmental Protection Agency (US-EPA) determined GUDI status. Rainfall collectors were deployed at four wells and are indicated by *blue triangles*. Well field regions are also labeled. Geologic units are modified from Stearns (1944).

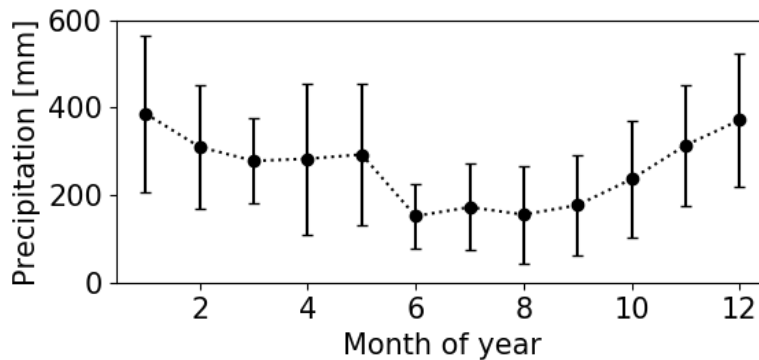


Figure 2.3: Seasonal precipitation cycle from the Pago Airport station, calculated June 1987 to May 2017. Error bars show  $1\sigma$  standard deviation.

## 2.2 Methods

### 2.2.1 Turbidity, Rainfall, and Video Log Data

Turbidity and local rainfall data from GUDI well tests were provided by ASPA for this study. Between 2012 and 2016, ASPA performed a total of thirty-eight tests on wells throughout the ASPA system. These tests were conducted one well at a time, during which an instrument package consisting of an in-line Turbidimeter (Hach model 1720E) and a tipping-bucket rain gage (RainWise model 804-1011) was installed at each well site for an average test period of roughly 2 months. Additionally, discrete water samples were periodically collected and analyzed at the AS-EPA microbiology laboratory for TC and *E. coli* concentrations. However, due to low sampling resolution, these microbial measurements are not analyzed in this study. Borehole video logging was also performed by ASPA on at least ten of the tested wells. Reports stored in ASPA files document methodology, and resulting GUDI status determinations for each well studied (e.g., Vold et al. 2013).

For this study, additional analysis of raw ASPA turbidity data was performed by filtering one-minute resolution turbidimeter measurements with a 1-hour rolling-median pass filter and smoothing with a Gaussian routine (*scipy.signal.general\_gaussian*, <https://scipy.org/>) to remove prevalent high-frequency spikes present in many of the datasets. These short duration spikes were assumed to be an artifact of bubbles within the supply line (Mauga 2016). An automated peak detection routine (*peakdet*, <https://gist.github.com/endolith/250860>) was then applied to identify the position of significant turbidity peaks. The start and end of each peak was defined as the point where turbidity levels departed significantly from a baseline turbidity value that was statistically determined for each dataset, except when a subsequent peak occurred before a previous peak had fully decayed. In this case, the inflection point between the two peaks was defined as both

the end of the first and the start of the second peak. Rainfall data from tipping-bucket gauges were consolidated into hourly totals and filled in with daily rainfall totals from the nearby Pago Pago Airport weather station (<https://www.weather.gov/ppg/>) where rainfall data at the well was missing. Heavy rainfall events were defined at the midpoint of any three-hour rolling-sum time-window with > 25 mm (1 inch) of recorded rainfall (Glickman 2000). Rainfall and turbidity peak data was plotted and manually inspected to define rain-event related turbidity peaks that occurred within 7 days of a heavy-rainfall event. Turbidity peaks not preceded by a heavy-rainfall event, or rainfall events not antecedent of a turbidity peak were ignored. Once rain-event turbidity-peak pairs were identified, the peak duration, time between rain event and start of the peak, and the time between rain event and maximum value of the peak were calculated for each event. For this study, borehole video logs were also reviewed to document depth to water, depth of well, casing depth, and any issues with casing integrity.

### **2.2.2 Indicator Bacteria on Annual Scales**

Indicator bacteria (TC and *E. coli*) were examined to assess microbial water quality variability in Tutuila's groundwater throughout different seasons and during selected rainfall events. Raw production well-water was regularly sampled at monthly intervals from well sample taps at four GUDI wells in the North Tafuna (N. Tafuna) well field and four non-GUDI wells throughout the island during the period spanning April 2016 and September 2017. Some additional samples were also collected during or after heavy rain events to ensure these conditions were well represented in the dataset. All microbial samples were collected in 100 ml sterilized plastic containers and cooled for transport to the laboratory at the American Samoa Community College (ASCC) for microbiological analyses. In the ASCC laboratory, Colilert®-18 kits and Quanti-Trays®/2000 (IDEXX Laboratories Inc., Westbrook, ME) were used to determine concentrations and 95% confidence intervals of TC and *E. coli* bacteria as most probable number (MPN) per 100 ml according to the manufacturer's protocol. Time between sample collection and analysis never exceeded 6 hours.

### **2.2.3 Water Isotopes in Precipitation and Groundwater**

Water isotope samples from precipitation and groundwater were collected at two distinct time resolutions. Annual variation was assessed through water isotope samples collected on a monthly basis for a three-year sampling period from both production wells and rainfall collectors located throughout the island. Precipitation was collected in cumulative precipitation collectors (CPC's) following the design used in Scholl et al. (1996). Collectors contained a 1-2 cm thick layer of high-purity mineral oil that floated on top of and prevented evaporation from collected water. All water was removed from collectors during sampling, thus each monthly sample represented the integrated water isotope composition of all precipitation falling during the whole month. Four collectors were deployed throughout Tutuila, at sites representative of various conditions that might affect precipitation isotope fractionation such as elevation or location. After 2 years, it was found that there was little

isotopic variation between collection sites, therefore sampling from three of the collectors was discontinued. Sampling continued for a total of three years at the collector located on the Tafuna side of the Plain, and the water isotope composition observed at this site was presumed to be representative of all precipitation within the study area. Water isotope composition of groundwater was assessed through samples collected each month over the three-year period from selected GUDI and non-GUDI production wells. Groundwater was always sampled from production well taps when well pumps were running.

To assess rainfall response at short time scales, a high-resolution time-series of water isotope samples was also collected at five GUDI wells and two non-GUDI wells during a three-week rainfall-event period in April, 2016. Water levels in each well were also measured through sounding tubes during sample collection with an electric water level indicator. Precipitation from just a single 3-day storm event at the beginning of the three-week period was collected separately from the precipitation collected for monthly sampling. Precipitation totals during this period were determined with rainfall data recorded by a weather station located at the nearby community college in Malaeimi Village (ASCC 2018), which is located about 1 km northwest of the N. Tafuna well field.

All water isotope samples were collected in 20 ml glass vials with no headspace, and were analyzed for  $\delta^{18}\text{O}$  and  $\delta^2\text{H}$  of water in a Picarro brand Cavity Ring-Down Spectrometer (L1102-i Isotopic Liquid Water Analyzer) at the University of Hawaii Stable Isotope Biogeochemistry Laboratory. Analytical uncertainty averaged  $\pm 0.07\text{‰}$  for  $\delta^{18}\text{O}$  and  $\pm 0.38\text{‰}$  for  $\delta^2\text{H}$ , and was assessed through computing the standard error of the estimate of duplicate samples, which made up about 15% of the dataset. All water isotope values referred to in this work are expressed in permil notation (‰) and are relative to the international standard V-SMOW.

## 2.3 Results

### 2.3.1 Results: Groundwater Turbidity and Response to Rainfall

Clearly defined rainfall-event related turbidity peaks up to 7 NTU were detected in all of the N. Tafuna wells, (Wells 33, 60, 61, 66, 72, 77, and 81), which are mostly designated as GUDI wells. On average, turbidity peaks in these wells generally had a sharp onset at  $17 \pm 11$  hours after rainfall events, reached their maximum value around  $36 \pm 21$  hours, and then trailed off with a subsequent exponential decay (Fig. 2.4a). Observed turbidity peaks lasted for a duration of 36 to 265 hours, although the length of many peaks was cut short when a subsequent peak interfered with the decay of the preceding peak (Table 2.1). Turbidity in most non-GUDI designated wells remained stable at very low levels (Fig. 2.4b), except in some cases where factors unrelated to rainfall seemed to stir up turbidity, such as daily cycles of pump activation. Also, Well 77 (located between wells 33 and 81) was originally designated

as the only non-GUDI well in N. Tafuna. However, turbidity data from Well 77 showed a well-defined 2 NTU magnitude peak, which was comparable to those in the other N. Tafuna wells (Fig. 2.4c). No other significant rain-event turbidity peak pairs were detected in any non-GUDI wells that are not specifically discussed in this section or noted in Table 2.1.

It should also be noted that the bimodal US-EPA designation of GUDI or non-GUDI for Tutuila's wells does not necessarily reflect the spectrum of variability in aquifer and well construction conditions observed in the field. While most of the GUDI wells show a similar response to rainfall, and most of the designated non-GUDI wells show little to no response, there are a number of outliers. Notable outliers include:

- Well 80 is the only GUDI well in Leone and shows a very subdued turbidity response.
- Wells 77 and 67 are located in the N. Tafuna and Malaeimi well fields and show a similar turbidity response to GUDI wells, yet are both designated as non-GUDI.
- Well 169 is designated as non-GUDI, but was found through video logging to have a significant flaw in the casing integrity.

The Malaeimi well field only has two active wells, GUDI Well 89, and non-GUDI Well 67. Turbidity data in both of these wells showed peaks that were less distinctive and had lower magnitudes than peaks in the N. Tafuna wells (Fig. 2.4d). The start of peaks occurred on similar timescales, within 4 to 13 hours after rain events, but in Well 67 peak maximums did not occur for roughly 3 days after the event. Unfortunately, only one peak was captured during the Well 89 study, and it appears that the turbidimeter was not operating correctly until just before this peak.

Only one well (Well 80) in the westerly Leone well field, and within the more ash-rich Leone Geologic Unit, was originally designated as a GUDI well. However, the turbidity response to rainfall at Well 80 was dissimilar to turbidity peaks observed in other GUDI wells, as it had a lower magnitude, was more dome shaped, and occurred more slowly (mean of 85 hours to peak maximum) than peaks in N. Tafuna wells (Fig. 2.4e). The most dramatic turbidity response observed in all profiles was in non-GUDI Leone Well 169, which had the highest maximum turbidity value (25 NTU), the shortest response time (3 hrs.), and the shortest peak duration (15 hrs.) of any well that was analyzed (Fig. 2.4f). This observation alone is enigmatic, as Well 169 was designated as non-GUDI, had minimal TC and no *E. coli* detections during the test period, is located far from other GUDI wells, and lies within the Pleistocene age rocks that have much lower permeabilities than the Tafuna lavas (Izuka et al. 2007). However, analysis of the borehole video log for Well 169 clearly shows a hole in the casing at 12.5 m below ground surface. This observation is discussed in greater detail in section 2.4.1.2.

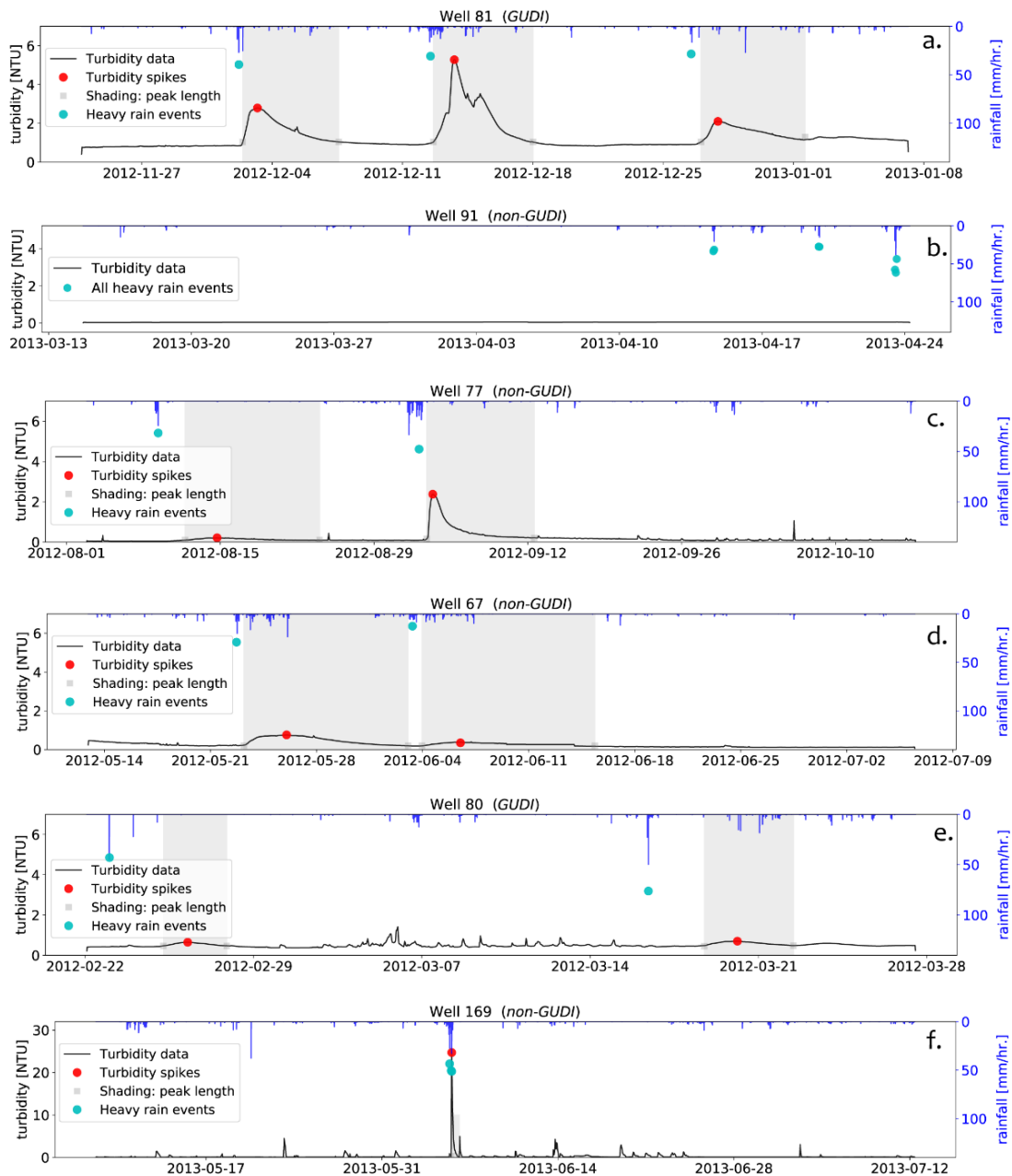


Figure 2.4: Selected ASPA GUDI well tests showing processed turbidity profiles (black lines) and rainfall (blue bars). Turbidity peaks (red dots) that correlate with preceding heavy-rainfall events (blue dots) are shown, and grey shaded fields represent durations of turbidity peaks. (a) Data from Well 81 shows the archetypical rainfall – turbidity peak response generally observed at all wells in the Tafuna wellfield. (b) Well 91 exemplifies the lack of response typical in most non-GUDI wells. (c and d) Well 67 and 77, despite being classified as non-GUDI, these wells show rainfall – turbidity responses similar to Tafuna GUDI wells, albeit subdued in magnitude and duration. (d) Well 80, located in Leone, is classified by AS-EPA as GUDI, but shows a subdued rainfall response of very low magnitude. (e) Well 169 is unique amongst all wells studied, as it is designated non-GUDI, but shows a dramatic response due to a hole in the casing (observed during a video log).

Table 2.1: Relevant statistics averaged across all rainfall-event turbidity peak pairs observed during continuous turbidity profiles. “Response to peak” indicates time between the defined rainfall event and the time of the maximum turbidity value. “Response to peak start” indicates time between the defined rainfall event and the point where turbidity departed from the baseline value. Wells are grouped by well field and only N. Tafuna wells are summarized with wellfield averages and 1 $\sigma$  standard deviations (S.D.) (in parentheses), as other well fields have fewer wells and more variability in response to rainfall.

<b>N. Tafuna Wells</b>	<b>Length of spike [hrs.]</b>	<b>Maximum Turbidity [NTU]</b>	<b>Response to peak [hrs.]</b>	<b>Response to peak start [hrs.]</b>	<b>Number of peaks recorded</b>
Well 33 (GUDI)*	36	1.1	26	13	3
Well 60 (GUDI)	35	1.5	33	22	3
Well 61 (GUDI)	37	5.4	12	7	3
Well 66 (GUDI)	86	2.2	37	15	3
Well 72 (GUDI)	127	6.2	42	16	3
Well 77 (non-GUDI)	265	2.4	79	38	2
Well 81 (GUDI)	129	5.3	30	7	3
<b>Average and S.D.</b>	<b>102 <math>\pm</math> (83)</b>	<b>3 <math>\pm</math> (2)</b>	<b>37 <math>\pm</math> (21)</b>	<b>17 <math>\pm</math> (11)</b>	<b>20 Total</b>
<b>Malaeimi Wells</b>					
Well 89 (GUDI)	119	1.1	18	4	1
Well 67 (non-GUDI)	267	0.8	78	13	2
<b>Leone wells</b>					
Well 80 (GUDI)	76	1	84	55	2
Well 70 (non-GUDI)	130	0.04	87	40	1
Well 169 (non-GUDI)**	15	25	4	3	1

\* Note GUDI designation was previously determined by ASPA, not during this study

\*\* Well 169 has a hole in casing, but was previously designated as non-GUDI

### 2.3.2 Results: Indicator Bacteria in GUDI and non-GUDI Wells.

Of the 69 microbial samples taken during this study at GUDI wells over the period April 2016 to September 2017, about 95% and 85% tested positive for TC and *E. coli*, respectively. In contrast, TC and *E. coli* detection rates in the 50 samples taken at non-GUDI wells were 28% and 0%, respectively. Concentrations of both TC and *E. coli* were highly variable in GUDI wells (< 1 to > 2419.6 MPN/100 ml), and when detected in non-GUDI wells, TC concentrations were always less than 10 MPN/100 ml. Correlation between TC and *E. coli* was moderate ( $r^2$  of 0.52 for all samples).

Microbial samples were taken during rainy periods and dry periods for about a year and a half on a monthly basis (Fig. 2.5). Three additional sample sets were collected during

targeted rainy periods to ensure all climatic conditions were well represented in the dataset. To find the most likely transport times for surface living bacteria detected at well pumps, correlation coefficients between *E. coli* concentrations and preceding rainfall totals calculated at various time-lags (defined as the number of hours before each sample was taken) were determined. This was accomplished for each of the four regularly sampled GUDI wells by calculating the least-squares coefficient of determination ( $r^2$ ) between sampled *E. coli* concentrations and an array of 12-hour rainfall totals at varying time-lags prior to the documented *E. coli* sample time. The array of time-lag values was created by summing all rainfall within a 12-hour window for every possible time-lag (on an hourly step), starting 168 hours (7 days) before and leading up to the time each sample was taken. Rainfall data was obtained from a weather station located at the nearby American Samoa Community College in Malaeimi Village (ASCC 2018). In Fig. 2.6 (top row),  $r^2$  values are shown as the dependent variable, with the time-lag used to calculate 12-hour rainfall totals serving as the independent variable. Figure 2.6 (bottom row) shows the correlation between *E. coli* concentrations and the 12-hour rainfall totals at the best-fitting (meaning maximum  $r^2$  value) time-lag window for each well.

Interestingly, there were two specific time-lags that consistently resulted in high correlation between rainfall and *E. coli* concentrations. Rainfall windows centered around 18 to 19 hours before sampling time produced high-correlations in three of the wells (Wells 33, 89, and 81) and in all four of the wells, a second correlation peak somewhere around 45 to 65 hours before sampling time was also observed. For time-lags preceding these local maxima, the correlation tended to drop off, except at Well 60, where the  $r^2$  value started to plateau around 0.9. Well 60 was also the well with the least number of samples. This analysis suggests a large proportion of the variability in these well's *E. coli* concentrations can be explained by the amount of rainfall occurring either the day before (18 to 19 hours) or a couple of days before (45 to 65 hours) sampling. The best-fitting travel times for the first of the two *E. coli* - rainfall correlation peaks are similar to the travel times observed between rainfall and the start of turbidity peaks in the N. Tafuna wells ( $17 \pm 11$  hours). Both of these processes would be expected to represent statistically extreme groundwater flowpaths. However, it is unclear what the correlation peaks at longer-time lags (45 to 65 hours) represent. The maximum values of turbidity breakthrough curves ( $37 \pm 21$  hours), which should represent average travel time for turbidity, occur at a slightly shorter time lag. Nonetheless, in individual wells, *E. coli* - rainfall peak timing and turbidity breakthrough timing do not show an explicit match, which may be due to a lack of microbial sample density, as well as having only a limited number of rain events represented in each turbidity profile.

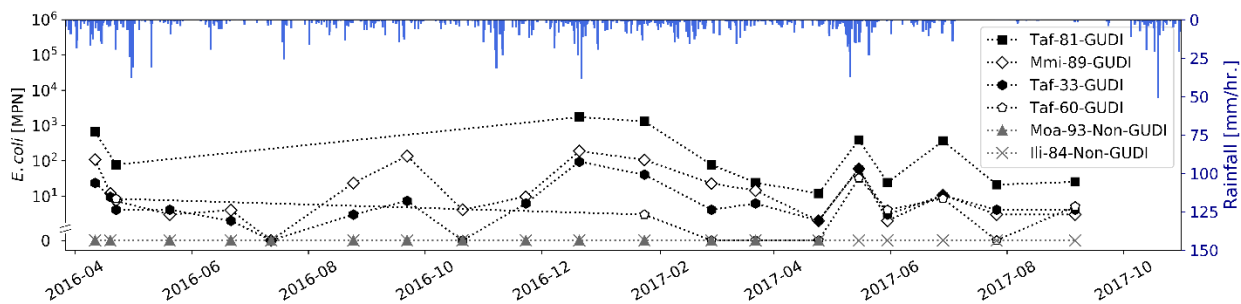


Figure 2.5: *E. coli* concentrations from monthly microbial sampling at GUDI and non-GUDI wells plotted with hourly rainfall totals from ASCC weather station. Note lines connecting sample points are shown for visual continuity only, and are not intended to infer concentrations between points.

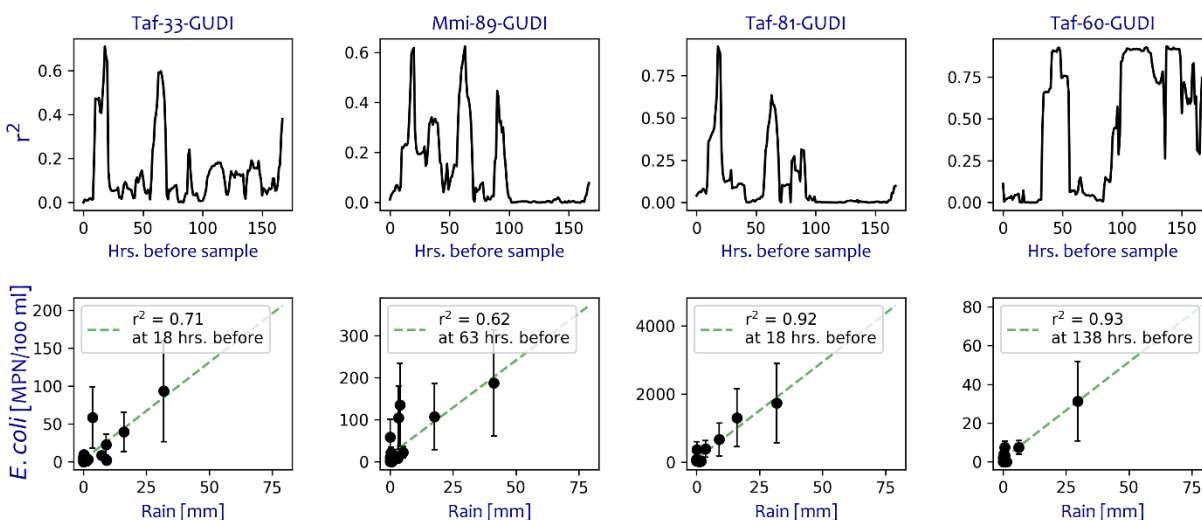


Figure 2.6: Correlation analysis between *E. coli* concentrations and rainfall totals used to estimate microbial travel time in groundwater. Top row of plots shows variation in  $r^2$  (y axis) as 12-hour rainfall totals are calculated at various the time-lags prior to the sample time (x axis). Bottom row shows scatter plots of *E. coli* concentrations vs. the rainfall total calculated at the best-fitting time-lag (maximum  $r^2$ ) from the plots directly above. *Green dashed lines* represent least-squares regressions, and the best-fit time lag in hours before sample time, and resulting  $r^2$  value at that time lag, are noted in the plot legends. Error bars represent 95% confidence intervals for MPN calculations and p-values for correlation analysis were all below 0.0003.

## 2.3.3. Results: Water Isotopes in Precipitation and Groundwater

### 2.3.3.1 Seasonal $\delta^{18}\text{O}$ and $\delta^2\text{H}$ Response

Three years of monthly rainfall sampling revealed strong, cyclical, and seasonal variation in water oxygen and hydrogen isotope compositions (Fig. 2.7). Precipitation  $\delta^2\text{H}$  and  $\delta^{18}\text{O}$  values during the austral winter were enriched in heavy isotopes, ranging up to +8‰ and -1‰, respectively, and were much more depleted in the austral summer, ranging down to -55‰ and -8‰, respectively. In the fall and spring seasons, precipitation  $\delta^2\text{H}$  and  $\delta^{18}\text{O}$  values transitioned between the extreme values recorded closer to the solstices. In contrast, monthly sampling at both GUDI and non-GUDI wells over the 3-year period showed limited variation in groundwater isotope compositions, which were generally close to the volume-weighted average-annual composition of precipitation (Table 2.2), and ranged between -3.5‰ and -5.6‰ for  $\delta^{18}\text{O}$  and -16.1‰ and -24.5‰ for  $\delta^2\text{H}$ . While the causes and patterns of observed  $\delta^2\text{H}$  and  $\delta^{18}\text{O}$  variation remain beyond the scope of this work, the pertinent implication to this study is that during months where the isotopic composition of precipitation is distinct from that of groundwater,  $\delta^2\text{H}$  and  $\delta^{18}\text{O}$  values in well samples can be used to determine the presence and even quantify the proportion of recently recharged water.

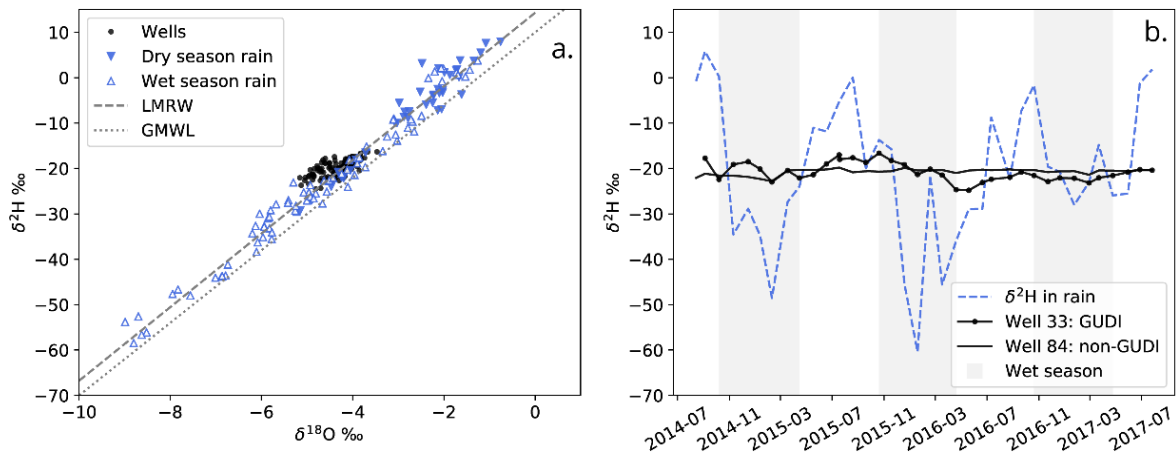


Figure 2.7: Water isotope values from rainfall collectors and groundwater wells. Dual-isotope diagram of  $\delta^2\text{H}$  and  $\delta^{18}\text{O}$  values (panel a), with regression through all rainfall samples showing the Local Meteoric Water Line (LMWR) plotted as dashed line, with the Global Meteoric Water Line (GMWR) shown as dotted line for reference. Seasonal variation (panel b) of water isotope ( $\delta^2\text{H}$ ) values in precipitation at the Ilili rainfall collector (*dashed line*) and in groundwater at selected wells (*solid lines*). Well 33 showed the most variation and Well 84 the least variation of all sampled wells. Grey shaded regions indicate the wet season. Note,  $\delta^{18}\text{O}$  values (not shown) followed the same pattern, and analytical uncertainties plot smaller than the symbol size.

### 2.3.3.2 Event-Scale $\delta^{18}\text{O}$ and $\delta^2\text{H}$ Response

Isotope tracers were most useful in this study for assessing recharge dynamics at a rain-event scale time resolution. Isotope samples and water levels collected roughly every other day from three GUDI and two non-GUDI wells formed a two-week long event-scale time-series where the effects of multiple heavy rainfall events and a subsequent period of drier weather could be observed (Fig. 2.8). The first day of well sampling took place as the most pronounced multi-day heavy-rain event was occurring. Two additional GUDI wells, 81 and 72 were sampled at a lower frequency, only once during the wet portion of the sampling period and once afterwards. These wells ended up showing the largest water isotope variations, and unfortunately their pre-rain event water isotope composition was not sampled. Instead, the pre-rain event isotopic compositions at Wells 81 and 72 was assumed to be equal to their measured values taken near the end of the sampling period. This assumption was considered reasonable as the substituted compositions were at most within 5% RPD of the pre-rain event compositions of Wells 33 and 46, which are located within 400 m of Wells 81 and 72.

The storm event precipitation was collected at Fagaalu Village, located about 6 km to the east of Tafuna, over a three-day period starting before the initial heavy rainfall event and ending as rainfall rates were declining. Additionally, a rain collector in the village of Iliili, located about 5 km to the southwest of N. Tafuna, was deployed for the entire month of April and integrated all precipitation that fell within the month. Both of these precipitation samples had isotopic compositions (-5.9‰ and -35.3‰ (storm event) and -5.8‰ and -34.1‰ (monthly sample) for  $\delta^{18}\text{O}$  and  $\delta^2\text{H}$ , respectively) that were distinct from average annual values of Tutuila's groundwater.

At four of the five GUDI wells, water isotope values generally started around -4.5‰ ( $\delta^{18}\text{O}$ ) and -22.5‰ ( $\delta^2\text{H}$ ), which are near but slightly depleted relative to the average annual composition of groundwater (Table 2.2). Within the first week of sampling,  $\delta^{18}\text{O}$  and  $\delta^2\text{H}$  values dropped towards the composition of storm-event precipitation, with values at Well 81 reaching -5.3‰ ( $\delta^{18}\text{O}$ ) and -28.3‰ ( $\delta^2\text{H}$ ). After the initial rainy portion of the sampling period, isotope compositions at the GUDI wells moved back towards the average groundwater composition, and were seen to dip slightly again as a final rain event occurred before the last day of the sampling period. On the other hand, water isotope compositions at the two sampled non-GUDI wells remained consistent throughout the sampling period. Water isotope values in these wells started and remained at a less depleted value than in the N. Tafuna wells. However, by the end of the time-series a very slight drop in  $\delta^{18}\text{O}$  and  $\delta^2\text{H}$  composition (on the order of 0.5‰ to 1‰ in  $\delta^2\text{H}$ ) was observed, which may indicate a delayed response to the recharge event. Additionally, Well 89, classified as GUDI and located almost 1 km from the center of the N. Tafuna wellfield, showed little response to precipitation, and displayed a subdued response comparable to the two non-GUDI wells. Water isotope magnitudes in Well 89 were also similar to the non-GUDI wells, in that the starting and ending isotopic

compositions, more closely matched the average annual groundwater  $\delta^{18}\text{O}$  and  $\delta^2\text{H}$  composition.

Water levels were also taken during each sampling, and all wells showed a significant though somewhat delayed response to rainfall, with water levels in the GUDI wells showing between 2 and 5.5 m of increase by the end of the rainy period (Fig. 2.9). At these wells, maximum water level measurements corresponded to times where minimum (most similar to recent rainfall)  $\delta^{18}\text{O}$  and  $\delta^2\text{H}$  values were observed. In non-GUDI wells a more subdued water level increase was recorded, up to about 1.5 m of rise, with notable differences from the GUDI wells being a slightly slower response, and also a much less precipitous and slower return back towards pre-event levels after the rainfall event had ceased. Since water levels are dependent on local hydrogeologic factors such as regional aquifer heads and aquifer connectivity, they are not simply a function of a volumetric addition of recharge. Nonetheless, these results show how heavy rainfalls significantly affect water availability in this region's aquifers.

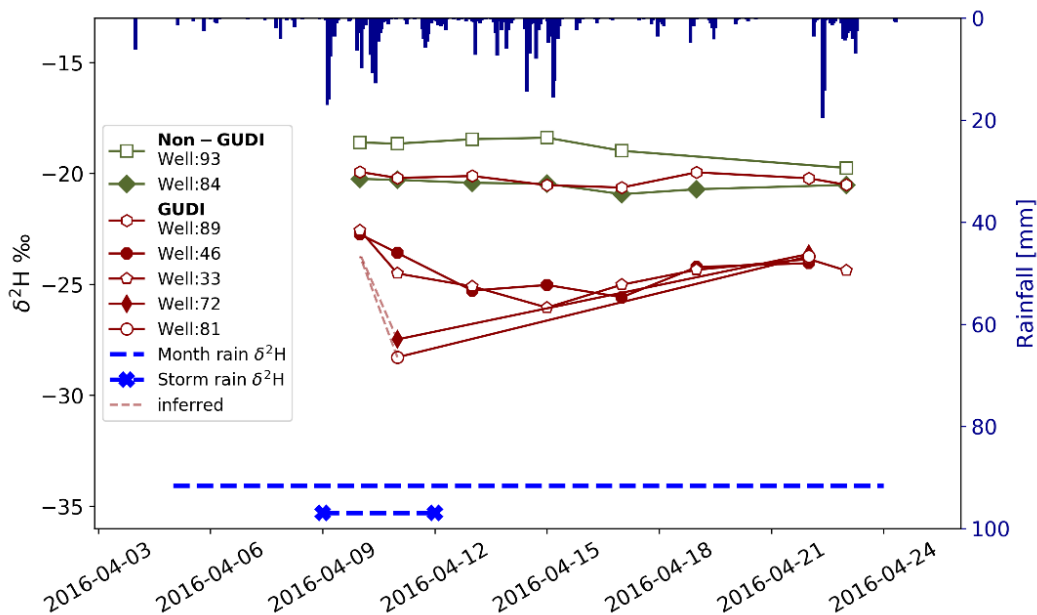


Figure 2.8: Water isotope values ( $\delta^2\text{H}$ ) from groundwater wells (red and green lines) and precipitation (dark blue bars) over a three-week heavy rain-event period. Wells were sampled at discrete times, whereas precipitation samples represent the volume weighted integration of all rain falling throughout two multi-day collection periods; (1) a 3-day period spanning the initial heavy rain event (dashed line with blue X) and (2) over the entire month of April (dashed line with no X). Note that analytical uncertainties plot at roughly the same magnitude as the symbol size, and only  $\delta^2\text{H}$  values are illustrated since  $\delta^{18}\text{O}$  values show similar patterns.

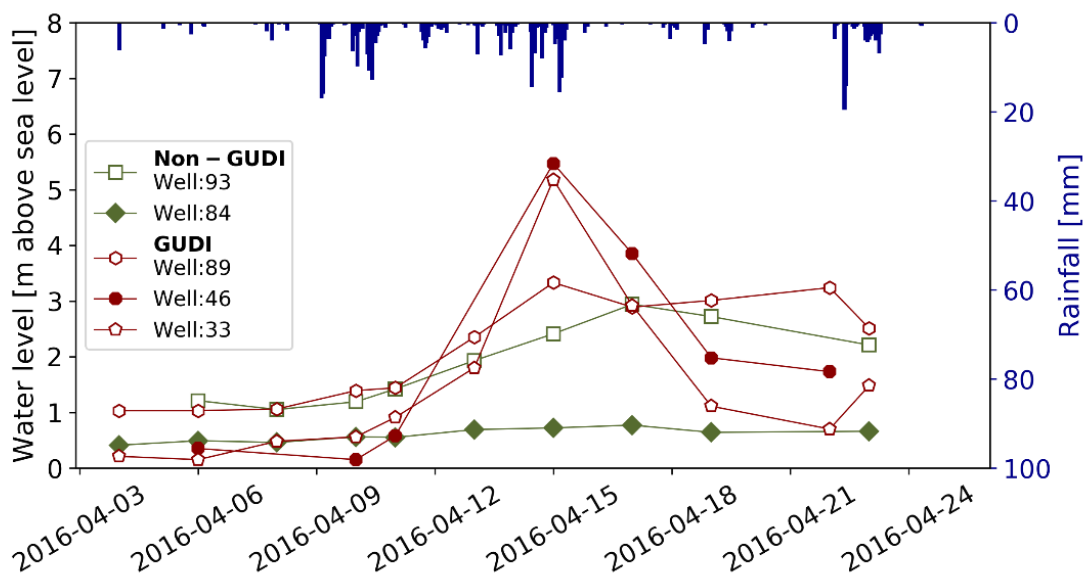


Figure 2.9: Water level variation at three GUDI and two non-GUDI wells measured concurrently with water isotope samples taken during the three-week heavy rain-event period.

Table 2.2: Average annual  $\delta^{18}\text{O}$  and  $\delta^2\text{H}$  values and  $1\sigma$  S.D. (in parentheses) as measured through monthly sampling of wells and precipitation collectors. Precipitation values are volume weighted to amount of water collected each month. Note, for volume weighted samples  $1\sigma$  S.D. is calculated for unweighted data to show the degree of seasonal variability.

Site	$\delta^{18}\text{O}$ [‰]	$\delta^2\text{H}$ [‰]
<b>Precipitation Collectors: Volume Weighted Averages</b>		
Aasu	-4.61 (1.98)	-22.07 (16.52)
Fagaalu	-5.01 (2.02)	-26.38 (16.2)
Iliili	-4.93 (1.87)	-25.96 (15.48)
Leone	-4.94 (1.91)	-25.99 (15.58)
<b>All collector average</b>	<b>-4.87 (1.95)</b>	<b>-25.10 (15.95)</b>
<b>Production Wells: Averages</b>		
Aasu 128	-4.22 (0.34)	-18.52 (1.00)
Fagaalu 179	-4.45 (0.29)	-21.18 (0.83)
Iliili 84	-4.26 (0.29)	-20.43 (0.67)
Malaeimi 89	-4.18 (0.25)	-19.06 (1.19)
Leone 93	-4.23 (0.22)	-20.21 (1.41)
Tafuna 33	-4.30 (0.31)	-20.42 (2.05)
<b>All well average</b>	<b>-4.27 (0.28)</b>	<b>-19.97 (1.19)</b>

## 2.4 Discussion

### 2.4.1 Expected Groundwater Travel Times

Comparing observed travel times from tracer based methods with expected travel times in aquifer material or through faulty casings allowed determination of which contamination mechanism is most likely. Expected travel times for each mechanism were estimated by assessing previously published information, as well as examination of turbidity and video log observations, as detailed below.

#### 2.4.1.1 Travel Time Through Aquifer Material

Overlooking dispersion effects, subsurface travel time is controlled by two primary factors, the distance traveled and the average rate at which water moves along the flow path. Thus, the depth of the pump at any given production well represents a minimum travel distance, with much longer distances possible. While rates of travel through the Tafuna-Leone Aquifers are probably variable, reasonable estimates of this parameter can be found in reported values for general cases of conduit flow, a likely flow mechanism in young basalt aquifers (Kiernan et al. 2003).

Kresic (2006) summarized and reported numerous measurements of groundwater velocity in karst terrains thought to be influenced by conduit flow. These estimates ranged between 400 to 2500 m/day and a typical average value of 716 m/day was suggested, as taken from 43 estimates at a West Virginia karst site. Although no reported measurements of groundwater velocity in aquifers of the Tafuna-Leone Plain have been found, Bentley (1975) reported an average transmissivity ( $T$ ) value of 1,149 m<sup>2</sup>/day from pump tests of Tafuna area wells, and, Izuka et al. (2007) reported horizontal hydraulic conductivity ( $K$ ) values specific to the Tafuna and Leone sides of the Plain of 945 m/day and 396 m/day, respectively, which were developed through calibration of a numerical model. Note also that these values are based on properties of the saturated zone whereas there exists scant information about the typically 20 to 30 m thick unsaturated zone, which like the saturated aquifer, is composed primarily of fractured basalts. A lack of information regarding matrix porosity, hydraulic gradients near pumping wells, and properties of the unsaturated zone precludes direct calculation of groundwater velocities using  $T$  or  $K$  values. However, the magnitudes of these values support the conclusion that groundwater velocities through the Tafuna side of the Plain are generally very high, and may be reasonably approximated with observed values from other conduit flow systems.

Expected groundwater travel times in the Tafuna-Leone Plain were approximated by multiplying groundwater velocities consistent with those suggested by Kresic (2006) (716 m/day) with flow distances through the Plain. Because groundwater infiltrates over an area, as opposed to a single point location, the distance recharge water travels is not a discrete number. Another complicating factor in this setting is the potential for groundwater to move through preferential pathways whose locations, conveyance rate, and prevalence of openings

is uncertain. The most reliable information regarding where water infiltrates in the Tafuna-Leone Plain was produced by Izuka et al. (2007), whereas their MODFLOW model applied the MODPATH particle tracking code to delineate areas contributing to recharge, or capture zones, for each well. If it is assumed that recharge to each well occurs only within this zone, that the actual well pumping rates are equivalent to those used in the Izuka et al., model, that the tracers used in this study (turbidity, soil bacteria, and rainfall) occur uniformly across the landscape, and that the likely heterogeneity of preferential pathways exists at a scale where openings are well distributed throughout the capture zone, then the distance parameter can be conceptualized as a distribution of distances between the well and all points throughout the capture zone. To represent this distribution, a 10 m grid of points was overlaid within each well's capture zone and the straight line distance from each point to the bottom of the well was calculated (Fig. 2.10). By dividing each of these distances by an estimated groundwater velocity from conduit flow systems, a distribution of estimated travel times was approximated (Table 2.3). Expected groundwater travel times from Table 2.3 are reasonably consistent with observed turbidity travel times in Table 2.1, which suggests overly-permeable aquifer material, as opposed to faulty well casings, is the more likely mechanism of contamination in the N. Tafuna wells.

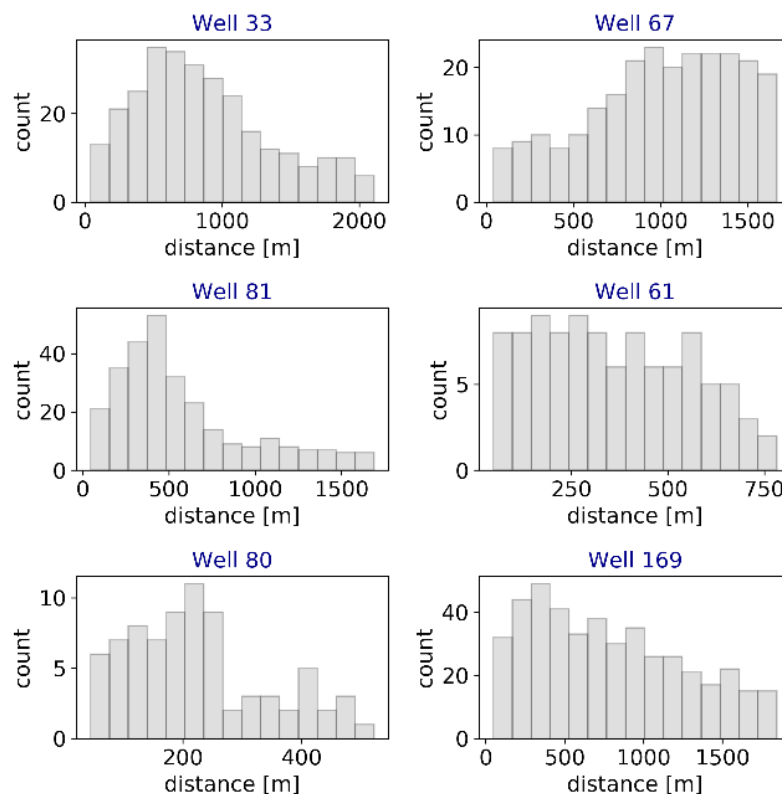


Figure 2.10: Histograms showing the distribution of distances from gridded points throughout capture zones to well pump locations for selected wells.

Table 2.3: Averages and standard deviations (in parentheses) of calculated travel distances from each well to all gridded points within each well's capture zone, and estimated average travel times derived via dividing travel distances by constant groundwater velocities taken from Izuka et al. (2007) and Kressic (2006). Travel time standard deviations (in parentheses) are propagated from travel distance standard deviations (SD).

<b>N Tafuna Wells</b>	<b>Average travel distance [m]</b>	<b>Travel time via Kresic (2006) velocities [hrs.]**</b>
Well 33 (GUDI)*	872 (494)	29 (16)
Well 60 (GUDI)	359 (188)	12 (6)
Well 61 (GUDI)	362 (192)	12 (6)
Well 66 (GUDI)	882 (501)	29 (16)
Well 72 (GUDI)	634 (425)	21 (14)
Well 77 (non-GUDI)	724 (461)	24 (15)
Well 81 (GUDI)	576 (388)	19 (13)
<b>Average and SD</b>	<b>-</b>	<b>21 (12)</b>
<b>Malaeimi Wells</b>		
Well 89 (GUDI)	847 (401)	28 (13)
Well 67 (non-GUDI)	995 (424)	33 (14)
<b>Average and SD</b>	<b>-</b>	<b>30 (13)</b>
<b>Leone wells</b>		
Well 80 (GUDI)	227 (117)	7 (3)
Well 70 (non-GUDI)	294 (166)	9 (5)
Well 169 (non-GUDI)**	788 (480)	26 (16)
<b>Average and SD</b>	<b>-</b>	<b>14 (8)</b>

\* Izuka et al. (2007) velocities were 473 m/day for Tafuna/Malaeimi and 198 m/day for Leone wells \*\* Kressic (2006) velocity used was 716 m/day

#### 2.4.1.2 Travel Time Through a Compromised Casing

The alternate hypothesis to contamination via overly-permeable aquifer material is that surface water travels down compromised casings or through preferential flow paths in the well packing material. In this scenario, maximum travel distance would be the pump depth. The velocity of water cascading down a well bore would be rapid, although this mechanism could still be subject to slower velocities while water percolates through the subsurface or well packing to the depth of a casing breach. Despite uncertainty in aquifer flow path travel-time estimates from section 4.1.1, it is reasonable to assume that surface water traveling through aquifer material will take significantly longer to reach a well pump than surface water traveling through and down a compromised well casing. Fortunately, this assumption can be validated here by examining the observed turbidity response in Well 169, where a hole in the casing was observed on video during a heavy rainfall event.

In the borehole video log performed on Well 169, water could clearly be seen cascading through a less than 2 cm wide hole in the casing, because the logging was coincidentally performed during a heavy-rain event (Fig. 2.11). Upon review of all ten borehole logs provided by ASPA, only Well 169 was observed to have a casing break with active leakage. Although it is unknown if rain events occurred during video logging of other wells, the turbidity profile for Well 169 (conducted a year prior to the video log) nonetheless shows a distinctive and rapid response to the single heavy rain event recorded during the GUDI test. Within 3 hours of rainfall, a large turbidity peak was initiated, peaked within 4 hours, and returned back to baseline in 15 hours. This peak was also the highest maximum turbidity value (25 NTU) observed in any analyzed well. This rapid response started, and more importantly ended, much faster than the average turbidity responses in the N. Tafuna GUDI wells, where turbidity spikes tended to show an exponential decay back to the baseline turbidity value, a phase which usually lasted for days. In contrast, the quick return to baseline at Well 169, within a matter of hours, likely indicates that the casing leak stops once surface water flooding subsides. This example helps validate the premise that surface-water travel time in wells with compromised casings is short, on the order of hours as opposed to days, and further supports the conclusion that overly-permeable aquifer material causes the N. Tafuna GUDI issue.



Figure 2.11: Horizontally oriented screen shot from borehole video log of Well 169 showing location of hole in casing and water actively cascading through the breach and down the well bore. Log was taken during a heavy rain event. Number in upper left corner indicates depth from surface in feet.

## 2.4.2 Isotope Mixing Model: Recent-Rainfall and Old-Groundwater Fractions

The high-resolution water-isotope well sampling in April 2016 took place during a period where  $\delta^{18}\text{O}$  and  $\delta^2\text{H}$  values in precipitation were substantially different from the reasonably consistent average annual isotopic composition of Tutuila's groundwater. This provided a short-term and seasonally dependent groundwater age dating tool, whereas recently recharged groundwater (i.e., recent-rainfall) and seasonally-integrated basal groundwater (i.e., old-groundwater) could be differentiated. By conceptualizing production well water as a mixture of these two isotopically-distinctive end-members, a basic isotope mixing model could be applied to quantify the fraction of water originating from each source. Isotope mixing models are commonly used for identifying the relative contribution of material in a mixed sample from different sources (e.g., Brooks et al. 2012; Fry 2013; Bishop et al. 2015). The isotope mass-balance approach is simple to apply for two end-member systems and results in a linear mixing relationship via integrating and solving a system of two equations of the form:

$$\delta_R \times F_R + \delta_{GW} \times F_{GW} = \delta_{MIX} \quad (2.)$$

$$F_R + F_{GW} = 1 \quad (3.)$$

Where

$\delta_R$  is the isotopic composition of recent-rainfall collected during the precipitation event,  
 $\delta_{GW}$  is the average annual isotopic composition (from monthly samples) of water at each well,  
 $\delta_{MIX}$  is the isotopic composition of well samples, as a mix of recent rainfall and old-groundwater,

$F_R$  is the calculated fraction of water originating from recent-rainfall,

$F_{GW}$  is the calculated fraction of old-groundwater originating from the basal aquifer.

When applied to each  $\delta^{18}\text{O}$  and  $\delta^2\text{H}$  value measured during the rain-event sampling period, the mixing model provided end-member fractions at each well and at each point in time. Table 2.4 summarizes these fractions as percentages of recent-rainfall (specifically from the storm event sample) in each groundwater sample. The fraction of old-groundwater can be inferred as one minus this percentage. Table 2.4 includes dates where maximum and minimum fractions were calculated for each well, and temporal variability in these fractions can be visualized through direct comparison to isotopic values in Fig. 2.8.

Maximum fractions of recent-rainfall were observed in GUDI wells, 33 and 46, on the 15<sup>th</sup> and 17<sup>th</sup> of April, respectively, about a week after the start of the rain event, and also about when the period of rainy weather was transitioning to drier conditions. Although GUDI wells 81 and 72 were sampled at low resolution, the two data points collected from these wells show significant variation within the event-scale survey, with 53% to 47% of their water being sourced from recent-rainfall, respectively, during the heavy rain event portion of the

sampling period on April 11<sup>th</sup>. When these wells were sampled again during the drier portion of the sampling period, their isotope compositions had returned much of the way to the average annual groundwater isotope composition as sampled monthly throughout the year at Well 81. Unfortunately, it is unknown how the isotopic composition of waters at Wells 81 and 72 varied throughout the sample-period.

In general, results from the isotope-mixing model support the conclusions from the other tracers applied in this study. In wells 33, 46, 81 and 72, which are located close together within the Tafuna Lavas, up to one-third of the water produced was seen to be recently recharged rainfall. However, this fraction was no more than 3-4% in wells 84 and 93, which are located in the more ash rich Leone geologic unit. Well 89 showed an intermediate amount of variation during the sampling period, which may be due to its location at the northern margin of the Tafuna Lavas. The spatial distribution of variation seen in water isotopes, water levels, and in other tracers, suggests that an additional sub-division of the Tafuna geologic unit may be warranted. Wells within the N. Tafuna area all display a similar tracer response that is consistent with the GUDI determinations, whereas this response is reduced with distance from this area, and non-existent in the southern Tafuna wells.

Table 2.4: Results from isotope mixing model applied to a series of eight rain-event samples taken every other day between 4/10/2016 and 4/22/2016. Maximum and minimum calculated fractions of the recently recharged groundwater end-member are shown as percentages with the sample date of minimum or maximum occurrence shown in parentheses. Average annual groundwater end member values are specific to each well.

Well #	Average annual groundwater end member [ $\delta^2\text{H}$ ]	Maximum recent fraction and date of occurrence (in parentheses)	Minimum recent fraction and date of occurrence (in parentheses)
81 (GUDI)**	-20.49 ‰	53% (4/11)	22% (4/22)
72 (GUDI)**	-20.49 ‰*	47% (4/11)	21% (4/22)
33 (GUDI)	-20.45 ‰	38% (4/15)	14% (4/10)
46 (GUDI)	-20.45 ‰*	35% (4/17)	15% (4/10)
89 (GUDI)	-20.35 ‰	9% (4/17)	5% (4/10)
93 (non-GUDI)	-19.33 ‰	3% (4/23)	-6% (4/15)
84 (non-GUDI)	-19.18 ‰	4% (4/17)	-1% (4/10)

\* Wells 46 and 72 were not measured monthly, end member values assumed from wells 81 and 33, respectively

\*\* Wells 81 and 72 were only sampled twice, on 4/11 and 4/22

Note: Only  $\delta^2\text{H}$  values and calculations shown,  $\delta^{18}\text{O}$  calculations showed nearly equivalent fractions

## 2.5 Conclusions

Contaminated groundwater from GUDI wells in American Samoa has necessitated one of the longest standing boil-water notices in U.S. history. Effective management of this issue relies on understanding if causes are rooted in well construction problems or aquifer structure problems. This question was explored here through field measurements of three independent multi-tracer datasets including turbidity, indicator bacteria, and water isotopes. Observed tracer responses to rainfall were assessed through the premise that surface-water derived contamination from faulty well construction should arrive at well pumps more quickly than contamination resulting from rapid aquifer transit. Specifically, as exemplified by Well 169, travel times of 3 to 4 hours were observed where a casing breach was found, whereas expected transit time through Tafuna aquifer material was estimated at 21 to 30 hours. Observations from N. Tafuna wells revealed average tracer breakthrough times of  $37 \pm 21$  hours for turbidity, 18 to 63 hours for bacteria, and 1 to 5 days for water isotopes. Travel times from all three methods are generally comparable, and all methods support the conclusion that overly-permeable aquifer material, as opposed to faulty well casings, is the most probable mechanism of contamination in the N. Tafuna GUDI wells.

Any one of the travel time estimates from the three methods used would probably be sufficient to determine which contamination mechanism is most likely. However, a coordinated assessment of all three tracers provided multiple opportunities for validation, gave deeper insight into the subtleties of aquifer conditions, and helped to explain the unique and sometimes enigmatic responses observed in some wells. Although Tutuila's wells have been categorized into a bimodal classification of GUDI or non-GUDI, in reality, each lies on a spectrum of influences controlled by heterogeneous and complex hydrogeology. The results of this study, at the very least can be used to confidently inform local water resource managers about the need for additional filtration infrastructure or abandonment of all wells in the N. Tafuna area. Repair or replacement will only result in continued GUDI contamination. However, observations of how tracer breakthroughs are shaped by heavy rainfall at each of the island's wells also provides insight into recharge dynamics, intra-aquifer variability, and subsurface flow characteristics of these and other highly-permeable young basaltic aquifers. The combination of physical, microbial, and isotopic tracers in this setting is a unique methodology that provides a valuable opportunity to better understand similarities and differences in how each tracer can be applied and interpreted to address water quantity and quality issues in geologically similar settings.

## References: Chapter 2

- ASCC - American Samoa Community College. 2018. Malaeimi weather station data. <https://www.wunderground.com/personal-weather-station/dashboard?ID=IWESTERN499> (accessed 2018-04-30).
- AS-DOC - American Samoa Department of Commerce. 2013. The 2013 Statistical Yearbook for American Samoa. Pago Pago, AS: American Samoa Department of Commerce. <http://doc.as.gov/wp-content/uploads/2011/06/2013-Statistical-Yearbook-Final-Draft.pdf>.
- Barrell, R.A.E., and M.G.M. Rowland. 1979. The relationship between rainfall and well water pollution in a West African (Gambian) village. *Epidemiology & Infection* 83, no. 1: 143--150.
- Birkel, C., J. Geris, M. Molina, C. Mendez, R. Arce, J. Dick, D. Tetzlaff, and C. Soulsby. 2016. Hydroclimatic controls on non-stationary stream water ages in humid tropical catchments. *Journal of hydrology* 542: 231--240.
- Bishop, J.M., C.R. Glenn, D.W. Amato, and H. Dulai. 2017. Effect of land use and groundwater flow path on submarine groundwater discharge nutrient flux. *Journal of Hydrology: Regional Studies* 11: 194--218.
- Brooks, J.R., P.J. Wigington, D.L. Phillips, R. Comeleo, and R. Coulombe. 2012. Willamette River Basin surface water isoscape ( $\delta^{18}\text{O}$  and  $\delta^2\text{H}$ ): temporal changes of source water within the river. *Ecosphere* 3, no. 5: 1--21.
- Byappanahalli, M., and R. Fujioka. 1998. Evidence that tropical soil environment can support the growth of *Escherichia coli*. *Water Science and Technology* 38, no. 12: 171--174.
- Byappanahalli, M.N., B.M. Roll, and R.S. Fujioka. 2012. Evidence for occurrence, persistence, and growth potential of *Escherichia coli* and enterococci in Hawaii's soil environments. *Microbes and environments* 27, no.2: 164--170.
- Calderon, H., and S. Uhlenbrook. 2016. Characterizing the climatic water balance dynamics and different runoff components in a poorly gauged tropical forested catchment, Nicaragua. *Hydrological Sciences Journal* 61, no. 14: 2465--2480.
- Cobb, K.M., J.F. Adkins, J.W. Partin, and B. Clark. 2007. Regional-scale climate influences on temporal variations of rainwater and cave dripwater oxygen isotopes in northern Borneo. *Earth and Planetary Science Letters* 263, no. 3-4: 207--220.
- Dansgaard, W. 1964. Stable isotopes in precipitation. *Tellus* 16, no.4: 436--468.
- Entry, J.A., and N. Farmer. 2001. Movement of coliform bacteria and nutrients in ground water flowing through basalt and sand aquifers. *Journal of Environmental Quality* 30, no. 5: 1533--1539.
- Fackrell, J.K. 2016. Geochemical evolution of Hawaiian groundwater. Honolulu, HI: Doctoral dissertation, University of Hawai'i at Manoa. [https://www.soest.hawaii.edu/GG/resources/theses/JFackrell\\_Dissertation.pdf](https://www.soest.hawaii.edu/GG/resources/theses/JFackrell_Dissertation.pdf).

- FAO - Food and Agriculture Organization of the United Nations. 2016. AQUASTAT website. [http://www.fao.org/nr/water/aquastat/water\\_use/](http://www.fao.org/nr/water/aquastat/water_use/) (accessed 2018-03-07).
- Foppen, J., and J. Schijven. 2006. Evaluation of data from the literature on the transport and survival of *Escherichia coli* and thermotolerant coliforms in aquifers under saturated conditions. *Water Research* 40, no. 3: 401--426.
- Freeze, R.A., and J.A. Cherry. Groundwater. (Englewood Cliffs, New Jersey: Prentice Hall, 1979).
- Fry, B. 2013. Alternative approaches for solving underdetermined isotope mixing problems. *Marine ecology progress series* 472: 1--13.
- Gat, J.R. 1996. Oxygen and hydrogen isotopes in the hydrologic cycle. *Annual Review of Earth and Planetary Sciences* 24: 225--262.
- Glickman, T.S. 2000. Glossary of Meteorology. American Meteorological Society, 2nd Edn. MA, USA: American Meteorological Society. <http://glossary.ametsoc.org/wiki/Rain>.
- Godfrey, S., F. Timo, and M. Smith. 2005. Relationship between rainfall and microbiological contamination of shallow groundwater in Northern Mozambique. *Water Sa* 31, no.4: 609--614.
- Goldscheider, N., M. Pronk, and J. Zopfi. 2010. New insights into the transport of sediments and microorganisms in karst groundwater by continuous monitoring of particle-size distribution. *Geologia Croatica* 63, no. 2: 137--142.
- Izuka, S.K., J.A. Perreault, and T.K. Presley. 2007. Areas contributing recharge to wells in the Tafuna-Leone Plain, Tutuila, American Samoa. Honolulu, HI: Geological Survey (US). Report no. 2007-5167. <https://pubs.er.usgs.gov/publication/sir20075167>.
- Keating, B.H., and B.R. Bolton. Geology and offshore mineral resources of the Central Pacific Basin. (New York, NY: Springer Science & Business Media, 1992).
- Kiernan, K., C. Wood, and G. Middleton. 2003. Aquifer structure and contamination risk in lava flows: insights from Iceland and Australia. *Environmental Geology* 43, no. 7: 852--865.
- Kirs, M., P. Moravcik, P. Gyawali, K. Hamilton, V. Kisand, I. Gurr, C. Shuler, and W. Ahmed. 2017. Rainwater harvesting in American Samoa: current practices and indicative health risks. *Environmental Science and Pollution Research* 24, no. 13: 12384--12392.
- Kresic, N. Hydrogeology and groundwater modeling. (Boca Raton, Fl: CRC press, 2006).
- Levitt, D.G., D.L. Newell, W.J. Stone, and D.S. Wykoff. 2005. Surface Water--Groundwater Connection at the Los Alamos Canyon Weir Site. *Vadose Zone Journal* 4, no. 3: 708--717.
- Massei, N., J. Dupont, B. Mahler, B. Laignel, M. Fournier, D. Valdes, and S. Ogier. 2006. Investigating transport properties and turbidity dynamics of a karst aquifer using correlation, spectral, and wavelet analyses. *Journal of hydrology* 329, no. 1-2: 244--257.
- Mauga, D. 2016. Personal Communication

- Nakamura, S., 1984, Soil Survey of American Samoa: U.S. Department of Agriculture Soil Conservation Service, 95 p.
- Pronk, M., N. Goldscheider, J. Zopfi, and F. Zwahlen. 2009. Percolation and particle transport in the unsaturated zone of a karst aquifer. *Groundwater* 47, no. 3: 361--369.
- Rhodes, A.L., A.J. Guswa, and S.E. Newell. 2006. Seasonal variation in the stable isotopic composition of precipitation in the tropical montane forests of Monteverde, Costa Rica. *Water Resources Research* 42, no. 11.
- Rozanski, K., L. Araguas-Araguas, R. Gonfiantini. 1993. Isotopic patterns in modern global precipitation. In: Swart, P.K., K.C. Lohmann, J. McKenzie (Eds.), *Climate Change in Continental Isotopic Records. Geophysical Monograph* 78: 1--36
- Scholl, M.A., S.B. Gingerich, and G.W. Tribble. 2002. The influence of microclimates and fog on stable isotope signatures used in interpretation of regional hydrology: East Maui, Hawaii. *Journal of Hydrology* 264, no. 1-4: 170--184.
- Scholl, M.A., S.E. Ingebritsen, C.J. Janik, and J.P. Kauahikaua. 1996. Use of precipitation and groundwater isotopes to interpret regional hydrology on a tropical volcanic island: Kilauea volcano area, Hawaii. *Water Resources Research* 32, no. 12: 3525--3537.
- Stearns, H.T. 1944. Geology of the Samoan islands. *Bulletin of the Geological Society of America* 55, no. 11: 1279--1332.
- Taylor, R., A. Cronin, S. Pedley, J. Barker, and T. Atkinson. 2004. The implications of groundwater velocity variations on microbial transport and wellhead protection--review of field evidence. *FEMS Microbiology Ecology* 49, no. 1: 17--26.
- US-EPA - U.S. Environmental Protection Agency. 1998. National Primary Drinking Water Regulations: Enhanced Surface Water Treatment Rule. Washington, DC.: U.S. Environmental Protection Agency. <https://www.epa.gov/dwreginfo/surface-water-treatment-rules>.
- US-EPA - U.S. Environmental Protection Agency. 2006. National Primary Drinking Water Regulations: Ground Water Rule. Washington, DC.: U.S. Environmental Protection Agency. <https://www.epa.gov/dwreginfo/ground-water-rule>.
- Vold, S., J. Regis, and J. Gambatese. 2013. Groundwater Under the Direct Influence of Surface Water Study: Well 81. unpublished report submitted to American Samoa Environmental Protection Agency. Pago Pago, AS: American Samoa Power Authority.

## Chapter 3:

# Understanding Surface Water - Groundwater Interaction, Submarine Groundwater Discharge, and Associated Nutrient Loading in a Small Tropical Island Watershed

### **Abstract**

Submarine groundwater discharge (SGD) provides important connectivity delivering land-based nutrients to coastal ecosystems in many oceanic islands. However, water quality management in these settings is typically focused on obvious surface waters, often ignoring SGD and nearshore groundwater-surface water interactions. In this study, we conducted a comprehensive radionuclide tracer based field investigation in tandem with watershed modeling to assess groundwater - surface water partitioning and to quantify nutrient loading from SGD and streamflow in a small embayment located in American Samoa. We used the Soil and Water Assessment Tool (SWAT) to produce water balance and nutrient loading estimates for locations, time periods, and hydrologic pathways not measured during fieldwork. Groundwater and surface water samples were analyzed for multiple tracers including  $^{222}\text{Rn}$  concentrations, nutrients, and nitrogen isotopes. Measurements indicated that SGD delivers a significant proportion of coastal nutrient loads, and upper-watershed baseflow delivers very little. Seepage run measurements informed a conceptual hydrogeologic model of groundwater-surface water interaction which was then used for interpreting model results. The SWAT simulated water fluxes matched flow observations well and the model simulated observed nutrient loads within an order of magnitude. The model also provided estimates of nitrogen loads in surface runoff and lateral flow, which were not measured, but together are likely to be smaller than those from SGD. By applying this integrated approach, our study demonstrates how watershed modeling can supplement limited field data to develop a more complete understanding of nutrient sources, transport, and fate in coastal watersheds with perennial streams.

Submitted to Journal of Hydrology (March 2019) as: Christopher K. Shuler, Henrietta Dulai, Olkeba T. Leta, Joseph Fackrell, Eric Welch, and Aly I. El-Kadi. Understanding Surface Water - Groundwater Interaction, Submarine Groundwater Discharge, and Associated Nutrient Loading in a Small Tropical Island

### 3.1 Introduction

Discharge of anthropogenic nutrients to coastal areas has the potential to significantly impact nearshore water quality and affect reef health (Bahr et al., 2015; Dulai et al., 2016). In recent decades, the effect of submarine groundwater discharge (SGD) on coastal nutrient budgets has become widely recognized (e.g., Johannes and Hearn, 1985; Dulaiova et al., 2006; Rodellas et al., 2015), and SGD has been found to be particularly significant in tropical volcanic island settings (Zektser, 2000; Moosdorf et al., 2015; Dulai et al., 2016). Nonetheless, environmental water quality management is typically focused on surface waters, often ignoring SGD. The U.S. Environmental Protection Agency's Clean Water Act (Section 303(d)) requires states and territories to establish water quality standards and Total Maximum Daily Loads (TMDLs) for nutrients in receiving waters. In many places, including the Territory of American Samoa, such standards apply only to fresh surface and open coastal waters (AS-EPA, 2013a), thereby overlooking potentially important nutrient pathways. Spatial variability in groundwater discharge directly to streams may also affect the validity of TMDL measurements, which are assumed to be from a surface water origin. Recent studies from streams (e.g., Avery et al., 2018), mangrove environments (e.g., Gleeson et al., 2013) and large tidal estuaries (e.g., Makings et al., 2014) indicate that groundwater has significant impacts on both coastal water quality and nearshore stream water quality, underscoring the importance of considering groundwater-surface water interaction when designing water quality monitoring protocols. However, accurate quantification of groundwater discharge to streams and coastlines is inherently challenging because available methods typically rely on measurements and conceptual models with high uncertainties. This underscores the need to develop an improved understanding of how land-use, groundwater, and surface water interact to deliver nutrients to the coast.

The naturally occurring noble gas radon-222 ( $^{222}\text{Rn}$ ) has become one of the most widely used tracers for determining SGD rates, (e.g., Burnett and Dulaiova, 2003; Charette et al., 2007; Sadat-Noori et al., 2015) and when combined with water quality sampling, this method is widely used for estimating associated coastal nutrient fluxes (e.g., Dulaiova et al., 2010; Gleeson et al., 2013; Wang et al., 2017). Radon has also been applied successfully in stream headwaters, channels, and estuaries for investigating the magnitude and locations of groundwater-surface water interactions (e.g., Peterson et al. 2010, Gleeson et al., 2018). Groundwater becomes enriched in  $^{222}\text{Rn}$  through prolonged contact with aquifer material, and pore-water  $^{222}\text{Rn}$  concentrations typically reach an equilibrium between ingrowth and radioactive decay within a couple of weeks. After leaving the aquifer, dissolved  $^{222}\text{Rn}$  has a short half-life of 3.8 days, exhibits conservative behavior through the full salinity range, and shows low concentrations in surface and ocean waters, making it an excellent tracer of recently discharged groundwater.

Predictable isotopic fractionation of nitrogen (N) in dissolved nitrate and nitrite ( $\delta^{15}\text{N}_{\text{N+N}}$ ) has been used extensively for tracing sources of nutrients in groundwater (e.g.

Kendall and Aravena, 2000; Cole et al., 2006; Hunt, 2007), stream water (e.g. Lindau, et al., 1989), and coastal surface waters (e.g. Garrison et al., 2007; Wong et al, 2014; Wiegner, 2016; Bishop et al., 2017). Commonly referenced ranges for  $\delta^{15}\text{N}$  values indicate synthetic fertilizer influenced waters have relatively low  $\delta^{15}\text{N}$  values (-5 ‰ to +5 ‰), natural soil processes typically produce porewaters with intermediate  $\delta^{15}\text{N}$  values (+2 ‰ to +6 ‰), and manure and human wastewater leachates generally produce higher  $\delta^{15}\text{N}$  values, albeit with a wide range (+4 ‰ to +25 ‰) (Kendall and Aravena, 2000; Dailer et al. 2010; 2012; Fenech et al., 2012, Abaya et al. 2018a,b). In tropical island settings wastewater  $\delta^{15}\text{N}$  values have been found to encompass almost this full range, from 5 ‰ to 23 ‰ (Bishop et al, 2017; Amato et al, 2016; Hunt and Rosa, 2009; Rogers et al, 2012).

Watershed and nutrient budget models are commonly applied to integrate diverse environmental datasets and to assess coastal water and nutrient fluxes at larger spatial and temporal resolutions (e.g. Alexander et al., 2002; Borah and Bera, 2004; Paul et al., 2017). These include the Soil & Water Assessment Tool (SWAT) (Arnold et al., 1998; Gassman et al., 2007), Gridded Surface/Subsurface Hydrologic Analysis (GSSHA) (Downer and Ogden, 2006), and Spatially Referenced Regression on Watershed Attribute (SPARROW) (Schwarz et al., 2006). The wide spatial coverage and often low development cost of models makes them useful for management agencies tasked with covering large areas that are difficult to fully characterize with field methods. However, the accuracy of model results directly relies on an appropriate conceptualization of the hydrologic system, as well as sufficient calibration and validation data to constrain uncertainty and ensure that results are accurate. Only a limited number of studies have integrated in-depth field investigations, conceptual hydrogeologic models, and distributed watershed models to characterize and assess nutrient delivery through all hydrologic pathways in small island watersheds (e.g., Oberdorfer, 2003; Michael, 2005; Gardner and Wilson, 2006; Zhu et al., 2017). To our knowledge, tropical island settings remain understudied in this regard.

Anthropogenic nutrient loading and sedimentation on American Samoan reefs have been identified as primary factors in reducing the reef's ability for recovery from increasing environmental stressors (McCook, 1999; Craig, 2009). Long-term studies of reefs on Tutuila, the territory's main island, suggest SGD is likely to be a significant explanatory variable in reef health (Houk et al., 2013; Whittall and Holst, 2015). However, prior to this study, there have been no known attempts to quantify SGD and its associated nutrient loading in American Samoa. To fill this gap, we used measurements of environmental tracers including  $^{222}\text{Rn}$ , dissolved nutrients, and nitrogen isotopes to a trace groundwater discharge, partition baseflow and SGD nutrient flux, and explore probable nutrient sources within a small, tropical-island watershed and embayment. Field observations provided insights for informing conceptual model development and were useful for model calibration and validation. Watersheds in American Samoa provide unique settings to examine nutrient budgets on a

basin-wide scale due to small drainage areas, relatively good accessibility, and high precipitation rates that drive measurably significant water fluxes.

In this study, we hypothesize that multiple hydrologic pathways, including groundwater, surface water, and SGD all act as significant controls on coastal nutrient loading within in a small watershed located in the Territory of American Samoa. To investigate this question, we integrated a detailed geochemical field investigation with watershed-nutrient modeling in order to partition the impact of water and nutrient discharge from different hydrologic pathways. Our primary objectives for this work are to develop a better understanding of groundwater – surface water interaction in these types of watersheds and to quantify coastal nutrient loading impacts from non-point sources in Faga’alu (Fong-uh ah-loo) Watershed on the island of Tutuila.

### 3.2 Study Area

Faga’alu Watershed consists of a small (2.1 km<sup>2</sup>), steep, heavily forested valley with one main perennial stream draining into Faga’alu Bay, a small arm of Pago Pago Harbor (Fig. 3.1). Geologically, the watershed is carved from dense inner-caldera basalts formed about 1.2 Mya, and the valley bottom is filled with a gently inclined wedge of terrestrial and marine alluvium that extends about 1 km upstream from the coast (Stearns, 1944). The regional scale aquifer permeability of the inter-caldera basalts is likely to be significantly lower than that of the terrestrial alluvium, based on aquifer properties of similar geologic units in Western Tutuila (Izuka et al., 2007). However, in Faga’alu the only known well is located in the alluvium, precluding direct comparison of each unit’s hydrogeologic properties. Significant springs found in the inter-caldera unit indicate that it contains high-level groundwater, which is likely to be impounded by sub-surface structures, such as dikes, perching layers, or potentially faults (Davis, 1963). In the upper watershed, the soil type is primarily silty clay to clay loam Lithic Hapludolls ranging from 20–150 cm deep, and the alluvial unit is covered with a fairly deep (>150 cm) mixture of well-drained very stony silty clay loams and poorly-drained silty clay to fine sandy loams (Nakamura, 1984). Faga’alu’s climate is warm and humid with year round average temperatures around 28 °C and annual rainfall between 3000 and 6000 mm/year, depending on elevation. The wet season extends from October to May and the drier season spans June to September.

In Faga’alu, anthropogenic activities have been connected to recent degradation of reef health and reduction of stream water quality, leading to its designation as a federal priority watershed management area by the United States Coral Reef Task Force (NOAA-CRCP, 2013). Both stream and coastal water quality in Faga’alu have been classified as ‘impaired’ since 2006 (AS-EPA, 2016) and AS-EPA coral reef monitoring suggests that Faga’alu’s benthic ecosystem is one of the most impacted on the island (Houk et al., 2005). Previous studies implicate the

stream as a pathway for terrigenous sediments and excessive nutrient loads to the bay (DiDonato, 2005; Messina, 2013; Messina & Biggs, 2016). However, the role of groundwater as a hydrologic pathway for terrigenous contamination remains unconstrained. The three primary anthropogenic nutrient sources on Tutuila have been previously determined to be: (1) On-Site wastewater Disposal Systems (OSDS), (2) widespread small-scale pig farming operations, and (3) agricultural fertilizers (Falkland et al., 2002; Polidoro et al., 2016; Shuler et al., 2017); but the relative impact of each source on coastal ecosystems remains poorly understood.

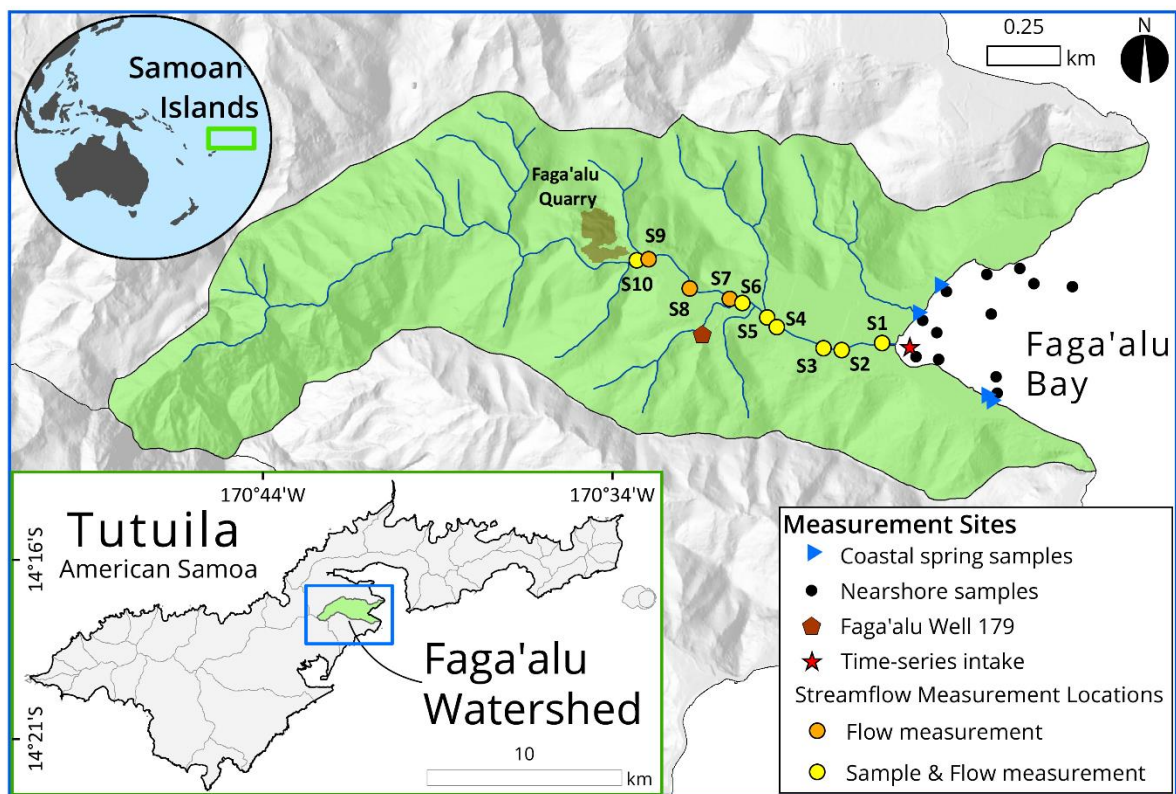


Figure 3.1: Study area and locations of sample sites in stream (colored circles), well (pentagon), coastal springs (triangles), and nearshore waters (black circles). Flow measurements were taken at all stream sites and yellow circles indicate where water samples were taken as well. The seepage run focused on the lower reach of Faga'alu Stream (below the quarry) as this reach encompassed the majority of human development within the valley.

## 3.3 Methods

### 3.3.1 Water Sampling and Stream Gauging Methods

We collected groundwater, coastal water, and stream water samples throughout a weeklong sampling campaign in the dry season of 2014 during a period with no significant rainfall. This included a longitudinal sampling and measurement transect up Faga'alu stream, hereafter referred to as a seepage run (Rosenberry and LaBaugh, 2008), which we conducted during a single 24-hour period through the lower 1 km stream section. During the seepage run, we measured streamflow at ten separate locations with a Price-type Pygmy Current Meter and the velocity-area-method (Turnipseed and Sauer, 2010) and sampled stream water at seven of those locations. During a boat-based coastal water survey (see section 3.2.2), we collected coastal water samples from Faga'alu Bay one day after the seepage run. We identified three areas along the shoreline of the bay with brackish coastal springs, and sampled these twice each at low tide throughout the week. We also sampled the only production well in the valley (Well #179). All sampling locations are shown on Fig. 3.1. To verify the seepage run results, we conducted a second seepage run on August 10<sup>th</sup>, 2016, and measured streamflow and dissolved <sup>222</sup>Rn concentrations (but not nutrients or other parameters) at many of the same sites as in 2014. To reduce measurement uncertainty, streamflow for the second seepage run was measured with a SonTek FlowTracker Handheld Acoustic Doppler Velocimeter, which has a higher velocity resolution and accuracy than the Pygmy meter we used in 2014. Sampling and analysis for <sup>222</sup>Rn concentrations was performed in the same way as was done in 2014.

For all nutrient samples, we also collected in situ temperature, salinity, pH, and dissolved oxygen data with a YSI multiparameter sonde (6600V2-4 model). Nutrient and isotope samples were collected in acid washed 60 ml HDPE bottles triple-rinsed with sample water before filling. Nutrient samples were kept refrigerated, whereas N-isotope samples were frozen until analysis. All nutrient and isotope samples were filtered through 0.45  $\mu\text{m}$  capsule filters, thus all measured nutrient concentrations and comparable modeled nitrogen concentrations reported here refer to dissolved species unless the particulate fraction is specifically indicated. We collected grab samples for <sup>222</sup>Rn in 250-ml glass bottles with no headspace and analyzed them the same day as collection with a RAD H<sub>2</sub>O radon in water analyzer, manufactured by Durrige Inc. (Billerica MA, USA). Because of <sup>222</sup>Rn's short half-life (3.8 days), <sup>222</sup>Rn grab sample values were decay corrected to the time of collection.

We analyzed all water samples for dissolved nutrients including nitrate and nitrite (N+N), ammonium (NH<sub>4</sub><sup>+</sup>), phosphate (PO<sub>4</sub><sup>3-</sup>), silicate (Si), total dissolved nitrogen (TDN), total dissolved phosphorus (TDP), dissolved <sup>222</sup>Rn concentration, and nitrogen isotope ( $\delta^{15}\text{N}_{(\text{N}+\text{N})}$ ) values of N+N in samples having > 1  $\mu\text{mol/L}$  of N+N. The only exceptions were samples collected in 2016, which were only analyzed for <sup>222</sup>Rn concentrations. Nutrient samples were analyzed within two weeks of collection at the University of Hawaii School of

Ocean and Earth Science and Technology (SOEST) Laboratory for Analytical Biogeochemistry using the methods described in Armstrong et al. (1967) and Grasshoff et al. (2007). Nitrogen isotope samples were measured within 4 months of collection at the University of Hawaii's Stable Isotope Biogeochemistry Lab using the denitrifier method of Sigman et al. (2001). Isotopic results are expressed here in per mil (‰) notation relative to the isotopic reference standard of AIR.

Since coastal groundwater is composed of both oceanic and fresh water, all reported nutrient concentrations for coastal springs were normalized to the fresh groundwater end-member salinity of 0.16, as measured at Well 179. This was done with an un-mixing calculation (e.g., Hunt and Rosa, 2009) that assumed conservative nutrient behavior during mixing and was based on an oceanic end member from Tutuila. This calculation allowed the derivation of nutrient fluxes solely contributed by fresh groundwater. We collected duplicate samples at five locations and analytical uncertainty was assessed using the relative percent difference (RPD) method, which is defined as the absolute value of the difference between two duplicates, expressed as a percentage of their mean. Average RPD was 1.4% for N+N, 0.5% for Si, 0.6% for  $\text{PO}_4^{3-}$ , 2.4% for  $\text{NH}_4^+$ , 0.8% for TDN, 1.9% for TDP, and 6.8% for  $\delta^{15}\text{N}_{(\text{N}+\text{N})}$ .

### 3.3.2 Radon-Based SGD Measurement

Dissolved  $^{222}\text{Rn}$  was used as a groundwater tracer in a temporally and spatially distributed non-steady-state radon flux model to calculate bay-wide SGD rates following the methods of Burnett & Dulaiova (2003) and Dulaiova et al. (2010). We assessed temporal (tide-dependent) variability with a time-series of  $^{222}\text{Rn}$  measurements taken from a fixed nearshore location over a 48-hour period. This was coupled with a coastal water survey to assess spatial variation in  $^{222}\text{Rn}$  throughout the inner bay. For both the time-series and survey,  $^{222}\text{Rn}$  concentrations were measured by pumping surface water through an air-water exchanger connected to a radon-in-air monitor (RAD AQUA, DurrIDGE Inc.). To obtain bay-wide SGD fluxes, we scaled up the tidally-averaged SGD flux from the stationary time-series to account for the additional SGD flux observed during the coastal survey in locations adjacent to the time-series location, as described below.

#### 3.3.2.1 Stationary $^{222}\text{Rn}$ Time-Series

The  $^{222}\text{Rn}$  time-series instrument package used a peristaltic pump that pumped surface water from the bay to an instream flow cell (with no headspace) attached to the YSI 6600-series sonde that continuously logged water salinity and temperature. The inlet hose for the pump was connected to a moored float located at a stationary point in the bay about 50 m away from the stream mouth (Fig. 3.1). After passing through the YSI, water flowed into an air-water-exchanger where  $^{222}\text{Rn}$  gas was extracted and pumped to the RAD7. Tidal height

was measured by a pressure transducer placed on the seafloor at the float anchor. We deployed the instrumentation for about 48 hours and the RAD7 was set to integrate measurements of  $^{222}\text{Rn}$  activity every 30 minutes. Typically, SGD manifests as a fresh or brackish plume that overlies denser seawater. We measured plume thickness at low tide by manually conducting salinity depth profiles at the water intake, and this plume thickness was used for volumetric calculations in the  $^{222}\text{Rn}$  mass-balance model. Change in plume thickness due to tidal dilution was calculated by subtracting the thickness of the underlying salt-water layer from the total depth of the water column.

### **3.3.2.2 Coastal Water Survey**

We performed the coastal water survey once the time-series was finished, during a 3-hour period bracketing low tide. We transferred the time-series instrument platform to a small boat and rowed throughout the bay while the air-water exchanger was supplied with surface water from a bilge pump tethered to the hull of the boat. The RAD7 was set to integrate  $^{222}\text{Rn}$  activity every 5 minutes and data was resampled to one minute intervals yielding a total of 205 points available for interpolation. During the survey, three distinct plumes of SGD were detected as low salinity and high  $^{222}\text{Rn}$  anomalies. We refer to these plumes as the southern, central, and northern plumes. During analysis, the surface area and geometry of each plume was determined by nearest neighbor interpolation of measurement points and contouring of the resultant  $^{222}\text{Rn}$  activity surface. Boundaries for each of the three plumes were defined as the  $^{222}\text{Rn}$ -isoline representing the mid-point of the range of measured activities (3.25 dpm/L). We defined the bottom boundary of each plume to be the salinity 28 isohaline, as indicated by salinity depth profiles that we took periodically during the survey; or if salinity was consistent throughout the whole water column, the full water depth was used as the plume thickness. Note that the time-series measurement described in section 3.2.1 was performed at a location that fell inside of the central plume. Additionally, during the survey, coastal water samples were collected for analysis in the same manner as stream and groundwater samples.

### **3.3.2.3 SGD Flux Scaling, Fresh and Recirculated Fractions**

The  $^{222}\text{Rn}$  flux model of Dulaiova et al. (2010) was used to calculate SGD fluxes for both survey and time-series data. The model uses a mass-balance approach that relies on accounting for  $^{222}\text{Rn}$  losses and additions from local and offshore processes that are not related to SGD. We assumed that ambient  $^{222}\text{Rn}$  activities from oceanic or atmospheric sources were comparable to those found in the Hawaiian Islands, and used an ambient  $^{222}\text{Rn}$  activity of 0.03 dpm/L (Kelly, 2012), a local excess  $^{222}\text{Rn}$  activity of 0.08 dpm/L supported by in situ  $^{226}\text{Ra}$  (Street et al., 2008), and an offshore  $^{222}\text{Rn}$  activity of 0.087 dpm/L, derived from the offshore  $^{226}\text{Ra}$  (Fröllje et al., 2016). We assumed residence time of SGD affected-groundwater

within Faga'alu's inner bay to be 12.2 hours, the length of one tidal cycle, which is within the ranges of published residence times from water circulation studies of Faga'alu (Storlazzi et al., 2014; Vetter and Vargas-Angel, 2014). Hourly measurements of local wind speed and air temperature were obtained from the American Samoa Observatory NOAA Earth System Research Laboratory (ESRL) weather station at Cape Matatula. To assess the SGD end-member composition, we collected groundwater samples from the only well in the valley and from four coastal spring locations at low tide. The  $^{222}\text{Rn}$  activity measured in coastal springs and the well showed a linear mixing relationship with salinity (Appendix C, Fig. C1), which suggests that while seawater recirculation does occur, the nearshore reef substrate or the re-infiltrated coastal water does not add a significant quantity of  $^{222}\text{Rn}$  to groundwater during this process; likely because circulation is rapid and recirculated seawater does not spend enough time in the subsurface to collect measurable radon. The linearity of this relationship also indicates the fresh coastal spring  $^{222}\text{Rn}$  end-members (when corrected for dilution by seawater) are quite consistent with the  $^{222}\text{Rn}$  activity measured at Well 179. Therefore, the  $^{222}\text{Rn}$  concentration from the well was used as the groundwater end member for SGD calculations.

The time-series calculations provided a temporally-integrated SGD rate, but for the central plume only, as this was where the water intake was located. On the other hand, the coastal water survey provided spatially distributed SGD rates, which allowed for the identification of three distinctive SGD plumes, but only as a snapshot in time. Therefore, to calculate temporally integrated SGD flux to the whole bay, the ratios of survey-measured SGD rates in the northern and southern plumes to the survey-measured SGD rate in the central plume were used as scaling factors to upscale the time-series derived, temporally-averaged SGD flux to include the other two plumes. Some limitations of this approach included needing to make the simplifying assumptions that tidal variation in the central plume was representative of the other two plumes, that SGD only discharged from the three identified plumes, and that the relative magnitudes of discharge from each plume stay consistent over time. These limitations could be addressed by replicating the survey at different times or repeating the time-series in different locations. However, due to the significant amount of time required for just one time-series and survey, we were unable to replicate the approach at a different time.

### 3.3.3 Watershed and Land-Use Modeling

For watershed modeling, we selected the SWAT model, which is a physically-based, semi-distributed, watershed scale, ecohydrological model (Arnold et al., 1998). The model served as a framework for integrating a diverse spread of field data and for estimating transient magnitudes of flow and nutrient flux through different hydrologic pathways (water budget components), such as surface runoff, lateral flow (i.e., subsurface stormflow), and baseflow at different spatial and temporal scales. The wide applicability of SWAT under

various conditions and to different environmental problems has been demonstrated worldwide (Gassman et al., 2007 and 2014).

The SWAT model development was based on the following datasets:

- A 3x3 m Digital Elevation Model (DEM) from the National Geophysical Data Center ([dataset] NGDC, 2013) and obtained from NOAA Ocean and Coastal Services Center.
- 1:24,000 scale soil maps from the Natural Resources Conservation Service - Soil Survey Geographic (SSURGO) database.
- A 2.4 x 2.4 m 2010 land-use map from the Coastal Change Analysis Program (C-CAP).
- Anthropogenic dissolved inorganic nitrogen (DIN) source locations and loading rates as detailed below.

Daily rainfall and streamflow were measured and provided for this study by A.M. Messina (2016 personal communication, with supporting methodology documented in (Messina, 2016)) at two sites within the Faga'alu Watershed for the period 2012 to 2014. Daily wind speed, relative humidity, and maximum and minimum temperatures were only available at one of these sites. Solar radiation was measured at the nearby American Samoa Community College ([Dataset] ASCC, 2018) and additional relative humidity data were obtained from the NOAA- Earth System Research Laboratory weather station. The watershed was divided into 26 sub-basins and 403 hydrological response units (HRUs), with zero threshold values for land-use, soil, and slope classes. The model simulation was run for the period of 2005 to 2014.

Nitrogen budget modeling was handled in SWAT by populating the model with locations and estimates of anthropogenic N sources, specifically agricultural applications, piggery waste, and household wastewater discharged via On-Site Disposal Systems (OSDS). Agricultural DIN was loaded as a fertilizer application, pig waste was simulated as a manure application, and OSDS leachate was simulated using SWAT's biozone algorithm module for OSDS simulation (Jeong et al., 2011). We obtained piggery locations and stock numbers from an AS-EPA piggery census GIS-dataset ([Dataset] Zennaro, 2007) provided by AS-EPA, and agricultural land-use areas were taken from the C-CAP land-use map mentioned above. Because no OSDS survey data is available for the Faga'alu area, we indirectly determined the locations of OSDS units, following Shuler et al. (2017), by taking all building locations, and geospatially subtracting those within 10 m of a sewer main or connection as indicated by wastewater as-built diagrams supplied by the American Samoa Power Authority (ASPA). The remaining buildings were assumed to be connected to an OSDS unit. Maps of input datasets used in the SWAT model are shown in (Fig. 3.2). We based the N-loading rate for pig manure on a reported value of 14 kg of N/pig/year (AS-EPA, 2013b), the agriculture loading rate was based on the synthetic fertilizer application rate of 2.81 kg-N/ha of arable land/year as

reported in Samoa ([Dataset] The World Bank, 2015). The loading rate for OSDS units was estimated to be 18.2 kg-N/unit/year, which was based on a published per capita N loading rate for failing septic systems (TCE, 2005) and the average number of occupants in American Samoan households (AS-DOC, 2013). Because most of the OSDS units in American Samoa are cesspools, we considered failing septic systems to be the best approximation for these types of units. Natural nitrogen cycling processes were automatically handled in SWAT based on the default ecological nitrogen production rates from each assigned land-use type.

Because SWAT’s ecological nitrogen cycling processes also act on anthropogenic nitrogen sources, the relationship between anthropogenic N input and N discharge due to each source is non-linear. To get around this issue we ran three different model scenarios, each with one of the three individual anthropogenic N source removed as an N input. In this way, source-specific loading rates to each hydrologic pathway could be calculated as the difference between the scenario and base-case N discharge to each pathway. A fourth scenario with all anthropogenic sources removed was also run to determine how much N is discharged when accounting for natural N cycling only.

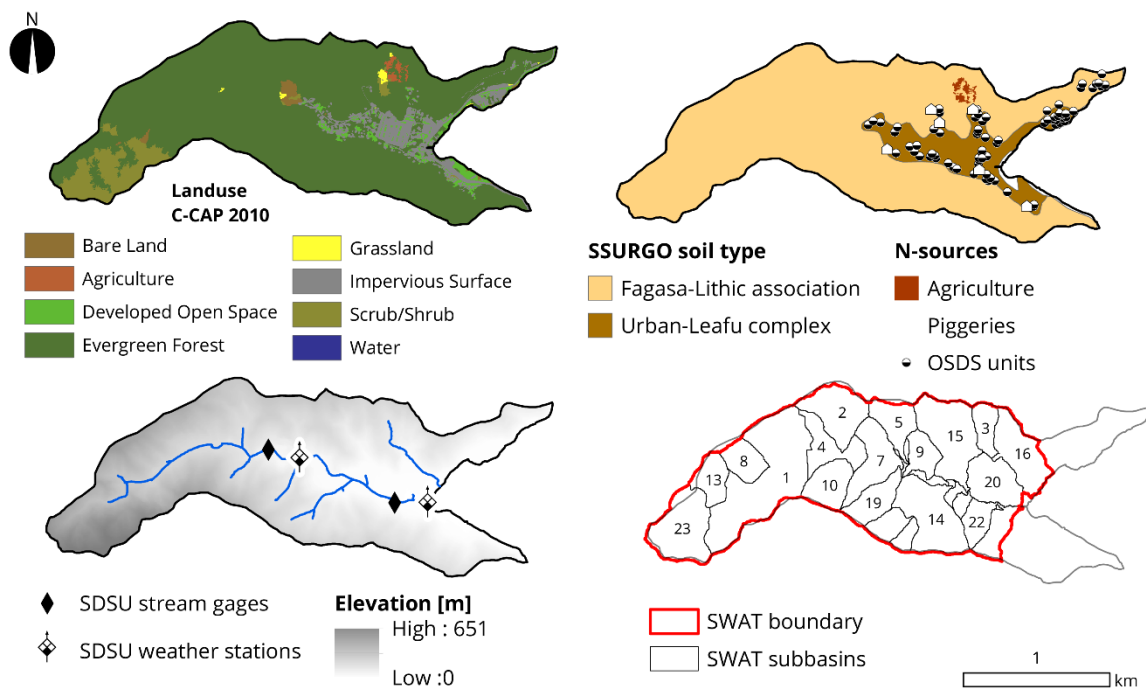


Figure 3.2: Input datasets used in SWAT model. These included (clockwise from top left) (1) land-use type, (2) soil type, with locations of N sources, (3) model boundaries, and (4) land surface elevation, and locations of weather and streamflow monitoring points.

## 3.4. Results

### 3.4.1 Conceptual Hydrogeologic Model

By integrating information about the study area's underlying geology with geochemical and physical measurements, we were able to develop a simple conceptual model of Faga'alu's groundwater-surface water interaction during baseflow conditions (Fig. 3.3). In its upper reaches, dense trachyte and older lava flows underlie the stream (Stearns, 1944), and dikes may also serve to impound groundwater in the shallow subsurface (Davis, 1963). On basaltic islands, dikes or low-permeability structures commonly impound groundwater at high-elevations (Takasaki and Mink, 1985). On a hike to the upper portion of the watershed, we observed numerous springs and small tributaries, indicating a general net transfer of groundwater to surface water in this area. Davis (1963) also documents the significance of springs in the upper Faga'alu watershed based on their historical water usage. Although this spring water is expected to be enriched in  $^{222}\text{Rn}$  upon discharge, numerous waterfalls and high turbulence throughout the upper-reaches promote evasion, which significantly reduces  $^{222}\text{Rn}$  concentrations as the water flows downhill. At Faga'alu Quarry, which lies at the upper edge of Faga'alu Village, the stream channel slope declines, and the lithology changes to an alluvial valley-fill, likely with higher permeability (Izuka et al., 2007). In the portion of the stream underlain by alluvial-fill, we observed low  $^{222}\text{Rn}$  levels and declining streamflow (except where two very small tributaries between sites S5 and S6 were seen to contribute water to the main branch), suggesting the stream is losing water to the aquifer in this reach (see section 4.2 below). Once the stream nears the coast, streamflow,  $^{222}\text{Rn}$ , and nutrient values spike, indicating this is an area of groundwater discharge, likely from a basal-lens aquifer within the alluvium. When corrected for mixing with high-level baseflow, the nutrient signature of this basal-lens baseflow is a fairly close match to the composition of salinity unmixed coastal spring discharge, suggesting that both of these water sources originate from the same nearshore aquifer.

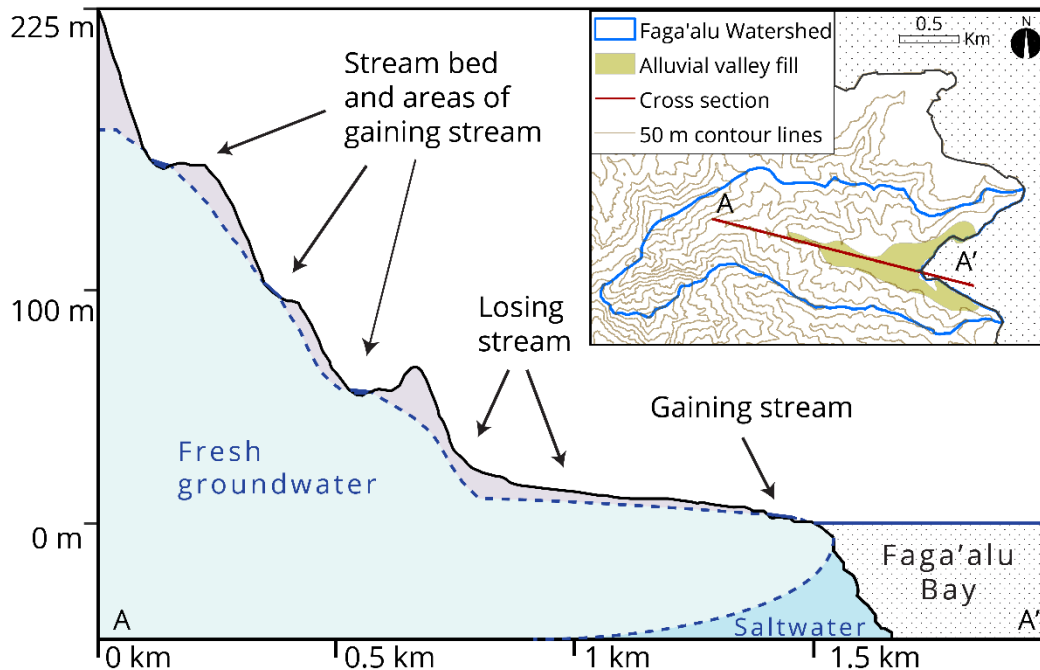


Figure 3.3: Conceptual schematic cross-section of groundwater-surface water interaction in Faga'alu watershed, based on geological information, geochemical data, and physical observations. The stream gains from high-level groundwater in its upper section and upon reaching the more permeable alluvial fill on the valley floor, begins to slowly lose water. The stream again intersects the water table near the coast where basal-lens groundwater discharges to the nearshore stream reach. Upper right panel shows map view of the valley topography and extent of alluvial valley fill.

### 3.4.2 Characterization of Baseflow Components

Dissolved  $^{222}\text{Rn}$  concentrations in the stream were generally low (6-10 dpm/L), except at the two sites nearest the coast (sites S1 and S2), where values increased up to 42 dpm/L. Coincident with increased  $^{222}\text{Rn}$  concentrations between the uppermost (S10) and lowermost (S1) sites, were increases in flow from 2,700 to 3,524  $\text{m}^3/\text{d}$ , DIN concentrations from 4 to 12  $\mu\text{mol}/\text{L}$ , and  $\delta^{15}\text{N}_{(\text{N}+\text{N})}$  values from 4.5 to 11.5‰ (Fig. 3.4). The simultaneous increase in  $\delta^{15}\text{N}_{(\text{N}+\text{N})}$  and DIN input suggests a portion of this DIN may be derived from human or animal waste, which both produce nitrogen with an elevated  $\delta^{15}\text{N}$  signature (Kendall, 1998). Because there were no observed surface tributaries above the lowest stream sampling sites, the coincident increases in water, nutrients, and  $^{222}\text{Rn}$  indicates the stream receives significant basal groundwater discharge just before exiting to the bay. The 2016 seepage run showed almost the exact same pattern, although  $^{222}\text{Rn}$  concentrations through the whole stream and particularly near the stream mouth were observed to be higher (up to 122 dpm/L).

Based on these observations, baseflow discharge to the bay can be viewed as a mixture of two distinct components, (1) baseflow sourced from high-level groundwater (Davis, 1963) (here referred to as high-level baseflow) and (2) baseflow sourced from basal-lens groundwater (here referred to as basal-lens baseflow). We estimated the fraction of high-level

baseflow ( $f_S$ ) to basal-lens baseflow ( $f_{GW}$ ) discharged in the stream estuary with a simple two end-member mixing model applied to  $^{222}\text{Rn}$  concentrations using the groundwater end member and surface water from the upper portion of the stream (as measured at site S3):

$$f_{GW} + f_S = 1 \quad (1)$$

$$f_S = \frac{C_{mix} - C_{GW}}{C_S - C_{GW}} \quad (2)$$

Where ( $C_S$ ) is the average concentration of  $^{222}\text{Rn}$  measured at site S3, ( $C_{GW}$ ) is the  $^{222}\text{Rn}$  concentration in groundwater at production well #179, and ( $C_{mix}$ ) is the mixed sample  $^{222}\text{Rn}$  concentration measured at the most coastal stream site, S1. Results from 2014 data indicate stream water at site S1 was composed of 67% high-level baseflow (2,368  $\text{m}^3/\text{d}$ ) and 33% (1,156  $\text{m}^3/\text{d}$ ) recently discharged basal-lens baseflow. Although this calculation assumes conservative radon behavior (no radioactive decay and no atmospheric evasion over the timescale of the water flow), the estimate compares reasonably well to the flow increase as directly measured by stream gauging, which showed an addition of 957  $\text{m}^3/\text{d}$ , or an additional 27% between site S3 and site S1 (Table 3.1). The 2016 seepage run was conducted at baseflow conditions as well. Total baseflow discharge at the lowest stream site in 2016 was 3,629  $\text{m}^3/\text{d}$ . When 2016 seepage run data was substituted into equations (1) and (2),  $^{222}\text{Rn}$  based partitioning of streamflow between high-level and basal-lens baseflow was very comparable to the 2014 results. The 2016 calculation indicated 66% of the stream's flow (2,412  $\text{m}^3/\text{d}$ ) originated from the high-level fraction and 34% (1,217  $\text{m}^3/\text{d}$ ) originated from the basal-lens. The 2016 streamflow measurements show a flow increase of 37% or an additional 1,339  $\text{m}^3/\text{d}$  between the lowest site (site S1) and flow at site S3. Because we did not take nutrient measurements or calculate SGD fluxes in 2016, we present the 2016 seepage run data as validation for streamflow partitioning only. For nutrient flux calculations we only used data from 2014.

We calculated baseflow nutrient flux rates by multiplying the respective measured flow rates by the nutrient concentrations observed in each baseflow component (high-level and basal-lens baseflow). Total baseflow loading of DIN and  $\text{PO}_4^{3-}$  to the bay were estimated to be  $0.72 \pm 0.05$  and  $0.38 \pm 0.03$   $\text{kg}/\text{d}$ , respectively. When partitioned with equations (1) and (2), basal-lens baseflow was estimated to have delivered  $0.47 \pm 0.05$   $\text{kg-DIN}/\text{d}$  and  $0.22 \pm 0.02$   $\text{kg-PO}_4^{3-}/\text{d}$ , whereas only  $0.25 \pm 0.03$   $\text{kg-DIN}/\text{d}$  and  $0.16 \pm 0.02$   $\text{kg-PO}_4^{3-}/\text{d}$  were delivered by high-level baseflow (Table 3.2).

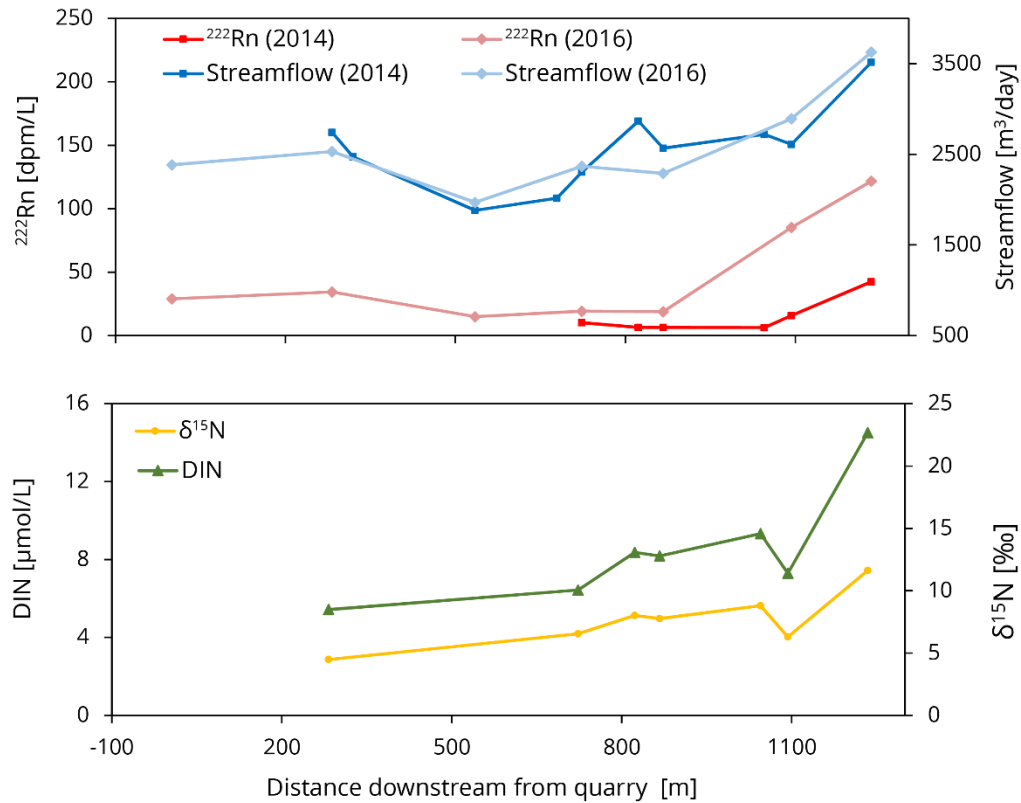


Figure 3.4: Physical (streamflow) and geochemical ( $^{222}\text{Rn}$ , DIN, and  $\delta^{15}\text{N}$ ) measurements from sampling points along seepage runs. The stream mouth, where the stream discharges into the bay, is located 1,250 m downstream from Faga'alu quarry, which marks the upper boundary of the lower reach of Faga'alu stream. Streamflow measurement uncertainty was not assessed, but was assumed to be 10 % of the measurement value. Note that for validation purposes, the same seepage run was reproduced in August 2016. Streamflow and  $^{222}\text{Rn}$  data from both 2014 and 2016 seepage runs are shown in top graph. The 2016 data is shown for validation only; all calculations were performed with 2014 data.

### 3.4.3 SGD Rates and Nutrient Fluxes

#### 3.4.3.1 Time-Series SGD Fluxes

During the stationary time-series,  $^{222}\text{Rn}$  concentrations at the intake point averaged 4.8 dpm/L (range of 2.9 to 8.2 dpm/L), salinities averaged 26.9 (range of 22.3 to 33.1), and the thickness of the SGD-affected brackish plume averaged 38 cm (range of 7 to 70 cm). While the highest  $^{222}\text{Rn}$  concentrations and the lowest salinities generally occurred at low-tide, as expected, a continuous input of higher  $^{222}\text{Rn}$  and lower salinity water from the nearby stream mouth was also detectable in the time-series data. Conversion of  $^{222}\text{Rn}$  concentrations to SGD fluxes with the transient radon balance model yielded an average fresh SGD rate of  $2959 \pm 891$  m<sup>3</sup>/d to the central plume where the intake was located. However, because the time-series measurement was taken just outside of the stream mouth, the time series and survey points

near this area were actually detecting a mixture of  $^{222}\text{Rn}$  from coastal SGD and recently discharged basal-lens baseflow from the nearshore tidally-affected part of the stream. Subtracting the basal-lens baseflow fraction ( $1,156 \pm 117 \text{ m}^3/\text{d}$ ) as calculated in section 4.2, left an estimated SGD rate of  $1,803 \pm 891 \text{ m}^3/\text{d}$  as groundwater coming from the coastal portion of the bay only. This does assume that most or all of the  $^{222}\text{Rn}$  from high-level baseflow has evaded by the time it reaches the coast, which if not, would bias the coastal SGD fraction of the total measured SGD to be a slight overestimate. Note that uncertainties associated with SGD fluxes represent the standard deviation of the temporal variation in discharge as this value is typically significantly larger than uncertainty propagated from individual model input parameters.

### 3.4.3.2 Spatial Distribution of SGD from Coastal Survey Measurements

The coastal water survey revealed three distinct groundwater discharge zones, or plumes, one each on the northern, central, and southern portions of the coastline (Fig. 3.5). We found the highest  $^{222}\text{Rn}$  concentrations, up to 7.4 dpm/L, and thus SGD fluxes with an average of  $2,623 \pm 1,653 \text{ m}^3/\text{d}$ , in the central plume, which was centered just to the south of the stream outlet. The southern plume had the lowest  $^{222}\text{Rn}$  concentrations and SGD fluxes, up to 4.7 dpm/L and average of  $266 \pm 138 \text{ m}^3/\text{d}$ , respectively, with the northern plume having  $^{222}\text{Rn}$  concentrations up to 5.0 dpm/L and SGD fluxes averaging  $846 \pm 78 \text{ m}^3/\text{d}$ .

### 3.4.3.3 Total SGD and Nutrient Flux Scaling with Coastal Survey Data

The time-series measurement provided critical information about temporal variability in SGD rates, but only for discharge to the central plume. Therefore, to calculate tidally-integrated average fresh SGD fluxes to the whole bay, the time-series measured discharge was upscaled to include discharge from the northern and southern plumes as well, using the spatially distributed SGD information from the survey as described in section 3.2.3.

Calculated scaling factors were 0.10 for the southern plume and 0.32 for the northern plume, or in other words, SGD rates measured during the survey showed the southern and northern plumes discharged 10 % and 32 %, respectively, of the central plume's SGD rate. Bay wide SGD flux was calculated by multiplying the scaling factors by the time-series derived tidally-averaged SGD flux for each plume then summing the results of all three plumes. Multiplying these factors by the central plume's true SGD rate ( $1,803 \pm 891 \text{ m}^3/\text{d}$ ) and summing flux from all three plumes yielded a SGD rate of  $2,587 \pm 899 \text{ m}^3/\text{d}$  to the whole inner-bay.

We calculated daily nutrient fluxes from SGD by multiplying coastal discharge rates by the average of salinity-unmixed, coastal-spring nutrient concentrations (Table 3.1). Salinity unmixing for coastal springs was performed with a standard solute unmixing calculation (Hunt and Rosa, 2009) based on the salinity and nutrient composition of a local oceanic end

member sample and an assumed freshwater salinity of 0.1. Fluxes were calculated to be  $1.76 \pm 1.28$  kg-DIN/d and  $0.49 \pm 0.31$  kg- $\text{PO}_4^{3-}$ /d (Table 3.2). Nutrient flux uncertainties were propagated from uncertainties in water discharge and nutrient concentration values.

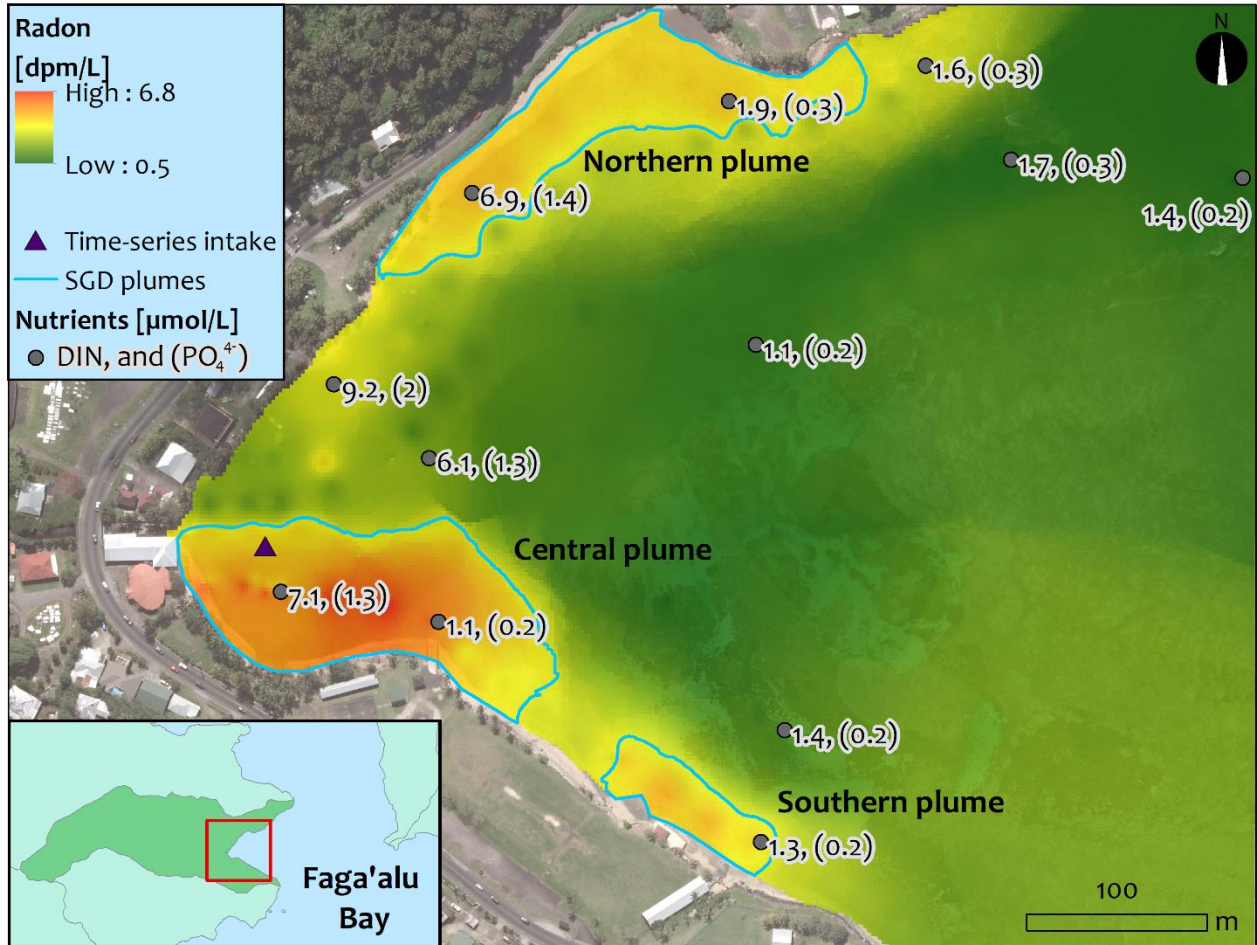


Figure 3.5: Results from coastal radon survey and surface water nutrient sampling. Dissolved radon concentrations are higher near the coast, indicating areas of groundwater discharge. Blue lines indicate defined boundaries of groundwater plumes, based on  $^{222}\text{Rn}$  iso-lines of 3.5 dpm/L. Water sample locations (grey dots) and concentrations of DIN (first number) and  $\text{PO}_4^{3-}$  (second number inside parentheses) are also shown in  $\mu\text{mol/L}$ .

Table 3.1: Measured nutrient and tracer concentrations in stream (S), well (W), and salinity unmixed samples from coastal springs (Csp)

Sample name	Latitude (°South)	Longitude (°West)	Salinity (PSU)	DO (mg/L)	<sup>222</sup> Rn (dpm/L)	N+N (µM)	PO <sub>4</sub> <sup>3-</sup> (µM)	SiO <sub>4</sub> <sup>4-</sup> (µM)	NH <sub>4</sub> <sup>+</sup> (µM)	DIN (µM)	Total N (µM)	Total P (µM)	δ <sup>15</sup> N (‰)
S1	14.29131	170.68340	0.2	6.6	42.5	12.5	3.5	522	2.00	14.5	19.7	3.4	11.61
S2	14.29153	170.68465	0.1	8.0	15.7	7.2	3.1	518	0.10	7.3	11.1	2.9	6.30
S3	14.29147	170.68521	0.1	7.6	6.3	9.1	2.9	530	0.27	9.4	14.4	2.9	8.79
S4	14.29082	170.68665	0.1	7.6	6.4	7.9	3.1	530	0.24	8.1	12.7	3.4	7.76
S5	14.29053	170.68694	0.1	7.6	6.4	7.9	3.6	519	0.41	8.3	12.7	3.4	8.01
S6	14.29008	170.68771	0.1	7.9	10.1	6.2	2.8	499	0.21	6.4	9.4	2.6	6.53
S10	14.28877	170.69096	0.1	8.0	-	5.4	2.4	502	0.03	5.4	7.8	2.3	4.47
Csp1	14.29173	170.68298	(9.6)*	0.3	1.3	5.3	3.3	197	10.9	16.2	24.3	3.3	7.47
Csp2	14.29046	170.68234	(8.1)*	0.9	62.3	0.0	8.7	299	14.1	14.1	17.7	7.9	-
Csp3	14.28960	170.68167	(4.7)*	6.0	101	65.9	4.3	522	0.00	65.9	60.9	4.1	7.09
Csp4	14.29316	170.68008	(26.7)*	2.5	7.5	39.7	4.1	586	1.49	41.2	54.7	3.5	5.50
Csp5	14.29315	170.68008	(26.2)*	0.7	1.2	8.2	7.5	453	21.5	29.7	51.7	6.5	-
W179	14.29092	170.68910	0.2	0.5	124.2	8.3	8.1	632.0	2.93	11.2	13.6	8.0	5.41
Bay1	14.29180	170.68167	34.8	9.3	6.9	0.5	0.2	3.4	0.58	1.1	5.3	0.4	-
Bay2	14.29290	170.68001	34.7	9.3	3.4	0.7	0.2	7.0	0.63	1.3	5.4	0.4	-
Bay3	14.29234	170.67989	34.9	7.7	1.1	1.0	0.2	1.1	0.41	1.4	5.3	0.4	-
Bay4	14.29041	170.68004	34.6	8.5	0.4	0.6	0.2	7.0	0.47	1.1	6.1	0.5	-
Bay5	14.28957	170.67754	34.9	7.8	0.1	1.0	0.2	3.5	0.41	1.4	5.2	0.5	8.17
Bay6	14.28948	170.67873	34.7	7.9	0.3	1.3	0.3	4.0	0.45	1.8	9.4	0.5	8.56
Bay7	14.29098	170.68172	27.2	7.6	2.7	5.1	1.3	149	1.00	6.1	10.2	1.4	-
Bay8	14.29061	170.68221	16.3	7.1	3.1	7.6	2.0	240	1.56	9.2	13.8	2.0	8.76
Bay9	14.28965	170.68150	19.4	7.1	4.5	5.9	1.4	161	1.06	7.0	11.0	1.4	9.27
Bay10	14.28919	170.68018	31.4	7.0	4.1	1.3	0.3	3.7	0.65	2.0	6.0	0.5	-
Bay11	14.28901	170.67917	34.8	6.2	3.1	1.5	0.3	2.7	0.15	1.7	5.2	0.5	8.62

\*Salinities in parentheses are original salinity prior to unmixing from seawater, unmixing was performed to a freshwater salinity of 0.1. Nutrient values in Csp. Samples represent fresh endmember values. Note DIN concentrations equal the sum of N+N and NH<sub>4</sub><sup>+</sup>.

### 3.4.4 Nearshore Water Quality

In Faga'alu's coastal waters, levels of DIN (1.1 to 9.2  $\mu\text{mol/L}$ ) and  $\text{PO}_4^{3-}$  (0.2 to 2.0  $\mu\text{mol/L}$ ) in samples taken near to the shore were higher than those found in those samples farther offshore (1.1 to 1.7  $\mu\text{mol -DIN/L}$ ) and (0.2 to 0.3  $\mu\text{mol - PO}_4^{3-}/\text{L}$ ) indicating local terrestrial nutrient sources have a detectable impact on the bay's water quality (Fig. 3.5). Typically N:P ratios in oceanic waters are near 16:1. However, N:P ratios in Faga'alu's baseflow and SGD are for the most part, disproportionately lower, averaging around 6:1. In Faga'alu's coastal waters, ratios ranged between 7:1 to 20:1 and averaged 12:1 suggesting nitrogen limiting conditions. This shows that SGD not only has an impact on the amount of N and P in the bay but also on the balance of these nutrients, which can have implications for biologic processes that control factors such as eutrophication. Within the bay, nutrient concentrations are elevated in the northern relative to the southern bay (Fig. 3.5), which is likely caused by circulation within the bay (Storlazzi et al., 2018) as well as heterogeneity in the spatial distribution of SGD. The northern and central plumes show discharge rates that are 5 and 10 times higher than the southern plume, respectively, and the persistent clockwise circulating current (Storlazzi et al., 2014) would be expected to transport stream water and its associated nutrient load to the north rather than to the south.

### 3.4.5 SWAT Model Results

#### 3.4.5.1 Model Calibration

For managing the calibration process, we used the SWAT Calibration and Uncertainty Program (SWAT-CUP) (Abbaspour, 2014) with the sequential uncertainty fitting (SUFI-2) method of Abbaspour, et al. (2007). We calibrated the hydrologic portion of model using daily streamflow observations for the period 2012 to 2014 from two sites on lower Faga'alu Stream. The deep-aquifer partitioning coefficient (RCHRG\_DP) was also manually adjusted to match measured SGD as well as possible (see section 4.5.2). The first seven years of the model simulation period (2005-2011) were assigned as model warm up, while the period from 2012 to 2013 was used for calibration. We used the year 2014 as a validation period. The temporal evolution of observed daily streamflow hydrographs was well reproduced by SWAT with a Nash-Sutcliffe Efficiency (NSE) (Nash and Sutcliffe, 1970) of 0.65 to 0.86 for both calibration and validation periods, indicating the ability of the model to simulate daily stream flow reasonably well (Fig. 3.6a). Considering the streamflow simulation uncertainty, 57% to 87% of the observations were bracketed at the NSE 95% confidence interval (CI) for both the calibration and validation periods.

We based calibration for the nutrient flux portion of the SWAT model on a set of twenty  $\text{NO}_3^-$  and  $\text{NH}_4^+$  nutrient measurements taken between March 2013 and February 2014 by A. M. Messina (2018, personal communication) and analyzed in the lab as described in McCormick

(2017). Measurement uncertainty reported by McCormick (2017) for these samples was assessed by concurrently analyzing independent standards with known concentrations. Measurement error alone ranged from 7 % up to 30 %. Considering the limited number and large measurement error of the nitrogen observations, we focused nutrient calibration on producing the distribution of model solutions that bracketed as many of the observations as possible within the NSE 95% CI (Abbaspour et al., 2007). The final model calibration produced a solution distribution with a 95% CI that bracketed nine of the  $\text{NH}_4^+$  measurements and fifteen of the  $\text{NO}_3^-$  measurements, which totaled to 60% of the calibration data (Fig 3.6b and 3.6c). Because of the high uncertainty in the nutrient calibration we interpreted these results as the full ranges of output values from all solutions that fell within the 95% CI distribution of the 1,000 best fitting model simulations (Table 3.2). In this way, large uncertainties in nutrient observations and in model parameterization were made explicit to avoid over interpretation of model results.

Sensitivity testing for all SWAT parameters was also performed with SWAT-CUP, and indicated the top three parameters to which the model was most sensitive for flow calibration were: (1) the runoff curve number, (2) the effective stream channel hydraulic conductivity, and (3) the threshold depth of water in the shallow aquifer required for return flow to occur. The top three most sensitive nutrient calibration parameters were: (1) the filtration capacity of stream edge, (2) the denitrification threshold soil water content, and (3) the in-stream rate constant for hydrolysis of organic N to  $\text{NH}_4^+$ . Lists of all calibration parameters used for flow and nutrient calibration are provided in Appendix C, Tables C3 and C4, respectively, and are ordered by the most to least sensitive parameter.

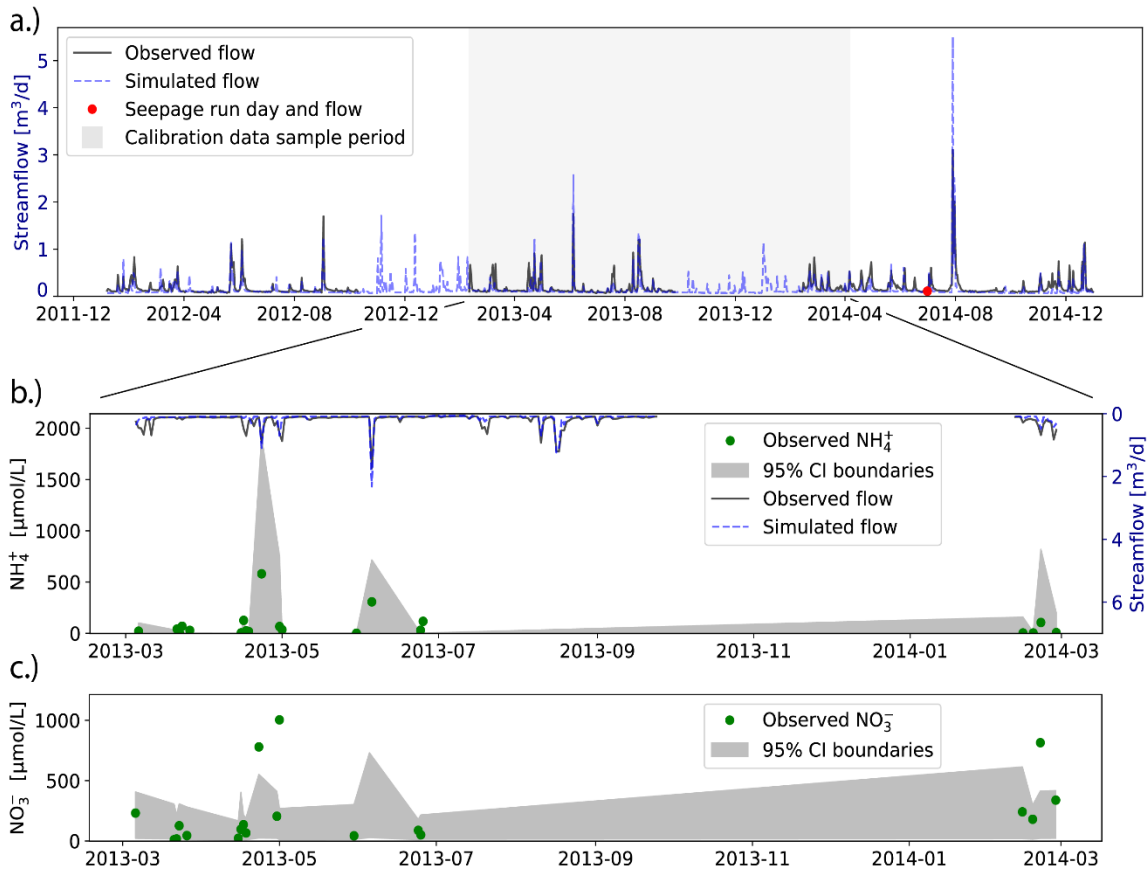


Figure 4.6: a) Daily streamflow hydrograph showing observed flow (from Messina, 2016) (black line) and SWAT modeled flow (blue dashed line). The date and flow value of our seepage run is indicated for comparative purposes (red dot). Shaded area corresponds to date range of nutrient calibration measurements as shown on lower panels. b) In-stream  $\text{NH}_4^+$  concentrations taken by A.M. Messina, and used as calibration data for the nutrient flux portion of the SWAT model (green dots). Margins of the grey band represent the upper and lower bounds of the 95% confidence interval of simulated  $\text{NH}_4^+$  concentrations from the distribution of solutions for which the model was calibrated. The model was able to bracket nine of the twenty  $\text{NH}_4^+$  observations within the 95% CI. Streamflow is also shown on upper x-axis for comparison. c) In-stream  $\text{NO}_3^-$  concentrations taken by A.M. Messina and used as calibration data for the nutrient flux portion of the SWAT model. The model was able to bracket fifteen of the twenty  $\text{NO}_3^-$  observations within the 95% CI.

### 3.4.5.2 Simulated Water and Nutrient Fluxes

All coastally discharging water budget components, otherwise referred to as hydraulic pathways, were simulated in SWAT. These included baseflow, lateral flow, surface runoff, and SGD, which was interpreted to be equivalent to deep-aquifer recharge, as SGD is not an explicit SWAT model output variable. The SWAT model partitions precipitation inputs into evapotranspiration, surface runoff, lateral flow, and groundwater recharge, which is itself partitioned between deep aquifer recharge and baseflow. Using the assumption that the island's groundwater system is in a steady-state, the deep-aquifer recharge calculated by SWAT of 2,578

m<sup>3</sup>/d was interpreted to represent the coastal SGD flux, as all water recharged to an island's deep aquifer must eventually discharge as SGD. High-level and basal-lens baseflow were also interpreted from SWAT results by applying our conceptual model, described in section 4.1. The conceptual model shows that stream baseflow originates from two distinctive aquifers, (1) the high-level aquifer and (2) the basal-lens aquifer. To approximate this scenario, we divided the SWAT-calculated baseflow into high-level baseflow and basal-lens baseflow by totaling baseflow from the sub-basins above and below the western margin of the alluvial unit, respectively. Based on this, the SWAT calculated baseflow of 3,203 m<sup>3</sup>/d was partitioned into 2,075 m<sup>3</sup>/d of high-level, or upper-watershed baseflow and 1,128 m<sup>3</sup>/d of basal-lens, or lower watershed baseflow. Comparison between modeled and measured water balance components showed good agreement (Table 3.2). Although streamflow via surface runoff and lateral flow were not measured, the SWAT model provided estimates of these components at 5,888 m<sup>3</sup>/d and 2,303 m<sup>3</sup>/d, respectively, which sums to about 59% of the total annual stream flow.

Anthropogenic DIN sources used for N input in the SWAT model included piggeries, OSDS units, and agricultural inputs, which together accounted for 2,317 kg-N/yr of N loading to the watershed. The remainder of N inputs to the model were internally calculated in SWAT from natural cycling of organic materials, based on SWAT land-use databases. Because of the high-uncertainty resulting from less-than-ideal nutrient calibration, we here report SWAT nutrient loading results as ranges based on the upper and lower 95% CI bounds of the distribution of model solutions created during model calibration. Annual DIN export to the coast included simulated DIN in surface runoff, lateral flow, baseflow, and SGD. These flux rates are individually presented in Table 3.2, and when summed, ranged between 712 and 3,384 kg-DIN/yr. Ranges in individual components were large, but were to an order of magnitude, somewhat comparable to the measured baseflow and SGD-derived DIN fluxes, when simulated values were resampled to average daily fluxes (Fig. 4.7).

For validation purposes, direct comparison between SWAT-simulated and field-measured nutrient concentrations was examined for the date of July 1<sup>st</sup>, 2014, when the seepage run was conducted. The daily streamflow nutrient concentrations calculated by SWAT on the seepage run day were extracted from the best-fitting model run produced during calibration. Simulated nutrient concentrations at each of the points where samples were taken matched the spatial distribution and magnitude of measurements fairly well, with a simulated- to-observed mean relative error of 1.3 μmol/L (Fig. 4.7).

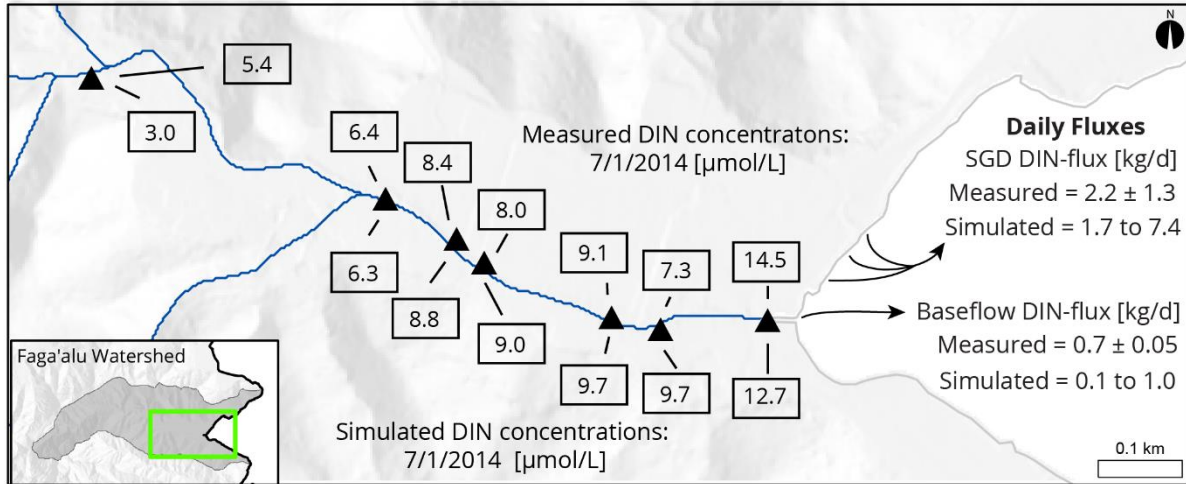


Figure 4.7: Comparison between measured and modeled nutrient results. Numbers in boxes show DIN concentrations (in  $\mu\text{mol}$ ) at each sampling site specifically on the seepage run day (7/1/2014), with measured values north of the stream and simulated values to the south. Coastal DIN fluxes for SGD and for total baseflow (high-level plus basal-lens baseflows) are shown as daily rates (in kg of DIN per day). Note that average annual modeled DIN fluxes were scaled into daily fluxes for comparison to measured rates. Simulated fluxes do not necessarily represent flux rates on any specific day.

Table 3.2: Comparison of measured and modeled flux rates of fresh water and nutrients into Faga'alu Bay. Field-based nutrient fluxes are valid for the sampling period only, and are presented as daily values whereas SWAT modeled nutrient fluxes can be calculated as yearly or daily values, and are presented as both for comparison to measured fluxes. Modeled nutrient fluxes are reported as the upper and lower values of the 95% CI distribution of the 1,000 best fitting model simulations. Note that PO<sub>4</sub><sup>3-</sup> fluxes were measured but not modeled due to lack of calibration data.

Measured in field				
Hydrologic pathway	Flow [m <sup>3</sup> /d]	DIN load [kg-N/d]	PO <sub>4</sub> <sup>3-</sup> load [kg-P/d]	
High-level baseflow fraction	2,368 ± 238	0.25 + 0.02	0.22 + 0.02	
Basal-lens baseflow fraction	1,157 ± 117	0.47 + 0.05	0.16 + 0.02	
Coastal SGD fraction	2,587 ± 899	1.76 + 1.28	0.49 + 0.31	
Modeled with SWAT				
Hydrologic pathway	Flow [m <sup>3</sup> /d]	DIN load [kg-N/yr]	Downsampled Daily DIN load for comparison [kg-N/d]	<b>Note: PO<sub>4</sub><sup>3-</sup> was not modeled</b>
Upper watershed baseflow fraction	2,075	1 to 169	0.01 to 0.46	
Lower watershed baseflow fraction	1,128	43 to 215	0.12 to 0.59	
Deep aquifer recharge (SGD) fraction	2,578	635 to 2,705	1.74 to 7.41	
Lateral flow fraction	2,303	19 to 507	0.05 to 1.39	
Surface runoff fraction	5,888	14 to 788	0.04 to 2.16	

### 3.4.5.3 Nutrient Loading Scenarios

We assessed the relative impact of each modeled non-point nutrient source within the watershed with four individual model scenarios, each with one, or all of the anthropogenic N sources removed. While these scenarios were not necessarily designed to reflect realistic future management actions, they were useful for estimating the relative impact each land-use practice has on coastal N loading. The N loading from each source was calculated by taking the difference of both the 95% CI lower and upper bounds, between the base-case and the scenario runs to produce 95% CI bracketed ranges of N-loading from each source. In general, scenarios suggested that of the three anthropogenic sources, OSDS units contribute the largest proportion of DIN, followed by piggeries, with agricultural loading as the least impactful. Interestingly, DIN transport from natural sources, which was assessed by removal of all anthropogenic sources, accounted for between 23 % and 99 % of the base-case DIN loads across the various hydrologic pathways (Table 3.3).

Table 3.3: Results of nutrient contribution scenarios. Base case values are presented as fluxes of nutrients in kg-DIN/yr and scenarios are presented as one minus the percent difference (% diff.) between each scenario and the base case. This indicates the fraction of the total DIN load contributed by each source to each hydrologic pathway.

<b>Transport vector</b>	<b>Base case [Kg-DIN/yr.]</b>	<b>Agriculture contribution [% diff.]</b>	<b>OSDS contribution [% diff.]</b>	<b>Piggery contribution [% diff.]</b>	<b>Anthropogenic sources contribution [% diff.]</b>	<b>Natural sources contribution [% diff.]</b>
<b>Upper watershed baseflow</b>	1 - 170	0.0% - 0.0%	0.0% - 0.0%	0.0% - 0.0%	0.0% - 0.0%	0.0% - 0.0%
<b>Lower watershed baseflow</b>	43 - 216	0.0% - 0.2%	99.0% - 44.7%	0.1% - 5.3%	99.1% - 50.0%	99.1% - 50.0%
<b>SGD</b>	636 - 2,705	0.0% - 0.4%	98.4% - 25.2%	0.2% - 8.9%	98.7% - 34.2%	98.7% - 34.2%
<b>Lateral flow</b>	20 - 507	0.0% - 0.1%	92.9% - 46.5%	3.1% - 1.5%	96.0% - 48.0%	96.0% - 48.0%
<b>Surface Runoff</b>	14 - 788	0.0% - 0.2%	6.9% - 5.0%	15.9% - 21.3%	22.8% - 26.3%	22.8% - 26.3%

## 3.5 Discussion

### 3.5.1 Implications for Natural Resources Management

Our results indicate SGD’s contribution to coastal nutrient loading in Faga’alu is significant, particularly during baseflow conditions. We found nutrient loading from nearshore groundwater to be an order of magnitude higher than loads from high-level baseflow, and the SWAT model suggested DIN loading via groundwater may be significantly higher than loading from surface runoff, though this estimate excludes particulate-N. In American Samoa, coastal resource management efforts have primarily concentrated on surface water quality for regulatory activities (AS-EPA, 2016). Even on islands where SGD has been extensively studied, such as the Hawaiian Islands (e.g. Glenn et al., 2013; Dulai et al., 2016), little to no regulatory action has been focused on groundwater as a hydrologic pathway for pollution. Our field measurements and model results suggest that SGD and nearshore baseflow are important coastal nutrient delivery mechanisms in steep basaltic-island watersheds with perennial streams. In these settings, coastal management may be more successful if both ground and stream water quality are considered when developing sampling protocols and applying TMDL standards. Additionally, consideration of factors that affect the spatial and temporal distribution of nutrient discharge, such as variation in groundwater-surface water interaction and rainfall timing, will provide more robust and accurate assessment of human impacts on coastal ecosystems.

### 3.5.2 Conceptual Model Implications

In high-island settings, human development is typically concentrated on near-shore coastal plains that are often underlain by alluvium or marine sediments. If these sediments happen to be more permeable than the surrounding rock, as appears to be the case in Faga'alu, they may facilitate a more direct connection between anthropogenic contaminant sources and basal groundwater. In these settings, groundwater may play a larger role in coastal nutrient transport than surface water. However, the reverse may be true in settings where development is concentrated above less-permeable layers, which is the case in some parts of Oahu, Hawaii, where a locally low-permeability marine carbonate formation known as "caprock" protects the underlying aquifer from contaminants (Oki et al., 1998). Therefore, in basaltic-island settings, the partitioning of nutrients from non-point sources into different hydrologic pathways is likely to be highly dependent on the relative permeabilities of different nearshore geologic layers. This further underscores the importance of developing a reasonably accurate conceptualization of local hydrogeologic systems when designing sampling schemes and assessing nutrient fluxes on a ridge-to-reef scale.

The high-resolution, locality specific understanding of groundwater-surface water interaction we developed for Faga'alu helped with construction and interpretation of the SWAT model. Discharge or loss between groundwater and a stream is generally controlled by water table elevation, which makes this parameter very important for predicting the distribution of baseflow in a watershed. However, the SWAT model uses a simplified linear reservoir model to control loss or gain from groundwater and does not consider water table elevations for baseflow partitioning. This gap is commonly filled by coupling surface water models with groundwater models (e.g. Kim et al., 2008; Guzman et al., 2015). However, subsurface models rely on calibrated parameterization of stream conductance and hydraulic conductivity, and in settings such as Faga'alu, the variable and steep terrain (Kampf and Burges, 2007) as well as a lack of groundwater elevation data (apart from one single well in the valley) imparts an unacceptable amount of uncertainty to groundwater modeling attempts. To cope with this challenge, we used a reasonable conceptual hydrogeologic model to determine where the water table was generally below the stream elevation (losing reach below the quarry) and where it was at or above the stream (gaining reach above the quarry). This provided the justification to allow for partitioning fluxes from high-level and basal-lens baseflow, likely within the same amount of certainty as would have been achieved through a more time-consuming and costly groundwater modeling process.

### 3.5.3 Nitrogen Source Tracing

While extensive source dependent nutrient tracing efforts were not performed in this study, reasonable correlation between elevated DIN concentrations and  $\delta^{15}\text{N}$  isotopes in baseflow and coastal surface water ( $r^2$  of 0.93 and 0.45, respectively) helped to validate the

transport history of nutrients from source to sink. High values of  $\delta^{15}\text{N}$  that are correlated with high DIN values suggests the majority of the DIN found in samples originates from a high  $\delta^{15}\text{N}$  source, such as wastewater or manure, as opposed to synthetic agricultural fertilizers, which typically have  $\delta^{15}\text{N}$  values near 0 ‰ (Kendall and Aravena, 2000). Finding this result in Faga'alu was not surprising, considering that most agricultural operations in the valley are small and focused on traditional Samoan crops that require few to no chemical inputs. However, a more pertinent need in American Samoa is to prioritize management of either piggeries or OSDS-sourced wastewater, because limited management resources could be more effectively spent if the relative impact from each source was better constrained (Carpenter et al., 2002; Shuler et al., 2017). Unfortunately, the overlap of  $\delta^{15}\text{N}$  values from animal manure and wastewater (Böhlke, 2003) does not allow DIN from these sources to be reliably partitioned with this method. Another complicating factor with isotopic N source tracing is mixing of nutrients from different sources, which would alter the final isotopic composition found in samples. More specific source-dependent tracers, like microbial source tracing (Scott et al., 2002; Kirs et al., 2011) or wastewater specific compounds (Petrie et al., 2015; Krall et al., 2018) would be useful for separating and prioritizing the impacts between wastewater and pigs in Samoa.

### 3.5.4 SWAT Model Applicability

The SWAT model was useful for providing insights into nutrient loading from processes and time periods that were not assessed during the field investigation. Due to the logistics of working in a remote area, our fieldwork was limited to a single week, thereby limiting the representativeness of measured nutrient fluxes to this time-period and season. For management priorities however, annual nutrient fluxes are more useful for assessing longer-term management questions. Compounding this is the fact that streams on small islands are generally steep and flashy, making it time-consuming to sample runoff events at a resolution that effectively characterizes annual nutrient fluxes (De Carlo et al., 2007). The SWAT model filled this gap in our study by providing daily resolution flows and loading rates that could be totaled to estimate annual discharge and DIN loading from each hydrologic pathway. This is highly beneficial for understanding processes that are prohibitively difficult or costly to observe, such as assessment of lateral flow or surface runoff, and allows a more comprehensive understanding of water and nutrient transport dynamics in difficult-to-study or remote watersheds.

Despite high uncertainties associated with simulated nutrient flux results, the model nonetheless proved useful for partitioning the impact from each anthropogenic non-point source through a scenario-based approach of modifying land-use inputs. When the effects of individual non-point sources were each removed from the input, results indicated a significant proportion of DIN in subsurface hydrologic pathways, including SGD, lateral flow, and baseflow, originating from OSDS sources. The proportion of OSDS sourced DIN in all

pathways, except for surface runoff, ranged from 25 % to 99 % of the base-case DIN discharge. On the other hand, OSDS loading appeared to contribute very little to DIN loads in surface runoff, less than 7 % (Table 3.3). Of the three modeled anthropogenic sources, piggeries appeared to contribute the most DIN to surface runoff, between 16 % and 21 %. The contribution of piggery DIN to groundwater was lower, less than 9 % of the total DIN in SGD or baseflow. This pattern is reasonable since OSDS leachate and manure are discharged into the environment in different ways. Subsurface OSDS units leach N directly below the soil, whereas pig manure is typically released directly on the land surface; and in American Samoa, manure is sometimes washed directly into streams, although this practice is currently illegal. This indicates that management focused on reducing OSDS impact is likely to primarily affect groundwater nitrogen loads, but if surface water quality is deemed to be more important, then management of piggeries may be a more effective strategy. As expected, removal of all agricultural sources did very little to affect modeled DIN fluxes considering the low magnitude of agricultural loading inputs.

While human land-use activities are often considered to be the primary cause of nutrient-based water quality impairment, nutrient inputs from natural plant and animal sources should not be ignored. For example, on Tutuila, Nimbus Environmental Services (2010) found that coastal water samples frequently exceeded local and federal water quality standards for  $\text{PO}_4^{3-}$  concentrations, even in lightly impacted areas. They concluded that geologic sources on Tutuila may produce naturally high levels of  $\text{PO}_4^{3-}$  in source waters. This has also been observed in the Hawaiian Islands (Vitousek et al. 2003). While an ideal approach to assess natural nutrient loads would be to duplicate study methodologies in pristine control watersheds, it is often difficult to even find pristine watersheds on islands where land is scarce, and if available, these areas often lack road access, which significantly complicates field logistics. Since this was not possible in our study, we estimated naturally-sourced DIN loading using a SWAT model scenario with all anthropogenic nutrient sources removed. Results suggested that coastal DIN loading from natural sources is somewhere between 20 and 2,734 kg-DIN/yr. When compared to the base case scenario, these results suggest that natural sources contribute between 74 % and 77% of DIN in surface runoff, 4 % to 52 % of DIN in lateral flow, 2 % to 70 % of DIN in baseflow and 1 % to 65 % of DIN in SGD. While these ranges are large, this result does suggest that natural nutrient sources are important to consider in this setting; however anthropogenic sources are still likely to be the main cause of elevated nutrient concentrations seen in Faga'alu Watershed. While complete removal of any of the watershed's non-point sources is not very realistic, the ability to run these different scenarios showed the relative impact of each source and also helped to validate the idea that management focused on different sources may benefit from adopting different sampling and assessment strategies.

### **3.5.5 Assumptions and Limitations of the SWAT Model**

1. The SWAT model uses a simplified linear reservoir model for the representation of the groundwater system, which applies a single parameter (RCHRG\_DP) for total

groundwater recharge partitioning to the deep aquifer (interpreted here as SGD). Hence, SWAT's SGD results are somewhat sensitive to this parameter (Appendix C, Table C3). Additionally, this interpretation hinges on the assumption that watershed boundaries also represent aquifer divides. Nonetheless, when the RCHRG\_DP parameter was calibrated to match measured SGD, the model was able to match streamflow observations well, suggesting that SWAT's parameterization was reasonable.

2. The daily N loading rates from anthropogenic sources (OSDS, piggeries, and fertilizers,) were assumed to be constant due to a lack of information about application timing. However, probably only OSDS loading is actually constant. Agricultural applications, and the number of pigs in a piggery at any given time likely fluctuates cyclically. Because agriculture is practiced year-round in American Samoa, it is difficult to predict when applications occur.
3. The SWAT model was calibrated with streamflow data from two stations, (*black diamonds* in Fig. 3.2) and therefore different parameter values were assigned for the upper watershed above the quarry, and for the lower watershed below. This was justified geologically, considering that the quarry location coincides with the contact between basalts and alluvium. However, in reality, the local geology is probably heterogeneous, particularly within the basalt unit itself. Thus the bi-modal parameterization of the model area is likely to be somewhat of an oversimplification.
4. Very limited information exists regarding septic system design in American Samoa. It is thought that many of the island's residents rely on cesspools (Falkland et al., 2002). However, exact numbers and specificities about system design remain unknown. Therefore, in SWAT, OSDS units were simulated with default parameters and an assumption that all systems were of a failing septic system type (TCE, 2005).
5. The lack of long term, multi-year measured in-stream nutrient data necessitated a heuristic approach where only order-of-magnitude scale nutrient fluxes could be confidently calculated and reported.

### 3.6 Conclusions

By combining a terrestrial and coastal hydrologic field investigation with model-based watershed characterization we were able to reveal the impact of different nutrient sources and hydrologic pathways in a small American Samoan watershed. This methodological framework demonstrates how snapshot scale observations and transient watershed modeling can be integrated to develop a fairly comprehensive understanding of water and nutrient dynamics in steep watersheds on tropical-basaltic islands. In Faga'alu Watershed, during low-flow conditions, our measurements suggested SGD and nearshore basal-lens baseflow contribute nearly all of the terrigenous DIN to the coastline with high level-baseflow contributing very little. Groundwater discharge was also found to be significant in coastal loading of dissolved  $\text{PO}_4^{3-}$ . Seepage run measurements indicated groundwater discharge to the stream occurs as two geochemically distinct fractions, (1) high-level baseflow and (2) basal-lens baseflow that discharges near the stream estuary. At baseflow conditions, high-level streamflow was seen to contribute about two-thirds of the stream's water, but nearshore basal-lens baseflow contributed the majority of the stream's nutrient load. This understanding of groundwater – surface water interaction proved useful for the conceptual foundation for developing the watershed model and for interpreting model results.

The SWAT model matched fluxes from measured water budget components well, within 2 %, 13 %, and 0.3 % RPD for basal-lens baseflow, high-level baseflow, and SGD, respectively. Despite limitations in nutrient calibration, SWAT was also able to provide order-of-magnitude estimates of nutrient fluxes over annual scales and from components such as surface runoff and lateral flow, which could not be measured during fieldwork. Though uncertainties were large, the model suggested that storm and lateral flow together deliver between 5 % and 31 % of the total annual DIN load. This leaves groundwater sources as the most impactful nutrient transport pathways, with SGD-derived DIN loading making up between 65 % to 92 % of the total annual DIN loading to the coast, and the remainder being delivered by baseflow. This suggests that both SGD and surface water are important coastal nutrient loading pathways and both should be considered when developing nutrient sampling and management plans. Although sampling surface runoff, baseflow, and groundwater nutrients would require a significant deviation from current water quality management practice and assessment in American Samoa, if watershed models can be developed to account for these processes, they can be a useful and money-saving tool in the land-manager's toolbox.

## References: Chapter 3

- Abbaspour, K.C., 2014. SWAT-CUP 2012: SWAT Calibration and Uncertainty Programs - A User Manual. Sci. Technol.  
[https://swat.tamu.edu/media/114860/usermanual\\_swatcup.pdf](https://swat.tamu.edu/media/114860/usermanual_swatcup.pdf) (accessed 2019-03-13).
- Alexander, R.B., Elliott, A.H., Shankar, U., McBride, G.B., 2002. Estimating the sources and transport of nutrients in the Waikato River Basin, New Zealand. *Water Resour. Res.* 38, 4-1-4-23. <https://doi.org/10.1029/2001wr000878>
- Amato, D.W., Bishop, J.M., Glenn, C.R., Dulai, H., Smith, C.M., 2016. Impact of submarine groundwater discharge on marine water quality and reef biota of Maui. *PLoS One* 11, e0165825. <https://doi.org/10.1371/journal.pone.0165825>
- AS-EPA - American Samoa Environmental Protection Agency, 2010. Territory of American Samoa Integrated Water Quality Monitoring and Assessment 2010.  
<https://www.epa.as.gov/sites/default/files/documents/surface/americansamoa2010integratedwaterqualityreport031910.pdf> (accessed 2019-03-13).
- Andreani, M., Galanter, M., Casciotti, K.L., Böhlke, J.K., Sigman, D.M., Barford, C., 2002. A Bacterial Method for the Nitrogen Isotopic Analysis of Nitrate in Seawater and Freshwater. *Anal. Chem.* 73, 4145-4153. <https://doi.org/10.1021/ac010088e>
- Armstrong, F.A.J., Stearns, C.R., Strickland, J.D.H., 1967. The measurement of upwelling and subsequent biological process by means of the Technicon Autoanalyzer® and associated equipment, in: *Deep-Sea Research and Oceanographic Abstracts*. pp. 381-389.  
[https://doi.org/10.1016/0011-7471\(67\)90082-4](https://doi.org/10.1016/0011-7471(67)90082-4)
- Arnold, J.G., Srinivasan, R., Muttiah, R.S., Williams, J.R., 1998. Large area hydrologic modeling and assessment part I: Model development. *J. Am. Water Resour. Assoc.* 34, 73-89.  
<https://doi.org/10.1111/j.1752-1688.1998.tb05961.x>
- ASCC - American Samoa Community College, 2018. Malaeimi weather station data. [Dataset].  
<https://www.wunderground.com/personal-weather-station/dashboard?ID=IWESTERN499> (accessed 2018-04-30).
- AS-DOC - American Samoa Department of Commerce, 2013. 2013 Statistical Yearbook for American Samoa. <http://doc.as.gov/wp-content/uploads/2011/06/2013-Statistical-Yearbook-Final-Draft.pdf> (accessed 2019-03-13).
- AS-EPA - American Samoa Environmental Protection Agency,, 2013. American Samoa Water Quality Standards 2013 Revision Administrative Rule No . 001-2013.  
<https://www.epa.gov/sites/production/files/2014-12/documents/aswqs.pdf> (accessed 2019-03-13).

- AS-EPA - American Samoa Environmental Protection Agency, 2013. American Samoa Watershed Management and Protection Program FY08 Annual Report.
- Avery, E., Bibby, R., Visser, A., Esser, B., Moran, J., 2018. Quantification of groundwater discharge in a subalpine stream using radon-222. *Water (Switzerland)* 10, 100. <https://doi.org/10.3390/w10020100>
- Babinec, J., Kennedy, J., Williamson, M., Kamenik, J., Waters, C.A., Jolly, J., Dulai, H., 2015. Autonomous long-term gamma-spectrometric monitoring of submarine groundwater discharge trends in Hawaii. *J. Radioanal. Nucl. Chem.* 307, 1865-1870. <https://doi.org/10.1007/s10967-015-4580-9>
- Bahr, K.D., Jokiell, P.L., Toonen, R.J., 2015. The unnatural history of Kāneʻohe Bay: coral reef resilience in the face of centuries of anthropogenic impacts. *PeerJ* 3, e950. <https://doi.org/10.7717/peerj.950>
- Barden, R., Kasprzyk-Hordern, B., Petrie, B., 2015. A review on emerging contaminants in wastewaters and the environment: Current knowledge, understudied areas and recommendations for future monitoring. *Water Res.* 72, 3-27.
- Böhlke, J.-K., 2003. Sources, transport, and reaction of nitrate., Residence times and nitrate transport in ground water discharging to streams in the Chesapeake Bay Watershed. *Water-Resources Investigations*.
- Buchanan, T.J., Somers, W.P., 1976. Discharge measurements at gaging stations, *Techniques of water-resources investigations of the United States Geological Survey - Book 3 - Applications of Hydraulics*.
- Burnett, W.C., Dulaiova, H., 2003. Estimating the dynamics of groundwater input into the coastal zone via continuous radon-222 measurements. *J. Environ. Radioact.* 69, 21-35. [https://doi.org/10.1016/S0265-931X\(03\)00084-5](https://doi.org/10.1016/S0265-931X(03)00084-5)
- Carpenter, C., Stubbs, J., Overmars, M., 2003. *Proceedings of the Pacific Regional Consultation On Water in Small Island Countries*.
- Carpenter, C., Stubbs, J., Overmars, M., 2003. *Proceedings of the Pacific Regional Consultation On Water in Small Island Countries*.
- Chadwick, O., Porder, S., Luers, A., Monastera, V., Kettley, L., Matson, P., Derry, L., Mecking, E., Allison, S., Vitousek, P., 2004. Erosion and the Rejuvenation of Weathering-derived Nutrient Supply in an Old Tropical Landscape. *Ecosystems* 6, 762-772. <https://doi.org/10.1007/s10021-003-0199-8>
- Charette, M. a, Moore, W.S., Burnett, W.C., 2007. CHAPTER-5 Uranium-and Thorium- Series Nuclides as Tracers of Submarine Groundwater Discharge CHAPTER-5 Uranium-and

- Thorium-Series Nuclides as Tracers of Submarine Groundwater Discharge. Uranium 13, 234-289.
- Cole, M.L., Kroeger, K.D., McClelland, J.W., Valiela, I., 2006. Effects of Watershed Land use on Nitrogen Concentrations and  $\delta^{15}\text{N}$  Nitrogen in Groundwater \h [electronic resource]. *Biogeochemistry* 77, 199-215.
- D. K. Borah, M. Bera, 2013. Watershed-Scale Hydrologic and Nonpoint-Source Pollution Models: Review of Applications. *Trans. ASAE* 47, 789-803.  
<https://doi.org/10.13031/2013.16110>
- Davis, D., 1963. Groundwater reconnaissance of American Samoa. U.S. Geological Survey Report No. 1608-C. US Government Printing Office.
- DiDonato, G.T., 2005. Nitrogen and phosphorus concentrations in tropical Pacific insular streams: historical data from Tutuila, American Samoa. *Micronesica-Agana-* 37, 235.
- Downer, C.W., Ogden, F.L., 2006. Gridded Surface Subsurface Hydrologic Analysis (GSSHA) User's Manual, Version 1.43 for Watershed Modeling System 6.1, US Army Corps of Engineers, Engineer Research and Development Center.
- Dulaiova, H., Burnett, W.C., Wattayakorn, G., Sojisuporn, P., 2006. Are groundwater inputs into river-dominated areas important? The Chao Phraya River - Gulf of Thailand. *Limnol. Oceanogr.* 51, 2232-2247. <https://doi.org/10.4319/lo.2006.51.5.2232>
- Dulaiova, H., Camilli, R., Henderson, P.B., Charette, M.A., 2010. Coupled radon, methane and nitrate sensors for large-scale assessment of groundwater discharge and non-point source pollution to coastal waters. *J. Environ. Radioact.* 101, 553-563.  
<https://doi.org/10.1016/j.jenvrad.2009.12.004>
- Fröllje, H., Fitzsimmons, J.N., Dulai, H., Schnetger, B., Brumsack, H.-J., Pahnke, K., 2016. Hawaiian imprint on dissolved Nd and Ra isotopes and rare earth elements in the central North Pacific: Local survey and seasonal variability. *Geochim. Cosmochim. Acta* 189, 110-131. <https://doi.org/10.1016/j.gca.2016.06.001>
- Gardner, L.R., Wilson, A.M., 2006. Comparison of four numerical models for simulating seepage from salt marsh sediments. *Estuar. Coast. Shelf Sci.* 69, 427-437.  
<https://doi.org/10.1016/j.ecss.2006.05.009>
- P. W. Gassman, M. R. Reyes, C. H. Green, J. G. Arnold, 2007. The Soil and Water Assessment Tool: Historical Development, Applications, and Future Research Directions. *Trans. ASABE* 50, 1211-1250. <https://doi.org/10.13031/2013.23637>
- Gassman, P.W., Sadeghi, A.M., Srinivasan, R., 2014. Applications of the SWAT Model Special Section: Overview and Insights. *J. Environ. Qual.* 43, 1.  
<https://doi.org/10.2134/jeq2013.11.0466>

- Garrison, V., Kroeger, K., Fenner, D., Craig, P., 2007. Identifying nutrient sources to three lagoons at Ofu and Olosega, American Samoa using  $\delta^{15}\text{N}$  of benthic macroalgae. *Mar. Pollut. Bull.* 54, 1830–1838. <https://doi.org/10.1016/j.marpolbul.2007.08.016>
- Gillespie, P., Kirs, M., Cornelisen, C., Fidler, A., Harwood, V., Blackwood, A., Fyfe, W., 2011. Source tracking faecal contamination in an urbanised and a rural waterway in the Nelson-Tasman region, New Zealand. *New Zeal. J. Mar. Freshw. Res.* 45, 43–58. <https://doi.org/10.1080/00288330.2010.535494>
- Gleeson, J., Santos, I.R., Maher, D.T., Golsby-Smith, L., 2013. Groundwater-surface water exchange in a mangrove tidal creek: Evidence from natural geochemical tracers and implications for nutrient budgets. *Mar. Chem.* 156, 27–37. <https://doi.org/10.1016/j.marchem.2013.02.001>
- Gleeson, T., Manning, A.H., Popp, A., Zane, M., Clark, J.F., 2018. The suitability of using dissolved gases to determine groundwater discharge to high gradient streams. *J. Hydrol.* 557, 561–572. <https://doi.org/10.1016/j.jhydrol.2017.12.022>
- Glenn, C.R., Whittier, R.B., Dailer, M.L., Dulaiova, H., El-kadi, A.I., Fackrell, J., Sevadjian, J., 2013. Lahaina Groundwater Tracer Study – Lahaina, Maui, Hawaii. Final Interim Report prepared from the State of Hawaii DOH, the U.S. EPA, and the U.S. Army Engineer Research and Development Center <https://scholarspace.manoa.hawaii.edu/handle/10125/50768> (accessed 2019-03-13).
- Grasshoff, K., Ehrhardt, M., Kremling, K., 1999. *Methods of Seawater Analysis*. Second, Revised and Extended Edition, 3rd ed. John Wiley & Sons.
- Guzman, J.A., Moriasi, D.N., Gowda, P.H., Steiner, J.L., Starks, P.J., Arnold, J.G., Srinivasan, R., 2015. Environmental Modelling & Software A model integration framework for linking SWAT and MODFLOW. *Environ. Model. Softw.* 73, 103–116. <https://doi.org/10.1016/j.envsoft.2015.08.011>
- Houk, P., Didonato, G., Iguel, J., & Van Woesik, R., 2005. Assessing the effects of non-point source pollution on American Samoa's coral reef communities. *Environ. Monit. Assess.* 107, 11–27.
- Houk, P., Benavente, D., Johnson, S., 2013. Watershed-based coral reef monitoring across Tutuila, American Samoa - Summary of decadal trends and 2013 assessment.
- Hunt, C.D., 2006. Ground-Water Nutrient Flux to Coastal Waters and Numerical Simulation of Wastewater Injection at Kihei , Maui , Hawaii. USGS Open Report 2006, 5283. <https://pubs.usgs.gov/sir/2006/5283/sir2006-5283.pdf> (accessed 2019-03-13).

- Hunt, Charles D., J., Rosa, S.N., 2009. A Multitracer Approach to Detecting Wastewater Plumes from Municipal Injection Wells in Nearshore Marine Waters at Kihei and Lahaina, Maui, Hawaii (USGS Scientific Investigations Report 2009-5253) 166.
- Izuka, S.K., Perreault, J.A., Presley, T.K., 2007. Areas contributing recharge to wells in the Tafuna-Leone Plain, Tutuila, American Samoa: U.S. Geological Survey Scientific Investigations Report 2007-5167.
- Johannes, R.E., Hearn, C.J., 1985. The effect of submarine groundwater discharge on nutrient and salinity regimes in a coastal lagoon off Perth, Western Australia. *Estuar. Coast. Shelf Sci.* 21, 789–800. [https://doi.org/10.1016/0272-7714\(85\)90073-3](https://doi.org/10.1016/0272-7714(85)90073-3)
- Kampf, S.K., Burges, S.J., 2007. A framework for classifying and comparing distributed hillslope and catchment hydrologic models. *Water Resour. Res.* 43. <https://doi.org/10.1029/2006WR005370>
- Kelly, J.L., Glenn, C., 2012. Identification and quantification of submarine groundwater discharge in the Hawaiian Islands. *Dep. Geol. Geophys.* [Honolulu]:[University of Hawaii at Manoa],[August 2012].
- Kendall, C., 2012. Tracing Nitrogen Sources and Cycling in Catchments, in: *Isotope Tracers in Catchment Hydrology*. Elsevier, pp. 519–576. <https://doi.org/10.1016/b978-0-444-81546-0.50023-9>
- Kendall, C., Aravena, R., 2011. Nitrate Isotopes in Groundwater Systems, in: *Environmental Tracers in Subsurface Hydrology*. Springer, pp. 261–297. [https://doi.org/10.1007/978-1-4615-4557-6\\_9](https://doi.org/10.1007/978-1-4615-4557-6_9)
- Kim, N. W., Chung, I. M., Won, Y. S., & Arnold, J.G., 2008. Development and application of the integrated SWAT-MODFLOW model. *Journal. of. Hydrol.* 356, 1–16.
- Krall, A.L., Elliott, S.M., Erickson, M.L., Adams, B.A., 2018. Detecting sulfamethoxazole and carbamazepine in groundwater: Is ELISA a reliable screening tool? *Environ. Pollut.* 234, 420–428. <https://doi.org/10.1016/j.envpol.2017.11.065>
- Lindau, Delaune, Patr, 1989. Assessment of stable n isotopes in fingerprinting surface water n source. *Water. Air. Soil Pollut.* 48, 489–496.
- Makings, U., Santos, I.R., Maher, D.T., Golsby-Smith, L., Eyre, B.D., 2014. Importance of budgets for estimating the input of groundwater-derived nutrients to an eutrophic tidal river and estuary. *Estuar. Coast. Shelf Sci.* 143, 65–76. <https://doi.org/10.1016/j.ecss.2014.02.003>
- Messina, A.M., Biggs, T.W., 2016. Contributions of human activities to suspended sediment yield during storm events from a small, steep, tropical watershed. *J. Hydrol.* 538, 726–742. <https://doi.org/10.1016/j.jhydrol.2016.03.053>

- McCormick, G.R., 2017. Water Quality and Sources of Nutrient Loads in Watersheds of American Samoa. Masters thesis, Dept. of Geography, San Diego State University. <https://search.proquest.com/openview/a236c90fb2b272eab29080873da04169/1?pq-origsite=gscholar&cbl=18750&diss=y> (accessed 2019-03-13).
- Messina, A.T., 2013. Terrestrial Sediment and Nutrient Fluxes to the Faga'alu Reefs in American Samoa, in: AGU Fall Meeting Abstracts. p. 08.
- Messina, A.T., 2016. Terrigenous Sediment Dynamics in a Small, Tropical Fringing-Reef Embayment, American Samoa. Doctoral dissertation Dept. of Geography, University of California, Santa Barbara. <https://www.alexandria.ucsb.edu/lib/ark:/48907/f3sj1kpt> (accessed 2019-03-13).
- Michael, H.A., 2005. Seasonal dynamics in costal aquifers: investigation of submarine groundwater discharge through field measurements and numerical models. Environ. Eng. Massachusetts Institute of Technology.
- Moosdorf, N., Stieglitz, T., Waska, H., Dürr, H., Hartmann, J., 2015. Submarine groundwater discharge from tropical islands: a review. *Grundwasser* 20, 53–67. <https://doi.org/10.1007/s00767-014-0275-3>
- Morrissey, A., Nolan, K., Rock, L., Fenech, C., Tobin, J., 2012. The potential for a suite of isotope and chemical markers to differentiate sources of nitrate contamination: A review. *Water Res.* 46, 2023–2041. <https://doi.org/10.1016/j.watres.2012.01.044>
- Nakamura, S., 1984. Soil Survey of American Samoa. USDA Soil Conservation Service, Washington, DC. 95 pp
- NGDC, 2013. American Samoa 1/3 Arc-second MWH Coastal Digital Elevation Model [dataset]. <https://catalog.data.gov/dataset/pago-pago-american-samoa-coastal-digital-elevation-model34341> (accessed 2015-12-10).
- Nimbus Environmental Services, 2012. US EPA National Coastal Assessment 2010, American Samoa Reef Flats, 2012.
- NOAA, 2013. Faga'alu Village Watershed Management and Conservation Plan. [ftp://ftp.library.noaa.gov/noaa\\_documents.lib/CoRIS/Faga'alu\\_Village\\_Watershed.pdf](ftp://ftp.library.noaa.gov/noaa_documents.lib/CoRIS/Faga%27alu_Village_Watershed.pdf)
- Oberdorfer, J.A., 2003. Hydrogeologic modeling of submarine groundwater discharge: Comparison to other quantitative methods. *Biogeochemistry* 66, 159–169. <https://doi.org/10.1023/B:BIOG.0000006096.94630.54>
- Oki, D.S., Souza, W.R., Bolke, E.L., Bauer, G.R., 1998. Numerical analysis of the hydrogeologic controls in a layered coastal aquifer system, Oahu, Hawaii, USA. *Hydrogeol. J.* 6, 243–263. <https://doi.org/10.1007/s100400050149>

- Paul, S., Cashman, M.A., Szura, K., Pradhanang, S.M., 2017. Assessment of nitrogen inputs into hunt river by onsite wastewater treatment systems via SWAT simulation. *Water (Switzerland)* 9, 610. <https://doi.org/10.3390/w9080610>
- Peterson, R.N., Santos, I.R., Burnett, W.C., 2010. Estuarine , Coastal and Shelf Science Evaluating groundwater discharge to tidal rivers based on a Rn-222 time-series approach. *Estuar. Coast. Shelf Sci.* 86, 165–178. <https://doi.org/10.1016/j.ecss.2009.10.022>
- Polidoro, B.A., Comeros-Raynal, M.T., Cahill, T., Clement, C., 2017. Land-based sources of marine pollution: Pesticides, PAHs and phthalates in coastal stream water, and heavy metals in coastal stream sediments in American Samoa. *Mar. Pollut. Bull.* 116, 501–507. <https://doi.org/10.1016/j.marpolbul.2016.12.058>
- Rengarajan, R., Sarma, V.V.S.S., 2015. Submarine groundwater discharge and nutrient addition to the coastal zone of the Godavari estuary. *Mar. Chem.* 172, 57–69. <https://doi.org/10.1016/j.marchem.2015.03.008>
- Rogers, K.M., Nicolini, E., Gauthier, V., 2012. Identifying source and formation altitudes of nitrates in drinking water from Réunion Island, France, using a multi-isotopic approach. *J. Contam. Hydrol.* 138–139, 93–103. <https://doi.org/10.1016/j.jconhyd.2012.07.002>
- Rosenberry, D.O., LaBaugh, J.W., 2008. Field Techniques for Estimating Water Fluxes Between Surface Water and Ground Water Techniques and Methods 4 – D2, U. S. Geological Survey.
- S. Pradhan, J. Jeong, K. Flynn, R. Srinivasan, J. G. Arnold, C. Santhi, 2013. Development of Algorithms for Modeling Onsite Wastewater Systems within SWAT. *Trans. ASABE* 54, 1693–1704. <https://doi.org/10.13031/2013.39849>
- Sadat-Noori, M., Santos, I.R., Sanders, C.J., Sanders, L.M., Maher, D.T., 2015. Groundwater discharge into an estuary using spatially distributed radon time series and radium isotopes. *J. Hydrol.* 528, 703–719. <https://doi.org/10.1016/j.jhydrol.2015.06.056>
- Saito, M., Onodera, S., Ohta, T., Shimizu, Y., Zhu, A., Jin, G., Chen, J., 2018. Evaluation of the spatial distribution of submarine groundwater discharge in a small island scale using the 222Rn tracer method and comparative modeling, in: editor, T. (Ed.), *Marine Chemistry*. Honolulu, HI. <https://doi.org/10.1016/j.marchem.2018.12.003>
- Schwarz, G.E., Hoos, A.B., Alexander, R.B., Smith, R.A., 2006. The SPARROW Surface Water-Quality Model: Theory, Application and User Documentation: U.S. Geological Survey Techniques and Methods Book 6, Section B, Chapter 3. US Geol. Surv. Tech. methods report, B. 6, 248.

- Scott, T.M., Rose, J.B., Jenkins, T.M., Farrah, S.R., 2002. Microbial Source Tracking : Current Methodology and Future Directions †. *Appl. Environ. Microbiol.* 68, 5796–5803. <https://doi.org/10.1128/AEM.68.12.5796>
- Shuler, C.K., El-Kadi, A.I., Dulai, H., Glenn, C.R., Fackrell, J., 2017. Source partitioning of anthropogenic groundwater nitrogen in a mixed-use landscape, Tutuila, American Samoa . *Hydrogeol. J.* 25, 2419–2434. <https://doi.org/10.1007/s10040-017-1617-x>
- Stearns, H.T., 2015. Geology of the Samoan Islands. *Geol. Soc. Am. Bull.* 55, 1279–1332. <https://doi.org/10.1130/gsab-55-1279>
- Storlazzi, C., Messina, A., Cheriton, O., Biggs, T., 2014. Eulerian and Lagrangian Measurements of Water Flow and Residence Time in a Fringing Coral Reef Embayment, in: AGU Fall Meeting Abstracts.
- Takasaki, K.J., Mink, J.F., 1985. Evaluation of major dike-impounded ground-water reservoirs, Island of Oahu, U.S. Geological Survey Water Supply Paper 2217. US Government Printing Office Washington, DC.
- TCE, 2005. OWTS 201: Overview of Advanced Wastewater Treatment Systems, Manual published by the Texas A&M University System. <https://ossf.tamu.edu/educational-materials-2/> (accessed 2015-12-10).
- The World Bank, 2014. Fertilizer consumption (kilograms per hectare of arable land). *World Dev. Indic.* <http://data.worldbank.org/indicator/AG.CON.FERT.ZS?page=2> (accessed 2017 -02 -17).
- Thomas, F., Ruttenberg, K., Dulai, H., Kleven, A., Briggs, R., 2016. Evaluation of Submarine Groundwater Discharge as a Coastal Nutrient Source and Its Role in Coastal Groundwater Quality and Quantity, in: Fares, A. (Ed.), *Emerging Issues in Groundwater Resources*. Springer, Prairie View, TX, pp. 187–221. [https://doi.org/10.1007/978-3-319-32008-3\\_8](https://doi.org/10.1007/978-3-319-32008-3_8)
- Thomas, F., Ruttenberg, K., Dulai, H., Kleven, A., Briggs, R., 2016. Evaluation of Submarine Groundwater Discharge as a Coastal Nutrient Source and Its Role in Coastal Groundwater Quality and Quantity, in: *Emerging Issues in Groundwater Resources*. Springer, pp. 187–221. [https://doi.org/10.1007/978-3-319-32008-3\\_8](https://doi.org/10.1007/978-3-319-32008-3_8)
- Vetter, O., Vargas-Angel, B., 2014. CRCP Project # 417 : Inter-Disciplinary Study of Flow Dynamics and Sedimentation Effects on Coral Colonies in Faga’alu Bay, American Samoa : Oceanographic Investigation Summary. Pago Pago.
- Weinstein, Y., Masqué, P., Feldman, M., Rodellas, V., Garcia-Orellana, J., 2015. Submarine groundwater discharge as a major source of nutrients to the Mediterranean Sea. *Proc. Natl. Acad. Sci.* 112, 3926–3930. <https://doi.org/10.1073/pnas.1419049112>

- Whitall, D.R., Rice, S.H., 2015. Pollution in surface sediments in Faga'alu Bay, Tutuila, American Samoa. NOAA Technical Memorandum NOS NCCOS 201. Silver Spring, MD. 54 pp.  
[https://coastalscience.noaa.gov/data\\_reports/pollution-in-surface-sediments-in-fagaalu-bay-tutuila-american-samoa/t](https://coastalscience.noaa.gov/data_reports/pollution-in-surface-sediments-in-fagaalu-bay-tutuila-american-samoa/t) (accessed 2019-03-13).
- Wiegner, T.N., Mokiao-Lee, A.U., Johnson, E.E., 2016. Identifying nitrogen sources to thermal tide pools in Kapoho, Hawai'i, U.S.A, using a multi-stable isotope approach. *Mar. Pollut. Bull.* 103, 63–71. <https://doi.org/10.1016/j.marpolbul.2015.12.046>
- Wong, W.W., Grace, M.R., Cartwright, I., Cook, P.L.M., 2014. Sources and fate of nitrate in a groundwater-fed estuary elucidated using stable isotope ratios of nitrogen and oxygen. *Limnol. Oceanogr.* 59, 1493–1509. <https://doi.org/10.4319/lo.2014.59.5.1493>
- Yang, J., Maximov, I., Srinivasan, R., Zobrist, J., Mieleitner, J., Abbaspour, K.C., Siber, R., Bogner, K., 2006. Modelling hydrology and water quality in the pre-alpine/alpine Thur watershed using SWAT. *J. Hydrol.* 333, 413–430.  
<https://doi.org/10.1016/j.jhydrol.2006.09.014>
- Young, C.W., Hoover, D.J., DeCarlo, E.H., MacKenzie, F.T., McManus, M.A., 2005. Impact of storm runoff from subtropical watersheds on coastal water quality and productivity. *Geochim. Cosmochim. Acta* 69, A760–A760.
- Zektser, I.S., Everett, L.G., 2000. *Groundwater and the Environment: Applications for the Global Community*. CRC Press.
- Zemann, J., Craig, P., 2005. Natural history guide to American Samoa. *Acta Crystallogr.* 18, 139.  
<https://doi.org/10.1107/S0365110X65000361>
- Zennaro, B.B., 2007. Regulating Illegal Piggery Waste Runoff.  
<http://www.esri.com/news/arcnews/fall07/articles/regulating-illegal.html> (accessed 2017-1-17)
- Zhang, M., Yang, J., Xiao, K., Li, H., Zheng, C., An, A., Zhang, Y., Wang, X., 2017. Nutrient inputs through submarine groundwater discharge in an embayment: A radon investigation in Daya Bay, China. *J. Hydrol.* 551, 784–792. <https://doi.org/10.1016/j.jhydrol.2017.02.036>

## Chapter 4:

# Assessment of Terrigenous Nutrient Loading to Coastal Ecosystems along a Human Land-Use Gradient, Tutuila, American Samoa

### Abstract

Anthropogenic nutrient loading is well recognized as a stressor to coastal ecosystem health. However, resource managers are often focused on addressing point source or surface water discharge, whereas the impact of submarine groundwater discharge (SGD) as a nutrient vector is often unappreciated. This study examines connections between land use and nutrient loading through comparison of four watersheds and embayments spanning a gradient of human use impact on Tutuila, a high tropical oceanic island in American Samoa. In each study location, coastal radon-222 measurements, dissolved nutrient concentrations, and nitrogen isotope values ( $\delta^{15}\text{N}$ ) in water and in situ macroalgal tissue were used to explore SGD and baseflow derived nutrient impacts, and to determine probable nutrient sources. In addition to sampling in situ macroalgae, pre-treated macroalgal specimens were deployed throughout each embayment to uptake ambient nutrients and provide a standardized assessment of differences between locations. Results show SGD-derived nutrient flux was more significant than baseflow nutrient flux in all watersheds, and  $\delta^{15}\text{N}$  values in water and algae suggested wastewater or manure are likely sources of elevated nutrient levels. While nutrient loading correlated well with expected anthropogenic impact, other factors such as differences in hydrogeology, distribution of development, and wastewater infrastructure also likely play a role in the visibility of impacts in each watershed.

As published in: Shuler, C.K.; Amato, D.W.; Veronica Gibson, V.; Baker, L.; Olguin, A.N.; Dulai, H.; Smith, C.M.; Alegado, R.A. Assessment of Terrigenous Nutrient Loading to Coastal Ecosystems along a Human Land-Use Gradient, Tutuila, American Samoa. *Hydrology* **2019**, *6*, 18.

## 4.1. Introduction

Coastal ecosystems on oceanic islands provide critical ecological services to geographically isolated populations. Indigenous residents are heavily dependent on nearshore farms for plant crops and adjacent reefs for protein. Increasing urbanization has made these ecosystems vulnerable to land-based sources of pollution arising from excessive sediment and nutrient delivery that stresses corals and drives persistent and harmful algal blooms [1,2]. Terrigenous nitrogen (N) loading, linked to variability in anthropogenic land use, provides a strong control on phytoplankton, turf algae and macroalgae growth in coastal environments [3,2]. Excessive algal growth is an economic and environmental concern, as the health of coastal areas is directly linked to tourism, a primary economic driver in tropical island locales [4]. For example, an economic assessment of the persistent algal bloom in waters adjacent to the town of Kihei, Maui demonstrated that algal blooms caused by anthropogenic N input, generated up to \$20 million / yr. of revenue loss from fewer vacation rentals, decreased tax-base property values, and beach clean-up costs [5]. Harmful macroalgal blooms in coastal environments are now common in many urban reefs [6,2,7,8] and in the extreme, have been tied with the onset of fibropapillomatosis, a disease in herbivorous green sea turtles [9,10].

Elemental analysis of macroalgal tissue from tropical-coastal regions is a reliable indicator of anthropogenic eutrophication derived from coastal wastewater inputs [11,12,7,13,8]. Through macroalgae have specific N and P requirements for growth [14,15], in oligotrophic marine environments one or more of these nutrients are often limited. As a survival mechanism, tropical marine algae store available excess N and P [16], increasing their resilience to temporary nutrient-limited conditions [17,18]. This adaptation allows macroalgal tissue composition to be used as a time-integrated record of recent nutrient inputs and sources, based on the amount of, and the isotopic composition of stored nutrients. Numerous studies have applied algal tissue analysis to compliment more common water-quality sampling efforts to better understand nutrient loading patterns across multiple-time scales in oligotrophic coastal waters [19,12,7,8].

While the focus of most coastal nutrient management is typically on point-source and surface water discharges, [20,21,22,23,24], the importance of submarine groundwater discharge (SGD) as a nutrient vector is becoming more recognized. On oceanic islands, SGD has potential to deliver nutrient loads 10 to 100 times higher than riverine inputs, in both pristine and human-impacted tropical watersheds [25,26,11,27]. Although quantifying SGD and associated nutrient loading is inherently more difficult than quantifying surface water inputs to coastal areas, well-established methods using dissolved radon-222 ( $^{222}\text{Rn}$ ) as a tracer of groundwater discharge [28,29] have been applied successfully in tropical island settings [30,31,32]. This naturally-occurring radiogenic noble gas is an ideal groundwater tracer as  $^{222}\text{Rn}$  has a short half-life of 3.8 days, is non-reactive through the full salinity range, and is typically found in very low concentrations in surface waters.

Predictable source dependent fractionation of the dual-isotopes of dissolved-aqueous nitrogen and oxygen ( $\delta^{15}\text{N}$ ,  $\delta^{18}\text{O}$ ) of nitrate have been applied globally as tracers for fingerprinting N sources in terrestrial groundwater [33,34,26] and in coastal surface waters [35,36,37,30]. Similarly, algal tissue characteristics such as %N and  $\delta^{15}\text{N}$  have also been used to effectively differentiate between nutrient sources. In ecosystems with excess N-loading from a wastewater source, macroalgae often have elevated N mass-fractions as well as enriched isotopic tissue-N compositions ( $\delta^{15}\text{N} \geq 7 \text{‰}$ ), whereas algae living in less-impacted areas typically have N-isotope compositions matching the composition ( $\delta^{15}\text{N} \leq 6 \text{‰}$ ) of oceanic-N sources [12,8].

This study examines water quality, macroalgal tissue N composition, and nutrient fluxes in SGD and baseflow across four watersheds on Tutuila, the main island in the U.S. Territory of American Samoa. These watersheds were selected because they span a gradient of human-use impact suggested by population density and land use. In American Samoa, land-use factors have been linked to degradation of surface water quality and reef health [38,39], but the role of SGD as a delivery mechanism for contaminants in the territory's coastal waters has so far only been speculated [40]. Prevalent on-site wastewater disposal systems (OSDS) (i.e., cesspools and septic tanks), numerous small-scale pig-rearing operations, and widespread agriculture have all been implicated as nutrient sources to Tutuila's fresh and coastal waters [41,42]. However, only limited source-tracking efforts have so far been applied in American Samoa [35,43].

The primary objective of this study is to develop a better understanding of how different land-uses interact with local hydrogeology to deliver nutrients or other contaminants to the nearshore environment. To accomplish this, two "snapshot" style measurement campaigns were conducted throughout the four study locations in August 2015 and 2016. During the first campaign, SGD derived nutrient fluxes were calculated using  $^{222}\text{Rn}$  as a groundwater tracer, and baseflow stage surface water nutrient fluxes were estimated through water sampling and using existing streamflow data. During both 2015 and 2016, water samples were collected from nearshore waters, coastal springs, streams at baseflow stage, and groundwater wells. *In situ* macroalgae were collected both years for analysis of tissue %N and  $\delta^{15}\text{N}$ , and in 2016, specimens of experimentally managed macroalgae were deployed at fixed locations throughout the coastal zone to control for variability affecting *in situ* macroalgae. Ultimately, this work provides insight into the magnitudes and sources of coastal nutrient discharge in a tropical island setting, and clarifies the need to support integrated terrestrial and coastal resource management in American Samoa.

### 4.1.1 Study Location descriptions

Located near 14° S and 170° W, the island of Tutuila (142 km<sup>2</sup> in area) hosts nearly 56,000 permanent residents and serves as the main population center of American Samoa [44]. Because of its position within the South Pacific Convergence Zone, the climate is hot and humid, has prevalent year-round rainfall, up to 6000 mm/year, and is subject to a wetter season from October to May. The four study locations selected for comparison each include a terrestrial watershed area and a coastal embayment. Listed from high to low population density, these locations are Pala Lagoon, Faga'alu Bay, Vatia Bay, and Oa Bay (Figure 4.1). Each watershed drains a steep forested upper section that generally transitions to an alluvial-coastal plain of variable size. For the most part, development is concentrated in coastal areas and villages are located on these alluvial plains, except for the nearly pristine Oa location, which has no road access or residents. At all study locations, nearshore zones contain well-developed fringing reefs, typically consisting of uniformly shallow (0.5 - 2 m deep) back-reef flats that extend roughly 50 to 300 m from shore to fore-reef crest; beyond which water depths rapidly increase. It is notable that soft sediments do not typically accumulate in nearshore areas except for in the interior portion of Pala Lagoon.

Geologically, Faga'alu, Vatia, and Oa are fairly typical examples of Tutuila's radial watersheds, with headwaters composed of heavily eroded Pleistocene basalts, erupted 1.5 Ma [45]. Since that time, alluvial transport of sediments and deposition of marine carbonates has created the small wedge-shaped coastal plains fronting the mouths of each bay. At least 30 other watersheds on Tutuila have a similar geologic structure, with Faga'alu and Vatia being two of the largest and Oa one of the smallest. In contrast, the hydrogeologic structure of the Pala Watershed, also referred to as the Tafuna Plain, differs significantly from the other study locations. The majority of the watershed is covered with a Holocene-age lava delta that has given the terrain a much lower slope and a much higher permeability to groundwater than the older Pleistocene rock that makes up the rest of the island [46].

Pala Lagoon drains the largest and the most developed watershed of the four study locations. Numerous farms and residences are scattered over the 12.2 km<sup>2</sup> lava plain, which has a population density of 480 people/km<sup>2</sup> [44]. Only one small perennial stream runs along the northeastern margin of the Tafuna Plain. Faga'alu bay, has been previously identified as a priority watershed management area by the US Coral Reef Task Force due to concerns of declining reef health and stream water quality. A single main stream drains to an embayment above a steep, forested 2.5 km<sup>2</sup> valley with a population density of 404 people / km<sup>2</sup> [44]. A sub-location consisting of a shallow reef flat fronting a rocky headland wrapping around and out the northern margin of Faga'alu Bay, termed Outer- Faga'alu, was also delineated as an algae sampling location for in this study. This location is adjacent to the Utulei Wastewater Treatment Plant, which discharges municipal wastewater effluent from a submerged outfall in the harbor channel. Vatia bay, drains three radially oriented perennial streams in a lightly impacted 3.6 km<sup>2</sup> watershed with a population density of 132 people / km<sup>2</sup>. Although anthropogenic impact

in Vatia has been categorized as minimal [47], reports of reef decline and increased algal growth, combined with a lack of wastewater infrastructure suggest more information is critically needed for natural resources management in Vatia [48]. Oa bay is located on the northern coast, drains a small 0.6 km<sup>2</sup> watershed, and is the least impacted of the study locations. The watershed contains no residents and has only a single stream that, at baseflow stage, infiltrates completely once it reaches the alluvial wedge. A large coastal spring is located near the dry stream mouth during low tide.

The four watersheds selected for this study span a gradient of human-impact and physical hydrogeologic properties that were defined through assessment of population density, and land-use analysis. Population data from the U.S. Census has been previously used to assign human impact classifications to Tutuila’s watersheds [47], and a recently released high-resolution wildlife habitat map [49] allows for geospatial assessment of land-use in each watershed. Land-use and population density metrics suggest Pala Lagoon should be subject to the highest anthropogenic impacts followed by Faga’alu then Vatia, and then Oa as its watershed is nearly 100% forested with no human residents (Table 4.1).

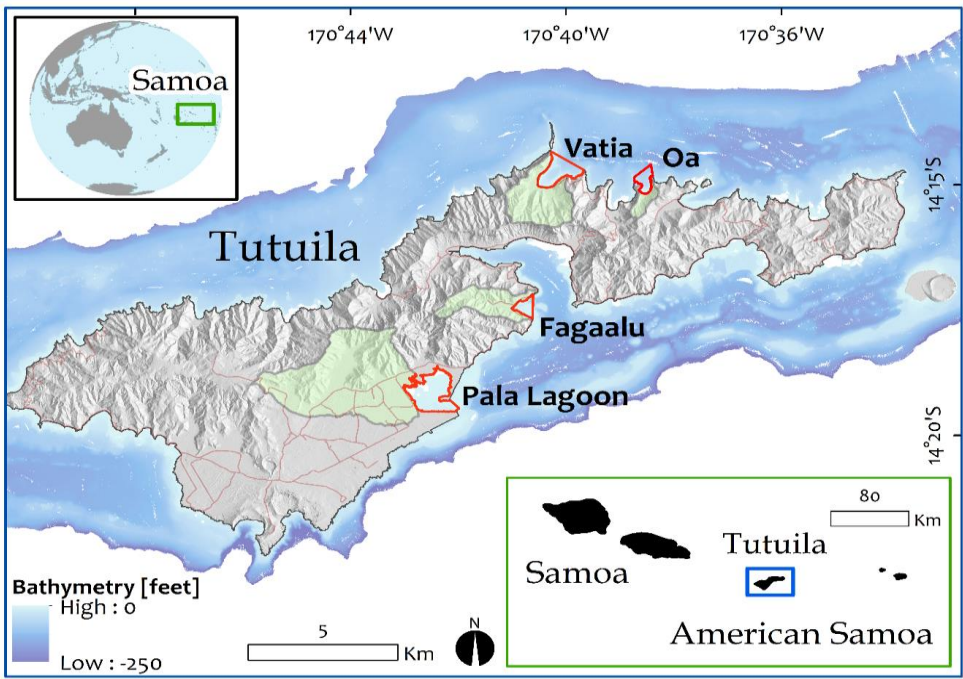


Figure 4.1: Location map showing Samoan archipelago and Tutuila with the four study watersheds highlighted in green and their bays outlined in red.

Table 4.1: Geospatial land-use analysis of study locations showing population data from the U.S. census [44], and land use data from a recently developed high-resolution habitat map [49].

Location	Total Area [km <sup>2</sup> ]	Population density [persons per km <sup>2</sup> ]	Developed proportion of watershed	Cultivated proportion of watershed	Natural proportion of watershed
<b>Pala Lagoon</b>	12.23	480	31%	15%	54%
<b>Faga'alu</b>	2.48	404	12%	6%	81%
<b>Vatia</b>	3.61	132	5%	7%	88%
<b>OA</b>	0.58	0	0%	0%	100%

## 4.2. Materials and Methods

### 4.2.1 Water Sample Collection and Analysis

Water samples were collected from local production wells, streams at baseflow stage, coastal groundwater springs (CGW), and coastal surface waters in all four study locations (Figure 4.2). Here CGW is defined as water (fresh to saline) obtained from shallow beach pore water or distinct coastal springs, and is assumed to be representative of the composition of the SGD endmember prior to release in the ocean. All samples were collected in acid washed 60 mL HDPE or new polypropylene bottles that were triple-rinsed with sample water during collection. Water samples were filtered on-site with 0.45  $\mu\text{m}$  hydrophilic polyethersulfone capsule filters (Pall AquaPrep 600).

At each sample site, water temperature, salinity, and dissolved oxygen were measured *in situ* with a multiparameter sonde (YSI, model V24 6600). Samples were immediately cooled for transport, frozen as soon as possible, and stored frozen until analysis. All samples were analyzed for total dissolved nitrogen (TDN) and dissolved inorganic nutrients (silica (Si), nitrate ( $\text{NO}_3^-$ ) + nitrite ( $\text{NO}_2^-$ ) herein referred to as (N+N), ammonium ( $\text{NH}_4^+$ ) and phosphate ( $\text{PO}_4^{3-}$ ) at the SOEST Laboratory for Analytical Biogeochemistry (S-LAB) using a Seal Analytical AA3 Nutrient Autoanalyzer. Dissolved inorganic nitrogen (DIN) was calculated as the sum of N+N and  $\text{NH}_4^+$ . The subset of samples containing sufficient N+N ( $> 0.8 \mu\text{mol/L}$ ) were analyzed for the isotopic composition of nitrogen and oxygen in dissolved N+N ( $\delta^{15}\text{N}$ ,  $\delta^{18}\text{O}$ ). Isotopic analysis was conducted at the University of Hawaii Stable Isotope Biogeochemistry Lab on a Thermo Finnigan MAT252 coupled to a GasBench II (Thermo Fisher Scientific Inc.) using the denitrifier method of Sigman et al. [50]. Nitrogen and oxygen isotope results are expressed in per mil (‰) notation relative to AIR for  $\delta^{15}\text{N}$  and V-SMOW for  $\delta^{18}\text{O}$ . Stream and CGW grab samples were also analyzed for concentrations of dissolved  $^{222}\text{Rn}$  gas with a radon in air

monitor RAD7 and its water accessory RADH2O (both manufactured by Durrige Inc.). Discrete samples were collected in 250 mL glass bottles with no headspace, were analyzed the same day as collection, and were corrected for radioactive decay between collection and analysis. To increase the number and temporal representativeness of end-member samples, thirteen CGW and six stream-baseflow samples collected in August 2014 were also included in the sample set. All other fieldwork was conducted during two field expeditions in July 2015 and August 2016, and took place in the dry season when rainfall was limited, streams remained at baseflow stage, and groundwater levels remained fairly stable. Duplicates were taken for 10% of the  $\delta^{15}\text{N}$  sample set and 5% of the nutrient analysis sample set. Significance of parameter averages were tested with one-way ANOVA and Tukey's range test for post hoc analysis [51].

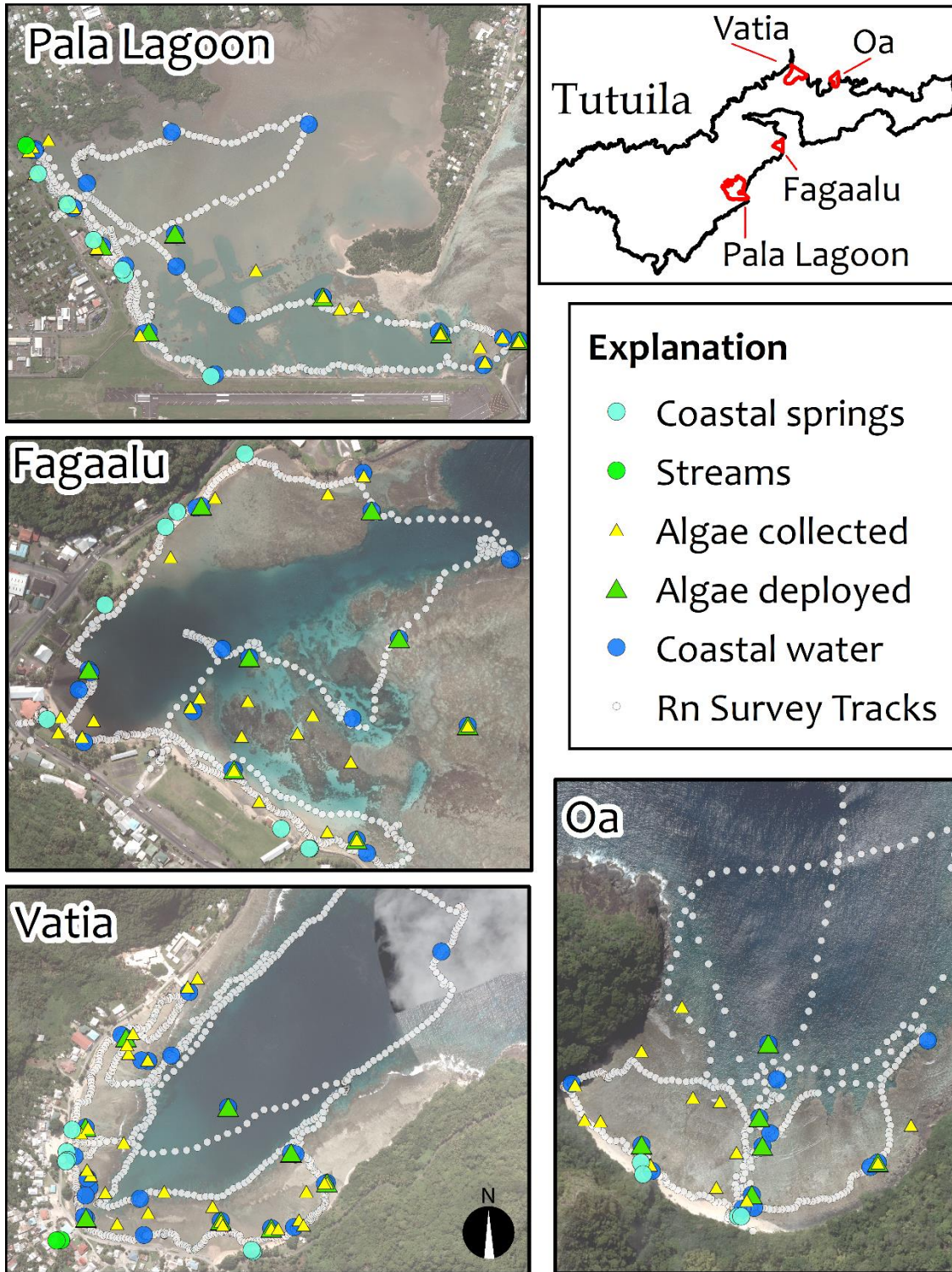


Figure 4.2: Study location maps showing sampling sites for coastal water (*small blue circles*), CGW (*large cyan circles*), streams at baseflow stage (*larger green circles*), *in situ* collected macroalgae (*smaller yellow triangles*), deployed macroalgae (*larger green triangles*), and tracks of  $^{222}\text{Rn}$  surveys (*grey dots*).

## 4.2.2 Time-Series and Survey Based $^{222}\text{Rn}$ Measurements

In each study location, SGD rates were calculated using dissolved  $^{222}\text{Rn}$  as a groundwater tracer. To account for the temporal (tide dependent) and spatial (geology dependent) variability of SGD in volcanic island settings, a fixed location time-series  $^{222}\text{Rn}$  measurement was coupled with a moving coastal water  $^{222}\text{Rn}$  survey in each embayment following the methods of Dulaiova et al. [52]. During the time-series, a peristaltic pump brought coastal water from a stationary point generally located within 40 m from shore to an instrument package on land that continuously measured  $^{222}\text{Rn}$  concentration and salinity (Figure 4.3a). Time-series measurements were conducted over one full tidal cycle ( $> 12.2$  h) at each location. Coastal water surveys were conducted either before or after each time-series, during a 3-hour period bracketing low tide. The same  $^{222}\text{Rn}$  and salinity sensors used in the time-series were mounted on a small inflatable boat that was motored through each bay in a series of shore parallel transects at roughly 0.75 m/s (Figure 4.3b). Shore-perpendicular transects were also conducted if time allowed. During each survey, eight to twelve coastal surface-water samples were collected. Time-series derived SGD fluxes were scaled with spatial information from the  $^{222}\text{Rn}$  surveys to calculate total-daily SGD fluxes to each of the four embayments.

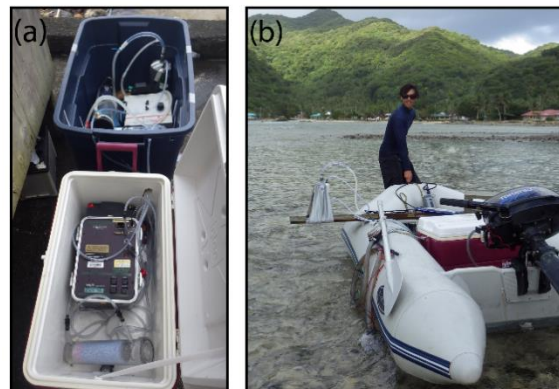


Figure 4.3: (a) Instrument package used for measuring dissolved  $^{222}\text{Rn}$  and water quality parameters for time-series measurements. (b) The same instrument package transferred and mounted to an inflatable boat for  $^{222}\text{Rn}$ -survey measurements.

## 4.2.3 SGD and Nutrient Flux Calculations

To convert  $^{222}\text{Rn}$  concentrations to SGD fluxes, the non-steady state  $^{222}\text{Rn}$  mass-balance model of Burnett and Dulaiova [28] was used. The survey area of each embayment was subdivided into Thiessen polygons, each surrounding a coastal-survey measurement point and all falling within the edges of each embayment. The volume of each polyhedron was calculated by multiplying the Thiessen polygon area by water depth on the back-reef flat, assumed to be the thickness of the SGD plume, as measured by a pressure transducer deployed at the time-

series location. This assumption was validated with depth profiles taken throughout the reef-flat, which showed salinity values typically remained constant as depth increased, indicating coastal waters were well mixed. For time-series measurements, the Thiessen polyhedron located around the time-series intake was used as the volumetric multiplier for flux calculations. Note that the volume of this polyhedron during time-series measurements changed dynamically with daily tidal fluctuations, whereas the polyhedron volumes used in processing survey data were calculated using a single water depth measured at low tide.

Non-SGD related losses and additions of  $^{222}\text{Rn}$  from local and offshore processes were also considered when calculating total SGD flux. These processes were assumed to be comparable in American Samoa to those of the Hawaiian Islands, and included accounting for: (1) atmospheric  $^{222}\text{Rn}$  activity of 0.03 dpm/L [53], (2) local excess  $^{222}\text{Rn}$  activity of 0.08 dpm/L supported by *in situ*  $^{226}\text{Ra}$  [54], (3)  $^{222}\text{Rn}$  activity of 0.087 dpm/L, from the offshore  $^{226}\text{Ra}$  pool [55], and (4) wind speed dependent evasion correction described in Burnett and Dulaiova [28] and calculated with hourly wind speed and air temperature recorded at the Pago Pago Airport. Mixing losses from tidal movement were calculated at each time-step in the time-series model and residence times for each bay (except for Pala Lagoon) were assumed to be the length of one tidal cycle (12.2 h), which is within the range of previously estimated residence times for these areas [56,57]. A conservative residence time of four tidal cycles (48.8 h) was chosen for Pala Lagoon to account for the lagoon's enclosed geometry and lack of available circulation data.

Groundwater end-member compositions were determined by averaging  $^{222}\text{Rn}$  activities for all sampled CGW sites and upgradient wells in each watershed. Salinities of CGW varied widely as SGD is typically composed of a fresh component mixed with a recirculated seawater component. The proportion of fresh and recirculated SGD was calculated with a two end member mixing analysis following the method used by Bishop et al. [30]. To calculate SGD nutrient fluxes, average CGW-endmember nutrient concentrations were simply multiplied by total (fresh + recirculated) SGD-flux rates for each study location. Nutrient fluxes in streams at baseflow stage were calculated similarly, using averaged, measured stream-nutrient concentrations and average annual baseflow discharge for streams in each watershed. These discharges were estimated using stream-gauging data collected by the United States Geological Survey (USGS) [58]. Note that runoff stage streamflow and associated nutrient fluxes are not addressed here, due to challenges in measuring Tutuila's short lived and difficult to sample runoff events.

#### 4.2.4 In Situ Algal Survey

At each study location, specimens of common-marine macroalgae were sampled at numerous sites on shallow back-reef flats (0.5- 2.0 m) during July 2015 and August 2016 (Figure 4.2). Species collected included *Chlorodesmis fastigiata*, *Hypnea pannosa*, *Dictyota bartayresiana*, and *Ulva intestinalis*, though not all species were found at each location. Algal tissues were initially

placed in plastic bags, cooled for transport, and processed within 12 h of collection. Sample processing included removal of any remaining holdfasts and triple rinsing tissues in distilled water to remove fouling organisms and excess salts. Algal tissues were towed dry before being placed in aluminum foil packets for dehydration. Initial dehydration commenced within 12 h of collection in a conventional oven at 71 °C before being transferred to a drying oven at University of Hawai'i and maintained at 60 °C for at least three months. After a constant mass was achieved, desiccated tissues were powdered with a mortar and pestle and placed in individual glass vials. Tissue  $\delta^{15}\text{N}$  (‰) and N % were measured using a Costech ECS 4010 Elemental Combustion System (Costech Analytical Technologies, CA, USA) interfaced with a ThermoFinnigan DeltaXP Mass Spectrometer (Thermo Fisher Scientific Inc.) at the University of Hawai'i Biogeochemical Stable Isotope Facility. Isotopic ratios of N in samples were normalized to reference materials NIST 3, USGS-32, USGS-34, and USGS-35 and are relative to AIR.

#### 4.2.5 Algal Deployments

On August 5<sup>th</sup> 2016, seventy-five specimens of *Hypnea pannosa* were collected at an open coastal location between Pala Lagoon and Faga'alu Bay and pre-treated in a 16 L indoor growth chamber filled with ambient ocean water to draw down tissue N levels, following Amato et al. [8]. An average irradiance of 5,700 lx (measured with a Digital Light Meter Model # FCM0-10M+, Phytotronics Inc.) was provided by six LED flood lights (Philips Model #9290002322) placed 25 cm above the water surface. On August 8<sup>th</sup>, 2016, reagent grade nutrients ( $\text{NaNO}_3$  and  $\text{NaPO}_4$ ) were added to the seawater to bring the nutrient levels to 0.5  $\mu\text{M}$  -  $\text{NO}_3$  and 0.05  $\mu\text{M}$  -  $\text{PO}_4$  (assuming the original seawater had negligible nutrient levels after 72 hours in algal culture). Salinity was monitored and distilled water was added every day to maintain a salinity of 35.

On August 10<sup>th</sup> -11<sup>th</sup>, 2016, thirty-six *H. pannosa* specimens, with an individual mass of 5 - 6 g were randomly assigned and deployed throughout the four study locations (Figure 4.2) in 8 cm x 20 cm cylindrical cages. The cages, which were constructed of 8 mm diameter plastic mesh and polyester fabric, were designed to allow water flow but exclude macroherbivores (Figure 4.4). At each site, a caged *H. pannosa* specimen was tethered 0.25 m below the surface to a small float and anchored to a cinder block. Eight cages were distributed throughout the bay at each study location. Three additional cages were deployed at Outer- Faga'alu at sites adjacent to the wastewater treatment facility. After eight days, all cages were retrieved and samples were prepared for tissue analysis as above. For comparison between each location, algal samples were grouped by study location and statistical tests were performed using SigmaPlot 11 (Systat Software Inc., CA, USA). One-way ANOVA (identified by the F-statistic) and Tukey's pairwise comparisons were used to compare parameters if test assumptions were not violated. The nonparametric Kruskal-Wallis ANOVA (identified by the H-statistic) was performed if the assumptions of normality or homoscedasticity were violated.



Figure 4.4. Deployed algae cage containing a single *H. pannosa* specimen.

## 4.3. Results

### 4.3.1 Water Quality Results: Nutrient Levels

To compare water quality between study locations, water samples were grouped by sample type (coastal surface water, CGW, streams, and wells), and study location before taking arithmetic means of each group (Figure 4.5). Concentrations of DIN in coastal surface waters and CGW showed statistically significant differences between all study locations (ANOVA  $p$ -values of  $> 0.002$ ), with Pala Lagoon having the highest ( $8.0 \pm 13.0 \mu\text{mol/L}$ ) and Oa Bay the lowest ( $1.2 \pm 1.5 \mu\text{mol/L}$ ) DIN values in coastal surface waters. Few statistically significant differences were found between locations for  $\text{PO}_4^{3-}$  concentrations, although some sample types, notably streams in Oa, well waters in Vatia, and coastal springs in Faga'alu and Vatia, had significantly higher levels of  $\text{PO}_4^{3-}$ . Silicate concentrations also showed few significant differences among sites, except for notably higher concentrations in Vatia's wells. All geochemical data are provided in Appendix C, Tables C5 through C9. It should be noted that because salinity varied widely amongst CGW samples, nutrient concentrations (DIN,  $\text{PO}_4^{3-}$ , and silicate) reported for CGW values as shown on Figure 4.5 were normalized to the freshwater salinity of 0.1 using an un-mixing calculation [11] based on the local-oceanic salinity and nutrient composition. Analytical uncertainties for nutrient concentrations and isotopic values were determined through applying the standard error of the estimate to duplicate samples. This yielded uncertainty values of  $\pm 3.1 \mu\text{mol/L}$  for TDN,  $\pm 2.8 \mu\text{mol/L}$  for N+N,  $\pm 6.2 \mu\text{mol/L}$  for Si,  $\pm 0.1 \mu\text{mol/L}$  for  $\text{PO}_4^{3-}$ , and  $\pm 0.01 \mu\text{mol/L}$  for  $\text{NH}_4^+$ , and  $\pm 0.26 \text{‰}$  for  $\delta^{15}\text{N}$  values.

### 4.3.2 Water Quality Results: Nitrate Isotopes

Most variability in  $\delta^{15}\text{N}$  values was found among sites within each individual study location. Many samples showed substantial enrichment above the commonly referenced ranges for  $\delta^{15}\text{N}$  of  $\text{NO}_3^-$  in natural soils, typically between +2 to +6 ‰ [33]. Few to no samples showed  $\delta^{15}\text{N}$  values within the typical range of synthetic fertilizer influenced waters (-5 to +5 ‰), suggesting agricultural inputs were not significant coastal N sources during the study period. Numerous CGW and coastal water samples in Vatia and Pala Lagoon had generally high-average  $\delta^{15}\text{N}$  values ( $8.6 \pm 0.5$ , and  $11.5 \pm 3$  ‰, respectively) which appeared to be indicative of a wastewater source. Typically, leachates from manure and wastewater have a wide but generally high  $\delta^{15}\text{N}$  range (+4 to +25 ‰) [12,7,59,60]. Studies in similar tropical island environments have reported wastewater  $\delta^{15}\text{N}$  values ranging from +5 to 23 ‰ [30,8,11,61]. Values matching these ranges were seen in Vatia, where the effect of exceptionally high  $\delta^{15}\text{N}$  values in CGW, sometimes above 14 ‰, were evident on Vatia's coastal waters, which had average  $\delta^{15}\text{N}$  values of  $10.3 \pm 0.9$  ‰. Faga'alu's coastal water had an unexpected distribution of  $\delta^{15}\text{N}$  values, whereas the highest values (ranging between 9.1 to 9.7 ‰) were observed in the outer part of the bay nearer to the Outer- Faga'alu location, with  $\delta^{15}\text{N}$  values in the inner bay ranging from 6.2 to 9.0 ‰. Unfortunately, the only water sample taken in the outer- Faga'alu area did not contain enough N+N for  $\delta^{15}\text{N}$  analysis. In Oa bay,  $\delta^{15}\text{N}$  values in coastal water and in the coastal spring ( $7.1 \pm 1.0$  ‰ and  $5.7 \pm 1.2$  ‰, respectively) were generally lower than those observed at other locations.

### 4.3.3 Water Quality Results: Nearshore – Offshore Gradient

Spatial trends in coastal-water geochemistry, and in algal-tissue samples, showed strong nearshore – offshore gradients within each study location. When all coastal-surface water sampled from sites located within 50 m of the coastline were pooled, they showed average DIN concentrations that were 124 %, 208 %, 332 %, and 610 % higher than samples taken more than 50 m offshore in Faga'alu, Oa, Vatia, and Pala Lagoon, respectively. Nearshore  $\text{PO}_4^{3-}$  levels were also generally about twice as high as offshore levels (Table 4.2). In Pala Lagoon and Vatia, only two coastal-water samples were taken within 50 m of a stream mouth (none at the other sites), and both had higher average DIN and  $\text{PO}_4^{3-}$  concentrations than samples taken farther from the stream. In all locations except Faga'alu, coastal-water samples taken within 50 m of coastal springs had markedly higher average DIN values, and slightly higher  $\delta^{15}\text{N}$  values than samples taken > 50 m from spring outlets. In Vatia, nearshore samples had up to 10 times higher DIN than offshore samples. Unlike all other study locations, in Faga'alu Bay, both  $\delta^{15}\text{N}$  and DIN values increased with distance from the stream mouth and coastline.

Table 4.2: Water quality parameters for coastal-water samples showing nearshore vs. offshore gradients

Study Location		Pala Lagoon	Faga'alu	Vatia	Oa
<b>DIN</b> [ $\mu\text{mol/L}$ ]	<b>Nearshore</b>	13.2 (16.0)	3.2 (2.9)	3.1 (6.7)	1.5 (1.9)
	<b>Offshore</b>	2.2 (4.3)	2.6 (1.1)	0.9 (0.6)	0.8 (0.5)
	<b>All</b>	8.0 (13.0)	3 (2.3)	2.3 (5.3)	1.2 (1.5)
<b><math>\delta^{15}\text{N}</math></b> [‰]	<b>Nearshore</b>	8.6 (0.7)	7.9 (1.1)	10.3 (0.8)	7.4 (1)
	<b>Offshore</b>	6.6 (-)	9.1 (0.7)	9.1 (-)	6.2 (-)
	<b>All</b>	8.3 (1)	8.6 (1.1)	10.0 (0.9)	7.1 (1)
<b><math>\text{PO}_4^{3-}</math></b> [ $\mu\text{mol/L}$ ]	<b>Nearshore</b>	1.0 (0.7)	1.4 (1.7)	0.5 (0.6)	0.6 (0.8)
	<b>Offshore</b>	0.5 (0.2)	0.9 (1)	0.2 (0.1)	0.2 (0)
	<b>All</b>	0.7 (0.6)	1.2 (1.5)	0.4 (0.5)	0.5 (0.7)

Number of samples (n) for nutrient samples in the nearshore was 11, 15, 15 and 10 and in the offshore was 10, 11, 9, and 6 for Pala Lagoon, Faga'alu, Vatia, and Oa, respectively.  
 Number of samples (n) for  $\delta^{15}\text{N}$  samples in the nearshore was 5, 5, 4, and 3 and in the offshore was 1, 7, 1, and 1 for Pala Lagoon, Faga'alu, Vatia, and Oa, respectively.

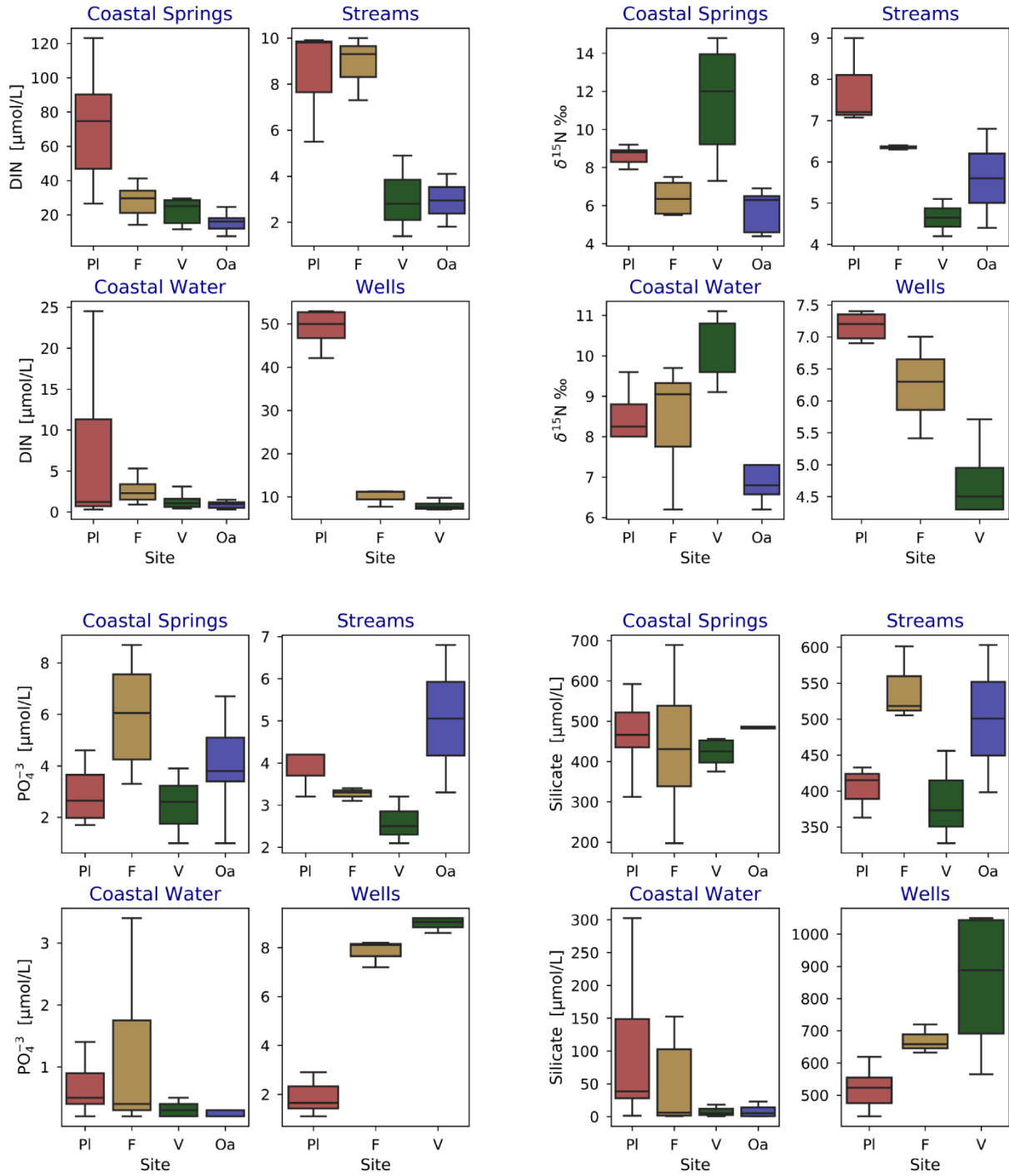


Figure 4.5: Box plots of water quality sample results. Box center lines represent median, edges represent interquartile range, and whiskers represent range. Site names are coded as, Pala Lagoon: PI, Faga'alu: F, Vatia: V, and Oa: Oa. Note that the stream in Oa bay was sampled in the perennial section above where it infiltrated into the ground.

#### 4.3.4 Hypnea Deployment Results

Significant differences in the tissue N content of deployed *Hypnea* tissue were detected among the four study locations ( $\delta^{15}\text{N}$ :  $p < 0.001$ ,  $H = 16.351$ ,  $\text{N}\%$ :  $p = 0.001$ ,  $F = 7.392$ ). Values of tissue  $\delta^{15}\text{N}$  and  $\text{N}\%$  values were highest in samples deployed at Faga'alu and lowest at Oa (Table 4.3); values were significantly higher at Faga'alu compared to Vatia and Oa. Trends in these values among study locations reflect gradients of impact/human density as discussed above. When data from all deployed samples are pooled, a positive relationship ( $r^2 = 0.26$ ,  $p = 0.004$ ,  $df = 28$ ) between  $\delta^{15}\text{N}$  and  $\text{N}\%$  is present. Exploratory deployments of three *Hypnea* tissue samples at the Outer- Faga'alu location had higher mean values for both N parameters than the four study locations (Table 4.3). In general, most  $\text{N}\%$  and  $\delta^{15}\text{N}$  values for deployed *Hypnea* samples were within a range that may indicate at least some wastewater impacts.

#### 4.3.5 In-situ Algal Survey Results

Mean tissue  $\delta^{15}\text{N}$  and  $\text{N}\%$  values from macroalgal species collected *in-situ* from coastal locations were similar to those of deployed *Hypnea* (Table 4.3). Significant differences in these N parameter values were detected among *in-situ* survey locations ( $p < 0.001$ ,  $H = 75.414$ ). Highest values of  $\delta^{15}\text{N}$  (mean  $\delta^{15}\text{N} = 9.6$ ) and  $\text{N}\%$  (mean  $\text{N}\% = 4.1$ ) from *in situ* algal tissues were collected at Outer- Faga'alu. *In-situ* algal tissues collected from Outer- Faga'alu had significantly higher  $\delta^{15}\text{N}$  than all other locations; samples from both Faga'alu and Pala Lagoon had significantly higher  $\delta^{15}\text{N}$  values than Vatia and Oa. Mean  $\text{N}\%$  values were above 1.0, but were not significantly different among locations ( $p = 0.071$ ,  $H = 8.637$ ). *In situ* tissue samples also generally had  $\text{N}\%$  and  $\delta^{15}\text{N}$  values consistent with some wastewater impact to these sampling locations.

In general, algal deployments and *in situ* surveys showed considerable intra-location fine scale variation in algal tissue  $\delta^{15}\text{N}$  values across each location) Similar to trends in water samples, algal tissue  $\delta^{15}\text{N}$  values in Vatia were generally higher near the shore and near groundwater-influenced springs and streams. In Pala Lagoon, both surface water and algal tissue  $\delta^{15}\text{N}$  values were highest where stream input and SGD flux was greatest (Figs. 4.6 and 4.7. However, in Faga'alu Bay, the opposite trend was again observed. In contrast, algal  $\delta^{15}\text{N}$  values were generally homogenous within Oa bay, ranging between 4.3 and 6.8 ‰. Algal tissue  $\delta^{15}\text{N}$  values of deployed samples were similar to *in situ* samples collected in close proximity. All measured algae parameters are provided in Appendix C, Tables C10 and C11.

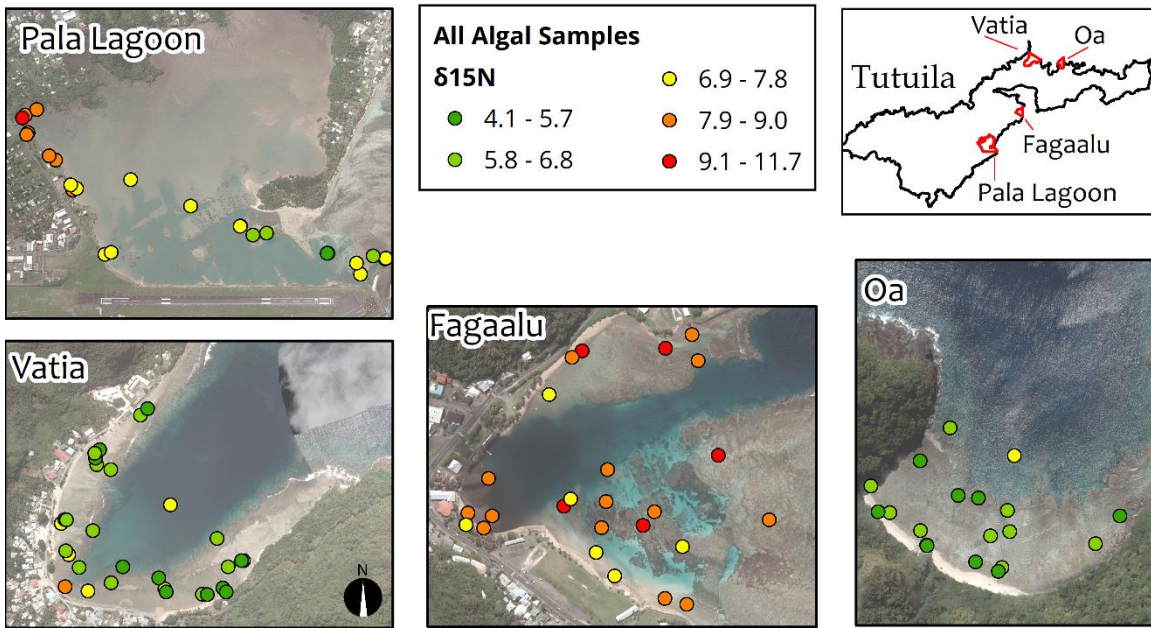


Figure 4.6: Map of  $\delta^{15}\text{N}$  values from in-situ and deployed algal samples at all four sample locations. Note that all species of in-situ samples are lumped together along with all deployed *Hypnea p.* samples, thus variation in this figure may also reflect natural inter-species variation in these parameters.

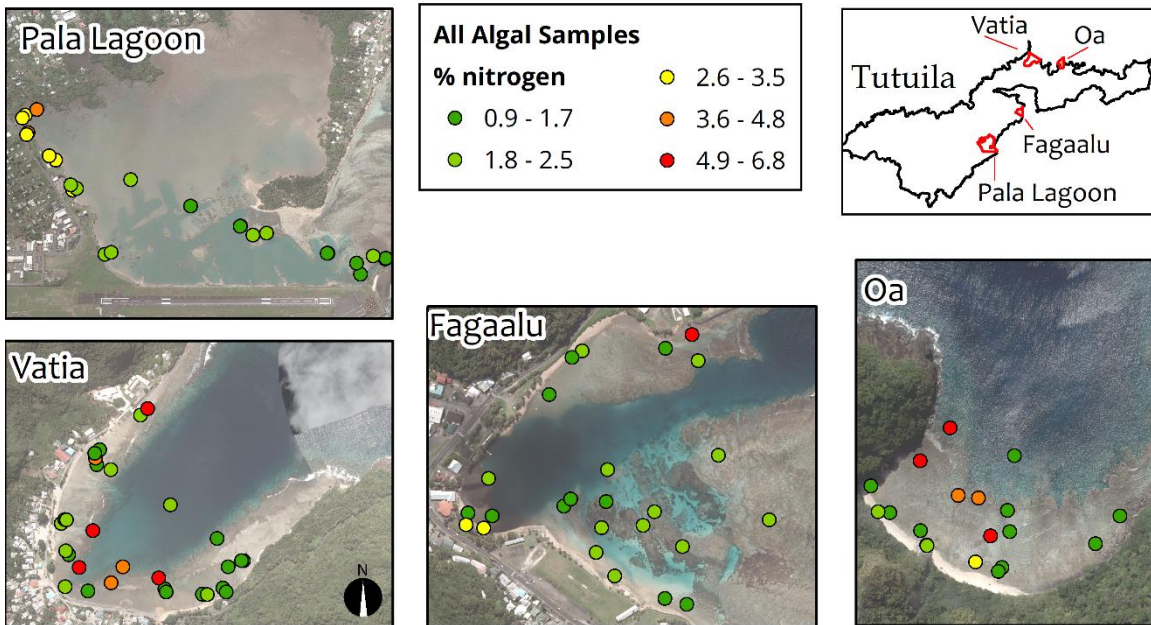


Figure 4.7: Map of % tissue N by weight from in-situ and deployed algal samples at all four sample locations. Note that all species of in-situ samples are lumped together along with all deployed *Hypnea p.* samples, thus variation in this figure may also reflect natural inter-species variation in these parameters.

### 4.3.6 SGD Rates and Associated Nutrient Fluxes

The highest coastal-water dissolved  $^{222}\text{Rn}$  concentration (24.3 dpm/L) and the lowest coastal-water salinity (11.6) from time-series measurements were observed in Pala Lagoon. In contrast, Vatia Bay had the lowest time-series  $^{222}\text{Rn}$  concentration (3.9 dpm/L), and the highest minimum salinity (30.3). When tidal-cycle averaged SGD rates from the  $^{222}\text{Rn}$  time-series were upscaled with spatially distributed SGD information from  $^{222}\text{Rn}$  surveys, Pala Lagoon showed the highest-absolute SGD magnitude and Oa Bay had the lowest (Table 4.4). However, when scaled by watershed area, both Pala Lagoon and Oa had higher per-km<sup>2</sup> SGD rates (9,490 and 8,522 m<sup>3</sup>/d/km<sup>2</sup>, respectively) than Faga'alu and Vaita bays, which had per-km<sup>2</sup> SGD rates of 5,398 and 1,274 m<sup>3</sup>/d/km<sup>2</sup>, respectively. This is reasonable considering perennial streams drain a significant proportion of water in Faga'alu and Vatia, whereas the single stream in Oa and the few streams in the Pala Watershed are intermittent and dry much of the year.

Dissolved  $^{222}\text{Rn}$ , and thus SGD, was concentrated in specific locations along the coastline, often near coastal springs, though not always (Figure 4.8, left panels). Tidal changes affected SGD rates significantly, with SGD peaking during low tide and nearly stopping during high tides, as would be expected (Figure 4.8, right panels). The fractions of fresh and recirculated SGD were assumed to be directly proportional to the average seawater fractions measured in coastal-spring samples at each location. In all locations except Vatia, this proportion was around 50% fresh and 50% recirculated SGD. In Vatia low observed CGW salinities increased the fresh fraction to about 90% of total SGD.

Nutrient flux rates from SGD were determined by multiplying total SGD by the average-measured DIN and  $\text{PO}_4^{3-}$  concentrations from all CGW and well samples taken in each study location. Nutrient flux rates in SGD followed the expected pattern of impact, with Pala Lagoon having almost two orders of magnitude higher nutrient fluxes than the other sites. Faga'alu and Vatia had intermediate SGD nutrient flux rates, with Faga'alu's exceeding Vatia's by two times, and Oa bay had the lowest (Table 4.4). Note that variance on nutrient flux estimates is large, in part because it is propagated from SGD standard deviation averaged over entire tidal cycles, and from averaging variable coastal spring nutrient concentrations. These measurements are both affected by high-temporal variability driven by tide changes, and high-spatial variability throughout each site, but nonetheless represent order-of-magnitude resolution estimates that are useful for relative comparison between study locations.

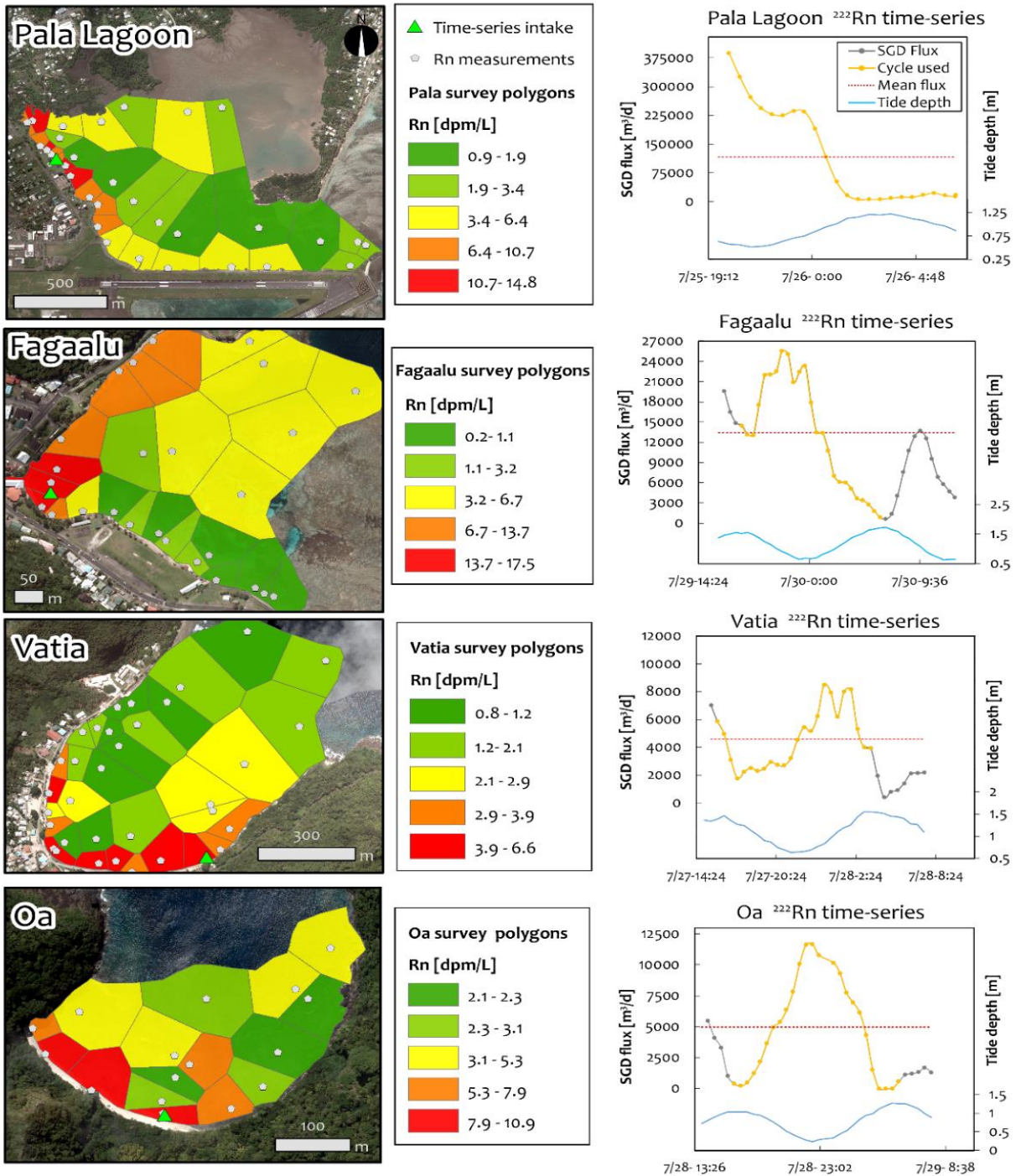


Figure 4.8: Radon survey and time-series results. Left map-panels show <sup>222</sup>Rn survey measurement locations (grey dots), time-series intake locations (green triangles) and geometries of Thiessen Polygons color coded by dissolved <sup>222</sup>Rn concentration at each measurement point for the four study locations. Note different color scales for each map. Right plot-panels show processed total SGD fluxes calculated from the time-series measurements after integration of spatial data from <sup>222</sup>Rn surveys. To standardize daily average fluxes, only measurements taken within a single tidal cycle (12.2 hours) were used (gold portion of grey lines). Note that mean-daily SGD fluxes (red dotted lines) represent total SGD (fresh + recirculated).

### 4.3.7 Stream Baseflow Estimates and Associated Nutrient Fluxes

Baseflow discharge rates for streams in Faga’alu, Vatia, and Pala watersheds were determined from existing streamflow data obtained from USGS stream gauging efforts, circa 1960 to 1995 and documented in Wong [58]. Wong reported median ( $Q_{50}$ ) and mean stream discharge values for numerous basins throughout Tutuila. Because Wong’s measurements did not include baseflow separation analysis, the  $Q_{50}$  was here assumed to be the most representative available estimate of baseflow discharge in Tutuila’s streams. Note that in Hawai‘i, stream baseflow has been shown to be equivalent to a flow value that falls within a range of the stream discharge ( $Q$ ) that is met or exceeded between 60% ( $Q_{60}$ ) and 80% ( $Q_{80}$ ) of the time [62]. Therefore, approximation of baseflow with the  $Q_{50}$  value is likely to bias stream baseflow and thus nutrient loads, towards over-estimation. Regardless of this, these baseflow discharges in each watershed were generally low ranging between 2,500 and 3,000  $m^3/d$ , and were generally similar across all watersheds except Oa, which had no baseflow discharge. The stream in Oa watershed is perennial in its headwaters but infiltrates by the time it reaches the coast. Estimates of nutrient flux via SGD were appreciably greater than fluxes via baseflow for all study locations, despite the potential for over-estimating baseflow amounts. Nutrient fluxes via baseflow ranged between  $0.21 \pm 0.05$  to  $0.34 \pm 0.08$   $kg/d$  for both DIN and  $PO_4^{3-}$  (Table 4.4). Also note that uncertainty in baseflow quantities were assumed to be 25% of the documented values.

Table 4.3. Mean values and standard deviation in N-parameter values for both deployed and in situ algal samples.  $1\sigma$  standard deviations are provided in parentheses.

Location	Deployed mean $\delta^{15}N$	<i>In situ</i> - mean $\delta^{15}N$	Deployed mean N%	<i>In situ</i> - mean N%	n deployed	n <i>in situ</i>
Pala Lagoon	7.4 (0.1)	7.4 (1.3)	1.9 (0.3)	2.6 (1.2)	6	58
Faga’alu	8.6 (0.4)	8.6 (1.0)	1.9 (0.2)	2.6 (1.5)	9	29
Outer Faga’alu	9.6 (0.7)	9.6 (0.7)	2.0 (0.3)	4.1 (1.5)	3	9
Vatia	7.2 (1.0)	6.0 (1.1)	1.5 (0.2)	2.7 (1.4)	8	58
Oa	6.6 (0.2)	5.5 (0.6)	1.4 (0.2)	3.3 (1.6)	6	18

Table 4.4: Measured and estimated volumetric SGD and baseflow discharges, end member nutrient concentrations, and calculated nutrient loads, both absolute and area-scaled. Values in parentheses are 1 $\sigma$  standard deviations for end member values or are propagated uncertainties for calculated fluxes.

Parameter	Pala Lagoon	Faga'alu Bay	Vatia Bay	Oa Bay
<b>Water Fluxes [m<sup>3</sup>/d]</b>				
SGD - fresh fraction [m <sup>3</sup> /d]	68,482 (74,126)	7,270 (4,455)	4,428 (2,027)	2,258 (1,891)
SGD - recirculated [m <sup>3</sup> /d]	47,586 (51,508)	6,115 (3,746)	168 (77)	2,684 (2,248)
Estimated baseflow [m <sup>3</sup> /d]*	2,886 (722)	2,691 (673)	2,642 (661)	-
<b>Averaged End Member Nutrient Values [<math>\mu</math>mol/L]</b>				
SGD DIN [ $\mu$ mol/L]	47.3 (21.5)	16.0 (15.0)	17.5 (11.7)	6.07 (0.94)
SGD PO <sub>4</sub> <sup>3-</sup> [ $\mu$ mol/L]	1.63 (0.54)	4.7 (2.69)	5.1 (3.48)	1.99 (1.24)
Baseflow DIN [ $\mu$ mol/L]	8.40 (2.5)	8.8 (1.4)	7.7 (9.5)	**2.97 (1.63)
Baseflow PO <sub>4</sub> <sup>3-</sup> [ $\mu$ mol/L]	3.90 (0.6)	3.3 (2.0)	2.7 (0.5)	**5.00 (2.4)
<b>Nutrient Fluxes [kg/d]</b>				
DIN flux via SGD [kg-N/d]	76.9 (46.3)	3.00 (1.15)	1.13 (0.04)	0.42 (0.15)
PO <sub>4</sub> <sup>3-</sup> flux via SGD [kg-P/d]	5.88 (3.22)	1.98 (0.64)	0.71 (0.16)	0.30 (0.18)
DIN flux via baseflow [kg-N/d]	0.33 (0.18)	0.33 (0.17)	0.28 (0.33)	-
PO <sub>4</sub> <sup>3-</sup> flux via baseflow [kg-P/d]	0.34 (0.08)	0.27 (0.14)	0.21 (0.05)	-
<b>Nutrient Fluxes Scaled by Area [kg/d/ km<sup>2</sup>]</b>				
SGD DIN flux [kg-N/d/ km <sup>2</sup> ]	3.7 (3.7)	0.65 (0.46)	0.30 (0.01)	0.33 (0.27)
SGD PO <sub>4</sub> <sup>3-</sup> flux [kg-P/d/ km <sup>2</sup> ]	0.23 (0.26)	0.32 (0.26)	0.09 (0.04)	0.28 (0.32)
Baseflow DIN flux [kg-N/d/ km <sup>2</sup> ]	0.02 (0.01)	0.13 (0.06)	0.07 (0.09)	-
Baseflow PO <sub>4</sub> <sup>3-</sup> flux [kg-P/d/ km <sup>2</sup> ]	0.02 (0.00)	0.10 (0.05)	0.05 (0.01)	-
Watershed Area [km <sup>2</sup> ]	12.2	2.5	3.6	0.6

\* stream samples in Oa were taken above where the stream infiltrates

### 4.3.8 Validation of SGD Measurements

To validate calculated magnitudes of SGD for each study location, existing water budget studies were examined. Because few water budgets explicitly calculate SGD rate, the water-budget derived recharge components minus baseflow and groundwater extraction components were assumed to be representative of the fresh-SGD fractions. These fractions were then compared to the calculated fresh-SGD rates measured in this study. For the island of Tutuila, two documented whole-island water budget studies were found, Eyre and Walker and Walters [63,64], and one that only covered Western Tutuila Izuka et al. [46,65] was found. Because

results from each study were presented in different formats (basin totalization, raster, and vector polygon, respectively), the output of each was converted into a standardized format for comparison with this study. Water budget results from Izuka et al. and Walters were converted into the basin totalization format of Eyre and Walker by summing the total water volumes for each component within the boundaries of each study watershed.

Expected SGD rates within each of the four watersheds were calculated as a function of water-budget derived recharge rate, minus the total watershed groundwater extraction rate, and stream baseflow rate estimate (Table 4.5). Locations and magnitudes of groundwater pumping were provided by the American Samoa Power Authority (ASPA) and baseflow rates from section 3.7 were used. While expected water-budget SGD estimates are subject to the uncertainties implicit in the approaches used in their calculation, each falls somewhere within or near the uncertainty bounds on <sup>222</sup>Rn based SGD measurements. Note that the Izuka et al. study area only covered Pala Lagoon, thus these results are not included in Table 4.5. The Izuka et al. recharge for the Pala Watershed was 108,746 m<sup>3</sup>/d and the expected SGD was 90,352 m<sup>3</sup>/d.

Table 4.5: Comparison of measured fresh- SGD rates from this study to expected SGD amounts determined from previously developed water budget studies by Walters (2013) and Eyre and Walker (1991), shortened to (Eyre..., 1991) in table heading.

Site	Estimated baseflow [m <sup>3</sup> /d]*	Well extraction [m <sup>3</sup> /d]	Recharge from water budgets [m <sup>3</sup> /d]		SGD from water budgets [m <sup>3</sup> /d]		Measured fresh- SGD [m <sup>3</sup> /d] (this study)
			(Walters, 2013)	(Eyre, 1991)	(Walters, 2013)	(Eyre..., 1991)	
<b>Pala Lagoon</b>	2,886	15,508	68,362	71,139	49,968	52,744	68,482 (74,126)
<b>Faga'alu</b>	2,691	131	13,669	7,570	10,847	4,748	7,270 (4,455)
<b>Vatia</b>	2,642	256	13,978	8,327	11,080	5,429	4,428 (2,027)
<b>Oa</b>	-	-	2,059	2,650	2,059	2,650	2,258 (1,891)

## 4.4. Discussion

Land use and hydrogeology both act as important controls on coastal water quality and terrestrial nutrient delivery in tropical oceanic island settings. At all of the studied locations, SGD is a major pathway for anthropogenic as well as naturally derived nutrients discharging to coastal waters. This is not surprising as studies on other Pacific Islands and even on a global scale have found SGD rates to be comparable to anywhere between 10 % and 1600 % of riverine water fluxes [13,66,67]. In all four locations studied on Tutuila, SGD rates were significantly higher than baseflow rates, as indicated by streamflow estimates by Wong [58]. Trends in island wide nutrient loading followed levels of expected human impact in each watershed, whereas fluxes of N and P were highest in the Pala watershed and lowest in Oa, with Faga'alu and Vatia in between. In the three inhabited study watersheds, elevated  $\delta^{15}\text{N}$  values in coastal groundwater, and onshore-offshore trends in algal and coastal water samples indicated wastewater or manure is likely to be a major source of coastal N in these areas. Additionally, high intra-location variation in water quality and algal parameters indicated the spatial distribution of nutrient loading is affected by heterogeneity in N-source locations and in subsurface flow paths, at remarkably fine scales.

### 4.4.1 Nutrient Levels in Coastal Management Context

While absolute magnitudes of nutrient concentrations found in Tutuila's coastal waters were relatively low when compared to other islands where waste-water injection wells or commercial-scale agricultural applications are present [11,30], observed N and P concentrations frequently exceeded local and federal water quality regulatory standards set for these environments. The American Samoa Water Quality Standards (ASWQS) were established by an AS-EPA [68] administrative ruling, which specifies coastal waters with median concentrations of TDN and total dissolved phosphorus (TDP) exceeding 10.7 and 0.65  $\mu\text{mol/L}$ , respectively, are in violation. Similarly, the National Coastal Assessment (NCA) Program of the U.S. EPA has established nutrient level "cutpoints" for assessing the condition of U.S. coastal resources, whereas tropical-coastal surface waters with DIN and  $\text{PO}_4^{3-}$  concentrations greater than 3.6 and 0.32  $\mu\text{mol/L}$ , respectively are considered to be in "poor" condition [69].

If all coastal water samples from this study are pooled, they exceeded NCA "poor condition" cutpoints for DIN and  $\text{PO}_4^{3-}$  17% and 55% of the time, respectively, and they exceeded the ASWQS for TDN and TDP 13% and at least 25% of the time, respectively (Table 4.6). Although the highest proportion of exceedances occurred in Pala Lagoon, it is also interesting to note that the NCA cutpoints for DIN and  $\text{PO}_4^{3-}$  were also exceeded 6 % and 18 % of the time respectively, in Oa Bay. While there is potential for sample location bias as sampling for this study was not spatially randomized, these data reveal that none of the study locations had water quality that always conformed to accepted standards, suggesting there are specific areas, or hotspots, within each location where nutrient input is concentrated to a level that is

worth management attention and continued study. On the other hand, observed NCA cutpoint exceedances in the pristine Oa location, may imply these particular standards simply need to be reviewed and revised.

Table 4.6: American Samoa water quality standards and NCA cutpoints defining “poor” water quality, with percentages of exceedance observed in coastal water samples from the four study locations, and aggregated for all locations.

Regulatory standard	US-EPA-NCA Cutpoints		AS-Water Quality Standards	
	DIN [ $\mu\text{mol/L}$ ]	$\text{PO}_4^{3-}$ [ $\mu\text{mol/L}$ ]	TDN [ $\mu\text{mol/L}$ ]	TP [ $\mu\text{mol/L}$ ]
Nutrient Value	> 3.6	> 0.32	> 10.7	> 0.64
Location	Percent of samples exceeding standard			
Pala Lagoon	33%	90%	33%	33%
Faga’alu Bay	23%	65%	12%	42%
Vatia Bay	4%	42%	8%	8%
Oa Bay	6%	18%	0%	12%
<b>All samples</b>	<b>17%</b>	<b>55%</b>	<b>13%</b>	<b>25%</b>

#### 4.4.2 Comparison of Watersheds Along an Expected Land Use Gradient

With increasing urbanization, coastal ecosystems on oceanic islands have become vulnerable to land-based nutrient loading, which causes stress to and ultimately can change benthic community composition [1,70,2,8]. Even in this relatively isolated Pacific island archipelago, the complex issues of island geology, hydrology and vulnerabilities from land-based sources of nutrients have led to significant gradients in impact.

##### 4.4.2.1 Highly Impacted

Pala Lagoon was expected to be the most impacted study location. Not surprisingly, the watershed’s combination of high population density, large area, and extremely permeable underlying bedrock contributed to the highest SGD flux and SGD-derived nutrient loading rates found in this study. Nutrient concentrations in Pala Lagoon’s CGW were high, likely due to both upgradient land use and limited nutrient attenuation through the conductive bedrock. This nutrient rich SGD, discharging from prevalent coastal springs along the western shoreline, appeared to drive a strong onshore-offshore nutrient gradient. Higher N and P concentrations and  $\delta^{15}\text{N}$  values in water and algal tissues near the coastline were observed to decrease with distance towards the lagoon outlet where mixing with offshore waters, biological uptake by the Lagoon’s well populated benthic-macroalgal community, or both served to attenuate nutrients.

This onshore-offshore gradient in  $\delta^{15}\text{N}$  and N concentration is indicative of terrigenous-N inputs and is commonly found at locations where wastewater is discharged via SGD or surface waters to coastal ecosystems [19,12,8].

Almost all spring and stream samples in Pala Lagoon showed some enriched  $\delta^{15}\text{N}$  values, ranging from 7.2 to 9.2 ‰, with little co-enrichment in  $\delta^{18}\text{O}$  values, which indicates this enrichment is likely not the result of denitrification. This, in combination with Pala Lagoon's high DIN flux indicates wastewater or manure sources within the watershed are the main sources of DIN, a conclusion that is also supported by land-use data. Although a municipal wastewater collection system exists in the Tafuna area, many households are likely not connected to it and thus still rely on OSDS units [44,43]. This in combination with the region's highly permeable geologic substrate allows effluent from OSDS or piggeries to move rapidly through the subsurface, with limited time and surface area for nutrient attenuation, resulting in high-N loading along the coastline.

#### 4.4.2.2 Moderately Impacted

In contrast to the expected onshore-offshore gradient in  $\delta^{15}\text{N}$  values, Faga'alu bay displayed an opposite and enigmatic trend. Measurements from *in situ* algal tissues collected near the northern-outside point of Faga'alu Bay in 2015 lead to suspicions that the Utulei Wastewater Treatment Plant (WWTP) may be a source of high- $\delta^{15}\text{N}$  nitrogen to Pago Pago Harbor and the bay. This WWTP discharges primary-treated effluent directly into the harbor via an ocean outfall located about 0.5 km to the north of Faga'alu. In 2016, additional *in situ* algal tissues, three deployed *Hypnea* samples, and a water sample were collected at the Outer-Faga'alu location to investigate this hypothesis further. Algal tissue  $\delta^{15}\text{N}$  values from this location were consistently higher than  $\delta^{15}\text{N}$  values of algal tissues and water collected from the stream, well, and coastal groundwater in the Faga'alu study location, indicating detectable levels of N from WWTP effluent do affect algae and water in the vicinity of the ocean outfall. Although this point-source nutrient discharge is monitored and regulated by AS-EPA, it is unknown as to if the extent of its effects within Faga'alu Bay have yet been considered by coastal resource managers.

In Vatia, co-enrichment in DIN,  $\delta^{15}\text{N}$  and  $\delta^{18}\text{O}$  values from coastal water and coastal springs suggests partially-denitrified N is present, likely from an OSDS source. In the bay, coastal spring samples on the north side had 2-3 times the DIN, elevated  $\text{NH}_4^+$  and generally higher  $\delta^{15}\text{N}$  values when compared to spring samples from the southern side of the bay; a trend that was consistent over the duration of this study. This geochemical signature is likely indicative of mixing with OSDS effluent, as there are number of homes served by OSDS within about 50 m of the northern coastline. In contrast, there are few homes upgradient of the more southerly Vatia springs, and these residences are all at least 150 m away from the coast. Coastal water samples in Vatia also showed high  $\delta^{15}\text{N}$  values in samples taken proximal to the northern

spring group, although these values were not observed along the central part of the bay front, which also faced many homes with OSDS units. The highest algal and water sample  $\delta^{15}\text{N}$  values observed in Vatia were found repeatedly in a single area of SGD discharge, and adjacent samples did not appear to be geochemically similar. This illustrates the potential for small-scale heterogeneity in subsurface flow paths or variability in source proximity to affect the geochemistry of SGD.

Estimates of nutrient loading to Faga'alu and Vatia Bays were similar with Faga'alu having about twice the nutrient loading as Vatia. This might be expected as Faga'alu has about twice population and developed land as Vatia. However, the population density of Faga'alu is over three times that of Vatia, and the natural land-use proportions of each watershed are fairly similar (Table 4.1). Therefore, it is likely that other factors also influence nutrient loading in these watersheds. An interesting difference between the two watersheds is the presence of a wastewater collection system that serves a portion of the residents in Faga'alu. According to self-reported 2010 U.S. Census information [44], of the 169 reported households in Faga'alu Village, 117 reported being connected to a public sewer and only 52 reported using an OSDS. Vatia in contrast, has no public sewer infrastructure, therefore all residents likely use some type of OSDS. This suggests that a number of the residents in Faga'alu are not contributing wastewater effluent to the watershed and therefore their impact is significantly reduced, which may help to explain why nutrient loading in Faga'alu is not larger than observed.

Another factor that may increase the impact of OSDS in Vatia village is the distribution of development. Many homes in Faga'alu are located up the valley whereas most of the residences in Vatia are located close to the shore. To quantify this idea, building location data were obtained from the American Samoa Department of Commerce [71], and the distribution of all buildings within Pala, Faga'alu, and Vatia Watersheds were calculated as a function of their straight-line distance to the coastline (Figure 4.9). The median distance from the coast for structures in Vatia is 87 m, whereas in Faga'alu and Pala Watershed median values for building distance from the coast are 152 and 1300 m, respectively. Because longer subsurface travel distance may provide increased time for attenuation reactions for nutrients (e.g. denitrification and sorption) the overall distance CGW travels between N-sources and the coast likely plays a role in final SGD nutrient compositions.

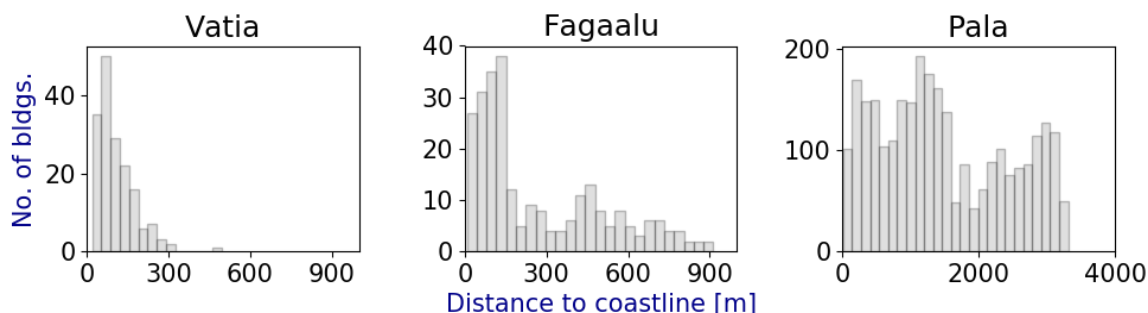


Figure 4.9: Histograms showing the distribution of straight-line distances from each building within the developed study watersheds to the nearest portion of the coastline.

#### 4.4.2.3 Least Impacted

Geochemical parameters observed in Oa Watershed were interpreted as reference values, reflecting the nutrient signature for pristine, unimpacted land use. Spring and stream samples from, Oa Watershed, had  $\delta^{15}\text{N}$  values within 4.4 to 6.9 ‰, indicating the expected range of source water  $\delta^{15}\text{N}$  lacking any anthropogenic impacts. Coastal waters in Oa generally reflected this  $\delta^{15}\text{N}$  signature, with the three of the four coastal samples that had enough N+N for analysis showing values of 6.2 to 6.9 ‰, and with one enigmatic sample located on the eastern edge of the bay that had a  $\delta^{15}\text{N}$  value of 8.5 ‰. The  $\delta^{15}\text{N}$  values of *C. fastigata* collected from Oa were generally within the upper range of values reported for this species located in other lightly impacted/pristine regions of American Samoa [35]. Calculated nutrient loads to Oa Bay were significantly lower than in other watersheds, which is a factor of both low concentrations of N in CGW and the watershed's small size (Table 4.4).

Although Oa Bay typically had lower DIN and  $\delta^{15}\text{N}$  values, area scaled  $\text{PO}_4^{3-}$  loading in Oa was found to be the second highest of the four studied watersheds. This relatively high  $\text{PO}_4^{3-}$  loading in a pristine location, as well as a general lack of correlation between  $\text{PO}_4^{3-}$  and expected land-use impact in the other watersheds, suggests that coastal P loading on Tutuila is likely to be controlled by factors other than land use. Across the four study locations, levels of phosphorus in most sample types appeared to be fairly consistent, yet were often high in comparison to national and local standards and cutpoints. Cho [67] approximates the global average P concentration in SGD to be around 0.75  $\mu\text{mol/L}$ , whereas the average P concentrations observed in unmixed coastal spring samples from this study was 2.3  $\mu\text{mol/L}$ . This apparent P surplus in Tutuila's waters may be attributed in part to natural weathering of volcanic rock. The oceanic basalts from which Tutuila is constructed contain amounts of phosphorus that are up to three-times higher than in continental rocks [72], and as this rock is weathered and dissolved by groundwater, high concentrations of TDP are able to leach out [69]. Chadwick et al. [73] suggests that higher P concentrations are found in younger Hawaiian soils, and these can be mobilized into groundwater and baseflow by erosion and weathering [74]. In terms of coastal ecosystem health, naturally high phosphate levels in themselves may not be

concerning; however, this does suggest that Tutuila's coastal waters are likely to be N, rather than P limited. Therefore, even small additions of N from anthropogenic sources into these environments could start to change species composition; excess N-loading could stimulate excessive algal growth and possible eutrophication more easily than if the system was P limited.

#### **4.4.3 Management Considerations and Future Directions**

Groundwater inputs can strongly influence watershed nutrient loading and cause impacts to coastal ecosystem health. In all four of this study's watersheds, calculated daily nutrient loads from SGD during the 2015 study period were significantly greater than loads from baseflow-stage stream inputs, underscoring the need to consider coastal groundwater quality in addition to surface water quality when undertaking management actions. Additionally, it is likely that there is significant interaction between coastal groundwater and stream baseflow in these watersheds, again showing the need for management of groundwater quality, as it directly affects surface-water quality. Future approaches to coastal land management and development would benefit from considering how changes in land use impact the quality of coastal groundwater, surface water, and therefore, nearshore reef health.

In Pala Lagoon and Vatia Bay, elevated N concentrations and  $\delta^{15}\text{N}$  values in both water and algal tissue suggest discharging N in these areas is primarily derived from a wastewater or manure source. This conclusion is also supported by the work of Shuler et al. [43] where it was found that OSDS sourced wastewater was the predominant N source to the aquifer underlying the Tafuna Plain. Detectable impact of wastewater on the coastal environment in these embayments is a strong motivation for the development of new wastewater collection systems or expansion of existing systems. On the other hand, elevated  $\delta^{15}\text{N}$  values observed within Faga'alu bay and adjacent to the Utulei WWTP warrant further investigation of this facility as a source of N to surrounding coastal and harbor areas.

Of equal concern to nutrient perturbation of coastal ecosystems is the potential risk of illness due to wastewater effluent from both WWTPs and OSDS units in American Samoa. The American Samoa EPA performs a limited amount of recreational water sampling for fecal indicator bacteria (FIB) and posts public warning signs about the risk of illness from swimming at local beaches [41]. However, the sources of FIB and the relationship of bacteria concentrations to physical conditions remain largely unknown. Future studies using a combination of the methods used in this study and DNA-derived source tracking could provide clarity on major waste/bacterial sources across small spatial scales. Although a handful of recent SGD investigations included a biotic component, there is a relative lack of knowledge regarding the effects of SGD on marine ecosystems and humans that use them. As concluded in a recent review by Lecher and Mackey [75], there are currently few studies that focus on the impact of groundwater at an ecosystem level, yet these were found to be the most insightful.

## 4.5. Conclusions

The results of this work suggest that on Tutuila, SGD is a major pathway for anthropogenic-nutrients discharging to coastal waters. Calculated nutrient loads from SGD in all four study watersheds were significantly greater than loads from baseflow-stage stream inputs. On an island wide scale, trends in nutrient loading followed levels of expected human impact in each watershed, whereas total N and P fluxes were both highest in the Pala Watershed and lowest in Oa Watershed, with Faga'alu and Vatia in between. Concentrations of coastal water DIN correlated well with land use impact, while concentrations of  $\text{PO}_4^{3-}$  did not. This suggests that DIN is a reliable indicator of anthropogenic impact to coastal areas and that phosphorus dynamics are probably more complicated and controlled by other factors including geology. Algal bioassays closely reflected the N content of Tutuila's coastal waters with deployed and *in-situ* algal bioassays showing very similar results. Use of macroalgae as a water quality proxy is a relatively inexpensive assessment that produces time-integrated information at relatively fine spatial scales. Similar magnitudes of nutrient loading in Faga'alu and Vatia Watersheds suggests that population or land-use fractions alone are probably not sufficient for accurately predicting anthropogenic impact on coastal areas. Instead, direct impacts from OSDS, livestock, and agricultural applications should also be considered when estimating nutrient impacts to coastal settings. All four study locations showed some exceedances in either local or federal water quality standards, suggesting that additional management of nutrient discharge on Tutuila may be warranted.

## References: Chapter 4

1. McCook, L. J. Macroalgae, nutrients and phase shifts on coral reefs: scientific issues and management consequences for the Great Barrier Reef. *Coral reefs* **1999**, *18*, 357-367.
2. Morton, S. L.; Shuler, A.; Paternoster, J.; Fanolua, S.; Vargo, D. Coastal eutrophication, land use changes and *Ceratium furca* (Dinophyceae) blooms in Pago Pago Harbor, American Samoa 2007--2009. *Chinese Journal of Oceanology and Limnology* **2011**, *29*, 790-794.
3. Smith, S. V.; Kimmerer, W. J.; Laws, E. A.; Brock, R. E.; Walsh, T. W. Kaneohe Bay sewage diversion experiment: perspectives on ecosystem responses to nutritional perturbation. *Pacific Science* **1981**, *35*, 279-395.
4. Pendleton, L. H. Valuing coral reef protection. *Ocean & Coastal Management* **1995**, *26*, 119-131.
5. Van Beukering, P.; Cesar, H. S. J. Ecological economic modeling of coral reefs: Evaluating tourist overuse at Hanauma Bay and algae blooms at the Kihei Coast, Hawai'i. *Pacific Science* **2004**, *58*, 243-260.
6. Koop, K.; Booth, D.; Broadbent, A.; Brodie, J.; Bucher, D.; Capone, D.; Coll, J.; Dennison, W.; Erdmann, M.; Harrison, P.; others. ENCORE: the effect of nutrient enrichment on coral reefs. Synthesis of results and conclusions. *Marine pollution bulletin* **2001**, *42*, 91-120.
7. Dailer, M. L.; Ramey, H. L.; Saephan, S.; Smith, C. M. Algal  $\delta^{15}\text{N}$  values detect a wastewater effluent plume in nearshore and offshore surface waters and three-dimensionally model the plume across a coral reef on Maui, Hawai 'i, USA. *Marine pollution bulletin* **2012**, *64*, 207-213.
8. Amato, D. W.; Bishop, J. M.; Glenn, C. R.; Dulai, H.; Smith, C. M. Impact of submarine groundwater discharge on marine water quality and reef biota of Maui. *PloS one* **2016**, *11*, e0165825.
9. Van Houtan, K. S.; Hargrove, S. K.; Balazs, G. H. Land use, macroalgae, and a tumor-forming disease in marine turtles. *PLoS One* **2010**, *5*, e12900.
10. Van Houtan, K. S.; Smith, C. M.; Dailer, M. L.; Kawachi, M. Eutrophication and the dietary promotion of sea turtle tumors. *PeerJ* **2014**, *2*, e602.

11. Hunt, C. D.; Rosa, S. N. A multitracer approach to detecting wastewater plumes from municipal injection wells in nearshore marine waters at Kihei and Lahaina, Maui, Hawai'i. Final Report. Honolulu (HI): 2009. Report No.: 2009--5253. *US Geological Survey*. Accessed January 2009.
12. Dailer, M. L.; Knox, R. S.; Smith, J. E.; Napier, M.; Smith, C. M. Using  $\delta^{15}\text{N}$  values in algal tissue to map locations and potential sources of anthropogenic nutrient inputs on the island of Maui, Hawai'i, USA. *Marine Pollution Bulletin* 2010, 60, 655-671.
13. Glenn, C. R.; Whittier, R. B.; Dailer, M. L.; Dulaiova, H.; El-Kadi, A. I.; Fackrell, J.; Kelly, J. L.; Waters, C. A.; Sevadjan, J. Lahaina groundwater tracer study--Lahaina, Maui, Hawaii. 2013.
14. Redfield, A. C. On the proportions of organic derivatives in sea water and their relation to the composition of plankton. *James Johnstone memorial volume* 1934, 176-192.
15. Taiz, L.; Zeiger, E.; Moller; Murphy, A. *Plant physiology and development*; Sinauer Press, 2016.
16. Atkinson, M. J.; Smith, S. V. C. N: P ratios of benthic marine plants1. *Limnology and Oceanography* 1983, 28, 568-574.
17. Lobban, C. S.; Harrison., P. J. *Seaweed ecology and physiology*; Cambridge University Press, 1997; p 366.
18. Littler, M. M.; Littler, D. S. Factors controlling relative dominance of primary producers on biotic reefs. *Proceedings of the Fifth International Coral Reef Congress, Tahiti* 1985, 4, 35-39.
19. Costanzo, S. D.; Udy, J.; Longstaff, B.; Jones, A. Using nitrogen stable isotope ratios ( $\delta^{15}\text{N}$ ) of macroalgae to determine the effectiveness of sewage upgrades: changes in the extent of sewage plumes over four years in Moreton Bay, Australia. *Marine Pollution Bulletin* 2005, 51, 212-217.
20. Board, O. S.; Council, N. R.; others. *Clean coastal waters: understanding and reducing the effects of nutrient pollution*; National Academies Press, 2000.
21. Fabricius, K. E. Effects of terrestrial runoff on the ecology of corals and coral reefs: review and synthesis. *Marine pollution bulletin* 2005, 50, 125-146.
22. Hoover, D. J.; Mackenzie, F. T. Fluvial fluxes of water, suspended particulate matter, and nutrients and potential impacts on tropical coastal water biogeochemistry: Oahu, Hawai'i. *Aquatic Geochemistry* 2009, 15, 547-570.

23. Holst-Rice, S.; Messina, A.; Biggs, T.; Vargas-Angel, B.; Whittall, D. Baseline Assessment of Faga'alu Watershed: A Ridge to Reef Assessment in Support of Sediment Reduction Activities and Future Evaluation of their Success. *Silver Spring, MD: NOAA Coral Reef Conservation Program. NOAA Technical Memorandum CRCP* **2016**, 23, 44.
24. Messina, A. T. *Terrigenous sediment dynamics in a small, tropical, fringing-reef embayment*; Ph.D. dissertation; University of California, Santa Barbara, 2016.
25. D'elia, C. F.; Webb, K. L.; Porter, J. W. Nitrate-rich groundwater inputs to Discovery Bay, Jamaica: a significant source of N to local coral reefs? *Bulletin of Marine Science* **1981**, 31, 903-910.
26. Hunt Jr, C. D. *Ground-water nutrient flux to coastal waters and numerical simulation of wastewater injection at Kihei, Maui, Hawaii*; Tech. rep.; Geological Survey (US), 2007.
27. Moosdorf, N.; Stieglitz, T.; Waska, H.; Dürr, H. H.; Hartmann, J. Submarine groundwater discharge from tropical islands: a review. *Grundwasser* **2015**, 20, 53-67.
28. Burnett, W. C.; Dulaiova, H. Estimating the dynamics of groundwater input into the coastal zone via continuous radon-222 measurements. *Journal of environmental radioactivity* **2003**, 69, 21-35.
29. Burnett, W. C.; Aggarwal, P. K.; Aureli, A.; Bokuniewicz, H.; Cable, J. E.; Charette, M. A.; Kontar, E.; Krupa, S.; Kulkarni, K. M.; Loveless, A.; others. Quantifying submarine groundwater discharge in the coastal zone via multiple methods. *Science of the total Environment* **2006**, 367, 498-543.
30. Bishop, J. M.; Glenn, C. R.; Amato, D. W.; Dulai, H. Effect of land use and groundwater flow path on submarine groundwater discharge nutrient flux. *Journal of Hydrology: Regional Studies* **2017**, 11, 194-218.
31. Dulai, H.; Kleven, A.; Ruttenberg, K.; Briggs, R.; Thomas, F. Evaluation of Submarine Groundwater Discharge as a Coastal Nutrient Source and Its Role in Coastal Groundwater Quality and Quantity. In *Emerging Issues in Groundwater Resources*; Springer, 2016; pp 187-221.
32. Richardson, C. M.; Dulai, H.; Whittier, R. B. Sources and spatial variability of groundwater-delivered nutrients in Maunaloa Bay, O'ahu, Hawaii 'i. *Journal of Hydrology: Regional Studies* **2017**, 11, 178-193.

33. Kendall, C.; Aravena, R. Nitrate isotopes in groundwater systems. In *Environmental tracers in subsurface hydrology*; Springer, 2000; pp 261-297.
34. Cole, M. L.; Kroeger, K. D.; McClelland, J. W.; Valiela, I. Effects of watershed land use on nitrogen concentrations and  $\delta^{15}\text{N}$  nitrogen in groundwater. *Biogeochemistry* **2006**, *77*, 199-215.
35. Garrison, V.; Kroeger, K. D.; Fenner, D.; Craig, P. Identifying nutrient sources to three lagoons at Ofu and Olosega, American Samoa using  $\delta^{15}\text{N}$  of benthic macroalgae. **2007**.
36. Wong, W. W.; Grace, M. R.; Cartwright, I.; Cook, P. L. M. Sources and fate of nitrate in a groundwater-fed estuary elucidated using stable isotope ratios of nitrogen and oxygen. *Limnology and Oceanography* **2014**, *59*, 1493-1509.
37. Wiegner, T. N.; Mokiao-Lee, A. U.; Johnson, E. E. Identifying nitrogen sources to thermal tide pools in Kapoho, Hawai'i, USA, using a multi-stable isotope approach. *Marine pollution bulletin* **2016**, *103*, 63-71.
38. Houk, P.; Didonato, G.; Iguel, J.; Van Woelik, R. Assessing the effects of non-point source pollution on American Samoa's coral reef communities. *Environmental monitoring and assessment* **2005**, *107*, 11-27.
39. Polidoro, B. A.; Comeros-Raynal, M. T.; Cahill, T.; Clement, C. Land-based sources of marine pollution: Pesticides, PAHs and phthalates in coastal stream water, and heavy metals in coastal stream sediments in American Samoa. *Marine pollution bulletin* **2017**, *116*, 501-507.
40. Houk, P.; Benavente; Johnson, S. *Watershed-based coral reef monitoring across Tutuila, American Samoa: Summary of decadal trends and 2013 assessment*; Monitoring program partnership between the American Samoa Environmental Protection Agency, Pacific Marine Resources Institute, and the University of Guam Marine Laboratory, 2013.
41. AS-EPA-American Samoa Environmental Protection Agency. *Territory of American Samoa integrated water quality monitoring and assessment report*; AS-EPA--American Samoa Environmental Protection Agency, 2016, Accessed 31 October 2018.
42. Carpenter, C.; Jeffrey, S.; Overmars, M. Proceedings of the Pacific Regional Consultation on Water in Small Island Countries., 2002, Sigatoka, Fiji Islands, 29 July<sup>3</sup> August 2002.

43. Shuler, C. K.; El-Kadi, A. I.; Dulai, H.; Glenn, C. R.; Fackrell, J. Source partitioning of anthropogenic groundwater nitrogen in a mixed-use landscape, Tutuila, American Samoa. *Hydrogeology Journal* **2017**, *25*, 2419-2434.
44. AS-DOC - American Samoa Department of Commerce. *2013 Statistical Yearbook for American Samoa, AS-DOC report, Pago Pago, AS*; AS-DOC--American Samoa Department of Commerce, 2013, Cited 31 October 2013.
45. Stearns, H. T. Geology of the Samoan islands. *Bulletin of the Geological Society of America* **1944**, *55*, 1279-1332.
46. Izuka, S. K.; Perreault, J. A.; Presley, T. K. *Areas contributing recharge to wells in the Tafuna-Leone Plain, Tutuila, American Samoa, USGS report No. 2007-5167. Honolulu, HI*; Tech. rep.; Geological Survey (US), 2007.
47. DiDonato, G. T. Developing an initial watershed classification for American Samoa. *Report from the American Samoa Environmental Protection Agency, Pago Pago, American Samoa* **2004**.
48. PIFSC-Pacific Islands Fisheries Science Center. *Benthic Surveys in Vatia, American Samoa since 2015: benthic images collected during belt transect surveys in 2015 from 2010-06-15 to 2010-08-15*; NOAA National Centers for Environmental Information, 2018.
49. Meyer, R. A.; Seamon, J. O.; Fa'aumu, S.; Lalogaufua, L. *Classification and Mapping of Wildlife Habitats in American Samoa: An object-based approach using high resolution orthoimagery and LIDAR remote sensing data*; 2016, Report in preparation for American Samoa Department of Marine and Wildlife Resources.
50. Sigman, D. M.; Casciotti, K. L.; Andreani, M.; Barford, C.; Galanter, M. B. J. K.; Böhlke, J. K. A bacterial method for the nitrogen isotopic analysis of nitrate in seawater and freshwater. *Analytical chemistry* **2001**, *73*, 4145-4153.
51. Tukey, J. W. Comparing individual means in the analysis of variance. *Biometrics* **1949**, *99*-114.
52. Dulaiova, H.; Camilli, R.; Henderson, P. B.; Charette, M. A. Coupled radon, methane and nitrate sensors for large-scale assessment of groundwater discharge and non-point source pollution to coastal waters. *Journal of Environmental Radioactivity* **2010**, *101*, 553-563.

53. Kelly, J. L. *Identification and quantification of submarine groundwater discharge in the Hawaiian Islands*; Ph.D. dissertation; [Honolulu]:[ University of Hawai'i at Mānoa],[August 2012], 2012.
54. Street, J. H.; Knee, K. L.; Grossman, E. E.; Paytan, A. Submarine groundwater discharge and nutrient addition to the coastal zone and coral reefs of leeward Hawai'i. *Marine Chemistry* **2008**, *109*, 355-376.
55. Fröllje, H.; Pahnke, K.; Schnetger, B.; Brumsack, H.-J.; Dulai, H.; Fitzsimmons, J. N. Hawaiian imprint on dissolved Nd and Ra isotopes and rare earth elements in the central North Pacific: local survey and seasonal variability. *Geochimica et Cosmochimica Acta* **2016**, *189*, 110-131.
56. Storlazzi, C.; Cheriton, O.; Rosenberger, K.; Logan, J.; Clark, T. B. *Coastal Circulation and Water-Column Properties in the National Park of American Samoa, February--July 2015*; Tech. rep.; US Geological Survey, 2017.
57. Vetter, O.; Vargas-Ángel, B. CRCP Project # 417 : Inter-disciplinary study of flow dynamics and sedimentation effects on coral colonies in Faga'alu Bay, American Samoa: oceanographic investigation summary. Pago Pago. **2013**.
58. Wong, M. F. *Analysis of streamflow characteristics for streams on the island of Tutuila, American Samoa*; US Geological Survey Water Resources Investigations Report No. 95-4185, 1996.
59. Abaya, L. M.; Wiegner, T. N.; Beets, J. P.; Colbert, S. L.; Kaile'a, M. C.; Kramer, K. L. Spatial distribution of sewage pollution on a Hawaiian coral reef. *Marine pollution bulletin* **2018**, *130*, 335-347.
60. Abaya, L. M.; Wiegner, T. N.; Colbert, S. L.; Beets, J. P.; Kaile'a, M. C.; Kramer, K. L.; Most, R.; Couch, C. S. A multi-indicator approach for identifying shoreline sewage pollution hotspots adjacent to coral reefs. *Marine pollution bulletin* **2018**, *129*, 70-80.
61. Rogers, K. M.; Nicolini, E.; Gauthier, V. Identifying source and formation altitudes of nitrates in drinking water from Réunion Island, France, using a multi-isotopic approach. *Journal of contaminant hydrology* **2012**, *138*, 93-103.
62. Bassiouni, M.; Oki, D. S. Trends and shifts in streamflow in Hawai 'i, 1913--2008. *Hydrological Processes* **2013**, *27*, 1484-1500.
63. Eyre, P.; Walker, G. *Geology and ground-water resources of Tutuila American Samoa*; Unpublished report in American Samoa Power Authority files, 1991.

64. Walters, M. O. *Documentation of Wellhead Analysis, Tutuila Hydrogeological Analysis for the U.S. EPA Clean Water Act – State Revolving Fund ASPA Consolidated Grant for the benefit of the Territory of American Samoa*; American Samoa Power Authority (ASPA), 2013, Report prepared for American Samoa Power Authority, Pago Pago, American Samoa.
65. Perreault, J. A. *Development of a water budget in a tropical setting accounting for mountain front recharge*; Master's thesis; UNIVERSITY OF HAWAII „I, 2010.
66. Rodellas, V.; Garcia-Orellana, J.; Masqué, P.; Feldman, M.; Weinstein, Y. Submarine groundwater discharge as a major source of nutrients to the Mediterranean Sea. *Proceedings of the National Academy of Sciences* **2015**, 201419049.
67. Cho, H.-M.; Kim, G.; Kwon, E. Y.; Moosdorf, N.; Garcia-Orellana, J.; Santos, I. R. Radium tracing nutrient inputs through submarine groundwater discharge in the global ocean. *Scientific reports* **2018**, 8, 2439.
68. AS-EPA - American Samoa Environmental Protection Agency. *American Samoa Water Quality Standards; 2013 Revision Administrative Rule No. 001-2013*; AS-EPA--American Samoa Environmental Protection Agency, 2013, Pago Pago, AS.
69. NES - Nimbus Environmental Services. *US EPA National Coastal Assessment 2010 American Samoa Reef Flats Project Report*; Tech. rep.; Report prepared for the American Samoa Environmental Protection Agency, 2012.
70. Smith, J. E.; Hunter, C. L.; Smith, C. M. The effects of top--down versus bottom--up control on benthic coral reef community structure. *Oecologia* **2010**, 163, 497-507.
71. AS-DOC - American Samoa Department of Commerce. *Buildings Shapefile*; AS-DOC--American Samoa Department of Commerce, 2009, Pago Pago, AS.
72. Certini, G. *Soils, Basic Concepts and Future Challenges*; Oxford University Press, 2006; p 328.
73. Chadwick, O. A.; Derry, L. A.; Vitousek, P. M.; Huebert, B. J.; Hedin, L. O. Changing sources of nutrients during four million years of ecosystem development. *Nature* **1999**, 397, 491.
74. Vitousek, P.; Chadwick, O.; Matson, P.; Allison, S.; Derry, L.; Kettleby, L.; Luers, A.; Mecking, E.; Monastera, V.; Porder, S. Erosion and the rejuvenation of weathering-derived nutrient supply in an old tropical landscape. *Ecosystems* **2003**, 6, 762-772.
75. Lecher, A.; Mackey, K. Synthesizing the Effects of Submarine Groundwater Discharge on Marine Biota. *Hydrology* **2018**, 5, 60.

76. Garrison, G. H.; Glenn, C. R.; McMurtry, G. M. Measurement of submarine groundwater discharge in Kahana Bay, O'ahu, Hawai'i. *Limnology and Oceanography* **2003**, *48*, 920-928.

## Chapter 5:

# Groundwater Recharge for Tutuila, American Samoa Under Current and Projected Climate as Estimated with SWB2, a Soil Water Balance Model

### **Abstract**

Groundwater is the primary water source on the island Tutuila in American Samoa, and accurate quantification of groundwater availability is essential for well-informed management of this limited resource. A water budget approach using SWB2, a soil water-balance model was applied to Tutuila with the primary objective of calculating spatially and temporally distributed net-infiltration, which directly controls groundwater recharge rate. Other water budget components such as evapotranspiration, canopy interception, runoff, and mountain front recharge were also quantified with the SWB2 model for average present-day climate conditions. Additionally, the potential effects of future climate change on water resources availability were simulated by integrating dynamically downscaled climate predictions for 2080 to 2099 derived from externally supplied global climate model results. Notable improvements in this model over previously developed water budget models for Tutuila include flow-routing based on land topography, inclusion of the mountain front recharge process, and consideration of direct net infiltration from anthropogenic sources such as on-site wastewater units and leaking water delivery lines. Model results indicated approximately 54% of Tutuila's rainfall infiltrates as groundwater recharge, 8% is lost to canopy evaporation, another 15% is lost to evapotranspiration from soils, and 21% is removed through surface-water features as stormflow-runoff. The model was able to simulate these processes with a high-spatial and temporal resolution with a 20 by 20 m grid-cell size, and a daily-resolution output time step. Climate scenarios suggested an increase in net-infiltration of 17 to 27% might be expected by the end of the century depending on the emissions scenario used.

## 5.1 Introduction

The island of Tutuila in the Territory of American Samoa relies on a limited groundwater supply for almost all of its water needs. In island settings, precipitation rates fundamentally constrain the availability of water. However, for all practical purposes, it is the partitioning of rainfall into different terrestrial reservoirs, along with aquifer storage capacity, that ultimately determines the amount of water accessible for human use. It is this subject, and specifically the quantification of groundwater recharge, that is the primary focus of this report. Accurate assessment of groundwater availability is often limited by uncertainty in the magnitude of recharge, because many critical processes influencing recharge are difficult if not impossible to directly measure. Commonly used approaches for recharge quantification range from simple analytical-regression equations where only limited input data is available (Shade and Nichols, 1996), to highly parameterized watershed models, such as the Soil and Water Assessment Tool (SWAT), which typically require more input data than is often available on regional scales (Arnold et al., 1994). For many applications, mass-balance based water budget models are frequently used to assess recharge and other water budget components on regional, or in this case, island wide scales. Quantitative water-budget models are valuable tools for accomplishing numerous water resource-management goals, including:

- Assessment of surface water availability
- Parameterization of groundwater models, which themselves can be applied in estimating groundwater availability
- Estimation of Submarine Groundwater Discharge (SGD) rates
- Assessing water quality and contaminant transport
- Integrated management of surface and groundwater resources
- Assessing floods and evaluating flooding potential

The water budget method allows integration of long-term climate data with geospatial information to address the high-spatial and temporal variability inherent in precipitation and other hydrologic processes found on steep tropical islands. Because groundwater recharge is typically the most difficult water budget component to directly measure, it is often calculated as a residual term after other significant components are subtracted from a metered amount of precipitation. In a simplified form, this approach was formulated by Thornthwaite and Mather (1955) as:

$$\text{Recharge} = \text{Rainfall} - \text{Runoff} - \text{Actual Evapotranspiration}$$

If it is determined that other inputs or losses, such as irrigation, streamflow infiltration, leaking water delivery lines, or leachate from septic systems are significant, these components can also be included to increase model accuracy. Recent examples of study locales in the Pacific where similar water budget methodologies have been applied include the Hawaiian Islands (Izuka et al., 2016), Guam (Johnson, 2012), and Jeju Island (Mair et al., 2013).

The primary objective for this study is to apply the Soil Water Balance 2 (SWB2) Model (Westenbroek et al., 2018) to create spatially distributed estimates of water balance components on Tutuila with a particular emphasis on groundwater recharge. These estimates are useful for assessing the availability of both groundwater and surface water resources. On Tutuila Island, only three previously documented recharge estimates have been found. These were developed by Eyre and Walker (1991), Izuka et al. (2007), and ASPA (2013). Of the three estimates only one, Izuka et al. (2007), is in a widely available published format, whereas the Eyre and Walker and ASPA water budgets are contained in internal reports, which reside at the ASPA headquarters in Tafuna, American Samoa. These estimates vary in methodology and accuracy of their input datasets, but all generally consider similar water budget components including precipitation, evapotranspiration, runoff, and streamflow infiltration to calculate recharge. However, none of these estimates have attempted to include the effects of leaking water lines or discharge from On-Site wastewater Disposal Systems (OSDS), both of which have the potential to influence localized water budgets significantly.

The first SWB model was originally developed by the U.S. Geological Survey (USGS) Wisconsin Water Science Center in 2010 and is based on a modified Thornthwaite-Mather soil-water balance approach. The SWB2 model is an updated form of the original SWB model with new methods of built in calculation, some of which include functionality from the Hawaii Water Balance Code (Izuka et al., 2010), thereby making it particularly suitable to modeling sites on tropical basaltic islands, such as Tutuila. Water balance components within the model are calculated at a daily-time resolution, and can be averaged into monthly or annual time steps. The model uses a rectangular grid to represent the spatial distribution of variability within the model domain, and the grid resolution can be modified to any desired size based on the resolution of input datasets. Westenbroek et al. (2018) provides detailed information regarding construction and use of the SWB2 model.

While the SWB2 model is applicable in a wide range of climatic and environmental conditions, it features a number of modified methods that are specifically intended to accurately represent hydrologic processes on tropical islands. These include the substitution of monthly runoff coefficients for curve-number generated estimates of runoff, use of Gash canopy interception in place of the bucket method, and modifications to land-use classification parameters that allow modeling of unique environments such as cloud forests. A type example application of the model on the Hawaiian island of Maui was developed for presentation in the SWB2 documentation (Westenbroek et al., 2018), and this example was used as a general guide in the selection of methods for the Tutuila model due to the similar geographic, geologic, and climatic attributes of these tropical island settings.

Datasets specific to the Tutuila model included:

- Gridded monthly precipitation data
- Precipitation gauge data used to represent temporal rainfall distributions
- Land use data
- Impervious surface ratios
- Canopy coverage ratios
- Soil type data consistent with the NRCS SSURGO database
- Geospatial data to represent direct infiltration from municipal water line leaks
- Geospatial data to represent direct infiltration from OSDS effluent discharge
- Watershed runoff-to-rainfall ratios, both measured and interpolated
- Potential evapotranspiration data in monthly gridded format
- Canopy evaporation data
- Gridded monthly maximum and minimum temperature data
- Mountain front recharge information

Details regarding sources and processing of each input dataset are provided in the sections below.

### 5.1.1 Study Area

The island of Tutuila (Fig. 5.1), located near 14° S and 170° W, is the main population center of American Samoa, and at 142 km<sup>2</sup> is the third largest island in the Samoan hot-spot island chain. Due to its position within the South Pacific Convergence Zone, the island experiences abundant year round rainfall, with increased precipitation amounts from October to May during the wetter season. Monthly average rainfalls in the wet season are roughly twice that of the dry season's still significant rainfall amounts. Rainfall varies considerably with location and elevation and ranges between 70 in./yr. near the Tafuna Airport up to more than 200 in./yr. along the crest of the highest mountains (NWS, 2000). Strong tropical storms and hurricanes also influence the region about once every other year, and an average of 25 to 30 significant thunderstorms affect the island annually (Kennedy et al., 1987). Tutuila consists of two distinct regions: The Tafuna-Leone Plain, a highly-permeable rejuvenated-phase lava delta, which due to its low slope contains concentrated human development; and a mountainous assemblage of Pleistocene age shield volcanoes that make up the bulk of the island and generally consist of lower-permeability rock. (Stearns, 1944).

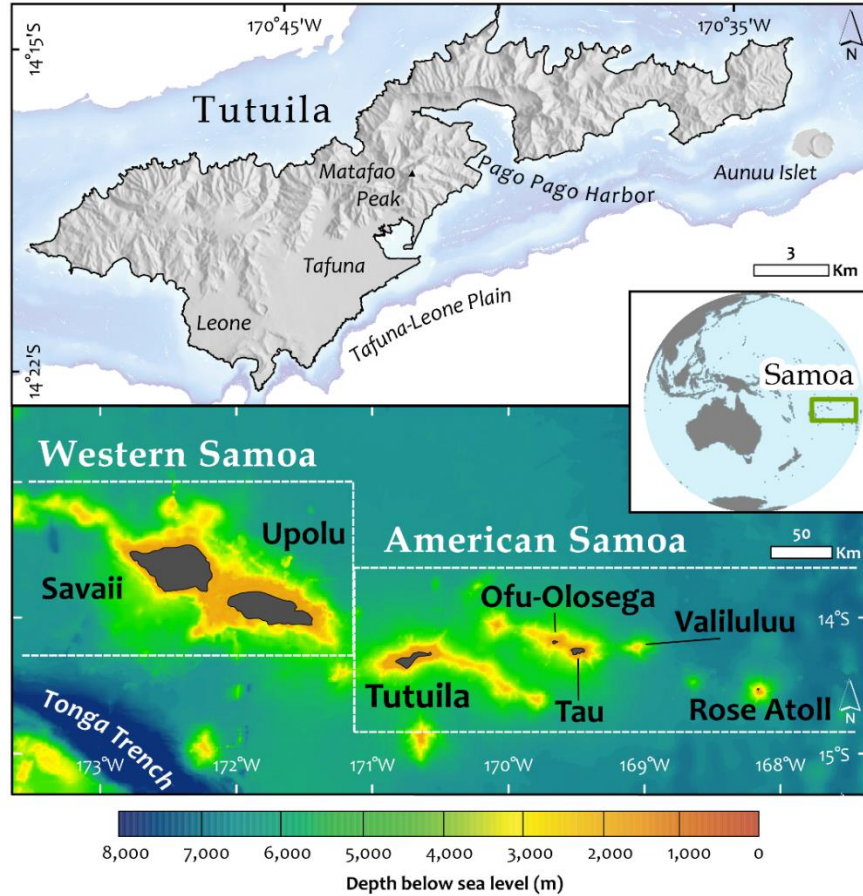


Figure 5.1: Map of Tutuila island (top) and bathymetric map of Samoan archipelago (bottom). Divisions between Western and American Samoa are drawn to mmshow political jurisdictions and do not constitute actual territorial boundaries. Regional location map shown in center-right inset.

## 5.2 Methods

Compiling and formatting input datasets comprised the bulk of model set up efforts. Except for a portion of the runoff-to-rainfall ratios and rainfall fragment sets, all input datasets used for this model were obtained from existing publications or databases, the details of each having been documented in the respective references cited in this report. Input data for determining rainfall timing and runoff-to-rainfall ratios were compiled from a combination of published and new rainfall and streamflow data collected specifically for use in this work. Where model parameters relating to hydrologic behavior throughout the different land-use and soil zones, specific to American Samoa were not available, the parameters from the Maui Case study were used as, the Hawaiian Islands were considered to be the closest available approximation for Tutuila's soils and land-cover. This approximation was justified because the islands of the Samoan and the Hawaiian island chains are affected by similar climatic patterns as they are both located in the tropics. American Samoa's climate differs from Hawaii in that it is situated closer to the equator and is more affected by the inter-tropical convergence zone.

However, both archipelagos share similar seasonality, steep rainfall gradients, tropical-forested land-cover, and geologic construction.

However, there remains the need for collection of new hydrologic and ecologic data to validate this approximation. The SWB2 model requires all spatially distributed input files to be in the ESRI ascii grid format, and for consistency, all input grids were pre-processed to have consistent boundaries and a 20 m cell-size. The model was run for a period of 10 years in order to average away any potential bias from the default initial soil-moisture conditions.

The SWB2 model runs on a daily time-step, and because of this it is preferred to use gridded daily precipitation data as rainfall input as this yields the most accurate results even when calculating water balance components on monthly or annual scales. However, because these data are not available at sufficient resolution for Tutuila, this application of SWB2 uses a stochastic approach, i.e., the Method of Fragments (described below), to synthesize daily-resolution precipitation data from available monthly precipitation data representing 30-year averages from 1971 to 2000. Rainfall pattern information from rain gauge data spanning the period 1955 to 2018 and streamflow data from 1958 to 2018 used for runoff calculations were also incorporated as model input data. Therefore, this model is rooted in steady-state paradigm, whereas model outputs do not necessarily reflect conditions on any particular day or month, but instead represent average conditions over long-term scales.

It should here be noted that groundwater recharge is defined as water that actually reaches the water table, whereas water-budget and watershed models typically calculate net-infiltration, defined as water that percolates below the root zone. Because vadose zone processes were not modeled as part of this work, it is possible that net-infiltration and groundwater recharge are not strictly equivalent. However, this possibility is typically ignored in basaltic island settings (Engott et al., 2015) because generally high hydraulic conductivities transport water quickly enough to avoid significant evaporative effects within the unsaturated zone. Although the term net-infiltration is often used in this report, it is used interchangeably with groundwater recharge and is intended to refer to the same process.

## 5.2.1 Gridded Monthly Precipitation

Gridded monthly precipitation data covering the entire island of Tutuila were produced by Oregon State University's PRISM Group using climate records from 1971 to 2000. The processing methodology is documented in Daly et al. (2006), and essentially involved integration of topographic data and rainfall information derived from 21 precipitation observation stations to interpolate a whole-island precipitation grid at a resolution of 90 m cell-size. Gridded precipitation data were produced in ascii grid format and could be directly used in the SWB2 code after pre-processing for cell-size and boundary extent. An example of the gridded data is shown as Fig. 5.2.

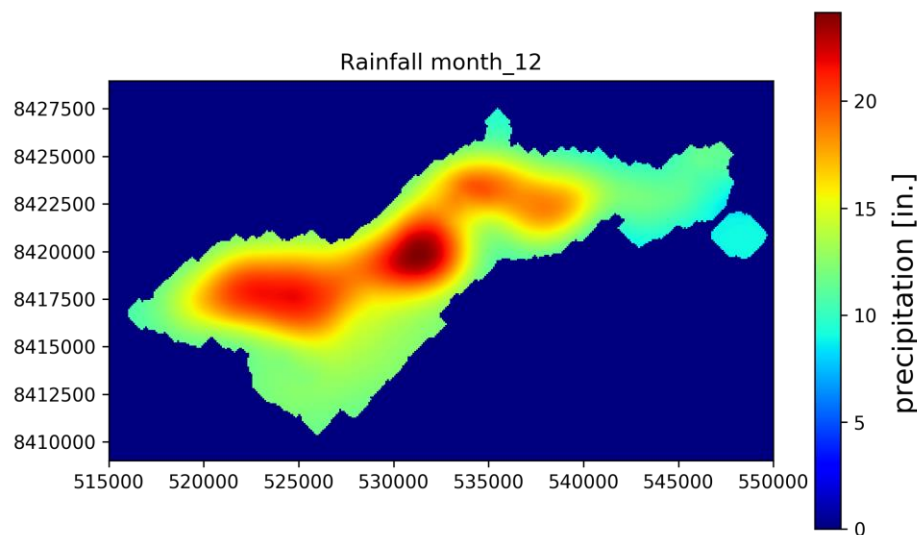


Figure 5.2: Gridded monthly rainfall data for the month of December from Daly et al. (2006). Note map units are in m relative to UTM zone 2S, WGS 84.

## 5.2.2 Rainfall Fragments

Although the outputs of water budget models are typically presented as monthly or annual totals, SWB2 uses a daily time step for soil moisture calculations, the output of which are subsequently downsampled to obtain monthly or annual results. Therefore, the model requires daily gridded-rainfall data in order to perform the soil-moisture processing step. However, daily gridded rainfall data at sufficient resolution are not currently available for Tutuila. Because this is a common issue on small islands, the SWB2 code contains a built in module to apply the Method of Fragments, which was used in this study to disaggregate the monthly gridded rainfall data (Daly et al., 2006) into daily-gridded rainfall estimates for use in model calculations. The Method of Fragments essentially creates a synthetic daily rainfall series for each modeled month by spreading the total monthly precipitation, taken from the gridded data,

into each day of the month following stochastically selected daily rainfall patterns observed at rain gauges. A synthetic rainfall dataset is created for each rain station, and applied only in the area geographically closest to each station, as defined by Thiessen polygons surrounding the gauge point locations (Fig. 5.3). For a more in-depth explanation of the Method of Fragments and its previous application see Oki (2002) and Westenbroek et al. (2018).

For this study, rainfall patterns or fragment sets were generated with daily precipitation records from 18 distinct rain gauging stations scattered throughout Tutuila. Since the method only indirectly uses rain gauge data, in order to obtain a representative temporal distribution of rain falling throughout the month, rain station periods of record do not need to and did not necessarily overlap. Periods of record for gauges used in this study ranged from 1955 to 2018.

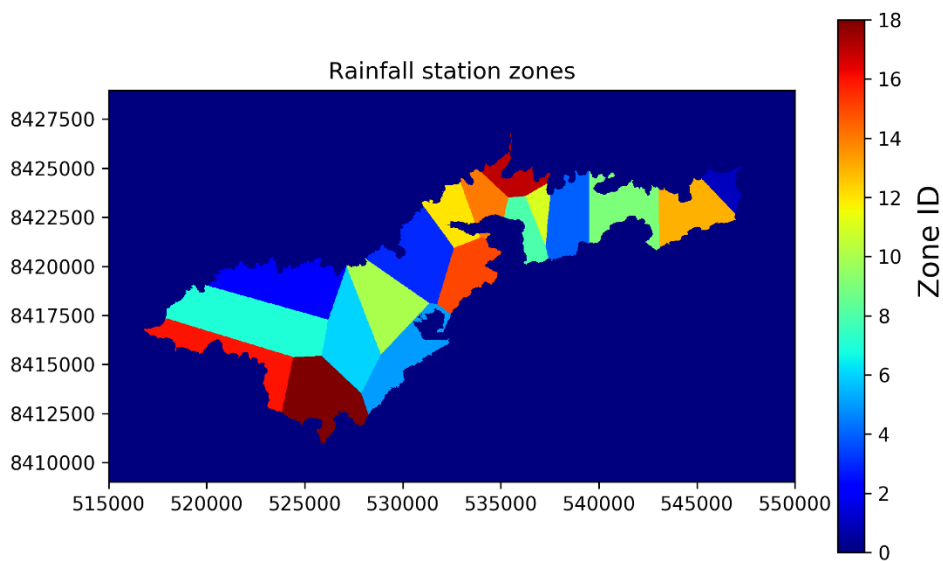


Figure 5.3: Gridded map of 18 rain gauge station zones as defined by the Thiessen polygons, used to define fragment sets for daily rainfall processing.

### 5.2.3 Land Use

The SWB2 model requires information about the spatial distribution of land use to assign site specific parameters that affect interception or infiltration rates. For this work, land-use data was obtained from a high-resolution wildlife habitat map developed by the American Samoa Department of Marine and Wildlife Resources (DMWR) (Meyer et al., 2016). This map was created using an object-based remote-sensing approach applied to high resolution orthoimagery and LIDAR data collected in 2012, and uses a classification scheme specific to the vegetation of American Samoa. For this study, each distinct land-use type was assigned a zone code, and the vector data supplied by the Meyer work was converted to a raster format, with each land-use type represented as a numerical zone code (Fig. 5.4)

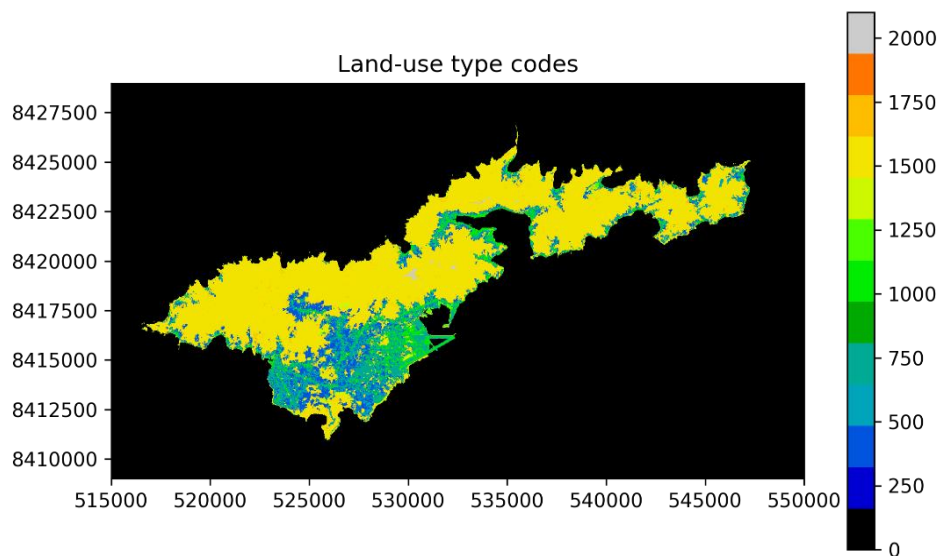


Figure 5.4: Gridded map showing the spatial distribution of different land-use types throughout Tutuila. Land-use code key provided in Table 5.1 below.

The SWB2 model applies parameters for each land-use type by assigning a specific zone code to each land-use and then the model matches these zone codes to parameter sets contained in a separate tabular land-use lookup table. Land-use parameters included rooting zone depth, canopy storage capacity, trunk storage capacity, stem-flow fractions, and certain factors related to irrigation or cropping timing, and those parameters used in the Tutuila model are given in Table 5.1. Because of the geologic and climatic similarities between the Hawaiian Islands and American Samoa, the land-use lookup table from the Maui SWB2 example (Westenbroek et al., 2018) was used to assign parameter values for Tutuila’s land uses. Although land-use classifications as defined by Meyer et al. (2016) were not exactly the same as classifications defined in the Maui case, analogous land use types from each model were matched (Table 5.1) to obtain the most-representative parameter values for the Tutuila land-uses.

Table 5.1: Mapping scheme used to transfer land-use parameters from the Maui case as defined in Westenbroek et al. (2018) to land uses in this model as defined by Meyer et al. (2016), and specific parameter values used in the Tutuila SWB2 model.

Tutuila Description (Meyer et al., 2016)	Land Use Code	Maui Description (Westenbroek et al., 2018)	Rooting depth [in]	Canopy Storage Capacity [in]	Trunk Storage Capacity [in]	Stemflow Fraction
Cultivated Land	400	Diversified Agriculture	10	0	0	0
Agroforest	500	Macadamia	60	0	0	0
Open Space	700	Developed Open Space	12	0	0	0
Developed Woodlands	800	Developed Low intensity	12	0	0	0
Buildings, Impervious Surfaces	1000	Developed High intensity	12	0	0	0
Marsh, Mangroves, Swamp	1200	Wetland	39	0	0	0
Landslips, Landfills and Quarries	1300	Sparsely vegetated	5	0	0	0
Grassland/Herbaceous	1400	Grassland	39	0	0	0
Upland Scrub, Coastal Scrub	1500	Shrubland	12	0	0	0
Lowland Rainforest, Coastal Forest	1600	Native forest	30	0.05	0.01	0.04
Successional Scrub Vegetation	1700	Alien forest	60	0.05	0.01	0.04
Montane Rainforest	2100	Native forest fog	30	0.05	0.01	0.04

## 5.2.4 Soils

The U.S. Natural Resources Conservation Service (NRCS) maintains a standardized database of soil types and properties for soils throughout the U.S. An island-wide soil study of Tutuila was completed by Nakamura (1984) and includes descriptions of each soil type, predictions of soil behavior, and suitability and limitation information of each soil for specified uses. The soil parameters specifically used in the SWB2 model are the hydrologic soil group, which categorizes soils into four groups based on runoff-producing characteristics, and soil moisture capacity, which indicates the total amount of water each soil can hold before losing water to infiltration into aquifer material below. For this study, a georeferenced soil map from Nakamura (1984) was obtained in shapefile format, and was used to develop gridded datasets of hydrologic soil groups (Fig. 5.5) and soil moisture capacity (Fig. 5.6).

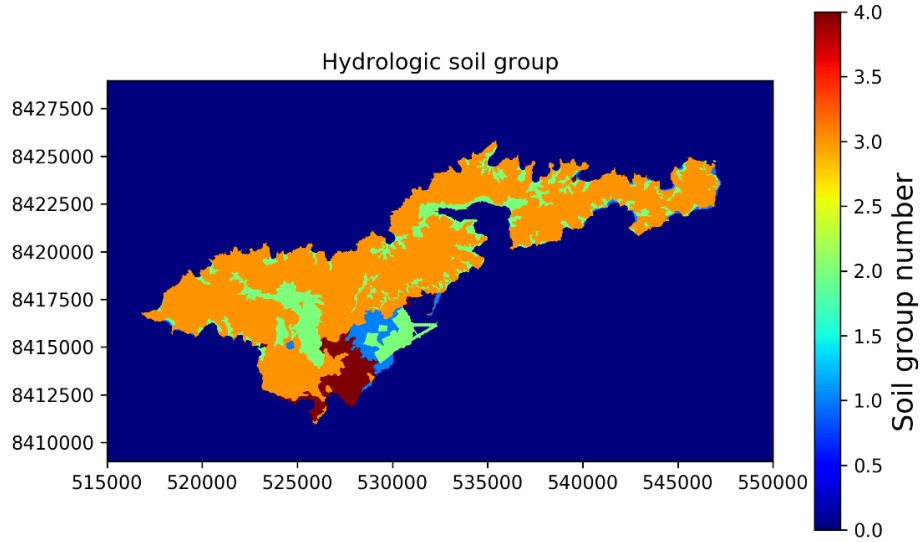


Figure 5.5: Gridded map of hydrologic soil groups derived from Nakamura (1984) for the study area.

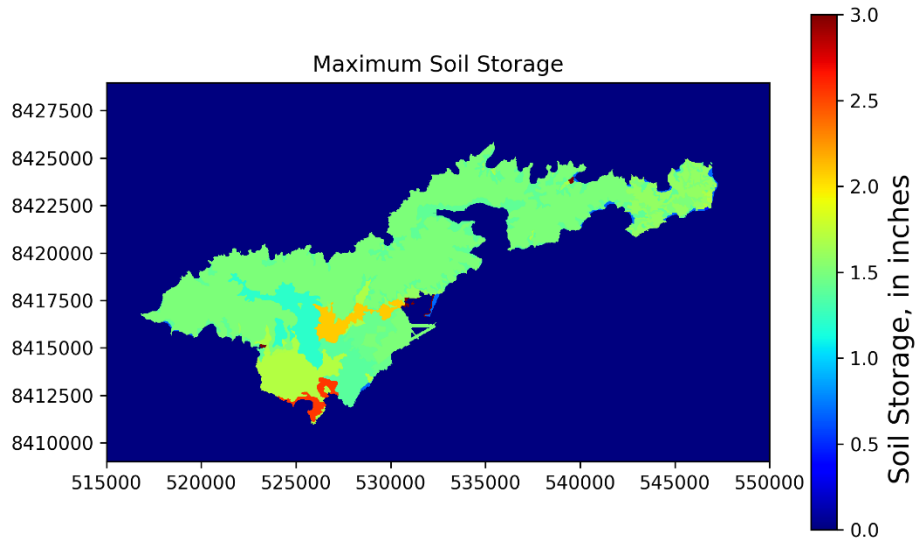


Figure 5.6: Gridded map of soil moisture capacity derived from Nakamura (1984) for the study area.

### 5.2.5 Runoff to Rainfall Ratios

Starting in the 1960s, the USGS began installation of continuous record stream gauges throughout Tutuila. Between this time and 2008, at least eleven continuous record stream gauges were operated over various periods of record. These data are available at the USGS National Water Information System (NWIS) database (<https://waterdata.usgs.gov/aq/nwis/sw>) and stream gauging methods are documented in

Wong (1996). However, in 2008, the USGS gauging operations ceased. To fill this data gap and to provide updated data for this study, a collaborative agreement was initiated between University of Hawaii (UH) and ASPA personnel to install eight new stream gauges and begin data collection again. For this study, streamflow data was primarily used in the calculation of runoff-to-rainfall ratios (R:R ratios), which represent the percentage of rainfall that becomes runoff within a given watershed basin, and is removed from the model through an assumed surface water feature. Note that the term runoff as used in this report refers specifically to stormflow generated and lost during and shortly after rainfall events and does not include baseflow, lateral flow, or any other water that has cycled through the aquifer or vadose zone.

To determine R:R ratios in gauged sub-basins, historical USGS streamflow data from eleven sub-basins were integrated with contemporary stream gauging data from UH/ASPA efforts. The integrated streamflow dataset included a total of fifteen sub-basins, seven of which had only USGS streamflow records and four of which had only data from UH/ASPA gauges, leaving the remaining four with non-overlapping streamflow hydrographs from both USGS and UH/ASPA records (Fig. 5.7). The runoff component of total streamflow was separated from the baseflow component with the Turning Point Baseflow Separation Method, (Wahl and Wahl, 1995) as described in Barlow et al. (2015). A graphical example of the baseflow separation results are shown in Fig. 5.7.

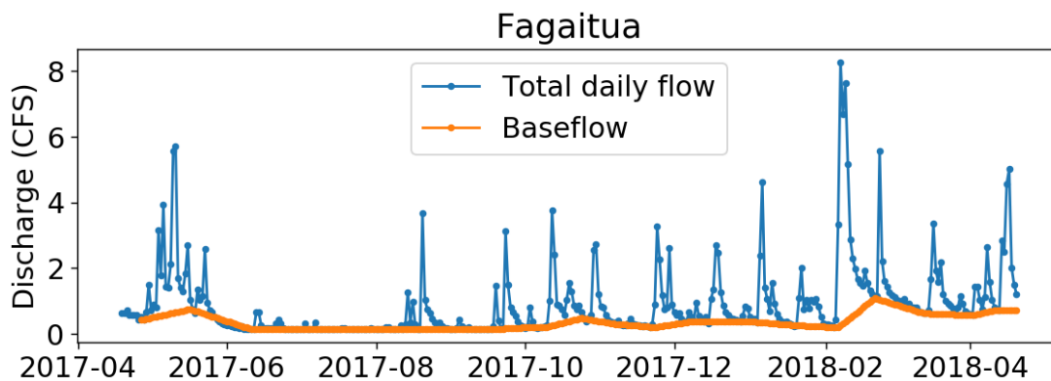


Figure 5.7: Example output of the Turning Point Baseflow Separation Method as performed on the UH/ASPA Fagaitua stream gauge data over a one-year period of record. The orange line indicates stream baseflow in cubic feet per second (CFS), while the blue line indicates total streamflow. Runoff is calculated as the difference between the baseflow and total flow for any given day.

Once the summed quantity of runoff during each month was separated from total stream flow, the runoff amount in each gauged sub-basin was divided by the sub-basin-total rainfall derived from monthly gridded precipitation data (Daly et al., 2006) to yield monthly-resolution R:R ratios. To interpolate R:R ratios to ungauged sub-basins, these measured R:R ratios were assigned to the major watersheds containing each gauged sub-basin, as shown in blue on Fig. 5.8, and watersheds in-between those with measured R:R ratios were assigned

averaged R:R values from the adjacent measured watersheds. If an ungauged watershed was only adjacent to a single measured watershed, then the R:R ratio of the measured watershed was directly assigned to it. This process was extended to each major watershed until a measured or interpolated R:R ratio was assigned in every watershed on the island, except in the Tafuna-Leone plain region where this method was modified to account for unique geologic conditions.

The geologic youth of the Tafuna-Leone basalts and the low slope of the plain's topography both contribute to a significantly higher hydraulic conductivity in this area (Davis, 1963; Bentley, 1975). This causes a reduction in runoff to rainfall ratios and thereby an increase in net-infiltration rates, an effect which has been previously described by Izuka et al. (2007) and Perreault (2010). This causes the plain's few developed stream channels to typically remain dry except during the heaviest rain events, making measurement of streamflow in the Tafuna-Leone region difficult. Thus there are currently no estimates of runoff in this the Tafuna-Leone area. Both Izuka et al. and Perreault assumed that most of the runoff in the plain likely infiltrates before running off, and they estimated this quantity to be approximately 75% of the total runoff generated in this region. For this study, the same assumption was made as no other information to better approximate this value was available. This was accomplished by multiplying the R:R ratio in each watershed adjacent to the Tafuna and Leone Plains, respectively, by a constant factor of 0.25 to obtain estimated R:R ratios in these areas.

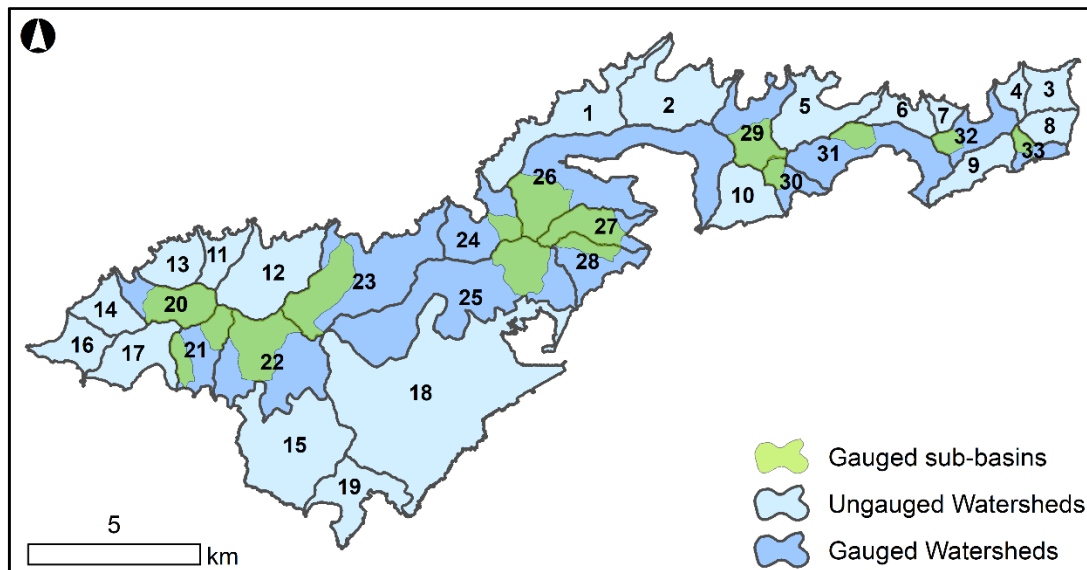


Figure 5.8: Measured sub-basins (green), major watersheds containing at least one continuous record stream gauge (dark blue), and ungauged major watersheds (light blue) lacking stream gauges. Labels indicate zone code number.

To assess the validity of this method, the R:R ratios calculated in this study were compared to ratios independently calculated by Perrault (2010), who determined R:R ratios for the eleven USGS streamflow records using baseflow separation method of (Wahl and Wahl, 1995), and sub-basin-total rainfall derived from Daly et al. (2006). In general, both datasets compared reasonably well, with the average relative percent differences (RPD) between R:R ratios at each station equaling about 10%, and with the correlation coefficient ( $r^2$ ) of the regression between the two datasets equaling 0.74 (Fig. 5.9). Note that the RPD is calculated as the difference between two values divided by the average of the two values.

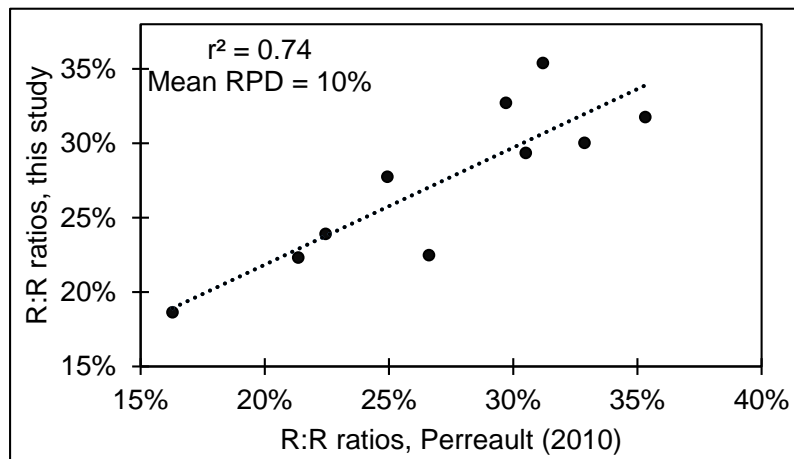


Figure 5.9: Comparison of runoff to rainfall ratios (R:R ratios) calculated in this study to those calculated by Perreault (2010), for the ten watersheds that both studies commonly assessed.

## 5.2.6 Direct Infiltration

Anthropogenic activities have the potential to significantly affect the spatial distribution of water balance components through water use, infrastructure leakage, and wastewater disposal. Unfortunately for sustainable water management goals, a significant fraction of the water produced by municipal wells is lost to underground water leakage from aging distribution mains and service laterals. This loss is referred to as non-revenue water (NRW). To assess the quantity of leaked NRW, total water production and consumption rates were obtained from ASPA. Over the last 5-years, island wide water production has ranged between 7.3 and 12.8 million gallons per day (Mgal/d) with an average of 10.8 Mgal/d. Customer service records indicate total metered-water use for the same period has averaged approximately 4.7 Mgal/d. Thus as of April 2018, the total island wide NRW was about 6 Mgal/d or about 55% of all water produced from pumping wells on Tutuila.

To model the contribution of NRW to groundwater recharge, the island-wide NRW total of 6 Mgal/d was distributed equally over all model cells that intersected with a water main. Locations of water mains were provided by ASPA in a georeferenced vector format. To

calculate the appropriate depth of NRW in each of the intersecting SWB2 grid cells, the island-wide NRW volume was divided by the number of cells intersecting a water line, and again divided by the area of each grid cell. This calculation yielded a depth of NRW water (in m/day) for each water-line grid cell, and was directly added to the infiltration component of the model (Fig. 5.10). It should also be noted that this method assumes that all water lines leak, and that they leak at an equal rate. Information regarding where subsurface leaks are actually located is lacking, thereby hindering a more accurate assessment of the spatial distribution of water leaks. However, the assumption we adopted here was considered reasonable considering the high proportion of NRW on the island, which indicates a large proportion of the water delivery system is likely to be compromised.

In addition to NRW, direct infiltration from OSDS leachate was also incorporated into the model. This was accomplished by indirectly determining the probable locations of OSDS units through geospatial subtraction of home or business sized buildings (> 120 m<sup>2</sup>) located within 10 m of a wastewater main or lateral. Note that the most recent geospatial Tutuila building location dataset (AS-DOC, 2009) was obtained from the American Samoa Department of Commerce (AS-DOC), and the locations of wastewater lines were provided by ASPA. Buildings larger than 120 m<sup>2</sup> and located more than 10 m away from a sewer line were assumed to require an OSDS unit for wastewater disposal. Per-unit effluent discharge rates from Shuler et al., (2017), equaling 1.45 m<sup>3</sup>/d per OSDS unit, were applied to calculate the total volume of additional water discharged by OSDS units in each grid cell. Island wide, the number of estimated OSDS units was approximately 5,750, which when multiplied by the above discharge rate, yielded a total OSDS discharge volume of about 2.2 Mgal/d. Effluent volume at each cell was converted to depth of water in the same manner as the additional NRW infiltration (Fig 5.11). Both NRW and OSDS effluent additions were supplied to the SWB2 model in a grid format, and were directly added to the calculated net-infiltration in each model cell.

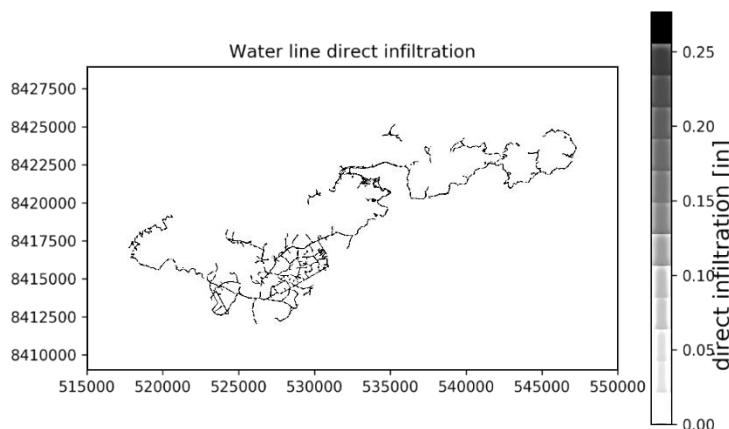


Figure 5.10: Estimated direct net-infiltration rates from leaking water lines, i.e. non-revenue water (NRW).

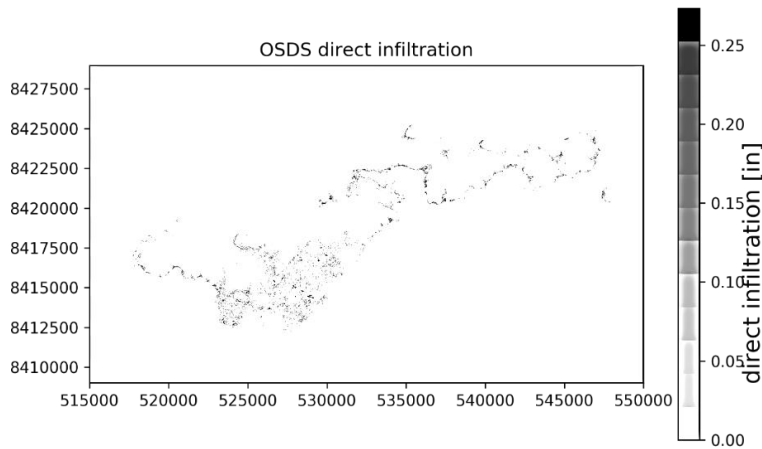


Figure 5.11: Estimated direct net-infiltration rates from OSDS discharge.

### 5.2.7 Potential Evapotranspiration

The SWB2 model has the ability to develop estimates of potential evapotranspiration (PET) from maximum and minimum air temperature data. However, if existing gridded monthly PET data exist, these data can be directly supplied to the model. Fortunately, PET maps for Tutuila were previously developed by Izuka et al. (2005). This study used the Penman (1948) method to analyze climate and pan-evaporation measurements from nine measurement stations throughout Tutuila to produce monthly PET maps for Tutuila Island (Fig. 5.12). For this study, these PET maps were first vectorized then converted to a gridded raster format with a spline interpolation method, so that they could be directly supplied to the SWB2 model. To determine actual evapotranspiration rates (AET), the SWB2 model was set to use the FAO-56 Method (Allen et al., 1998), which essentially sets AET values equal to PET values until soil moisture reaches a threshold value near the soil-wilting point, at which point the AET begins to linearly decrease with time to zero.

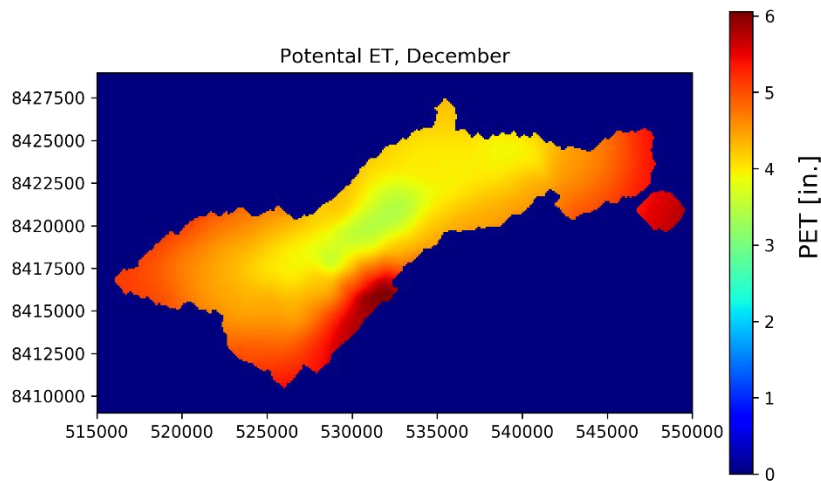


Figure 5.12: Gridded monthly potential evapotranspiration map for the month of December. Data was derived from hardcopy maps taken from Izuka et al. (2005).

## 5.2.8 Canopy Interception and Losses

As precipitation falls on a forested landscape, most raindrops are intercepted by vegetation before reaching the land surface. While much of this water ultimately falls to the forest floor, a proportion of it evaporates while still on vegetative surfaces. This process, termed canopy evaporation, is defined as the amount of intercepted precipitation that evaporates from leaves, stems, and trunks of a forest. The SWB2 code provides multiple ways to model interception and evaporative losses in forested areas. Because the Gash et al. (1995) conceptual model and computational method was determined to be most applicable to the tropical forests modeled in the Maui case study (Westenbroek et al., 2018) this method was chosen to represent canopy processes on Tutuila as well. The Gash method assigns parameters controlling canopy cover, canopy storage capacity, trunk-storage capacity, and the proportion of precipitation diverted to stem-flow to forested land-use zones. With this method, canopy interception is calculated on a daily-time step where water that remains in canopy or trunk storage after precipitation has stopped is subject to a user specified canopy evaporation rate.

The Gash et al. (1995) method requires canopy evaporation data to calculate evaporative losses from the canopy over the course of modeled rainfall events. On Oahu, estimated-gridded canopy-evaporation data have been successfully developed by applying an empirically derived linear relationship between average annual wind-speeds and annual rainfall rates (Engott et al., 2015). Therefore, to develop estimates of average annual canopy evaporation on Tutuila, the same linear model between rainfall and wind speed at 30 m height that was previously described for the island of Oahu, was applied for Tutuila for input in the SWB2 model (Fig. 5.13).

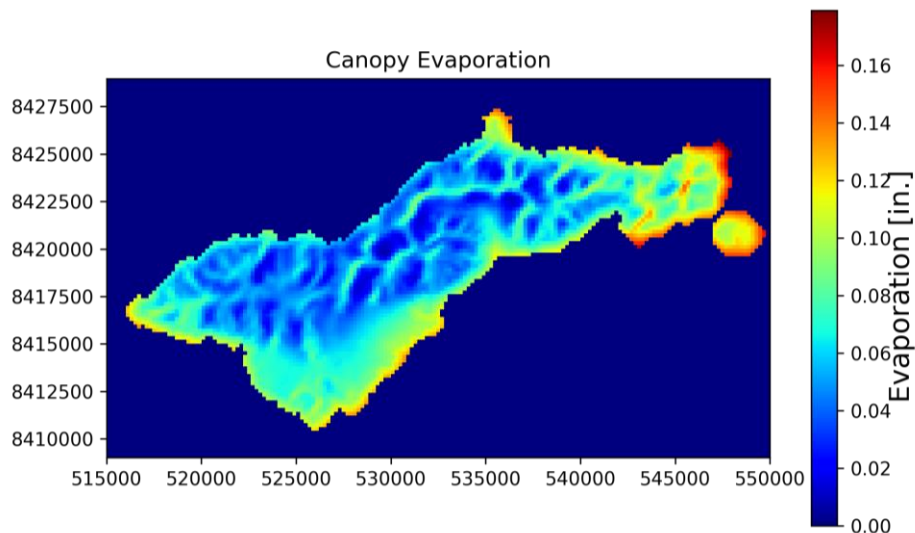


Figure 5.13: Processed map of canopy evaporation derived from average annual wind speed and average annual precipitation gridded datasets.

## 5.2.9 Mountain Front Recharge

Infiltration on the Tafuna-Leone Plain is enhanced by the process of Mountain Front Recharge (MFR), where surface waters and overland runoff from watersheds above the plain infiltrate into streambeds or soil once reaching a more permeable geologic substrate. This process is analogous to the MFR frequently observed in arid climates (Wilson and Guan, 2004). On the highly-permeable Tafuna-Leone Plain, the majority of direct precipitation has been observed to infiltrate before it has a chance to runoff due to the high permeability of the Holocene-age lavas (Perreault, 2010). There are only a few well developed stream channels on the plain and no perennial streams. In contrast, the older volcanic shields that lie above the plain have much lower permeabilities and contain perennial streams and springs that drain to the sea or terminate at the Tafuna-Leone Plain (Izuka et al., 2007). Actual points of infiltration likely vary depending on stream discharge or rainfall rate, thus a MFR zone located at the base of the mountains has been previously defined (Izuka et al., 2007; Perreault, 2010). While MFR is most significant in the Tafuna-Leone Plain, it has also been observed to a limited extent in Tutuila's alluvial-fill valleys.

The MFR process was simulated in this work by calculating the total volume of runoff produced within an MFR capture area above the Tafuna-Leone Plain, and applying a fraction of this runoff as direct infiltration within the downgradient MFR zone. The MFR infiltration zone boundaries were delineated by Izuka et al. (2007) as the northern portion of the Tafuna-Leone plain that lies within the Pavaiai stony clay loam soil unit, as surveyed by Nakamura (1984). This soil unit overlies the highly conductive Tafuna-Leone lavas and was described as a deep, well-drained soil with moderately high permeability. The area along the floor of Malaeimi Valley was also included in the MFR infiltration zone for this study, based on direct observations of streams infiltrating into the ground in this area. The extent of the MFR capture area included the watershed boundaries between the mountain crest and the northern boundary of the MFR infiltration zone is illustrated in Fig. 5.14. Izuka et al. (2007) and Perreault (2010) previously estimated that 75% of runoff generated in the MFR capture zone likely soaks in to the infiltration zone, and because there exists no new information to update this assumption, the total volume of MFR added as direct infiltration in the MFR infiltration zone (7.6 MGD) was calculated as 75% of the MFR capture-zone runoff from a preliminary run of the SWB2 model.

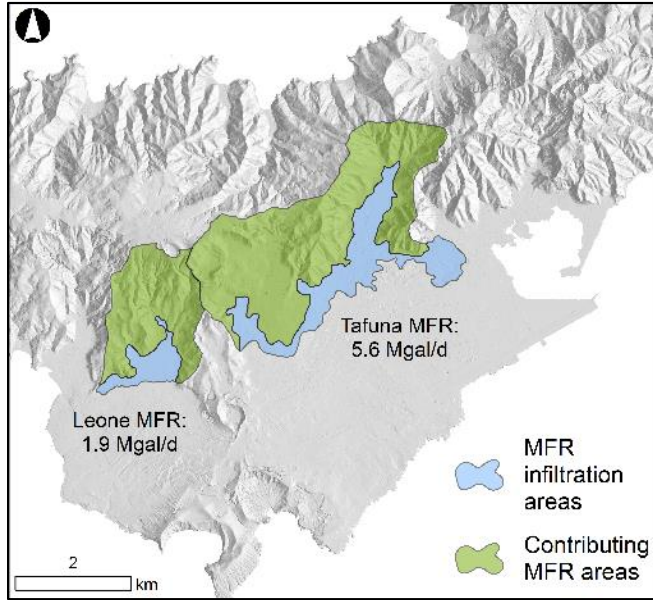


Figure 5.14: Mountain front recharge (MFR) capture and infiltration zone boundaries for the Tafuna and Leone sides of the Plain as applied to the SWB2 model. Total volumes of MFR added to model cells within each MFR infiltration zone are labeled.

## 5.3 Results and Discussion

The SWB2 model produces spatially and temporally-distributed datasets for each output parameter in a NetCDF file format. Each NetCDF file contains one spatially-distributed gridded dataset for every day for which the model was run. Because the Tutuila model was run for a total of ten years, each NetCDF file contained 3653 two-dimensional grid files, each of which specified a depth of water (in inches) for the given parameter at each grid cell during each of the modeled days. For interpretation, these highly distributed multi-dimensional datasets were summarized by first calculating average annual water depths in each cell to create an average annual gridded dataset for each parameter. The output datasets were then summarized spatially by calculating the total volume of water contained in each component on an island-wide scale, as well as calculating the total volumes of water in each component within each major watershed on the island. Annual gridded-parameter datasets are shown below in Figs. 5.15 to 5.20. At the annual, whole-island resolution, the water budget model can be conceptualized as a simple equation, despite the more complicated internal daily processing steps. This equation takes the form:

$$\textit{Water inputs} = \textit{Water outputs}$$

On the water input side, precipitation inputs equaled 394 Mgal/d (as an annual average), which was summed with an additional 8 Mgal/d of water representing direct infiltration due to OSDS and leaking water line discharge. Together, these represent an initial water input value of 402 Mgal/d. For this work, the MFR amount was calculated as a function of the runoff component from the watersheds above the Tafuna-Leone Plain. Therefore, an initial model run was performed to determine the quantity of MFR, which totaled 7.6 Mgal/d. This volume of water was distributed to the MFR infiltration zones as direct recharge during the second and final model run.

Significant water budget components on the water outputs side included canopy interception, AET, runoff, and net infiltration. Of these, SWB2 calculated a loss of 33 Mgal/d or 8% of total water inputs to canopy interception, and a loss of 61 Mgal/d or 15% of water inputs to evapotranspiration, as determined by soil-moisture processing. Island wide runoff was initially calculated to be 92 Mgal/d or 23% of total water inputs, of which 5.7 Mgal/d was captured and re-introduced to the model as MFR, thereby reducing the amount of water lost to runoff to 86 Mgal/d or 21% of water inputs. This left the remaining 54% of inputs, totaling 221 Mgal/d, as the total island wide net-infiltration estimate. When summed, all output parameters yielded 399 Mgal/d, which accounts for 99.4% of the 402 Mgal/d of water inputs, thereby leaving a modeled error of less than 1% likely due to rounding error or differences in resolution during results post-processing.

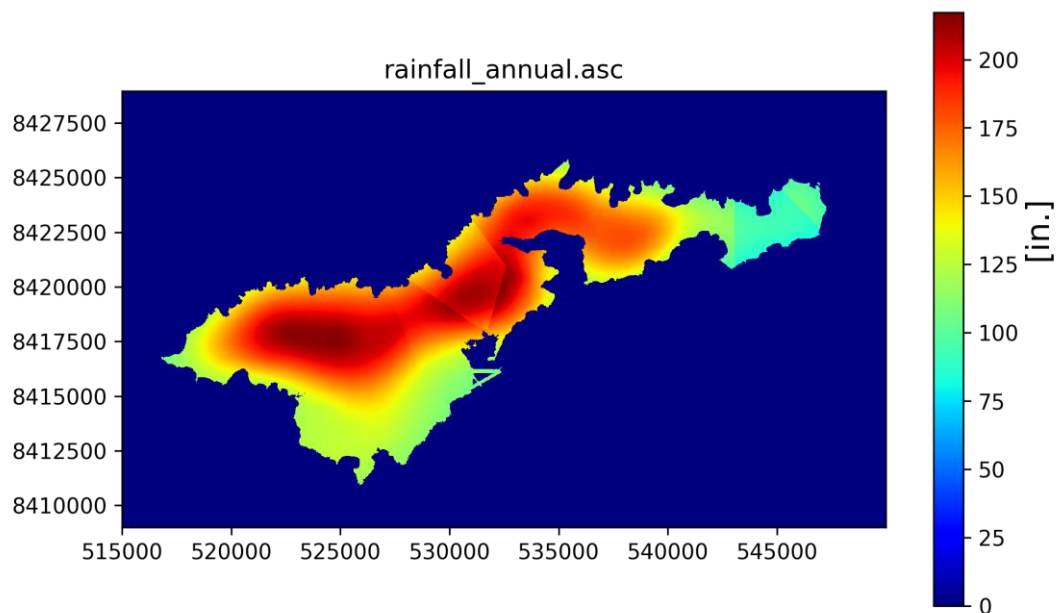


Figure 5.15: Average-annual rainfall after rainfall fragment processing, used as model input.

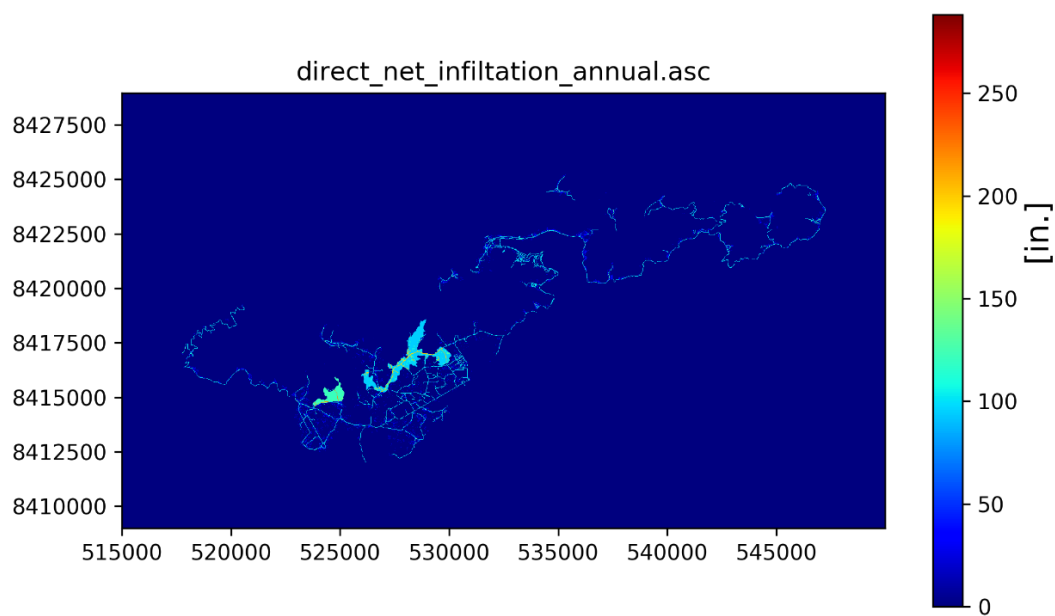


Figure 5.16: Final average-annual direct infiltration additions from OSDS effluent, leaking water lines, and MFR.

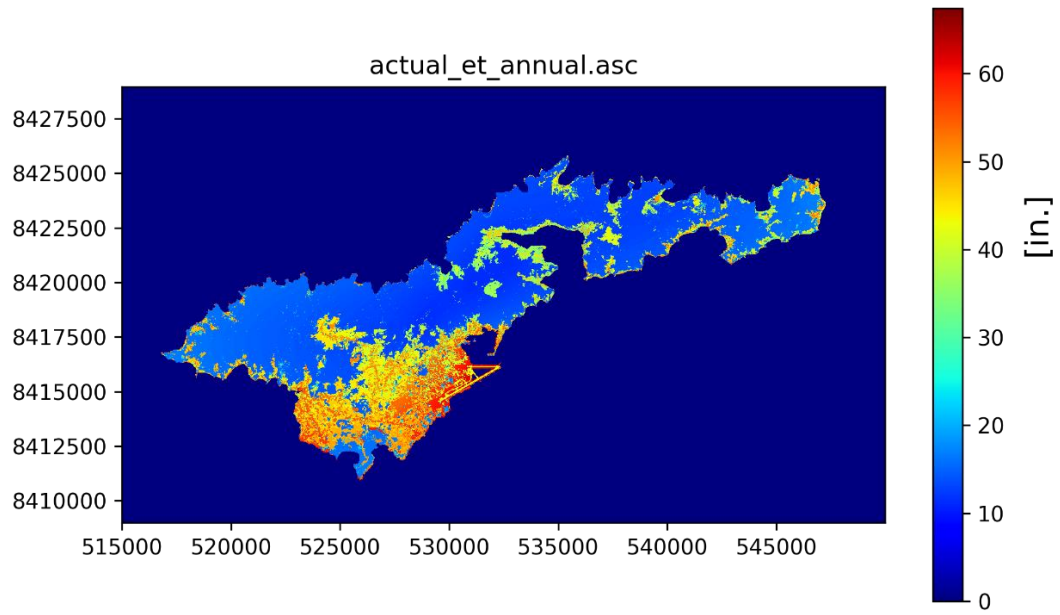


Figure 5.17: Final model output of average-annual actual evapotranspiration (AET).

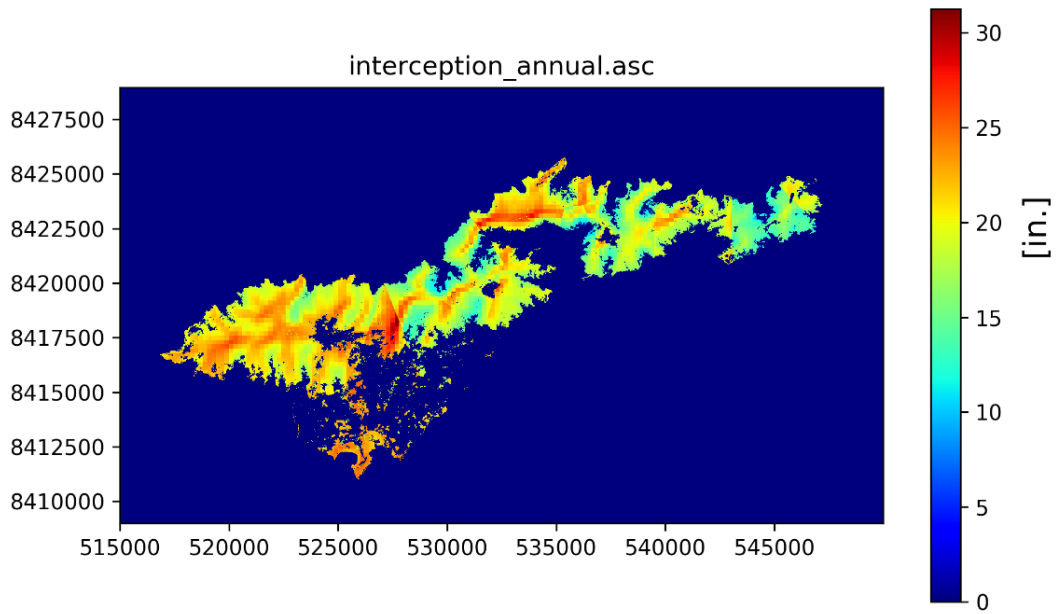


Figure 5.18: Final model output of average-annual canopy interception and subsequent evaporative losses.

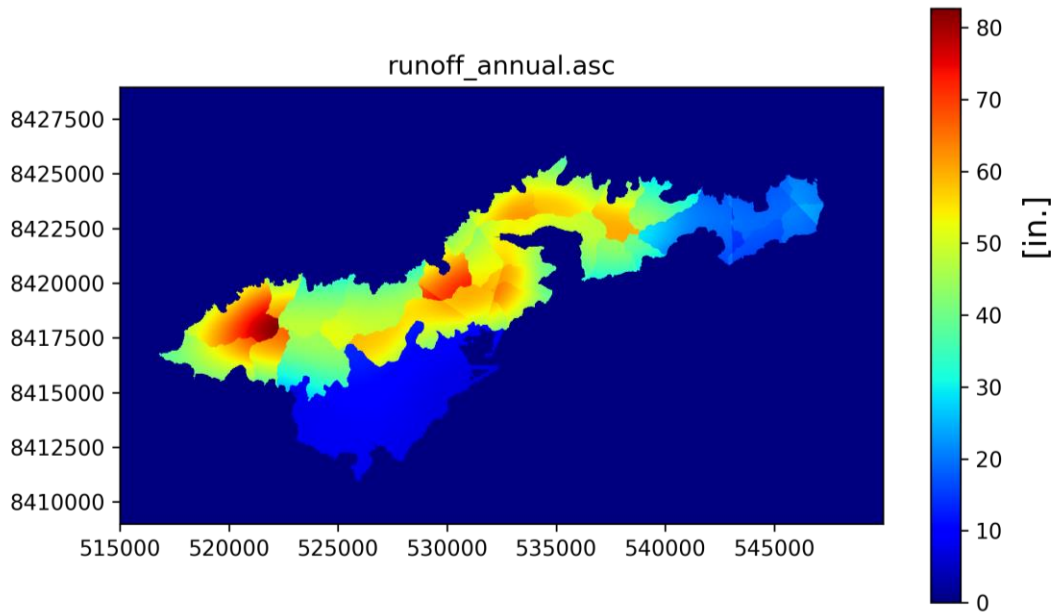


Figure 5.19: Final average-annual runoff totals.

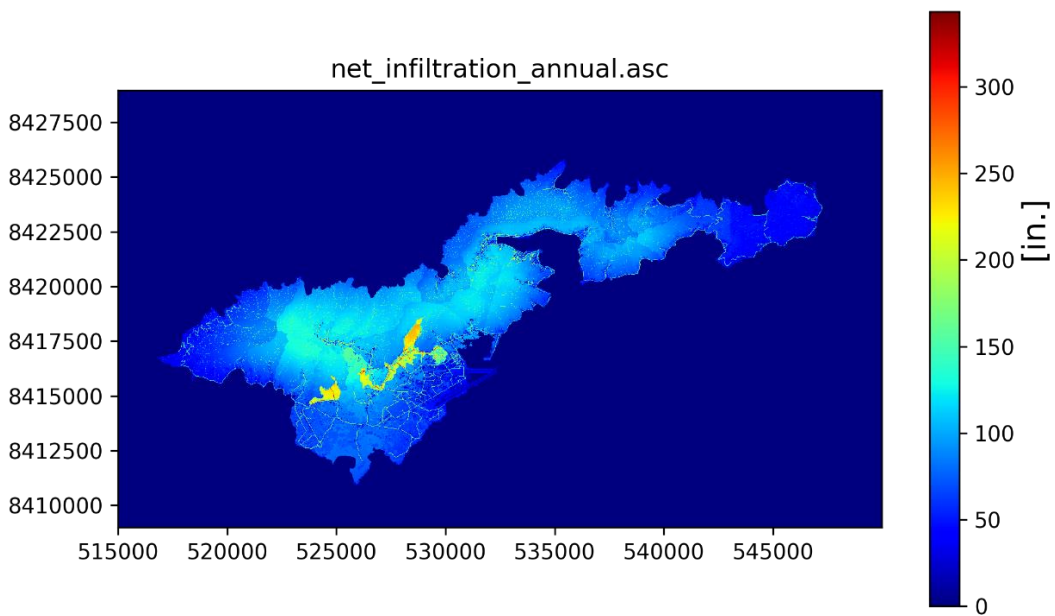


Figure 5.20: Final model calculated net-infiltration, presented at an annual average resolution. Also see Fig, 5.26 for a high resolution detail map of this net infiltration result.

### 5.3.1 Future Climate Scenarios

The water budget calculations discussed so far utilize climate data collected in the late 20<sup>th</sup> and early 21<sup>st</sup> centuries, and therefore represent estimates of hydrologic conditions during this period. However, the climate of the late 21<sup>st</sup> century, and likely beyond, will undeniably be significantly different than it has been in the short period of time since the start of the industrial revolution. The availability of water resources will be most affected by changes in amount and distribution of rainfall, as well as an increase in temperature, which is a major driver of ET. To estimate the potential effects of future climate change on water budget components, and thus future water resources availability in American Samoa, the Tutuila SWB2 model was run with modified input files derived from dynamically-downscaled climate projections for American Samoa. These projections were developed by Wang and Zhang (2016) using a physically-based global climate model. These authors produced gridded-hourly data for precipitation and temperature at 800 m by 800 m grid resolution and simulated three specific scenarios: (1) present-day climate for the years 1990 to 2009, (2) future climate during the years 2080-2099 reflecting a lower-carbon emissions scenario (RCP4.5), and (3) 2080-2099 climate reflecting on a higher emissions scenario (RCP8.5).

To assess the effects of these possible-future climates on SWB2 calculated net-infiltration rates, the Wang and Zhang (2016) rainfall and temperature projections were transformed into monthly-average grids of rainfall and maximum and minimum average monthly temperatures. The PET calculation method used in the model was also switched so that the effects of higher-future temperatures on ET could be assessed. Note that this method does not include other factors affecting ET such as differences in solar radiation or CO<sub>2</sub> concentrations, and this is a limitation with the method. The original model (henceforth referred to as the high-resolution model for reasons explained below) used externally-calculated reference ET values developed with rainfall, temperature, and energy flux measurements taken by Izuka et al. (2005). However, since these values are representative of that study's data collection period and could not be directly recalculated to include modified parameters, a built-in PET estimation method (the Hargreaves-Samani Method) was activated within the SWB2 code to calculate PET during the model run itself. This method utilizes an energy balance approach and is parameterized with user-supplied maximum and minimum air temperature data while applying default values based on vegetation types and latitude-based solar radiation. The effect of changing only the PET method as described above was tested on the high-resolution model, to ensure that the change of ET calculation method would not significantly affect water budget results. When these two methods were tested on an otherwise identical model, the RPD of the run using the Izuka et al. PET values and run using the Hargreaves-Samani calculations was relatively small, at 8.0% for AET and 2.3% for net-infiltration, with all other water budget components having RPD's below 0.1%.

The Wang and Zhang (2016) climate projections included a scenario for the present-day climate (1990 to 2009), but it was found that rainfall totals within this scenario were

significantly lower than present-day rainfall totals measured at physical rain gauge stations and reflected in the precipitation data from Daly et al. (2006), which was used in the original high-resolution model. Additionally, the grid resolution of the of the climate projections dataset (800 m) was much courser than the original high-resolution gridded precipitation input (90 m). Because of these discrepancies, output from the high-resolution model run was not directly comparable to output from the models parameterized with the climate projection datasets. Instead, the percent changes in each water budget component between the downscaled present-day and future (RCP4.5 and RCP 8.5) scenarios were assessed to determine how future climates may, in a relative sense, affect water resources availability (Fig. 5.21 and Table 5.2). If desired, these calculated percent-change values could conceivably be applied to the output from the high-resolution water budget model to produce predictions of volumetric change in water budget components. On an average annual scale, simulation results showed that both of the future climate scenarios predict significant increases in both precipitation and temperature, which translate into overall increases in all water budget components as calculated by the modified SWB2 runs. Most notably, the 11 to 18% increase in precipitation predicted by the RCP8.5 and RCP4.5 scenarios, respectively, drove increases in net-infiltration rates of 17 to 27%, respectively. This would suggest that in the future, the availability of Tutuila's groundwater-resources may significantly improve, though the costs of this will likely also include problems with flooding and groundwater inundation of buried infrastructure. It should also be noted that these results are contingent on the accuracy of these downscaled climate predictions, which do not necessarily represent the only or best predictions available.

Table 5.2: Results for present and future climate scenarios, as well as the results from the original high-resolution model output, given as volumetric totals in upper rows. Lower rows provide the same results but scaled as the percent change between the downscaled-present-day scenario and the future climate scenarios. Note that precipitation totals from the downscaled present-day run are significantly lower than the totals calculated with present-day data from Daly et al (2006), and thus are not directly comparable.

Scenario	Precip. [Mgal/D]	Dir. Infl. [Mgal/D]	AET [Mgal/D]	Intcept. [Mgal/D]	Runoff [Mgal/D]	MFR [Mgal/D]	Net Infiltration [Mgal/D]
<b>High-res. model</b>	393.7	15.7	61.4	33.3	92.3	7.6	220.9
<b>Downscaled: present</b>	228.6	13.3	54.2	31.7	51.9	4.4	105.9
<b>rcp45: 2080 - 2099</b>	269.4	13.9	54.9	34.4	61.2	5.2	134.6
<b>rcp85: 2080 - 2099</b>	253.9	13.6	54.9	33.4	57.8	4.9	123.4

Percent change between downscaled present-day and future climate scenarios, annual averages

Scenario	Precip. [% change]	Dir. Infl. [% change]	AET [% change]	Intcept. [% change]	Runoff [% change]	MFR [% change]	Net Infiltration [% change]
<b>RCP45: 2080 - 2099</b>	17.83%	4.74%	1.15%	8.46%	17.81%	19.23%	27.18%
<b>RCP85: 2080 - 2099</b>	11.06%	2.86%	1.22%	5.22%	11.30%	11.60%	16.57%

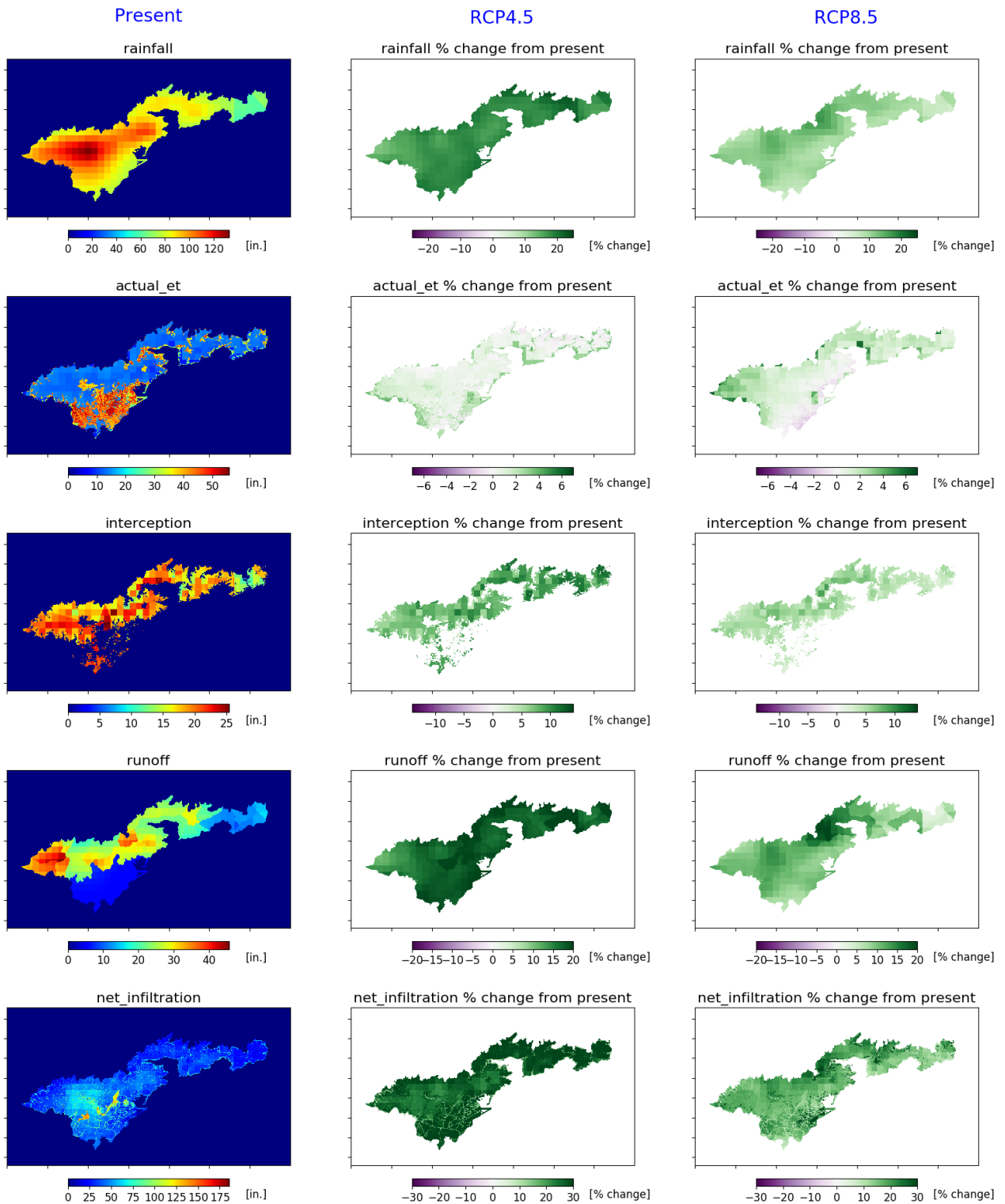


Figure 5.21: Water budget results using downscaled rainfall and temperature predictions (Wang and Zhang, 2016). Present-day predictions are shown as depth of water (left column) whereas future predictions are shown as % change from the present-day scenario for the RCP4.5 (center column) and RCP8.5 (right column) scenarios.

### 5.3.2 Sensitivity Analysis

Although input datasets and parameter choices used in this model were considered to be those that were most reasonable, uncertainty nonetheless exists in both. Thus, a sensitivity analysis was completed to assess the effect of parameter uncertainty on whole island net-infiltration, as well as to determine which parameters have the most control on model output values. Sensitivity testing only assessed changes in the net-infiltration output, as this parameter is the primary focus of this report.

Parameters chosen for sensitivity analysis included:

- Gridded precipitation
- Tabular runoff to rainfall ratios
- Gridded PET
- Trunk storage coefficient
- Gridded canopy evaporation
- Gridded water line leakage
- Gridded OSDS discharge
- Percent of mountain runoff becoming MFR
- Stem-flow coefficient
- Cell-size
- Flow routing option
- Selection of rainfall fragment sets

For the first nine test parameters listed above, input values were multiplied by test factors of 75%, 90%, 110%, and 125% of the parameter value used in the base case model. When the dataset being tested was formatted as a spatially variable gridded dataset, the entire gridded dataset was multiplied by each test factor and the model was run with each of the modified gridded datasets to test model response through the range of test constants. If the test parameter took the form of single or even multiple coefficients supplied to the model through a lookup table, then multiple lookup tables with the parameter of interest multiplied by each test factor were generated and the model was run with each. Of the eleven tested parameters, three were not formatted in a way that allowed simple multiplication by a constant percentage. The effects of cell-size were tested by running the model with multiple different cell-sizes; the effect of the built-in SWB2 flow routing option was tested by turning the option on and off; and the effect of using different sets of rainfall fragments to develop synthetic daily precipitation sequences was assessed by generating multiple randomly selected fragment sets and comparing output from each one. Detailed descriptions of sensitivity test results are provided below. As mentioned earlier, the sensitivities of results were only limited to net infiltration.

#### 5.3.2.1 Cell-Size

The input file preparation code was set up in a manner that allowed modification of the model cell-size. This not only allowed for faster processing times while building the model, but

also provided the opportunity to determine if cell-size resolution is a factor that affects output parameters. Thus, the model was tested at cell-sizes of 200, 100, 50, and 20 m. Results indicated whole-island model output parameters were only marginally sensitive to cell-size, showing RPD's of less than 7% at 200 m cell-sizes and less than 3% at 50 m cell-sizes (Fig. 5.22), when tested against the base case model at 20 m cell-size. Because a higher-resolution result is often desirable, the final model was run at the lowest practical cell-size, in consideration of model run time and file size (> 35 Gb at 20 m cell-size). Also, because of the small difference between the output at the 20 m and 50 m cell resolutions, all other sensitivity tests were performed at 50 m cell-size to avoid unnecessarily long processing times.

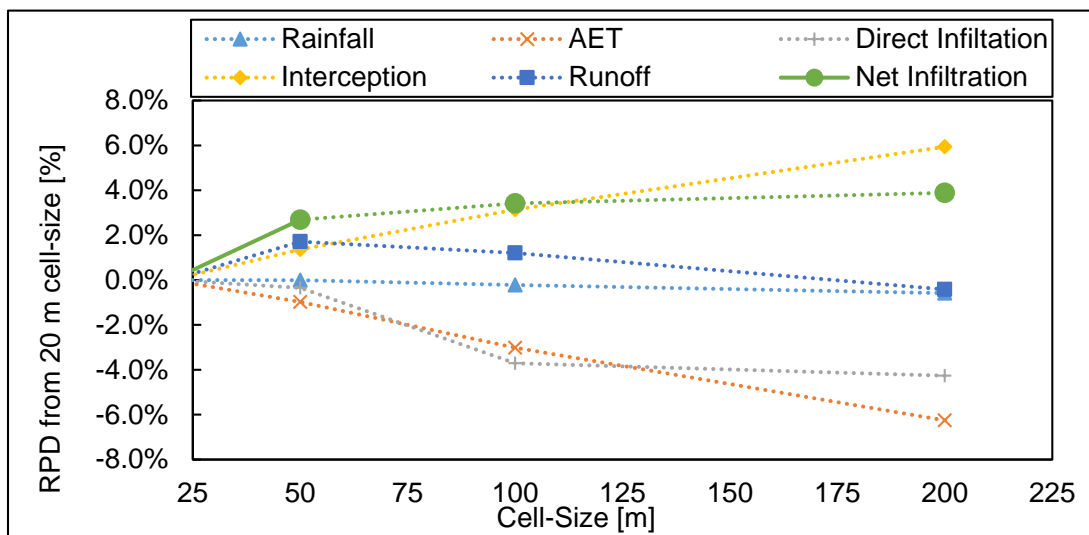


Figure 5.22: Pertinent model output results calculated over runs with different model cell-sizes. Values are shown as relative percent differences (RPD) between values from the model run at 20 m cell-size and the same values at other cell-sizes, up to 200 m.

### 5.3.2.2 Flow Routing

The SWB2 model contains a flow routing option to more realistically model the transport of surface runoff by considering the effects of steep or hilly terrain on the movement of overland flow. The model uses a D8 flow routing scheme (O'Callaghan and Mark, 1984) that allows surface water generated at a grid cell to flow into the next downslope cell where it is processed along with the runoff component of that cell. Because most water-budget models do not include this option, it was desirable to assess the effects of this method on total net-infiltration. With this method activated, sensitivity testing revealed an increase in island-wide net infiltration by 3.6% (at 50 m cell-size). Therefore, it appears that on an island-wide scale the model is only marginally affected by use of the flow routing method. However, the spatial distribution of infiltration on the sub-basin scale is significantly different as can be seen in Fig.

5.26. This would suggest that this method is most useful in applications where higher resolution results are desired.

### 5.3.2.3 Rainfall Fragment Set Selection

The Method of Fragments involves randomly selecting different sets of rainfall fragments for each month to generate synthetic daily gridded rainfall datasets from the monthly gridded rainfall data supplied to the model. This method begs the question of how much stochastic variability is introduced through the process of randomly selecting rainfall fragments. To assess this question, the model run time was reduced to one year to maximize the potential variability between different selected sets of rainfall fragments, and the model was run a total of five times, each with a different set of randomly selected fragment sets. Results indicated minimal differences between each model run with RPD between net-infiltration values of < 0.8 %. When all output parameters were assessed, most had RPD values (between each run and the average value of all five runs) of less than 1% with only a few outliers, which were still below 2% (Fig. 5.23). Therefore, this test indicates that selection of different fragment sets will only affect model results by 2% at most, and more likely will affect them by much less considering the final model was run for 10 years, thereby averaging the stochastic variability from each year over the entire time period.

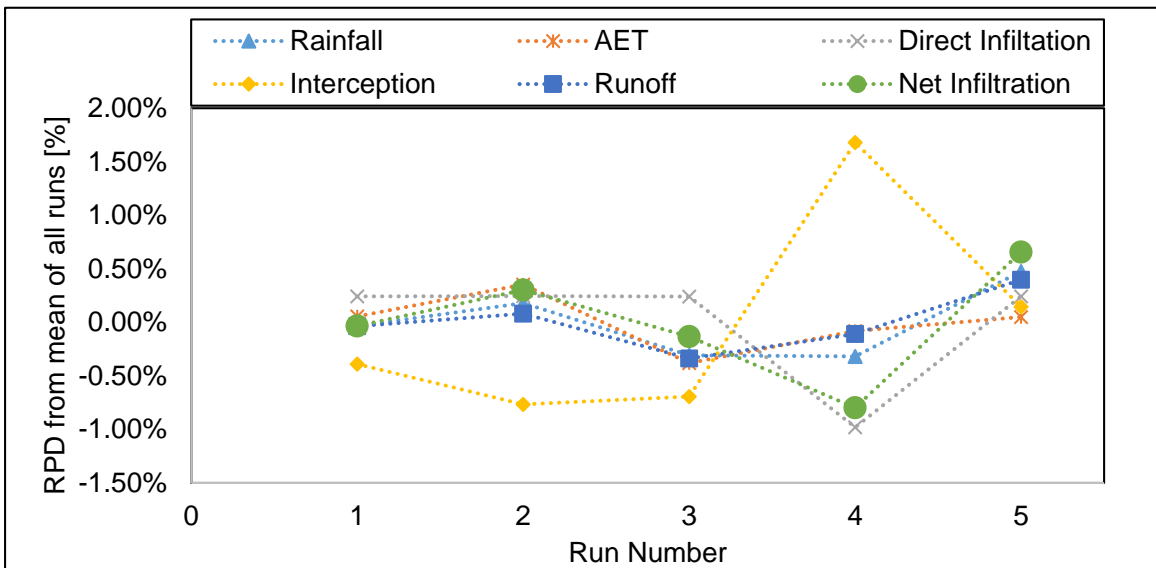


Figure 5.23: Pertinent model output results calculated over five different runs each using a different sequence of randomly selected rainfall fragment sets. Values are shown as the relative percent differences (RPD) between average parameter values across all five runs and the same parameter values for each individual run.

### 5.3.2.4 Input Parameters Tested with Discrete Constants

Of all input parameters examined with sensitivity testing, the model was only found to be highly sensitive to precipitation inputs, with 'highly-sensitive' meaning that a given percentage change in input values produces a larger percentage change in the net-infiltration output. This result supports the not-unexpected conclusion that rainfall is the strongest control on net infiltration and thus groundwater recharge. The model was less sensitive to all other parameters, with the next most important ones being runoff and PET. Changes in all other parameters tested with these constants yielded relative changes in output that were less than 1/10<sup>th</sup> of the magnitude of the change in the input parameter. Table 5.3 shows the RPD in net infiltration values between the base case model run and each of the sensitivity test runs for the gridded or look-up table values.

Table 5.3: Sensitivity test results expressed as relative percent differences (RPD) in model calculated net infiltration between the base case model and sensitivity test runs. For each parameter, individual model input parameters were multiplied by test constant values of 75%, 90%, 110% and 125%. Values for RPD are based off of the difference between net infiltration calculated in the base case model run and net infiltration from the run where the given input parameter was multiplied by each test constant.

Input parameter undergoing change	Input values x 75%	Input values x 90%	Input values x 100%	Input values x 110%	Input values x 125%
Relative percent difference in modeled net infiltration values					
Precipitation [RPD]	-37.81%	-13.65%	-	12.06%	27.68%
R:R ratios [RPD]	8.22%	3.37%	-	-3.48%	-8.92%
PET [RPD]	5.82%	2.31%	-	-2.27%	-5.61%
Trunk storage [RPD]	1.98%	0.79%	-	-0.78%	-1.94%
Canopy evaporation [RPD]	1.42%	0.55%	-	-0.63%	-1.52%
Water line leakage [RPD]	-0.87%	-0.35%	-	0.34%	0.86%
Percent of mountain runoff becoming MFR [RPD]	-0.66%	-0.26	-	0.26%	0.65%
OSDS discharge [RPD]	-0.24%	-0.10%	-	0.10%	0.24%
Stem-flow [RPD]	0.08%	0.03%	-	-0.02%	-0.05%

### 5.3.3 Comparison to Previous Tutuila Water Budget Studies

Direct calibration or validation of the SWB2 model was not possible due a lack of sufficient net-infiltration measurements to represent hydrologic processes at the regional scale. Nonetheless, comparisons to previously developed water-budget models can help to provide confidence in this model's results. For the island of Tutuila, only two documented whole island water budget studies (Eyre and Walker, 1991; ASPA, 2013), and one partial-island model covering Western Tutuila (Izuka et al., 2007) were found. The methods of computation, and indeed the accuracy of input datasets appear to be variable between each of the studies. Nonetheless, because of the difficulties inherent in calibration and validation of the water-budget method, it is primarily the user acknowledged reasonableness of input and output data that provides insight into the accuracy of results. The Izuka et al. (2007) study was the only water budget model produced by a national agency (the USGS) in a formally published and internally reviewed format. This study was also the only one of the three comparison studies that included the effects of MFR, and also used daily time-step processing to simulate soil moisture processes. The ASPA model was documented in an internal report within the ASPA-water division. The ASPA study was limited in its explanation of methodologies and appeared to be fairly simplistic in its computational rigor, but unlike the Izuka et al. study, covered the entire island in its extent. The Eyre and Walker study methodology was well documented in a report intended to be publicly available as a USGS report, but was never released. The Eyre and Walker study also covered the whole island in its extent and primarily used simple analytical computations to estimate recharge on a basin-wide scale.

The net-infiltration estimates from each of the three comparison studies were produced in different formats (basin totalization, raster, and vector polygon, for the Eyre and Walker (1991), ASPA (2013), and Izuka et al. (2007) studies, respectively), thus the output of each was converted into a standardized format to assess the reasonableness of the magnitude and spatial distribution of recharge to that of this study (the SWB2 model). This was done by summing total net-infiltration within the boundaries of each major watershed to obtain a basin total infiltration rate for each. A summary of watershed-scale comparisons is shown in Fig. 5.24 and basin-total net-infiltration rates are presented graphically in Fig 5.25. In general, correlation coefficients ( $R^2$ ) between the SWB2 model and the other studies are high, indicating the spatial distribution of recharge is similar in all studies. However, only the Izuka et al. comparison had a linear regression slope close to 1, whereas the regression slopes are around 1.4 in comparisons to the other two models, indicating these models, comparatively, are systematically under-predicting infiltration rates. This may be due to the addition of MFR in the SWB2 and Izuka et al. models, but not in the other two. The RPD in calculated net-infiltration rates between the watersheds from each study provided another way to directly compare models on the watershed scale. This analysis yielded a mean RDP between the SWB2 and the Izuka et al. model of only 17%, while mean RPDs between the SWB2 model and the ASPA and Eyre and Walker models were 67% and 107%, respectively. Overall, the high  $R^2$  low RPD, and the linear-regression slope between the Izuka et al. and SWB2 models suggests that the results of both of these models are fairly reliable.

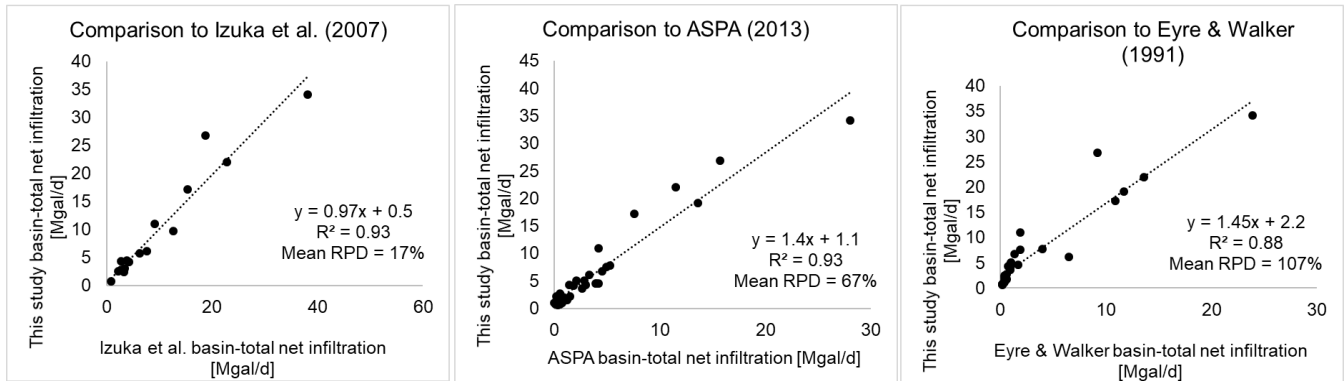


Figure 5.24: Quantitative comparisons of watershed-total net-infiltration amounts between the SWB2 model of this study and the three available Tutuila water-budget model comparison studies of Eyre and Walker (1991), ASPA (2013), and Izuka et al. (2007).

## 5.4 Summary and Conclusions

The SWB2 water budget model code created by the USGS (Westenbroek et al. 2018) was developed to specifically address unique hydrologic processes occurring in a wide array of settings, with a specific emphasis on high-tropical islands. For this study, the SWB2 code was applied to the island of Tutuila in American Samoa in order to calculate water budget components with a focus on net-infiltration, as this parameter directly relates to water resources availability via groundwater recharge. Water inputs to the model included monthly-gridded precipitation data developed by the PRISM Group (Daly et al., 2006) as well as direct-net infiltration resulting from anthropogenic sources such as leaking water lines and OSDS discharge. Land use, soil type, land slope, PET, wind speed, and surface water flow data were also used to parameterize the model. The SWB2 model used a stochastic approach where random sets of monthly rainfall patterns were used to disaggregate monthly-gridded precipitation data into a sequence of synthetic daily-gridded precipitation inputs, allowing the model to perform soil-moisture processing on a daily time step. The daily-resolution output was subsequently post-processed to reflect annual average totals of water budget components, and also within each major watershed on the island. The calculated water-budget components of interest included precipitation, ET, canopy interception, direct net-infiltration, runoff, and net infiltration. Results indicate 54% of Tutuila’s rainfall ends up infiltrating to be available as potential groundwater recharge, 8% is lost to canopy evaporation, another 15% is lost as ET from soils, and 21% is lost as stormflow-runoff to surface water features.

Sensitivity testing revealed that rainfall was the parameter to which the modeled net-infiltration result was the most sensitive. This was followed by the R:R ratios and PET. Variation in other parameters by 25% yielded changes in net infiltration of less-than 2%, suggesting the model was not very sensitive to these parameters. Therefore, high uncertainties in poorly constrained parameters, such as MFR ratios and the spatial distribution of NRW leakage are mitigated by the lack of sensitivity to these parameters in final recharge results. On the other hand, the model is more sensitive to R:R ratios, and the measurement uncertainty is likely to be high on this parameter, due to uncertainty in the empirical relationships used to calculate streamflow and the subjectivity inherent in baseflow-separation analysis. Conversely, even though the model is most sensitive to precipitation, the uncertainty on this parameter is probably fairly low, as it was interpolated from numerous measurement stations and averaged over a 30-year period. Therefore, the model's weakest link is probably the R:R ratios. This indicates that future efforts targeted at developing better constraints of streamflow, especially in MFR affected areas would be very useful for improving estimates of groundwater recharge.

The effects of future climate change on water resources availability was also tested with the parameterized water budget model. This was accomplished by integrating dynamically downscaled climate predictions for 2080 to 2099 derived from a global climate model (Wang and Zhang, 2016) into the SWB2 model input files. Specifically, modified rainfall and temperature datasets were supplied to the model, and an increase in net-infiltration of 17 to 27% was predicted depending on the emissions scenario used. Sensitivity testing was performed with all model parameters and the effect of precipitation was found to have the most impact on net-infiltration amounts. Model results were validated by comparison to three other previously documented water budget models and the SWB2 model produced results that were reasonably consistent with the most reliable of the previous models, showing an average RPD of just 17% for overlapping watersheds.

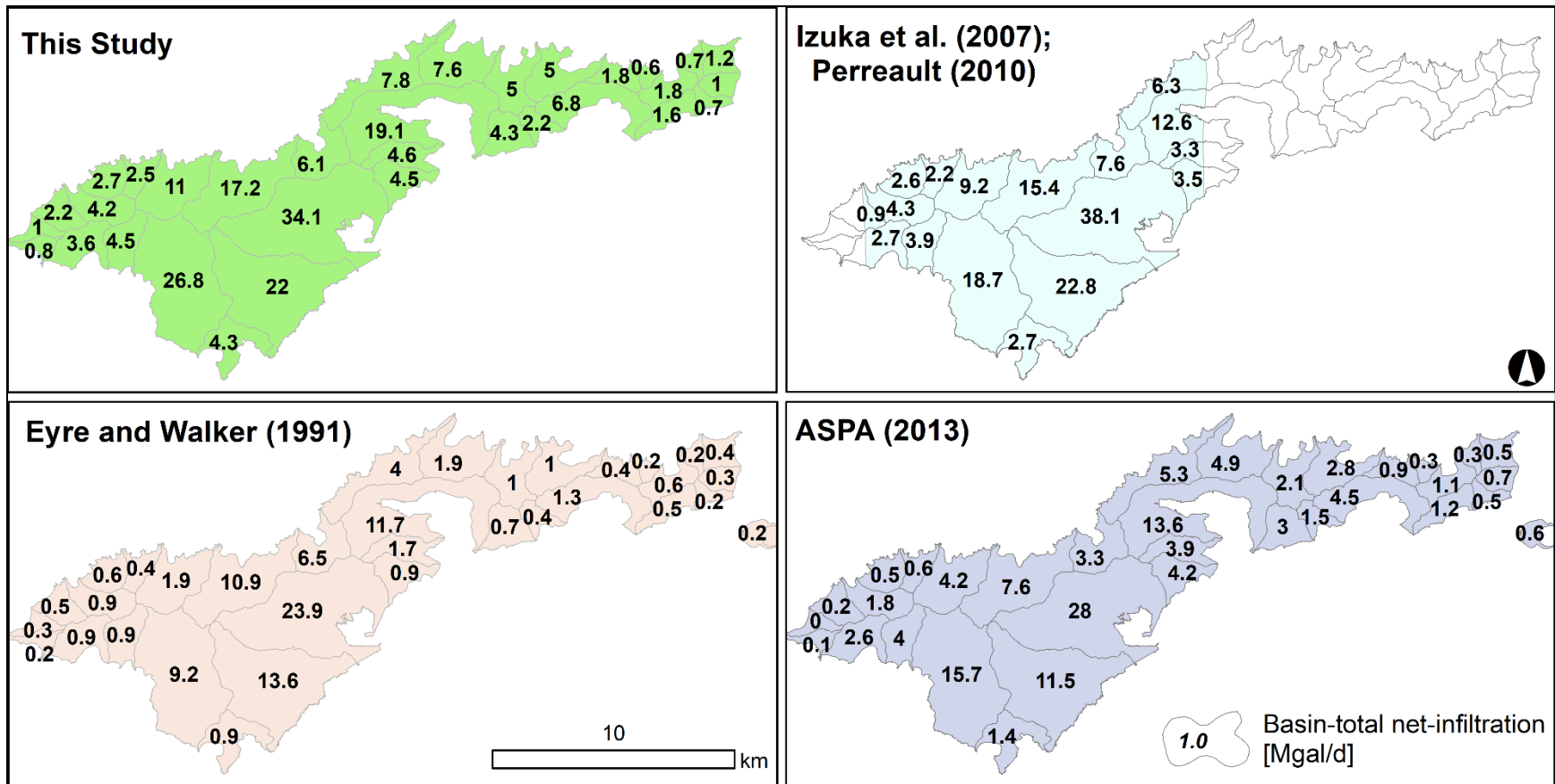


Figure 5.25: Comparison of basin-total net-infiltration amounts, in Mgal/d, between this study and three other documented Tutuila water-budget models. Only the model from Izuka et al. (2007) study was formally published, with the other two being contained in unpublished reports. Also the Izuka et al. model is the only other one that includes the effects of MFR on the Tafuna-Leone Plain.

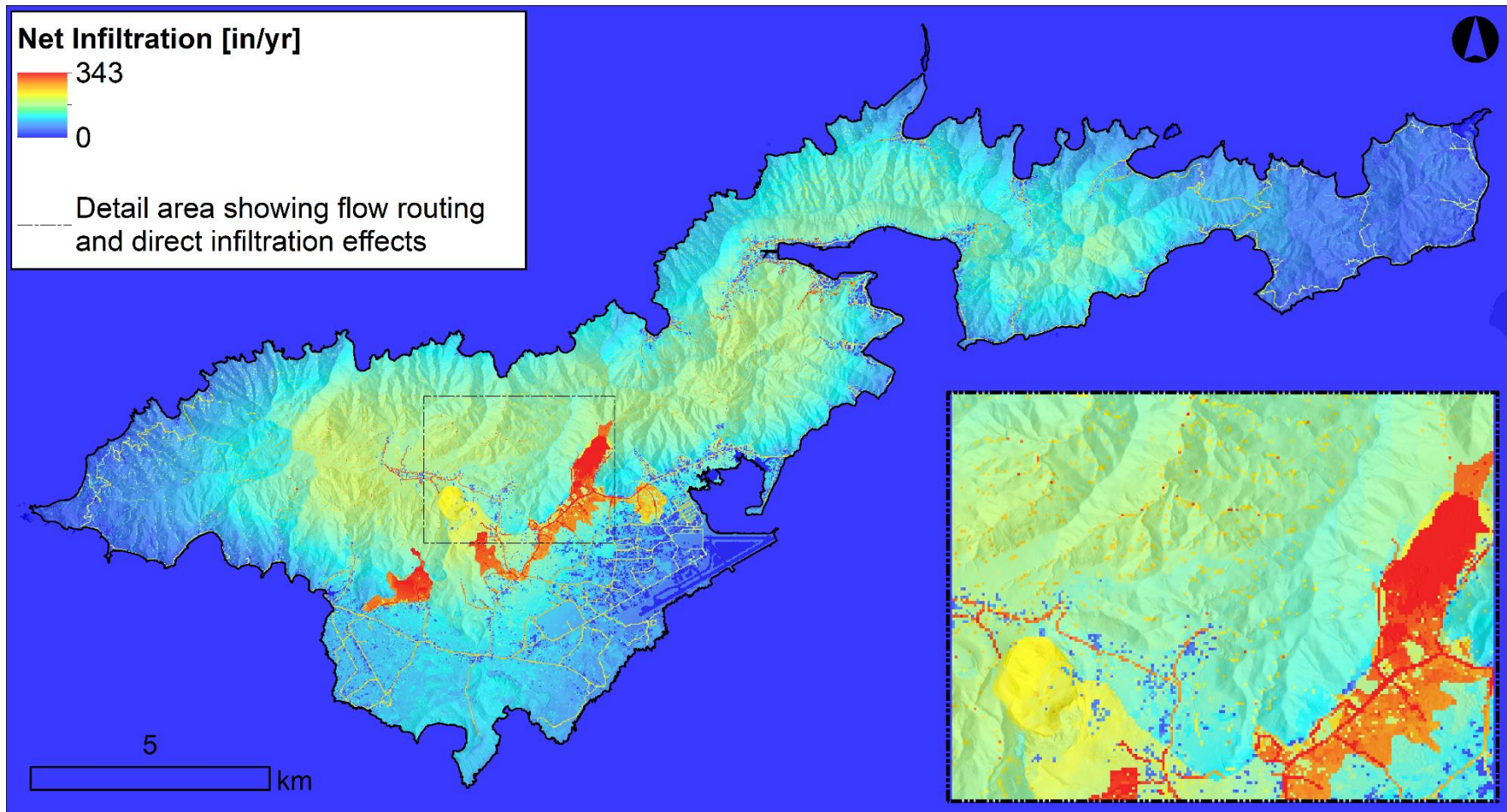


Figure 5.26: Detail map of model calculated average-annual net infiltration at 20 m cell-size resolution. Inset map shows detail of (1) flow routing effects, seen as higher recharge squares at the bottom of drainage channels, (2) direct infiltration from leaking water lines, seen as linear zones of higher infiltration, and (3) MFR zones seen as larger patches of high-infiltration.

## 5.4.1 SWB Technology Transfer

The implementation of this model is not intended to be a static-finished product. As different climate projections are developed or updated parameterization datasets are released the model can and should be revised to reflect newer or more accurate data sources. Therefore, the model code and the directory tree with all of the raw-input datasets are hosted at <https://github.com/UH-WRRC-SWB-model>. This repository contains all the necessary files to completely regenerate the model on any other computer with a Python interpreter and the required modules. To run the model, the user simply needs to download or 'clone' the Github repository (UH-WRRC-SWB-model) and run the code following the instructions in the online-readme file and using a python interpreter such as jupyter notebook. It should be noted that the model was constructed using a number of required python modules, which are listed in the first code block of the model script. All of these modules are open-source except for one, whereas the model uses functionality included with ESRI's ArcPy module, thus the user must have an active ArcGIS or ArcPRO license to run the model and access these functions.

### List of input datasets included in repository

- SWB control file: "Tutuila200\_controlFile.ctl"
- Shapefile of model boundary: "grid\_bound.shp"
- Shapefile of land use zones: "Land\_use\_wRO\_codes2.shp"
- Shapefile of soil zones: "Tut\_Soil\_clip2.shp"
- Shapefile of rainfall station Thissen polygons: "Thissen\_poly\_rain\_clip\_modified2.shp"
- Shapefile of watersheds: "All\_major\_WS\_modified3.shp"
- Shapefile of municipal water lines: "Transmission\_water\_mains.shp"
- Shapefile of OSDS units: "OSDS\_units\_pts.shp"
- Raster format DEM: "10M\_DEM.tif"
- Annual rainfall grid: "An\_pcip\_in.tif"
- 30 m winds speed map: "wndsp\_30m.tif"
- Set of 12 monthly gridded rainfall maps: "PRISM\_ppt\_tutuila\_30yr\_normal\_80mM1\_{ month }\_asc.asc"
- Monthly gridded Max temperatures: "PRISM\_tmax\_tutuila\_30yr\_normal\_80mM1\_{ month }\_asc.asc"
- Monthly gridded Max temperatures: "PRISM\_tmin\_tutuila\_30yr\_normal\_80mM1\_{ month }\_asc.asc"
- Monthly gridded evapotranspiration maps: "{month}\_ET.shp"
- Modified land-use lookup table: "Landuse\_lookup\_maui\_mod5.txt"
- Tabular file of runoff to rainfall ratios: "RO\_Rf\_ratios\_real\_monthly3\_2000\_2010.txt"
- Externally generated rainfall fragment set file: "Rainfall\_fragments\_2001.prn"
- Sequence file for rainfall fragment order: "Sequence\_file\_2002.prn"
- Shapefile of mountain font recharge contributing areas: "Contributing\_MRF\_Areas\_leone.shp, Contributing\_MRF\_Areas\_tafuna.shp"
- Shapefile of mountain font recharge receiving areas: "MFR\_infiltration\_area\_leone.shp", MFR\_infiltration\_area\_Tafuna.shp"

### Example list of output datasets included in repository

- "actual\_et\_annual.asc"
- "direct\_net\_infiltration\_annual.asc"
- "direct\_soil\_moisture\_annual.asc"
- "interception\_annual.asc"
- "net\_infiltration\_annual.asc"
- "rainfall\_annual.asc"
- "runoff\_annual.asc"

## References: Chapter 5

- Allen, R.G., Pereira, L.S., Raes, Dirk, and Smith, Martin. (1998). Crop evapotranspiration – Guidelines for computing crop water requirements: Rome, Food and Agriculture Organization of the United Nations, FAO Irrigation and Drainage Paper No. 56, 174 p.
- Arnold, J.G., Srinivasan, R., Muttiah, R.S., Williams, J.R., (1998). Large area hydrologic modeling and assessment – Part 1: model development J. Am. Water Resour. Assoc., 34 (1) (1998), pp. 73-89, 10.1111/j.1752-1688.1998.tb05961.x.
- AS-DOC - American Samoa Department of Commerce. (2009). Buildings layer for Tutuila Island. [Data file]. <http://doc.as.gov/>
- ASPA - American Samoa Power Authority. (2013). Documentation of Wellhead Analysis, Tutuila Hydrogeological Analysis for the U.S. EPA Clean Water Act – State Revolving Fund ASPA Consolidated Grant for the benefit of the Territory of American Samoa. Report prepared for American Samoa Power Authority, Pago Pago, American Samoa. Author Walters, M.O.
- Barlow, P. M., Cunningham, W. L., Zhai, T., & Gray, M. (2015). US Geological Survey groundwater toolbox, a graphical and mapping interface for analysis of hydrologic data (version 1.0): user guide for estimation of base flow, runoff, and groundwater recharge from streamflow data. US Department of the Interior, US Geological Survey.
- Bentley, C.B. (1975). Ground-water resources of American Samoa with emphasis on the Tafuna-Leone Plain, Tutuila Island. US Geological Survey Report No. 75-29.
- Daly, C., J. Smith, M. Doggett, M. Halbleib, and W. Gibson. (2006). High-resolution climate maps for the Pacific basin islands, 1971–2000. Final Report. National Park Service, Pacific West Regional Office.
- Davis, D.A. (1963). Ground-water reconnaissance of American Samoa. U.S. Geological Survey Water-Supply Paper 1608-C.
- Engott, J. A., Johnson, A. G., Bassiouni, M., & Izuka, S. K. (2015). Spatially distributed groundwater recharge for 2010 land cover estimated using a water-budget model for the island of O'ahu, Hawaii (No. 2015-5010). US Geological Survey.
- Eyre, P., and G. Walker. (1991). Geology and ground-water resources of Tutuila American Samoa. Unpublished report in American Samoa Power Authority files.
- Gash, J.H.C., Lloyd, C.R., and Lachaud, G., (1995). Estimating sparse forest rainfall interception with an analytical model: Journal of Hydrology, v. 170, no. 1, p. 79–86.
- Izuka, S. K., Giambelluca, T. W., & Nullet, M. A. (2005). Potential Evapotranspiration on Tutuila.

- American Samoa. U.S. Geological Survey Scientific Investigations Report 2005-5200. U.S. Geological Survey
- Izuka, S.K., J.A. Perreault, and T.K. Presley. (2007). Areas contributing recharge to wells in the Tafuna-Leone Plain, Tutuila, American Samoa. Honolulu, HI: Geological Survey (US). Report no. 2007-5167. <https://pubs.er.usgs.gov/publication/sir20075167>.
- Izuka, S.K., Oki, D.S., and Engott, J.A., (2010). Simple method for estimating groundwater recharge on tropical islands: *Journal of Hydrology*, v. 387, no. 1, p. 81-89.
- Izuka, S. K., Engott, J. A., Bassiouni, M., Johnson, A. G., Miller, L. D., Rotzoll, K., & Mair, A. (2016). Volcanic aquifers of Hawai 'i – Hydrogeology, water budgets, and conceptual models (No. 2015-5164). US Geological Survey.
- Johnson, A.G., (2012). A water-budget model and estimates of groundwater recharge for Guam: U.S. Geological Survey Scientific Investigations Report 2012-5028, 53 p
- Kennedy, Jenks, and Chilton Consulting Engineers. (1987). Groundwater contamination study Tafuna-Leone Plain Tutuila Island. Final report for the Environmental Quality Commission, Office of the Governor, Tutuila, American Samoa. 168 p.
- Mair, A., Hagedorn, B., Tillery, S., El-Kadi, A. I., Westenbroek, S., Ha, K., & Koh, G. W. (2013). Temporal and spatial variability of groundwater recharge on Jeju Island, Korea. *Journal of hydrology*, 501, 213-226.
- Meyer, R.A., Seamon, J.O., Fa'aumu, S., and Lalogafuafua, L. (2016). Classification and Mapping of Wildlife Habitats in American Samoa: An object-based approach using high resolution orthoimagery and LIDAR remote sensing data. Report prepared for American Samoa Department of Marine and Wildlife Resources.
- Nakamura, S., 1984. Soil survey of American Samoa. U.S. Department of Agriculture Soil Conservation Service, Pago Pago. 95 p.
- National Weather Service (NWS). (2000). Precipitation records from 1971-2000. Data Set.
- O'Callaghan, J.F., and Mark, D.M., (1984). The extraction of drainage networks from digital elevation data: *Computer vision, graphics, and image processing*, v. 28, no. 3, p. 323-344.
- Oki, D.S., (2002). Reassessment of ground-water recharge and simulated ground-water availability for the Hawi area of north Kohala, Hawaii: US Department of the Interior, US Geological Survey, 62p.
- Penman, H.L., (1948). Natural evaporation from open water, bare soil, and grass: *Proceedings of the Royal Society of London*, A193, p. 120-146.

- Perreault, J.A. (2010). Development of a water budget in a tropical setting accounting for mountain front recharge. Masters Thesis, University of Hawaii at Manoa. Honolulu, HI.
- Shade, P. J., & Nichols, W. D. (1996). Water budget and the effects of land-use changes on ground-water recharge, Oahu, Hawaii (Vol. 1412). US Geological Survey.
- Shuler, C. K., El-Kadi, A. I., Dulai, H., Glenn, C. R., & Fackrell, J. (2017). Source partitioning of anthropogenic groundwater nitrogen in a mixed-use landscape, Tutuila, American Samoa. *Hydrogeology Journal*, 25(8), 2419-2434.
- Thorntwaite, C.W., and J.R. Mather. (1955). The water balance. *Publications in Climatology (Laboratory of Climatology)* 8(1): 1-86.
- Stearns, H.T. (1944) Geology of the Samoan islands. *Geological Society of America Bulletin* 55(11): 1279-1332.
- Wang, Y. and Zhang, C. (2016). Project Final Report - 21st Century High-Resolution Climate Projections for Guam and American Samoa. Retrieved from: <https://www.sciencebase.gov/catalog/item/583331f6e4b046f05f211ae6>
- Wahl, K. L., and Wahl, T. L., (1995). Determining the Flow of Comal Springs at New Braunfels, Texas, Texas Water '95, American Society of Civil Engineers, August 16-17, 1995, San Antonio, Texas, pp. 77-86.
- Westenbroek, S. M., Engott, J. A., Kelson, V. A., & Hunt, R. J. (2018). SWB Version 2.0—A Soil-Water-Balance Code for Estimating Net Infiltration and Other Water-Budget Components (No. 6-A59). US Geological Survey.
- Wilson, J.L., and H. Guan. (2004). Mountain-block hydrology and mountain-front recharge. In *Groundwater Recharge in a Desert Environment: The Southwestern United States*, ed. J.F. Hogan, F.M. Phillips, and B.R. Scanlon, 113-137. American Geophysical Union, Washington, D.C.
- Wong, M.F. (1996). Analysis of streamflow characteristics for streams on the island of Tutuila, American Samoa. US Geological Survey Water Resources Investigations Report No. 95-4185, Honolulu, HI.

## Chapter 6:

# Collaborative groundwater modeling: Open source, cloud-based, applied science at a small-island water utility scale

### **Abstract**

The process traditionally used to execute most groundwater modeling projects has several drawbacks. The typical client-consultant relationship is expensive, produces products with limited longevity, and is technologically dated. Recent advancements in cloud-computing and social-networking are influencing how we communicate professionally, work collaboratively, and approach data-science tasks. Here we show how the groundwater modeling process is especially well positioned to benefit from these technological advancements. This work presents a case study detailing a vertically-integrated, collaborative modeling framework jointly developed by participants at the American Samoa Power Authority and at the University of Hawaii Water Resources Research Center. The framework includes a chain of modular components extending from the direct collection and analysis of climatic and streamflow data through the development of a water budget model and a dynamic regional groundwater model. The process we present is entirely open-source and employs newly available data-science infrastructure such as Python-based tools compiled with Jupyter Notebooks, GitHub, Binder and Microsoft Azure. These resources facilitate the collaborative model development process and deliver seamless integration of multiple computational components into a dynamic cloud-based workflow that is immediately accessible by stakeholders, resource managers, or anyone with an internet connection.

## 6.1 Introduction

For the last half-century, computational modeling has become one of the primary tools in the water resource manager's toolbox. Groundwater models have become indispensable, industry standard methods for estimating the availability and sustainability of groundwater resources (e.g. Young & Bredehoeft 1972; Cummings & McFarland, 1974; Willis & Yeh 1987). However, because of the inherent complexity of numerical models and the significant time, effort, and expertise needed for their development, it is often challenging for stakeholders and water managers to access models that are appropriate for their needs (Essawy et al. 2018). Oftentimes smaller water utilities or resource management agencies simply do not have the resources to develop their own models or the in-house expertise to assess the validity, conceptualization, calibration, or usefulness of existing models. Within the traditional model development paradigm, water management agencies usually take one of two approaches, (1) dedicate significant resources to building internal modeling capacity or (2) contract with outside 'experts' to deliver models that typically cannot be interacted with once completed. The latter approach generally produces static models that may lose relevance quickly, and are often produced in a format that does not allow end-users to easily modify parameters or address new questions. This approach also suffers from the inherent temporariness of typical funding mechanisms, whereas the modeling process lasts only as long as the project account is solvent, after which a final report is delivered and model files are archived for long-term storage on a server in the back of an office somewhere. Compounding the issue, is the fact that these sorts of models typically require proprietary software or specialized computational environments to run, making it prohibitively challenging for end-users to open and interact with the model. On the other hand, a major drawback to the approach of handling all modeling tasks in-house, is the high cost of training, software, and salary required for agencies to retain personnel with sufficient skills to create and maintain effective models. This level of resource dedication is often only possible for larger utility companies or management agencies, thereby leaving small, remotely located agencies with few to no options for accessing quality modeling tools.

Here we document the ongoing development of a collaborative modeling framework conceived as a joint effort between the University of Hawaii Water Resources Research Center (UHWRRRC) and the American Samoa Power Authority (ASPA). Our intended outcomes for the models developed within this framework are commensurate with the motivations behind the participatory and collaborative modeling movement that has, in recent decades, become a highly utilized approach in environmental management. These outcomes are centered around addressing the need for enhanced researcher - stakeholder engagement (e.g. Argent and Grayson, 2003; Liu et al., 2008) and producing, practical, defensible models that sufficiently address stakeholder needs and promote model use in guiding important water management decisions. Such models are intended to incorporate the views, needs, and knowledge of as many stakeholders as possible, including scientists, policy makers, and resource managers.

The terms collaborative and participatory modeling are often used interchangeably in the literature to describe modeling endeavors that involve scientists, modelers, stakeholders, or community members in decision making processes. Basco-Carrera et al. (2017) distinguishes these terms, defining collaborative modeling as a more intensive sub-discipline of participatory

modeling. With collaborative modeling, the actual model development responsibilities are more equally shared between participants and the decision making process has a higher level of participation across all levels. Moran (2016) describes the collaborative process as one where, *“...model developers, decision-makers, stakeholders and others work together to develop a shared understanding of [the region’s] management objectives and the model’s role in supporting those objectives.* Langsdale et al. (2013) further refines collaborative modeling as a process where, *“Both the model and the process remain accessible and transparent to all participants, Collaborative modeling builds trust and respect among parties.”* Participatory and collaborative modeling methods have been applied across many disciplines ranging from computer science (e.g. Bidarra et al., 2001), to economics (e.g. Mendoza and Prabhu, 2006), and social sciences (e.g. Flint et al., 2017). This approach is especially pertinent in water resource management, as water’s indispensable and ubiquitous nature inherently makes any issue a multi-stakeholder concern. In the water resources field, collaborative or participatory approaches have been applied in numerous case studies across a range of technical foci including watershed modeling (e.g. Liu et al., 2008), groundwater modeling (e.g. Barfield, 2009; Beall et al., 2011), and water policy and planning (e.g. Tidwell et al., 2004).

It is incontrovertible that the adoption of research results by decision makers relies on the usability of the information produced. Such information must be both scientifically credible as well as tailored to the priorities of managers and policy-makers. This means models should be easy for managers and end-users to understand and to interact with. In this context, the success of a model is measured by more than just its calibration, a successful model is able to provide stakeholders with the opportunity to dynamically change model inputs, assess future scenarios, and evaluate model uncertainties. This requires a model design that is physically accessible, i.e. based on open-source codes, and conceptually accessible, meaning the modeling process facilitates sharing of the required core skills for data management, workflow efficiency, and visualization (Pease et al, 2018). Accessible models should also be portable, flexible, use small file sizes, and have short run times to enhance their ease of adoption (Argent and Grayson, 2003). This paradigm views model development as a process, not necessarily an end-goal. Such a process-based approach does require some redefinition of the typical client-consultant relationship, requiring a longer period of interaction and collaboration. However, without this time commitment, it is difficult to support the type of continuous model development that allows updated information to be incorporated as new data or changing conditions are encountered.

The cooperative paradigm is beneficial to both model developers and end users, as it not only encourages the adoption and trust of models but also encourages their responsible use, as users are more aware of limitations, assumptions, and appropriate uses of their tools (Argent and Grayson, 2003). Another benefit is simply the more effective use of limited resources and avoidance of duplicative efforts. When a model is built cooperatively, there is less need for technology transfer, since participating stakeholders are already familiar with the model and its development. This helps to reduce user error leading to poor decision making, which can result from miscommunication of model application or results. Perhaps most importantly, this paradigm allows decision making to be an exploratory process by accommodating new data or

information and simulating alternative ideas quickly (Barfield, 2009; Langsdale et al., 2013). The collaborative framework facilitates interaction and dynamic management, by allowing models to be modified based on stakeholder discussion, concerns, and ideas (Pease et al, 2018).

### 6.1.1 Objectives

The main objective of this chapter is to present a framework for, and a case study of, a small scale, vertically integrated, collaborative groundwater modeling process that takes advantage of recent advancements in cloud-computing and open-source modeling tools. We refer to this framework as vertically integrated because it includes a diverse chain of modular components extending from the direct collection and processing of basic hydrologic parameters, through to the development of a dynamic regional groundwater model. A primary objective of this process is to make every part of it publically available online, so that the process is transparent, reproducible, and easy to understand for interested stakeholders. Anyone with the skill and interest is able to modify inputs, test scenarios, and continue model development for their own ends, and where stakeholders do not wish to interact directly with the model, the open-source code and in-line documentation facilitates discussion and planning between participants. Another objective of the chapter is to demonstrate the ease of use and the applicability of modern code sharing and cloud-computing tools in a scientific modeling setting involving participants at different and remotely located institutions. The tools presented are able to connect researchers and stakeholders through ready-built data science infrastructure that allows advanced modeling techniques to be easily shared, even when either party has limited software development experience.

## 6.2 Case Study Setting

The island of Tutuila is the main population center of the U.S. territory of American Samoa. It is located near 14° S and 170° W, and at 142 km<sup>2</sup> is the third largest island in the Samoan hot-spot island chain. Geologically, Tutuila contains two distinct provinces. The bulk of the island is composed of an older, highly eroded basaltic shield edifice (1.5 to 1.0 Ma), henceforth referred to as the older-volcanics. Recent (Holocene age) rejuvenation-stage volcanism erupting through the eroded southwestern flank of the older shields created the Tafuna-Leone Plain, a lava delta composed mostly of thin bedded pahoehoe lava flows (Stearns, 1944; McDougall, 1985). The pahoehoe flows of the plain impart a significantly higher overall hydraulic conductivity than is found in the Older-Volcanic Unit, which is composed of a heterogeneous mixture of a'ā lava flows, pyroclastic materials, and trachyte domes (Stearns, 1944; Eyre and Walker, 1991). Geological subdivisions within each of these units exist, and may be used as the basis for further refinement into zones with different hydrogeologic properties (Izuka et al., 2007). Tutuila's climate is warm and humid with abundant, year-round rainfall due to its position within the South Pacific Convergence Zone. The island experiences a wetter season with increased precipitation amounts from October to May, and a drier season with less, though still significant, precipitation from June to September. Rainfall varies considerably with

location and elevation, and ranges between 1,800 mm/yr near the Tafuna Airport up to more than 5,000 mm/yr along the crest of the highest mountains (Daly et al., 2006). The region is also influenced by tropical storms and hurricanes, and an average of 25 to 30 significant thunderstorms affect the island annually (Kennedy et al., 1987).

In American Samoa, groundwater resources supply over 90% of domestic, and nearly 100% of industrial water use. However, these resources are afflicted by multiple threats to their long-term sustainability. Since 2009, portions of the public water supply system have been unsafe to drink, necessitating one of the longest standing boil-water-advisories in U.S. history. This is partly caused by the vulnerability of Tutuila's young and highly-permeable aquifers to anthropogenic and surface water contamination (Shuler et al., 2017; Shuler et al., 2018). Other aquifers on Tutuila produce high salinity water, presumably caused by salt-water intrusion (Izuka, 1999). In some cases, the island's wells produce water with Cl<sup>-</sup> concentrations exceeding the U.S. Environmental Protection Agency drinking water standards by four to five times. Multiple local stakeholders see groundwater models as a tool that will greatly facilitate management of these issues (ASPA, 2013, Anderson-Taggarino personal communication Oct, 2018). While development of groundwater models has been a long standing priority for ASPA, the island's only water utility, limitation of financial and personnel resources has so far, precluded realization of that goal. As of this writing, there have been four known groundwater models developed for portions of Tutuila (Izuka et al., 2007; ASPA, 2013, Shuler et al., 2014, Shuler et al., 2017). While each of these models addressed a specific question, ranging from defining well-capture zones to modeling nutrient transport, none have satisfied the requirements to fully address ASPA's water management needs. The static nature of these models also restricts their ability to be modified, and by nature, most small-scale water utilities do not have the time or resources needed to support building and maintaining the technical capacity necessary for maintaining active modeling projects.

## 6.2.1 Collaborative Groundwork

The foundation for this collaborative modeling project was based on a formalized working relationship between ASPA and UHWRRRC. The American Samoa Power Authority is the sole water utility in American Samoa, and is also responsible for all municipal power, wastewater, and solid waste services. American Samoa is a unique environment as it is small (population of approximately 60,000), geographically isolated (4,000 km to the nearest continent), and a sovereign society still retaining much of its indigenous culture and tradition. Therefore, ASPA is particularly invested in not only meeting customer needs, but also in conservation and responsible stewardship of the island's limited natural resources. The Water Resources Research Center is a technical research unit at the University of Hawaii, and its stated mission is, "*To promote understanding of critical state and regional [including the U.S. Affiliated Pacific Islands] water resource management and policy issues through research, community outreach, and public education.*" To fulfil this mission in American Samoa, UHWRRRC has been working with ASPA and other agencies since 2013 to develop an integrated water resources research program in the territory that strives to incorporate on-island stakeholder concerns into research priorities. The relationship between UHWRRRC and ASPA was officially ratified in 2015 through

a memorandum of understanding (MOU) focused on collaborative water resources related work. The MOU established long-term goals specifically to (1) develop infrastructure for collection of hydrologic and climatic data, and (2) generate and apply hydrologic data in support of ASPA's water resources management priorities. Additionally, a formal mechanism for identifying stakeholder needs and research priorities was conceived by UHWRRRC through establishment of the American Samoa Water Resources Stakeholders Committee. Water-related agency heads were invited to serve as committee members. Since its formation, the committee has participated in annual stakeholder input workshops and meetings on Tutuila, and also provides annual review of Water Resources Research Institute Program grant proposals. A consistently identified priority by the committee is a need for additional groundwater modeling.

## 6.3 Methods

### 6.3.1 Modeling Framework

The modeling framework presented in this chapter was developed using a collaborative modeling paradigm, where input, feedback, and participation between ASPA and UHWRRRC participants were integrated into the development process from its beginning. Because ASPA's and UH-WRRRC's interests overlap in terms of groundwater modeling, development of a management focused groundwater model was prioritized as an end-goal of this effort. The first step identified for achieving this goal was to begin collecting hydrologic data after a 7-year long data gap resulting from the cessation of U.S. Geological Survey (USGS) monitoring operations in 2008. Prior to this time, the USGS maintained numerous weather stations, rain gauges, and stream gauges, many with decades long periods of record. These datasets are imperative for estimating groundwater recharge, which is perhaps the most important input variable for development of groundwater models, especially in island settings with very steep rainfall gradients. To fill this need, UHWRRRC and ASPA collaboratively created and now currently maintain a monitoring network consisting of eight stream gauging stations and six weather monitoring stations. ASPA took responsibility for regular station maintenance and downloading data, and UHWRRRC covered the initial equipment costs and took responsibility for data processing, quality assurance / quality control (QA/QC) procedures, as well as archiving and distribution of data. To accommodate the extra field-based workload of this project, ASPA agreed to develop a full-time position for a hydrologic technician. This step was a cornerstone in the success of the participatory process, as it significantly increased ASPA's ability to commit to the program success.

These weather stations and stream gauges continually produce raw data in need of QA/QC processing and integration into each complete station record with previous data. This is accomplished with cloud-based processing routines that create output datasets, which can subsequently be supplied as input to a water budget model. We selected the Soil-Water Balance 2 (SWB2) water budget mode developed by the USGS (Westenbroek et al., 2018) to calculate spatially distributed groundwater recharge rates. All water budget inputs and outputs can be

processed in the same Python development environment as the aforementioned monitoring network data, resulting in a seamless integration of processing steps, including running the SWB2 code itself. While linking these steps creates a complex network of interdependencies, consistency and organization are maintained through the cloud-based version management application GitHub.

Groundwater model development is the final step in this collaborative modeling process, and this step like those previously described, is performed in the same Python-based development environment, again resulting in seamless integration of all modeling steps to achieve a cohesive workflow. Specifically, the Python module FloPy was selected for most of the necessary pre- and post-processing tasks. The primary input from the ASPA-UHWRRRC processing/modeling workflow to the groundwater modeling component is the SWB2 generated groundwater recharge coverage, which is formatted so that it can be used as direct input in a FloPy script. As of this writing, groundwater model calibration is ongoing and dynamic Python based inverse-modeling optimization procedures are currently being explored. The adaptability of this framework greatly facilitates updating the existing model, for example, as ASPA drills more wells and additional water level observations and new pump test results become available. Figure 6.1 shows the entire data and modeling workflow for the ASPA-UHWRRRC cooperative modeling case study and these components are individually described in the sections below.

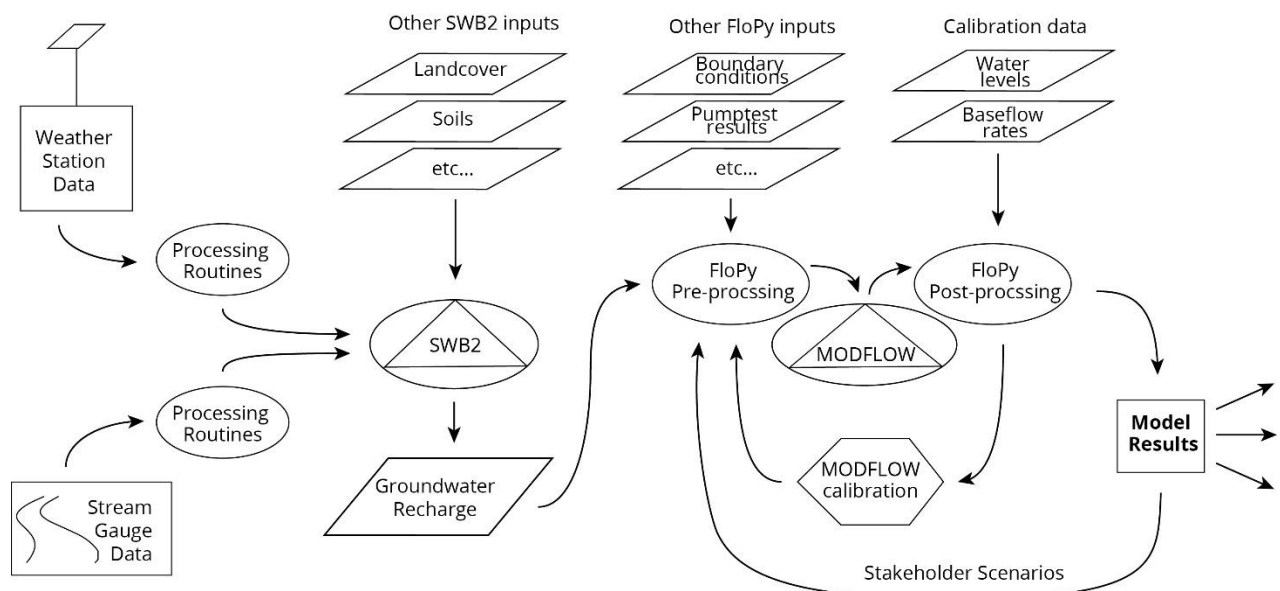


Figure 6.1: Schematic of data and modeling workflow for the ASPA-UHWRRRC case study. Datasets or geospatial layer components are shown in quadrilaterals, code-based processes are contained in ovals, and external model executables are contained in triangles, which are themselves within ovals since they are run as Python sub-processes.

### 6.3.2 Cyber-infrastructure Framework

The cloud based cyber-infrastructure framework used in the UHWRRRC-ASPA modeling process was imperative for facilitating communication, providing the ability to collaboratively code, and for taking care of the basic cloud-computing needs that would have been overwhelmingly resource intensive for either participant to develop independently. The selection of processing and computing tools was originally based on the need to make the weather station processing routines and data accessible to both parties, and also to store data in a way that allowed automatic updates to results each time new data became available. We selected Jupyter Notebooks (<https://jupyter.org>) for coding and project development, GitHub (<https://github.com>) for project storage and version control, Skype and Google Hangouts ([www.skype.com](http://www.skype.com) and <https://hangouts.google.com>) for communication, and (Binder or Microsoft Azure) (<https://mybinder.org> or <https://azure.microsoft.com>) for live, cloud-based code execution. All of these services are intuitive, simple, open-source, and integrable with each other, as well as with other widely used cloud-computing services.

The computing languages Python, R, and MATLAB are ubiquitous and commonly used tools in the sciences, especially for model development and application. (e.g. Borah and Bhattacharjya, 2013; Bakker et al., 2016; Yin et al., 2017). However, these tools have historically been difficult for non-experts to access, with steep learning curves and sometimes requiring costly licenses. While mastery of any of these languages can take a lifetime, recent developments in code compilation, support, and shareability are opening up these tools to non-traditional users in ways that have not been previously possible (Perez and Granger, 2015). Jupyter Notebooks (previously called ipython notebooks) are designed to bridge the gap between “coders” and the uninitiated by integrating live code, equations, visualizations, web links, and explanatory documentation, thereby drastically increasing their accessibility to more novice users (Kluyver et al., 2016). A key aspect of Jupyter Notebooks is a code-cell based modularity where blocks of code can be run independently, making the learning or exploration process more manageable and allowing explanations or visualizations to augment each step (Fig. 6.2). While these advances may seem unimportant to those more familiar with coding, in a collaborative framework where team members with variable degrees of expertise wish to be involved in the modeling process, simplicity and ease of access is paramount for everyone’s engagement. Owing to its current popularity, this format is very well supported in the development community and a large number of tools are being made available to increase the shareability and accessibility of notebooks. Almost every step in the Tutuila modeling framework project is compiled in Jupyter Notebook format (.ipynb). These notebooks can then directly integrated into the GitHub and Binder or Azure platforms to allow remote access for sharing, developing, and collaboration.

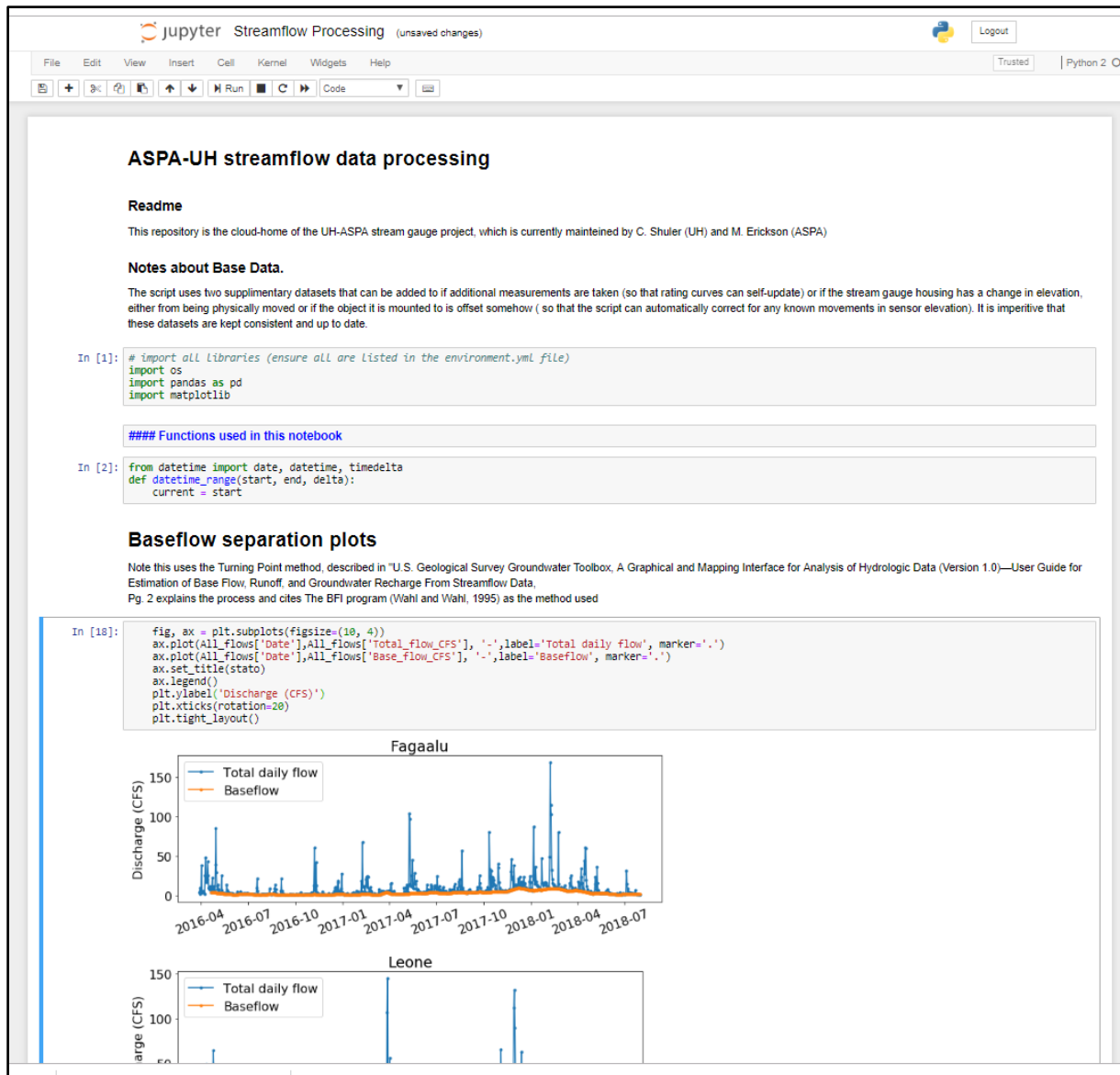


Figure 6.2: Example of a Jupyter Notebook showing code execution cells, live code with notes/comments, explanatory markdown cells, and in-line visualizations. These attributes make notebooks significantly more user friendly to team members with limited data science backgrounds.

GitHub is a free cloud-based file hosting service for version control and management of multi-participant coding projects, and it is becoming increasingly popular as a collaborative coding and data-driven project management tool (Dabbish et al., 2012). It is presently the computer-science industry-standard application for storing, managing, and tracking changes to code. Over 80% of professional developers indicate they use GitHub on a regular basis (Stack Overflow, 2018). GitHub is free (for open-access code) and provides unlimited data storage (as long as each file is under 100 mb). More importantly, the platform provides version control and

workflow organization, keeping track of changes made by different users and providing a browser friendly graphical user interface (GUI) to view and explore files, datasets, and results without needing specialized software or computing resources. For this project, GitHub was used to share processing routines and models and also to store and organize all data. Projects are managed in individual units termed “repositories”, which contain all of the data, the code, and the file structure for a process to run. The project repository can be directly downloaded from the web by anyone, providing the ability to share, reproduce, and work on models from start to finish. The repository can be pushed (uploaded) back to GitHub (by authorized team members), and any changes can be viewed and managed before incorporation into the master branch of the model. This not only allows for direct collaborative model development by multiple parties, but also acts as a system for archiving and distributing an entire modeling process including input, historical development, and output files. It also allows the modeling process to be completely transparent, as all the input data, and everything done with it is visible and reproducible by anyone.

There are numerous online video telecommunications services currently available, and we primarily used Skype or Google Hangouts as the main channels of communication between participants on different islands. While this is a fairly simple part of the framework, it nonetheless was one of the most important, as it facilitated simple, affordable communication and helped to avoid expensive international calling charges to American Samoa. The ability to share computer screens, so that users can see visual output directly, was especially helpful for the modeling process.

While GitHub provides online file storage and organization, it does not provide facilities for running models. Although it is not difficult to install the required open-source software modules needed to run these models on a user’s own computer, it does require the user to install Python and ensure version compatibility between the developer’s and the user’s installed software. This equates to a couple of extra steps and more importantly, introduces the potential for creating problems from incompatible software versions or operating systems. However, there are a number of small scale, cloud-computing resources available online that are dedicated to simplifying this particular issue. These services operate by opening a cloud-based Python environment on a remote server and installing all needed software at the time of use. Current options include Microsoft Azure, Google Colaboratory, and Binder, all of which allow for seamless integration with Jupiter Notebooks and GitHub. Binder is perhaps the most intuitive and straightforward of these options, simply requiring the web address of a GitHub project repository to start a live Python instance. Microsoft Azure, operates in essentially the same way, but does require an account login. At present, we are experimenting with both of these services to determine which will be most useful for this project. These recent advancements in cloud-based, remote-collaboration computing technologies have so far proved to be incredibly useful for facilitating participation between participants in the ASPA-UHWRRC modeling project, despite that fact that we are separated by 3000 km of ocean.

### 6.3.3 Weather Station Infrastructure

Because of the data gap created in 2008 when the USGS left American Samoa, historical, spatially-distributed rainfall and weather parameter data was becoming more and more outdated. To address this need and to supply data for our modeling purposes, UHWRRRC and ASPA worked collaboratively to develop and maintain a network of seven weather stations throughout the island (Fig. 6.3). The stations all have the capability to record precipitation, temperature, relative humidity (RH), wind speed and direction, and solar radiation (SR). The network was initially developed using Spectrum Technologies Inc. WatchDog 2900ET weather stations (Spectrum item number 3350WD2) and Davis Vantage Pro2 Plus weather stations (Davis Item #61612) (Fig. 6.4). These less-expensive and less robust instruments are currently being replaced by solar powered Campbell Scientific stations consisting of an RM Young Wind Sentry Set (03002-L12-PT), a CSL Temperature/RH Probe (CS215-L7-PT), an Apogee SP-110 Pyranometer (CS300-L12-PT), and a Texas Electronics Rain Gauge (TE525-L10-PT) (part numbers refer to Campbell Scientific catalog numbers). All stations are mounted on 2-3 m poles and placed at sites with the best balance of station-siting characteristics considering the available terrain (WMO, 1983; USEPA, 1987). Specifically, the ASPA-WRRRC weather station sites were selected based on the following criteria:

- 1) **Land ownership**—sites already leased or owned by ASPA were highly prioritized.
- 2) **Minimizing obstructions**— open fields or locations with fewer trees were prioritized.
- 3) **Spatial distribution**— Representativeness of the variability in Tutuila’s climate based on elevation, aspect, location was a priority in site distribution.

All weather stations were set to log data every 15 minutes, and data is downloaded in csv format every 1 to 3 months by the ASPA hydrologic technician. Once downloaded, the ASPA technician simply uploads the raw data files to the project repository on GitHub for processing and for long-term storage. Additional metadata and information about the ASPA-UHWRRRC network is presented in Shuler and El-Kadi (2017).

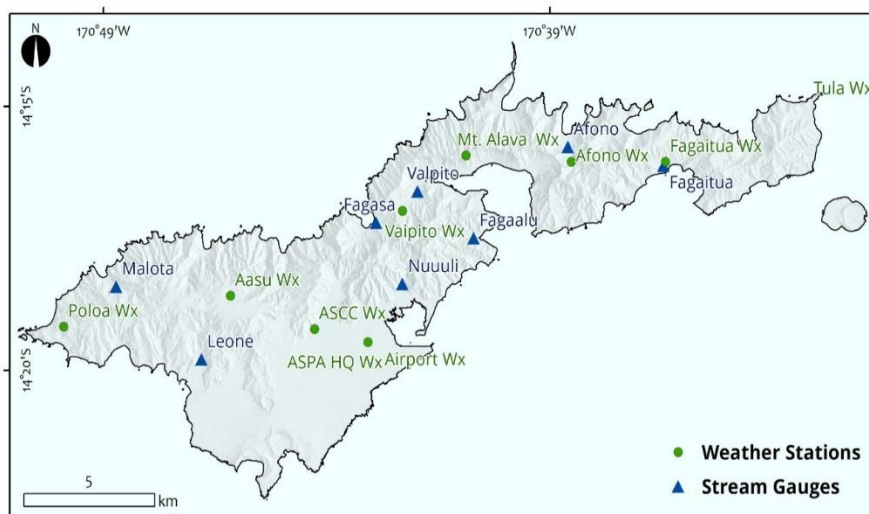


Figure 6.3: Monitoring network instrument map for Tutuila Island with weather stations shown as green circles and stream gauges shown as blue triangles.

### 6.3.4 Stream Gauge Infrastructure

The ASPA-UHWRRC collaborative framework also included developing on-island capacity for continuous streamflow measurement. Stream gauges were installed cooperatively by staff from both UHWRRC and ASPA over the course of two years. At present, the stream network consists of eight separate continuous record gauges located on different streams throughout Tutuila, and two open-air barometers, all recording at 15 minute intervals. The gauges consist of stainless steel, water level logging, pressure transducers (PT) (HOBO model # U20-001-01) installed in durable steel housings, which are permanently mounted to immobile structures such as bridges or bedrock outcroppings. Housings are made from perforated square galvanized steel pipe with a locking mechanism at the top (Fig. 6.4). The site selection process involved field scoping and soliciting input from multiple departments at ASPA, other on-island stakeholders such as the American Samoa EPA, and also with hydrologists at UH to ensure maximization of data utility. Site selection criteria included considering site access, proximity to historical gauges, bank and channel-control stability, and representativeness of the variability in Tutuila’s different climatic and geological regions. Additional metadata and information about the stream gauge network is available in Shuler and El-Kadi (2017).

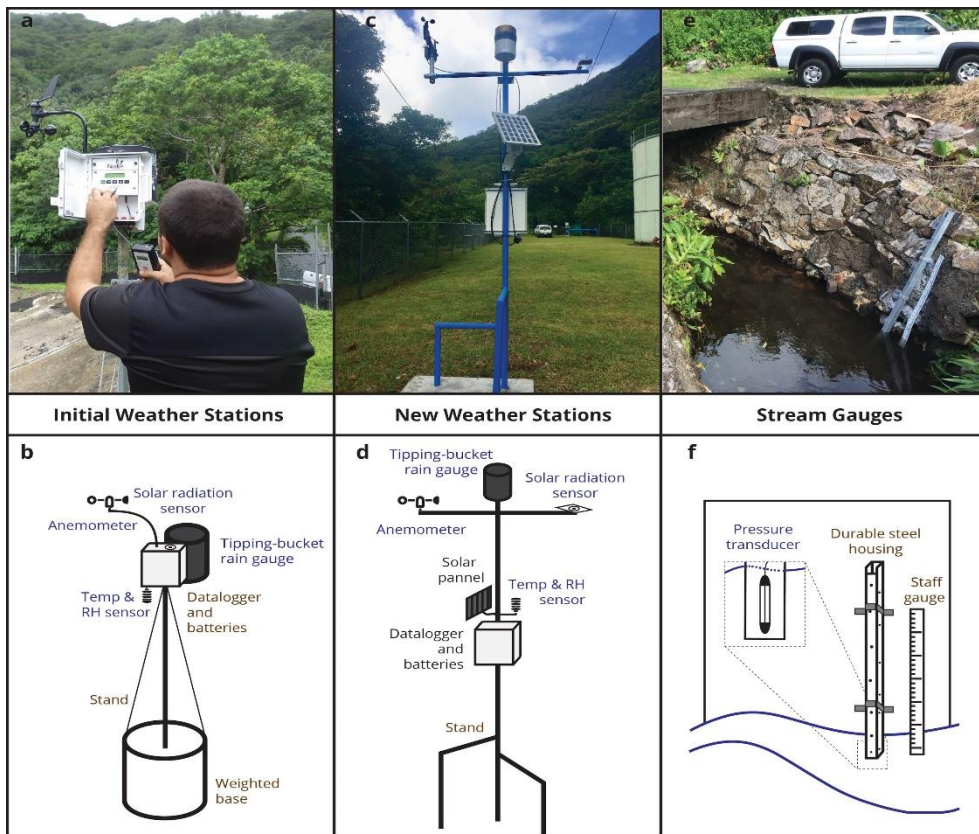


Figure 6.4: Examples of ASPA-UHWRRC weather station and stream gauge network instruments with schematics. Lower grade weather stations (a and b) initially deployed in 2015, are being replaced with new higher-quality stations (c and d) as time and funding permits. Stream gauges are shown in panels e and f. Blue text on schematics indicates sensors and brown text indicates infrastructure used.

### 6.3.5 SWB2 Model Development

The USGS developed the SWB2 Model (Westenbroek et al., 2018) to allow users to easily calculate water budget components, and specifically groundwater recharge. For this study SWB2 was used to develop a groundwater recharge coverage, which could then be used as an input to the FloPy groundwater model. The SWB2 model is based on a modified Thornthwaite-Mather (1955) soil-water balance approach, which in a simplified form is represented by the following:

$$\text{Recharge} = \text{Rainfall} - \text{Runoff} - \text{Actual Evapotranspiration}$$

The SWB2 model also includes recent updates based on the Hawaii Water Balance Code (Engott et al., 2017) that make the model better suited to modeling tropical basaltic islands such as the Hawaiian or Samoan Islands. All water balance components are calculated at a daily resolution and output files are produced in NetCDF format. This format can be post-processed with most geospatial software or python scripts can be used to process data into different temporal or spatial resolutions. Runoff-to-rainfall ratios and temporal rainfall distributions derived from our monitoring network data were used as key input variables to the SWB2 model. All other input datasets used for the SWB2 model were obtained from existing publications or databases, with each being described in the respective documentation as cited in Chapter 5 of this dissertation. All SWB2 inputs are either in the form of tabular lookup tables or if spatially-distributed data are used, they are required to be in the ESRI ascii grid format. Input files and sources included:

- Gridded monthly precipitation data (Daly et al., 2006)
- Precipitation gauge data used to represent temporal rainfall distributions (this study)
- Land use data (Meyer et al., 2016)
- Impervious surface ratios (Meyer et al., 2016)
- Canopy coverage ratios (Meyer et al., 2016)
- Soil type data consistent with the NRCS SSURGO database (Nakamura, 1984)
- Direct infiltration data from municipal water line leaks (ASPA, personal communication)
- Direct infiltration data from OSDS effluent discharge (AS-DOC, 2009)
- Runoff-to-rainfall ratios (this study; Perrault (2010); Wong 1996)
- Potential evapotranspiration data in monthly gridded format (Izuka et al., (2005).
- Canopy evaporation data (Engott et al., 2015; AWS Truepower, 2014)
- Gridded monthly maximum and minimum temperature data (Daly et al., 2006)
- Mountain front recharge information (Izuka et al., 2007)

The water budget model, just like the other routines and models used in this project, was designed to be used in a collaborative processed-based manner. Newly downloaded streamflow or rainfall datasets can be used to update the model on an ongoing basis, and if desired, participants can modify input files, change model parameters, run the model, and post-process model results. The version control capabilities of GitHub help to manage different participant's contributions or new scenarios, and also provides the ability to track the model's evolution. Although UHWRRRC performed the majority of SWB2 model development, ASPA provided advice in designing portions of the model, specifically relating to the magnitude and

distribution of non-revenue water / leaking water lines and direct net-infiltration from OSDS units. Additionally, as of this writing, we are developing additional future land-use scenarios with local stakeholders to assess the effects of possible land-use change on groundwater recharge. Full documentation of the SWB2 model development is provided in Chapter 5 of this dissertation.

### 6.3.6 FloPy Model Development

Although calibration and validation of the groundwater modeling component of the framework remains ongoing as of this writing, a fully functioning MODFLOW modeling process has been established. One of the primary motivations for development of this component is to ensure that all steps are directly integrable into the existing cyber-infrastructure framework and that the model only depends on tools that can be seamlessly implemented in the Python environment. Additional stipulations for the groundwater modeling process included:

1. Input data need to be simple to modify
2. Recharge from SWB2 has to be seamlessly integrated with future SWB2 updates
3. Updated observation data must be easily incorporated into calibration routines
4. Cell size resolution needs to be simple to modify
5. All model files, need to be small enough to be hosted on GitHub

Meeting these requirements was simplified by using FloPy, an open-source Python package developed by the USGS (Bakker et al., 2016). The primary functionality of FloPy is to support pre-and post-processing methods for the MODFLOW family of models, such as MODFLOW (Harbaugh et al., 2000), MT3DMS (Zheng and Wang, 1999), or SEAWAT (Guo and Langevin, 2002). Presently, the FloPy package is relatively new, but it is rapidly gaining in popularity due to its modularity, open-source availability, and use and support by USGS modelers (e.g. Rotzoll et al., 2016; Feo et al., 2018, Foglia et al., 2018). The bulk of the work in model development typically lies in converting and standardizing input datasets from variable formats into the grid-based formats accepted as input by the MODFLOW executable. FloPy contains many functions to perform pre-processing tasks, and since it is open-source and continually in-development, new functionality is constantly being added. Once input files are converted to appropriate formats, FloPy organizes the input data into a model object, which is input to MODFLOW and run by FloPy as a sub-process. FloPy also contains functionality to post-process, visualize, or reformat output data as desired by the user.

Key benefits of the FloPy method for model construction include: (1) model building and pre-processing steps are quick to execute, (2) the entire process is trivial to reproduce, (3) specific inputs are easy to modify, for example, changing cell size, and (4) the whole modeling process is transparent and easy to share with modeling team participants, as well as with end-users, other researchers, or reviewers. The ease of directly changing the model contributes to its utility in a process-based paradigm, allowing continuous model evolution based on new stakeholder needs, development of new procedures, and incorporation of updated data.

## 6.4 Process Implementation and Discussion

### 6.4.1 Weather Data Process Implementation

Weather stations are maintained, and data is downloaded at least quarterly by the ASPA technician. Protocols for data collection and maintenance were developed collaboratively between UHWRRC and ASPA and these are documented in Shuler and El-Kadi (2017). Once downloaded, the ASPA technician uploads raw weather station datasets to the cloud-based repository on GitHub (<https://github.com/cshuler/ASPA-UH-Integrated-Modeling-Framework>) and new datasets are automatically incorporated with previous datasets once the repository is accessed and the routine is run. Processing the available set of weather station data is simple and can be done by anybody with an internet connection. To process the raw data into summarized files, the user can download the repository from GitHub and run the routine on a personal computer, provided Jupyter Notebook is installed, or online using Binder or Azure. A user with contribution permissions to the GitHub repository, can then upload processed data back to the repository with the push of a button.

Once the weather data processing routine is open in a Python environment, the user can run through the existing steps to update the output with all raw weather data contained in the repository. If desired, the processing routine itself can be modified to change processing steps, generate different visualizations or reformat output data. The processing routine currently includes steps to consolidate and organize raw data files, perform QA/QC checks, remove previously identified bad data, visualize datasets, and summarize data at different time resolutions (Fig. 6.5). The primary output from the weather station processing routine used as input to the SWB2 model, is daily rainfall data and this dataset is directly taken in by the SWB2 pre-processing to ultimately inform calculation of the groundwater recharge coverage.

### 6.4.2 Streamflow Data Process Implementation

Stream gauge instruments are inspected and downloaded on a monthly basis and streamflow measurements are taken as frequently as possible, especially during high flow events. Once data is collected, the ASPA technician can upload raw water level files, and append new streamflow measurement data to the project repository on GitHub. The repository can be downloaded and processed on a personal computer or on a remote server as described for the weather station data. The streamflow processing steps include barometric compensation, removal of false readings, corrections for physical changes at gauge sites, automated development of rating curves, and summarization of data into daily series, monthly averages, and annual averages (Fig. 6.6). Monthly streamflow summaries produced by this routine are directly used as input in the SWB2 water budget model pre-processing routine to determine runoff to rainfall ratios, which are a key component in determining groundwater recharge rates.

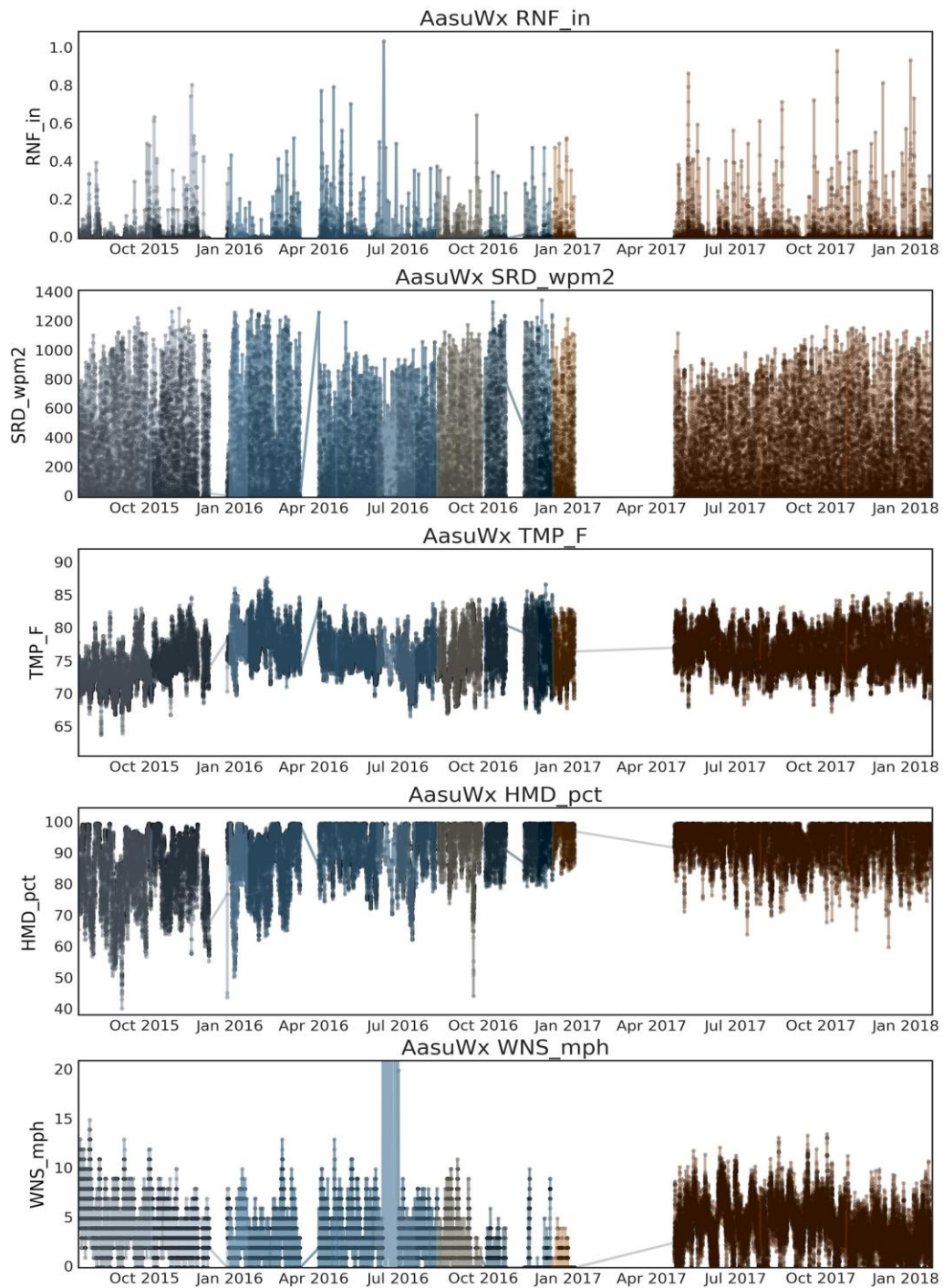


Figure 6.5: Example of consolidated weather station data for one of the ASPA-UHWRRC weather stations (Aasu site). Black line and dots represent consolidated data and colored shaded lines indicate extent of each individual raw weather station data file downloaded by ASPA technician. Note the gap in data where the original station went down, and was later replaced with a new high-quality weather station.

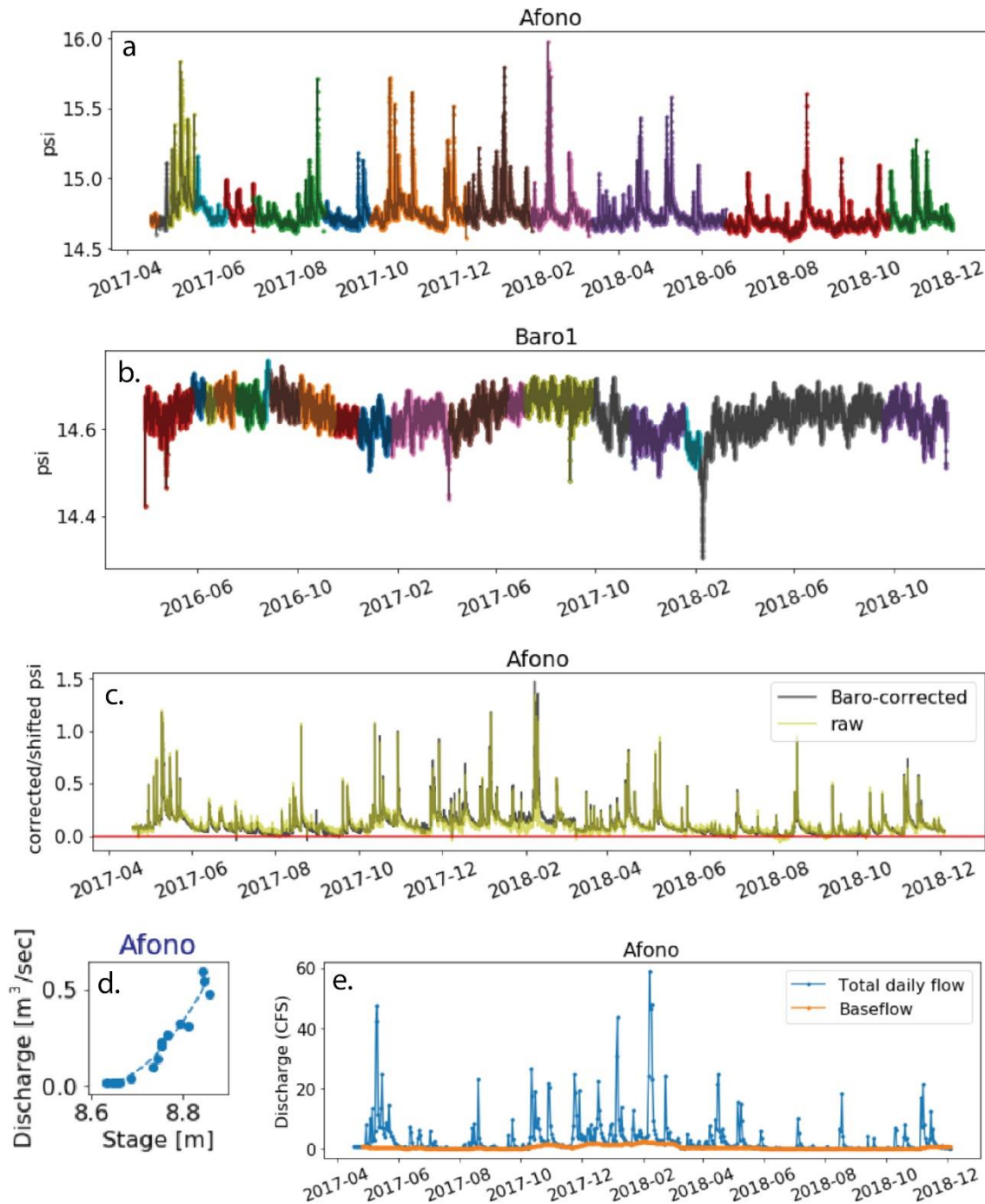


Figure 6.6: Example visualizations for a selection of the procedures implemented in streamflow processing for the Afono Stream Gauge. Steps include but are not limited to, a) consolidation of individual downloaded files (each color represents an individual data file) b) consolidation and incorporation of barometer data (each color represents an individual data file) c) barometric correction of stream stage, d) rating curve calculation, and e) baseflow separation.

### 6.4.3 SWB Implementation

The SWB2 model component was designed to be run as a series of modular cells, the first of which contain pre-processing routines that format shapefile or raster datasets into ascii grids for use in the SWB2 model. It is possible to modify or substitute different input datasets during any of these steps if desired, to update the model or to assess different scenarios. The SWB executable, which can be downloaded at no cost from the developer's website (<https://github.com/smwesten-usgs/swb2>), is run as a sub-process from the Jupyter Notebook. Once the SWB2 code is executed, the next set of cells, which contain code for post-processing the model output, are run to produce output data at any resolution or spatial aggregation the user desires. The SWB2 model produces spatially and temporally-distributed datasets for each output parameter in NetCDF file format. These datasets are computed on a daily time step, though it is typically common to summarize water budget results by month or year. At present, the SWB2 notebook is setup to produce volumetric annual totals for each water budget component. With the present array of input datasets, the SWB2 output indicates Tutuila receives a total of 402 Mgal/d as precipitation inputs, and of these inputs, 33 Mgal/d or 8% are lost to canopy interception, 61 Mgal/d or 15% are lost to evapotranspiration, 84 Mgal/d or 21% are lost to island wide runoff, leaving the remaining 54% of inputs, totaling 221 Mgal/d, as the total island wide groundwater recharge estimate (Fig. 6.7). The annual resolution groundwater recharge layer produced by SWB2 is directly integrable in the FloPy pre-processing routine to supply the MODFLOW model with recharge rates at the desired spatial resolution.

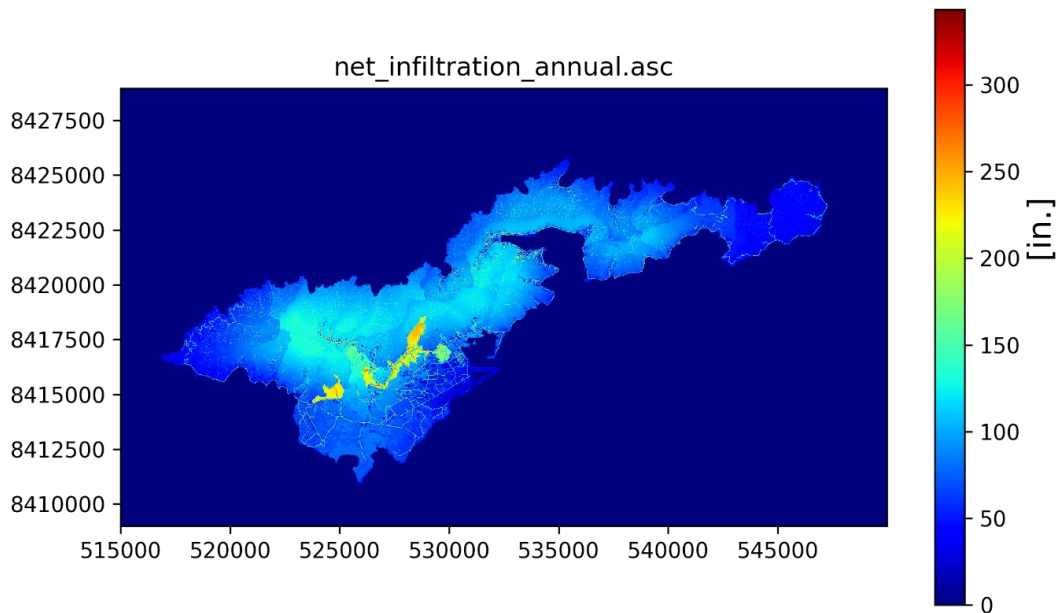


Figure 6.7: Annual average groundwater recharge (net-infiltration) as calculated by most recent SWB2 run, and in appropriate format to be supplied as input to FloPy model. Axes are labeled with UTM coordinates.

It should be noted that because this modeling process is considered to be dynamic, with additions of updated streamflow and weather station data continually being produced by the monitoring network, that this particular model output only represents the latest model iteration at the time of this writing, and may be subject to change as new rainfall, runoff or other input variable data are gathered, or as new information becomes available warranting change of the original conceptual model or decision making process. This also makes it simple to incorporate different scenarios into the model to assess possible future changes. For example, we incorporated future climate scenarios based on gridded dynamically-downscaled climate projections for American Samoa (Wang and Zhang 2016) into the SWB2 model to assess potential climate change effects on the island's water resources, and future land-use scenarios are currently under development through a participatory approach with local stakeholders.

Wang and Zhang (2016) produced 800 m x 800 m gridded-hourly precipitation and temperature predictions within three specific scenarios: (1) present-day climate for the years 1990 to 2009, (2) future climate during the years 2080-2099 reflecting a lower-carbon emissions scenario (RCP4.5), and (3) 2080-2099 climate reflecting on a higher emissions scenario (RCP8.5). This set of climate predictions suggests that under both emissions scenarios future climate may see significant increases in both precipitation and temperature. When integrated into the water budget model, this translated into overall increases in all water budget components as calculated by the modified SWB2 runs. Most notably, the 11 to 18% increase in precipitation predicted by the RCP8.5 and RCP4.5 scenarios, respectively, drove increases in net-infiltration rates of 17 to 27%, respectively. However, because these scenarios are only one of the many predictions that are possible, the model framework has the ability to incorporate scenarios from other predictions (such as statistically-downscaled climate predictions) once these are made available. Future land-use scenarios will be incorporated into the SW2 model in a similar manner once the participatory scenario development process with stakeholders in American Samoa is completed.

#### **6.4.4 FloPy Implementation**

The MODFLOW model input is structured into a discrete set of required and optional packages, and each are represented by separate input files. Required packages include the basic package (.bas), the discretization package (.dis), and the output control package (.oc). While these files are generally human-readable text or ascii grid files that can be modified by hand, FloPy contains highly useful data formatting functionality to easily take shapefile- or raster-based input data and generate the MODFLOW package files in required formats. Implementation of the Tutuila groundwater modeling framework accomplished all pre-processing steps using FloPy or other Python modules within a dedicated Jupyter Notebook. FloPy also provides functionality to run the MODFLOW code, which needs to be downloaded as a separate executable file ([https://water.usgs.gov/water-resources/software/MODFLOW-2005/MF2005.1\\_12.zip](https://water.usgs.gov/water-resources/software/MODFLOW-2005/MF2005.1_12.zip)). FloPy runs MODFLOW as a sub-process and prints output directly to the notebook cell. Once the MODFLOW code is run and output files are saved, these can be accessed within the notebook for post-processing routines that display model output or conduct

statistical analysis. The Tutuila groundwater model workflow currently includes definition of the required MODFLOW packages as well as those representing boundary conditions (.ghb), hydraulic conductivity zones (.lpf), head observations (.obs), spatially-resampled recharge rates (.rch) derived directly from SWB2, and salt-water interface predictions as described in sections 6.4.4.1 to 6.4.4.6 below.

It should be noted that this iteration of the Tutuila model workflow is presented as an example / proof-of-concept only. Any results presented here are not necessarily accurate or representative of reality, due to the need for additional constraint on many of the model parameters. However, as the cooperative modeling process evolves and as more specific modeling objectives are identified, better constrained parameters can be easily integrated into the existing modeling framework to generate results with lower levels of uncertainty.

#### 6.4.4.1 MODFLOW Model Package Development: Model Geometry

The discretization package (.dis) defines the model geometry and establishes cell size and dimensions, georeferenced coordinates, cell elevations, and model stress periods. The Tutuila case study model cell size can be modified to any desired rectangular dimension and presently, the model has been developed with only one layer, although more can be easily added. The Tutuila model basic package (.bas) establishes the spatial model boundaries, which encompass the shallow marine areas surrounding the island (above 50 m below sea level) and the starting groundwater head levels. Model top elevations are shown in Figure 6.8. A general head boundary (.ghb package), with a head of 0.001 m elevation, is also defined within the region between the model boundary and the island's coastline (Fig. 6.9). This boundary condition is intended to represent the effect of ocean water overlying the submarine island slope, which can discharge water flux, thereby representing the process of submarine groundwater discharge.

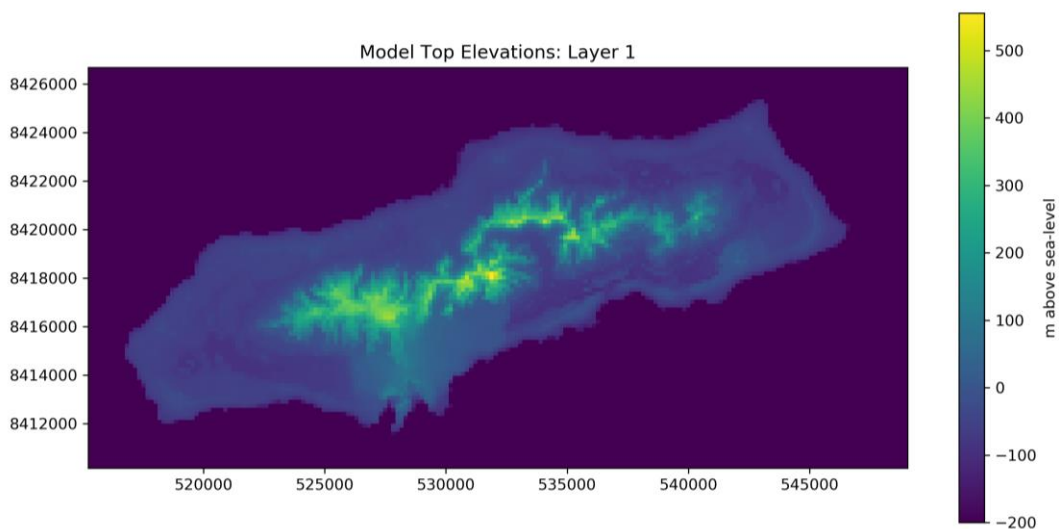


Figure 6.8: Plot of Tutuila case study model grid top elevations derived from a publically available 1/3 arc second digital elevation model.

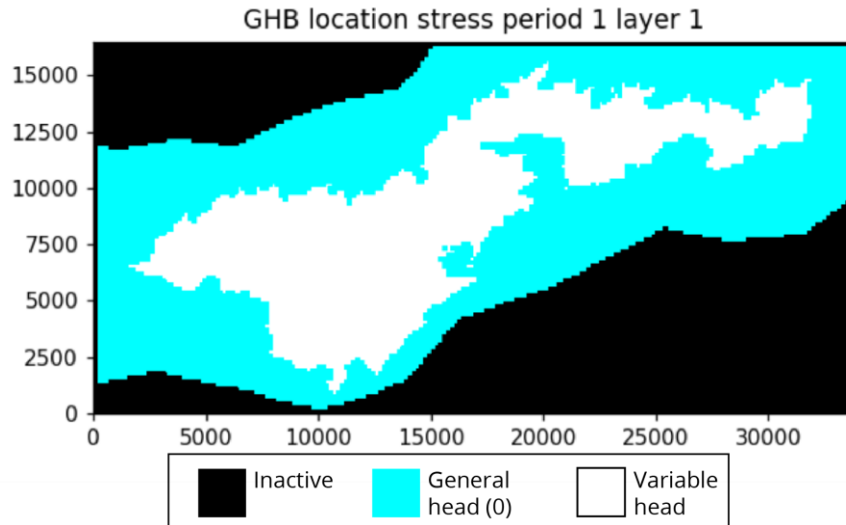


Figure 6.9: Plot of Tutuila case study model grid (at 169 x 165 m cell size) showing model active area (blue and white), and area of general head (.ghb) boundary condition (blue).

#### 6.4.4.2 MODFLOW Model Package Development: Recharge

Spatially distributed groundwater recharge is a key input to the MODFLOW model, and for the Tutuila case study, is provided as an output file from the SWB2 water budget component. The SWB2 model produces a gridded groundwater recharge file in ascii format, and this file is spatially resampled in the groundwater modeling component to a desired grid size (Fig 6.10). Generally, a larger grid size is desirable to speed FloPy processing time. Once resampled, FloPy reformats the groundwater recharge into the MODFLOW input .rch file.

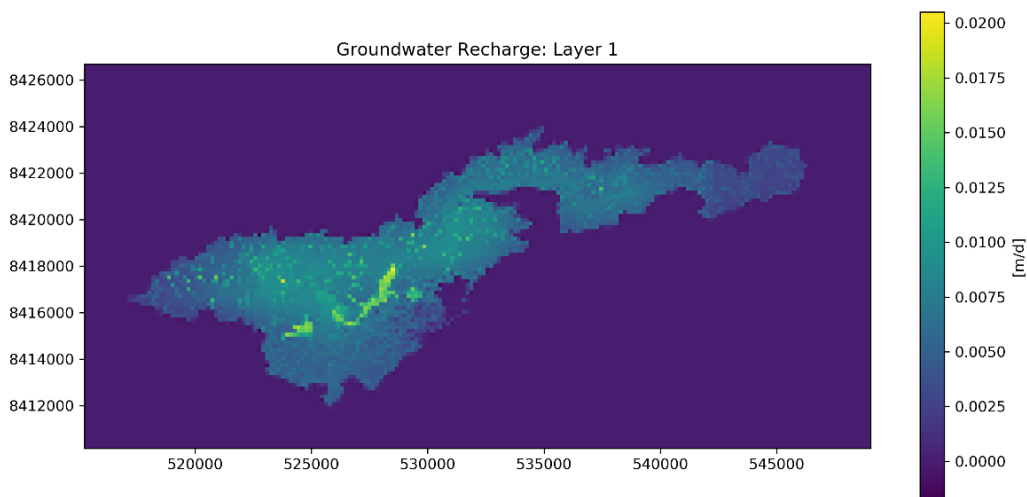


Figure 6.10: Plot of Tutuila case study MODFLOW input groundwater recharge values, resampled from SWB2 water budget model results.

### 6.4.4.3 MODFLOW Model Package Development: Hydraulic Conductivity

The .lpf package and input file can be used to provide subsurface-flow parameters to the MODFLOW model. These parameters include hydraulic conductivity in both the vertical and horizontal directions, and other parameters affecting subsurface flow such as inter-block transmissivity and cell wetting parameters. Groundwater models are highly sensitive to horizontal hydraulic conductivity values, and thus this property is an important, though difficult to measure parameter due to typically high spatial heterogeneity. Therefore, spatially distributed hydraulic conductivity values used in models are typically obtained through calibration. Numerous optimization approaches exist for this process and many are straightforward to execute in Python. At present, development of an appropriate hydraulic conductivity calibration method for the Tutuila case study remains ongoing. Zone based calibration using a simple Python-based optimizer was applied to develop a first-order estimate of the spatial conductivity distribution and an example of this result is shown in Figure 6.11. As the modeling process and objectives evolve, we intend to apply other techniques for conductivity calibration as well.

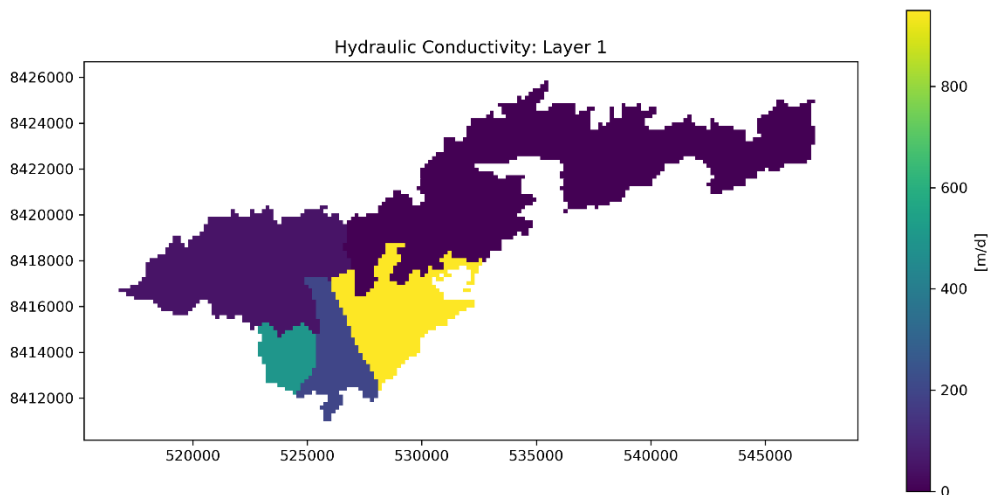


Figure 6.11: Example of hydraulic conductivity zone definition based on simplified geologic units from Stearns (1944). In the current iteration of the Tutuila case-study model each zone is assigned a single value of hydraulic conductivity. Other more distributed parameterization approaches are currently being explored as well.

### 6.4.4.4 MODFLOW Model Package Development: Head Observations

While essentially any variable calculated by MODFLOW can be used as a calibration parameter, water table elevations, i.e. head observations, are typically used as the primary calibration variable in groundwater models. FloPy is able to quickly format observation data into a MODFLOW-readable .obs file. For Tutuila, pre-development water level observations from wells were compiled from drillers logs and pump test records provided by ASPA or as found in documented literature. Locations of these observation points are shown in Fig. 6.12,

left panel, and metadata regarding their sources and uncertainties is provided in Appendix B. To provide a basic example of conductivity calibration here, a simplified zonal calibration approach was applied to the Tutuila model to develop a first-order estimate of a possible hydraulic conductivity distribution. The resulting comparison between observed and simulated water table elevations is shown in Figure 6.12, right panel, and error analysis can either be accomplished through manual calibration, or the model can be wrapped into an object that almost any Python based optimization routine can be applied to further minimize the error. For the purpose of demonstration, the `scipy.optimize.minimize` solver was implemented here to develop a first order estimate of hydraulic conductivities in the zones delineated in the section above (<https://docs.scipy.org/doc/scipy.14.0/reference/generated/scipy.optimize.minimize.html>).

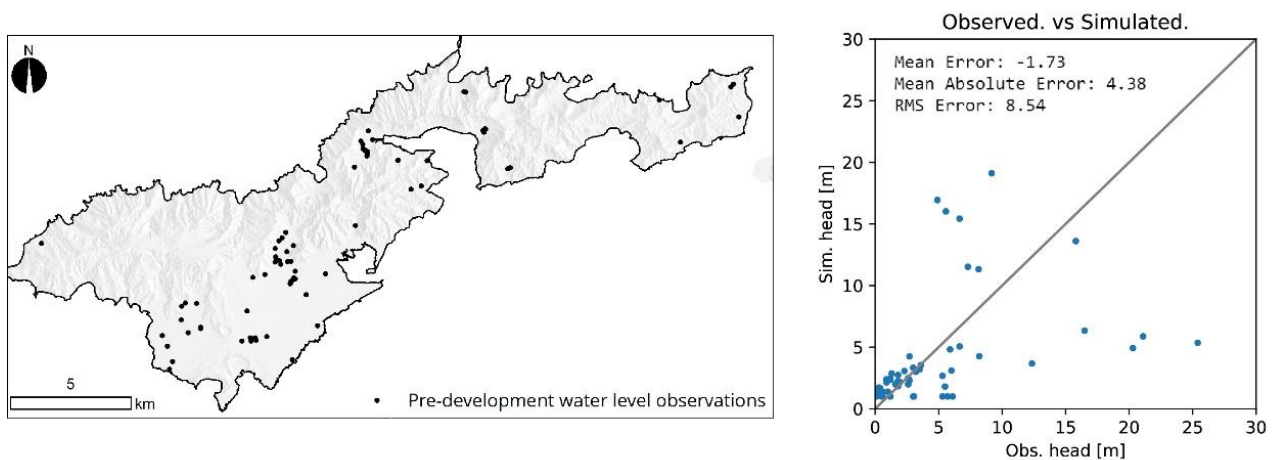


Figure 6.12 (left): Map of water level observation locations and (right): example plot of observed vs. simulated water levels and error statistics as calculated by the manually calibrated FloPy MODFLOW model, demonstrating post-processing visualization. Note grey line in scatter plot is the 1 to 1 line.

#### 6.4.4.5 MODFLOW Model Package Development: Seawater Intrusion

The interaction between salt and freshwater is often modeled with dispersive solute transport models such as SUTRA (Voss and Provost, 2010) or SEAWAT or (Langevin et al., 2008), which are often computationally expensive and require fine vertical discretization of model cells. However, the Seawater Intrusion (SWI2) package for MODFLOW uses a vertically integrated variable-density formulation to simulate vertically integrated variable-density groundwater flow and seawater intrusion. This allows for the position of the 50% freshwater-seawater interface within the saltwater transition zone to be estimated as a discrete sharp-interface or density isosurface. This methodology is simpler and less computationally intensive than that used in dispersive solute transport models. However, because it does not account for diffusion and dispersion, SWI2 cannot definitively predict salt concentrations; it can only approximate the location of the middle of the transition zone.

The primary management utility of this package is to assess the effects of pumping on underlying seawater, which has implications for the salinity or chloride content of produced water. Because the hydraulic conductivity field is the primary control on the position of the seawater interface, at this point in the Tutuila model development, results of the SWI2 analysis should not be considered reliable and are presented for demonstration purposes only. Additionally, due to the lack of direct salinity monitoring information from depths that represent the transition zone, salinity or interface position predictions cannot be calibrated at this time. This underscores the need to enhance Tutuila’s groundwater monitoring capacity and encourages development of deeper monitoring wells. As an example visualization, the position of the interface as created by the first-order calibrated model is shown in Figure 6.13.

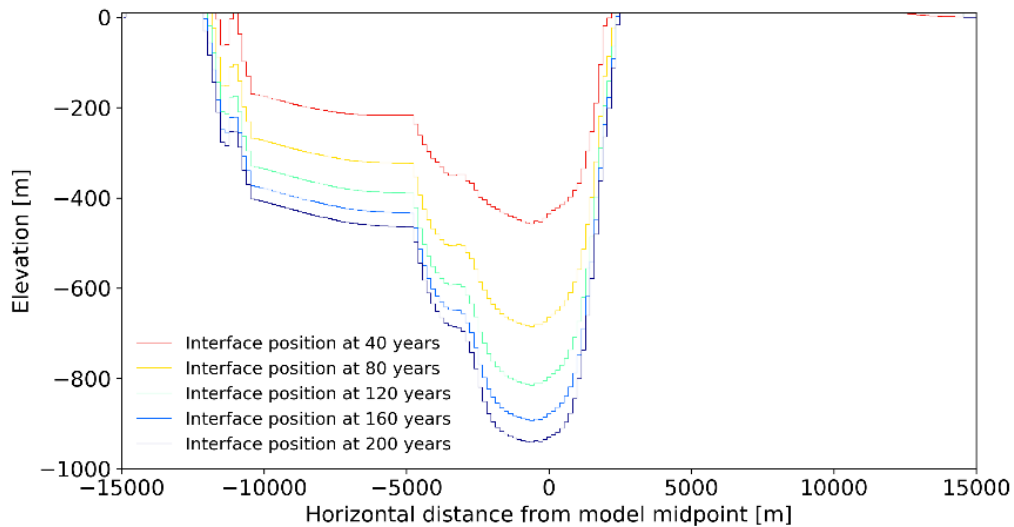


Figure 6.13 Demonstration visualization of the position of the salt-freshwater interface midpoint generated by the SWI2 package as applied to the first-order calibrated Tutuila model. Different colors represent the evolution of the interface position at different time steps as the model runs and moves towards equilibrium. Note that results are not reliable are presented for demonstration purposes only.

#### 6.4.4.6 MODFLOW Model Output: Post-Process Visualization

Since the MODFLOW code is not able to generate plots or any type of graphical or statistical output, the FloPy module provides basic functionality for plotting contour maps and creating other output visualizations. Other Python-based methods for data visualization can be applied as well, simply by reading output files and converting data into the desired format. As an example visualization, a contour plot from the output of the Tutuila case-study model, as parameterized by the first-order zonal calibration method is shown in Figure 6.14. Note again that results are not reliable are presented for demonstration purposes only.

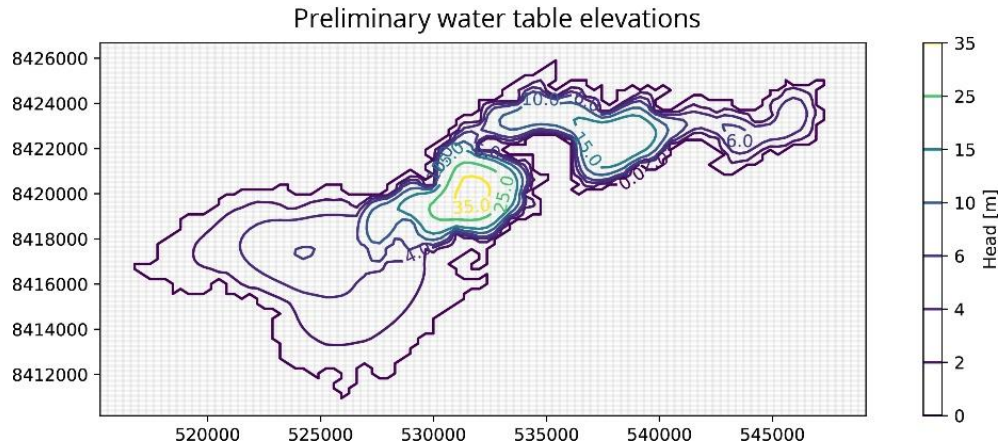


Figure 6.14: Preliminary water table elevations as produced by the Tutuila case-study MODFLOW model. Note that results are shown only for demonstration purposes as the model calibration remains, as of this writing, in an oversimplified state.

## 6.5 Conclusions

The modeling framework developed for this project integrates weather station data, streamflow data, water budget modeling, and groundwater modeling into a seamless data-to-model workflow. The workflow is made entirely open-source, reproducible, and dynamic by using innovative cloud-computing tools such as Jupyter Notebooks, GitHub, and Binder/Azure. These tools manage the data-science infrastructure, so the project team can focus on communicating with each other and developing models that are scientifically relevant and useful for water resources management. While this framework was deployed in American Samoa it could be easily scaled to other islands or localities.

### 6.5.1 Continuing Work

This case-study demonstrates a long-term, process-based groundwater modeling approach, that as of this writing is evolving and under active development. While the goals, methods, and preliminary results have been established, there remain numerous planned, and likely many unplanned additions and modifications to be made as stakeholders weigh in, and as our experience with these tools grows. Planned future objectives include continued development with the groundwater modeling component, as well as some additions to the monitoring network. Continued development of the weather station network includes installation of at least one additional station, to be located on Aunuu Island off the south-eastern coast of Tutuila, as well as replacement of older low-quality stations with higher-quality stations. One additional streamflow station is planned for installation at an old USGS gauging site on Aasu Stream located on the northern coast of Tutuila. Collection of streamflow measurements for rating curve updates remains ongoing. The SWB2 model results continues to incorporate updated rainfall and streamflow information future land use predictions are currently being developed with stakeholders and these will be incorporated once completed. The groundwater modeling process is ongoing with continued model calibration, validation using baseflow data, and running groundwater pumping scenarios to assess potential rise in

transition zone. The groundwater model has already, and will likely continue to expose data gaps, which can be prioritized in the future. So far these include, (1) developing additional monitoring well capacity, especially in Western Tutuila, (2) development of deep monitoring wells or nearshore wells to monitor the saltwater-freshwater transition (3) Management plan for existing deep geothermal wells, and possible repurposing as salinity monitoring points, and (4) additional constraint on mountain front recharge behavior in the Tafuna-Leone Plain area.

### **6.5.2 Final Thoughts**

The traditional approach to groundwater modeling has several significant drawbacks. It is expensive, it produces products with limited longevity, and it is technologically dated. Recent advancements in social-networking are spilling over into how we communicate professionally, how we work collaboratively, and how we approach data-science. Scientific endeavors, and especially computational tasks such as groundwater modeling, are well poised to take advantage of these new developments. Improvement in the sharability of information is revolutionizing how we work with each other, and this allows for a new process-based paradigm that promotes the maintenance of long-standing project partnerships. While collaborative process-based approaches do require more commitment than static, product-based ones, they allow smaller size agencies or utilities to obtain the benefits of having in-house expertise while being able to defer some of the costs of maintaining dedicated personnel. This also benefits institutions or universities dedicated to providing scientific expertise to large regions with many independent stakeholders. By using cloud-based collaborative tools, institutional staff and researchers can maintain relationships with more agencies in spread out locations while deferring the travel cost and time that would otherwise be required to retain this level of involvement.

The collaborative, process-based approach is especially well suited to development of groundwater models on small islands such as Tutuila, where there is a critical management need for environmental models, but limited resources to develop and maintain the scientific capacity to use them. Groundwater modeling is a complex process and within the traditional paradigm, often takes multiple years of project development to obtain results. During this period, the original research questions may become outdated, and newer more relevant questions may not be appropriate to answer with a model designed for an older objective. For example, in the Tutuila case study, initial modeling efforts were targeted at finding new sites for well development (ASPA, 2013). However, several years later, ASPA's well drilling program has gotten well underway and now addressing sustainable yield and salt-water intrusion is a more pertinent need. When stakeholders are involved in the modeling process at a collaborative level, products can easily evolve to remain relevant to management needs as priorities shift. Additionally, stakeholders will also be more aware of the uncertainties involved with using preliminary results and may be able to apply them to pertinent needs without having to wait for delivery of a polished product. This is evidenced by the vertical integration of multiple different components used in this study, which enhanced all of the participant's understanding of not only the data collection process leading up to the model, but also to the uncertainties implicit in the approaches used and the weight that can be placed upon results.

## References: Chapter 6

- Argent, R. M., & Grayson, R. B. (2003). A modelling shell for participatory assessment and management of natural resources. *Environmental Modelling & Software*, 18(6), 541-551.
- AS-DOC - American Samoa Department of Commerce. (2009). Buildings layer for Tutuila Island. [Data file]. <http://doc.as.gov/>
- ASPA - American Samoa Power Authority. (2013). Documentation of Wellhead Analysis, Tutuila Hydrogeological Analysis for the U.S. EPA Clean Water Act – State Revolving Fund ASPA Consolidated Grant for the benefit of the Territory of American Samoa. Report prepared for American Samoa Power Authority, Pago Pago, American Samoa. By Walters, M.O.
- AWS Truepower (2014). Wind Resource Maps and Data of American Samoa: Final Report. Report prepared for the American Samoa Power Authority. [https://www.asrec.net/wp-content/uploads/2016/03/Wind-Resource-Study\\_2014\\_DRAFT\\_2014-10-27-4378826.pdf](https://www.asrec.net/wp-content/uploads/2016/03/Wind-Resource-Study_2014_DRAFT_2014-10-27-4378826.pdf)
- Bakker, M., Post, V. +., Langevin, C. D., Hughes, J. D., White, J. T., Starn, J. J., & Fienen, M. N. (2016). Scripting MODFLOW model development using Python and FloPy. *Groundwater*, 54(5), 733-739.
- Barfield, D. W. (2009). Collaborative groundwater model development. In World Environmental and Water Resources Congress 2009: Great Rivers (pp. 1-3).
- Basco-Carrera, L., Warren, A., van Beek, E., Jonoski, A., & Giardino, A. (2017). Collaborative modelling or participatory modelling? A framework for water resources management. *Environmental modelling & software*, 91, 95-110.
- Beall, A., Fiedler, F., Boll, J., & Cosens, B. (2011). Sustainable water resource management and participatory system dynamics. Case study: Developing the Palouse basin participatory model. *Sustainability*, 3(5), 720-742.
- Bidarra, R., Van Den Berg, E., & Bronsvort, W. F. (2001, September). Collaborative modeling with features. In *Proceedings of DET* (Vol. 1, p. 2001).
- Borah, T., & Bhattacharjya, R. K. (2013). Solution of source identification problem by using GMS and MATLAB. *ISH Journal of Hydraulic Engineering*, 19(3), 297-304
- Cummings, R. G., & McFarland, J. W. (1974). Groundwater management and salinity control. *Water Resources Research*, 10(5), 909-915.
- Dabbish, L., Stuart, C., Tsay, J., & Herbsleb, J. (2012, February). Social coding in GitHub: transparency and collaboration in an open software repository. In *Proceedings of the ACM 2012 conference on computer supported cooperative work* (pp. 1277-1286). ACM.

- Daly, C., J. Smith, M. Doggett, M. Halbleib, and W. Gibson. (2006). High-resolution climate maps for the Pacific basin islands, 1971–2000. Final Report. National Park Service, Pacific West Regional Office.
- Engott, J. A., Johnson, A. G., Bassiouni, M., & Izuka, S. K. (2015). Spatially distributed groundwater recharge for 2010 land cover estimated using a water-budget model for the island of O'ahu, Hawaii (No. 2015-5010). US Geological Survey.
- Essawy, B. T., Goodall, J. L., Zell, W., Voce, D., Morsy, M. M., Sadler, J., ... & Malik, T. (2018). Integrating scientific cyberinfrastructures to improve reproducibility in computational hydrology: Example for HydroShare and GeoTrust. *Environmental Modelling & Software*, 105, 217-229.
- Eyre, P., and G. Walker. (1991). Geology and ground-water resources of Tutuila American Samoa. Unpublished report in American Samoa Power Authority files.
- Feo, A., Zanini, A., Petrella, E., & Celico, F. (2018). A Python script to compute isochrones for MODFLOW. *Groundwater*, 56(2), 343-349.
- Flint, C. G., Jones, A. S., & Horsburgh, J. S. (2017). Data management dimensions of social water science: The iUTAH experience. *JAWRA Journal of the American Water Resources Association*, 53(5), 988-996.
- Foglia, L., Borsi, I., Mehl, S., De Filippis, G., Cannata, M., Vasquez-Suñe, E., ... & Rossetto, R. (2018). FREEWAT, a Free and Open Source, GIS-Integrated, Hydrological Modeling Platform. *Groundwater*, 56(4), 521-523.
- Guo, W., & Langevin, C. D. (2002). *User's guide to SEAWAT; a computer program for simulation of three-dimensional variable-density ground-water flow* (No. 06-A7).
- Harbaugh, A. W., Banta, E. R., Hill, M. C., & McDonald, M. G. (2000). MODFLOW-2000, The U. S. Geological Survey Modular Ground-Water Model-User Guide to Modularization Concepts and the Ground-Water Flow Process. *Open-file Report. U. S. Geological Survey*, (92), 134.
- Izuka, S.K. (1999). Summary of ground-water eata for Tutuila and Aunuu, American Samoa, for October 1987 Through September 1997. U.S. Geological Survey, Pacific Islands Water Science Center, Open-File Report No. 99-252.
- Izuka, S. K., Giambelluca, T. W., & Nullet, M. A. (2005). Potential Evapotranspiration on Tutuila, American Samoa. U.S. Geological Survey Scientific Investigations Report 2005-5200. U.S.Geological Survey
- Izuka, S.K., J.A. Perreault, and T.K. Presley. (2007). Areas contributing recharge to wells in the Tafuna-Leone Plain, Tutuila, American Samoa. U.S. Geological Survey Scientific Investigations Report 2007-5167. [<http://pubs.usgs.gov/sir/2007/5167/>].

- Engott, J. A., Johnson, A. G., Bassiouni, M., Izuka, S. K., & Rotzoll, K. (2017). Spatially distributed groundwater recharge for 2010 land cover estimated using a water-budget model for the Island of O‘ahu, Hawai‘i (No. 2015-5010). US Geological Survey.
- Kennedy, Jenks, and Chilton Consulting Engineers. 1987. *Groundwater contamination study Tafuna-Leone Plain Tutuila Island*. Final report for the Environmental Quality Commission, Office of the Governor, Tutuila, American Samoa. 168 p.
- Kluyver, T., Ragan-Kelley, B., Pérez, F., Granger, B. E., Bussonnier, M., Frederic, J., ... & Ivanov, P. (2016, May). Jupyter Notebooks-a publishing format for reproducible computational workflows. In *ELPUB* (pp. 87-90).
- Langevin, C.D., Thorne, D.T., Jr., Dausman, A.M., Sukop, M.C., and Guo, Weixing, (2008). SEAWAT Version 4 – A computer program for simulation of multi-species solute and heat transport: U.S. Geological Survey Techniques and Methods, book 6, chap. A22, 39 p
- Langsdale, S., Beall, A., Bourget, E., Hagen, E., Kudlas, S., Palmer, R., ... & Werick, W. (2013). Collaborative modeling for decision support in water resources: Principles and best practices. *JAWRA Journal of the American Water Resources Association*, 49(3), 629-638.
- Liu, Y., Gupta, H., Springer, E., & Wagener, T. (2008). Linking science with environmental decision making: Experiences from an integrated modeling approach to supporting sustainable water resources management. *Environmental Modelling & Software*, 23(7), 846-858.
- McDougall, I. 1985. Age and evolution of the volcanoes of Tutuila, American Samoa. *Pac. Sci.* 39(4): 311-320.
- Mendoza, G. A., & Prabhu, R. (2006). Participatory modeling and analysis for sustainable forest management: Overview of soft system dynamics models and applications. *Forest Policy and Economics*, 9(2), 179-196.
- Meyer, R.A., Seamon, J.O., Fa‘aumu, S., and Lalogafuafua, L. (2016). Classification and Mapping of Wildlife Habitats in American Samoa: An object-based approach using high resolution orthoimagery and LIDAR remote sensing data. Report prepared for American Samoa Department of Marine and Wildlife Resources.
- Moran, T. (2016). Projecting Forward: A framework for groundwater model development under the Sustainable Groundwater Management Act. Stanford Water in the West, Stanford Law School.
- Nakamura, S., 1984. Soil survey of American Samoa. U.S. Department of Agriculture Soil Conservation Service, Pago Pago. 95 p.
- Pease, E. C., Pfeil, A., Ibarra, V., Reid, M., Siddique, S., Apango, F., ... & Pierce, S. A. (2018, December). Groundwater Modeling with Informatics and Automated Workflows for Water Resource Management: A Case Study from the Northern Trinity Aquifer. In *AGU Fall Meeting Abstracts*.

- Perez, F., & Granger, B. E. (2015). Project Jupyter: Computational narratives as the engine of collaborative data science. *Retrieved September, 11(207)*, 108.
- Perreault, J.A. (2010). Development of a water budget in a tropical setting accounting for mountain front recharge. Masters Thesis, University of Hawaii at Manoa. Honolulu, HI.
- Rotzoll, K., Izuka, S. K., Nishikawa, T., Fienen, M. N., & El-Kadi, A. I. (2016, December). Quantifying effects of humans and climate on groundwater resources of Hawaii through sharp-interface modeling. In *AGU Fall Meeting Abstracts*.
- Shuler, C. K., El-Kadi, A.I., & Dulaiova, H. (2014, October). Hunting for High-Level Groundwater on Tutuila, American Samoa. In 2014 GSA Annual Meeting In Vancouver, British Columbia.
- Shuler and El-Kadi, (2017). WRRRC-ASPA Hydrologic Monitoring Network Handbook. WRRRC Special Report SR-2018-02, Water Resources Research Center University of Hawai'i at Manoa, Honolulu, Hawai'i 96822
- Shuler, C.K.; El-Kadi, A.I.; Dulai, H.; Glenn, C.R.; Fackrell, J. (2017) Source partitioning of anthropogenic groundwater nitrogen in a mixed-use landscape, Tutuila, American Samoa. *Hydrogeol. J.* (25), 2419-2434.
- Shuler, C. K., Dulai, H., DeWees, R., Kirs, M., Glenn, C. R., & El-Kadi, A. I. (2018) Isotopes, Microbes, and Turbidity: A Multi-Tracer Approach to Understanding Recharge Dynamics and Groundwater Contamination in a Basaltic Island Aquifer. *Groundwater Monitoring & Remediation*.
- Stack Overflow. (2018). *Stack Overflow Developer Survey*. [online] Available at: <https://insights.stackoverflow.com/survey/2018/#work-version-control> [Accessed 24 Mar. 2019].
- Stearns, H.T. (1944). Geology of the Samoan islands. *Geological Society of America Bulletin* 55(11): 1279-1332.
- Thorntwaite, C.W., and J.R. Mather. (1955). The water balance. *Publications in Climatology* (Laboratory of Climatology) 8(1): 1-86.
- Tidwell, V. C., Passell, H. D., Conrad, S. H., & Thomas, R. P. (2004). System dynamics modeling for community-based water planning: Application to the Middle Rio Grande. *Aquatic sciences*, 66(4), 357-372.
- U.S. EPA - United States Environmental Protection Agency (1987). On-Site Meteorological Program Guidance for Regulatory Modeling Applications, EPA-450/4-87-013 Office of Air Quality Planning and Standards, Research Triangle Parks, North Carolina 27711
- Voss, C.I., and Provost, A., (2010). SUTRA – A model for saturated-unsaturated variable-density ground-water flow with solute or energy transport: U.S. Geological Survey Water-

Resources Investigations Report 02-4231 (Version of September 22, 2010 (SUTRA Version 2.2).

Wang, Y. and Zhang, C. (2016). Project Final Report - 21st Century High-Resolution Climate Projections for Guam and American Samoa. Retrieved from:

<https://www.sciencebase.gov/catalog/item/583331f6e4b046f05f211ae6>

Westenbroek, S. M., Engott, J. A., Kelson, V. A., & Hunt, R. J. (2018). SWB Version 2.0 – A Soil-Water-Balance Code for Estimating Net Infiltration and Other Water-Budget Components (No. 6-A59). US Geological Survey.

Willis, R and Yeh W., (1987) Groundwater Systems Planning and Management, Prentice-Hall, Englewood Cliffs, New Jersey.

Wong, M.F. (1996). Analysis of streamflow characteristics for streams on the island of Tutuila, American Samoa. US Geological Survey Water Resources Investigations Report No. 95-4185, Honolulu, HI.

WMO - World Meteorological Organization (1983). Guide to Meteorological Instruments and Methods of Observation. World Meteorological Organization No. 8, 5th edition, Geneva Switzerland

Yin, D., Liu, Y., Padmanabhan, A., Terstriep, J., Rush, J., & Wang, S. (2017, July). A CyberGIS-Jupyter framework for geospatial analytics at scale. In *Proceedings of the Practice and Experience in Advanced Research Computing 2017 on Sustainability, Success and Impact* (p. 18). ACM.

Young, R. A., & Bredehoeft, J. D. (1972). Digital computer simulation for solving management problems of conjunctive groundwater and surface water systems. *Water Resources Research*, 8(3), 533-556.

Zheng, C., & Wang, P. P. (1999). *MT3DMS: a modular three-dimensional multispecies transport model for simulation of advection, dispersion, and chemical reactions of contaminants in groundwater systems; documentation and user's guide*. Alabama Univ University.

# Appendix A: Conceptual Hydrologic Model Data

## A1 Compilation and Interpretation of Subsurface Logs

Borehole logs from well drilling or other belowground exploratory operations allow a direct assessment of subsurface structure, materials, and conditions. Available logs from Tutuila show the island is constructed of a complex arrangement of lava flows, associated clinker zones, a limited amount of marine and terrestrial sedimentary units, and pyroclastic materials – including pockets of cinder and ash layers.

Throughout Tutuila there have been numerous shallow (< 100 m) boreholes drilled during the last 30 years, primarily as production wells. Two deep exploratory boreholes were also drilled in 2015, one on the northern Leone Plain in the village of Upper Malaeloa (TGH-1) and the other on the southern Tafuna Plain in the village of Iliili (TGH-3). Driller’s logs of varying quality were found for about one-third of the shallow holes. Excellent logs were made, and core samples were collected, for nearly the full depth of the deep boreholes. Trenches dug for archaeological purposes, though usually only < 2 m deep, also provided information about the shallow subsurface. The locations of each log or trench are shown in Figure A1. Despite significant variation in the quality and terminology used between logs, they were nonetheless useful for comparing the subsurface characteristics of different areas and assessing the subsurface elevations of recognizable geologic features.

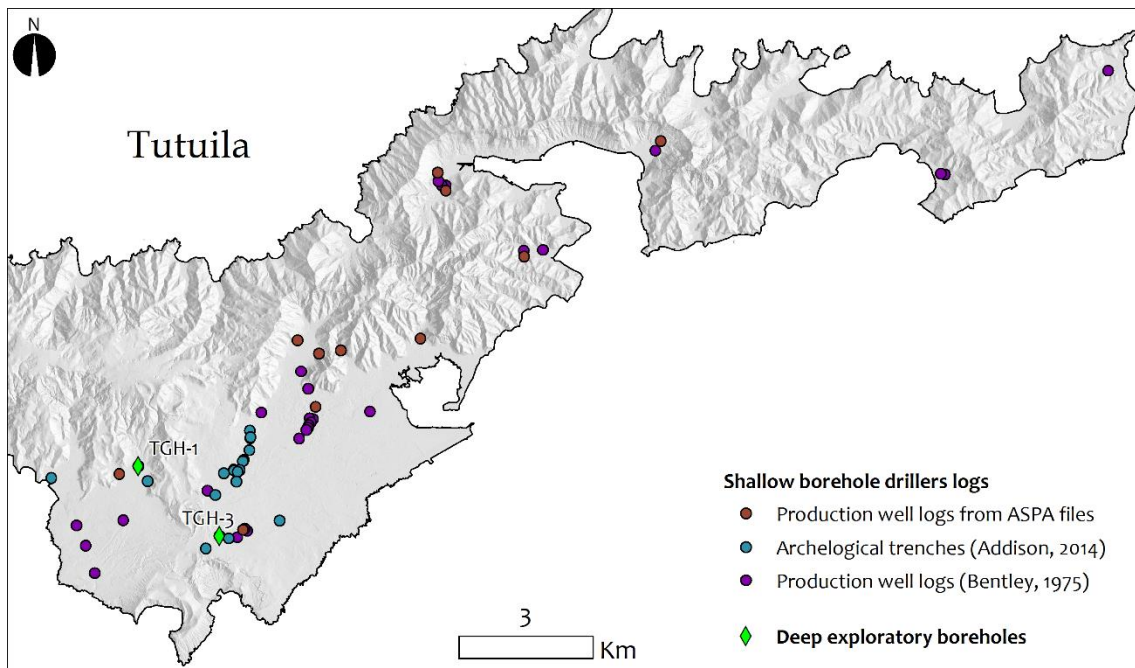


Figure A1. Location of boreholes (Bentley 1975, ASPA files) and archeologic trenches (Addison 2014). Note: Symbols represent log sources.

## A1.1 Shallow Borehole Logs

For this study, lithologic sections from shallow production-well borehole logs were classified into a simplified database. Terminology between the logs was highly variable since they were recorded over several decades by different drillers. The driller's logs often lacked clear lithological descriptions, and frequently only documented changes in drilling speed as "hard" or "soft." In volcanic island settings, these terms have been interpreted to signify the difference between massive-impermeable lava sections (hard) and more-permeable rubble or clinker zones (soft) (Eyre and Walker, 1991). However, this assumption may be an oversimplification, as drilling speed can also increase if a lower-permeability clay or weathered volcanic rock horizon is encountered. Nonetheless, the logs do provide general indications of geologic structures, as well as a statistical basis upon which Tutuila's extreme subsurface heterogeneity may be crudely understood. For simplicity here, each lithologic section was classified into one of ten categories: unconsolidated, hard basalt, vesicular basalt, no-circulation, clay, soft basalt or fractured rock, cinder, ash, non-carbonate sand, carbonate sand, or carbonate reef. The proportions of each material, averaged over the logs available in the different well fields or regions is presented in Table A1. Many of the logs show massive lavas (or hard drilling zones) interlayered with cinders, weathered basalt, rubble, or other soft materials, indicating that small scale heterogeneity may be so localized as to not have much control over regional aquifer properties.

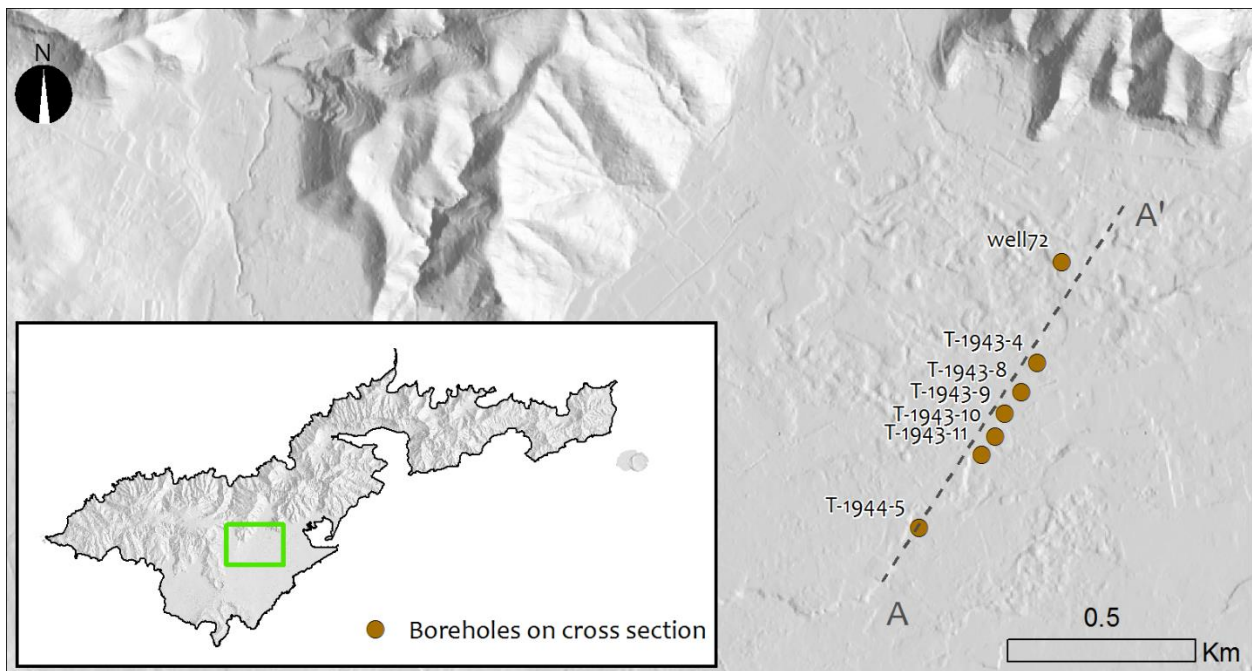
Table A1. Interpretation of shallow borehole logs, grouped by region. The proportion of each material type (% of total thickness) is averaged over the logs within each region.

Well field	n*	Hard basalt	Vesicular basalt	Soft or fractured	Cinder	Ash	Clay	Sand
Tafuna	13	52%	5%	26%	3%	0%	4%	0%
Iliili	6	46%	16%	17%	9%	1%	1%	5%
Leone	6	43%	5%	28%	4%	1%	1%	8%
Tula & Alofau	3	11%	0%	0%	4%	21%	53%	10%
Aua & Pago Pago	9	16%	12%	9%	12%	6%	13%	4%
Fagaalu	3	7%	1%	15%	11%	0%	33%	23%
Malaeimi	3	31%	0%	46%	0%	0%	11%	0%
<b>All</b>	<b>43</b>	<b>35%</b>	<b>7%</b>	<b>20%</b>	<b>6%</b>	<b>3%</b>	<b>11%</b>	<b>5%</b>

\*n = number of logs available in each region.

Note: not all material types are shown, thus percentages do not sum to 100%

The heterogeneous subsurface structure of the Tafuna Plain is displayed in a cross section at seven closely spaced shallow borehole logs in the Tafuna Plain (Bentley, 1975). These logs provide a unique high-resolution opportunity to examine the subsurface structure of the region. These boreholes lie along an 850-m-long southwest to northeast profile (Fig. A2). Despite their spatial proximity, the geologic sections encountered are poorly correlated between boreholes (Fig. A3). This lack of correlation illustrates the plain's complex structure, which is shown in the logs as alternating sequences of massive lavas and rubble or fractured zones that are clearly not aerially extensive. Figure A4 shows a conceptualized schematic interpretation of how these alternating permeable and impermeable sections might create borehole observations that fit the log data shown. This conceptual model again supports the conclusion that Tutuila's subsurface is hydrogeologically, very complex.



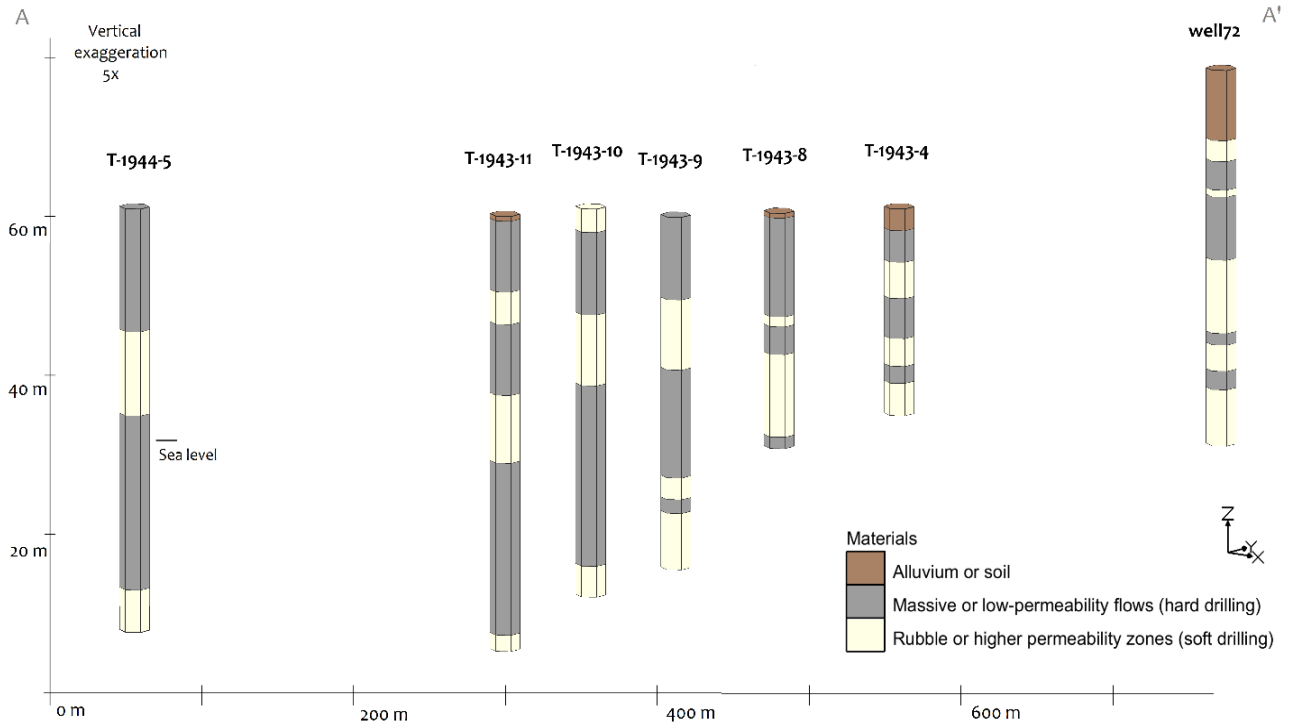


Figure A3. Interpretation of driller's logs (from Fig. A1) into lithologic units with simplified hydrological properties (Bentley, 1975). Note: Reference datum is arbitrary.

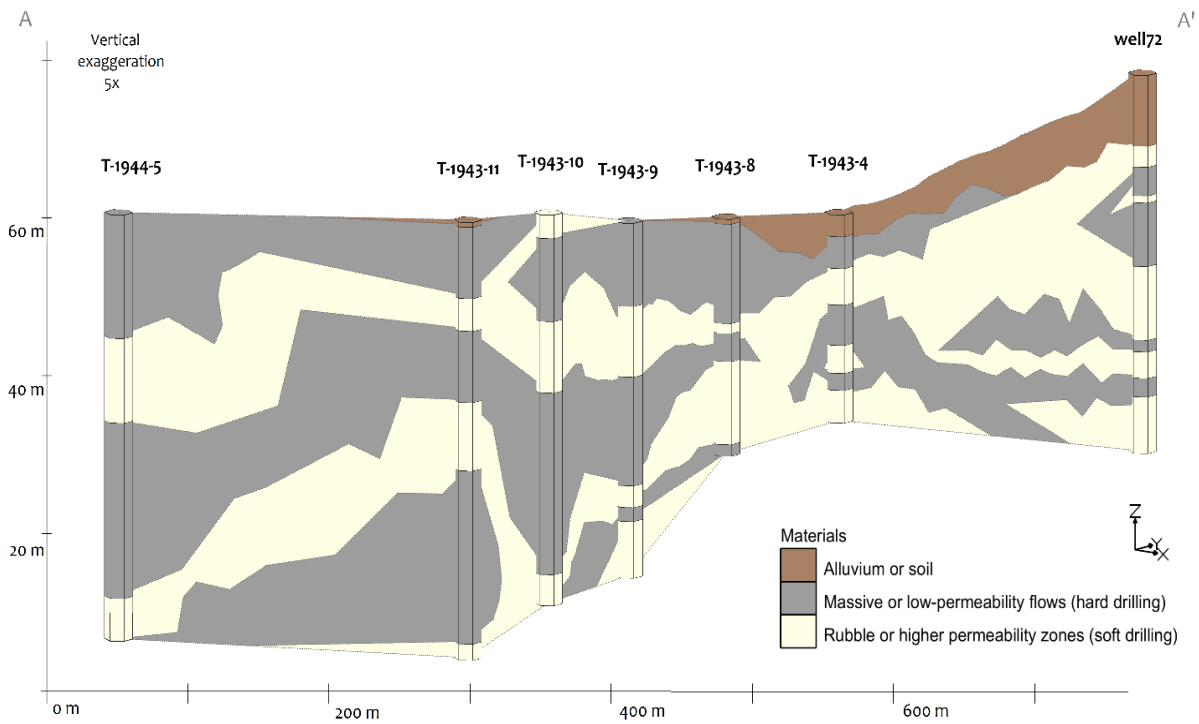


Figure A4. Conceptualized cross section of the Tafuna-Leone lava delta. The model is based on conceptual occurrence of lava delta formation when overlaid on seven borehole logs shown in Figure A3.

## **A1.2 Deep Exploratory Boreholes (TGH-1 and TGH-3)**

The data collected from the two deep boreholes in the Tafuna-Leone area provides an informative visualization of subsurface conditions and lithology at each point. The core samples recovered from these holes provide a record of the geologic past via visual inspection, radiocarbon ( $^{14}\text{C}$ ) dating methods, and major/minor element chemistry. The Leone Series rocks can be distinguished from the underlying Taputapu rocks by distinctive geochemical signatures, where the Leone rocks have approximately 10% less magnesium oxide and 20% more zirconium (both normalized by weight) than what is contained in the Taputapu rocks (Reinhard et al., 2019).

As expected, the lithologic column in the boreholes consists primarily of dense lava sections that are interbedded with rubble and/or pyroclastic materials. The column at TGH-1 shows a thick layer of mountain-front talus and alluvium covering the Leone Volcanic Unit, which overlies the Taputapu rocks; thus indicating that the well is probably located in a lava filled paleo-valley. At TGH-3, the alluvial overburden is relatively thin, and the Leone Volcanics contains two marine carbonate layers above the contact with the Taputapu Volcanics. This indicates the well must be located north of the lava-covered inland margin of the carbonate bench surrounding the island. Three distinct hydrogeologic units and a handful of notable geologic events (e.g., debris flows) can be interpreted based on known geologic history and inspection of the cores and logs. The sequence of these events and a hydrogeological interpretation of significant units are presented in Tables A2 and A3, with photos from Geologica Geothermal Group, Inc. (2016).

Table A2. Simplified log from TGH-1 core interpretation.

Depth (bottom of unit, m)	Height (above MSL, m) <sup>a</sup>	Geologic Unit and Hydrologic Notes	Unit Thickness (m)	Core Samples <sup>b</sup>
24.2	18.9	Sediments, alluvium, pyroclastics, and basalts? No core recovered. Unsaturated zone. Reports of poorly sorted material suggest moderate permeability.	24.2	
34.1	9.0	Sediments, alluvium, and pyroclastics, core recovered. Unsaturated zone, limited permeability.	9.9	
61.6	-18.5	Leone volcanics, fractured vesicular basalt. High permeability. Water table encountered at 39.6 m depth (3.5 m above MSL), unconfined aquifer below. <sup>c</sup> (sampled at 42.7 m deep)	27.4	
76.2	-33.1	Leone volcanics, vesicular basalt, mixed with clinker, scoriaceous zones, and massive units. Heterogeneous permeability, but generally high. One geochemical sample <sup>c</sup> at 75 m deep looks Taputapu in origin, may not be in situ.	14.6	
89.0	-45.9	Sediments, alluvium, massive boulders, clay. Likely a debris flow. Probably low permeability.	12.8	
114.9	-71.8	Loss of circulation, no data. Assumption that circulation loss indicates highly permeable formation is reasonable.	25.9	
279.5	-236.4	Taputapu volcanics alternating zones of massive and vesicular basalt, lapili tuff, clinker, and scoria. Thin paleohorizons and debris flows present. Heterogeneous permeability, with zones of potentially high permeability. Notable rubble zone at 231 to 236 below MSL. <sup>c</sup> (sampled at 118 & 124 m deep)	164.6	
>663	-620 (bottom of hole)	Taputapu volcanics. Basalt and volcanoclastics, predominantly massive texture, most pore spaces filled with secondary mineralization. Generally lower permeability than upper Taputapu.	>383	

<sup>a</sup>Ground elevation at TGH-1 estimated at 43.1 m above Mean Sea Level (MSL).

<sup>b</sup>Photos from Geologica Geothermal Group, Inc. (2016), depths shown in photos are in feet below ground surface.

<sup>c</sup>Geochemical rock samples taken at given depths, used to delineate Taputapu Volcanics from Leone Volcanics.

Table A3. Simplified log from TGH-3 core interpretation.

Depth (bottom of unit, m)	Height (above MSL, m) <sup>a</sup>	Geologic Unit and Hydrologic Notes	Unit Thickness (m)	Core Samples <sup>b</sup>
74.4	1.9	Leone basalts, unsaturated zone. Fractures and vesicularity suggest high permeability. Terrigenous soil and surface sediments from 0 to 4.5 m, no returns	74.4	
82.3	-6.0	Leone basalts and ash layer at bottom. Upper water table encountered at 74.4 m, unconfined saturated zone. Basalts look permeable, ash may have low permeability. <sup>c</sup> (sampled at 77.4 m)	7.9	
91.4	-15.1	Carbonate. Coral sand, intact reef, and fine grained marl. Probably more permeable than lower carbonates.	9.1	
134.1	-57.8	Leone basalts between carbonates. Mostly vesicular. Fractures and vesicularity suggest high permeability. <sup>c</sup> (sampled at 93.6 m deep)	42.7	
150.3	-74.0	Second carbonate unit. Mostly carbonate marl, some coral fragments. High clays suggest low permeability. Potentially a confining unit?	16.2	
157.3	-81.0	Leone basalts and tuff. Iron oxide and secondary mineralization visible in fractures. Low vesicularity, thus potentially low permeability. <sup>c</sup> (sampled at 150 & 153 m deep)	7.0	
167.8	-91.5	Debris flow, mud, clay, and clasts. Potentially a confining layer?	10.5	
>645	-568 (bottom of hole)	Taputapu volcanics. Many alternating units of basalt and lithic lapili tuff. Some scoriaceous units. Heterogeneous permeability distribution. Large rubble zone at 199 to 232 below MSL. <sup>c</sup> (sampled at 188 & 214 m deep)	>480	

<sup>a</sup>Ground elevation at TGH-3 estimated at 76.3 m above MSL. <sup>b</sup>Photos from Geologica Geothermal Group, Inc. (2016), depths shown in photos are in feet below ground surface.

<sup>c</sup>Geochemical rock samples taken at given depths, used to delineate Taputapu Volcanics from Leone Volcanics.

The lithology of the Leone and Taputapu Units was analyzed and statistics are compiled in Table A4. The data shows that in both boreholes, the Taputapu and Leone Volcanic Units are composed of similar materials and have lithological sections ranging from massive basalt, vesicular basalt, fractured basalt, pyroclastic materials, and unconsolidated regions to sedimentary horizons, many of which seem to alternate frequently (average section thickness in both holes was between 2.0 and 2.4 m) in a non-regular sequence. Each layer was classified based on its lithology as well as an assumption of its permeability with vesicular basalt, rubble, and unconsolidated zones having a higher-assumed permeability and massive lavas, while ash and clay have a lower assumed permeability. This analysis indicates the Taputapu Series generally has more secondary mineralization in voids and a higher proportion of clays or other minerals that reduce permeability, whereas the Leone series is constructed of a greater proportion of rock types that are assumedly more permeable. Notably large rubble zones were seen in the Taputapu Series in both holes, ranging from -231 to -236 m and -199 to -232 m below sea level at TGH-1 and TGH-3, respectively. It remains unclear if these zones are connected between holes. Below this zone the ratio of permeable to impermeable rock is reduced from 25% to 35%. Temperature logging was also performed during and after drilling, and showed a distinct anomaly in the TGH-3 rubble zone. Overall the heterogeneity seen in these logs emphasizes the futility of aquifer characterization based on individual geologic sections, thus emphasizing the need to assess integrated regional hydrological properties through aquifer tests.

Table A4. Physical characteristics of deep borehole logs based on visual examination of core.

<b>Borehole (Unit)</b>	<b>Total Thickness of Unit (m)</b>	<b>Proportion of Basalt Layers: Pyroclastic Layers (%)*</b>	<b>Proportion of Massive Basalt: Vesicular/Clinker/Rubble Rock (%)</b>	<b>Proportion of Less-Permeable: More-Permeable Flow Units (%)**</b>
TGH-1 (Leone Series)	89.0	85:15	47:53	48:52
TGH-1 (Taputapu Series)	548.3	92:8	58:42	87:13
TGH-3 (Leone Series)	153.0	96:4	37:63	33:67
TGH-3 (Taputapu Series)	477.3	85:15	50:50	79:21

\*Only the first 215 m of each hole was analyzed due to difficulty in distinguishing pyroclastics in lower layers.

\*\*Permeability interpreted based on material type, was not measured.

### **A1.3 Temperature Logging of Deep Boreholes**

Although, aquifer tests were not performed on the deep boreholes TGH-1 and TGH-3, temperature logging was performed during and after drilling. This technique is useful for indicating areas of fluid flow because meteoric or ocean waters have distinctive temperatures that are likely to disrupt the geothermal temperature gradient of the surrounding rock. Survey results from Geologica Geothermal Group, Inc. (2016) are shown in Figures A5 and A6, both show low temperature plateaus and thus the presence of the known freshwater aquifer between about +3 to -85 m above sea level at TGH-1, and about +1 to -25 m above sea level at TGH-3.

#### **Iliili Borehole**

The temperature profile in Iliili at TGH-3 shows a decrease in the air-filled hole from the ground surface to near sea level where the water table is encountered (Fig. A5). From near sea level to a depth of -15 m below sea level, the water temperature is relatively cool and consistent, and matches the temperature (25°C to 26°C) of the groundwater pumped from the unconfined freshwater lens in the nearby wells. The limited thickness of the freshwater lens, as shown on the temperature profile, was corroborated by salinity measurements of groundwater within the Iliili well field, which does become saltier during dry times or when over-pumped. Heads in the Iliili well field ranged from 0.3 to 2 m above sea level, and well depths ranged from -2 to -10 m below sea level. Despite uncertainties in elevations and depths in the temperature-depth profile, this data suggests a flowing freshwater lens extends to about -15 m below sea level. Inaccuracies in the ground elevation data and equipment used to measure depth, the shallow penetration of the Iliili wells below the water table, and the potential for vertical flow within the aquifer only allow the elevation of the bottom of the lens to be roughly approximated, which could potentially range from -15 to over -40 m below sea level.

With one major exception, a typical geothermal temperature gradient is observed in TGH-3 from -15 m to the bottom of the hole. However, between -175 to -280 m below sea level an anomalous 'low'-temperature plateau is observed. However, the interpretation of this anomaly is complicated by a lost circulation event that required drillers to cement a small interval at about -225 m below sea level. Since hydration of cement releases heat, a corresponding temperature spike is seen on the temperature profile, coincident with the upper portion of the low-temperature plateau. Despite this complication, the temperature profile still shows a plateau below the spike, which could indicate fluid flow. It was reported that the plugs were placed in an unstable zone of coarse volcanic "gravel" that occupies the local lithologic column from -200 to -230 m below sea level (Geologica Geothermal Group, Inc. 2016). The plateau's temperature of over 31°C, exceeds typical freshwater or even regional sea surface temperatures ( $\approx 29^\circ\text{C}$ ) and suggests some geothermal heating of freshwater or saltwater may be occurring, regardless of its salinity.

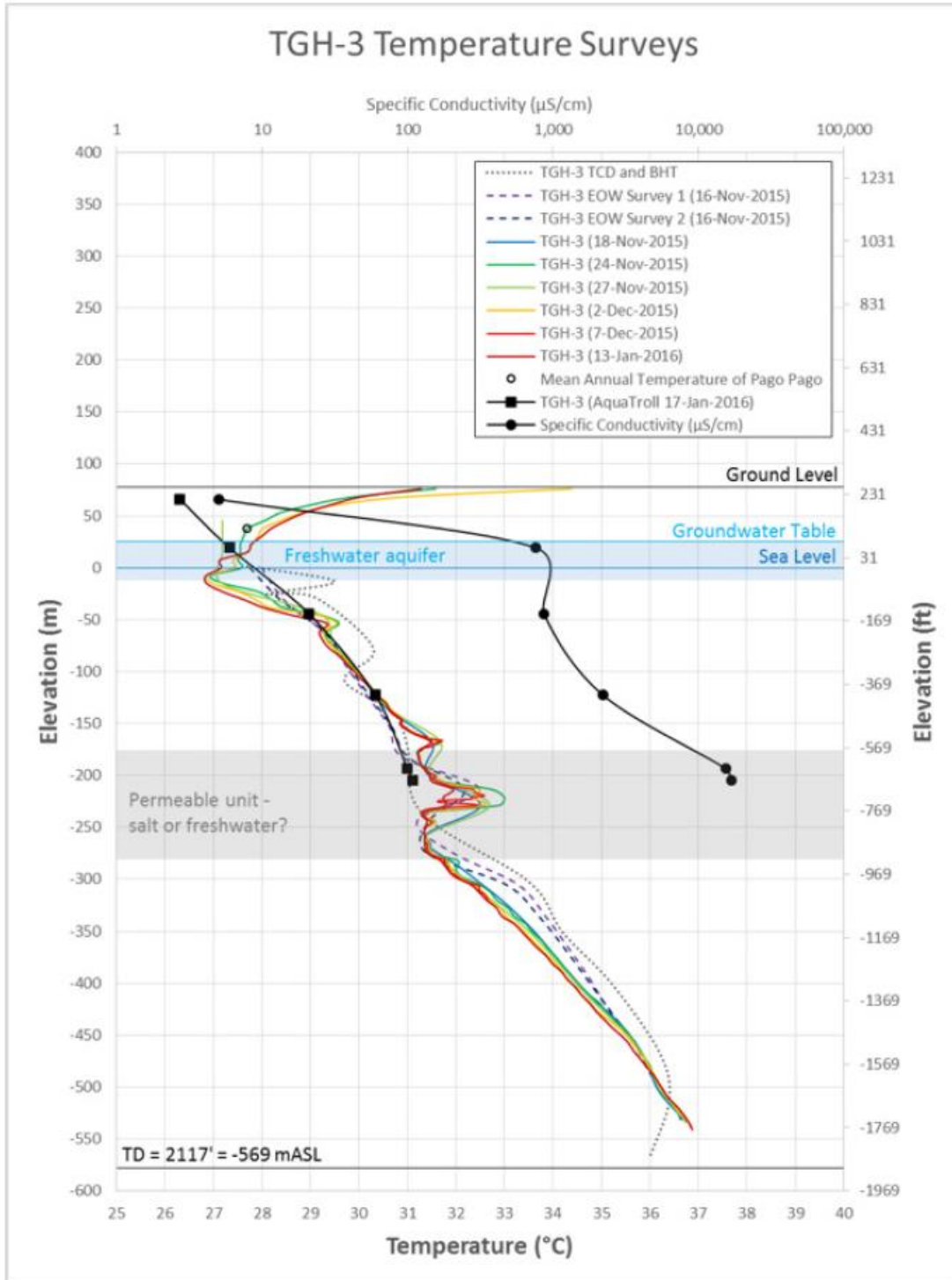


Figure A5. Temperature and conductivity survey log data of TGH-3. Colored lines are repeated temperature logging measurements for TGH-3, black line with circles shows conductivity log in  $\mu\text{S}/\text{cm}$ , and dashed line is series of Bottom Hole Temperatures (BHT) collected by maximum recording thermometers while drilling progressed downward. Reprinted from Geologica Geothermal Group, Inc. (2016) with permission.

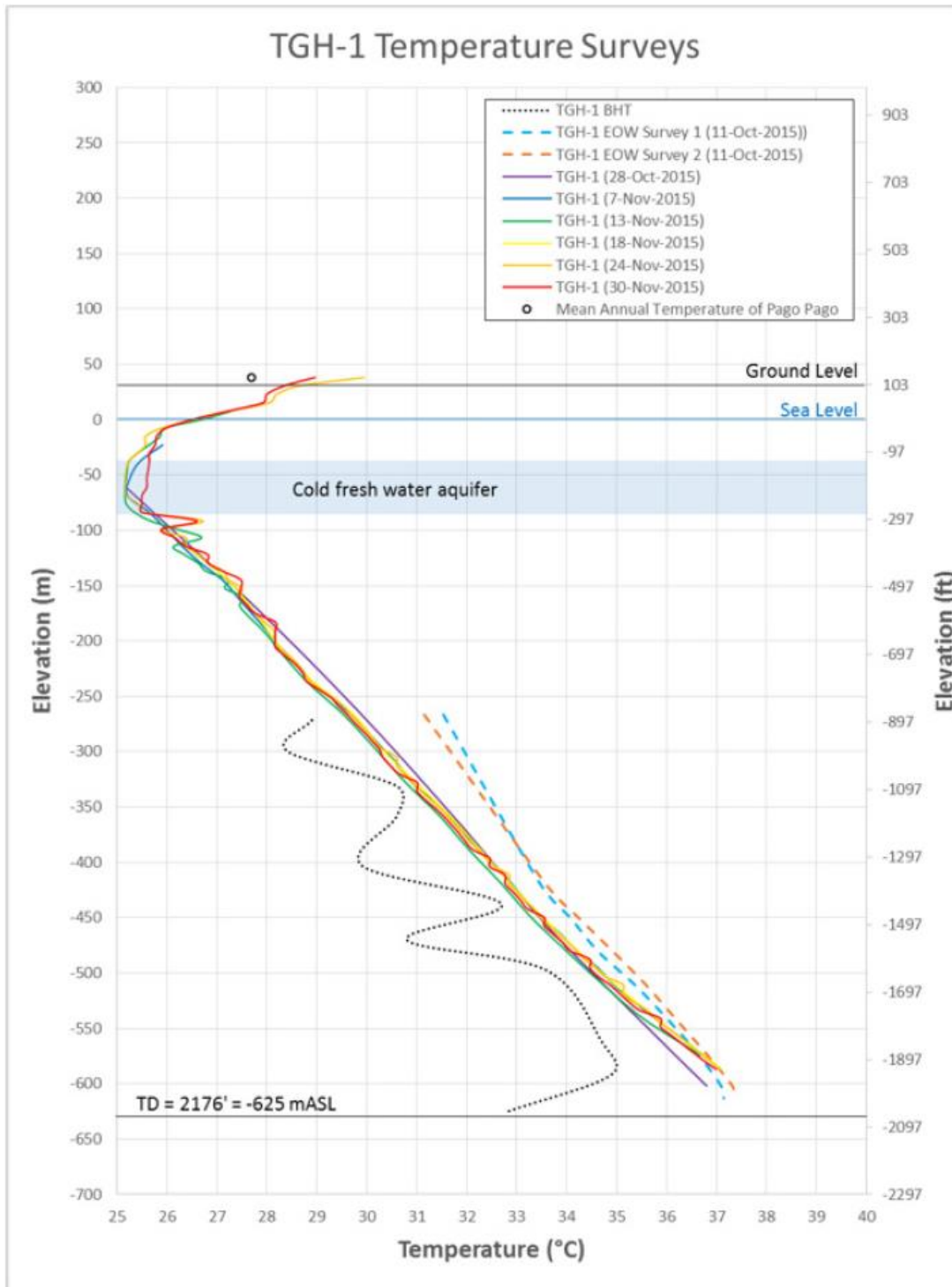


Figure A6. Temperature survey logs data of TGH-1. Colored lines are repeated temperature logging measurements for TGH-1, dashed line is a series of Bottom Hole Temperatures (BHT) collected by maximum recording thermometers while drilling progressed downward. Reprinted from Geologica Geothermal Group, Inc. (2016) with permission.

The zone of constant temperature in TGH-3 from -175 to -280 m below sea level indicates a region where the flow of water is sufficient to overcome the geothermal gradient. This might be interpreted to be evidence of a deep freshwater aquifer extending from the interior of the Taputapu Shield to below the plain. The zone of flowing water does not extend deeper than -260 m below sea level and the geothermal gradient is reestablished at that depth. A head of 6.5 m is theoretically required for a basal lens to reach -260 m below sea level. Although there are no existing measurements of basal heads within the interior of Taputapu Shield, the relatively low-permeability of the rocks and substantial amount of groundwater recharge suggests that such heads are possible. However, the temperature anomaly could also be caused by tidally-forced inflow of seawater. Water sampling from TGH-3 in this zone after extensive cleanout of the borehole would help to constrain the salinity of water in this zone.

### **Malaeloa Borehole**

The temperature profile in Malaeloa at TGH-1 (Fig. A6) is similar to the profile at TGH-3 with the exception that TGH-1 lacks any deep temperature anomalies. Below the cooler freshwater lens zone, the geothermal gradient is stable and consistent with global values. As would be expected, the low-temperature freshwater lens portion of the profile at TGH-1 is thicker, which corresponds to higher observed heads in the Malaeloa well field (1.5 to 2 m above sea level). The bottom of the shallow freshwater lens indicated by the temperature profile (-75 m below sea level), is nicely positioned at the theoretical location of the transition zone as predicted by the Ghyben-Herzberg principal.

## **A2 Examination of Lava Outcrops in Pleistocene Volcanic Rocks**

Although the large fraction of a'a rubble in the Pleistocene aquifers seems to suggest a high overall permeability, aquifer tests shows the opposite (see Section 2.4). This discrepancy may be caused by the presence of low-permeability features that reduce the connectivity and aerial extensiveness of the rubble zones, effectively reducing the overall permeability. The subaerial extent of Tutuila is highly dissected by erosion and dikes intrude on much of the land remaining above sea level. The island experienced other disruptive events such as small eruptions, faulting, landslides, and other types of mass wasting. These events produce small and large pockets of talus breccia, debris flow material, cinders, or intrusive bodies (e.g. Fig. A7). These features alter the aquifer's permeability and are heterogeneously dispersed throughout the body of the island. Although subsurface structures are nearly impossible to observe with certainty below ground, surface outcrops can provide valuable clues to what lies below in locations where erosion or other processes have cleared Tutuila's prolific vegetation.

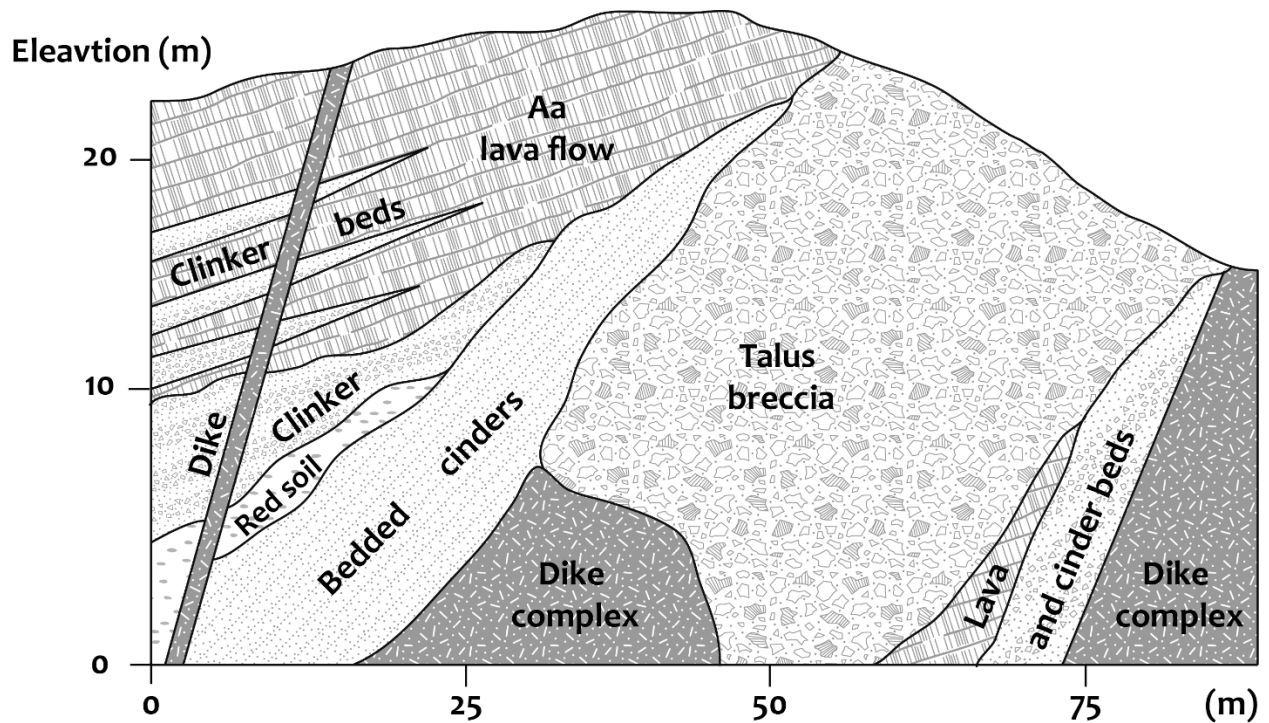
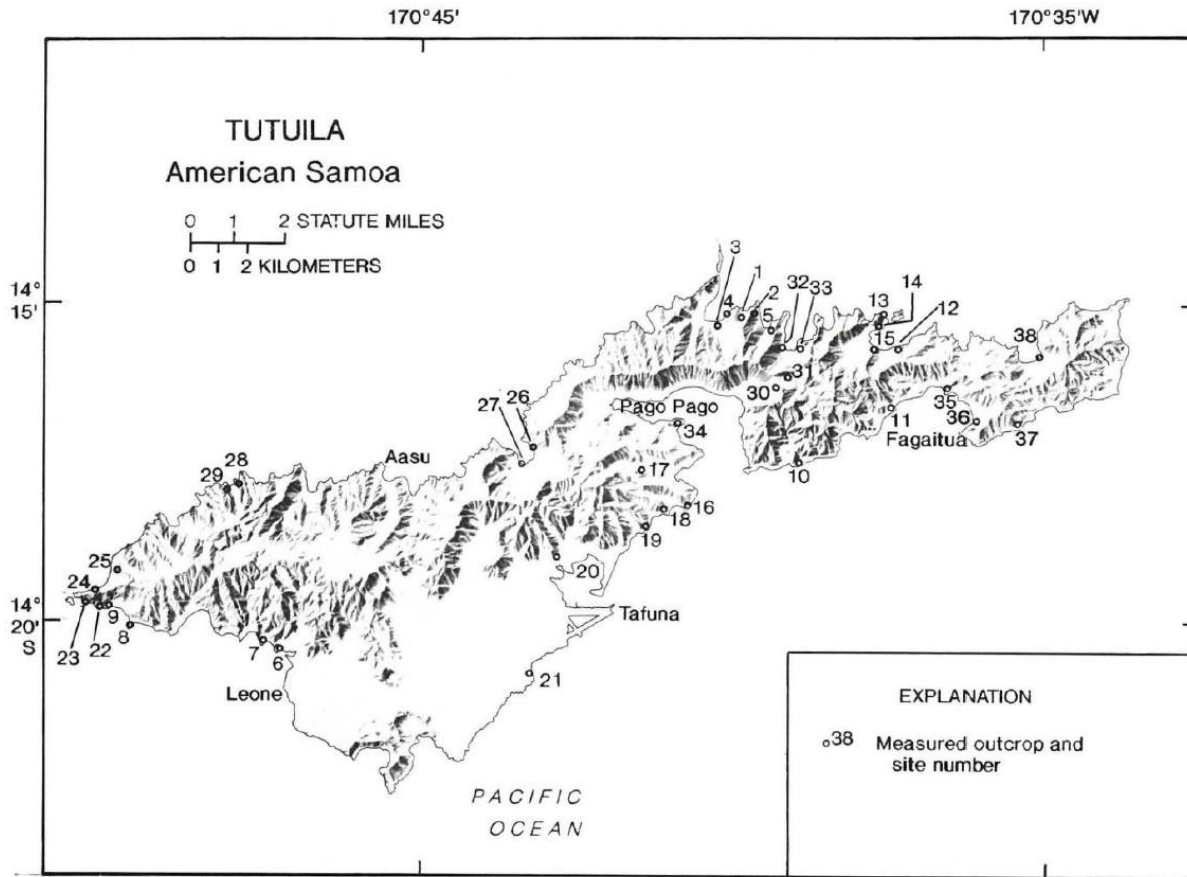


Figure A7. Diagram of the geologic components of the Pleistocene volcanics in an outcrop at Masfau Bay. Modified from Stearns 1944 with permission.

Over 50 quantitative measurements of outcrop characteristics in the Pleistocene Volcanic rocks were made by Eyre and Walker (1991). Measurements of the following were taken at road cuts, coastal cliffs, and promontories throughout the island: (1) thickness of each lava flow section, (2) the separate thickness of the flow interior and rubble layers of a'a flows, (3) the vesicularity of the flow interior, and (4) overall dip of lavas (Figure A8, Table A5). As shown in Table A5, only 2.4% of the total flow thicknesses of the Pleistocene rocks were classified as pahoehoe – the majority consisted of a'a. Within the a'a flows, massive a'a cores were distinguished from rubble or clinker layers. Rubble was seen to make up about half (46%) of the total a'a flow thickness. The proportion of rubble to massive sections in the measured outcrops is proportionally similar to the amounts of these materials observed in the driller's logs from the Pleistocene rocks.



Base from Atlas of American Samoa,  
University of Hawaii Cartographic Laboratory, 1981

Figure A8. Locations of measured outcrops of Pleistocene Volcanic rocks. From Eyre and Walker (1991) with permission.

Table A5. Statistics from selected lava flows on Tutuila.

Site No. <sup>a</sup>	Location	No. of Measured Flows	Total Column Thickness (m)	A'a Unit Thickness: Massive Section (m)	A'a Unit Thickness: Rubble Section (m)	Pahoehoe Unit Thickness (m)	Dip Angle (°)	Rubble (%) <sup>b</sup>
1	Vatia	21	57.2	18	39.2	0	22	69
2	Vatia	2	10.9	5.2	5.7	0	23	52
3	Afono	1	8.2	4.2	4	0	20	49
4	Vatia	5	20.2	6.9	13.3	0	20	66
7	Leone	6	13.3	8.5	4.8	0.9	7	36
8	Amanave	11	17	12.2	1.7	0	small	28
11	Fagaitua	2	11.7	5.9	5.6	0	small	50
12	Masefau	12	55	33	22	0.1	small	40
13	Masefau	5	13.6	9.6	3.9	0	small	29
15	Masefau	2	9.9	8.8	1.1	0	small	12
18	Fatumafuti	2	13.1	6.3	6.8	0	<5	52
19	Faganeane	3	9.8	4.5	5.3	0	15	54
20	Nuuuli	2	34	23	11	0	–	32
23 + 24	Cape Tapu	6	30.3	17.2	13.1	0	small	43
25	Poloa	6	23	14.6	8.4	0.8	small	37
26	Fagasa	15	18.3	10.6	7.7	0.6	20	42
27	Fagasa	10	11.1	5.7	5.4	0.7	25	49
28	Fagamalo	6	14.1	6.8	7.3	0	10	52
29	Fagamalo	4	6.9	3.6	3.2	2.3	15	47
32	Afono	11	38.6	22.4	16.2	0	–	42
34	Utulei	1	5.9	4	1.9	4.1	–	32
37A	Amouli	4	27.6	14	13.6	0	15	49
37B	Amouli	5	2.3	1.5	0.8	0	15	34
38	Aoa	3	8.9	5.1	3.8	0	small	43

Source: Data from Eyre and Walker (1991).

<sup>a</sup>See Appendix Figure A.8 for site locations.

<sup>b</sup>Mean weight of rubble (%) = 45.4 (includes ~10% of thermally-welded rubble of low-permeability).

### A3 Interpretation of New Geophysics and Well Logging

A magnetotelluric (MT) survey of subsurface electrical resistivity beneath the Tafuna-Leone Plain and the Taputapu Volcano was conducted by Geologica Geothermal Group, Inc. (2014) for the purpose of exploration for a geothermal resource. In addition, these results are useful for interpreting the hydrogeology of the subsurface. The profiles indicate less-resistive zones that could be inferred to be saturated with seawater, and highly-resistive areas that may indicate the unsaturated zones. Moderately resistive areas could be interpreted as either permeable basalt saturated with freshwater or as regions of dense but unsaturated rock. The hydrology in these moderately resistive areas is difficult to discern on the profiles. An approach to resolve this issue with additional surveys might include a time-lapse sequence of MT imaging, which would evaluate transient changes based on water saturation and density conditions.

These profiles of subsurface resistivity (Figs. A8 and A9) vary in the specifics for different areas but share the common characteristic of an approximately 500 m thick high-conductivity layer, with resistivities of less than 10  $\Omega\cdot\text{m}$ . This layer extends from the coast (sea level) to two to three miles inland (-600 m below sea level) where it fades into more resistive material. This high conductivity layer is overlain, underlain, and bounded towards the central part of the island by more resistive material (20 to 400  $\Omega\cdot\text{m}$ ). The high-conductivity layer seems to occur in the Tafuna-Leone lavas, the underlying carbonate reef platform, and into the edifice of the Taputapu Mountain. This layer is very likely the result of conductive seawater that underlies the freshwater lens. The more resistive materials that bound the conductive layer on three sides (top, bottom, and inland margin) have resistivities that correspond to either unsaturated or saturated basalt with freshwater. The overlying highly resistive layers ( $>10 \Omega\cdot\text{m}$ ) most likely represents unsaturated basalt, and the moderately resistive layers in this region ( $\approx 20$  to 120  $\Omega\cdot\text{m}$ ) may represent the same material saturated with freshwater. The inland resistive material at depth may well represent the island's rift zone where numerous volcanic dikes either (1) prevents the intrusion of seawater and possibly allows freshwater to penetrate hundreds of meters below sea level, or (2) creates a material of such low porosity that no significant amount of water (fresh or salt) penetrates it, thus yielding the resistivity of basalt with low moisture content.

In the Geologica profiles, high resistivities plotted underneath the conductive layer seaward of the island's interior are surprising and contrast to typical salinity profiles on islands; saltwater saturation would be expected. Either the material is of such low porosity that no significant amount of water penetrates it, yielding the resistivity of basalt with a low moisture content; or the development of the resistivity profiles, which are based on a data inversion process, were not performed in a manner that accurately reflects conditions in the region in question. Note that temperature and resistivity-conductivity depths mentioned in the Geologica data are approximate due to potential inaccuracies in measurements and in estimation of depths from the MT profiles.

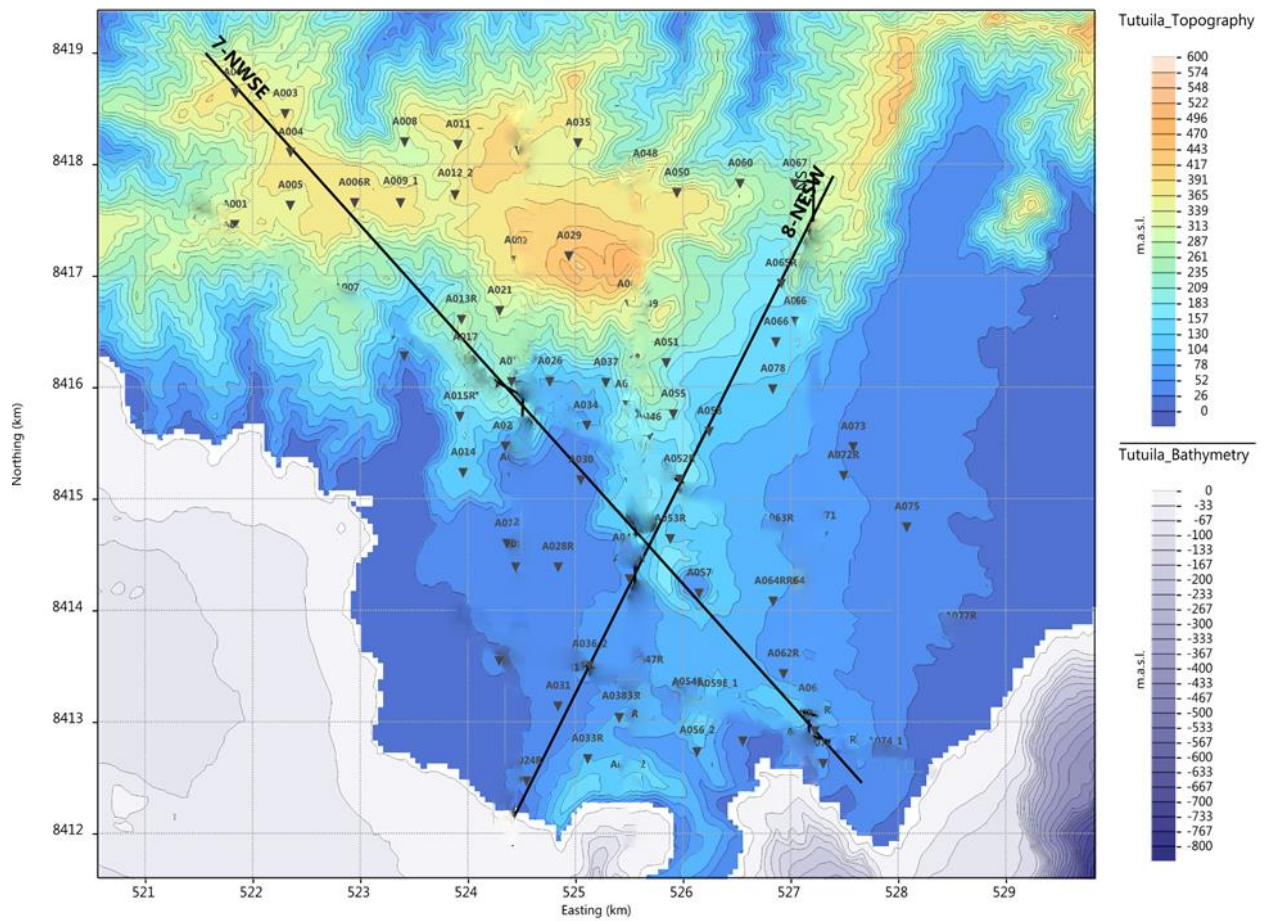


Figure A9. Map of the Tafuna-Leone Plain area showing locations of MT station measurements and cross sections (illustrated in Figure A10). Reprinted from Geologica Geothermal Group, Inc. (2014) with permission.

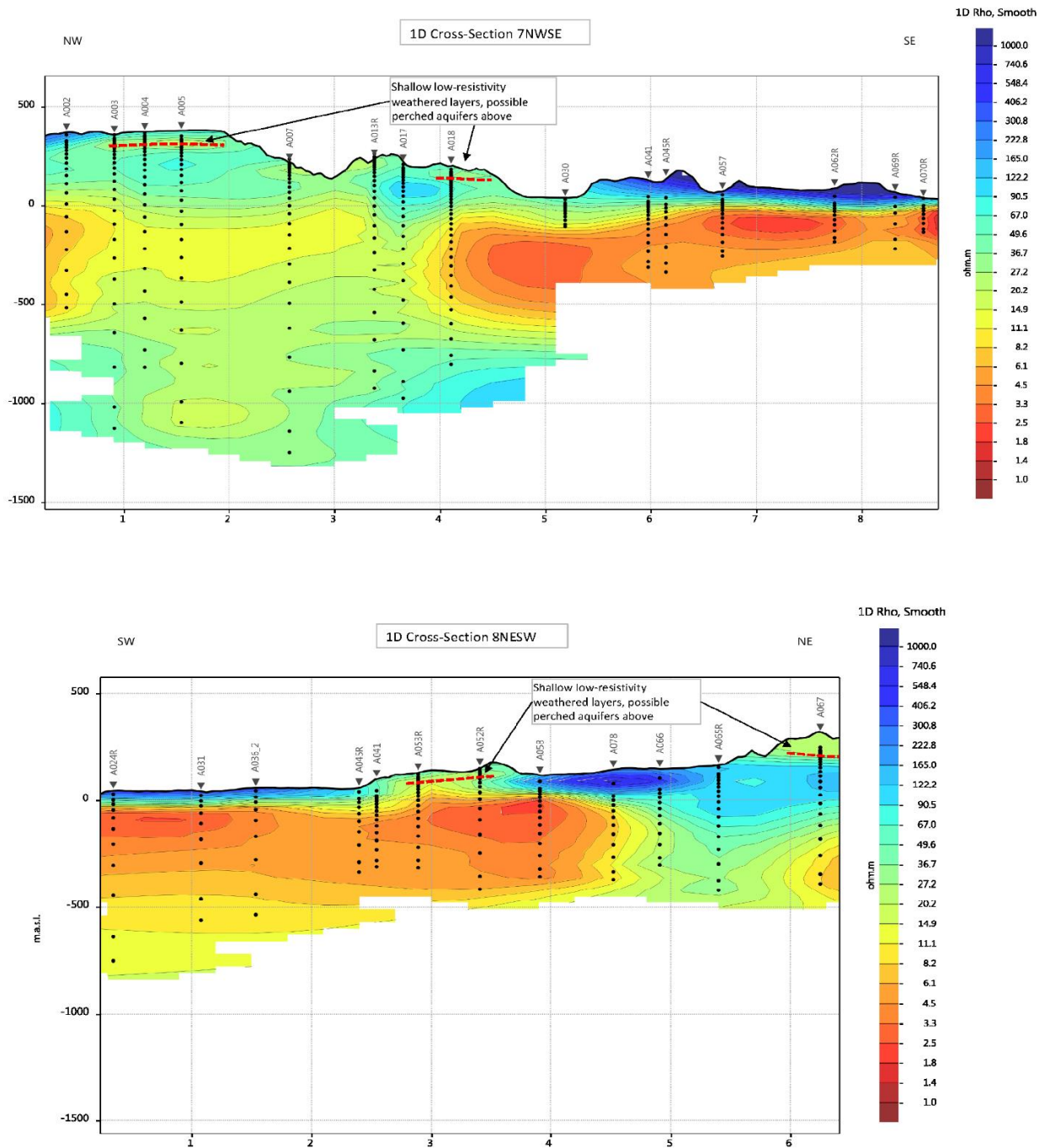


Figure A10. Cross sections of western Tutuila showing subsurface resistivity from Geologica Geothermal Group MT survey. Warmer colors indicate less resistive materials, interpreted to show conductivity from seawater saturation in the subsurface. Reprinted from Geologica Geothermal Group, Inc. (2014) with permission.

## A4 Hydrogeologic Data from Wells and Pumping Tests

### A4.1 Water Levels

Basic water level information can be used to assess the direction of groundwater flow, to infer aquifer properties, and to estimate magnitudes of hydraulic connectivity in different areas. Near sea level water levels in the Tafuna-Leone Plain generally support observations of high hydraulic conductivity, whereas wells in valley-fill alluvial aquifers and Pleistocene rocks have more variable water levels suggesting these areas have more heterogeneous conductivity distributions. Historical U.S. Geological Survey (USGS) reports authored by Izuka (1996, 1997, 1999a) contain water levels from American Samoa Power Authority (ASPA) records from 1984 to 1997. Eyre and Walker (1991) summarized water level data from USGS records from 1975 to 1991. Reported water levels from all known sources are summarized in Table A6 (Fig. A11). Note that the discrete (one time) measurements compiled in this report are subject to uncertainties in recharge variation, previous pumpage, and tidal or atmospheric fluctuations.

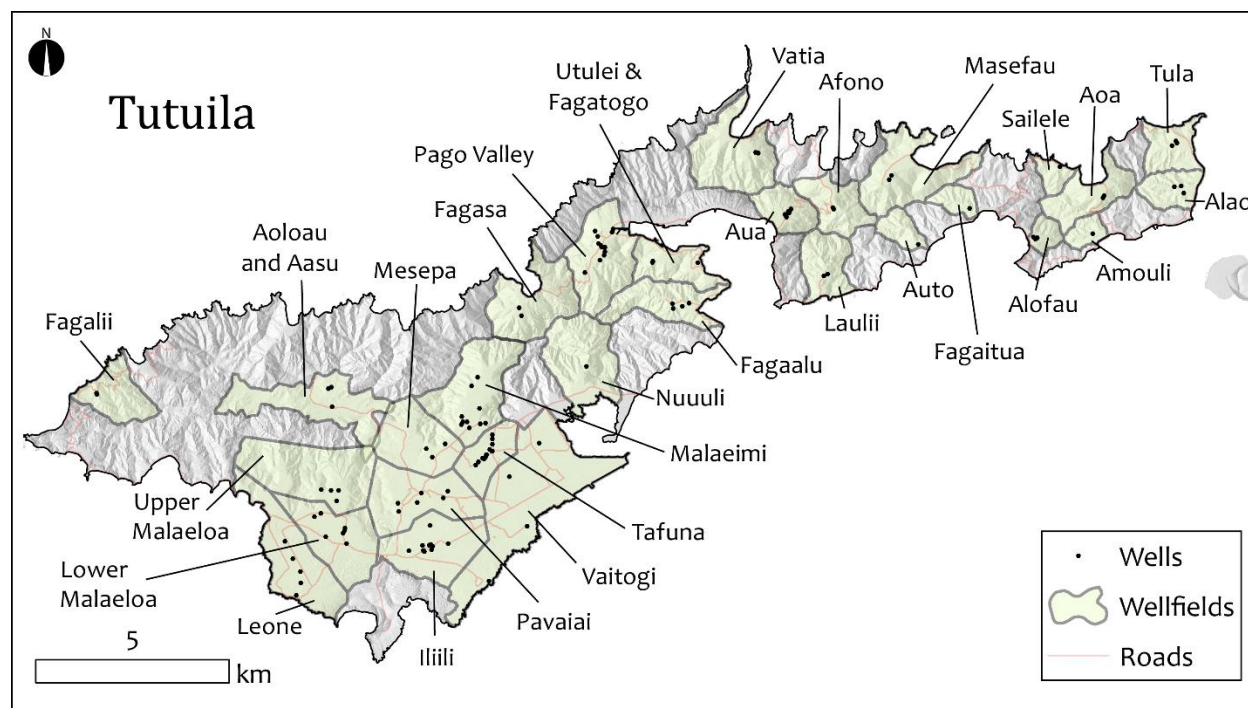


Figure A11. Location map of selected watersheds or wellfield areas where water level data is available.

Table A6. Compilation of historical water level data by well field, in meters relative to mean sea level

<b>Well Field</b>	<b>Drilling Water Level Range [m]</b>	<b>Pumping Water Level Range [m]</b>	<b>Geologic unit(s)</b>
Afono	-	-1.5	Pago Outer-Caldera
Vatia	8	-9 to 7	Pago Outer-Caldera
Laulii	6 to 7	-8	Pago Outer-Caldera
Pago Valley	1 to 62	-45 to 61	Alluvial or Pago Outer-Caldera
Fagaitua	-	-1	Alluvial or Pago Outer-Caldera
Masefau	-	1 to 2	Alluvial or Pago Outer-Caldera
Fagasa	-	4 to 25	Alluvial or Pago Outer-Caldera
Nuuuli	22	-	Pago Inner-Caldera
Fagaalu	3 to 27	-1	Alluvial or Pago Inner-Caldera
Aua	1 to 6	-10 to -22	Alluvial or Pago Inner-Caldera
Utulei & Fagatogo	6 to 7	-1 to 5	Alluvial or Pago Inner-Caldera
Tula	3	-5	Alluvial or Olomana Shield
Aoa	-	-8 to 1	Alluvial or Olomana Shield
Alao	6	-5 to -1	Alluvial or Olomana Shield
Amouli	5.5	4	Alluvial or Alofau Shield
Alofau	0 to 2.3	-	Alluvial or Alofau Shield
Sailele	2.5	-	Alluvial or Alofau Shield
Tafuna	0.5 to 2.5	-5 to 0.5	Leone Volcanics (Tafuna Lavas)
Pavaiai	1.5		Leone Volcanics (Tafuna Lavas or Pyroclastics)
Iiili	1 to 3	-1 to 1	Leone Volcanics (Tafuna Lavas or Pyroclastics)
Mesepa	3	1	Leone Volcanics (Tafuna Lavas)
Malaeimi	2 to 35	-1 to 24	Leone Volcanics, Pago Outer, or Alluvial
Lower Malaeloa	1 to 3	1 to 2	Leone Volcanics (Leone Lavas)
Leone	0 to 0.5	-	Leone Volcanics (Leone Lavas)
Upper Malaeloa	4 to 14	2.5	Taputapu or Leone Volcanics
Fagalii	5.5	5	Taputapu Shield
Aoloau and Aasu	382	344 to 346	Leone volcanics (Pyroclastics)

Note: Water levels are in meters above sea level.

Sources: Bentley (1975); Eyre and Walker (1991); Izuka (1996, 1997, 1999a); Unpublished ASPA records and drillers logs

## A4.2 Water Level Variability in the Tafuna-Leone Plain

Water levels in the Tafuna-Leone Plain aquifers are quite variable in response to rainfall or extended dry periods, and baseflow and spring flow throughout the island has been reported to be significantly reduced by extended dry periods (Davis, 1963; Bentley, 1975). In the Pleistocene rocks, water-level drawdowns of up to 15 m are observed in response to pumping (Eyre and Walker 1993). Although the plain's water levels do not seem to respond strongly to variations in pumpage (Shuler, unpublished data, July 2014), Kennedy et al. (1987) notes that water levels in Tafuna-Leone wells were found to increase and subsequently decrease rapidly in response to high rainfall events. Water level declines and increased salinity have also been observed in Tafuna-Leone wells during droughts. An extreme example of rapid change in water levels from recharge events is the recent observation made in a non-pumping well in Lower Malaeloa Village during a period of heavy rain events (Fig. A12). Over the course of ten days, during and following these events, the water level in Malaeloa Well 80 rose by over 2 m. Periods of heavy rainfall leading to large increases in water levels have also been correlated with increase in turbidity and *Escherichia coli* detections in some Tafuna-Leone wells, which is the primary issue that has mandated the island's long standing boil-water notice.

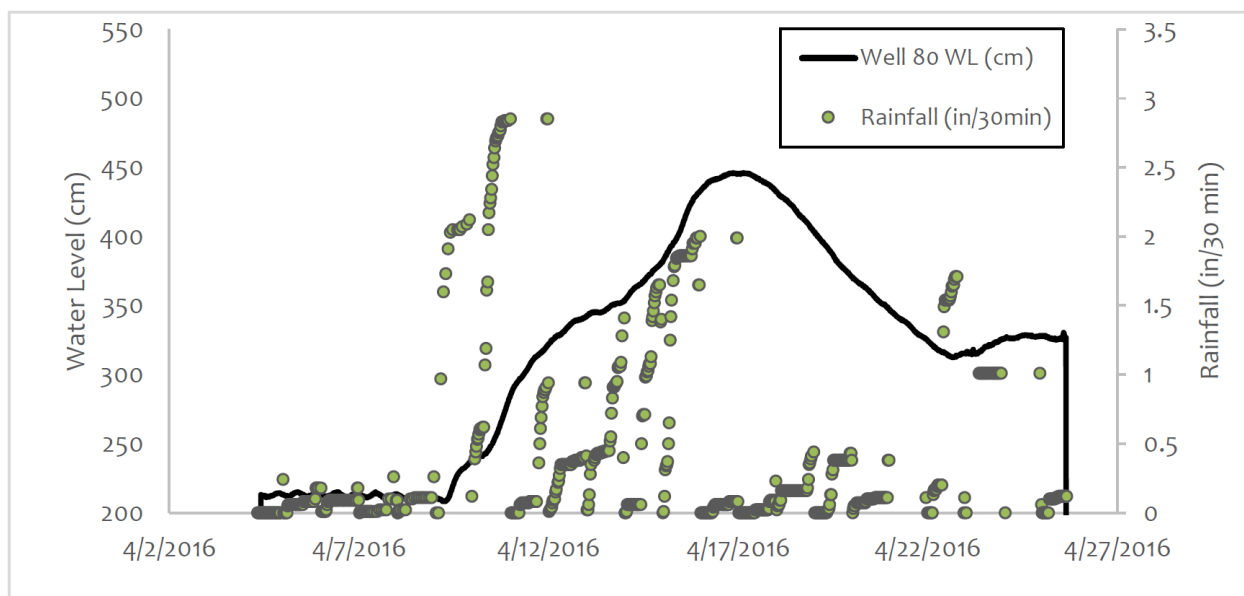


Figure A12. Time series measurement of water levels (WL) taken over an extended period of heavy rain events in Lower Malaeloa monitoring Well 80 as recorded at a WRRC weather station located in Malaeimi Village.

## A4.3 Specific Capacity

In production wells where static and pumping water levels are available, the ratio of pump-rate to drawdown can be assessed. This measurement, known as specific capacity, is reported here in gallons per minute (GPM) per meter of drawdown. In general, higher specific capacities indicate better producing wells. While this parameter can indicate the productivity of

a well, it is of limited use in describing aquifer characteristics, as drawdowns from both aquifer loss and the well loss (head loss resulting from attributes of well construction) are both included in water level measurements. Depending on the drilling and well construction methods, well loss can be, and often is, greater than aquifer loss. Measurements of specific capacity from past studies, ASPA records, and recently conducted University of Hawaii (UH) Water Resources Research Center (WRRC) tests shown in Figure A13, display expected regional variability. Specific capacity measurements on Tutuila indicate that in general, wells in the Tafuna-Leone Plain region yield more water per unit of drawdown than wells in other parts of the island.

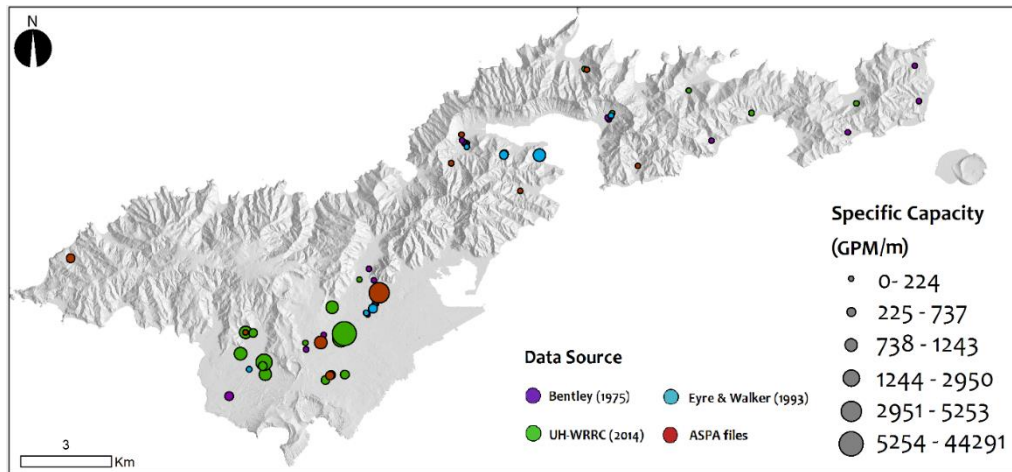


Figure A13. Distribution and magnitude of specific capacity values derived from historical records and from recently conducted WRRC tests. Colored circles indicate data source, circle size indicates specific capacity value (GPM/m).

#### A4.4. Aquifer Transmissivity and Hydraulic Conductivity

Transmissivity ( $T$ ) and hydraulic conductivity ( $K$ ) describe how fast water is able to move through saturated aquifer material over a given hydraulic gradient. These data are commonly gathered through constant-rate pumping, step-drawdown, and recovery tests when a new well is developed. The two parameters are related,  $K$  describes the rate of flow through a unit cross sectional area of aquifer, whereas  $T$  describes the rate of flow in regards to the entire thickness of the aquifer ( $b$ ). This essentially means that  $T$  equals  $K$  times  $b$  (Freeze and Cherry 1979).

To develop the most comprehensive estimates of aquifer parameters on Tutuila, all available pump test, step-drawdown, and recovery test data were compiled from USGS records (Bentley 1975, Eyre and Walker 1991), archived ASPA records, and the recently performed WRRC aquifer tests. Values of  $T$  and  $K$  from Bentley (1975) and Eyre and Walker (1991) are estimates derived from pump tests performed by USGS or from data recorded during well development testing, and their analytical methods are detailed in the aforementioned reports.

Different analytical methods were used to derive  $T$  and  $K$  estimates from an array of sources. Values of  $K$  from ASPA records and WRRC tests were obtained with the Jacob-Zangar

Method (Zangar, 1953; Jacob, 1947). Pumping and recovery tests performed by WRRRC in 2014 were analyzed with the Cooper-Jacob Straight-Line Method to obtain values of  $T$  (Halford and Kuniansky, 2002). Since the thicknesses of Tutuila's aquifers are unknown,  $T$  values were converted to  $K$  values by assuming the effective thickness of the aquifer  $b$  is equal to the saturated length of the well (i.e., well depth minus depth to water or bottom of casing, whichever is deeper). Values of  $T$  reported in Bentley (1975), were converted to  $K$  values in the same way. It should be noted that these estimates are based on methods that have implicit assumptions such as isotropic and homogeneous aquifer conditions, wells are fully penetrating, aquifers have infinite areal extent, and well-losses are adequately represented by the second degree Jacob equation. Tutuila's wells seldom meet these ideal conditions. Nonetheless, these data represent the best available estimates for the range and magnitude of Tutuila's aquifer parameters.

Compiled aquifer parameter values of  $K$ ,  $T$ , and specific capacity from all data sources are summarized in Table A7 and shown in Figure A14. The data is summarized with three different measures of central tendency, these being the arithmetic mean [ $\mu = E(x)$ ], the harmonic mean [ $1/\mu = E(1/x)$ ], and the geometric mean [ $\ln(\mu) = E[\ln(x)]$ ], where  $E$  is the sum of individual values divided by the number of values. Considering the heterogeneous character of the Pleistocene aquifers, it is reasonable to assume that when characterizing  $T$  and  $K$  for the entire hydrologic unit, the best estimate of these parameters is probably represented by the harmonic or geometric means, rather than the arithmetic mean, of individual values from well tests (Eyre and Walker, 1991).

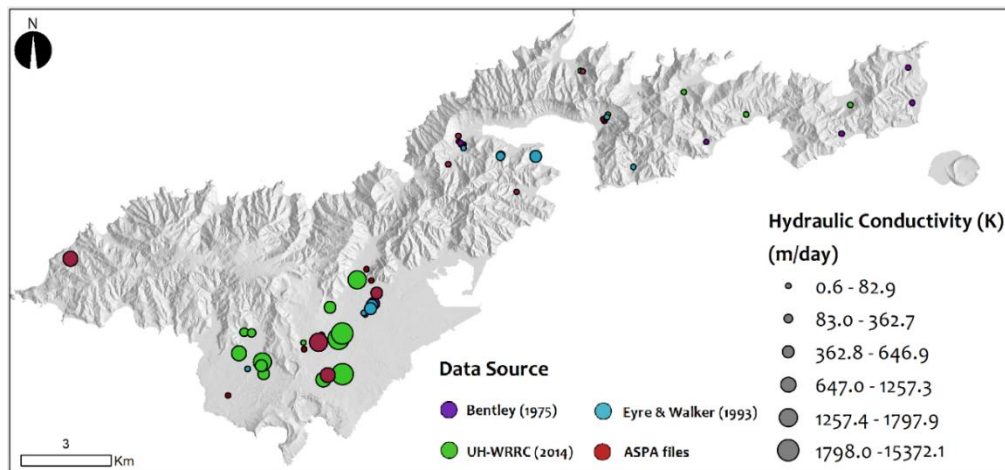


Figure A14. Distribution and magnitude of  $K$  values derived from ASPA historical records and from recently conducted WRRRC recovery tests. Colored circles indicate data source, circle size indicates value of  $K$  (m/d).

Table A7. Summary of aquifer and well production characteristics from existing wells on Tutuila from 1973 to 2014.

<b>SPECIFIC CAPACITY (GPM/m)</b>				
Hydrogeologic Unit	n*	Arithmetic Mean	Geometric Mean	Harmonic Mean
Tafuna lavas	20	2,882	228	12
Leone lavas and ash	7	783	449	194
Pyroclastics of Leone Series	5	368	94	2
Taputapu Shield	4	628	524	426
Pago Outer-Caldera Shield	14	13	10	4
Pago Inner-Caldera Shield	5	26	15	9
Olomoana or Alofau Shields	2	19	19	19
Alluvial-fill valleys	10	309	32	4
<b>TRANSMISSIVITY (m<sup>2</sup>/d)</b>				
Hydrogeologic Unit	n*	Arithmetic Mean	Geometric Mean	Harmonic Mean
Tafuna lavas	19	11,894	3,512	1,112
Leone lavas and ash	5	4,782	3,379	1,584
Pyroclastics of Leone Series	3	3,882	3,070	2,369
Taputapu Shield	5	7,791	5,984	5,002
Pago Outer-Caldera Shield	12	176	124	73
Pago Inner-Caldera Shield	4	210	129	85
Olomoana or Alofau Shields	2	181	110	66
Alluvial-fill valleys	9	1	278	70
<b>HYDRAULIC CONDUCTIVITY (m/d)</b>				
Hydrogeologic Unit	n*	Arithmetic Mean	Geometric Mean	Harmonic Mean
Tafuna lavas	13	7,652	708	98
Leone lavas and ash	5	1,270	635	130
Pyroclastics of Leone Series	3	837	355	86
Taputapu Shield	3	410	323	270
Pago Outer-Caldera Shield	10	6	4	3
Pago Inner-Caldera Shield	3	7	3	1
Olomoana or Alofau Shields	1	9	9	9
Alluvial-fill valleys	4	261	121	22

Source: Bentley 1975, Eyre and Walker 1991, UH-WRRC aquifer tests, and ASPA file cabinets.

\*n = number of wells.

### A4.5 High Chloride Wells

A number of Tutuila's wells produce water with levels of chloride ( $\text{Cl}^-$ ) that exceed the U.S. Environmental Protection Agency (EPA) recommended limit of 250 mg/L. The salinity of a well on Tutuila will ultimately be a function of the well depth, pumping rate, hydraulic conductivity of the aquifer tapped, and the geometry of the well placement, specifically its proximity to the coast. Many of the higher salinity wells on Tutuila are located near to the coast (Fig. A15).

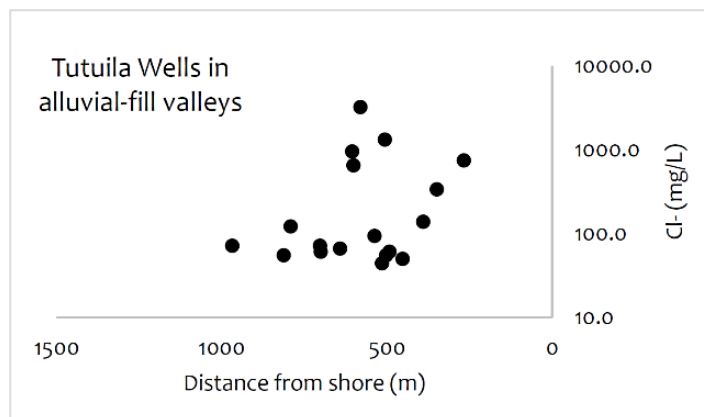


Figure A15. Graph showing correlation between  $\text{Cl}^-$  concentration (mg/L) and distance of well from shore (for all wells located in Tutuila's Pleistocene shield alluvial-fill valleys). Note that distance from shore is not necessarily the primary factor that controls groundwater  $\text{Cl}^-$  concentrations.  $\text{Cl}^-$  measurements are from unpublished WRRC data.

Freshwater lens thickness is a primary consideration in setting well target depths when developing new groundwater sources. Although well depth is not the only factor controlling groundwater  $\text{Cl}^-$  concentrations, an assessment of existing production wells in the Pleistocene rocks shows that only wells deeper than approximately -20 m are currently producing water with elevated  $\text{Cl}^-$  levels (Fig. A16). However, it should be noted that any well below sea level has the potential to be affected by seawater if over-pumped. Although groundwater production below -20 m below sea level is not recommended, exploratory drilling below this depth would certainly be useful to assess the location of the saltwater-freshwater interface.

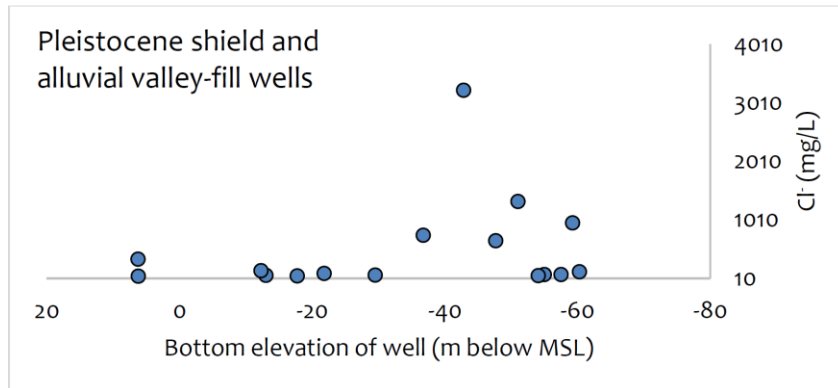


Figure A16. Graph showing correlation between Cl<sup>-</sup> concentrations (mg/L) and well depth (in m below sea level) located in selected Pleistocene shield and alluvial valley-fill wells. Note that well depth is not necessarily the primary factor that controls groundwater Cl<sup>-</sup> concentrations. Well depth is taken from various sources and is not confirmed. Cl<sup>-</sup> measurements are from unpublished WRRC data.

## A5 Numerically Modeled Values of Hydraulic Conductivity

Another method for estimation of  $K$  values is through parameterization of numerical models that are calibrated with water level observations. This approach yields a regionally integrated estimate of  $K$ , as opposed to well tests that only provide point based data. Groundwater models use subsurface flow equations (essentially partial differential forms of Darcy's Law) and parameterize them with recharge rates, geographic geometry, well characteristics, and well flowrates. Generally, the most poorly constrained parameter (often  $K$ ) is numerically solved for using a calibration process.

Two groundwater models of Tutuila have thus far been developed, and each used its own paradigm for parameterizing values of  $K$ . Izuka et al. (2007) measured elevations of the water table at wells and assumed locations of mountain springs. Values of  $K$  were then found through calibration so that the simulated water table elevations matched the observed and assumed data. For the older volcanic unit, this procedure yielded a calibrated  $K$  value of approximately 0.1 m/d. In contrast, the model developed by ASPA (2013) assumed that a measured estimate of  $K$ , based on an aquifer test and geologic conditions, was valid throughout all of the Pleistocene rocks. This value was used as an input parameter in the model, which was then solved for the water table elevation.

The Izuka et al. (2007) model focused on the Tafuna-Leone Plain region only, and used static water levels in six monitoring wells to determine modeled values of hydraulic conductivity ( $K$ ) (Table A8), via model calibration. The Pleistocene rocks were modeled as a fully saturated homogeneous anisotropic system. The ASPA (2013) model on the other hand, utilized many of the parameters from the Izuka et al. (2007) model, but the Pleistocene rocks were assumed to contain both disconnected high-level groundwater (which was not explicitly simulated by the model) and basal groundwater. This alternate conceptual model for the older-

volcanic region was represented in the model by a change in  $K_h:K_v$  and an increase in the  $K_h$  of the older volcanic unit by a factor of about 50, from the Izuka et al. (2007) model. Although the ASPA (2013) model's  $K_h$  value is a better match with the measured  $K$  values from the pump tests in the Pago Shield (1–7 m/d), it is significantly lower than pump-test values measured from the Taputapu Shield (270–410 m/d). Hence, both of these models may overestimate water levels, and underestimate the productivity of potential wells in the Taputapu Shield. The Izuka et al. (2007) and ASPA (2013) numerical models present fundamentally different conceptualizations of the flow of groundwater through the Pleistocene volcanics, but it remains unclear as to which is more representative of the actual conditions, as each model has both weaknesses and strengths.

Table A8. Numerically modeled values of hydraulic conductivity.

<b>IZUKA MODEL<sup>a</sup></b>		
<b>Geologic Unit</b>	<b><math>K_h:K_v</math></b>	<b><math>K_h</math> (m/d)</b>
Alluvium	100:1	260
Leone lava and ash	100:1	1,300
Pyroclastics	100:1	10
Rift-zone	10:1	0.03
Tafuna lava	10:1	945
Old-volcanics	100:1	0.14
<b>ASPA MODEL<sup>b</sup></b>		
<b>Geologic Unit<sup>c</sup></b>	<b><math>K_h:K_v</math></b>	<b><math>K_h</math> (m/d)</b>
Old-volcanics	44:1	6.7

<sup>a</sup>Izuka et al. 2007.

<sup>b</sup>ASPA 2013.

<sup>c</sup>Other geologic unit values are same as Izuka model.

## A6 High-Level Spring Occurrence and Geochemistry

The existence of Tutuila's high-level groundwater is clearly indicated by the occurrence of perennial streams and springs throughout upper elevations on Tutuila. Davis (1963), Eyre and Walker (1991), and Izuka et al. (2007) noted that streamflow from the Pleistocene age volcanic rocks is generally fed by numerous and dispersed springs with low-flow rates. Davis (1963) describes high-level seepage zones that release small volumes of water, often along a lineation of some sort, and often with flow rates so low that they easily escape detection when seeping out under soil or thick vegetation. These observations imply high-level reservoirs in the Pleistocene volcanic rocks are dispersed, and may only contain insignificant quantities of water. Nonetheless, additional documentation of a few notable high-flow springs throughout the

island suggests that some of these reservoirs may be larger than others. Locations of perennial high-level springs and streamflow characteristics may provide clues for assessing the significance of an area's high-level water supply. Springs with exceptional flow rates were often documented in reports because of their historical use in village or U.S. Navy water systems. Prior to groundwater development in the 1970s, surface water supplies were the primary source of drinking water on the island. A spring with a high flowrate suggests that the subsurface source reservoir contains significant storage or that the recharge area for the reservoir is extensive.

A major limitation for the development of high-level groundwater is the nature of Tutuila's Pleistocene aquifers, which are not well understood. Typically in volcanic island environments, structures such as dikes, faults, or aerially extensive perching layers are thought to control the locations and size of the larger pockets of high-level water. However, it is also possible due to the high and frequent rainfall (up to 5,700 mm/yr [200 in./yr]) in the island's interior, that instead of being fed by structurally controlled aquifers contained in bedrock, some high-level springs and streams may be fed by lateral flow from reservoirs consisting of continually wetted soil. To estimate the residence time of water in the subsurface, and therefore better constrain the magnitude of storage, a number of environmental tracers can be applied.

Assessments of water-isotope ( $\delta^2\text{H}$  &  $\delta^{18}\text{O}$ ) compositions in precipitation and groundwater have been widely used in tropical island environments to assess recharge source, elevation, or timing. (Scholl et al. 2002, Rhodes et al. 2006, Fackrell 2016). On Tutuila, a strong seasonal trend in precipitation  $\delta^2\text{H}$  &  $\delta^{18}\text{O}$  values has been observed (Fig. A17a) (Shuler et al., 2017). Because of this predictable seasonal variation, the isotopic composition of surface or groundwaters can indicate how recently their source was recharged. Recently infiltrated water moving to streams via lateral-flow would be expected to show an isotopic signature that matches that of recent precipitation. On the other hand, groundwater from an extensive aquifer would be expected to have a longer subsurface residence time and show an isotopic signature that integrates or averages the isotopic composition of precipitation events over multiple seasons. To test this hypothesis, six production wells throughout the island (ASPA wells 33, 84, 89, 93, 128, and 179) were sampled on a monthly basis and precipitation was collected at four well sites over a period of three years. Rainfall was collected in cumulative precipitation collectors (CPCs) following the design used in Scholl et al. (1996). Samples were collected in 20 ml glass vials with no headspace and analyzed for  $\delta^{18}\text{O}$  and  $\delta^2\text{H}$  of water in a Picarro brand Cavity Ring-Down Spectrometer (L1102-i Isotopic Liquid Water Analyzer) at the University of Hawaii Stable Isotope Biogeochemistry Lab. Water isotope values reported here are in per mil (‰) notation relative to the international water isotope standard of VSMOW.

This assessment showed that the average annual  $\delta^2\text{H}$  and  $\delta^{18}\text{O}$  values in groundwater from all the wells were -4.25‰ and -20.01‰, respectively. This isotopic signature is quite close to the annual volume weighted average for  $\delta^2\text{H}$  and  $\delta^{18}\text{O}$  values measured at all precipitation collectors (-4.87‰ and -25.01‰, respectively). Additionally, numerous samples of high-level

groundwater at upland springs, and baseflow from streams throughout the island were collected over the period spanning from 2013 to 2018. Water isotopes from these springs and streams were plotted against observed isotope values in precipitation and groundwater (Fig. A17b). In general, the isotopic composition of springs and streams more closely resembled the average annual composition of groundwater than precipitation during the month in which they were taken. This result suggests that the sampled springs and streams, for the most part, originate from groundwater sources having multi-season residence times.

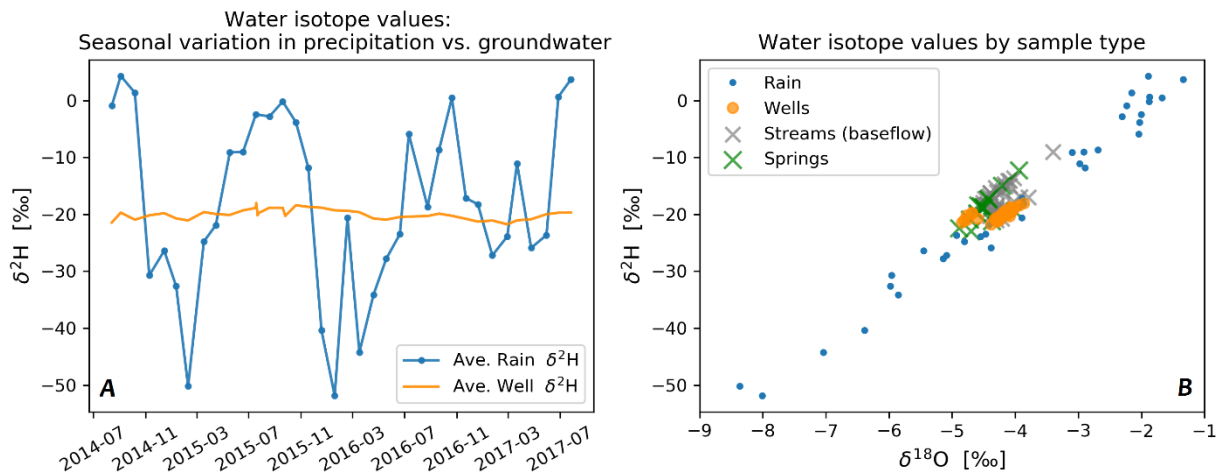


Figure A17: Panel a, Monthly average water isotope values in rainfall measured with precipitation collectors (*blue line*) and monthly average water isotope values in groundwater measured at six production wells located throughout Tutuila (*orange line*) over a 3 year period. Panel b, Values of  $\delta^2\text{H}$  plotted against  $\delta^{18}\text{O}$  values in precipitation (*blue dots*) well waters (*orange dots*), high-level springs (*green crosses*), and stream baseflow samples (*grey crosses*). Samples from different sources will plot in different fields.

Another useful tracer for determining residence time of groundwater is the noble gas radon-222 ( $^{222}\text{Rn}$ ). Radon has a short half-life (3.8 days), is produced underground by geologic material, and reaches an equilibrium concentration in groundwater after about 15 days (Snow and Spalding, 1997). Radon quickly escapes to the atmosphere when water is exposed on the surface, thus its presence in spring or stream waters indicates these waters were recently discharged from an aquifer. In addition, recently recharged – and subsequently discharged – subsurface water will not have substantial  $^{222}\text{Rn}$  concentrations because it may take up to two weeks for  $^{222}\text{Rn}$  to reach equilibrium levels. Many springs and streams sampled for water isotopes were also sampled for  $^{222}\text{Rn}$ . Radon grab samples were collected in 250-ml glass bottles and analyzed with a RAD7 radon detector and RAD H2O water analyzer, both manufactured by DurrIDGE Inc. Because of  $^{222}\text{Rn}$ 's short half-life, grab sample values were corrected for radioactive decay between collection and analysis. From 2013 to 2018, over 150 samples from Tutuila production wells were collected and analyzed for  $^{222}\text{Rn}$ . Although  $^{222}\text{Rn}$  concentrations were variable throughout different parts of the island, the arithmetic mean of all well water samples was 250.2 dpm/L, and the median was 160 dpm/L. In spring waters,  $^{222}\text{Rn}$

concentrations fell into two distinct groups, those with concentrations below 15 dpm/L and those with concentrations above 80 dpm/L. Springs that fall into the latter group likely originated from a groundwater source with a residence time exceeding rain-event timescales.

Springs located during WRRC field expeditions that showed high ( $> 80$  dpm/L)  $^{222}\text{Rn}$  concentrations and  $\delta^2\text{H}$  and  $\delta^{18}\text{O}$  signatures matching average annual groundwater values are presented in Table A9 and Figure A18, along with locations and anecdotal information about ‘exceptional’ springs documented in Davis (1963), Bentley (1975), Eyre and Walker (1991), and Burger (1981). It should be noted that the spring locations sampled through these efforts do not constitute a comprehensive, or necessarily representative assessment of all areas on Tutuila. Due to the difficulty in accessing mountain springs located on steep and overgrown terrain, the sites presented in this study are probably a small subset of the full population of springs that exist in Tutuila’s Pleistocene shields. It should also be understood that any water development in high-level reservoirs areas will most likely result in reduction of spring and associated streamflow. Such actions have consequences for aquatic ecosystems as well as for the residents who rely on village water systems that are dependent on springs. These consequences should be fully assessed prior to the development of groundwater near significant springs.

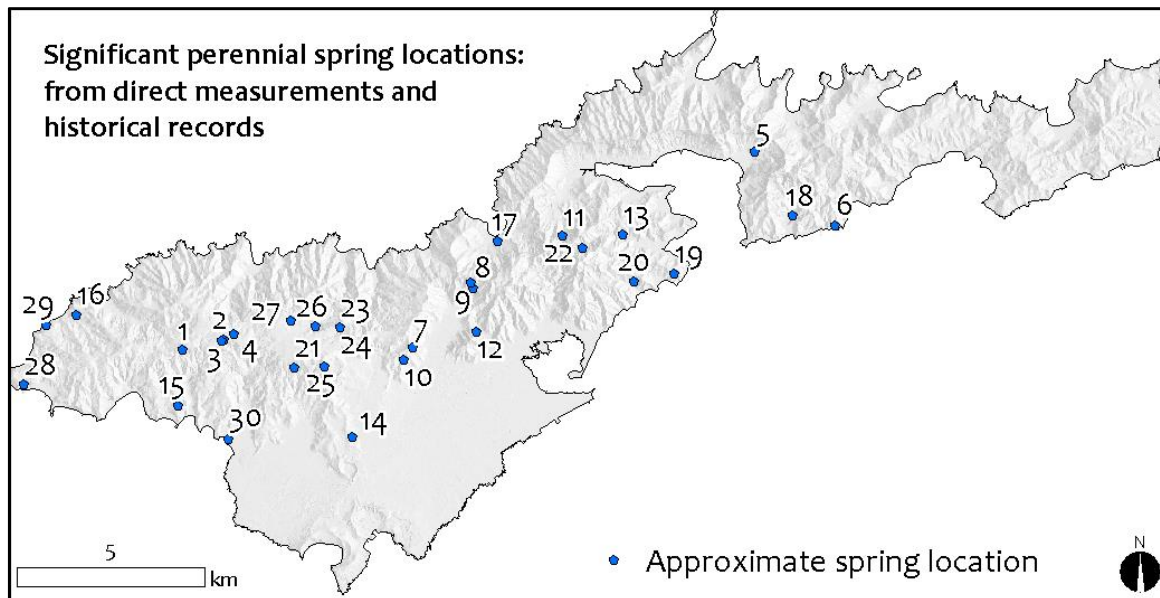


Figure A18. Locations of documented and/or observed freshwater springs that may have significant flow rates or are confirmed through geochemical analysis to be sourced from groundwater reservoirs with significant residence times. Geochemical data and anecdotal details for each spring are provided in Table A9.

Table A9: Geochemical data and details provided in literature sources for notable springs.

Number	Data Source	<sup>222</sup> Rn [dpm/L]	δ <sup>18</sup> O [‰]	δ <sup>2</sup> H [‰]
1	Uh-WRRC	134	-4.37	-21.2
2	Uh-WRRC	209	-4.55	-18.51
3	Uh-WRRC	485	-4.72	-20.9
4	Uh-WRRC	291	-4.6	-19.81
5	Uh-WRRC	266	-4.5	-18.88
6	Uh-WRRC	133	-4.89	-22.41
7	Uh-WRRC	164	-4.59	-18.39
8	Uh-WRRC	559	-4.43	-17.4
9	Uh-WRRC	89	-4.21	-14.99
10	Uh-WRRC	266	-4.01	-19.44

Number	Data Source	Notes
11	Uh-WRRC	High volume, used for Tuna Cannery supply
12	Uh-WRRC	Dike impounded, significant flow rate, tapped by local family
13	Uh-WRRC	Significant seepage from quarry face
14	Uh-WRRC	Significant discharge from pyroclastic ridge
15	Davis (1963)	Documented on map
16	Davis (1963)	Documented on map
17	Davis (1963)	Flow rate of a few gallons per minute
18	Davis (1963)	Documented on map
19	Davis (1963)	Developed tunnel, Flow rate of 5 GPM
20	Davis (1963)	Documented on map
21	Davis (1963)	Two springs noted with combined flow rate of 20 GPM
22	Davis (1963)	Davis notes as exceptional, estimated flow rate of 350 GPM
23	Bentley (1975)	Flow rate of 50 - 150 GPM, flow in dry season may be halved
24	Bentley (1975)	Flow rate of 50 - 150 GPM, flow in dry season may be halved
25	Burger (1981)	Mapped due to biological significance
26	Burger (1981)	Mapped due to biological significance
27	Burger (1981)	Mapped due to biological significance
28	Burger (1981)	Mapped due to biological significance
29	Burger (1981)	Mapped due to biological significance
30	Burger (1981)	Mapped due to biological significance

## A7 Streamflow Analysis

Streamflow statistics such as variation in flow, baseflow quantity, and runoff to rainfall ratios between different basins can indicate aquifer parameters; primarily the ability of the rocks in a basin to store and then slowly release water. Aquifers with higher water holding capacities will generally retain more precipitation as recharge, and streams in these basins will discharge a higher proportion of their total flow as baseflow, as opposed to direct runoff. Extensive stream gauging on Tutuila was performed by the USGS between the 1950s and 2008. The data from this effort remains a significant asset to the understanding of American Samoa's hydrology. A summary of Tutuila's streamflow data and an analysis of low-flow characteristics are given by Wong (1996). Wong compiled the analyses for 83 streams and tributaries in 63 basins or sub-basins. These included statistics regarding low flows at various recurrence intervals, mean and median flows, drainage basin characteristics, and variation in baseflow. Of particular interest to this work is Wong's Baseflow Index (BFI), which is described in detail below. Continuous flow measurements were collected at eleven of the USGS stations and the data were run through a baseflow separation analysis by Perreault (2010). Station locations are shown in Figure A19.

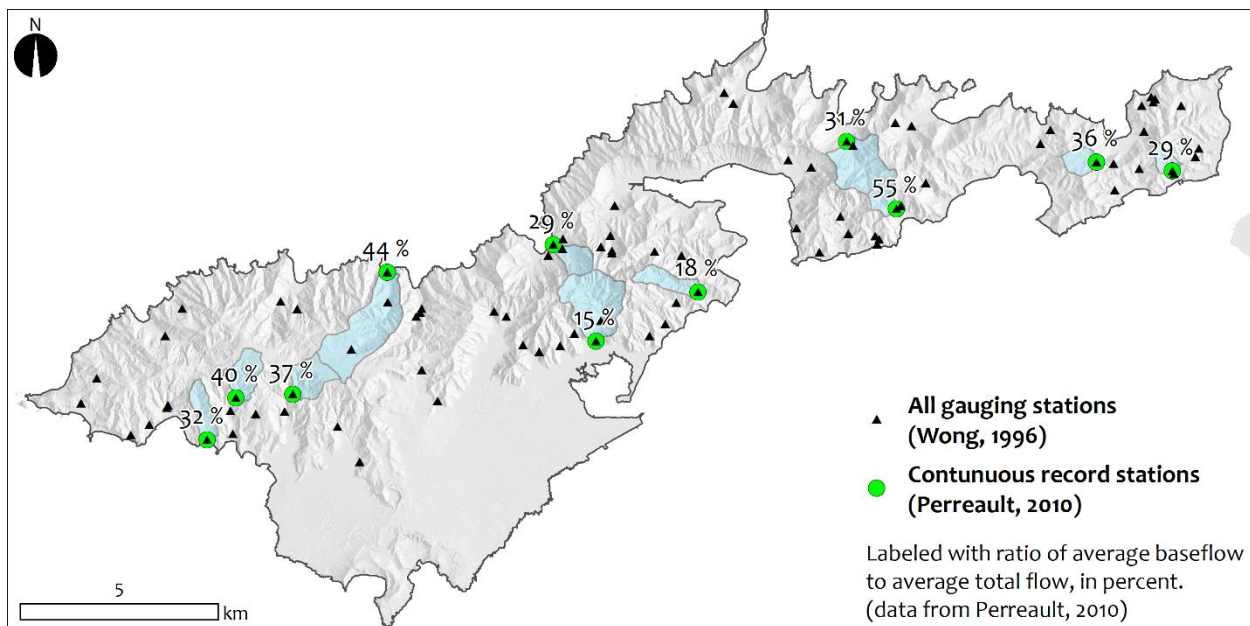


Figure A19. Locations of continuous and partial-record streamflow gauging stations maintained and reported by the USGS. Continuous record stations are shown as green dots with upgradient watershed areas (blue patches), and are labeled with the station's ratio of average baseflow to average flow as determined by baseflow separation analysis (Perreault 2010).

Streamflow is often broken into two basic components – baseflow and runoff. The runoff component is defined as the portion of streamflow that reaches the stream via overland flow or through inner-event lateral flow, and primarily occurs during heavy rains. Baseflow, on the other hand, originates from a groundwater aquifer and is discharged consistently to the stream at all times, during and between rainfall events. Also note that lateral flow, which is defined as

water that reaches streams via lateral (across bedding) movement through soil layers, is sometimes classified in either of the aforementioned categories depending on separation methods because it shares characteristics of both runoff and baseflow. Most lateral flow occurs during or shortly after rainfall events and is thus often grouped with surface runoff. In American Samoa, rainfall is generally heavy, the land is steep, and streams are short. These conditions create short-lived runoff events. However, the majority of the time baseflow or slower moving lateral flow supplies the water that sustains streamflow in Tutuila's drainages. Based on data from Perreault (2010), the eleven analyzed drainages discharged (on average) 33% of their flow as baseflow and 66% as runoff.

In Hawaii, stream baseflow is equivalent to a flow value that falls within a range of the  $Q_{60}$  and  $Q_{80}$  exceedance values (Bassiouni and Oki, 2013). These values are defined as the stream discharge ( $Q$ ) that is met or exceeded 60% of the time ( $Q_{60}$ ) or 80% of the time ( $Q_{80}$ ). Although Wong (1996) did not calculate values for true baseflow in Tutuila's streams, median flows ( $Q_{50}$ ) were reported. Comparison of the  $Q_{50}$  reported by Wong, to average baseflows as reported by Perreault (2010) for each of the continuous record sites shows that the ratio of median flow to baseflow is about 1.4. Thus  $Q_{50}$  (Wong 1996) averages about 40% higher than the stream's mean baseflow discharge. With appropriate scaling (multiplying by 0.72), median flows can be used to approximate the relative differences in baseflow characteristics between streams, assuming the runoff to rainfall ratios are fairly stable across the watersheds.

A BFI calculated by Wong (1996), was reported for each gauged stream on Tutuila. This measurement is essentially a stream's  $Q_{90}$  value standardized by its basin size and indexed to the closest continuous record station. Despite the fact that the  $Q_{90}$  does not explicitly represent the mean baseflow value, Wong's BFI is nonetheless a useful relative indicator of the magnitude of groundwater discharge in each stream. The locations of stream gauges and the BFI of each gauged basin are shown in Figure A20. The BFI for streams in the Taputapu area are clearly higher than those in the eastern portion of the island, probably because of the addition of the discharge from the many springs that issue from the cinder cap at Aoloau Mountain (Wong, 1996). Overall, there are a number of basins whose median flows and BFIs suggest that more substantial aquifers may contribute a larger proportion of groundwater to the stream flow. These basins are shown in Figure A20 and include watersheds in the Taputapu Shield region, above the Tafuna-Leone Plain, in Nuuuli, and also around Rainmaker Mountain (Pioa Plug). Eastern Tutuila has less overall baseflow, and generally shows lower stream BFIs, indicating a lower potential for productive and sustainable high-level aquifers.

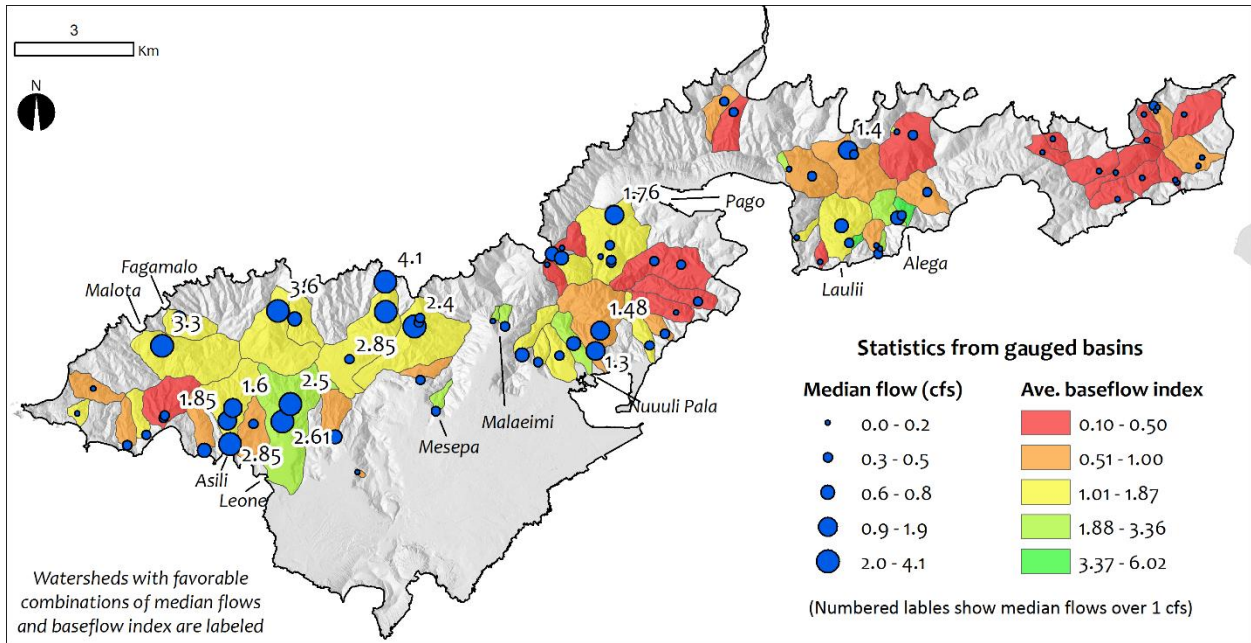


Figure A20. Summary of low-flow streamflow characteristics for Tutuila, data from Wong (1996).

## Appendix B: Consolidated Aquifer and Well Monitoring Data

Data obtained from existing wells is a key resource for understanding the condition of aquifers and assessing future groundwater development potential. This appendix organizes available well data by wellfields (Fig. B1), that are generally defined by existing groupings of wells, topographic basins, geologic units, or geographic regions throughout Tutuila. Three subsections group these wellfields based on a qualitative determination of current aquifer conditions and the perceived viability of future groundwater development. The first subsection presents data for areas with a minimal amount of groundwater development in comparison to their likely potential for groundwater development capacity, as well as areas where data limitations preclude a confident assessment of capacity. The second subsection includes areas where moderate to extensive groundwater resources are currently developed, yet aquifer data does not show trends suggesting withdrawal rates are unsustainable. The third subsection includes heavily developed wellfields with water level and chloride trends suggesting groundwater withdrawals may already exceed the aquifer's capacity to sustainably supply water.

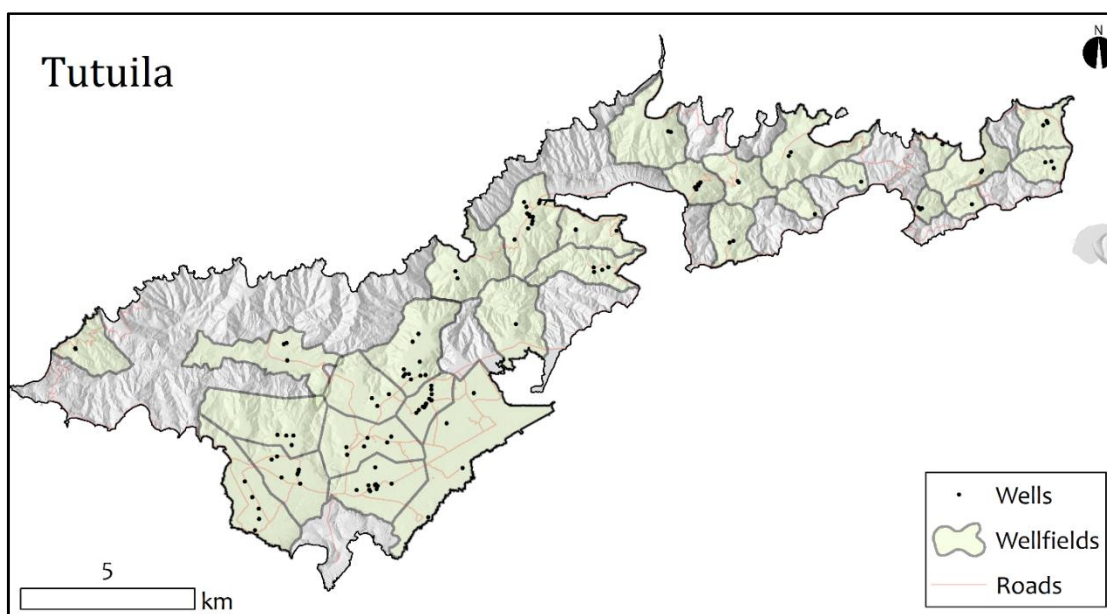


Figure B1: Map of existing wellfield boundaries on Tutuila

Aquifer data included in this section are intended to inform a dialog about past and present groundwater conditions on Tutuila. Additionally, assessment of temporal trends may be useful for understanding the current trajectory that may occur for future groundwater resources, should controlling factors remain as they are. For example, measured chloride concentrations in many of the island's wells have been increasing for the last three years. The sustainability of Tutuila's groundwater supply is limited by the effects of saltwater upconing and intrusion, which may be a warning sign that the rate of groundwater extraction in these areas exceeds the sustainable supply. However, these trends are not in themselves predictive of future conditions as numerous factors may affect their magnitude and direction.

Currently available groundwater datasets include: well locations and elevations, pumping rates, pre-production and pumping water levels, chloride (Cl<sup>-</sup>) concentrations, specific capacity values, and transmissivity (*T*) and hydraulic conductivity (*K*) values from aquifer tests. Although not all wells have records available for each of these parameters, every effort was made to compile as much of this information from as many sources as possible. These sources include published reports, values obtained through fieldwork, and unpublished datasets or reports. Because multiple sources were compiled to develop these datasets, some wells have multiple values from different sources for a given parameter. The values presented here were selected based on the trustworthiness and completeness of the available sources and a source-preference ranking for each parameter is described below.

Chloride concentrations reported here are from the following sources in the preferred order of (1) average Cl<sup>-</sup> from ASPA records spanning January 2015 to April 2017, (2) discrete Cl<sup>-</sup> measurements as directly sampled by WRRC from 2013 to 2017, and (3) discrete Cl<sup>-</sup> measurements as reported by Bentley (1975). An existing data gap to fill is obtaining higher resolution Cl<sup>-</sup> information from production wells. Aquifer test values, such as specific capacity, *K*, and *T*, are reported from the following sources in the preferred order of: (1) WRRC recovery tests, (2) values of *K* derived by Zangar's equation from Eyre and Walker (1991), (3) values of *T* reported by Bentley (1975), and (4) values of *K* that were calculated with *T* values from Bentley and records of the well's open interval thickness. Some existing wells have no documented aquifer test information and this is a data gap that could be filled through performing pumping and recovery tests in the future.

Water levels can vary dramatically through time and during different hydrologic conditions. Documented pre-development water levels are here reported from the following sources in the preferred order of: (1) actual drillers logs or pre-development pump test reports, (2) water levels reported by Bentley (1975), and (3) drilling water levels from Eyre and Walker (1991, 1993). Pumping water levels, are distinct from static water levels as they are recorded while a well is operational. These water levels are subject to both aquifer and well losses. Pumping water levels are here reported as an average of monthly ASPA data spanning the period January 2008 to September 2013. When water level records for wells were not available in the ASPA files, pumping water levels from the observed discrete production drawdown measurements taken during WRRC recovery tests done in 2014 are reported.

Water level elevations are reported relative to mean sea level and are calculated as the difference of the depth to water measurement and the well's measuring point elevation. Unknown accuracy of measuring point elevations adds uncertainty to the water level elevation, so every attempt was made to determine the most accurate measuring point elevations. The preferred order of the sources for the measuring point elevations are (1) ASPA wellhead survey information, (2), land-surface altitude reported in Bentley (1975), (3) well elevations reported by Eyre and Walker (1991, 1993), and (4) when documented elevations were not available elevations were taken from a 1 m resolution digital elevation mode.

Well ID numbers on Tutuila have been documented in two different systems. The USGS developed a well ID system that consists of a four-digit map quadrant identifier with a dash separating a separate well number (e.g., 1642-01). ASPA well ID numbers are one to three digit numeric identifiers, (e.g. Well 179) and do not have any relation to USGS well IDs. In general, older wells have only USGS IDs, newer wells only have an ASPA ID number, and many wells have both. Data tables are indexed by both ID's where available.

As mentioned earlier, recharge is the source of all groundwater on the island, thus recharge rate is a fundamental control on groundwater availability. Determining the ratio of recharge rate to extraction rate (referred to here as the use ratio) in each region can be a helpful metric for assessing the relative development potential of different regions throughout the island. Extraction is measured as a volume of water per time, while recharge is generally calculated as a volume per unit area per time. Therefore, to determine the amount of recharge available for extraction, a boundary delineating the area that supplies groundwater to the region's wells must be specified. Since aquifer boundaries have not been conclusively delineated, the island was partitioned into twelve geographic zones based on surface expressions of inferred subsurface geologic features. Recharge estimates from three sources, Eyre and Walker (1991), Izuka et al. (2007), and ASPA (2013), were summed for each geographic zone and the area weighted portion of recharge in each wellfield region was determined by dividing the wellfield region area by the geographic zone area. Wellfield region boundaries were delineated with topographic watershed boundaries in the Pleistocene unit, or as the consolidated area of Thiessen polygons defined for all wells in each wellfield on the Tafuna-Leone Plain. Estimates based on these calculations have an inherent amount of uncertainty because it cannot be assumed that true aquifer boundaries conform to the wellfield region boundaries. However, they may be useful for making some very rough assessments of groundwater availability. This methodology could be greatly improved by developing improved recharge coverages and also by improved assessments of aquifer boundaries.

## B1 Underutilized or Unexplored Areas

These areas are characterized as having a minimal amount of groundwater development in comparison to their potential for groundwater storage capacity (Fig. B2). Some of these areas have been subject to more extensive groundwater development in the past, such as the Pago Inner-Caldera region, but currently experience extraction rates that are significantly lower than their expected extraction potential, based on a qualitative assessment of recharge quantities and aquifer parameters. It should be noted that any future groundwater development in these areas is likely to be more successful if it is carried out farther from present and past extraction sites, and as far inland as possible. Also included in this section are relatively unexplored regions where a limitation in data precludes a confident assessment of the area's capacity, such as the Taputapu Shield.

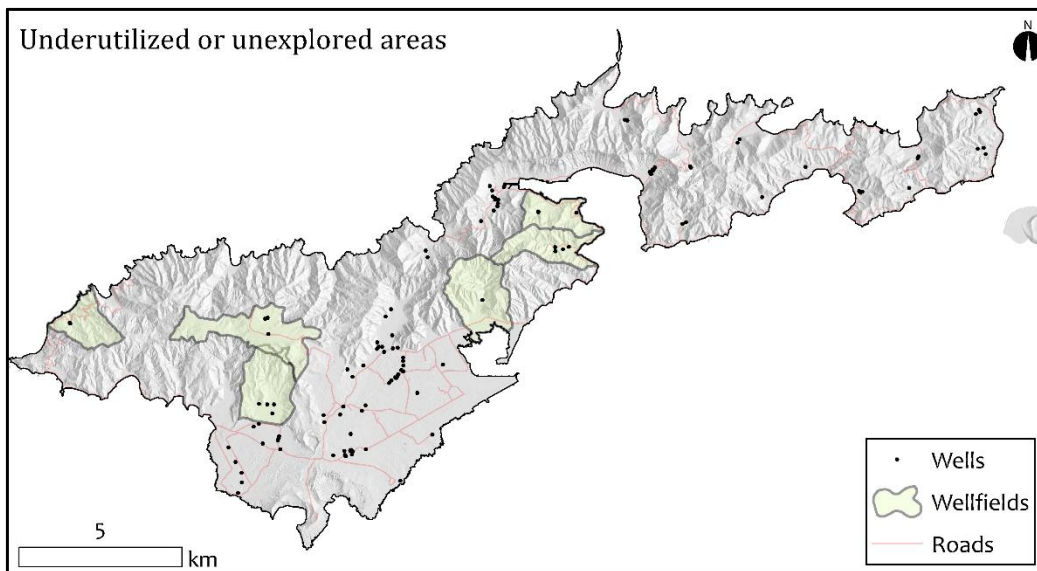


Figure B2: Map of wellfields with minimal amount of groundwater development in Tutuila

## B1.1 Aasu and Aoloau Region

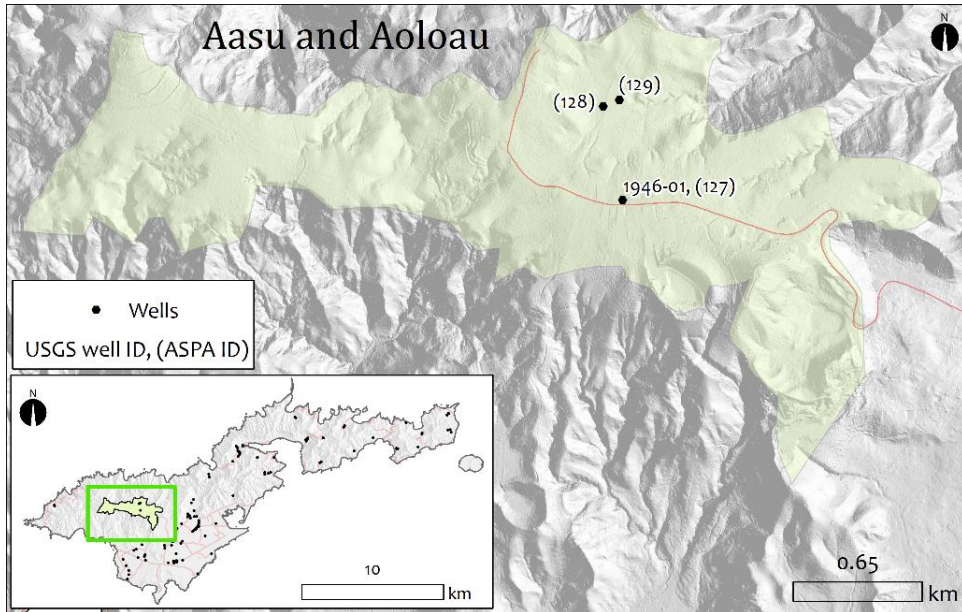


Figure B3: Location map of the Aasu and Aoloau region. Green shading denotes the inferred area of cinder deposits that may contain a potentially perched aquifer.

In the Aasu-Aoloau aquifer (Figs. B3, B4, and B5) only Well 128 is currently active. This well extracts about 0.03 Mgal/d (22 GPM). Section 2.1.2 provides a description of the region's geology and groundwater occurrence. Eyre and Walker (1993) estimate this area receives about 6 Mgal/d of recharge, which suggests that regional withdrawal rates could be sustainably increased. It should be noted however, that an increase in groundwater development in this region is likely to reduce flow at springs on the unit's periphery and subsequently reduce streamflow to the perennial streams that flow across the flanks of the Taputapu Shield and to the Tafuna-Leone Plain below (Table B1).

The region is estimated to receive about 6 mgal/d of recharge (Eyre and Walker, 1991), whereas the extraction at well 128 averages 0.03 Mgal/d (22 GPM). The roughly estimated area weighted recharge use ratio for Aasu-Aoloau is 0.4%

Table B1: Aasu and Aoloau region aquifer parameters.

Well # [USGS ID]	Well # [ASPA ID]	Drilling WL [m]	Pumping WL [m]	Pump rate [GPM]	Specific capacity [GPM/m]	T [m <sup>2</sup> /day]	K [m/d]	Avg. Cl <sup>-</sup> [mg/L]	Cl <sup>-</sup> trend [mg/L/yr.]
1946-01	127	382.2	-	-	-	-	-	-	-
-	<b>128</b>	-	<b>345.5</b>	<b>22</b>	-	-	-	<b>21</b>	<b>↑, 2</b>
-	129	-	343.6	40	-	-	-	23	-

\* Pump rates and Ave. Cl<sup>-</sup> values are taken from 2015-2017 ASPA data, ↓ denotes decreasing Cl<sup>-</sup> trend, ↑ denotes increasing Cl<sup>-</sup> trend. Values for inactive wells were taken from sources as described in Section 4.0. Records in bold are active wells as of 2016.

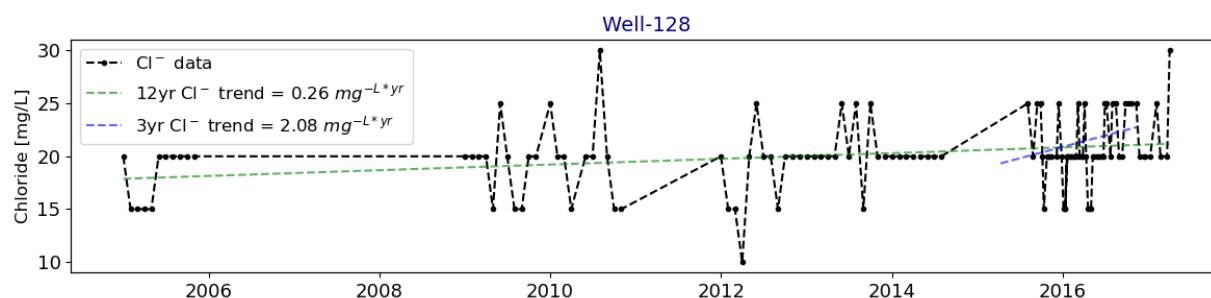


Figure B4: Cl<sup>-</sup> concentrations for most recent 3-year period, 2015-2017 at Well 128. *Green dashed line* shows the linear regression trend line for all data, generally about 12 years, and *blue dashed line* shows the linear regression trend line for 2015-2017.

### Preliminary recommendations for sustainable aquifer management

**Existing wells:** Pumping water levels from the period of 2008 to 2013 as reported by ASPA (ASPA unpublished data) indicate that the aquifer tapped by Wells 128 and 129 is fairly stable at current pumping rates. Since these wells most likely tap a perched high-level aquifer, saltwater intrusion is not a concern. To assess the viability of additional withdrawals from Wells 128 and 129 measurements of specific capacity or pumping tests would be very useful for developing numerical or analytical estimates of sustainable withdrawal rates.

**Future development:** It is unclear as to why Wells 127 and 129 were decommissioned. However, it does appear that additional water could be withdrawn from the aquifer without significantly affecting the sustainability of groundwater supplies in this area. A possible issue with developing water from this likely unconfined aquifer is the existence of high numbers of On-Site Wastewater Disposal Systems and piggeries located within the villages of Aoloau and Aasu. These villages are, however, concentrated within the eastern side of the unit, whereas the western side currently has no development on it. Despite these potential sources of contamination, the well in Aasu Village, does not show levels of contaminants (including bacteriological indicators) that are above Environmental Protection Agency limits. Additionally, withdrawals in this region are likely to reduce discharge from the numerous natural springs that are located on the margins of the cinder unit. These springs feed perennial streams that in turn create aquatic habitats. It is unknown if springs serve village water systems. Springs and subsurface flows feed basal aquifers, primarily in the Malaeloa and Pavaii wellfields, and if withdrawals are significant enough, basal water supplies may be affected.

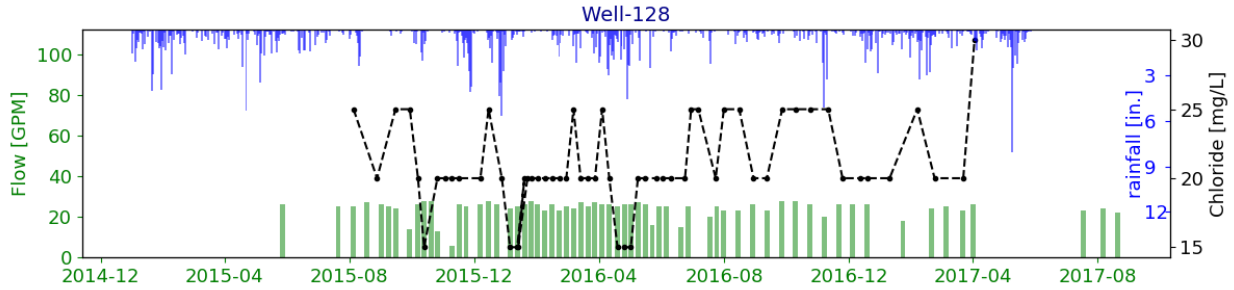


Figure B5: Plot of pump rates (green bars), Cl<sup>-</sup> values (black line), and rainfall (blue bars) for Well 128 for the period 2015-2017.

### B1.2 Taputapu Shield Including Upper Malaeloa Wellfield

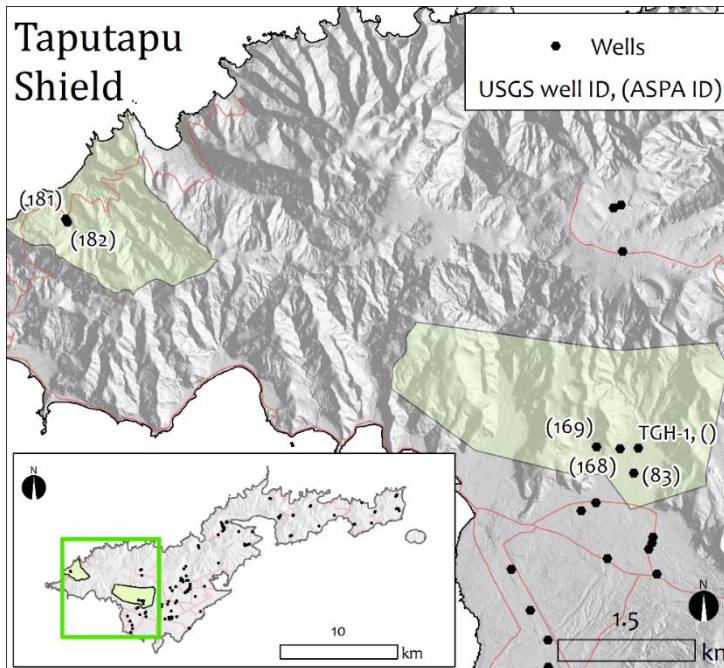


Figure B6: Location map of wellfields in the Taputapu region with locations of active and abandoned wells. *Green shading* denotes local watershed or wellfield boundaries, which do not necessarily delineate aquifer extent. Labels indicate well ID numbers.

Although the Taputapu Shield Region (Figs. B6, B7, and B8) is quite extensive, only a limited amount of groundwater development has occurred throughout the region. One well (Well 182) on the shield's northwestern flank and two wells on its southern margin (Wells 169 and 168) likely tap the Taputapu rocks. Well 83 lies to the southeast of Well 168 and probably penetrates alluvial sediments for much of its depth, although it may also be partially completed in Taputapu Volcanics.

Existing wells are generally drilled with a substantial buffer in distance or elevation from the coast, and thus show very low Cl<sup>-</sup> concentrations. Extraction rates in these wells are not insignificant, yet Cl<sup>-</sup> trends are stable, possibly due to the thickness of the freshwater lens at these locations, and the high amount of recharge that feeds the area. Only about 0.5 to 1 m of pumping drawdown is seen in

the few wells with complete records, indicating reasonably high conductivities and further supporting the idea that these wells draw from an aquifer that is supported by ample recharge (Table B2).

The Northern Taputapu Region is estimated to receive between 6 and 19.2 Mgal/d of recharge (range of all estimates), whereas the extraction at Well 182 averages 0.15 Mgal/d (105 GPM). The roughly estimated area weighted recharge use ratio for the Fagalii Watershed is between 6 and 24% (average of 15%).

The Leone Plain Region is estimated to receive between 8.7 and 18.7 Mgal/d of recharge (range of all estimates), whereas the extraction at wells 169, 168, and 83 averages 1.2 Mgal/d (815 GPM). The roughly estimated area weighted recharge use ratio for the Upper Malaeloa region is between 19 and 41% (average of 25%).

Table B2: Taputapu Shield region aquifer parameters.

Well # [USGS ID]	Well # [ASPA ID]	Drilling WL [m]	Pumping WL [m]	Pump rate [GPM]	Specific capacity [GPM/m]	T [m <sup>2</sup> /day]	K [m/d]	Avg. Cl <sup>-</sup> [mg/L]	Cl <sup>-</sup> trend [mg/L/yr.]
-	181	-	-	-	-	-	-	-	-
-	<b>182</b>	<b>5.5</b>	<b>5.0</b>	<b>105</b>	<b>202</b>	<b>5700</b>	<b>312</b>	<b>31</b>	-
-	<b>83</b>	-	<b>0.8</b>	<b>270</b>	-	-	-	<b>24</b>	→, <b>0</b>
-	<b>168</b>	-	<b>2.4</b>	<b>245</b>	<b>471</b>	<b>4100</b>	<b>147</b>	<b>25</b>	→, <b>0</b>
-	<b>169</b>	<b>3.5</b>	<b>2.5</b>	<b>300</b>	<b>1154</b>	<b>5600</b>	<b>199</b>	<b>25</b>	→, <b>0</b>
-	15	14.2	-	-	-	-	-	-	↑, <b>1</b>
-	TGH-1	3.6	-	-	-	-	-	-	-

\* Pump rates and Ave. Cl<sup>-</sup> values are taken from averages of the last 3 years of ASPA data, ↓ denotes decreasing Cl<sup>-</sup> trend ↑ denotes increasing Cl<sup>-</sup> trend. Values for inactive wells were taken from sources as described in Section 4.0. Records in bold are active wells as of 2016.

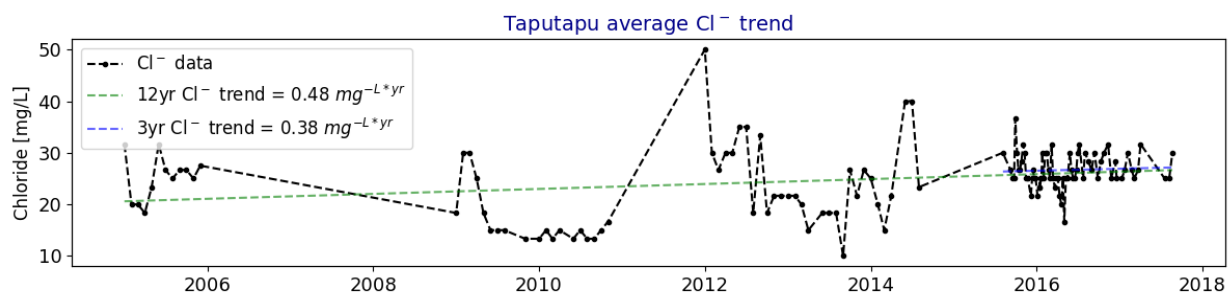


Figure B7: Averaged Cl<sup>-</sup> concentrations for most recent 3-year period, 2015-2017 at Taputapu wells. *Green dashed line* shows the linear regression trend line for all data, generally about 12 years, and *blue dashed line* shows the linear regression trend line for 2015-2017.

## **Preliminary recommendations for sustainable aquifer management**

### **Existing wells:**

Flat trends in water levels and Cl<sup>-</sup> concentrations suggest the few existing wells in the Taputapu Region are being sustainably managed at their current extraction rates. Well 15 was recently drilled just to the south of Well 169, and will soon be online in the Upper Malaelo Valley area. Regardless, the behavior of existing wells suggests this well should be able to extract a significant quantity of water without affecting the water levels or Cl<sup>-</sup> concentrations at the nearby wells. Presently the well in Fagalii Valley has not been put into heavy production and the low water demand in the area keeps extraction rates at this well quite low.

### **Future development:**

Although previous conceptual models have combined all of Tutuila's older shields into a single hydrologic unit with uniform properties, some recent observations suggest that the Taputapu Shield may have better water development potential than the island's other shields. Groundwater recharge is significantly higher over the Taputapu Region and specific capacities and *K* values measured in the Taputapu wells are generally higher than in the other older shield rocks. The distribution of geologic features throughout the island suggests that the Taputapu Shield contains less impermeable intrusive bodies, such as dike complexes that would serve to reduce permeability and aquifer connectivity. There remains significant exploration potential for groundwater resources in the Taputapu region. Primary recommendations for exploration and development in this area are to (1) drill new wells as far inland as possible to avoid saltwater intrusion, and (2) to spread development centers out to avoid excessive drawdown caused by overlapping cones of depression.

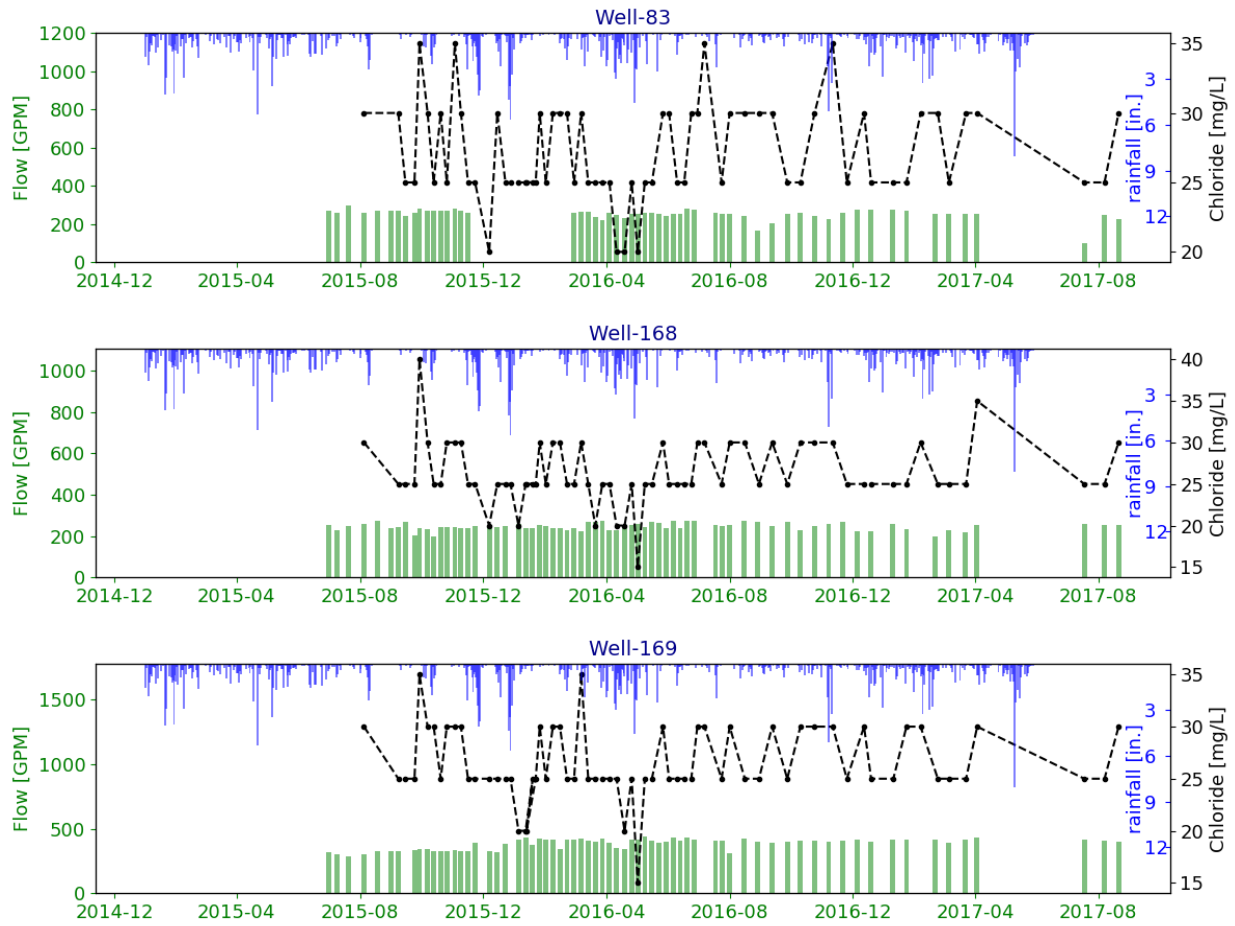


Figure B8: Plots of pump rates (green bars), Cl<sup>-</sup> values (black line), and rainfall (blue bars) for Taputapu region wells during the period 2015-2017.

### B1.3 Mesepa Wellfield

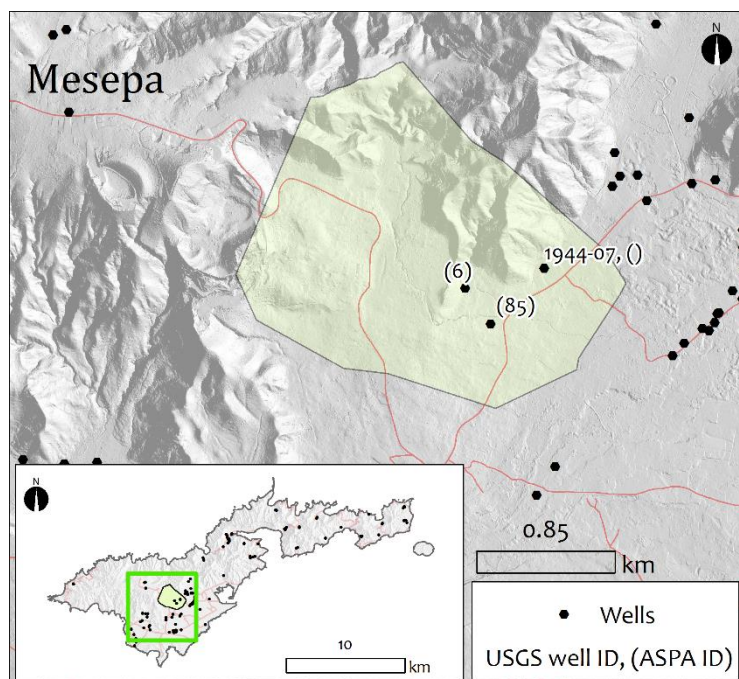


Figure B9: Location map of the Mesepa wellfield with locations of active and abandoned wells. *Green shading* denotes wellfield boundary, which does not necessarily delineate aquifer extent. Labels indicate well ID numbers.

The Mesepa wellfield (Figs. B9, B10, and B11) lies on the northwesterly portion of the Tafuna Plain. This area is geologically distinctive in that it has a steeper slope and is likely to be composed of lava flows lying upon the flanks of the Taputapu Shield below. There are only two wells drilled in the area, Well 85 is active and Well 6 has not yet been connected to the system. Well 85 is relatively new and is located near the boundary of the Malaeimi area. The Pavaiai wells are located to the south of the Mesepa area, but are located on the flatter portion of the plain. No published documentation is available regarding wells in this area. Existing data for Well 85 shows low Cl<sup>-</sup> values that are not affected by rainfall and seem to be increasing slightly through time. Values of T and K from two relatively new wells in the area indicate that the aquifer probably shares some characteristics with the Tafuna Aquifer to the southeast, but likely there are lower conductivity and Cl<sup>-</sup> concentrations due to the proximity to denser lava flows in the nearby Pleistocene unit (Table B3).

The Tafuna Plain Region is estimated to receive between 24.5 and 45.9 Mgal/d of recharge (range of all estimates), whereas the extraction at the only active well in Mesepa area averages 0.4 Mgal/d (280 GPM). The roughly estimated area weighted recharge use ratio for the current wellfield is between 7 and 13% (average of 10%). However, this value is likely to increase once the newly drilled Well 6 is put into production.

Table B3: Mesepa Wellfield aquifer parameters.

Well # [USGS ID]	Well # [ASPA ID]	Drilling WL [m]	Pumping WL [m]	Pump rate [GPM]	Specific capacity [GPM/m]	T [m <sup>2</sup> /day]	K [m/d]	Avg. Cl <sup>-</sup> [mg/L]	Cl <sup>-</sup> trend [mg/L/yr.]
1944-07	-	3.0	-	-	-	-	-	23	
-	<b>85</b>	-	<b>0.8</b>	<b>280</b>	<b>1244</b>	<b>9195</b>	<b>647</b>	<b>28</b>	<b>↑, 4</b>
-	6	0.0	-43.9	130	3	3810	18	25	

\* Pump rates and Ave. Cl<sup>-</sup> values are taken from averages of last 3 years ASPA data, ↓ denotes decreasing Cl<sup>-</sup> trend ↑ denotes increasing Cl<sup>-</sup> trend. Values for inactive wells were taken from sources as described in Section 4.0. Records in bold are active wells as of 2016.

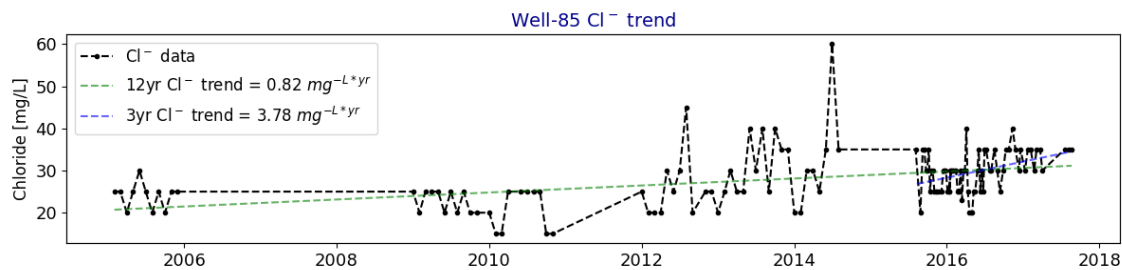


Figure B10: Averaged Cl<sup>-</sup> concentrations for most recent 3-year period, 2015-2017 at Well 85. Green dashed line shows the linear regression trend line for all data, generally about 12 years, and blue dashed line shows the linear regression trend line for 2015-2017.

### Preliminary recommendations for sustainable aquifer management

#### Existing wells:

Since only one well is currently active in this area, and this well seems to be producing water with relatively low Cl<sup>-</sup> concentrations, it appears that this extraction rate can be sustainably maintained. Once Well 6 is put into production it will be useful to reassess the effects of increased pumping in this area.

#### Future development:

The recharge use ratio of this well averages around 10%, which is not insignificant for a single well. Thus drastic increases in extraction rates in this area may quickly overwhelm the area's natural storage potential. Nonetheless, the upgradient portion of the Mapasagafou area remains fairly unexplored, and likely hosts rock with a relatively high **K** distribution, as is indicated by geophysical cross-sections (Geologica Geothermal Group, Inc., 2014). This certainly warrants further groundwater exploration within the Mesepa and Mapasagafou areas.

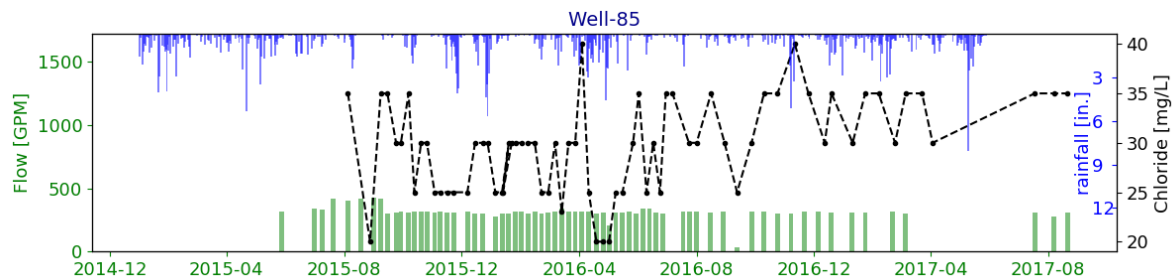


Figure B11: Plot of pump rate (green bars), Cl<sup>-</sup> values (black line), and rainfall (blue bars) for Well 85 during the period 2015-2017.

## B1.4 Pago Inner-Caldera Geologic Unit

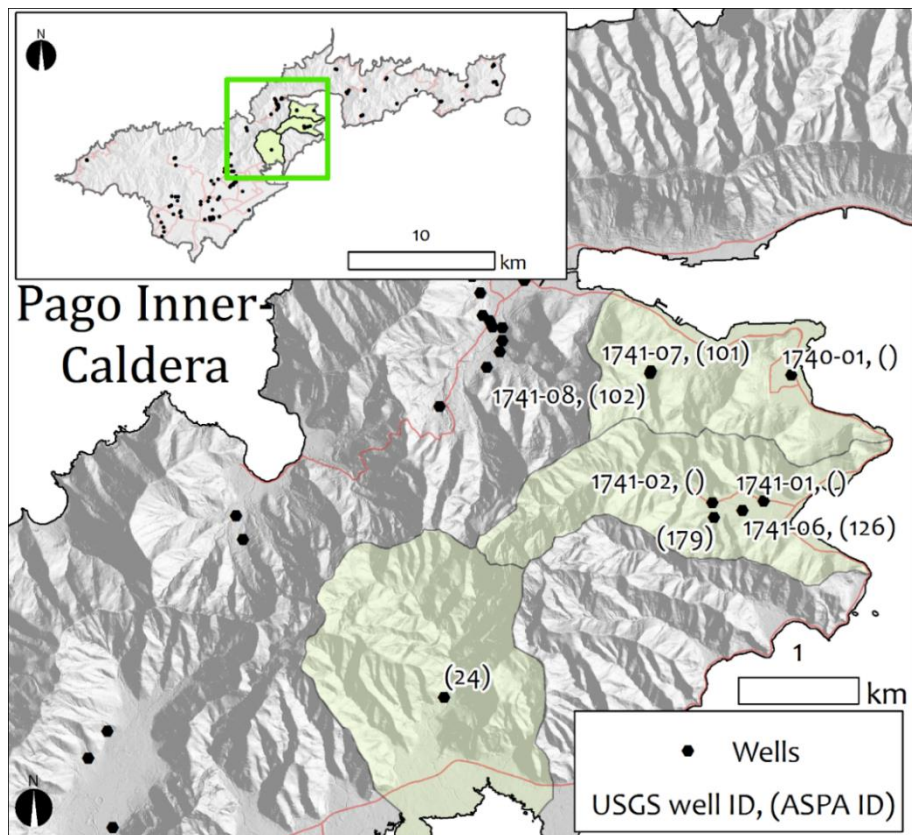


Figure B12: Location map of distinct watersheds in the Pago Inner-Caldera unit with locations of active and abandoned wells. Green shading denotes local watershed boundaries, which do not necessarily delineate aquifer extent. Labels indicate well ID numbers.

Although a number of wells have previously been developed in this geologic unit (Figs. B12, B13, and B14), only two wells are currently active. In Fagaalu Valley Well 179 produces an average of 19 GPM and has a pumping water level drawdown of 2 to 4 m. At the head of Fagaalu Valley is an exceptionally large high-level spring was recorded to have been used by the U.S. Navy in recent historical times (Davis, 1963). This spring was said to have a flow rate of 0.5 Mgal/d. The large spring feeds the headwaters of Fagaalu Stream and its flow has long since been captured by a reservoir located at the base of Mt. Matafao. Use of the reservoir has been discontinued, although it and the dam remain intact. Groundwater behavior observed in this area indicates how geologic features such as faults and low-permeability layers can control subsurface water flow on Tutuila. These conditions were described by Eyre and Walker (1991) as,

*“The fault separating these two formations is visible at the base of the dam. The occurrence of the large spring is controlled by the interrelations of infiltrating rainwater, the trachyte plug, the Pago volcanic rocks, and the location of the fault.”*

A number of now abandoned moderately producing (30-60 GPM) wells have been drilled in Fagaalu Valley and their development histories are described in greater detail in Eyre and Walker (1991) (Table B4).

Groundwater development in the Fagatogo/Utulei Region has an enigmatic history. The aquifer in this area currently yields a significant amount of water from Well 101 (520 GPM) while showing only a moderate pumping drawdown, and maintaining stable long-term Cl<sup>-</sup> concentrations. Eyre and Walker (1991) noted that upon drilling of the Fagatogo wells, artesian conditions below hard basalt were encountered at -3 m below sea level with water rising to about 7 m above sea level. Wells 101 and 102 have been used in alternating cycles of pumping and observation in the past. The producing zone was said to be about 6 m thick. Also a now abandoned well, (1740-01), was drilled in Utulei, the valley south of Fagatogo. This well was shallow, 4 m deep, and pumped at 90 GPM. The Cl<sup>-</sup> concentrations were reported to have ranged from 30 to 200 mg/L. It is unusual for a well so near to the shore to produce water this fresh, and it would seem that this area must receive a disproportionate share of recharge from nearby areas, and have aquifer properties that allow for a significant amount of storage. Geologically this unit would be expected to have a high-proportion of less-permeable material, and it has been hypothesized that the prevalence of fresh water, as well as the observed occurrence of marshes in this area, prior to being filled for urban development, may result from the discharge of an underlying artesian volcanic aquifer (Eyre and Walker, 1991).

Only recently have any known wells been developed in the Nuuli area. Well 24 was drilled in 2015 and has not yet been pumped. This well is fairly shallow and may experience some hydraulic connection to the nearby stream.

The Pago Harbor Region is estimated to receive between 15.6 and 16.6 Mgal/d of recharge (range of all estimates), whereas the extraction at Well 179 averages 0.03 Mgal/d (19 GPM). The roughly estimated area weighted recharge use ratio for the Fagaalu Watershed averages less than 1%.

The Pago Harbor Region is estimated to receive between 15.9 and 16.6 Mgal/d of recharge (range of all estimates), whereas the extraction at Well 101 averages 0.8 Mgal/d (520 GPM). The roughly estimated area weighted recharge use ratio for the Fagatogo Watershed is between 30 and 32% (average of 31%).

Table B4: Pago Inner-Caldera Unit aquifer parameters

Well # [USGS ID]	Well # [ASPA ID]	Drilling WL [m]	Pumping WL [m]	Pump rate [GPM]	Specific capacity [GPM/m]	T [m <sup>2</sup> /day]	K [m/d]	Avg. Cl <sup>-</sup> [mg/L]	Cl <sup>-</sup> trend [mg/L/yr.]
-	24B	22.4	-	-	-	-	-	0	
1740-01	-	0.0	-	-	-	-	-	425	
<b>1741-07</b>	<b>101</b>	<b>6.9</b>	<b>-0.4</b>	<b>520</b>	<b>711</b>	<b>3270</b>	<b>244</b>	<b>50</b>	<b>↑, 7</b>
1741-08	102	6.4	5.5	310	363	3317	363	-	
1741-01	-	6.1	-	-	-	-	-	-	
1741-02	-	27.4	-	-	-	-	-	-	
1741-06	126	10.7	-	-	-	-	-	-	
-	<b>179</b>	<b>2.7</b>	<b>-1.1</b>	<b>19</b>	<b>19</b>	<b>561</b>	<b>18</b>	<b>38</b>	<b>↑, 1</b>
1741-09	-	7.5	-	-	-	-	-	-	

\* Pump rates and Ave. Cl<sup>-</sup> values are taken from averages of last 3 years ASPA data, ↓ denotes decreasing Cl<sup>-</sup> trend ↑ denotes increasing Cl<sup>-</sup> trend. Values for inactive wells were taken from sources as described in Section 4.0. Records in bold are active wells as of 2016.

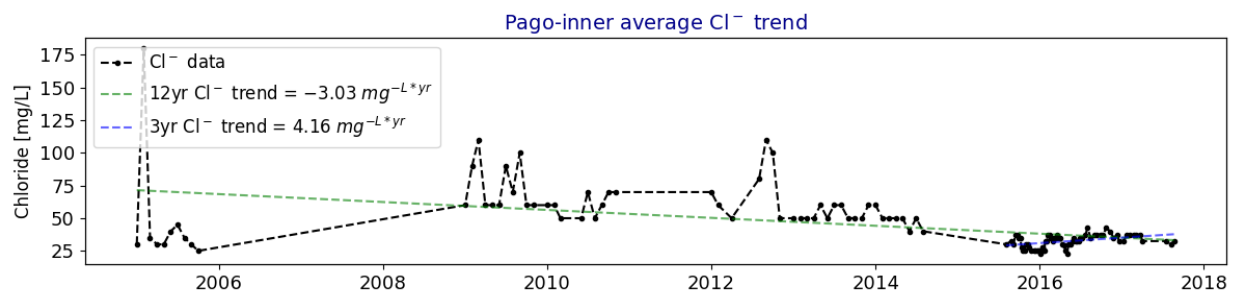


Figure B13: Averaged Cl<sup>-</sup> concentrations for most recent 3-year period, 2015-2017 at Pago Inner-Caldera Unit wells. *Green dashed line* shows the linear regression trend line for all data, generally about 12 years, and *blue dashed line* shows the linear regression trend line for 2015-2017.

### Preliminary recommendations for sustainable aquifer management

**Existing wells:** Although this unit has contained numerous wells in the past, many have been abandoned. Considering the very favorable groundwater producing conditions reported and observed in the Fagatogo and Utulei Valleys it is unclear as to why additional development has not occurred in these areas. The wells in Fagatogo however, do pump at a fairly high rate, and although this rate appears to be sustainable, additional extraction has the potential to exceed the sustainability of the areas resources.

**Future development:**

Current production rates and Cl<sup>-</sup> trends at active wells seem to indicate that it may be reasonable to explore new sites for future groundwater development. The geologic characteristics of this region would indicate that keeping an expectation for low to moderate extraction rates would be prudent, although Well 102 provides an example of how the island's heterogeneity can sometimes produce outliers from expectations. The Utulei Watershed currently has no active wells, and while the southern portion contains a fuel tank farm and a wastewater treatment plant, upgradient portions of the northern portion of the watershed may be viable locations to explore for groundwater. In general, a strategy of siting wells above development and farther from the coast should help to protect against issues related to contamination or salinization.

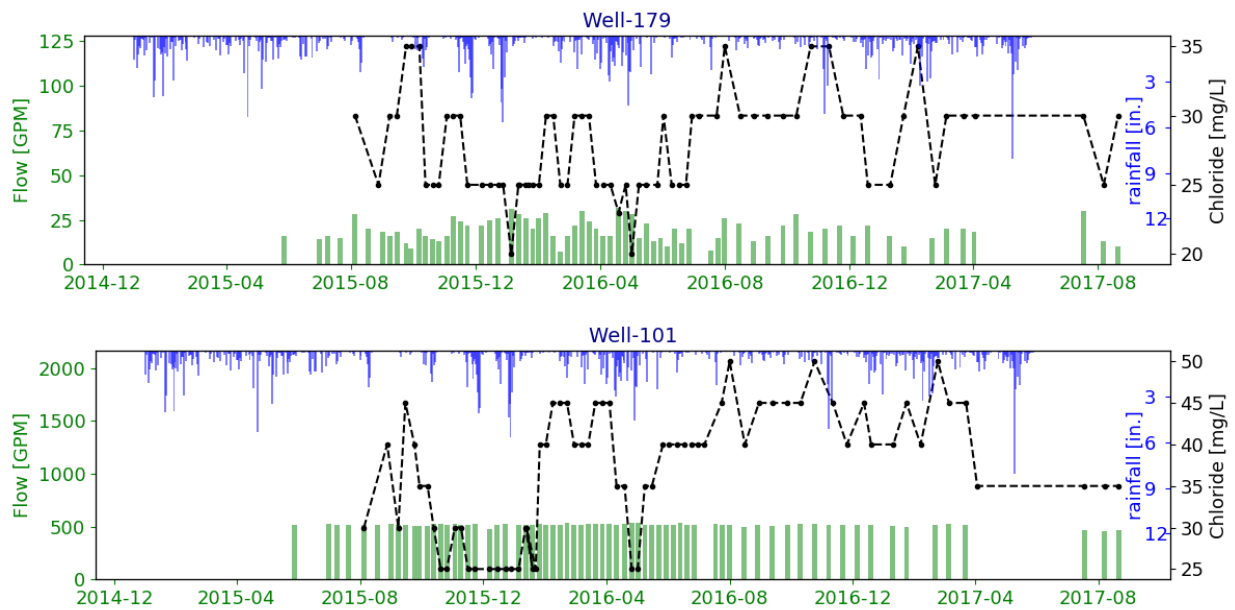


Figure B14: Plots of pump rates (*green bars*), Cl<sup>-</sup> values (*black line*), and rainfall (*blue bars*) for active Pago Inner-Caldera Unit wells during the period 2015-2017.

## B2 Moderately Utilized Areas

Moderately utilized areas have been grouped based on characteristics of a having light to moderate groundwater development in place, but where aquifer data for the most part does not show trends suggesting that extraction rates are clearly unsustainable (Fig. 4.15). While additional development may be possible without affecting water levels or Cl<sup>-</sup> concentrations in existing wells, consideration of aquifer conditions at existing extraction sites should be informative for siting future wells. A number of these regions are fairly large and may contain some areas that already seem to experience extraction rates that exceed freshwater supply. In particular, the Pago Valley area has one well with a Cl<sup>-</sup> concentration and trend that is dramatically higher than other upgradient wells. This could be due to tapping a different aquifer, or simply a different portion of the same basal lens. Regardless, abandonment of this well, and replacement with another in a different, more upgradient location, may allow for extraction of the same amount of water at a higher quality.

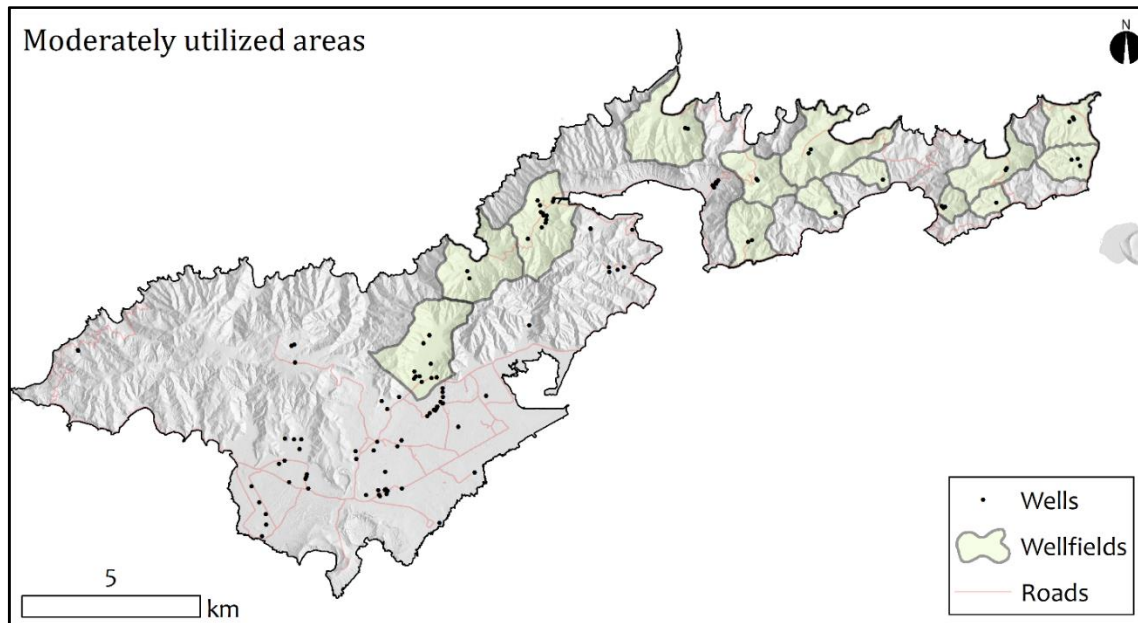


Figure B15: Map of wellfields that show characteristics suggesting current extraction rates may currently be close to water supply capacity.

## B.2.1 Eastern Tutuila Region

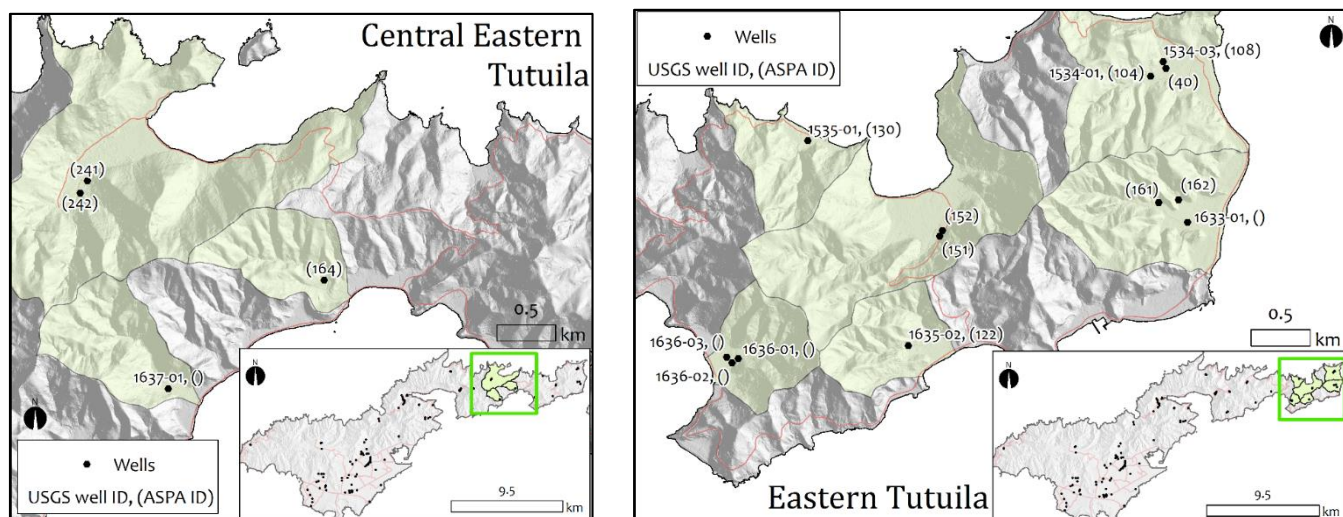


Figure B16: Location map of small distinct watersheds in the Eastern Tutuila Region with locations of active and abandoned wells. *Green shading* denotes local watershed boundaries, which do not necessarily delineate aquifer extent. Labels indicate well ID numbers.

Many wells have been completed in Eastern Tutuila (Figs. B16, B17, and B18). Most of these are connected to satellite systems and develop only small quantities of water for small localized population centers. The dispersed satellite system strategy is well suited to this region since groundwater development conditions, recharge rates, and storage volumes, are somewhat less favorable than in Western Tutuila. Many of the wells in this region tap small basal lenses in alluvial or marine sedimentary wedges that fill the mouths of valleys. The water quality from these alluvial aquifers is variable and often affected by saltwater intrusion or sometimes by excessive organic material within the shallow aquifer. Drilling water levels in these wells generally ranged from approximately 0 to 6 m above sea level; however, current pumping water levels are often below sea level indicating that even with low pump rates, aquifer yield would be expected to remain fairly small. Some wells do produce relatively fresh water, but most wells in this region are drilled close to the coast and in thin lenses, thus they are prone to producing high  $\text{Cl}^-$  water. However, this is not necessarily an indication that this region is overexploited, as these high  $\text{Cl}^-$  concentrations may be due to well placement rather than local groundwater availability (Table B5).

Eyre and Walker (1993) described developed groundwater resources in this region to be primarily derived from thin and sometimes brackish basal lenses:

*“Flow into the well(s) may occur evenly along the submerged length of the well, but more commonly, flow occurs from a narrow water-producing zone. Pumping at rates of 50 gal/min or less yields water with chloride concentrations between 150 and 2,000 mg/L. These data indicate that thin fresh- to-brackish water lenses occur in this area in both sedimentary and volcanic rocks.”*

While there are springs that feed a few perennial streams in this region, there are generally more intermittent streams than there are in Western Tutuila, which indicates that ground water supplies (high-level or otherwise) in the mountainous interior are typically limited in extent.

The total Eastern and Central Eastern Tutuila Regions are estimated to receive between 7.3 and 17.9 Mgal/d of recharge.

The North-Central Eastern Tutuila Region is estimated to receive between 2.7 and 5.6 Mgal/d of recharge (range of all estimates), whereas the extraction at Wells 241 and 242 averages 0.1 Mgal/d (69 GPM). The estimated area weighted recharge use ratio for Masefau Watershed is between 5 and 9% (average of 7%).

The South-Central Eastern Tutuila Region is estimated to receive between 2.3 and 8.1 Mgal/d of recharge (range of all estimates), whereas the extraction at Well 164 averages 0.04 Mgal/d (28 GPM). The roughly estimated area weighted recharge use ratio for Fagaitua Watershed is between 5 and 21% (average of 13%).

The Eastern Tutuila Region is estimated to receive between 2.3 and 4.2 Mgal/d of recharge (range of all estimates), whereas the extraction at Wells 151 and 152 averages 0.04 Mgal/d (30 GPM). The roughly estimated area weighted recharge use ratio for Aoa Watershed is between 4 and 8% (average of 6%).

The Eastern Tutuila Region is estimated to receive between 2.3 and 4.2 Mgal/d of recharge (range of all estimates), whereas the extraction at Well 104 averages 0.02 Mgal/d (13 GPM). The roughly estimated area weighted recharge use ratio for the Tula Watershed is between 2 and 4% (average of 3%).

Table B5. Eastern Tutuila Region aquifer parameters.

Well # [USGS ID]	Well # [ASPA ID]	Drilling WL [m]	Pumping WL [m]	Pump rate [GPM]	Specific capacity [GPM/m]	T [m <sup>2</sup> /day]	K [m/d]	Avg. Cl <sup>-</sup> [mg/L]	Cl <sup>-</sup> trend [mg/L/yr.]
1637-01	-	-	-	-	-	-	-	-	
-	<b>164</b>	-	<b>-0.7</b>	<b>28</b>	<b>13</b>	<b>610</b>	<b>46</b>	<b>1113</b>	<b>↑, 83</b>
-	<b>241</b>	-	<b>0.9</b>	<b>33</b>	-	-	-	<b>30</b>	<b>↑, 3</b>
-	<b>242</b>	-	<b>2.2</b>	<b>36</b>	<b>10</b>	<b>51</b>	<b>1</b>	<b>28</b>	<b>↑, 4</b>
1633-01		5.7	-	-	-	-	-	38	
-	161	-	-0.7	-	-	-	-	-	
-	162	-	-4.9	-	-	-	-	-	
1635-02	122	5.3	3.8	25	16	325	16	-	
-	<b>151</b>	-	<b>-7.9</b>	<b>2</b>	-	-	-	<b>168</b>	<b>↓, 120</b>
-	<b>152</b>	-	<b>0.7</b>	<b>28</b>	<b>21</b>	<b>37</b>	<b>3</b>	<b>414</b>	<b>↓, 51</b>
1636-01	-	0.0	-	-	-	-	-	12	
1636-02	-	-	-	-	-	-	-	-	
1636-03	-	2.3	-	-	-	-	-	106	
1535-01	130	2.7	-	-	-	-	-	-	
<b>1534-01</b>	<b>104</b>	<b>3.1</b>	<b>-5.1</b>	<b>13</b>	<b>2</b>	<b>28</b>	<b>1</b>	<b>75</b>	<b>↑, 13</b>
1534-03	108	3.0	-	-	-	-	-	-	
	40	-	-	-	-	-	-	-	

\* Pump rates and Ave. Cl<sup>-</sup> values are taken from averages of last 3 years ASPA data, ↓ denotes decreasing Cl<sup>-</sup> trend ↑ denotes increasing Cl<sup>-</sup> trend. Values for inactive wells were taken from sources as described in Section 4.0. Records in bold are active wells as of 2016.

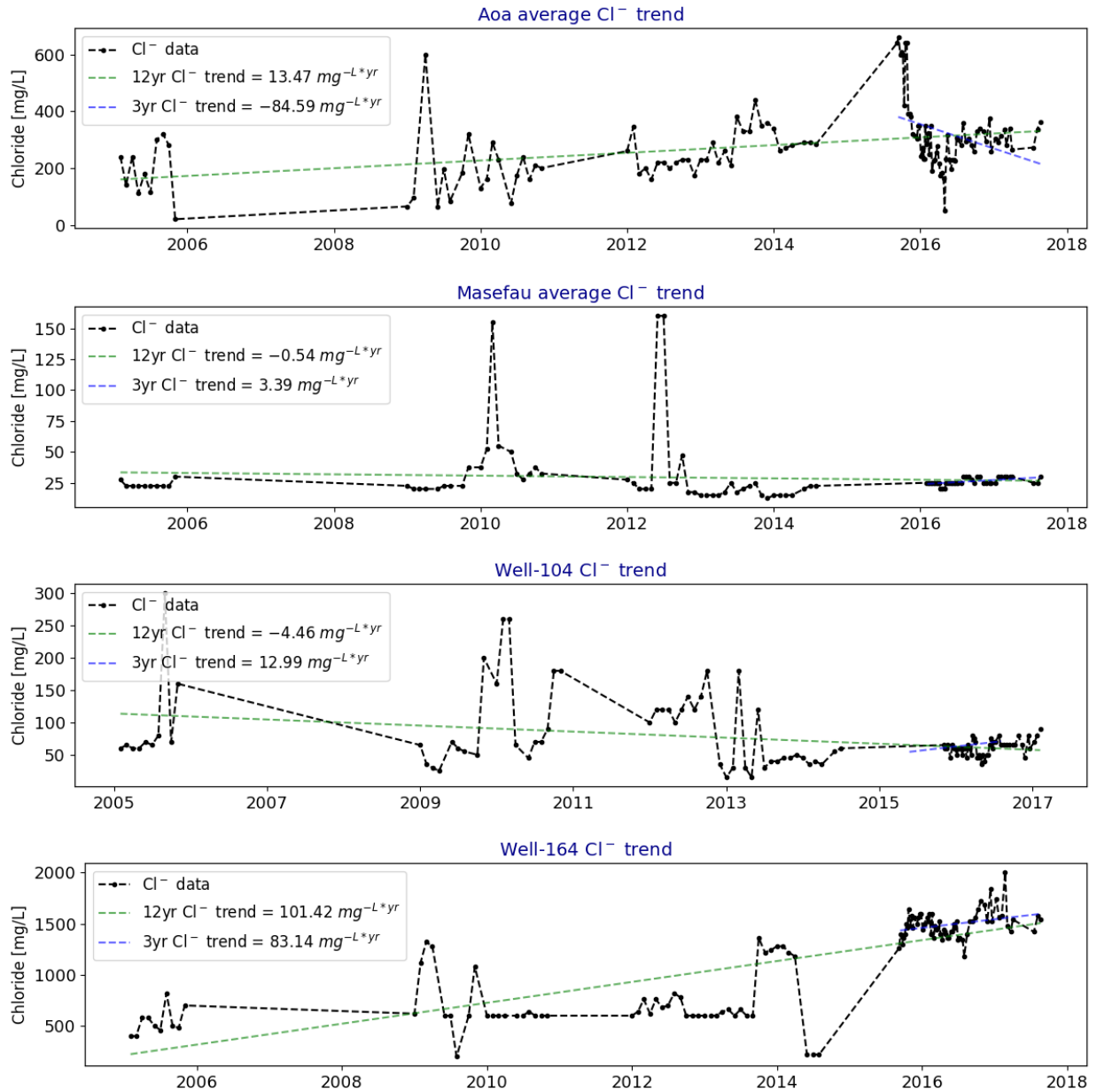


Figure B17: Cl<sup>-</sup> concentrations and trends for active wells in the Eastern Tutuila Region. Tula (Well 104) and Fagaitua (Well 164) have only one active well each and Aoa and Masefau have two wells each, with averaged Cl<sup>-</sup> concentrations presented here. *Green dashed lines* show the linear regression trend line for all data, generally about 12 years, and *blue dashed lines* show the linear regression trend line for the most recent 3-year period, 2015-2017.

## Preliminary recommendations for sustainable aquifer management

**Existing wells:** Many of the existing wells are located adjacent to the coast and are set to a depth where saltwater intrusion is a consistent problem. Where possible, abandonment of existing salty wells and replacement with wells that utilize the same aquifer, but are located farther inland in a thicker part of the freshwater lens may provide similar yields with lower Cl<sup>-</sup> concentrations.

**Future development:** It appears that aquifers in this region have the potential to provide small yields (< 20 GPM) of groundwater. However, pumping in excess of this rate may easily cause saltwater intrusion. Continuing the strategy of developing multiple low-yield wells, dispersed to avoid concentrating the effects of drawdown or upconing, to supply a low-level of demand will likely be sustainable until population increases to the point where demand is increased beyond what the region can supply. Pumping in excess of this amount may not be feasible, due to apparently low *K* values combined with overall low recharge rates in this area.

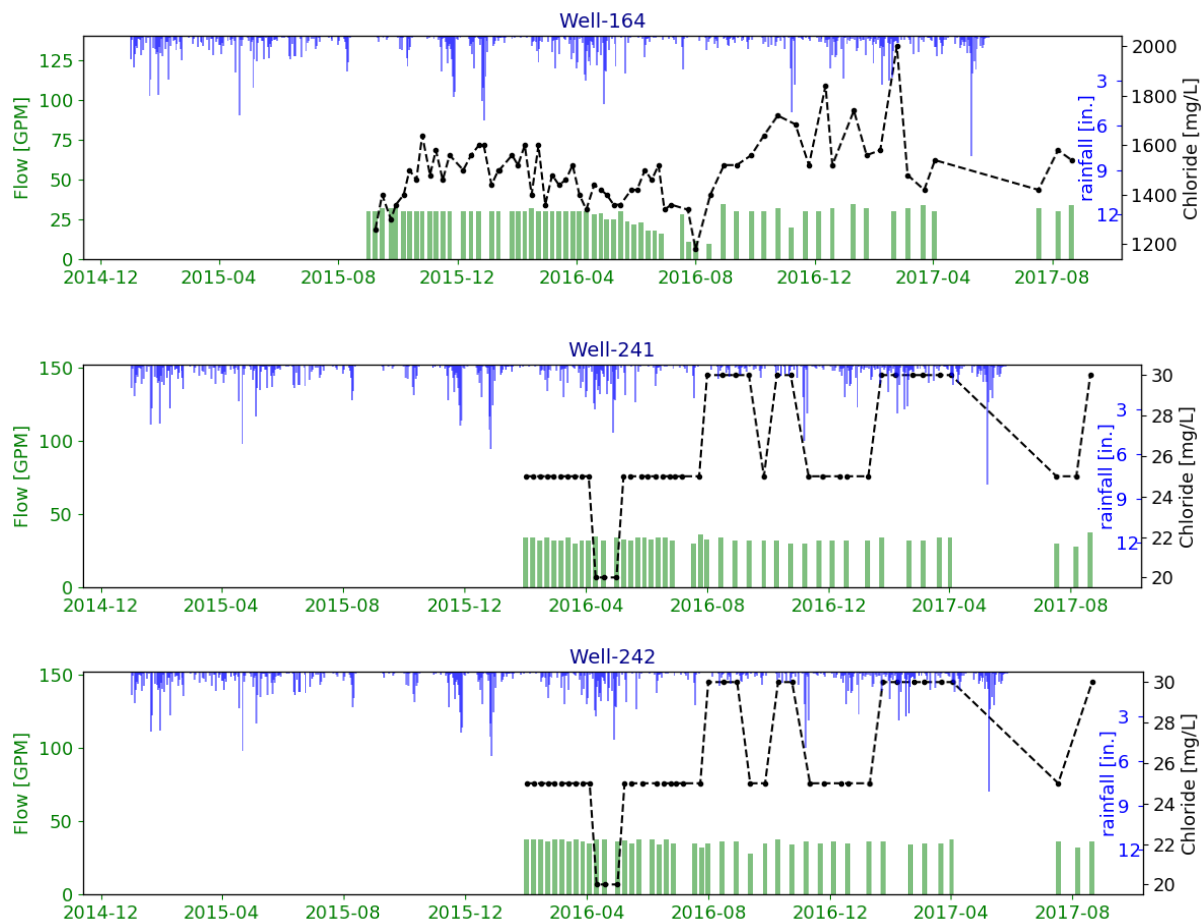


Figure B18: Plots of pump rates (*green bars*), Cl<sup>-</sup> values (*black line*), and rainfall (*blue bars*) for each active well in the Eastern Tutuila Region for the period 2015-2017.

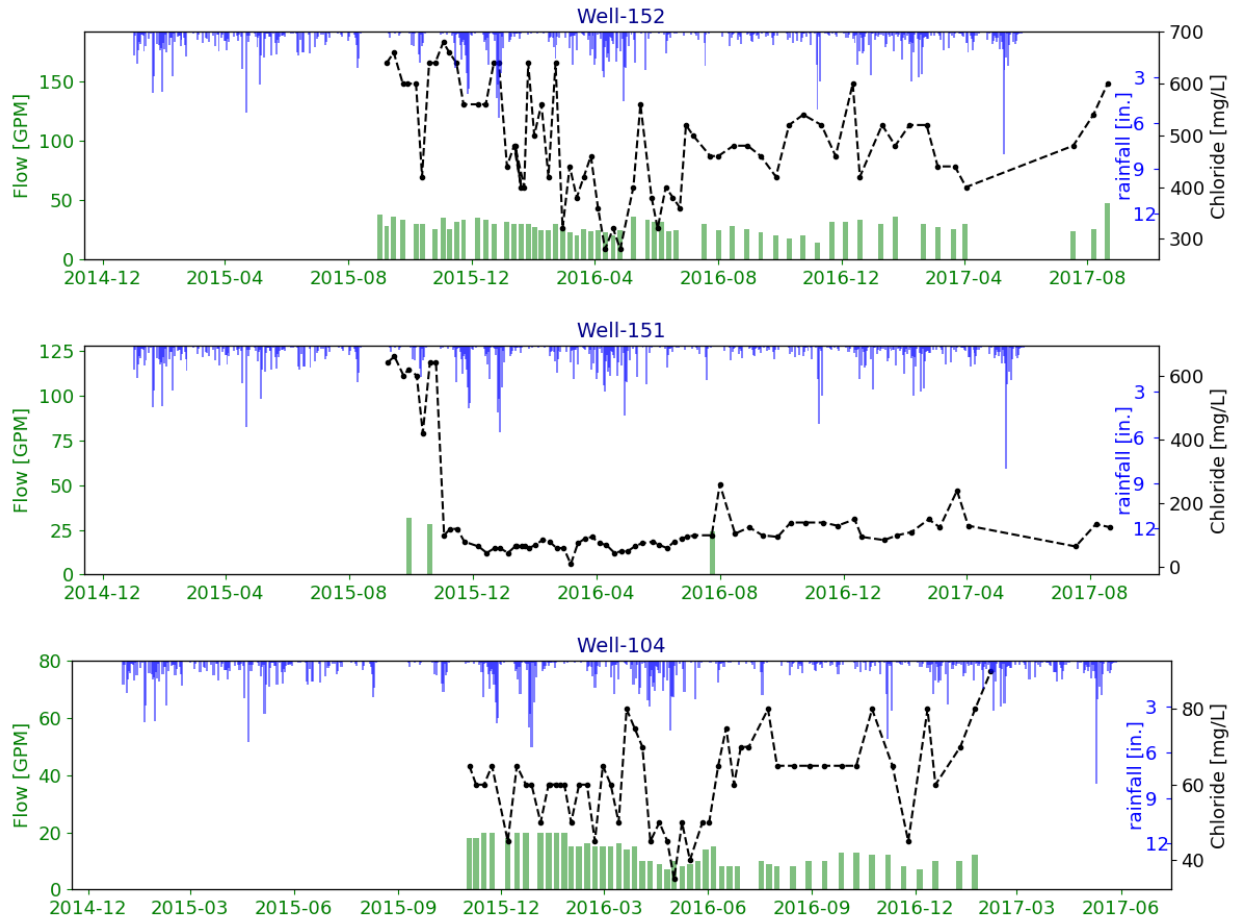


Figure B18 continued: Plots of pump rates (*green bars*), Cl<sup>-</sup> values (*black line*), and rainfall (*blue bars*) for each active well in the Eastern Tutuila Region for the period 2015-2017.

## B2.2 Pago Outer-Caldera Geologic Unit

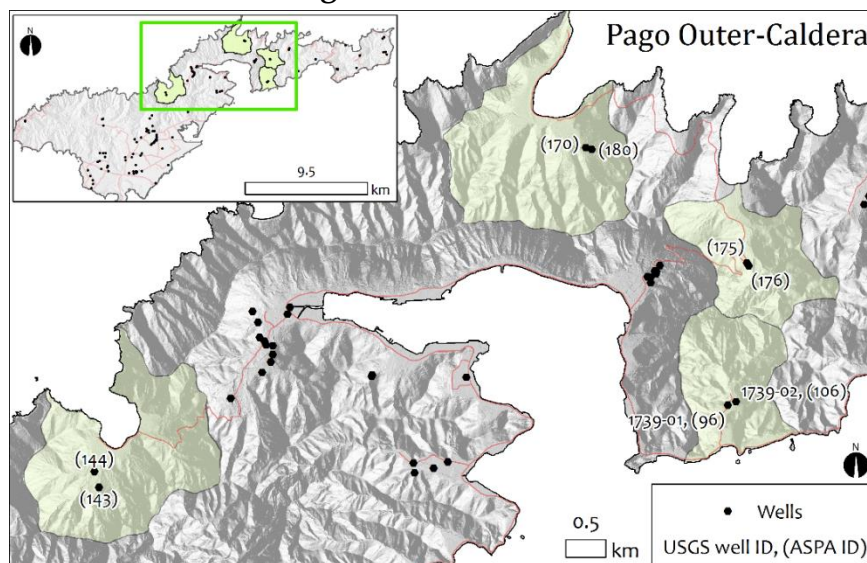


Figure B19: Location map of watersheds in the Pago Outer-Caldera Unit with locations of active and abandoned wells. *Green shading* denotes local watershed boundaries, which do not necessarily delineate aquifer extent. Labels indicate well ID numbers.

Wells drilled into the basalt aquifers of the outer-caldera region of the Pago Shield (Figs. B19, B20, and B21) generally show low  $K$  values, low specific capacity, and low  $Cl^-$  concentrations. This supports the idea that overall conductivities in the unit are low, which contributes to the development of a thick basal-lens. However, due to the low  $K$  values, these areas may be susceptible to high aquifer drawdowns. Water levels in each of the unit's wells are variable. However, it appears that local barriers to water movement may drastically control groundwater levels in the unit as is shown by the historical account of groundwater development in Laulii Village from Eyre and Walker (1991):

*"[Laulii] well 96 entered the major water-producing formation at 150 feet below sea level. Water with a chloride concentration of 25 mg/L rose in the well to an altitude of 19 feet above sea level. Another well, 150 feet deep and drilled 400 feet to the north of well 96, encountered only massive rock, yielded no water, and was abandoned. Well 106 was drilled across the stream 500 feet to the east of well 96 to a depth of 320 feet below sea level. Prior to pumping well 96, water levels at well 106 ranged from 22 to 24 feet above sea level"* (pg. 36).

Interestingly there have been a few accounts of finding confined conditions during drilling of some, but not all, of the wells in Aua, Laulii, and the Pago Valley watersheds. This is shown by observations of pre-development heads in localized portions of these aquifers that are significantly above sea level and in some cases above the ground surface, encountered after drilling through dry often massive lava formations above (Eyre and Walker, 1991). Extraction of water from these wells subsequently produced large drawdowns, indicating the confined water bodies are likely to be limited in extent. This supports the conclusion that aquifer connectivity in the Pago Volcanics is

typically low and may be controlled by the locations of low-conductivity formations such as massive lava flows, pyroclastics, or potentially dikes (Table B6).

The Central Northern Coast Region is estimated to receive between 9.6 and 10.4 Mgal/d of recharge (range of all estimates), whereas the extraction at Wells 170 and 180 averages 0.4 Mgal/d (31 GPM). The roughly estimated area weighted recharge use ratio for the Vatia Watershed averages less than 1%.

The North-Central Eastern Tutuila Region is estimated to receive between 2.7 and 5.6 Mgal/d of recharge (range of all estimates), whereas the extraction at Well 176 averages 0.14 Mgal/d (100 GPM). The roughly estimated area weighted recharge use ratio for Afono Watershed is between 12 and 25% (average of 18%).

The Western Central Northern Coast Region is estimated to receive between 10.7 and 19.6 Mgal/d of recharge (range of all estimates), whereas the extraction at well 143 averages 0.16 Mgal/d (110 GPM). The roughly estimated area weighted recharge use ratio for Fagasa Watershed is between 2 and 4% (average of 3%).

Table B6: Pago Outer-Caldera Unit aquifer parameters

Well # [USGS ID]	Well # [ASPA ID]	Drilling WL [m]	Pumping WL [m]	Pump rate [GPM]	Specific capacity [GPM/m]	T [m <sup>2</sup> /day]	K [m/d]	Avg. Cl <sup>-</sup> [mg/L]	Cl <sup>-</sup> trend [mg/L/yr.]
-	175	-	-	-	-	-	-	-	
-	<b>176</b>	-	<b>-1.3</b>	<b>100</b>	-	-	-	<b>23</b>	<b>↑, 2</b>
-	<b>143</b>	-	<b>25.3</b>	<b>110</b>	-	-	-	<b>35</b>	<b>↑, 2</b>
-	144	-	4.3	120	-	-	-	25	
1739-01	96	5.5	-7.5	47	4	38	1	-	
1739-02	106	7.3	-	-	-	-	-	-	
-	<b>170</b>	<b>8.1</b>	-	<b>14</b>	<b>1</b>	<b>13</b>	<b>7</b>	<b>24</b>	<b>↑, 5</b>
-	<b>180</b>	<b>7.9</b>	-	<b>17</b>	<b>9</b>	<b>461</b>	<b>18</b>	<b>24</b>	<b>↑, 5</b>

\* Pump rates and Ave. Cl<sup>-</sup> values are taken from averages of last 3 years ASPA data, ↓ denotes decreasing Cl<sup>-</sup> trend ↑ denotes increasing Cl<sup>-</sup> trend. Values for inactive wells were taken from sources as described in Section 4.0. Records in bold are active wells as of 2016.

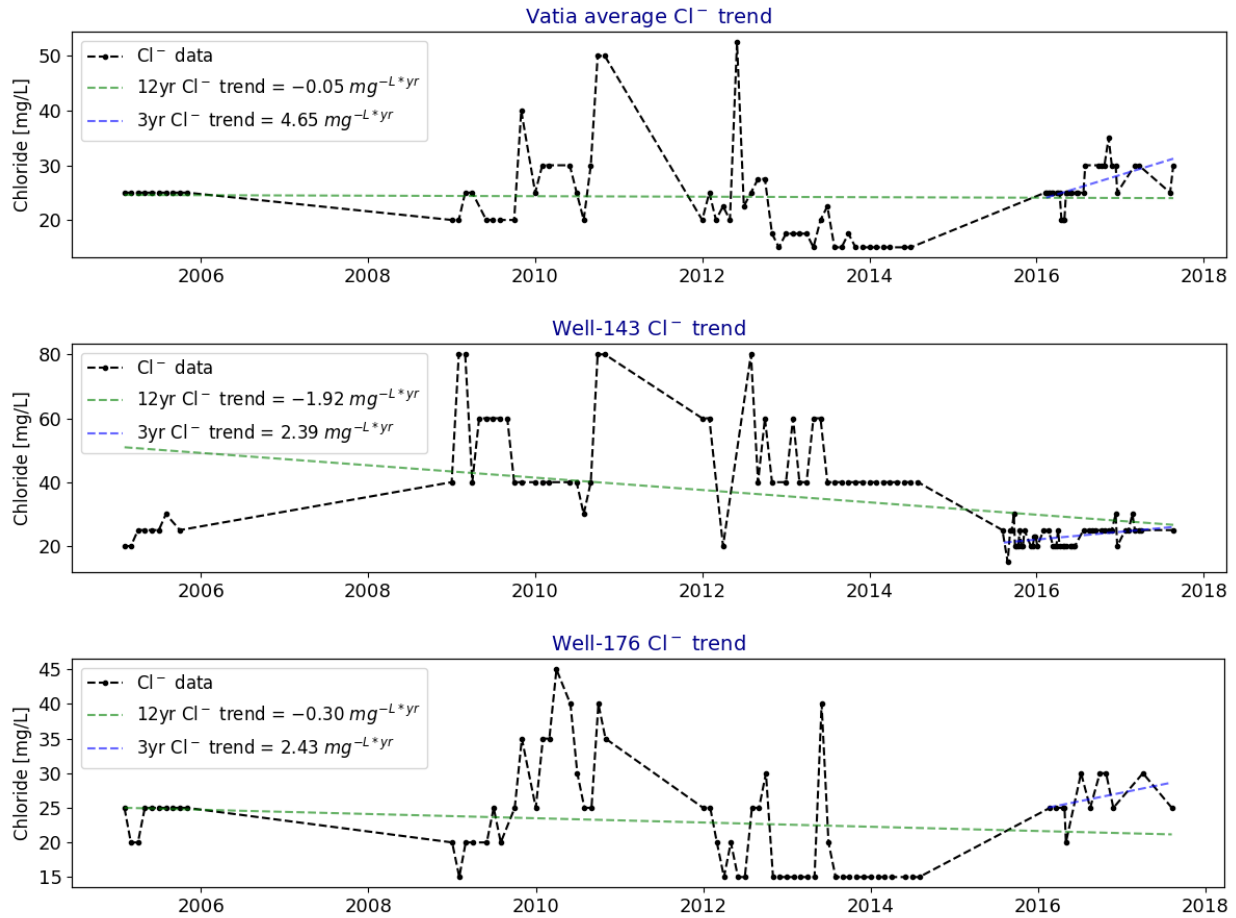


Figure B20: Cl<sup>-</sup> concentrations and trends for active wells in the Pago Outer-Caldera unit. Fagasa (Well 143) and Afono (Well 176) have only one active well each and Vatia has two wells, with averaged Cl<sup>-</sup> concentrations presented here. *Green dashed lines* show the linear regression trend line for all data, generally about 12 years, and *blue dashed lines* show the linear regression trend line for the most recent 3-year period, 2015-2017.

### Preliminary recommendations for sustainable aquifer management

**Existing wells:** The satellite systems in Vatia, Afono, and Fagasa Villages appear to be maintaining stable Cl<sup>-</sup> concentrations and water levels, based on data from ASPA records (from 2006 to 2017). This suggests these wells are currently pumped at a sustainable rate, and indeed, in general pump rates at these wells do not exceed 120 GPM and some pump at rates as low as 15 GPM. As long as demand does not increase, these wells are likely to be able to continue supplying high-quality water at current rates.

**Future development:** Since this is a large and diverse region, localized aquifer conditions are also likely to be diverse. However, as long as lower yielding wells are acceptable, it is likely that new wells could be sustainably developed. Individual site characteristics will be variable, in general targeting areas that are likely to encounter continuous water bodies near sea level will be the most conservative approach. As wells are deepened below sea level, the risk of dewatering a surficial aquifer of limited extent is exchanged for the risk of drilling through the basal lens and invoking

saltwater intrusion via pumping. Both of these risks can be minimized by drilling as far inland as possible where the main groundwater body is expected to be thicker, or by utilizing angled drilling methods to further gain access to more inland parts of the lens. Based on available data, it would be conservative to expect wells in the Pleistocene shields to yield water at an order of magnitude less than wells in the Tafuna-Leone aquifers.

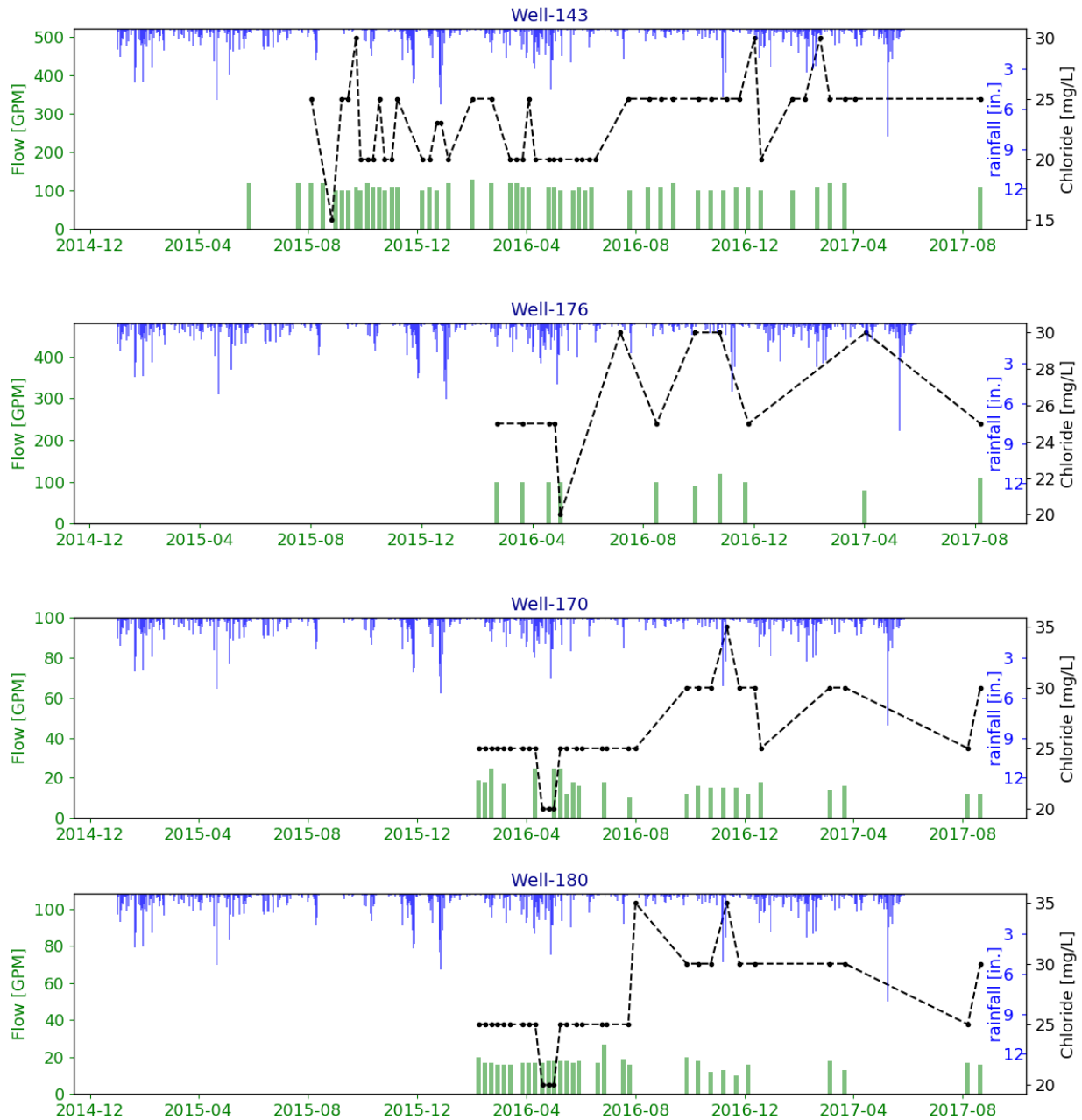


Figure B21: Plots of pump rates (*green bars*), Cl- values (*black line*), and rainfall (*blue bars*) for each active well in the Pago Outer-Caldera Unit for the period 2015-2017.

### B2.3 Malaeimi Watershed

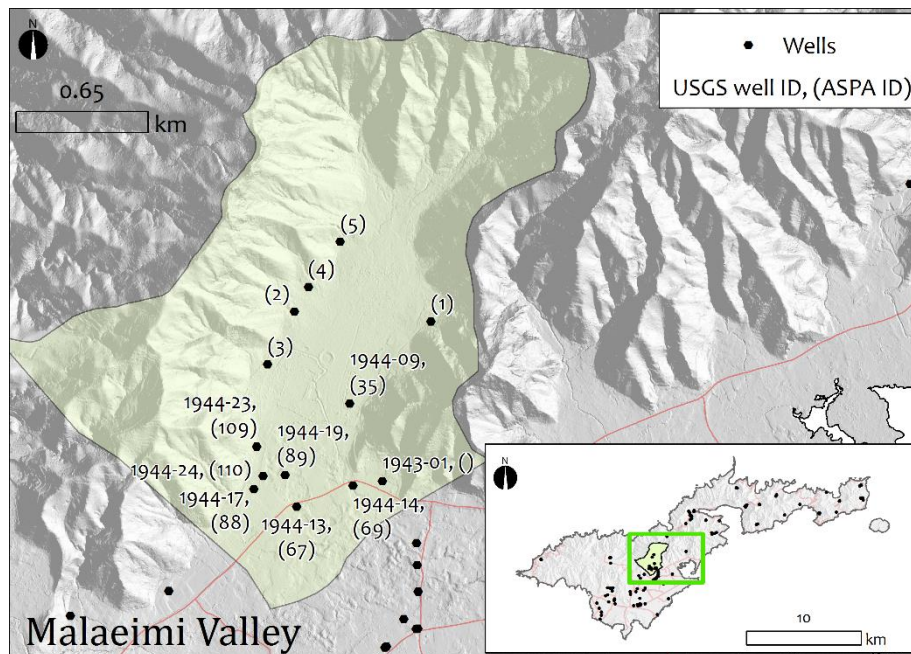


Figure B22: Location map of Malaeimi Watershed with locations of active and abandoned wells. *Green shading* denotes local watershed boundary, which does not necessarily delineate aquifer extent. Note, new well locations (Wells 1 to 5) are estimated, and are still awaiting surveyed locations from ASPA. Labels indicate well ID numbers.

The Malaeimi Valley area (Figs. B22, B23, and B24) has been widely recognized as having valuable water resource characteristics. This is due to underlying geologic features, as well as relatively high recharge rates for Tutuila. The valley is a primary recharge capture zone for the heavily utilized Tafuna Plain aquifer. Currently the valley's land use is mostly undeveloped and second growth forest. While some agro-forestry and light habitation exists in the valley, there are presently few residents. The valley has been recognized as possessing all three of the needed qualifications for designation an area as a "Special Management Area" under American Samoan Law. These qualifications include unique and irreplaceable habitat, products or materials offering beneficial functions, and products or materials affecting the cultural values or quality of life that are significant to the general population of the Territory of American Samoa and Fa'a Samoa. Multiple studies to assess Malaeimi's water resources value have been performed, and in 2004 it was recommended that the watershed be legally protected as a special management area (Shuler et al. 2014, Pedersen Planning Consultants 2004). Unfortunately, this recommendation was not legislated upon and no management protections for Malaeimi Valley exist at this time (Table B7).

Geologically, the area is unique in that it lies at the boundary of two very hydrogeologically different rock units. Subsurface water flow and storage is affected by the physical structure of the Leone lava flow and the underlying topography of the valley carved into the Pleistocene Pago Inner-Caldera volcanics. Surface water draining off of the Pleistocene mountains has been observed to quickly infiltrate into the alluvial deposits that fill the valley bottom. These deposits are bounded to the south by Tafuna lavas, which are likely to be even more permeable than the alluvium, thereby increasing the proportion of MFR that occurs at the valley mouth.

High observed drilling water levels in wells with reasonably high T and K values, such as those at Wells 1, 88, 89, 109, 110, that rapidly drop off further down the valley near Wells 67 and 69 suggest that wells in the valley may tap different hydrogeologic units. Pumping shows that some high water levels are unstable and may decline rapidly when pumped or potentially even when they are directly connected to the underlying basal aquifer via a high permeability pathway such as a well. All of the Malaeimi wells show low Cl<sup>-</sup> levels, which also support the idea that these wells tap a thick freshwater lens with a potential partial disconnection from underlying seawater.

The Tafuna Plain Region is estimated to receive between 24.5 and 45.9 Mgal/d of recharge (range of all estimates), whereas the extraction at the two active well in Malaeimi averages 0.7 Mgal/d (460 GPM). The roughly estimated area weighted recharge use ratio for the current wellfield is between 9 and 16% (average of 12%). However, this value is likely to drastically increase once five new wells are put into production in this area.

Presently, Wells 1-5 are awaiting connection to the water distribution system, and available data should be considered to be provisional. Once these wells are connected, elevations can be more accurately surveyed, and pumping water levels can be monitored this analysis should be revisited.

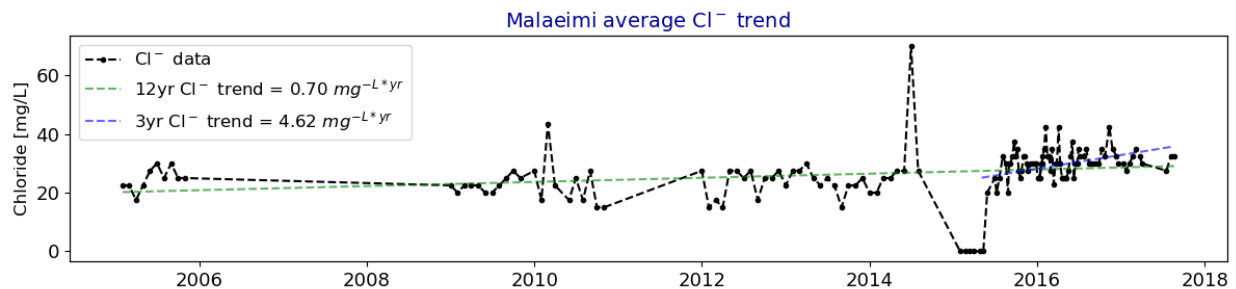


Figure B23 Cl<sup>-</sup> concentrations averaged across active Malaeimi Wells 89 and 67. *Green dashed line* shows the linear regression trend line for all data, generally about 12 years, and *blue dashed line* shows the linear regression trend line for the most recent 3-year period, 2015-2017.

## Preliminary recommendations for sustainable aquifer management

### Existing wells:

Presently, only two wells are producing water in the watershed. These wells have low Cl<sup>-</sup> concentrations and do not appear to produce unsustainable drawdowns, therefore current extraction rates can be sustainably maintained. However, five new wells have been drilled in this area and once they are put into production it will be important to reassess the effects of increased pumping in this area.

### Future development:

The recharge use ratio of this well averages around 12%, but it is unclear as to how well the recharge estimates incorporate the addition of MFR to the local aquifer. The area is soon to be subject to what are likely to be drastic increases in extraction rates from five new wells that are not yet online. It would be prudent to assess the effects of this recent development prior to planning any future groundwater development in the watershed.

Table B7: Malaeimi region aquifer parameters.

Well # [USGS ID]	Well # [ASPA ID]	Drilling WL [m]	Pumping WL [m]	Pump rate [GPM]	Specific capacity [GPM/m]	T [m <sup>2</sup> /day]	K [m/d]	Avg. Cl <sup>-</sup> [mg/L]	Cl <sup>-</sup> trend [mg/L/yr.]
1943-01	-	8.8	-	-	-	-	-	20	-
1944-09	35	25.4	23.9	15	10	-	-	-	-
<b>1944-13</b>	<b>67</b>	<b>3.2</b>	<b>-0.5</b>	<b>280</b>	-	-	-	<b>28</b>	<b>↑, 1</b>
1944-14	69	1.8	-	-	-	-	-	-	-
1944-17	88	19.2	-	300	-	-	-	-	-
<b>1944-19</b>	<b>89</b>	<b>30.7</b>	<b>-1.1</b>	<b>180</b>	<b>41</b>	<b>30000</b>	<b>1798</b>	<b>26</b>	<b>↑, 4</b>
1944-23	109	35.4	-	-	-	-	-	-	-
1944-24	110	23.5	-	-	-	-	-	-	-
-	1	20.3	-19.6	120	3	1107	5	-	-
-	2	8.0	2.8	300	58	2830	24	25	-
-	3	5.9	5.8	60	984	1301	637	-	-
-	4	16.5	-6.7	200	30	740	4	20	-
-	5	34.2	27.6	50	2	81	0.4	25	-

\* Pump rates and Ave. Cl<sup>-</sup> values are taken from averages of last 3 years ASPA data, ↓ denotes decreasing Cl<sup>-</sup> trend ↑ denotes increasing Cl<sup>-</sup> trend. Values for inactive wells were taken from sources as described in Section 4.0. Records in bold are active wells as of 2016.

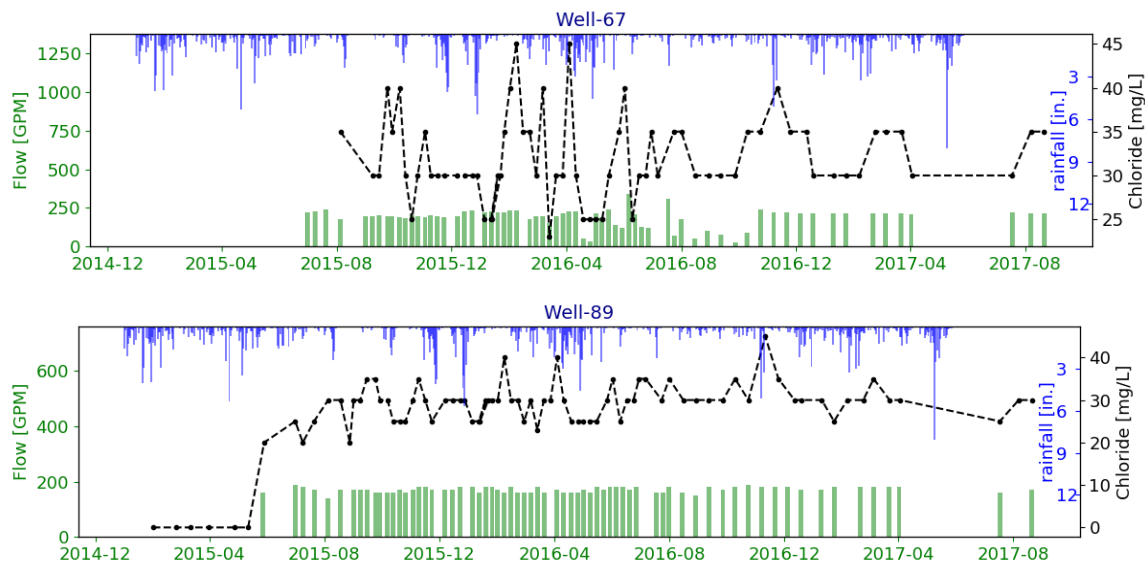


Figure B24 Plots of pump rates (green bars), Cl<sup>-</sup> values (black line), and rainfall (blue bars) for each active well in the Malaeimi Valley Wellfield for the period 2015-2017.

## B2.4 Pago Valley Wellfield

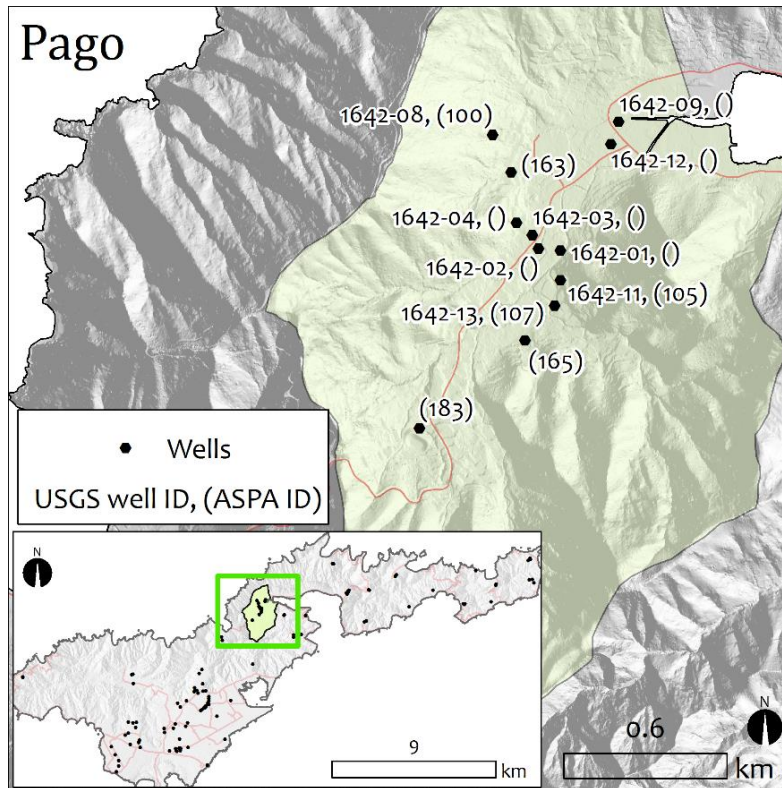


Figure B25: Location map of Pago Valley Watershed with locations of active and abandoned wells. *Green shading* denotes local watershed boundary, which does not necessarily delineate aquifer extent. Labels indicate well ID numbers.

The alluvial-fill valley of Pago Pago, also known as Vaipito Valley, is here referred to as Pago Valley (Figs. B25, B26, B27 and B28), is one of the largest and most populated on Tutuila. Groundwater development in this region dates back to the 1940's when Stearns selected a site for a water tunnel (Pago shaft, Well 1642-04) in a ridge of Pago inter-caldera rocks on the north side of the valley. Eyre and Walker (1993) provide an account of the construction and use of the Pago shaft:

*"Pago shaft 2 is a water tunnel excavated at sea level and accessible through a vertical shaft 56 feet deep. The infiltration gallery is composed of several nearly horizontal tunnels that penetrate massive ponded lavas, volcanic ejecta, breccia, dikes, and faults, as well as a small amount of thin-bedded vesicular lava. The materials penetrated are typical of the rocks found in the central part of Tutuila. The artesian aquifer tapped by the tunnels had a head of 30 feet above sea level. Storage of 0.3 million gallons is available in the tunnels, only one of which contributes significantly to the gallery yield of about 60 gal/min."*

Numerous other wells have been drilled in the valley, generally through a relatively thick (15 to 30 m) veneer of alluvium into either the layered a'a flows of the Pago Outer-Caldera Unit or the massive flows of the Pago Inner-Caldera Unit. The fault boundary separating the inner and outer unit likely lies somewhere between Pago shaft 1642-04 and Well 1642-08 based on different

lithologies documented in their driller's logs. Higher pre-development water levels and low *K* values in the more southerly of Pago valley's wells may indicate that they are located within the Pago Inner-Caldera Unit. Also an artesian aquifer was reported to have been found in 1985 very near to the shore at the Pago Plaza in Wells 1642-09 and 1642-12. The productive formation at about 20 m depth consisted of basalts overlain by 5 m of alluvium and scapolite. Drilling water levels were about 0.5 m above ground surface with low (10 mg/L) Cl<sup>-</sup> concentrations (Eyre and Walker, 1993). With pumping, Cl<sup>-</sup> concentrations in these wells rose to an average of 250 mg/L, though the eventual fate of these wells remains unreported. A number of other anecdotal reports of lithology and drilling conditions of wells in the Pago region are reported by Eyre and Walker (1991; 1993) (Table B8).

Currently five wells produce about 1.7 Mgal/d of water from the valley. While most wells in this area show low Cl<sup>-</sup> concentrations, Well 163 has concentrations that are significantly higher. This is enigmatic as the other wells are drilled to similar depths and have similar extraction rates. It is possible that this discrepancy could be caused by heterogeneous subsurface structures that connect the location of Well 163 to coastal water more directly than other parts of the local formation. This hypothesis could be tested through the use of tidal efficiency tests at each of the wells in this region. Also the geologic unit boundary between the Pago Outer-Caldera Unit and the Inner-Caldera Unit, is thought to lie somewhere proximal to Well 163, thus the behavior of this well might be controlled by faulting or other types of fractures. Nonetheless Well 163 is only about 0.5 km from the Vaipito Stream estuary and may serve as an example of the risks involved in drilling in thinner portions of the freshwater lens.

Although pre-development water levels in the region were generally high (up to 10 or 20 m) pumping water levels are primarily below sea level. This indicates the low hydraulic conductivity of this area and the high risk of thinning of the freshwater lens. Water level and Cl<sup>-</sup> concentration trends in the Pago area are similar to that of the Aua region, though not as dire. Because of this, and the already high Cl<sup>-</sup> concentration in Well 163, the sustainability of additional water development in this area is questionable.

The Pago Harbor Region is estimated to receive between 15.7 and 16.6 Mgal/d of recharge (range of all estimates), whereas the extraction at the valley's active wells averages 1.5 Mgal/d (1045 GPM). The roughly estimated area weighted recharge use ratio for the Pago Valley Watershed is between 33 and 35% (average of 34%).

Table B8: Pago Valley aquifer parameters.

Well # [USGS ID]	Well # [ASPA ID]	Drilling WL [m]	Pumping WL [m]	Pump rate [GPM]	Specific capacity [GPM/m]	T [m <sup>2</sup> /day]	K [m/d]	Avg. Cl <sup>-</sup> [mg/L]	Cl <sup>-</sup> trend [mg/L/yr.]
1642-01	-	10.7	-	-	-	-	-	30	-
1642-02	-	8.2	-	-	-	-	-	-	-
1642-03	-	10.5	-	-	-	-	-	13	-
1642-04	-	7.3	-	-	-	-	-	-	-
1642-08	100	1.2	-	35	-	-	-	-	-
1642-09	-	3.0	-	-	-	-	-	250	-
<b>1642-11</b>	<b>105</b>	<b>12.4</b>	<b>-44.8</b>	<b>88</b>	<b>11</b>	<b>78</b>	<b>2</b>	<b>51</b>	<b>↑, 3</b>
1642-12	-	3.0	-	-	-	-	-	250	-
<b>1642-13</b>	<b>107</b>	<b>20.3</b>	<b>-21.2</b>	<b>380</b>	-	-	-	<b>91</b>	<b>↑, 2</b>
-	<b>163</b>	<b>7.3</b>	<b>-35.9</b>	<b>150</b>	<b>8</b>	<b>140</b>	<b>5</b>	<b>846</b>	<b>↑, 273</b>
-	<b>183</b>	<b>62.5</b>	<b>61.0</b>	<b>224</b>	<b>20</b>	<b>140</b>	<b>10</b>	<b>28</b>	<b>↑, 2</b>
-	<b>165</b>	-	<b>-31.5</b>	<b>203</b>	-	-	-	<b>41</b>	<b>↑, 2</b>

\* Pump rates and Ave. Cl<sup>-</sup> values are taken from averages of last 3 years ASPA data, ↓ denotes decreasing Cl<sup>-</sup> trend ↑ denotes increasing Cl<sup>-</sup> trend. Values for inactive wells were taken from sources as described in Section 4.0. Records in bold are active wells as of 2016.

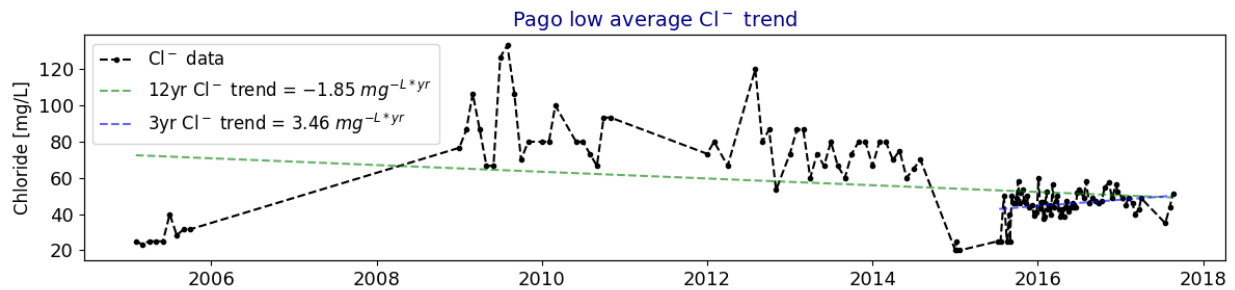


Figure B26: Cl<sup>-</sup> concentrations averaged across active wells in the Pago Valley, except for Well 163, which has Cl<sup>-</sup> concentrations that are significantly higher than other wells in the area. *Green dashed line* shows the linear regression trend line for all data, generally about 12 years, and *blue dashed line* shows the linear regression trend line for the most recent 3-year period, 2015-2017.

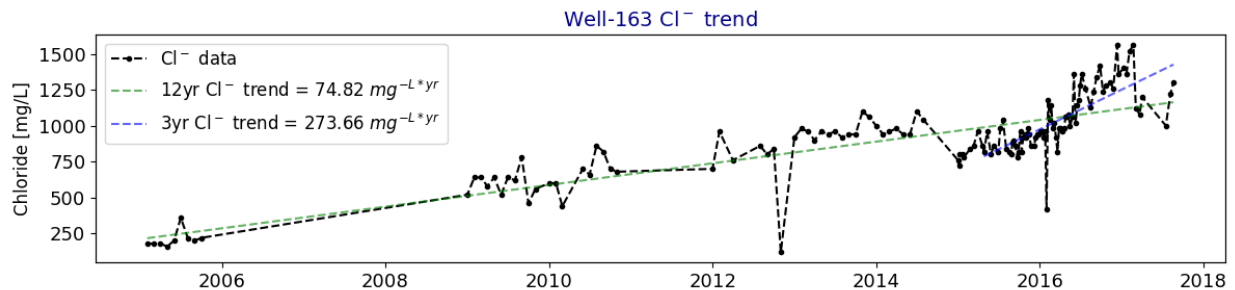


Figure B27: Cl<sup>-</sup> concentrations for Well 163, which has distinctively higher Cl<sup>-</sup> concentrations than the other Pago area wells. *Green dashed line* shows the linear regression trend line for all data, generally about 12 years, and *blue dashed line* shows the linear regression trend line for the most recent 3-year period, 2015-2017.

## **Preliminary recommendations for sustainable aquifer management**

**Existing wells:** The wells in Pago Valley can be classified into three groups based on their potential sustainability: (1) Well 183, which may utilize a high-level reservoir; (2) Well 163, which must develop a thin part of the basal aquifer or be drilled in a different lithology; and (3) all the other wells, which utilize a seemingly thicker part of the basal lens. Cl<sup>-</sup> concentrations at Well 163 clearly indicate that this well is experiencing saltwater upconing and the issue is only being exacerbated with continued pumping. While this well is the closest of its neighbors to the coast, it is located only about 150 m closer to the Vaipito Stream estuary than Wells 105 and 107, and is drilled to a similar depth (-50 to -60 m) as nearby wells. Regardless, it is clear that Well 163 would benefit from a reduction in pumpage or in abandonment.

The other wells that utilize the basal aquifer (group 2 above) seem to have relatively low and stable Cl<sup>-</sup> concentrations in comparison to Well 163, despite having production water levels that are similar and below sea level. These wells may tap an aquifer system that has less connectivity to coastal saltwater and more connectivity to freshwater recharge zones located above. These wells seem to have fairly stable Cl<sup>-</sup> trends suggesting that if their pump rates are not increased current production levels may be maintained without detriment to local water quality.

Well 183, which is located at a higher elevation, seems to tap an aquifer that is significantly elevated above the basal water levels that are found at the Valley's other wells. This suggests the aquifer tapped by Well 183 is perched or elevated in some other manner. The water produced at this well has a Cl<sup>-</sup> concentration that is not affected by underlying saltwater at all, further supporting the idea that it is disconnected from the basal system below.

**Future development:** Additional exploration could be undertaken in the upper sections of the watershed to assess the development potential of the elevated water system found at Well 183. Additional development in the lower watershed area is not recommended based on the already high extraction in this area.

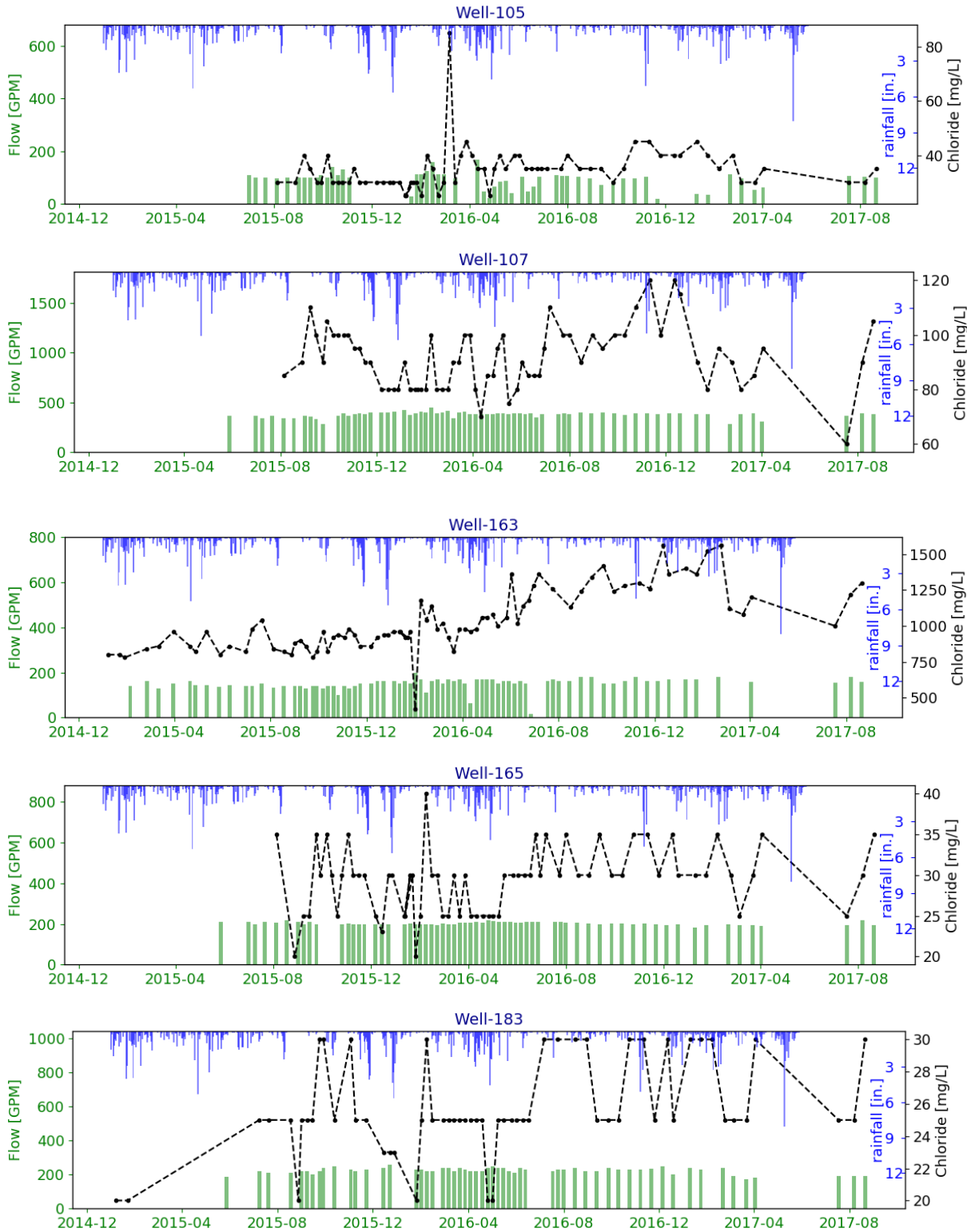


Figure B28: Plots of pump rates (*green bars*), Cl- values (*black line*), and rainfall (*blue bars*) for each active well in the Pago Valley Wellfield for the period 2015-2017.

### B3 Heavily Developed Areas

Regions or wellfields grouped in this section already have a significant amount of existing groundwater development in place. Many of these areas have increasing Cl<sup>-</sup> trends or decreasing water level trends (Fig. B29). Additionally, groundwater recharge to extraction ratios in many of these areas are generally higher than the in areas in other sections. While each area is influenced by each these factors to a different degree, in general, these indicators suggest that groundwater withdrawals may be occurring at a rate exceeding the capacity of the aquifer to sustainably supply water. In consideration of these concerns future development of groundwater in these areas is generally not recommended.

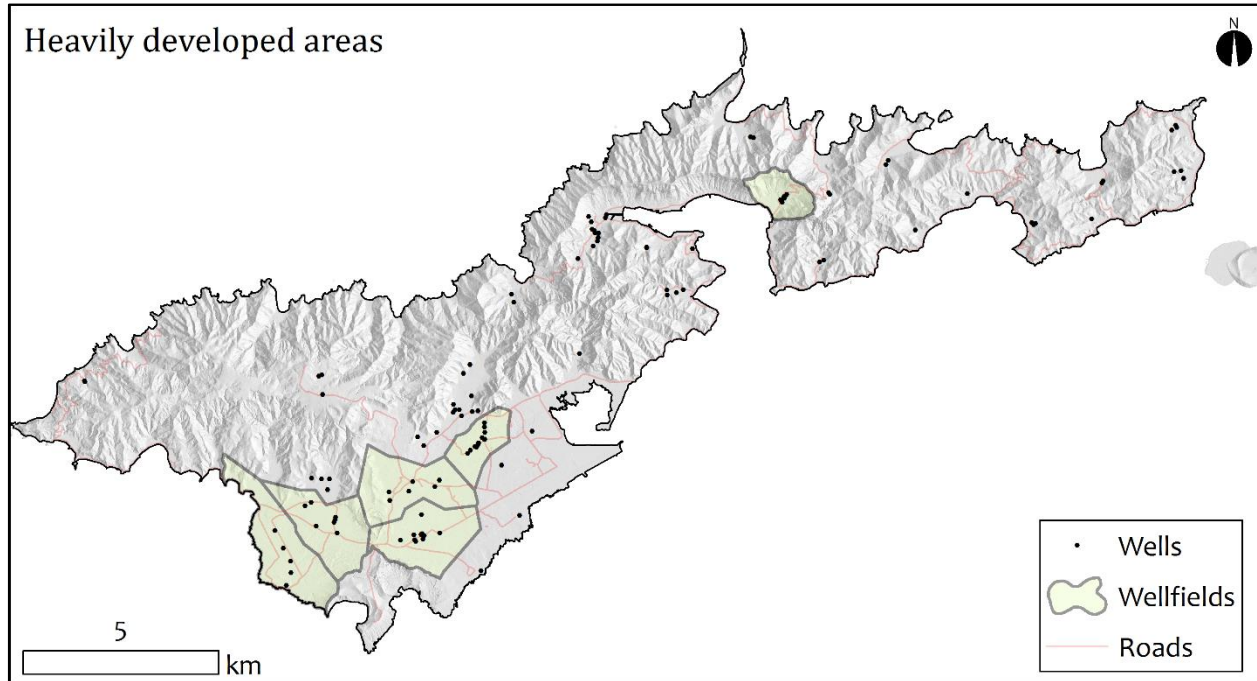


Figure B29: Map of wellfields showing characteristics where current extraction rates may exceed the water supply capacity in Tutuila.

### B3.1 Aua Watershed

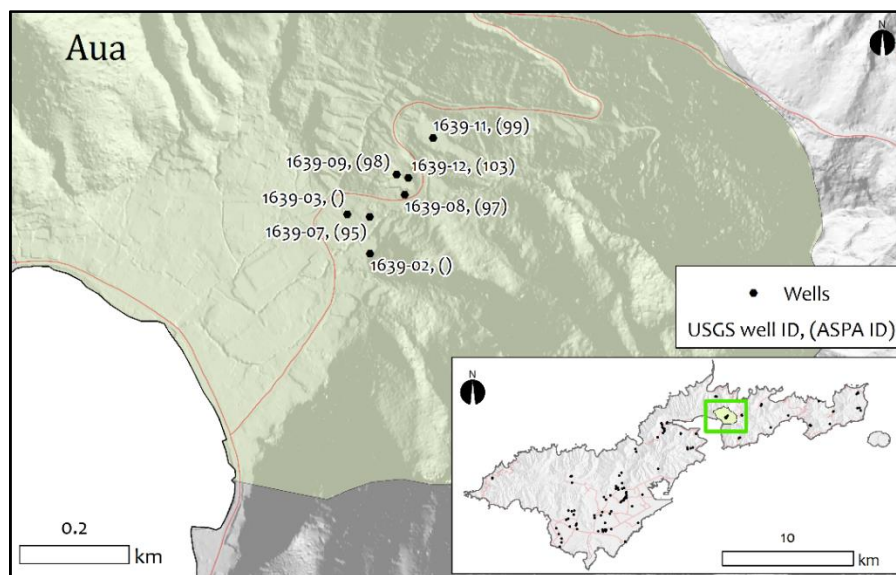


Figure B30: Location map of Aua Watershed with locations of active and abandoned wells. *Green shading* denotes local watershed boundary, which does not necessarily delineate aquifer extent. Labels indicate well ID numbers.

The Aua Region (Figs. B30, B31, and B32) provides a clear example of consequences that may be expected when rates of groundwater withdrawal exceed the sustainable capacity of an aquifer. In Aua, these consequences have taken the form of large water level drawdowns (up to 15 m) and progressively increasing Cl<sup>-</sup> concentrations. In 1983 total extraction in this area was 0.28 Mgal/d (233.5 GPM), this rose to 0.93 Mgal/d (775.5 GPM) in 1985, and then in 1989 was scaled back to 0.22 Mgal/d (183.5 GPM), following a rise in chloride concentration. Currently only Wells 97 and 99, are active in this watershed and together they now produce an average of 0.39 Mgal/d (229 GPM). Present day Cl<sup>-</sup> concentrations in these wells are some of the highest on the island, generally exceeding the USEPA recommended maximum level of 250 mg/L by 4 to 7 times. In addition to high Cl<sup>-</sup> levels, these wells also show large pumping water level drawdowns, 11 m in Well 97, and 15 m in Well 99. While some of this drawdown can be attributed to well losses, the temporal trend in regional water levels clearly indicates that dewatering of the aquifer has taken place. This trend is evident in pre-development water level observations, which dropped from an average of about 5 m above sea level when the first wells were drilled in this area to over -7 m below sea level when now inactive Well 103 was drilled in 1985. At Well 99 a static water level of -1.2 m below sea level was recorded in 2014 after a 24-hour cessation in pumping. Eyre and Walker (1991) provide a summary of the area's hydrogeology and development history.

*"The producing zone of the volcanic aquifer in Aua valley, west of Laulii, is overlain by approximately 100 feet of saturated sediments and several tens of feet of poorly permeable basalt. The alluvial aquifer has not been developed because of its generally low permeability and its susceptibility to contamination. By drilling to sufficient depths a productive artesian aquifer, with a potentiometric surface 20 feet above sea level, has been tapped. Apparently, recharge to the deep aquifer is by way of fractures*

*in the overlying rock... The water level at the deeper of two adjacent alluvial wells was 18 feet above sea level, while the water level at the shallower well was 16 feet above sea level (Bentley, 1975). A source of this alluvial water is apparently upward flow from the deeper artesian volcanic aquifer....During the drilling of deep Aua wells 95, 97, 98, 99, a substantial flow of water was not found until productive zones between 40 and 140 feet below sea level were tapped. The water rose to 20 feet above sea level at well 95 when it was completed in 1981. Subsequent wells encountered progressively lower water levels. A single aquifer has been tapped by these wells, as evidenced by the decline of water levels at each well in response to pumpage from the others.”*

The similar water chemistry and water level behavior in the Aua wells indicates that the wells tap a common aquifer, which is probably fairly limited in extent and bounded by impermeable structures that do not provide a hydraulic connection to distant reservoirs. This idea is supported by the results of a pumping test performed in 1982 and documented in Eyre and Walker (1991):

*“When well 97 was pumped steadily at a rate of 263 GPM, water levels declined 38 feet in 27.7 hours and remained at that level, or rose slightly, for the next 44.3 hours (test data is in the files of the U.S. Geological Survey, Honolulu, Hawaii). ...a step drawdown test shows that the aquifer loss was about 23 feet at that pumping rate. Because the cone of depression is generally steep in aquifers of low permeability, water levels several hundred feet from well 97 would be expected to be little affected. Certainly the static water levels of -6 and -20 feet relative to sea level, eventually reached at wells 99 and 103, respectively, could not have been predicted from the 72-hour pumping test. These large drawdowns, far from the pumping wells, were most likely be caused by dewatering of an aquifer of limited size.”*

The Pago Harbor Region is estimated to receive between 15.6 and 16.6 Mgal/d of recharge (range of all estimates), whereas the extraction at wells 97 and 99 averages 0.3 Mgal/d (229 GPM). The estimated area weighted recharge use ratio for Aua Watershed is between 17 and 18% (average of 17%) (Table B9).

Table B9: Aua region aquifer parameters.

Well # [USGS ID]	Well # [ASPA ID]	Drilling WL [m]	Pumping WL [m]	Pump rate [GPM]	Specific capacity [GPM/m]	T [m <sup>2</sup> /day]	K [m/d]	Avg. Cl <sup>-</sup> [mg/L]	Cl <sup>-</sup> trend [mg/L/yr.]
1639-02	-	5.5	-	30	1	-	-	-	-
1639-03	-	5.1	-	45	16	-	-	-	-
1639-07	95	6.1	-	-	-	-	-	-	-
<b>1639-08</b>	<b>97</b>	<b>5.5</b>	<b>-10.2</b>	<b>190</b>	<b>24</b>	<b>190</b>	<b>4</b>	<b>1586</b>	<b>↑, 114</b>
1639-09	98	4.3	-	-	-	-	-	271	-
<b>1639-11</b>	<b>99</b>	<b>1.2</b>	<b>-15.1</b>	<b>139</b>	<b>10</b>	<b>150</b>	<b>5</b>	<b>942</b>	<b>↑, 91</b>
1639-12	103	-7.6	-21.9	280	20	183	5	-	-

\* Pump rates and Ave. Cl<sup>-</sup> values are taken from 2015-2017 ASPA data, ↓ denotes decreasing Cl<sup>-</sup> trend ↑ denotes increasing Cl<sup>-</sup> trend. Values for inactive wells were taken from sources as described in Section 4.0. Records in bold are active wells as of 2016.

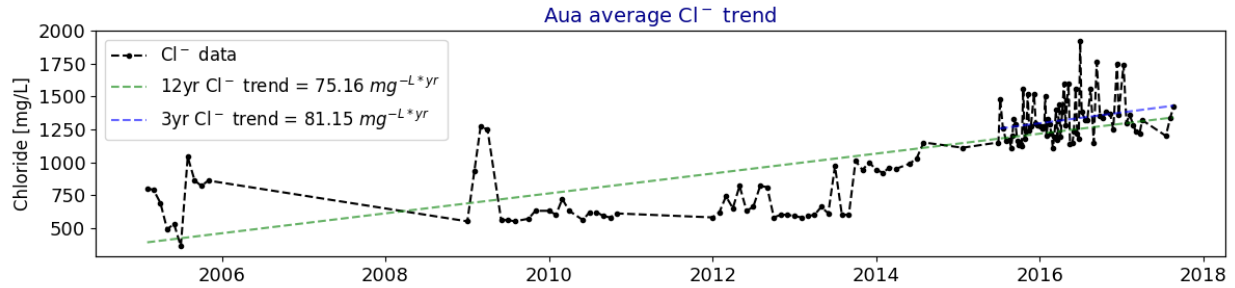


Figure B31: Cl<sup>-</sup> concentrations averaged across all active wells in the Aua Region. Green dashed line shows the linear regression trend line for all data, generally about 12 years, and blue dashed line shows the linear regression trend line for the most recent 3-year period, 2015-2017.

### Preliminary recommendations for sustainable aquifer management

**Existing wells:** Considering high observed aquifer drawdown and chloride levels observed in Wells 97 and 99, the pumping rates in these wells could be reduced to allow recovery of the aquifer and reduction of Cl<sup>-</sup> concentrations.

**Future development:** Due to the groundwater development history in the Aua area, drilling additional wells in the already over-utilized aquifer is not recommended. If additional wells are necessary in this area, they could be used to offset the pumpage of existing wells, thereby allowing all the wells in the aquifer to pump at lower rates. This may spread out the effects of withdrawals to a larger area, and potentially serve to reduce local drawdown and Cl<sup>-</sup> at each well. This would require locating new wells as far from existing wells as possible.

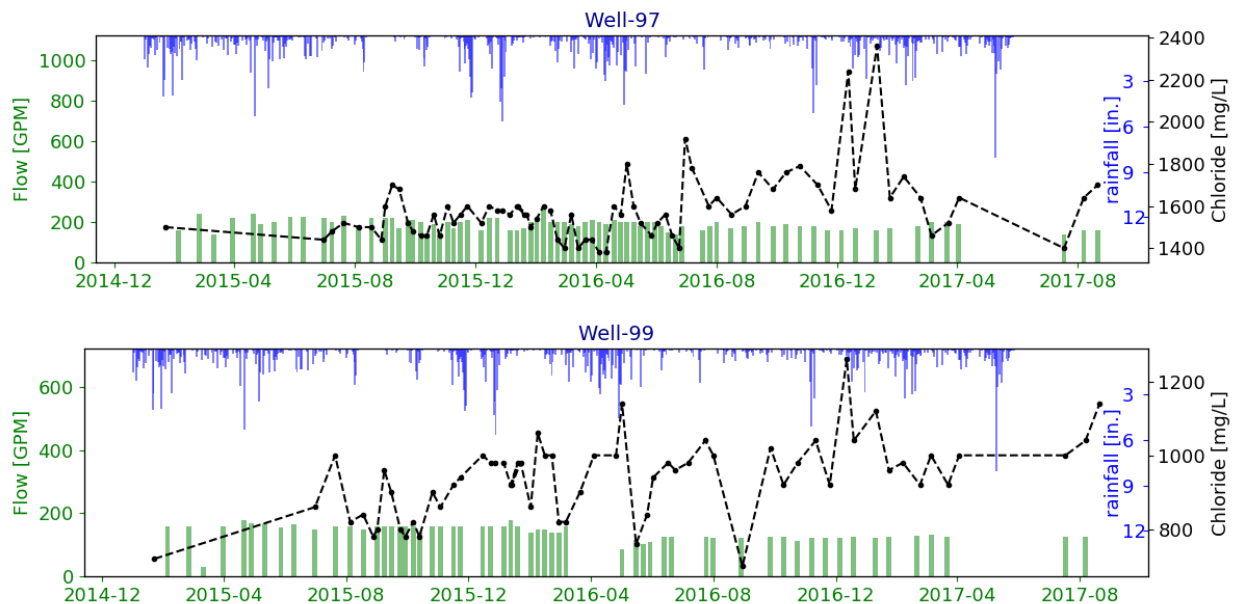


Figure B32: Plots of pump rates (*green bars*), Cl<sup>-</sup> values (*black line*), and rainfall (*blue bars*) for each active well in the Aua Region for the period 2015-2017.

## B3.2 Iliili Wellfield

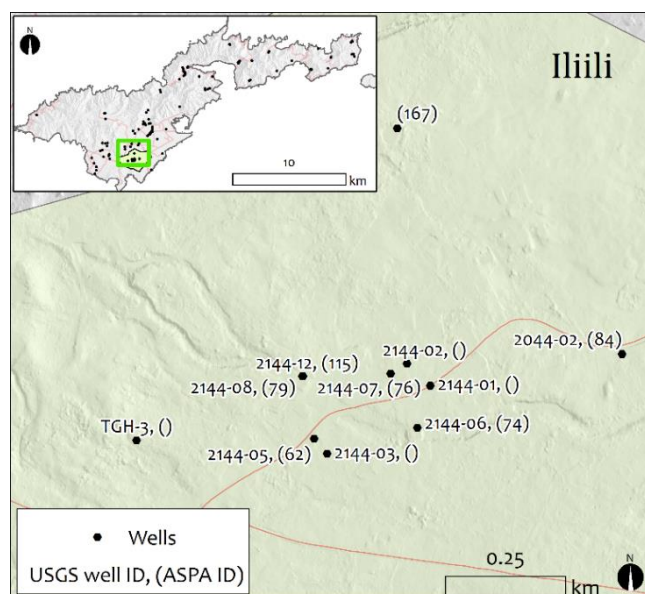


Figure B33: Location map of Iliili Region with locations of active and abandoned wells. *Green shading* denotes Thiessen polygon boundary based on clustering of wells into wellfields. This boundary is not intended to delineate aquifer extent. Labels indicate well ID numbers.

The Iliili Wellfield (Figs. B33, B34, and B35) is located in the southwestern region of the Tafuna-Leone Plain. Iliili is near the Pavaiai Wellfield and it is likely that the thin basal-lens aquifer is interconnected through the Iliili, Pavaiai, and Tafuna Wellfields since there is a generally high hydraulic conductivity throughout the whole area. However, the Iliili Wellfield may be distinct in its local permeability distribution as it is located closer to the ash cones on the southern portion of the Leone Rift. The geology is inferred to be relatively more pyroclastic rich (Stearns, 1944) and thus there is likely to be a significantly lower vertical hydraulic conductivity in this area than the more northeasterly wellfields. Levels of total coliform and *Escherichia coli* bacteria in Well 84 (Shuler, unpublished data, 2016) are generally lower than in the Tafuna and Malaeimi Wellfields, indicating that there may indeed be longer travel times or more aquifer filtration in the Iliili Region. Also the deep borehole TGH-3 was drilled in the western portion of the wellfield and the lithologic log and core samples give a detailed record of the aquifer structure at that point (Table B10).

Although there have been numerous wells drilled in this area, there are only four active wells in the wellfield that together produce about 1.2 Mgal/d. Pumping rates are relatively high and drawdowns are relatively low indicating the high overall hydraulic conductivity in this region. Well 84 has an exceptionally high Cl<sup>-</sup> level which averages about two times the U.S. standard, indicating this well's and potentially the whole region's susceptibility to saltwater upconing. The annual average composite chloride concentration has increased from 30 mg/L in 1975 to about 175 mg/L in 1989, and now averages about 210 mg/L. The long term trend of increasing salinity in conjunction with measurements of a relatively thin fresh water lens in this area suggests that current rates of groundwater extraction have already begun to impact the sustainability of the resource in this area. Further groundwater development in the lower elevations of the Iliili Region are not recommended, though there may be some potential to tap thicker aquifers in the lower permeability area of the rift zone.

The Tafuna Plain Region is estimated to receive between 24.5 and 45.9 Mgal/d of recharge (range of all estimates), whereas the extraction at the wellfields active wells averages 1.5 Mgal/d (1012 GPM). The roughly estimated area weighted recharge use ratio for Ilili Wellfield is between 22 and 41% (average of 32%).

Table B10. Ilili region aquifer parameters.

Well # [USGS ID]	Well # [ASPA ID]	Drilling WL [m]	Pumping WL [m]	Pump rate [GPM]	Specific capacity [GPM/m]	T [m <sup>2</sup> /day]	K [m/d]	Avg. Cl <sup>-</sup> [mg/L]	Cl <sup>-</sup> trend [mg/L/yr.]
<b>2044-02</b>	<b>84</b>	<b>1.8</b>	<b>0.6</b>	<b>283</b>	<b>577</b>	<b>11000</b>	<b>3825</b>	<b>475</b>	<b>↑, 91</b>
2144-01	-	-	-	-	-	-	-	44	-
2144-02	-	-	-	-	-	-	-	76	-
2144-03	-	-	-	-	-	-	-	45	-
<b>2144-05</b>	<b>62</b>	<b>2.6</b>	<b>0.4</b>	<b>239</b>	<b>736</b>	<b>7000</b>	<b>1126</b>	<b>121</b>	<b>↑, 11</b>
2144-06	74	1.8	-	-	-	-	-	-	-
<b>2144-07</b>	<b>76</b>	<b>1.4</b>	<b>-0.8</b>	<b>265</b>	<b>478</b>	<b>3446</b>	<b>992</b>	<b>101</b>	<b>↑, 15</b>
2144-08	79	0.9	-	-	-	-	-	-	-
2144-12	115	1.8	-	-	-	-	-	-	-
-	<b>167</b>	-	<b>1.0</b>	<b>225</b>	-	-	-	<b>101</b>	<b>↑, 17</b>
TGH-3	TGH-3	1.9	-	-	-	-	-	-	-

\* Pump rates and Ave. Cl<sup>-</sup> values are taken from averages of last 3 years ASPA data, ↓ denotes decreasing Cl<sup>-</sup> trend ↑ denotes increasing Cl<sup>-</sup> trend. Values for inactive wells were taken from sources as described in Section 4.0. Records in bold are active wells as of 2016.

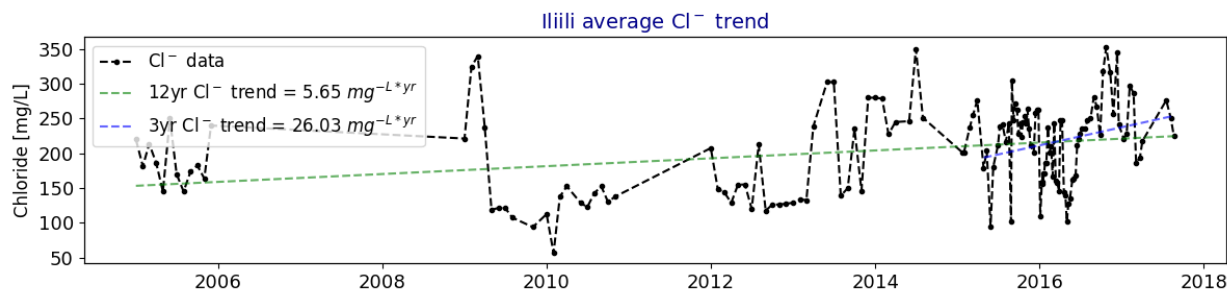


Figure B34: Cl<sup>-</sup> concentrations averaged across all active wells in the Ilili Wellfield. *Green dashed line* shows the linear regression trend line for all data, generally about 12 years, and *blue dashed line* shows the linear regression trend line for the most recent 3-year period, 2015-2017.

### Preliminary recommendations for sustainable aquifer management

**Existing wells:** The Ilili area shows thinning of the freshwater lens and as such, the wells in this area produce groundwater with fairly high Cl<sup>-</sup> concentrations, with Well 84 producing the highest. This is to be expected, as Well 84 is the closest to the coast and is located in the thinnest part of the lens. Shifting production towards more upgradient wells, such as Well 167, and reducing withdrawals at Well 84 may help to alleviate the issue somewhat.

**Future development:** If future groundwater development is considered in this area, locating wells closer to the Leone Rift Zone, near the TGH-3 location, and as far from the coast or Well 84 as possible will decrease chances of encountering continued issues with salinization.

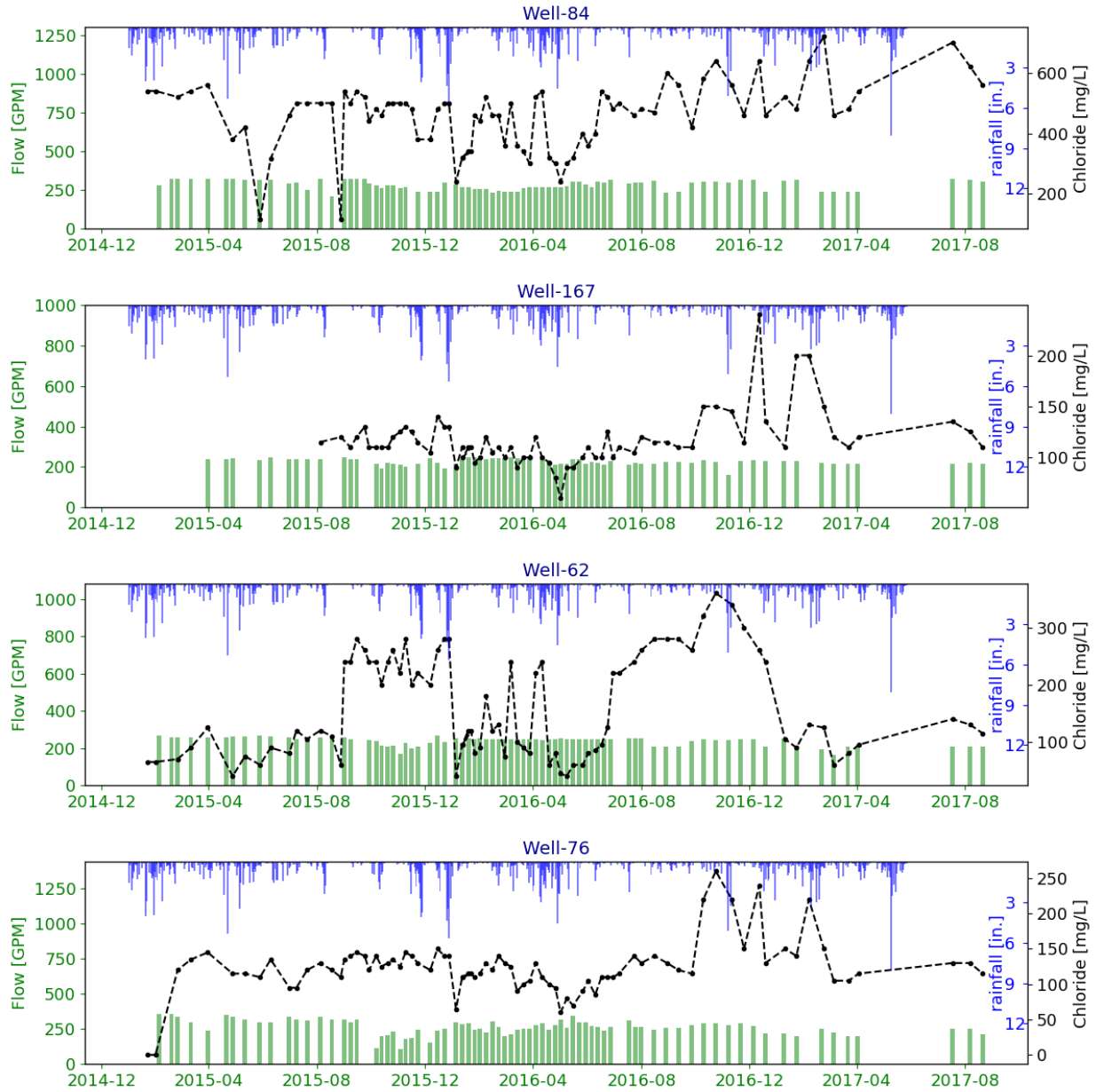


Figure B35: Plots of pump rates (green bars), Cl<sup>-</sup> values (black line), and rainfall (blue bars) for each active well in the Iliili Wellfield for the period 2015-2017.

### B3.3 Pavaiai Wellfield

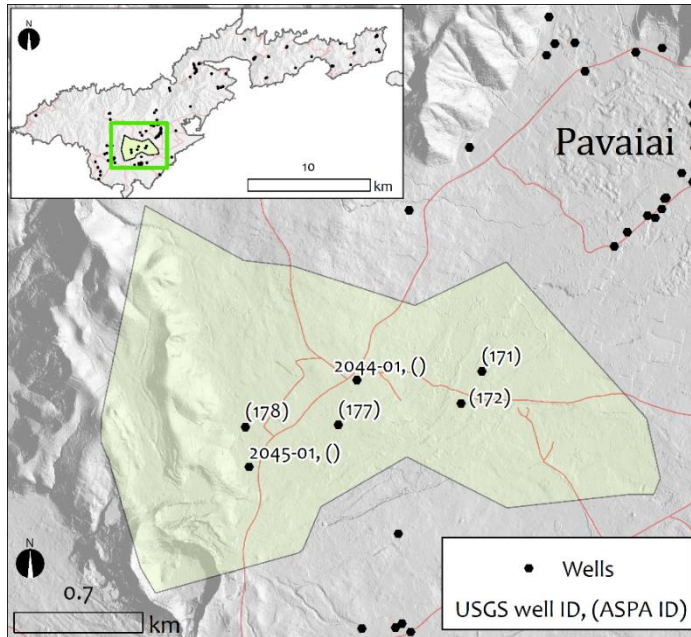


Figure B36: Location map of Pavaiai Wellfield with locations of active and abandoned wells. *Green shading* denotes Thiessen polygon boundary based on clustering of wells into wellfields. This boundary is not intended to delineate aquifer extent. Labels indicate well ID numbers.

The Pavaiai Wellfield (Figs. B36, B37, and B38) could be considered to be an extension of the Tafuna or the Iliili Wellfields, which are all likely share the same aquifer. The Pavaiai field is distinguished here because it shares aquifer characteristics with the Tafuna Wellfield, high-hydraulic conductivities and large specific capacities, but produces groundwater that does not seem to show the same effects of surface water contamination that the Tafuna field is subject to. Similar to Iliili, some wells produce water with high  $\text{Cl}^-$  concentrations and have static water levels that are near to sea level. These observations suggest the basal lens is thin in this region as well (Table B11).

The Tafuna Plain Region is estimated to receive between 24.5 and 45.9 Mgal/d of recharge (range of all estimates), whereas the extraction at the wellfields active wells averages 1.4 Mgal/d (962 GPM). The roughly estimated area weighted recharge use ratio for Pavaiai Wellfield is between 20 and 38% (average of 29%).

Table B11: Pavaiai Wellfield aquifer parameters.

Well # [USGS ID]	Well # [ASPA ID]	Drilling WL [m]	Pumping WL [m]	Pump rate [GPM]	Specific capacity [GPM/m]	T [m <sup>2</sup> /day]	K [m/d]	Avg. Cl <sup>-</sup> [mg/L]	Cl <sup>-</sup> trend [mg/L/yr.]
2044-01	-	-	-	-	-	-	-	-	-
2045-01	-	-	-	-	-	-	-	15	-
-	<b>171</b>	-	<b>1.0</b>	<b>245</b>	<b>44291</b>	<b>99753</b>	<b>4616</b>	<b>456</b>	↑, 55
-	<b>172</b>	-	<b>0.8</b>	<b>242</b>	<b>2947</b>	<b>21778</b>	<b>5372</b>	<b>481</b>	↑, 63
-	<b>177</b>	<b>1.3</b>	<b>1.0</b>	<b>380</b>	<b>691</b>	<b>6300</b>	<b>870</b>	<b>241</b>	↑, 27
-	<b>178</b>	-	<b>1.7</b>	<b>95</b>	<b>100</b>	<b>1200</b>	<b>77</b>	<b>28</b>	0

\* Pump rates and Ave. Cl<sup>-</sup> values are taken from averages of last 3 years ASPA data, ↓ denotes decreasing Cl<sup>-</sup> trend ↑ denotes increasing Cl<sup>-</sup> trend. Values for inactive wells were taken from sources as described in Section 4.0. Records in bold are active wells as of 2016.

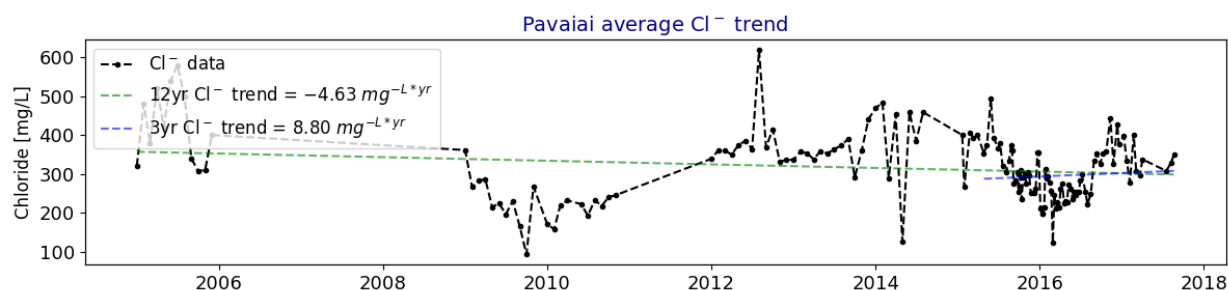


Figure B37: Cl<sup>-</sup> concentrations averaged across all active wells in the Pavaiai Wellfield. *Green dashed line* shows the linear regression trend line for all data, generally about 12 years, and *blue dashed line* shows the linear regression trend line for the most recent 3-year period, 2015-2017.

### Preliminary recommendations for sustainable aquifer management

**Existing wells:** Wells in the Pavaiai Wellfield pump at fairly high rates and produce water with Cl<sup>-</sup> concentrations reflecting the effect of these rates in a hydraulically conductive aquifer with a thin basal lens. The generally high Cl<sup>-</sup> concentrations in this area seem to decrease in response to rainfall events, thus pumping rates could be reduced in these wells during periods of low rainfall. Any additional reduction in pumping rates in this well field would likely help to alleviate the currently observed problems of high Cl<sup>-</sup> levels and increasing Cl<sup>-</sup> trends.

**Future development:** If future groundwater development is considered in this area, locating wells closer to the Leone Rift Zone, near the elevation of Well 178, may increase the chances of reducing continued issues with salinization. Well 178 is located in an area with a higher proportion of volcanic ash, the Leone Pyroclastics Geologic Unit, and as such would be expected to have lower *K* values, with a thicker freshwater lens.

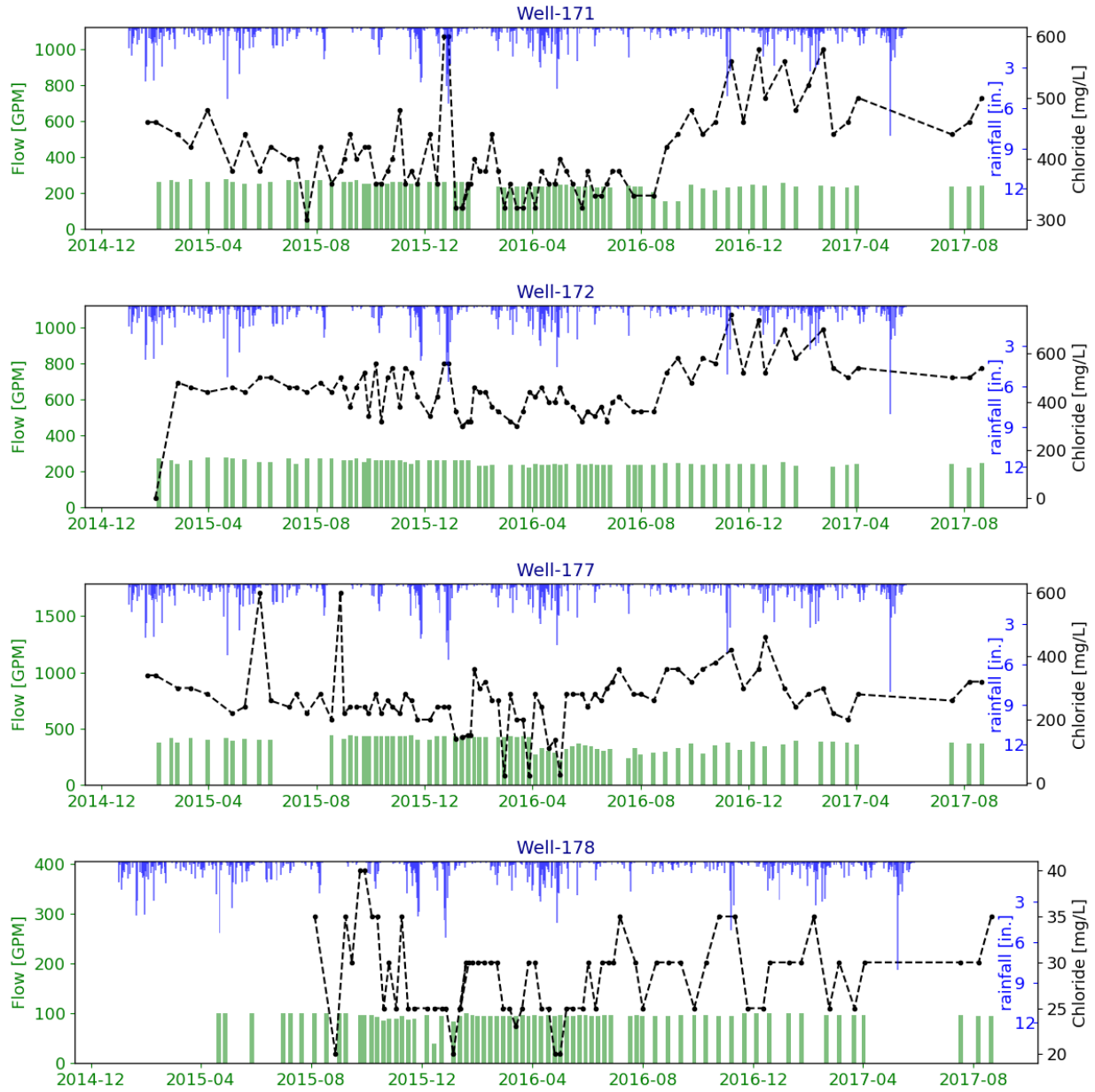


Figure B38: Plots of pump rates (green bars), Cl<sup>-</sup> values (black line), and rainfall (blue bars) for each active well in the Pavaai Wellfield for the period 2015-2017.

### B3.4 Lower Malaeloa Wellfield

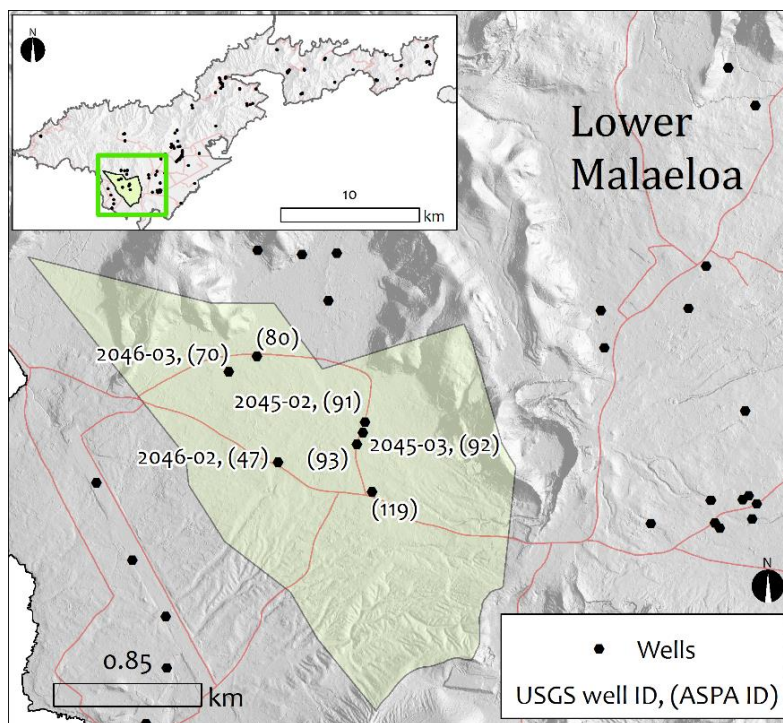


Figure B39: Location map of Lower Malaeloa region with locations of active and abandoned wells. *Green shading* denotes Thiessen polygon boundary based on clustering of wells into wellfields. This boundary is not intended to delineate aquifer extent. Labels indicate well ID numbers.

The Lower Malaeloa Wellfield (Figs. B39, B40, and B41) is one of the most productive on Tutuila. Historically, total extraction from this wellfield increased from 0.1 Mgal/d in 1977 to 1.7 Mgal/d in 1989, and it currently produces a total of 3.0 Mgal/d from eight wells. In this report the Lower Malaeloa wells are distinguished from the upper Malaeloa wells based on proximity to the mountains composed of Taputapu Shield rocks. The more northerly wells are likely to tap into the Taputapu unit, whereas the southerly wells only encounter Holocene age Leone Volcanics. While the aquifers are likely to be hydraulically connected, they probably have different overall properties. The Lower Malaeloa Wellfield contains five active pumping wells that together produce 1.6 Mgal/d of generally low Cl<sup>-</sup> water. The exception is the most southerly well (119), which has had an average Cl<sup>-</sup> concentration of about 290 mg/L since 1989. In addition to direct recharge this area also gains additional recharge from MFR processes. Pre-development water levels in this portion of the Leone Plain were approximately 1.0 to 1.5 m and even relatively high extraction rates do not cause substantial aquifer drawdown. This observation is supported by relatively high values of *T* and *K*, which are expected in the young Holocene Volcanics. Although NO<sub>3</sub><sup>-</sup> levels in Malaeloa wells are currently only about 1/10<sup>th</sup> of the U.S. drinking water maximum contaminant limit, the Malaeloa Wellfield is located in an area of high on-site disposal system density and is downgradient from some of the island's most significant row crop agricultural operations. These potential contaminant sources are a consideration for future water development in this region. Since the majority of contaminant sources are located downgradient of the Upper Malaeloa Wellfield, this

portion of Maleloa is a more conservative area for future development. Salinity values are generally low except at Well 119, which shows a higher Cl<sup>-</sup> concentration as well as a steeper rate of Cl<sup>-</sup> increase with time (84 mg/L/yr) (Table B12).

The Leone Plain Region is estimated to receive between 8.7 and 18.7 Mgal/d of recharge (range of all estimates), whereas the extraction at the wellfield’s active wells averages 1.6 Mgal/d (1134 GPM). The roughly estimated area weighted recharge use ratio for Lower Malaeloa Wellfield is between 37 and 80% (average of 53%).

Table B12: Lower Malaeloa Wellfield aquifer parameters.

Well # [USGS ID]	Well # [ASPA ID]	Drilling WL [m]	Pumping WL [m]	Pump rate [GPM]	Specific capacity [GPM/m]	T [m <sup>2</sup> /day]	K [m/d]	Avg. Cl <sup>-</sup> [mg/L]	Cl <sup>-</sup> trend [mg/L/yr.]
<b>2045-02</b>	<b>91</b>	<b>1.8</b>	<b>1.2</b>	<b>245</b>	<b>2063</b>	<b>6900</b>	<b>1765</b>	<b>27</b>	<b>↑, 1</b>
2045-03	92	1.2	-	-	-	-	-	-	-
2046-02	47	1.2	0.0	80	66	-	-	15	-
<b>2046-03</b>	<b>70</b>	<b>2.6</b>	<b>0.8</b>	<b>372</b>	<b>1129</b>	<b>6500</b>	<b>1257</b>	<b>30</b>	<b>↑, 4</b>
-	80	-	2.4	-	-	-	-	20	-
-	<b>93</b>	-	<b>1.0</b>	<b>263</b>	<b>718</b>	<b>3800</b>	<b>406</b>	<b>27</b>	<b>↑, 2</b>
-	<b>119</b>	-	<b>0.9</b>	<b>254</b>	<b>826</b>	<b>6300</b>	<b>496</b>	<b>245</b>	<b>↑, 84</b>

\* Pump rates and Ave. Cl<sup>-</sup> values are taken from averages of last 3 years ASPA data, ↓ denotes decreasing Cl<sup>-</sup> trend ↑ denotes increasing Cl<sup>-</sup> trend. Values for inactive wells were taken from sources as described in Section 4.0. Records in bold are active wells as of 2016.

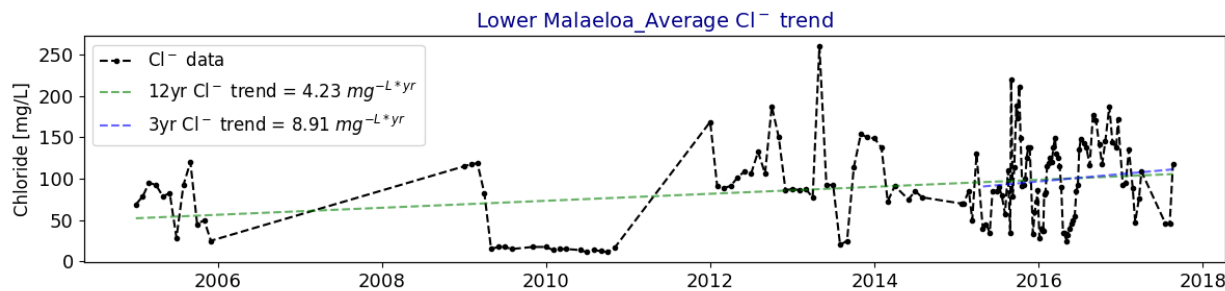


Figure B40: Cl<sup>-</sup> concentrations averaged across all active wells in the Lower Malaeloa Region. Green dashed line shows the linear regression trend line for all data, generally about 12 years, and blue dashed line shows the linear regression trend line for the most recent 3-year period, 2015-2017.

## Preliminary recommendations for sustainable aquifer management

**Existing wells:** Most of the wells in this area show fairly low Cl<sup>-</sup> concentrations with the exception of Well 119, which is located closest to the coast and thus in the thinnest part of the lens. Cl<sup>-</sup> concentrations at Well 119 can be seen to fluctuate with rainfall. Shifting production towards more upgradient wells, and reducing withdrawals at Well 119 may help to alleviate the issue somewhat.

**Future development:** Due to already significant extraction rates, additional groundwater development is not recommended in the Lower Malaeloia Wellfield.

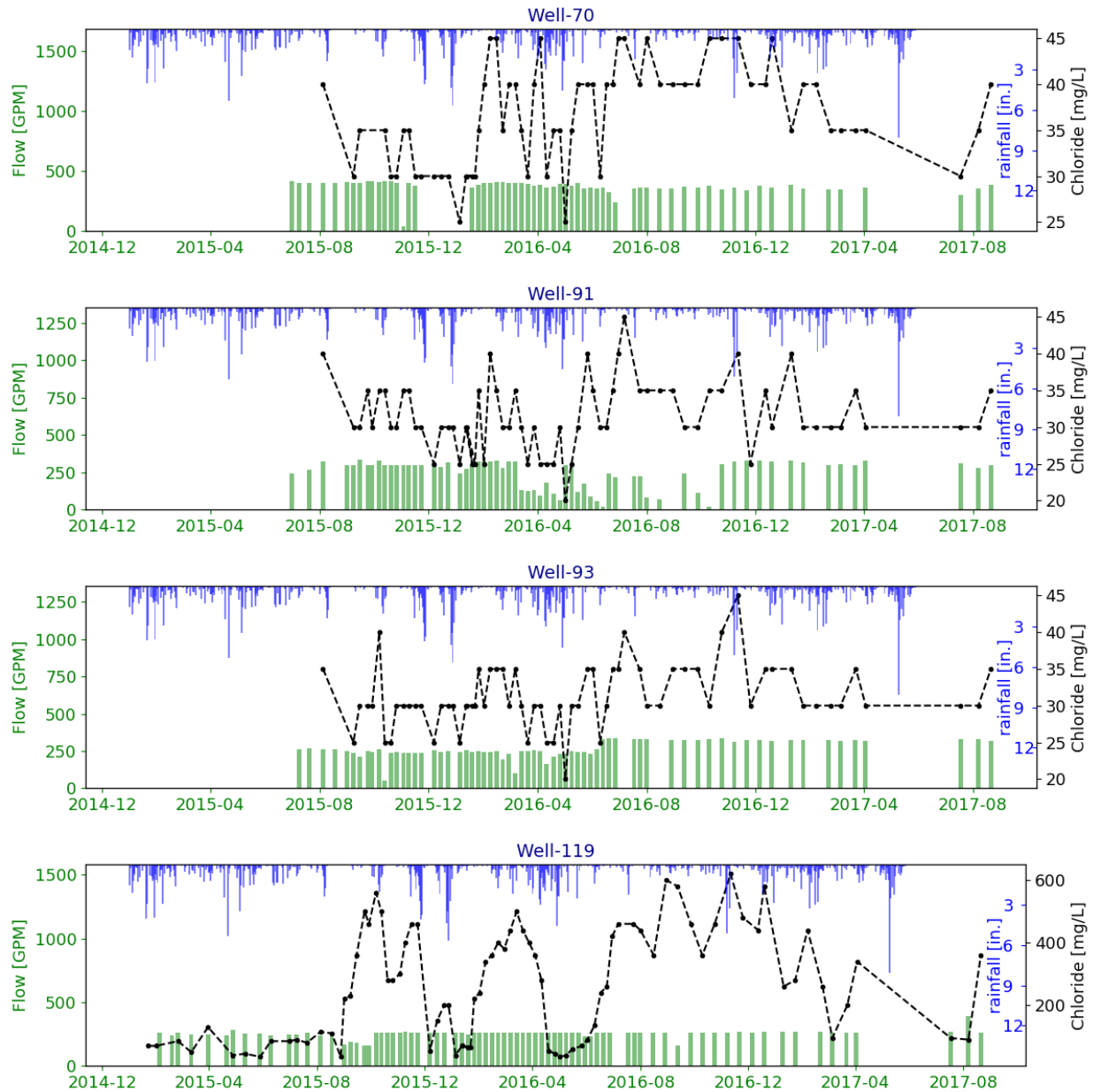


Figure B41: Plots of pump rates (*green bars*), Cl<sup>-</sup> values (*black line*), and rainfall (*blue bars*) for each active well in the Lower Malaeloia Wellfield for the period 2015-2017.

### B3.5 Leone Abandoned Wellfield

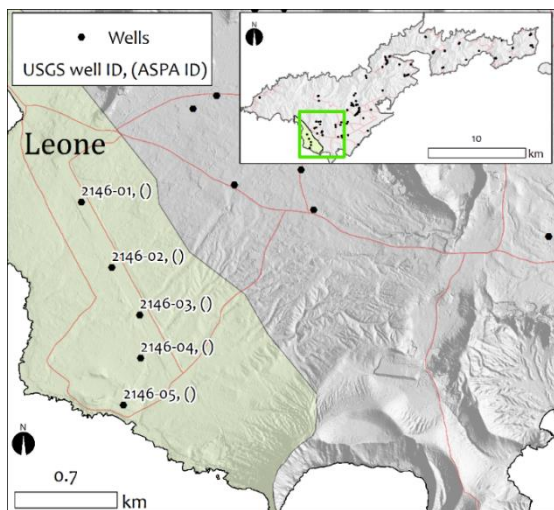


Figure B42: Location map of the coastally proximal Leone region with locations of now abandoned wells. *Green shading* denotes Thiessen polygon boundary based on clustering of wells into wellfields. This boundary is not intended to delineate aquifer extent. Labels indicate well ID numbers.

While the Leone area (Fig. B42) no longer has active pumping wells, it is described in this section as it is likely to be hydraulically connected to the heavily utilized Lower Malaeloa Wellfield. The old wells in this region were likely abandoned due to salinization, which is an expected effect of pumping from a thin nearshore freshwater lens. Pre-development water

levels indicate that the lens height above sea level was never more than a meter even before pumping began. It is unknown whether reported Cl<sup>-</sup> values are from pre-development or from production samples. Since this area has already been abandoned from previous groundwater development, future development in this region would likely prove to be un-sustainable. Additionally, this area is downgradient from a high OSDS and other non-point source pollution source density, and water quality may subject to anthropogenic impacts (Table B13).

#### Preliminary recommendations for sustainable aquifer management

**Existing wells:** Not applicable, all wells have been abandoned.

**Future development:** Additional groundwater development is not recommended in the Lower Leone area.

Table B13: Leone region aquifer parameters

Well # [USGS ID]	Well # [ASPA ID]	Drilling WL [m]	Pumping WL [m]	Pump rate [GPM]	Specific capacity [GPM/m]	T [m <sup>2</sup> /day]	K [m/d]	Avg. Cl <sup>-</sup> [mg/L]	Cl <sup>-</sup> trend [mg/L/yr.]
2146-01	-	0.2	-	-	-	-	-	94	-
2146-02	-	0.4	-	-	-	-	-	73	-
2146-03	-	-	-	-	-	-	-	260	-
2146-04	-	0.6	-	-	-	-	-	257	-
2146-05	-	0.0	-	-	-	-	-	-	-

\* Pump rates and Ave. Cl<sup>-</sup> values are taken from averages of last 3 years ASPA data, ↓ denotes decreasing Cl<sup>-</sup> trend ↑ denotes increasing Cl<sup>-</sup> trend. Values for inactive wells were taken from sources as described in Section 4.0.

### B3.6 Tafuna Wellfield

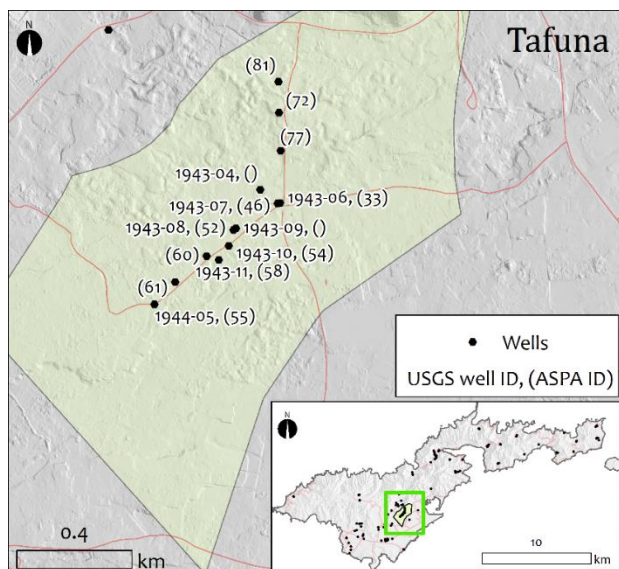


Figure B43: Location map of Tafuna Wellfield with locations of active and abandoned wells. *Green shading* denotes Thiessen polygon boundary based on clustering of wells into wellfields. This boundary is not intended to delineate aquifer extent. Labels indicate well ID numbers.

While the Tafuna Wellfield (Figs. B43, B44, and B46) is currently one of the production workhorses of the ASPA municipal water system, this area may be destined for abandonment in the near future due to USEPA designation of seven of its highest producing wells as groundwater under the direct influence (GUDI) of surface water wells. This designation has necessitated the island's current Boil-Water-Advisory for nearly a decade. This issue is likely to be a consequence of very high hydraulic conductivity of the Tafuna Aquifer, which greatly exceeds the conductivities of any other region on the island (Bentley, 1975; Kennedy, 1987; Izuka et al. 2007). Numerous aquifer tests and water level measurements performed by multiple investigators support this conclusion. Since the region is generally constructed of thin bedded pahoehoe flows, the high permeability is likely to be manifest as secondary porosity in the form of fractures or lava tubes (Table B14).

Currently, the Tafuna Wellfield consists of eight closely-spaced active wells that together produce a total of 2.9 Mgal/d. Pre-development water levels averaged about 1.2 m above sea level, static water levels are reported to be about 1 m above sea level, and pumping water levels are around -1 m below sea level (note, this measurement includes well losses). While the unconfined basal aquifer is highly productive, relatively high chloride levels in many wells indicate that the freshwater lens is thin and at risk of overexploitation. Izuka (1999) observes that  $\text{Cl}^-$  concentrations in the Tafuna Wellfield vary with rainfall, slowly increasing during dry periods and rapidly decreasing during high-recharge events. Eyre and Walker (1993) note that exceptionally dry periods (droughts) such as those observed in 1979, 1983, and 1987 cause significant saltwater upconing and a subsequent rise in average  $\text{Cl}^-$  concentrations to over 350 mg/L. Bentley (1975) noted that wells in this region drilled to a depth of more than -6 m below sea level, experienced higher  $\text{Cl}^-$  concentration peaks during dry periods.

Two abandoned Wells, 2043-01 and 2043-02, that lie to the east of the tightly grouped active Tafuna wells show water levels that grade towards sea level and were documented to have produced fairly brackish water. The records of these abandoned wells illustrate the shape and the limited vertical extent of the of the Tafuna Region's freshwater lens.

The Tafuna Plain Region is estimated to receive between 24.5 and 45.9 Mgal/d of recharge (range of all estimates), whereas the extraction at the Tafuna Wellfields active wells averages 2.23 Mgal/d (1552 GPM). The roughly estimated area weighted recharge use ratio for Tafuna Wellfield is between 69 and 130% (average of 99%).

Table B14: Tafuna Wellfield aquifer parameters. Records in **bold** are active wells as of 2016

Well # [USGS ID]	Well # [ASPA ID]	Drilling WL [m]	Pumping WL [m]	Pump rate [GPM]	Specific capacity [GPM/m]	T [m <sup>2</sup> /day]	K [m/d]	Avg. Cl <sup>-</sup> [mg/L]	Cl <sup>-</sup> trend [mg/L/yr.]
1943-02	17	1.0	-	-	-	-	-	450	-
1943-04	-	0.8	-	-	-	-	-	8	-
<b>1943-06</b>	<b>33</b>	<b>2.6</b>	<b>-1.1</b>	<b>211</b>	-	-	-	<b>230</b>	<b>↑, 68</b>
1943-07	46	2.4	-1.3	150	57	576	83	145	-
1943-08	52	0.6	0.2	95	208	4069	621	15	-
1943-09	-	1.1	-	-	-	-	-	45	-
1943-10	54	0.9	-4.5	200	37	446	18	15	-
1943-11	58	0.9	0.3	250	410	1087	38	820	-
1944-05	55	-	-	50	137	483	23	280	-
2043-01	-	0.3	-	-	-	-	-	280	-
-	<b>60</b>	-	<b>-1.4</b>	<b>325</b>	-	-	-	<b>298</b>	<b>↑, 107</b>
-	<b>61</b>	-	<b>0.5</b>	<b>226</b>	-	-	-	<b>306</b>	<b>↑, 124</b>
-	<b>72</b>	<b>1.8</b>	<b>-0.6</b>	<b>243</b>	<b>108</b>	<b>5880</b>	<b>478</b>	<b>85</b>	<b>↑, 36</b>
-	<b>77</b>	-	<b>-0.3</b>	<b>240</b>	-	-	-	<b>385</b>	<b>↑, 233</b>
-	<b>81</b>	-	<b>-2.5</b>	<b>307</b>	-	-	-	<b>6</b>	<b>↑, 20</b>
2043-02	-	0.5	-	-	-	-	-	1060	-
2143-01	-	0.6	-	-	-	-	-	1650	-

\* Pump rates and Ave. Cl<sup>-</sup> values are taken from averages of last 3 years ASPA data, ↓ denotes decreasing Cl<sup>-</sup> trend ↑ denotes increasing Cl<sup>-</sup> trend. Values for inactive wells were taken from sources as described in Section 4.0. Records in bold are active wells as of 2016.

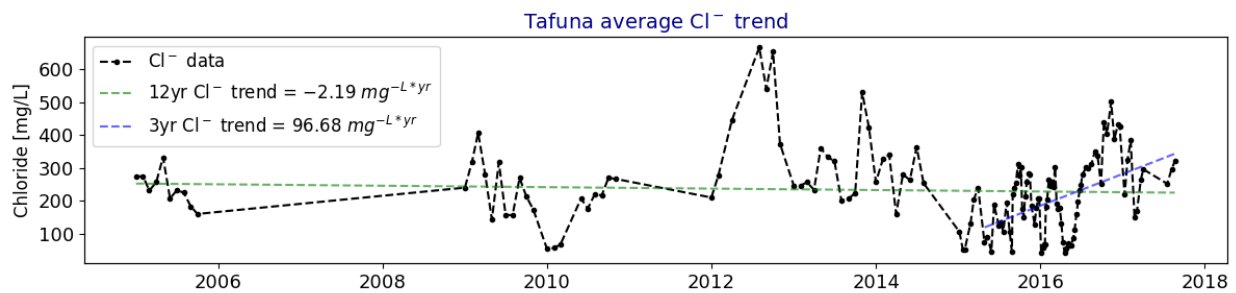


Figure B44: Cl<sup>-</sup> concentrations averaged across all active wells in the Tafuna Wellfield. *Green dashed line* shows the linear regression trend line for all data, generally about 12 years, and *blue dashed line* shows the linear regression trend line for the most recent 3-year period, 2015-2017.

## Preliminary recommendations for sustainable aquifer management

### Existing wells:

Concentrations of Cl<sup>-</sup> in this area decrease in response to heavy rainfalls and this is accompanied by (or basically caused by) an increase in water levels during these high-recharge events (Fig. B45). Cl<sup>-</sup> concentrations show seasonal cycles in this wellfield, whereas concentrations are lower during the wet season than in the dry season. This rapid response is one symptom of the very high hydraulic conductivities in this area, another of which is detections of surface water contamination during high-rainfall events. Combined, these factors make production water from this wellfield less-desirable, because the salinity increases with low rainfall, and bacterial contamination increases with ample rainfall. Reduction of extraction rates can help with the salinization issue, but the contamination issue may be best solved by abandonment of wells in this area.

**Future development:** Additional groundwater development is not recommended in the Tafuna Wellfield area, specifically considering the ongoing issues presently experienced with groundwater affected directly by surface water

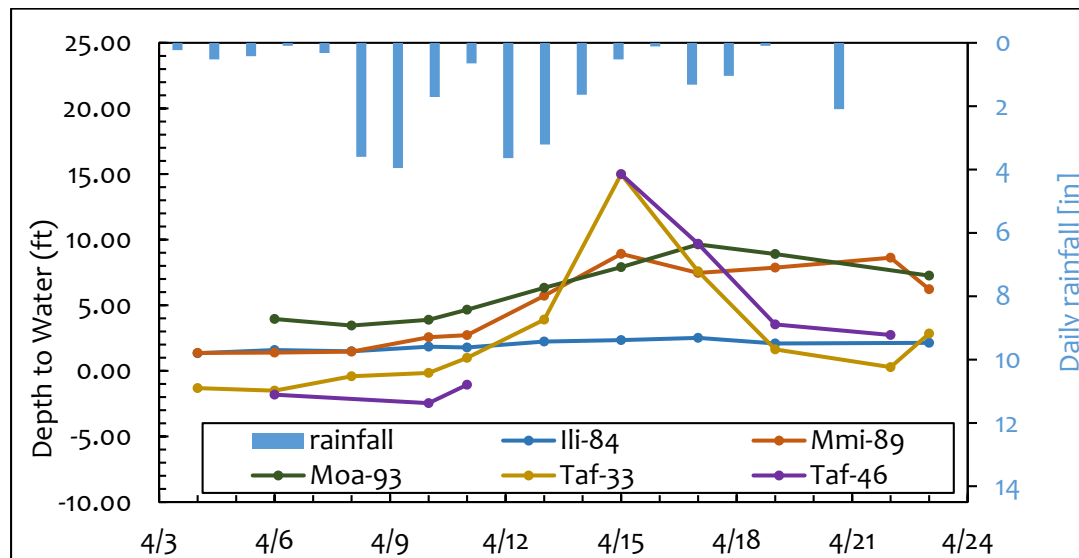


Figure B45: Results of water level monitoring for April 2016 at Tafuna-Leone Plain wells. Note: Rapid water level response due to high-rainfall events.

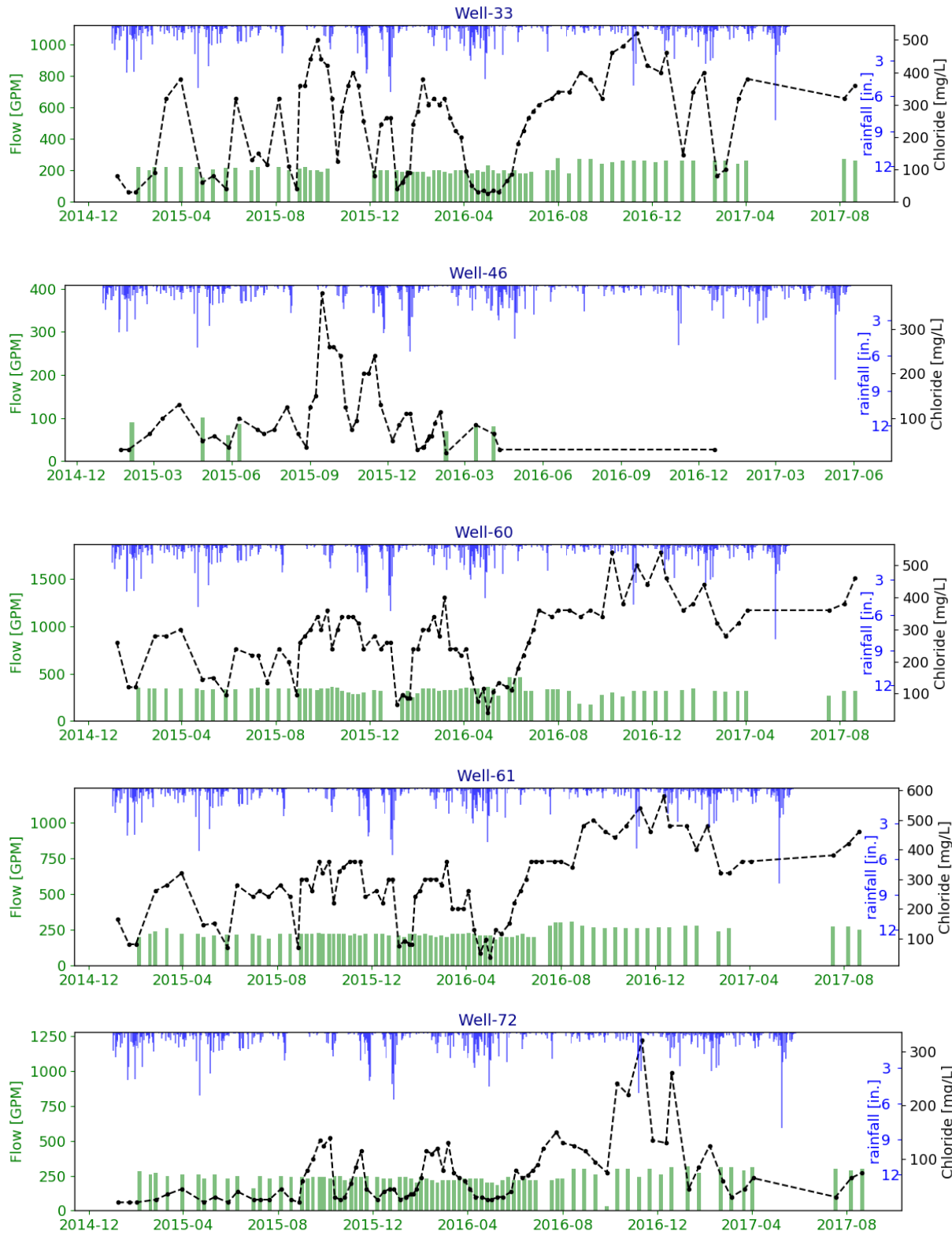


Figure B46: Plots of pump rates (*green bars*), Cl<sup>-</sup> values (*black line*), and rainfall (*blue bars*) for each active well in the Tafuna Wellfield for the period 2015-2017.

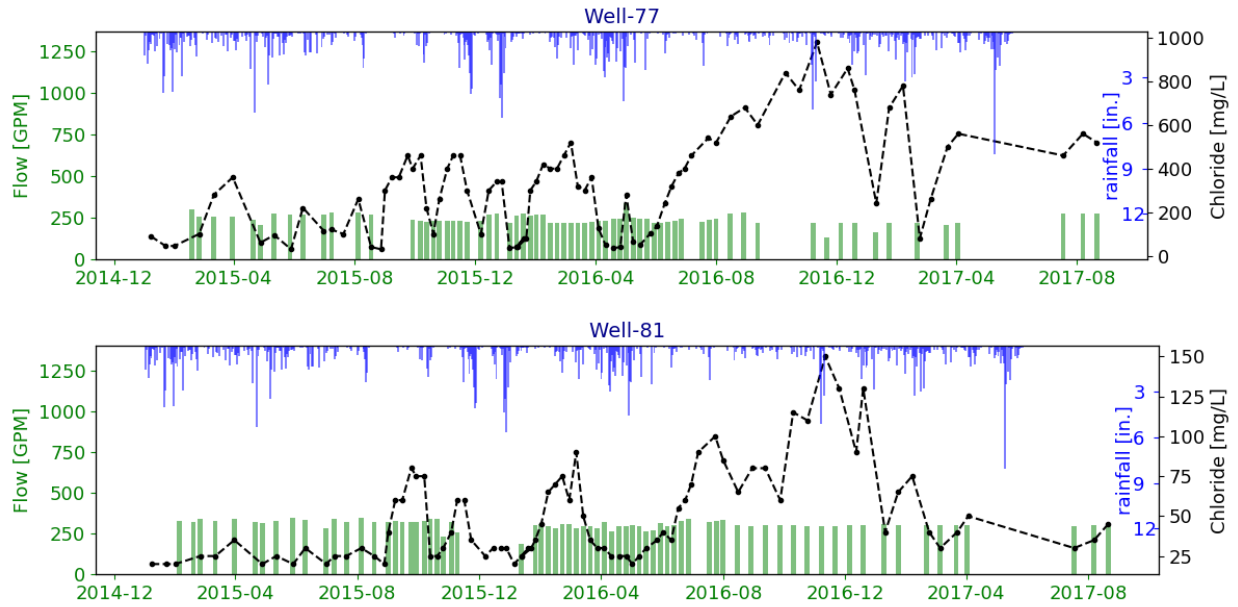


Figure B46 continued: Plots of pump rates (*green bars*), Cl<sup>-</sup> values (*black line*), and rainfall (*blue bars*) for each active well in the Tafuna Wellfield for the period 2015-2017.

## REFERENCES: Chapter 1 and Appendices A and B

- Addison, D.J. 2014. *Late-Holocene Volcanics on Tutuila Island, American Samoa: an archaeological perspective on their chronological and spatial distribution*. Report prepared for American Samoa Power Authority, Pago Pago, American Samoa.
- Addison, D.J., and T.S. Asaua. 2006. One hundred new dates from Tutuila and Manu'a: additional data addressing chronological issues in Samoan prehistory. *The Journal of Samoan Studies* 2:95–117.
- American Samoa Department of Commerce (ASDOC). 2013. *2013 Statistical yearbook for American Samoa*. Pago Pago, American Samoa.
- American Samoa Environmental Protection Agency (ASEPA). 2010. *Territory of American Samoa integrated water quality monitor and assessment report*. [305[b] report]. Pago Pago, American Samoa.
- American Samoa Environmental Protection Agency (ASEPA). 2016. *Territory of American Samoa Integrated water quality monitor and assessment report*. [305[b] report]. Pago Pago, American Samoa.
- American Samoa Power Authority (ASPA). (2013). Documentation of Wellhead Analysis, Tutuila Hydrogeological Analysis for the U.S. EPA Clean Water Act – State Revolving Fund ASPA Consolidated Grant for the benefit of the Territory of American Samoa. Report prepared for American Samoa Power Authority, Pago Pago, American Samoa. By Walters, M.O.
- Bassiouni, M., and D.S. Oki. 2013. Trends and shifts in streamflow in Hawaii, 1913–2008. *Hydrological Processes* 27(10): 1484–1500.
- Bentley, C.B. 1975. *Ground-water resources of American Samoa with emphasis on the Tafuna-Leone Plain, Tutuila Island*. US Geological Survey Report No. 75-29.
- Betancur, T., Palacio C.A., Escobar, J.F. (2012). Conceptual models in hydrogeology, methodology and results. In *Hydrogeology-A Global Perspective*. InTech.
- Burger, I. L., and J.A. Maciolek. 1981. Map inventory of nonmarine aquatic resources of American Samoa with on-site biological annotations. Review draft. US Fish and Wildlife Service Report. National Fisheries Research Center, Seattle, Washington. Available at Hamilton Library, Pacific Collection, University of Hawaii, Honolulu.
- Custodio, E., 1989. Groundwater characteristics and problems in volcanic rock terrains. *Isotopic Techniques in the Study of the Hydrology of Fractures and Fissured Rocks*. IAEA, Vienna, pp. 87–137.
- Custodio, E., & Cabrera, M. C. 2008. Synthesis of the Canary Islands hydrogeology. *Hydrogeology of volcanic rocks, SIHD-2008, Djibouti*, 51-56.

- Daly, C., J. Smith, M. Doggett, M. Halbleib, and W. Gibson. 2006. *High-resolution climate maps for the Pacific basin islands, 1971–2000. Final Report*. National Park Service, Pacific West Regional Office.
- Davis, D.A. 1963. *Ground-water reconnaissance of American Samoa*. U.S. Geological Survey Water-Supply Paper 1608-C.
- Eyre, P. 1994. *Ground-water quality reconnaissance, Tutuila, American Samoa, 1989*. U.S. Department of the Interior, US Geological Survey Report. Honolulu, HI.
- Eyre, P., and G. Walker. 1991. *Geology and ground-water resources of Tutuila American Samoa*. Unpublished report in American Samoa Power Authority files.
- Eyre, P., and G. Walker. 1993. *Geology and ground-water resources of Tutuila American Samoa (revised)*. Unpublished report in American Samoa Power Authority files.
- Fackrell, J. K. 2016. *Geochemical evolution of Hawaiian groundwater* (Doctoral dissertation, University of Hawai'i at Manoa).
- Freeze, R.A., and J.A. Cherry. 1979. *Groundwater*. Prentice-Hall: Englewood Cliffs, New Jersey, 604 p.
- Geologica Geothermal Group, Inc. 2014. *Phase 2 evaluation of the geothermal resource potential of Tutuila Island, American Samoa*. Report Prepared for the American Samoa Power Authority. San Francisco, California.
- Geologica Geothermal Group, Inc. 2016. *Tutuila Holocene Rift Zone Phase 3 geothermal exploration final report*. Report Prepared for the American Samoa Power Authority. San Francisco, California.
- Halford, K. J., & Kuniandy, E. L. 2002. Documentation of spreadsheets for the analysis of aquifer-test and slug-test data. U.S. Geological Survey, Branch of Information Services, Open-File Report No. No. 2002-197.
- Houk, P., Benavente, D., Johnson, S., 2013. Watershed-based coral reef monitoring across Tutuila, American Samoa - Summary of decadal trends and 2013 assessment.
- Izuka, S.K. 1996. *Summary of ground-water and rainfall data for Tutuila and Aunu'u Islands, American Samoa, for July, 1984 through September, 1995*. U.S. Geological Survey, Earth Science Information Center, Open-File Report No. 96-116.
- Izuka, S.K. 1997. *Summary of ground-water data for Tutuila and Aunu'u, American Samoa, for July 1985 through September 1996*. U.S. Geological Survey, Branch of Information Services, Open-File Report No. 97-654.
- Izuka, S.K. 1999a. *Summary of ground-water data for Tutuila and Aunu'u, American Samoa, for October 1987 Through September 1997*. U.S. Geological Survey, Pacific Islands Water Science Center, Open-File Report No. 99-252.

- Izuka, S.K. 1999b. *Hydrogeologic interpretations from available ground-water data, Tutuila, American Samoa*. U.S. Geological Survey, Water-Resources Investigations Report No. 96-116.
- Izuka, S. K., & Gingerich, S. B. 2003. A thick lens of fresh groundwater in the southern Lihue Basin, Kauai, Hawaii, USA. *Hydrogeology Journal*, 11(2), 240-248.
- Izuka, S.K., J.A. Perreault, and T.K. Presley. 2007. *Areas contributing recharge to wells in the Tafuna-Leone Plain, Tutuila, American Samoa*. U.S. Geological Survey Scientific Investigations Report 2007-5167. [<http://pubs.usgs.gov/sir/2007/5167/>].
- Jacob, C. E. (1947). Drawdown test to determine effective radius of artesian well. *Transactions of the American Society of Civil Engineers*, 112(1), 1047-1064.
- Johnson, R.H. 1977. *Exploration of three submarine volcanos in the South Pacific*. Hawaii Institute of Geophysics Report, University of Hawaii. Honolulu, HI.
- Join, J. L., Folio, J. L., Bourhane, A., & Comte, J. C. 2016. Groundwater Resources on Active Basaltic Volcanoes: Conceptual Models from La Réunion Island and Grande Comore. In *Active Volcanoes of the Southwest Indian Ocean* (pp. 61-70). Springer Berlin Heidelberg.
- Keating, B.H., and B.R. Bolton (eds). 1992. *Geology and Offshore Mineral Resources of the Central Pacific Basin*, Volume 14. Springer Science & Business Media: New York.
- Kennedy, Jenks, and Chilton Consulting Engineers. 1987. *Groundwater contamination study Tafuna-Leone Plain Tutuila Island*. Final report for the Environmental Quality Commission, Office of the Governor, Tutuila, American Samoa. 168 p.
- Knight Enterprises Inc. 2014. *Assessment for alternative water resources on Tutuila, American Samoa*. Report submitted to American Samoa Power Authority. Honolulu, HI. Author: Michael D. Knight
- Koppers, A.A., J.A. Russell, M.G. Jackson, J. Konter, H. Staudigel, and S.R. Hart. 2008. Samoa reinstated as a primary hotspot trail. *Geology* 36(6): 435-438.
- Lau, L. K. S., & Mink, J. F. 2006. *Hydrology of the Hawaiian Islands*. University of Hawaii Press.
- Lim, E., L.A. Taylor, B.W. Eakins, K.S. Carignan, P.R. Grothe, R.J. Caldwell, and D.Z. Friday 2010. *Digital elevation models of Pago Pago, American Samoa: procedures, data sources and analysis*. NOAA Technical Memorandum NESDIS NGDC-36, Dept. of Commerce, Boulder, CO.
- Machesky, L.F. 1965. Gravity relations in American Samoa and the Society Islands. *Pacific Science* 19(3): 367-373.
- Mayor, A.G. 1920. The reefs of Tutuila, Samoa, in their relation to coral reef theories. *Proceedings of the American Philosophical Society* 59(3): 224-236.
- McDougall, I. 1985. Age and evolution of the volcanoes of Tutuila, American Samoa. *Pac. Sci.* 39 (1987): 311- 320.

- National Parks Service (NPS). 2008. *National Park of American Samoa geologic resource evaluation report*. National Park Service Report. No. 2008/025. Denver, Colorado: Geologic Resources Division.
- National Weather Service (NWS). 2000. *Precipitation records from 1971–2000*. Data Set.
- Natland, J.H. 1980. The progression of volcanism in the Samoan linear volcanic chain. *Am. J. Sci.* 280:709–735.
- Natland, J.H. 2003. The Samoan Chain: a shallow lithospheric fracture system. <http://www.mantleplumes.org/Samoa.html>
- Nunn, P.D., 1998. Sea-level changes over the past 1,000 years in the Pacific. *Journal of Coastal Research*, pp.23-30.
- Pedersen Planning Consultants, 2004 Malaeimi Valley Special Management Area Proposal. Report to: American Samoa Environmental Protection Agency Granby, CO. Edna Buchan
- Perreault, J.A. 2010. *Development of a water budget in a tropical setting accounting for mountain front recharge*. Masters Thesis, University of Hawaii at Manoa. Honolulu, HI.
- Regional Consultation Workshop on Water (RCWW). 2002. Proceedings of the Pacific Regional Consultation on Water in Small Island Countries – American Samoa Briefing Paper Sigatoka, Fiji, 29 July–3 August 2002.
- Reinhard, A.A., Jackson, M.G., Blusztajn, J., Koppers, A.A., Simms, A.R. and Konter, J.G., 2019. “Petit Spot” Rejuvenated Volcanism Superimposed on Plume-Derived Samoan Shield Volcanoes: Evidence From a 645-m Drill Core From Tutuila Island, American Samoa. *Geochemistry, Geophysics, Geosystems*.
- Rhodes, A.L., Guswa, A.J., Newell, S.E., 2006, Seasonal variation in the stable isotopic composition of precipitation in the tropical montane forests of Monteverde, Costa Rica: *Water Resources Research*, v. 42, 17 p.
- Scholl, M.A., S.E. Ingebritsen, C.J. Janik, and J.P. Kauahikaua. 1996. Use of precipitation and groundwater isotopes to interpret regional hydrology on a tropical volcanic island: Kilauea volcano area, Hawaii. *Water Resources Research* 32, no. 12: 3525--3537.
- Scholl, M.A., Gingerich, S.B., Tribble, G.W., 2002, The influence of microclimates and fog on stable isotope signatures used in interpretation of regional hydrology: East Maui, Hawaii: *Journal of Hydrology*, v. 264, p. 170-184.
- Shuler, C., A. El-Kadi, and H. Dulaiova. 2014. *Hunting for high-level groundwater on Tutuila, American Samoa*. Poster Presentation at the 2014 GSA Annual Meeting in Vancouver, British Columbia.
- Shuler, C. K., El-Kadi, A. I., Dulai, H., Glenn, C. R., & Fackrell, J. (2017). Source partitioning of anthropogenic groundwater nitrogen in a mixed-use landscape, Tutuila, American Samoa. *Hydrogeology Journal*, 25(8), 2419-2434.

- Snow, D. D., & Spalding, R. F. (1997). Short-term aquifer residence times estimated from  $^{222}\text{Rn}$  disequilibrium in artificially-recharged ground water. *Journal of environmental radioactivity*, 37(3), 307-325.
- Stearns, H.T. 1944. Geology of the Samoan islands. *Geological Society of America Bulletin* 55(11): 1279-1332.
- Takasaki, K.J., and J.F. Mink. 1985. *Evaluation of major dike-impounded ground-water reservoirs, Island of Oahu*. Washington, DC: US Government Printing Office.
- Tarling, D.H. 1966. The palaeomagnetism of the Samoan and Tongan Islands. *Geophysical Journal International* 10(5): 497-513.
- Tribble, Gordon, 2008, Ground water on tropical Pacific Islands--understanding a vital resource: U.S. Geological Survey Circular 1312, 35 p. <https://pubs.usgs.gov/circ/1312/>.
- Walker, G.P. 1991. Structure, and origin by injection of lava under surface crust, of tumuli, "lava rises", "lava-rise pits", and "lava-inflation clefts" in Hawaii. *Bulletin of Volcanology* 53(7): 546-558.
- Walker, G.P., and P.R. Eyre. 1995. Dike complexes in American Samoa. *Journal of Volcanology and Geothermal Research* 69(3): 241-254.
- Whitall, D.R., Rice, S.H., 2015. Pollution in surface sediments in Faga'alu Bay, Tutuila, American Samoa. NOAA Technical Memorandum NOS NCCOS 201. Silver Spring, MD. 54 pp. [https://coastalscience.noaa.gov/data\\_reports/pollution-in-surface-sediments-in-fagaalu-bay-tutuila-american-samoa/t](https://coastalscience.noaa.gov/data_reports/pollution-in-surface-sediments-in-fagaalu-bay-tutuila-american-samoa/t) (accessed 2019-03-13).
- Wong, M.F. 1996. *Analysis of streamflow characteristics for streams on the island of Tutuila, American Samoa*. US Geological Survey Water Resources Investigations Report No. 95-4185, Honolulu, HI.
- Zangar, C.N. 1953. *Theory and problems of water percolation*. U.S. Department of the Interior and Bureau of Reclamation Report Engineering Monograph No. 8.

# Appendix C: Supplementary Data

## C1 Chapter 3

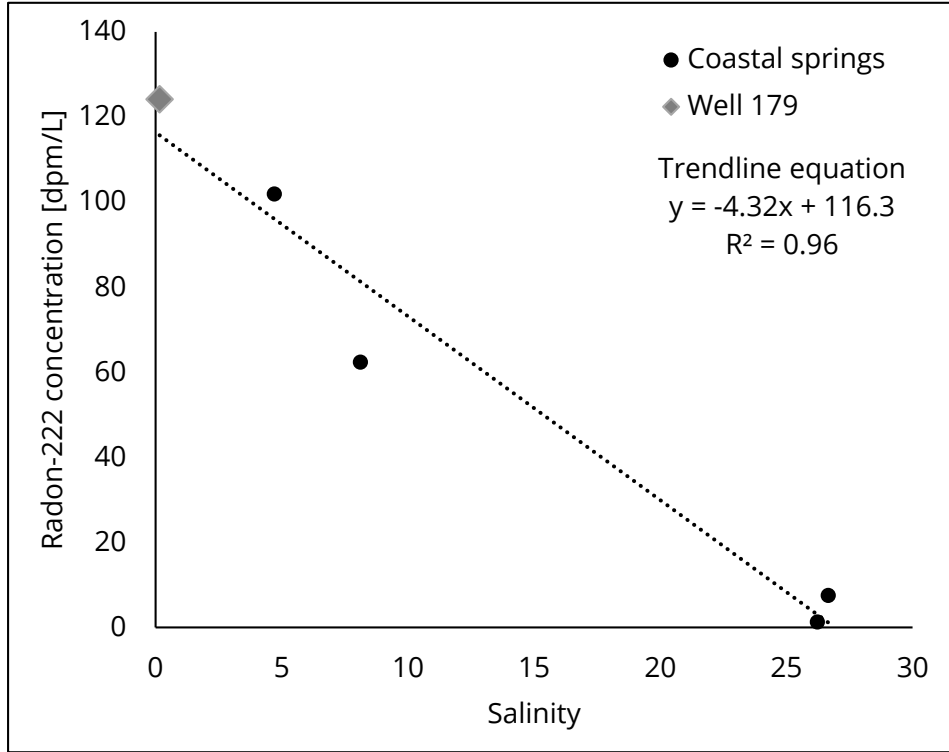


Figure C1: Plot of coastal spring and well water salinity against  $^{222}\text{Rn}$  concentrations. A linear trend indicates conservative mixing of high  $^{222}\text{Rn}$  fresh-groundwater with low  $^{222}\text{Rn}$  but high salinity seawater. The y-intercept of the regression line indicates the  $^{222}\text{Rn}$  concentration of the fresh end-member, which is nearly equivalent to the  $^{222}\text{Rn}$  concentration measured in the only well in the valley, Well 179.

Table C1: Streamflow data measured during stream survey on July 1, 2014. Coordinates are in WGS 84 datum.

Site Name	Latitude	Longitude	Distance from coast [m]	<sup>222</sup> Rn [dpm/L]	Flow [CFS]	Flow [m <sup>3</sup> /d]
S10	-14.2888	-170.6910	993	-	1.12	2,742
S9	-14.2887	-170.6906	957	-	1.01	2,474
S8	-14.2896	-170.6893	741	-	0.77	1,881
S7	-14.2900	-170.6881	597	-	0.82	2,017
S6	-14.2901	-170.6877	553	10.1	0.94	2,305
S5	-14.2905	-170.6869	453	6.4	1.23	3,021
S4	-14.2908	-170.6867	409	6.4	1.23	3,021
S3	-14.2915	-170.6852	231	6.3	1.11	2,720
S2	-14.2915	-170.6847	183	15.7	1.07	2,610
S1	-14.2913	-170.6834	42	42.5	1.44	3,517
<b>Average Flow</b>					<b>1.06</b>	<b>2,631</b>

Table C2: Streamflow data measured during stream survey on August 10, 2016. Coordinates are in WGS 84 datum. Note not all sites from 2014 were re-measured, and one additional site (S11) located at the western margin of the quarry was added.

Site Name	Latitude	Longitude	Distance from coast [m]	<sup>222</sup> Rn [dpm/L]	Flow [CFS]	Flow [m <sup>3</sup> /d]
S11	-14.28813	-170.69337	1,234	28.9	0.97	2,384
S10	-14.2888	-170.6910	993	34.3	1.03	2,531
S9	-	-	-	-	-	-
S8	-14.2896	-170.6893	741	14.9	0.81	1,969
S7	-	-	-	-	-	-
S6	-14.2901	-170.6877	553	19.2	0.97	2,367
S5	-	-	-	-	-	-
S4	-14.2908	-170.6867	409	18.8	0.94	2,289
S3	-	-	-	-	-	-
S2	-14.2915	-170.6847	183	85.1	1.18	2,894
S1	-14.2913	-170.6834	42	121.8	1.48	3,628
<b>Average Flow</b>					<b>1.05</b>	<b>2,581</b>

Table C3: Sensitivity test results for SWAT flow parameters. Note that lower p-value and higher absolute magnitude of t-Stat indicates the model is more sensitive to the given parameter. Table is sorted in order of most to least sensitive parameters.

<b>Parameter code</b>	<b>Parameter</b>	<b>t-Stat</b>	<b>p-Value</b>
CN2	SCS runoff curve number.	25.400	0.000
CH_K2	Effective hydraulic conductivity in main channel alluvium.	8.063	0.000
GWQMN	Threshold depth in the shallow aquifer for return flow to occur.	2.305	0.021
GW_REVAP	Groundwater "revap" coefficient.	-2.063	0.039
ALPHA_BF	Baseflow alpha factor.	-2.015	0.044
LAT_TTIME	Lateral flow travel time.	1.935	0.053
SOL_Z	Depth from soil surface to bottom of layer.	-1.493	0.136
RCHRG_DP	Deep aquifer percolation fraction.	1.307	0.192
HRU_SLP	Average slope steepness.	-1.229	0.220
SOL_AWC	Available water capacity of the soil layer.	-0.918	0.359
EPCO	Plant uptake compensation factor.	0.895	0.371
SURLAG	Surface runoff lag time.	-0.873	0.383
REVAPMN	Threshold depth of water in shallow aquifer for "revap" to occur.	0.776	0.438
SOL_K	Saturated hydraulic conductivity.	0.562	0.574
ESCO	Soil evaporation compensation factor.	-0.311	0.756
GW_DELAY	Groundwater delay.	-0.247	0.805

Table C4: Sensitivity test results for SWAT nutrient parameters. Note that lower p-Value and higher absolute magnitude of t-Stat indicates the model is more sensitive to the given parameter. Table is sorted in order of most to least sensitive parameters.

<b>Parameter code</b>	<b>Parameter</b>	<b>t-Stat</b>	<b>p-Value</b>
FILTERW	Width of edge-of field filter strip.	-18.501	0.000
SDNCO	Denitrification threshold water content.	-2.948	0.003
BC3	Rate constant for hydrolysis of organic N to NH4 in the reach.	2.420	0.016
ERORGN	Organic N enrichment ratio.	2.128	0.034
BC1	Rate constant for biological oxidation of NH4 to NO2 in the reach.	1.639	0.102
NPERCO	Nitrogen percolation coefficient.	1.622	0.105
RS3	Benthic source rate for NH4-N in the reach.	1.473	0.141
CDN	Denitrification exponential rate coefficient.	1.313	0.190
P_N	Algal preference factor for ammonia.	-1.258	0.209
BIOMIX	Biological mixing efficiency	1.240	0.216
AI2	Fraction of algal biomass that is phosphorus.	-1.180	0.238
RSDCO	Residue decomposition coefficient.	1.171	0.242
RS4	Rate coefficient for organic N settling in the reach.	1.096	0.274
BC2	Rate constant for biological oxidation of NO2 to NO3 in the reach.	1.033	0.302
CMN	Rate factor for humus mineralization of active organic nitrogen.	0.990	0.323
SOL_CBN	Organic carbon content.	-0.876	0.382
BC4	Rate constant for mineralization of organic P to dissolved P.	0.734	0.463
HLIFE_N	Half-life of nitrogen in groundwater.	-0.669	0.504
RS5	Organic phosphorus settling rate in the reach.	-0.549	0.583
N_UPDIS	Nitrogen uptake distribution parameter.	-0.483	0.629
SOL_ORGN	Initial organic N concentration in the soil layer.	0.412	0.681
AI1	Fraction of algal biomass that is nitrogen.	0.388	0.698
RCN	Concentration of nitrogen in rainfall.	0.190	0.849
RS2	Benthic sediment source rate for dissolved phosphorus in the reach.	-0.149	0.881
ANION_EXCL	Fraction of porosity (void space) from which anions are excluded.	-0.089	0.929

## C2 Chapter 4

Table C5: Coastal surface water geochemical data

Sample ID	Date	Latitude	Longitude	Salinity	DIN [ $\mu\text{mol/L}$ ]	TDN [ $\mu\text{mol/L}$ ]	PO4 [ $\mu\text{mol/L}$ ]	Silicate [ $\mu\text{mol/L}$ ]	D <sup>15</sup> N [‰]	D <sup>18</sup> O [‰]
V-C-1	8/17/2016	-14.24867	-170.67504	31.0	27.1	29.5	2.6	183	11.1	1.5
V-C-2	8/17/2016	-14.25049	-170.67503	34.0	1.6	7.4	0.4	17	10.8	1.0
V-C-3	8/17/2016	-14.24918	-170.67092	35.8	1.1	5.6	0.2	0	-	-
V-C-4	8/17/2016	-14.24978	-170.67020	32.6	0.6	5.4	1.0	2	-	-
V-C-5	8/17/2016	-14.25069	-170.67132	35.6	1.3	6.3	0.3	8	-	-
V-C-6	8/17/2016	-14.25055	-170.67233	33.2	0.4	5.9	0.2	3	-	-
V-C-7	8/17/2016	-14.24688	-170.67423	35.3	1.3	6.7	0.2	2	-	-
V-C-8	8/17/2016	-14.24827	-170.67218	35.5	2.2	6.6	0.4	5	9.1	0.1
V-C-9	8/17/2016	-14.24987	-170.67496	33.8	2.6	6.8	0.4	5	9.6	-1.7
V-C-10	8/17/2016	-14.24970	-170.67500	35.3	3.1	6.7	0.5	6	9.6	0.3
V-C-11	8/17/2016	-14.25003	-170.67504	35.2	2.1	7.2	0.4	6	-	-
V-C-12	8/17/2016	-14.24734	-170.67378	33.6	0.4	5.5	0.2	1	-	-
V-C-13	8/17/2016	-14.24732	-170.67392	35.4	1.2	5.0	0.2	1	-	-
V-C-14	7/27/2015	-14.24925	-170.67526	33.2	0.8	5.7	0.3	13	-	-
V-C-15	7/27/2015	-14.24596	-170.67296	34.6	1.3	13.4	0.3	3	-	-
V-C-16	7/27/2015	-14.24682	-170.67432	35.3	0.5	5.4	0.2	6	-	-
V-C-17	7/27/2015	-14.25046	-170.67507	33.0	1.6	6.3	0.3	18	-	-
V-C-18	7/27/2015	-14.25083	-170.67387	33.1	0.4	5.3	0.3	16	-	-
V-C-19	7/27/2015	-14.25067	-170.67086	31.5	1.0	5.6	0.4	38	-	-
V-C-20	7/27/2015	-14.24980	-170.67024	34.7	0.6	6.2	0.2	3	-	-
V-C-21	7/27/2015	-14.24921	-170.67083	34.8	0.8	5.6	0.2	2	-	-
V-C-22	7/27/2015	-14.24515	-170.66791	34.6	0.5	5.3	0.2	3	-	-
V-C-23	7/27/2015	-14.24723	-170.67332	34.6	0.8	5.6	0.2	2	-	-
V-C-24	7/27/2015	-14.25010	-170.67395	33.8	0.9	5.6	0.3	11	-	-
O-C-1	8/18/2016	-14.25248	-170.64336	35.4	1.4	6.4	0.2	5	6.7	-0.7
O-C-2	8/18/2016	-14.25294	-170.64234	34.0	0.4	6.4	0.3	23	-	-
O-C-3	8/18/2016	-14.25264	-170.64117	35.5	1.5	6.6	0.2	9	8.5	3.6
O-C-4	8/18/2016	-14.25249	-170.64224	35.8	1.1	5.5	0.3	1	-	-
O-C-5	8/18/2016	-14.25223	-170.64227	35.9	1.1	5.1	0.2	0	6.2	1.6
O-C-6	8/18/2016	-14.25154	-170.64219	36.0	1.0	5.2	0.2	0	-	-
O-C-7	8/18/2016	-14.25306	-170.64232	0.0	6.5	8.8	2.6	219	6.9	-2.5
O-C-8	8/18/2016	-14.24807	-170.64178	0.0	0.7	5.4	0.2	0	-	-
O-C-9	7/28/2015	14.24472	170.64095	34.9	0.0	5.2	0.2	1	-	-
O-C-10	7/28/2015	14.25289	170.64245	34.3	0.3	6.2	0.2	14	-	-
O-C-11	7/28/2015	-14.25151	-170.64071	34.9	0.5	5.4	0.2	2	-	-
O-C-12	7/28/2015	-14.25268	-170.64124	34.1	0.9	6.4	0.3	15	-	-
O-C-13	7/28/2015	-14.25307	-170.64243	21.6	2.5	7.1	1.7	162	-	-
O-C-14	7/28/2015	-14.25272	-170.64327	34.7	0.8	6.5	0.2	6	-	-
O-C-15	7/28/2015	-14.25191	-170.64401	34.9	0.5	5.6	0.2	2	-	-
O-C-16	7/28/2015	-14.25237	-170.64217	34.6	0.4	5.9	0.2	6	-	-
O-C-17	7/28/2015	-14.25187	-170.64211	35.0	1.0	6.6	0.2	1	-	-
P-C-1	8/16/2016	-14.31781	-170.71644	13.4	34.4	44.4	2.1	302	8.9	0.2
P-C-2	8/16/2016	-14.31983	-170.71512	12.8	48.5	57.7	2.1	368	8.5	-0.2
P-C-3	8/16/2016	-14.32414	-170.71252	22.3	12.7	25.8	1.1	174	9.6	3.3
P-C-4	8/16/2016	-14.32419	-170.70240	31.2	0.9	5.1	0.5	39	-	-
P-C-5	8/16/2016	-14.32074	-170.71161	33.6	1.9	6.4	0.4	32	6.6	-0.4
P-C-6	8/16/2016	-14.32442	-170.69969	33.2	2.0	6.6	0.3	23	8.0	-0.5
P-C-7	8/16/2016	-14.32293	-170.70649	33.2	0.7	5.8	0.3	21	-	-
P-C-8	8/16/2016	-14.32116	-170.71414	24.8	7.7	11.2	0.9	92	8.0	2.3
P-C-9	8/16/2016	-14.32528	-170.70093	33.7	0.7	7.0	0.2	23	-	-

P-C-10	7/26/2015	-14.31985	-170.71513	21.2	24.5	30.4	1.3	185	-	-
P-C-11	7/26/2015	-14.31786	-170.71648	15.3	11.3	30.5	1.4	258	-	-
P-C-12	7/26/2015	-14.32184	-170.71333	31.5	1.6	6.5	0.5	46	-	-
P-C-13	7/26/2015	-14.32418	-170.71269	32.1	1.2	5.5	0.4	37	-	-
P-C-14	7/26/2015	-14.32560	-170.71022	32.8	0.9	5.1	0.4	28	-	-
P-C-15	7/26/2015	-14.32434	-170.70026	34.9	0.6	5.7	0.2	1	-	-
P-C-16	7/26/2015	-14.32412	-170.70247	33.4	0.6	5.5	0.3	19	-	-
P-C-17	7/26/2015	-14.32356	-170.70946	32.4	0.7	5.1	0.4	32	-	-
P-C-18	7/26/2015	-14.32187	-170.71156	32.2	1.1	5.7	0.4	36	-	-
P-C-19	7/26/2015	-14.31899	-170.71466	23.9	14.3	20.4	0.9	149	-	-
P-C-20	7/26/2015	-14.31722	-170.71172	25.4	0.3	6.6	0.6	131	-	-
P-C-21	7/26/2015	-14.31695	-170.70698	28.5	0.6	6.1	0.6	87	-	-
F-C-1	8/19/2016	-14.28937	-170.68127	35.3	1.6	5.8	0.4	10	6.2	-2.0
F-C-2	8/19/2016	-14.29118	-170.68252	32.2	2.3	6.4	1.3	38	7.6	-0.7
F-C-3	8/19/2016	-14.29229	-170.68091	32.9	5.3	12.5	5.6	152	-	-
F-C-4	8/19/2016	-14.29306	-170.67956	31.2	3.4	9.7	4.3	118	7.8	0.3
F-C-5	8/19/2016	-14.29105	-170.68074	35.4	2.2	6.1	0.7	18	9.4	2.8
F-C-6	8/19/2016	-14.28942	-170.67939	35.6	2.6	7.3	0.4	1	9.3	-1.1
F-C-7	8/19/2016	-14.28995	-170.67783	35.9	2.3	5.7	0.3	1	9.1	-1.3
F-C-8	8/19/2016	-14.29084	-170.67908	35.9	3.2	8.0	0.4	1	9.7	-0.8
F-C-9	8/19/2016	-14.29180	-170.67832	0.0	3.0	6.8	0.3	1	9.5	-1.3
F-C-10	8/19/2016	-14.29520	-170.67678	0.0	1.8	6.3	0.2	2	9.1	-1.3
F-C-11	8/19/2016	-14.29164	-170.68136	31.5	3.3	7.8	1.9	72	9.0	-0.4
F-C-12	8/19/2016	-14.29164	-170.68136	31.8	3.8	7.8	2.3	82	-	-
F-C-13	8/19/2016	-14.29164	-170.68136	31.8	4.5	8.5	3.2	112	7.5	0.5
F-C-14	8/19/2016	-14.29306	-170.67956	35.9	1.6	6.1	0.3	2	8.6	-1.9
F-C-15	8/19/2016	-14.29306	-170.67956	35.9	1.4	5.4	0.2	2	-	-
F-C-16	8/19/2016	-14.29306	-170.67956	35.9	1.6	6.2	0.3	2	-	-
F-C-17	7/29/2015	-14.29229	-170.68093	34.8	1.0	6.0	0.2	3	-	-
F-C-18	7/29/2015	-14.29321	-170.67944	34.9	0.9	6.1	0.2	2	-	-
F-C-19	7/29/2015	-14.29198	-170.68257	15.7	7.9	11.5	2.1	255	-	-
F-C-20	7/29/2015	-14.29140	-170.68263	2.0	11.1	13.6	3.4	451	-	-
F-C-21	7/29/2015	-14.29121	-170.68250	26.3	4.1	8.9	1.3	123	-	-
F-C-22	7/29/2015	-14.28939	-170.68133	27.6	2.9	8.3	1.2	109	-	-
F-C-23	7/29/2015	-14.28900	-170.67948	34.7	1.5	6.8	0.3	3	-	-
F-C-24	7/29/2015	-14.28996	-170.67786	34.9	1.3	6.2	0.3	1	-	-
F-C-25	7/29/2015	-14.29172	-170.67960	35.0	1.3	6.1	0.3	1	-	-
F-C-26	7/29/2015	-14.29095	-170.68104	34.4	1.2	6.0	0.3	9	-	-
OUT-F-C-1	8/19/2016	-14.28310	-170.67561	35.9	0.3	5.5	0.2	0	-	-

Notes: Site Id's are coded to indicate study location, F – Fagaalu, P – Pala, V – Vatia, and O – Oa, sample type, C – coastal surface water, and sample number of each type at each location.

Table C6: Coastal spring water geochemical data

Sample ID	Date	Latitude	Longitude	Salinity	DIN [ $\mu\text{mol/L}$ ]	TDN [ $\mu\text{mol/L}$ ]	PO <sub>4</sub> [ $\mu\text{mol/L}$ ]	Silicate [ $\mu\text{mol/L}$ ]	D <sup>15</sup> N [‰]	D <sup>18</sup> O [‰]	Radon [dpm/L]
F-CSP-1	8/19/2016	-14.28879	-170.68079	14.11	18.0	23.8	3.5	246.1	-	-	91
F-CSP-2	8/19/2016	-14.29294	-170.68039	28.4	6.5	10.0	1.7	69.2	-	-	32
F-CSP-3	7/30/2015	-14.28943	-170.68154	5.71	19.1	19.3	5.4	579.5	5.6	-2.7	257
F-CSP-4	7/9/2014	-14.29316	-170.68007	26.23	7.9	13.8	2.1	116.9	-	-	1
F-CSP-5	7/9/2014	-14.29173	-170.68298	9.55	12.0	18.0	2.5	144.7	7.5	2.2	1
F-CSP-6	7/9/2014	-14.29046	-170.68234	8.12	10.9	13.8	6.7	231.7	-	-	62
F-CSP-7	7/15/2014	-14.29316	-170.68008	26.66	10.4	13.9	1.1	144.1	5.5	0.3	7
F-CSP-8	7/15/2014	-14.28960	-170.68167	4.71	57.3	53.0	3.8	453.9	7.1	-0.5	102
O-CSP-1	8/18/2016	-14.25314	-170.64247	15.97	6.7	10.9	2.9	264.8	6.9	-3.4	131
O-CSP-2	8/18/2016	-14.25314	-170.64247	22.13	6.3	9.9	2.6	181.9	6.3	-3.5	112
O-CSP-3	8/18/2016	-14.25264	-170.64337	27.17	4.4	6.8	0.9	141.2	4.4	-2.1	111
O-CSP-4	7/28/2015	-14.25275	-170.64335	26	6.7	12.3	0.4	128.7	4.6	-0.4	
O-CSP-5	7/28/2015	-14.25314	-170.64244	6.94	6.2	7.3	3.1	328.0	6.5	-3.8	189
P-CSP-1	8/14/2016	-14.31969	-170.71535	5.13	22.9	65.3	1.5	267.4	7.9	-0.2	141
P-CSP-2	7/15/2015	-14.31969	-170.71535	3.36	68.8	69.7	2.0	392.8	8.9	0.4	142
P-CSP-3	7/25/2014	-14.32567	-170.71036	26.55	10.1	13.0	1.3	116.1	-	-	-
P-CSP-4	7/25/2014	-14.32214	-170.71335	26.15	28.1	35.3	1.0	130.2	-	-	20
P-CSP-5	7/25/2014	-14.31973	-170.71533	7.64	66.4	68.2	1.5	366.5	9.2	0.5	36
P-CSP-6	7/25/2014	-14.31865	-170.71635	17.81	24.6	25.4	1.6	294.4	-	-	28
P-CSP-7	7/25/2014	-14.32095	-170.71443	15.53	69.3	73.0	1.2	244.8	8.3	0.5	23
P-CSP-8	7/25/2014	-14.32198	-170.71344	31.55	8.1	10.5	0.6	62.5	8.8	0.7	6
V-CSP-1	8/15/2016	-14.25116	-170.67168	0.46	11.9	15.9	2.7	545.4	7.3	-1.4	572
V-CSP-2	8/15/2016	-14.24872	-170.67531	6.32	41.3	49.4	3.3	363.4	14.3	2.8	272
V-CSP-3	7/23/2015	-14.24916	-170.67542	0.325	29.3	29.4	1.0	390.4	14.8	3.7	197.4
V-CSP-4	7/27/2015	-14.24932	-170.67540	0.93	23.7	26.1	1.5	400.6	11.1	0.8	519.9
V-CSP-5	8/7/2014	-14.24935	-170.67543	0.25	25.6	35.4	2.5	373.4	12.9	2.8	239
V-CSP-6	8/7/2014	-14.25113	-170.67171	0.41	11.5	12.5	3.4	452.1	8.6	-1.3	198

Notes: Site Id's are coded to indicate study location, F – Fagaalu, P – Pala, V – Vatia, and O – Oa, sample type, Ux- CSP – coastal spring (measured value), and sample number of each type at each location.

Table C7: Salinity-unmixed coastal spring water geochemical data

Sample ID	Date	Latitude	Longitude	Salinity	DIN [ $\mu\text{mol/L}$ ]	TDN [ $\mu\text{mol/L}$ ]	PO <sub>4</sub> [ $\mu\text{mol/L}$ ]	Silicate [ $\mu\text{mol/L}$ ]	D <sup>15</sup> N [‰]	D <sup>18</sup> O [‰]	Radon [dpm/L]
F-Ux-CSP-1	8/19/2016	-14.28879	-170.68079	0.1	29.6	39.1	5.7	409	-	-	150
F-Ux-CSP-2	8/19/2016	-14.29294	-170.68039	0.1	31.7	48.6	7.7	352	-	-	156
F-Ux-CSP-3	7/30/2015	-14.28943	-170.68154	0.1	22.7	22.9	6.4	689	5.6	-2.7	306
F-Ux-CSP-4	7/9/2014	-14.29316	-170.68007	0.1	29.7	51.7	7.5	453	-	-	-
F-Ux-CSP-5	7/9/2014	-14.29173	-170.68298	0.1	16.3	24.3	3.3	198	7.5	2.2	1
F-Ux-CSP-6	7/9/2014	-14.29046	-170.68234	0.1	14.1	17.7	8.7	300	-	-	80
F-Ux-CSP-7	7/15/2014	-14.29316	-170.68008	0.1	41.2	54.7	4.1	587	5.5	0.3	23
F-Ux-CSP-8	7/15/2014	-14.28960	-170.68167	0.1	65.9	60.9	4.3	522	7.1	-0.5	117
O-Ux-CSP-1	8/18/2016	-14.25314	-170.64247	0.1	12.0	19.2	5.1	482	6.9	-3.4	237
O-Ux-CSP-2	8/18/2016	-14.25314	-170.64247	0.1	16.1	25.3	6.7	486	6.3	-3.5	295
O-Ux-CSP-3	8/18/2016	-14.25264	-170.64337	0.1	18.1	27.2	3.4	611	4.4	-2.1	473
O-Ux-CSP-4	7/28/2015	-14.25275	-170.64335	0.1	24.6	44.9	1.0	487	4.6	-0.4	-7
O-Ux-CSP-5	7/28/2015	-14.25314	-170.64244	0.1	7.6	8.9	3.8	407	6.5	-3.8	234
P-Ux-CSP-1	8/14/2016	-14.31969	-170.71535	0.1	26.6	76.1	1.7	312	7.9	-0.2	164
P-Ux-CSP-2	7/15/2015	-14.31969	-170.71535	0.1	75.8	76.8	2.2	433	8.9	0.4	156
P-Ux-CSP-3	7/25/2014	-14.32567	-170.71036	0.1	39.8	50.5	4.6	466	-	-	-
P-Ux-CSP-4	7/25/2014	-14.32214	-170.71335	0.1	107.4	134.2	3.5	500	-	-	72
P-Ux-CSP-5	7/25/2014	-14.31973	-170.71533	0.1	84.4	86.6	1.9	466	9.2	0.5	45
P-Ux-CSP-6	7/25/2014	-14.31865	-170.71635	0.1	49.2	50.6	3.1	592	-	-	55
P-Ux-CSP-7	7/25/2014	-14.32095	-170.71443	0.1	123.2	129.6	2.0	436	8.3	0.5	40
P-Ux-CSP-8	7/25/2014	-14.32198	-170.71344	0.1	73.5	93.7	4.1	586	8.8	0.7	41
V-Ux-CSP-1	8/15/2016	-14.25116	-170.67168	0.1	12.1	16.0	2.7	551	7.3	-1.4	578
V-Ux-CSP-2	8/15/2016	-14.24872	-170.67531	0.1	50.1	59.8	3.9	441	14.3	2.8	330
V-Ux-CSP-3	7/23/2015	-14.24916	-170.67542	0.1	29.5	29.6	1.0	393	14.8	3.7	199
V-Ux-CSP-4	7/27/2015	-14.24932	-170.67540	0.1	24.3	26.7	1.5	410	11.1	0.8	532
V-Ux-CSP-5	8/7/2014	-14.24935	-170.67543	0.1	25.7	35.6	2.5	375	12.9	2.8	240
V-Ux-CSP-6	8/7/2014	-14.25113	-170.67171	0.1	11.6	12.6	3.4	456	8.6	-1.3	199

Notes: Site Id's are coded to indicate study location, F – Fagaalu, P – Pala, V – Vatia, and O – Oa, sample type, Ux-CSP – salinity unmixed coastal springs (to a salinity of 0.1), and sample number of each type at each location.

Table C8: Well water geochemical data

Sample ID	Date	Latitude	Longitude	Salinity	DIN [ $\mu\text{mol/L}$ ]	TDN [ $\mu\text{mol/L}$ ]	PO <sub>4</sub> [ $\mu\text{mol/L}$ ]	Silicate [ $\mu\text{mol/L}$ ]	D <sup>15</sup> N [‰]	D <sup>18</sup> O [‰]	Radon [dpm/L]
F-W-1	8/13/2016	-14.31969	-170.71535	0.1	7.7	11.6	8.2	719	7.0	-3.3	334
F-W-2	7/22/2015	-14.29092	-170.68910	0.1	11.3	12.3	7.2	658	6.3	-1.6	354
F-W-3	7/21/2014	-14.29092	-170.68910	0.2	11.2	13.6	8.1	632	5.4	-2.5	124
P-W-1	8/13/2016	-14.32065	-170.73203	0.2	52.9	69.8	2.9	552	7.4	-0.9	261
P-W-2	8/9/2016	-14.32436	-170.73219	0.6	47.9	66.9	1.8	619	7.2	-0.5	170
P-W-3	7/19/2015	-14.32438	-170.73213	0.2	52.0	52.6	1.1	434	7.2	-0.1	169
P-W-4	7/19/2015	-14.31756	-170.73825	0.1	42.1	42.8	1.4	495	5.6	-0.1	245
P-W-5	7/25/2015	-14.32065	-170.73203	0.1	46.3	46.0	2.5	469	6.9	-0.1	308
P-W-6	7/21/2014	-14.32438	-170.73213	0.9	83.6	78.3	1.5	556	8.2	-0.1	68
V-W-1	8/15/2016	-14.25476	-170.66857	0.1	7.3	9.0	9.2	1049	4.3	-2.2	1170
V-W-3	7/27/2015	-14.25478	-170.66858	0.1	8.0	9.2	8.6	565	4.7	-1.3	-
V-W-4	8/1/2014	-14.25478	-170.66858	0.2	9.8	10.6	8.9	734	5.7	-1.9	644

Notes: Site Id's are coded to indicate study location, F – Fagaalu, P – Pala, V – Vatia, and O – Oa, sample type, W – wells, and sample number of each type at each location.

Table C9: Stream water geochemical data

Sample ID	Date	Latitude	Longitude	Salinity	DIN [ $\mu\text{mol/L}$ ]	TDN [ $\mu\text{mol/L}$ ]	PO <sub>4</sub> [ $\mu\text{mol/L}$ ]	Silicate [ $\mu\text{mol/L}$ ]	D <sup>15</sup> N [‰]	D <sup>18</sup> O [‰]	Radon [dpm/L]
F-S-1	8/10/2016	-14.29137	-170.68379	0.1	10.0	13.0	3.4	601	-	-	122
F-S-2	7/23/2015	-14.29143	-170.68383	0.1	9.3	11.7	3.3	505	6.4	0.1	101
F-S-3	7/2/2014	-14.29153	-170.68465	0.1	7.3	11.1	3.1	518	-	-	16
O-S-1	8/18/2016	-14.25457	-170.64335	0.1	4.1	10.3	6.8	603	4.4	-2.5	23
O-S-2	7/28/2015	-14.25683	-170.64386	0.0	1.8	4.0	3.3	398	6.8	-2.5	58
P-S-1	8/11/2016	-14.31768	-170.71676	3.5	9.8	12.7	3.2	363	9.0	1.2	58
P-S-2	7/23/2015	-14.31779	-170.71791	0.1	5.5	9.7	4.2	433	7.2	-0.2	13
P-S-3	8/6/2014	-14.31800	-170.71846	0.1	9.9	14.7	4.2	415	-	-	1
V-S-1	8/16/2016	-14.25093	-170.67553	0.2	4.9	9.8	3.2	373	5.1	-5.3	29
V-S-2	8/16/2016	-14.25239	-170.67273	0.1	1.4	5.8	2.1	456	-	-	23
V-S-3	7/23/2015	-14.25094	-170.67562	0.1	2.8	7.9	2.5	328	4.2	-3.0	19
V-S-4	8/7/2014	-14.25059	-170.67525	1.1	21.8	27.7	2.8	323	-	-	43

Notes: Site Id's are coded to indicate study location, F – Fagaalu, P – Pala, V – Vatia, and O – Oa, sample type, S – streams, and sample number of each type at each location.

Table C10: Algae N and C parameter data for deployed algal samples

Sample ID	Sample year	Latitude	Longitude	Nitrogen by weight [%]	D15N [‰]	Carbon by weight [%]	Carbon to nitrogen ratio
F-Dep-Hp-1	2016	-14.289371	-170.6812731	1.6	8.2	15.2	9.5
F-Dep-Hp-2	2016	-14.291182	-170.6825189	2.3	8.3	22.4	9.6
F-Dep-Hp-3	2016	-14.292286	-170.6809127	1.7	8.7	15.7	9.2
F-Dep-Hp-4	2016	-14.293061	-170.679555	1.7	8.6	16.7	9.6
F-Dep-Hp-5	2016	-14.291047	-170.6807421	1.8	8.5	16.4	8.9
F-Dep-Hp-6	2016	-14.289422	-170.6793883	2	8.5	17.6	8.8
F-Dep-Hp-7	2016	-14.290835	-170.6790841	1.8	9.4	16.3	9.1
F-Dep-Hp-8	2016	-14.291801	-170.6783233	2.1	8.9	17.9	8.5
F-Dep-Hp-9	2016	-14.295201	-170.676782	1.7	8.2	16.5	9.7
Oa-Dep-Hp-1	2016	-14.252478	-170.6433634	1.1	6.4	15.3	13.6
Oa-Dep-Hp-2	2016	-14.25294	-170.6423413	1.3	6.4	18.2	14.5
Oa-Dep-Hp-3	2016	-14.252642	-170.6411735	1.3	6.5	16.6	12.3
Oa-Dep-Hp-4	2016	-14.252489	-170.6422443	1.5	6.6	16.4	10.8
Oa-Dep-Hp-5	2016	-14.252226	-170.6422722	1.7	6.8	17.7	10.3
Oa-Dep-Hp-6	2016	-14.251539	-170.6421883	1.4	7	16.6	11.9
Pl-Dep-Hp-1	2016	-14.32414	-170.712521	2	7.4	17.4	8.7
Pl-Dep-Hp-2	2016	-14.324187	-170.7024008	1.7	7.4	18.1	10.8
Pl-Dep-Hp-3	2016	-14.32074	-170.7116105	1.9	7.5	17	8.9
Pl-Dep-Hp-4	2016	-14.324424	-170.6996857	1.6	7.2	15.1	9.3
Pl-Dep-Hp-5	2016	-14.322926	-170.7064932	1.6	7.1	15.5	9.5
Pl-Dep-Hp-6	2016	-14.321162	-170.7141373	2.3	7.5	20	8.7
V-Dep-Hp-1	2016	-14.248673	-170.6750382	1.2	8.8	14.4	12.2
V-Dep-Hp-2	2016	-14.250488	-170.6750312	1.8	8.6	17.1	9.5
V-Dep-Hp-3	2016	-14.249185	-170.6709203	1.7	6.6	14.9	8.7
V-Dep-Hp-4	2016	-14.249785	-170.6702002	1.2	6.2	14.7	11.8
V-Dep-Hp-5	2016	-14.25069	-170.671316	1.5	6.2	16.7	11.3
V-Dep-Hp-6	2016	-14.250546	-170.6723282	1.5	7	16.8	11.2
V-Dep-Hp-7	2016	-14.246878	-170.6742287	1.3	6.7	16.4	12.2
V-Dep-Hp-8	2016	-14.24827	-170.6721811	1.8	7.7	17.3	9.7
X-Dep-Hp-1	2016	-14.283105	-170.6756103	2.3	9.3	18	8
X-Dep-Hp-2	2016	-14.281954	-170.6783773	1.7	9.2	15.6	9
X-Dep-Hp-	2016	-14.286124	-170.6754757	1.9	9.2	16.7	8.8

Table C11: Algae N and C parameter data for collected *in situ* algal samples

Sample ID	Sample year	Latitude	Longitude	Nitrogen by weight [%]	D15N [‰]	Carbon by weight [%]	Carbon to nitrogen ratio
F-Dep-Hp-1	2016	-14.295201	-170.676782	1.9	9.6	18	9.4
F-Dep-Hp-2	2016	-14.291881	-170.6802107	1.8	9.8	19.2	10.4
F-Dep-Hp-3	2016	-14.293506	-170.6768181	5.9	9.2	44.7	7.6
F-Dep-Hp-4	2016	-14.289235	-170.679873	1.5	10.2	22.2	14.6
F-Dep-Hp-5	2016	-14.291594	-170.6813936	1.5	8.5	23.3	15.4
F-Dep-Hp-6	2016	-14.291594	-170.6813936	1.6	9.2	16.4	10.2
F-Dep-Hp-7	2016	-14.289275	-170.6811212	4	10.1	34.2	8.5
F-Dep-Hp-8	2016	-14.289275	-170.6811212	1.8	9.8	24.1	13
F-Dep-Hp-9	2016	-14.291801	-170.6783233	4.7	10.1	41.9	8.9
F-Dep-Hp-10	2016	-14.291801	-170.6783233	2.2	10.5	19.6	8.7
F-Dep-Hp-11	2016	-14.29192	-170.6825919	2.6	8.1	28.2	10.7
F-Dep-Hp-12	2016	-14.291698	-170.6828267	1.6	8	21.4	13.5
F-Dep-Hp-13	2016	-14.291743	-170.6824654	1.5	8.7	24.7	15.9
F-Dep-Hp-14	2016	-14.292286	-170.6809127	1.4	8.5	23.2	16.2
F-Dep-Hp-15	2016	-14.293061	-170.679555	1.3	9.3	17.7	13.2
F-Dep-Hp-16	2016	-14.292972	-170.6798812	1.4	8.6	21.1	15.3
F-Dep-Hp-17	2015	-14.292635	-170.680634	4.6	7.8	41.5	9
F-Dep-Hp-18	2015	-14.2922	-170.6796198	5.3	7.7	42.6	8.1
F-Dep-Hp-19	2015	-14.286812	-170.6760387	4.8	9	39.4	8.3
F-Dep-Hp-20	2015	-14.289033	-170.679477	6.8	8.2	44.8	6.6
F-Dep-Hp-21	2015	-14.289929	-170.6816141	1.7	7.7	24.5	14.6
F-Dep-Hp-22	2015	-14.292286	-170.6809127	2	7.6	30	15.3
F-Dep-Hp-23	2015	-14.292635	-170.680634	2.1	7.2	30.2	14.2
F-Dep-Hp-24	2015	-14.2922	-170.6796198	2.1	7.8	18.9	9
F-Dep-Hp-25	2015	-14.29168	-170.6800413	1.9	8.2	18.8	10.1
F-Dep-Hp-26	2015	-14.291525	-170.6807598	1.5	8.3	18.1	11.8
F-Dep-Hp-27	2015	-14.291487	-170.6812898	1.6	7.6	17.7	11.2
F-Dep-Hp-28	2015	-14.291914	-170.6808262	2	7.9	19.7	9.9
F-Dep-Hp-29	2015	-14.291871	-170.6828564	3	7.3	26.4	8.8
Oa-Dep-Hp-1	2016	-14.252642	-170.6411735	5.3	5.3	36.5	6.9
Oa-Dep-Hp-2	2016	-14.252036	-170.6428887	4.7	5.7	43.7	9.2
Oa-Dep-Hp-3	2016	-14.252545	-170.6424856	5	6.1	45.1	9.1
Oa-Dep-Hp-4	2016	-14.25287	-170.6426722	3.4	5.2	42.9	12.7
Oa-Dep-Hp-5	2016	-14.252657	-170.6432849	1.7	5.3	29	16.9
Oa-Dep-Hp-6	2016	-14.252072	-170.642638	4.4	5.5	40.2	9.2
Oa-Dep-Hp-7	2016	-14.251919	-170.6439818	5.2	6.5	44.8	8.6
Oa-Dep-Hp-8	2016	-14.251919	-170.6439818	1.7	6.8	24.8	14.4
Oa-Dep-Hp-9	2016	-14.251192	-170.6429906	5.1	6.2	44.4	8.7
Oa-Dep-Hp-10	2016	-14.252255	-170.6437463	1.3	6.1	22.6	17.7
Oa-Dep-Hp-11	2015	-14.251606	-170.643366	5	4.9	40.3	8.1
Oa-Dep-Hp-12	2015	-14.252243	-170.6438936	4.9	4.3	36.2	7.5

Oa-Dep-Hp-13	2015	-14.252665	-170.6432801	2.7	5	33.8	12.7
Oa-Dep-Hp-14	2015	-14.252243	-170.6438936	1.9	5.3	31.6	16.5
Oa-Dep-Hp-15	2015	-14.252665	-170.6432801	1.9	4.9	33.1	17.1
Oa-Dep-Hp-16	2015	-14.252988	-170.6423885	1.7	5	30.7	18.6
Oa-Dep-Hp-17	2015	-14.252294	-170.6408672	1.5	5.1	29.6	19.5
Oa-Dep-Hp-18	2015	-14.251304	-170.6403125	2.4	5.3	32.5	13.3
Pl-Dep-Hp-1	2016	-14.328442	-170.7015466	1.3	7.1	20.1	15.3
Pl-Dep-Hp-2	2016	-14.324454	-170.6997225	5	6.2	41.1	8.3
Pl-Dep-Hp-3	2016	-14.324454	-170.6997225	1.7	7	16.8	9.6
Pl-Dep-Hp-4	2016	-14.321988	-170.7088063	1.2	7.3	21.1	17.5
Pl-Dep-Hp-5	2016	-14.319826	-170.7151175	3.3	8.3	29.3	8.8
Pl-Dep-Hp-6	2016	-14.317731	-170.7165364	3.5	8.7	29.8	8.5
Pl-Dep-Hp-7	2016	-14.318555	-170.7164019	3.9	7.9	33.6	8.6
Pl-Dep-Hp-8	2016	-14.321237	-170.7143268	2.9	8.5	29.3	10
Pl-Dep-Hp-9	2016	-14.32424	-170.7128188	2.4	7	25.6	10.8
Pl-Dep-Hp-10	2016	-14.323245	-170.7052629	1.8	6.8	29.3	16.6
Pl-Dep-Hp-11	2016	-14.322903	-170.7064723	1.3	6.8	22.4	16.9
Pl-Dep-Hp-12	2016	-14.324168	-170.7024108	0.9	6.1	18.4	19.5
Pl-Dep-Hp-13	2016	-14.325165	-170.7008813	1.1	7.3	15.2	13.6
Pl-Dep-Hp-14	2016	-14.325165	-170.7008813	1.7	7.1	15.5	9.1
Pl-Dep-Hp-15	2016	-14.325165	-170.7008813	4.6	6.9	43.1	9.4
Pl-Dep-Hp-16	2016	-14.325165	-170.7008813	1.3	7.2	14.5	10.8
Pl-Dep-Hp-17	2015	-14.32465	-170.7010565	4.2	6.4	37.9	9
Pl-Dep-Hp-18	2015	-14.324196	-170.7024293	1.4	5.6	24.3	18
Pl-Dep-Hp-19	2015	-14.323337	-170.7059016	2	6.2	31.4	15.5
Pl-Dep-Hp-20	2015	-14.324311	-170.7002821	2.1	6.6	18.4	9
Pl-Dep-Hp-21	2015	-14.32465	-170.7010565	1.4	7	21.4	14.8
Pl-Dep-Hp-22	2015	-14.31748	-170.715993	4	8	27.7	6.9
Pl-Dep-Hp-23	2015	-14.320985	-170.7144163	2.5	7.4	24.3	9.7
Pl-Dep-Hp-24	2015	-14.319639	-170.7154152	2.7	8.3	25.4	9.5
Pl-Dep-Hp-25	2015	-14.318646	-170.7164634	3.3	8	29.2	8.9
Pl-Dep-Hp-26	2015	-14.317874	-170.7166678	3	11.7	26.1	8.8
V-Dep-Hp-1	2016	-14.24732	-170.6737941	2.3	6.8	23.1	10.2
V-Dep-Hp-2	2016	-14.24878	-170.6751368	2.4	8.4	28.2	11.9
V-Dep-Hp-3	2016	-14.24878	-170.6751368	1.9	7.7	28.5	15
V-Dep-Hp-4	2016	-14.250378	-170.6737846	4.3	6.4	38	8.8
V-Dep-Hp-5	2016	-14.247187	-170.6741775	1.7	5.9	28	16.9
V-Dep-Hp-6	2016	-14.247014	-170.6742087	3.9	5.6	35.5	9.1
V-Dep-Hp-7	2016	-14.249627	-170.6749364	1.4	7.8	22.1	15.7
V-Dep-Hp-8	2016	-14.248972	-170.6742767	4.9	6.8	44.3	9
V-Dep-Hp-9	2016	-14.245848	-170.6729926	2.5	5.8	32.4	12.7
V-Dep-Hp-10	2016	-14.24995	-170.6706178	1.1	6	20.9	18.9
V-Dep-Hp-11	2016	-14.249785	-170.6702002	1.5	5.4	26.2	17.4
V-Dep-Hp-12	2016	-14.25069	-170.671316	1.7	5.6	26.6	16.1

V-Dep-Hp-13	2016	-14.250546	-170.6723282	3.1	6.4	32.3	10.4
V-Dep-Hp-14	2016	-14.250546	-170.6723282	1.1	6.6	20.5	18.3
V-Dep-Hp-15	2016	-14.246786	-170.6740902	1.6	5.7	27.1	17.1
V-Dep-Hp-16	2016	-14.250522	-170.6707607	1.4	5.2	23.4	16.9
V-Dep-Hp-17	2015	-14.249517	-170.6750146	2.8	7.1	32.1	11.6
V-Dep-Hp-18	2015	-14.250627	-170.6722927	3.1	5.2	34.6	11.3
V-Dep-Hp-19	2015	-14.242078	-170.670777	3.5	5.6	39.9	11.5
V-Dep-Hp-20	2015	-14.245673	-170.6727996	5	4.4	41.4	8.4
V-Dep-Hp-21	2015	-14.249952	-170.6734651	4.8	5	42	8.7
V-Dep-Hp-22	2015	-14.249971	-170.674648	5.9	5.9	45.6	7.7
V-Dep-Hp-23	2015	-14.250252	-170.6724957	5.3	5.5	43.6	8.2
V-Dep-Hp-24	2015	-14.248678	-170.67499	2.3	6.8	33.3	14.2
V-Dep-Hp-25	2015	-14.249517	-170.6750146	2.2	6.4	32.9	14.8
V-Dep-Hp-26	2015	-14.250599	-170.6744079	1.7	7.4	25.7	15.1
V-Dep-Hp-27	2015	-14.250627	-170.6722927	1.6	5.2	27.2	17.1
V-Dep-Hp-28	2015	-14.2507	-170.6711816	1.9	4.5	31.3	16.6
V-Dep-Hp-29	2015	-14.250626	-170.6706727	1.7	4.2	27.3	15.9
V-Dep-Hp-30	2015	-14.249785	-170.6702535	1.5	4.1	26.5	17.2
X-Dep-Hp-1	2015	-14.284088	-170.6767402	5	8.4	38.2	7.7
X-Dep-Hp-2	2015	-14.283345	-170.6774462	3	8.4	26.5	8.8
X-Dep-Hp-3	2016	-14.284311	-170.6756585	4.6	9.9	40.2	8.8
X-Dep-Hp-4	2016	-14.283181	-170.6759416	5.7	10.3	44.9	7.9
X-Dep-Hp-5	2016	-14.283939	-170.6766093	5.3	9.8	43	8.1
X-Dep-Hp-6	2016	-14.282973	-170.6761598	4.9	9.8	40.5	8.2
X-Dep-Hp-7	2016	-14.281977	-170.6785069	4.5	9.7	36.2	8.1
X-Dep-Hp-8	2016	-14.281977	-170.6785069	2.1	10	16.5	8
X-Dep-Hp-9	2016	-14.280538	-170.6808764	1.5	10.3	12	8.1